Lipid II-binding antibiotics – differential antibiotic activities beyond sequestration of the central peptidoglycan precursor

Dissertation

zur Erlangung des Doktorgrades (Dr. rer. nat.)

der

Mathematisch-Naturwissenschaftlichen Fakultät

der

Rheinischen Friedrich-Wilhelms-Universität Bonn

vorgelegt von

Kevin Christopher Ludwig

aus

Kirchen (Sieg)

Bonn, 2022

Angefertigt mit Genehmigung der Mathematisch-Naturwissenschaftlichen Fakultät
der Rheinischen Friedrich-Wilhelms-Universität Bonn

1. Gutachterin: Prof. Dr. Tanja Schneider

2. Gutachterin: Priv.-Doz. Dr. Christiane Dahl

Tag der Promotion: 20.04.2023

Erscheinungsjahr: 2023

To my family

” Vaccines and antibiotics have made many infectious diseases a thing of the past; we've come to expect that public health and modern science can conquer all microbes. But nature is a formidable adversary. “

Tom R. Frieden, 16th CDC director

Abbreviations

AG	arabinogalactan
AMR	antimicrobial resistance
ApoA-I	apolipoprotein A-I
ATP	adenosine triphosphate
BGC	biosynthetic gene cluster
C_{55}-P	undecaprenyl phosphate
C_{55}-PP	undecaprenyl pyrophosphate
cAMP	cationic antimicrobial peptide
CCCP	carbonyl cyanide *m*-chlorophenylhydrazone
CL	cardiolipin
CP	capsular polysaccharide
CRAB	carbapenem-resistant *Acinetobacter baumannii*
CRE	carbapenem-resistant *Enterobacterales*
CRPA	carbapenem-resistant *Pseudomonas aeruginosa*
cryo-EM	cryogenic electron microscopy
Da	Dalton
DAP^R	daptomycin-resistant
DNA	desoxyribonucleic acid
ECA	enterobacterial common antigen
EMA	European Medicines Agency
FDA	Food and Drug Administration
Fruc	fructose
FucNAc	*N*-acetylfucosamine
FQR	fluoroquinolone-resistant
FQRGC	fluoroquinolone-resistant *Neisseria gonorrhoeae*
FQRP	fluoroquinolone-resistant *Pseudomonas aeruginosa*
GISA	glycopeptide-intermediate *S. aureus*
Glc	glucose
GlcNAc	*N*-acetylglucosamine
HIV	human immunodeficiency virus
HPV	human papilloma virus
HS-AFM	high-speed atomic force microscopy
HTS	high-throughput screening
kDa	kilodalton
LAM	lipoarabinomannan
LCP	LytR-CpsA-Psr
LM	lipomannan
LPS	lipopolysaccharide
LRSA	linezolid-resistant *Staphylococcus aureus*
LTA	lipoteichoic acid
ManNAc	*N*-acetylmannosamine
ManNAcA	*N*-acetylmannosaminuronic acid
*m*DAP	*meso*-diaminopimelic acid
MD	molecular dynamics
MDR-TB	multidrug-resistant *Mycobacterium tuberculosis*

MIC	minimum inhibitory concentration
MOP	multidrug/oligosaccharidyl-lipid/polysaccharide
MRSA	methicillin-resistant *Staphylococcus aureus*
MSSA	methicillin-susceptible *Staphylococcus aureus*
MurNAc	*N*-acetylmuramic acid
NMR	nuclear magnetic resonance
NRP	non-ribosomally synthesized peptides
NRPS	non-ribosomal peptide synthetase
PAP2	phosphatidic acid phosphatases of type 2
PBP	penicillin-binding protein
PG	phosphatidylglycerol
PGN	peptidoglycan
PK/PD	pharmacokinetics and pharmacodynamics
PRSA	penicillin-resistant *Staphylococcus aureus*
PRSP	penicllin-resistant *Steptococcus pneunmoniae*
RBC	red blood cell
R&D	research and development
RIF	region of increased fluidity
RiPP	ribosomally synthesized and post-translationally modified peptides
RNA	ribonucleic acid
SAR	structure-activity relationship
SEDS	shape, elongation, division, and sporulation
TA	teichoic acids
TCS	two-component system
TEM	transmission electron microscopy
THCz	tetrahydrocarbazole
TIRF	total internal reflection fluorescence
UDP	uridine diphosphate
UDP-MurNAc-5p	uridine diphosphatidyl-*N*-acetylmuramic acid-pentapeptide
UPP	undecaprenyl pyrophosphate phosphatase
USD	US dollar
VISA	vancomycin-intermediate *Staphylococcus aureus*
VRE	vancomycin-resistant enterococci
VRSA	vancomycin-resistanripp*taphylococcus aureus*
WHO	World Health Organization
WTA	wall teichoic acid
XDR-TB	extensively drug-resistant *Mycobacterium tuberculosis*

Amino acids are abbreviated according to the IUPAC amino acid single letter or three letter code.

Table of contents

I. Summary

Antibiotic resistance has reached crisis proportions and is a leading mortality factor worldwide. Despite the relevance for public health globally, the antibiotic-discovery pipeline is drying up. The reason for the steep decline of novel antibiotics approved is manifold and complex, including overmining of antibiotic sources, decreased economic attractiveness, as well as regulatory hurdles.

Besides the identification of new antibiotic compounds, it is essential to arrive at a better understanding of their mechanisms of action and the cellular function(s) of the target molecule(s). Most successful antibiotics trigger pleitropic cellular consequences upon primary target inhibition. Understanding the complex antibiotic downstream effects that follow primary target attack is of utmost importance for rational drug development.

Bacterial cell wall biosynthesis is historically known as a most attractive target pathway for antibiotic intervention. Cell wall targeting antibiotics usually inhibit enzymes or block lipid-bound intermediates of the multistep cell wall biosynthesis process. Among the latter, the ultimate peptidoglycan prescuror lipid II represents a most relevant target structure. This thesis particularly focuses on the mechanisms of action elucidation of natural and synthetic cell wall biosynthesis inhibitors from distinct chemical classes.

Chapters 1 to 4 describe the mode of action analysis of natural products. The antibacterial activity of the *Streptomyces*-derived lasso peptide siamycin-I was shown to be based on interference with membrane-bound steps of peptidoglycan biosynthesis through specific interaction with the pyrophosphate moiety of lipid II (**chapter 1**). The identification of a tripartite complex of the clinically approved lipopeptide daptomycin with undecaprenyl-coupled cell wall intermediates and the membrane phosholipid phosphatidylglycerol deciphers the long-time enigmatic molecular target and reconciles previous controversial mechanism of action studies. In a refined model, daptomycin captures the essential undecaprenyl-coupled intermediates and hence blocks cell wall biosynthesis which consequently leads to bacterial cell death (**chapter 2**). The novel cyclodepsipeptides hypeptin and clovibactin, that both share structural features with teixobactin, block cell wall biosynthesis by specificially binding to multiple cell wall precursors that have an undecaprenyl pyrophosphate-moiety in common. Both peptides efficiently kill bacterial pathogens without detectable resistance (**chapters 3 and 4**).

Lipid II-binding antibiotics are generally large and complex natural products. **Chapters 5 and 6** describe the mode of action analysis of synthetic small molecule inhibitors. The 1-amino substituted tetrahydrocarbazole (THCz) class represents the first synthetic small molecule (<500 Da) lipid II binder described. THCz block cell wall biosynthesis by binding to undecaprenyl pyrophospate-containing lipid intermediates of peptidoglycan, teichoic acid and capsule biosynthesis pathways. Importantly, the central diamino motif of THCz was required for target interaction (**chapter 5**). The chlorine-substituted carbazole compound DCAP was previously anticipated to exclusively disrupt the bacterial membrane. However, the mechanism of action of DCAP was found to be more targeted and multifaceted than previously anticipated. DCAP binds to lipid II and undecaprenyl pyrophosphate-coupled lipid intermediates of wall teichoic acid and capsule biosynthesis, thereby blocking cell wall biosynthesis and cell division leading to strong lytic effects (**chapter 6**).

II. Introduction

The antibiotic resistance crisis

Antibiotics are powerful medicines that fight routine and life-threatening bacterial infections, thus, reducing morbidity and mortality and increasing life expectancy and quality. Infectious diseases are the second major cause of death worldwide (Nathan, 2004). More, antibiotics are indispensable pillars of modern medicine as they enable surgeries, bone marrow and organ transplants, artificial joint replacements, and management of immunocompromised patients.

The classes of nearly all major antibiotics in nowadays use were found during the so-called golden era of antibiotic discovery in the 1940s to mid 1960s (Figure 1A). This era was heralded by the discovery of penicillin (Fleming, 1929) and in the following years most antibiotics in todays clinical use have been identified, by systematic screening of soil-derived streptomycetes for antimicrobial activity against a susceptible bacterium grown on solid agar plates and detection of growth inhibition zones (Schatz and Waksman, 1944). However, this rational screening approach, termed the Waksman platform, reached its limits by the end of the 1960s, resulting in the rediscovery of already known compounds terminating the golden era of antibiotic discovery. Depending on the frequency of natural occurrence and the total number of screened strains, Richard Baltz estimated that since then 10 million actinomycetes strains would need to be screened to discover a novel class of antibiotics (Baltz, 2005). With the breakdown of the Waksman platform, companies focused on extending the functional lifetimes of marketed antibiotics by chemical modification of molecular scaffolds to bypass resistance development. However, antibiotics within the same class still act by a similar mechanism of action. As a result, resistance emerged soon after introduction on the market. The lipopeptides, with daptomycin discovered in 1987, represent the latest approved antibiotic class. Since then every newly approved antibiotic belongs to a iterative derivative of a known chemical class (Silver and Mobashery, 2014). With the technological progress including the ability to sequence whole genomes by the 1990s, screening approaches shifted towards high-throughput screenings (HTS) of huge synthetic compound libraries against conserved essential bacterial targets (Silver, 2011). Despite enormous efforts and investments by pharmaceutical industry numerous HTS programmes (e.g. 70 and 65 campaigns conducted by GlaxoSmithKline and by AstraZeneca, respectively) failed to deliver suitable lead scaffolds for further drug development, since bioactivity against whole cells beyond the direct drug–target interactions was not considered and physicochemical parameters were not applicable to the human body (Cook *et al.*, 2014; Gwynn *et al.*, 2010; Payne *et al.*, 2007; Tommasi *et al.*, 2015). Importantly, most successful antibiotics are natural products and do not follow the Lipinski's rule of five (Lipinski *et al.*, 2012); criteria to which rational pharmaceutical compound libraries have been composited (O'Shea and Moser, 2008). Natural product antibiotics are often large, consist of rigid and complex chemical structures, are mostly hydrophilic, and have a positive net charge (Atanasov *et al.*, 2021).

The steady decline in the pipeline of newly discovered and effective antibiotics, the intensive overuse and misuse of antibiotics in healthcare and agriculture combined with improper disposal and environmental contamination, the acquisition of resistance via mutations in chromosomal genes and by horizontal gene transfer, as well as the resistance-associated persistence of drug-resistant pathogens has

led to a global antimicrobial resistance crisis (Berendonk *et al.*, 2015; Harms *et al.*, 2016; Larsson and Flach, 2022; Milani *et al.*, 2019; Munita and Arias, 2016; OECD, 2020).

According to the World Health Organization (WHO) antimicrobial resistance poses one of the most serious threats to public health. Drug-resistant infections were estimated to kill at least 1.27 million people globally each year (Murray *et al.*, 2022) and that number increased as a result of mostly inappropriate antibiotic treatment of the COVID-19 disease (Pan American Health Organization, 2022). 10 million deaths attributable to antimicrobial resitance are predicted globally per year by 2050 accompanied by financial burden of 100 trillion USD on healthcare systems under the scenario that no action is taken (O'Neill, 2014).

Pathogens that have emerged (multi)drug-resistance include members of the so-called 'ESKAPE' group (***E****nterococcus faecium*, ***S****taphylococcus aureus*, ***K****lebsiella pneumoniae*, ***A****cinetobacter baumannii*, ***P****seudomonas aeruginosa*, and ***E****nterobacter* spp.), which are responsible for the majority of nosocomial infections (De Oliveira *et al.*, 2020; Rice, 2008). These and further antibiotic-resistant pathogens of particular global concern (e.g. *Streptococcus pneumoniae*, *Haemophilus influenzae*, and *Shigella* spp.) were categorized in the WHO global priority list of antibiotic-resistant bacteria, also including bacteria responsible for community-acquired infections such as *Salmonella* spp., *Campylobacter* spp., *Neisseria gonorrhoeae*, and *Helicobacter pylori* (Figure 1B; Tacconelli *et al.*, 2018; WHO, 2017). Notably, 15 of the 18 listed drug-resistant bacteria represent Gram-negative species. In addition to this list, multidrug-resistant *Mycobacterium tuberculosis* (MDR-TB) and extensively drug-resistant *M. tuberculosis* (XDR-TB) are of already globally long-established priority (WHO, 2020). Notably, infections caused by difficult- or impossible-to-treat antibiotic-resistant bacteria are becoming increasingly common (Simonsen, 2018).

To date, there is no antibiotic in clinical use to which resistance has not yet emerged. Therefore, one of the key recommendations is to safeguard the efficacy of new antibiotics by restricting them for treatments of last resort. Paradoxically, the relatively short revenue periods and low purchase prices of antibiotics compared to other drugs reduced the commercial interest in antibiotic research and forced large pharmaceutical companies to divest from antibiotic development, as sale volumes for new antibiotics remain minimal and thus affect profitability (Nathan and Goldberg, 2005). Currently, only four big pharmaceutical companies continue to develop new antibiotics (Figure 1A). Although small and mid-sized companies are involved in 92% of new drugs (as of December 31th, 2019) being developed (Dheman *et al.*, 2020; Munos, 2009), only (partnerships with) large companies in combination with cost-lowering interventions (so-called push incentives) have the means to process an antibiotic from its discovery to market approval (Cama *et al.*, 2021; Miethke *et al.*, 2021). According to the WHO, only about 14% of antibiotics in phase I clinical trials are likely to accomplish approval and the process from discovery to approval typically takes more than a decade and costs about 1.4 billion USD without marketing and surveillance costs included (DiMasi *et al.*, 2016; McKenna, 2020). The combination of scientific, economic and regulatory hurdles yielded only three approved new antibiotic classes within the past 30 years (Figure 1A).

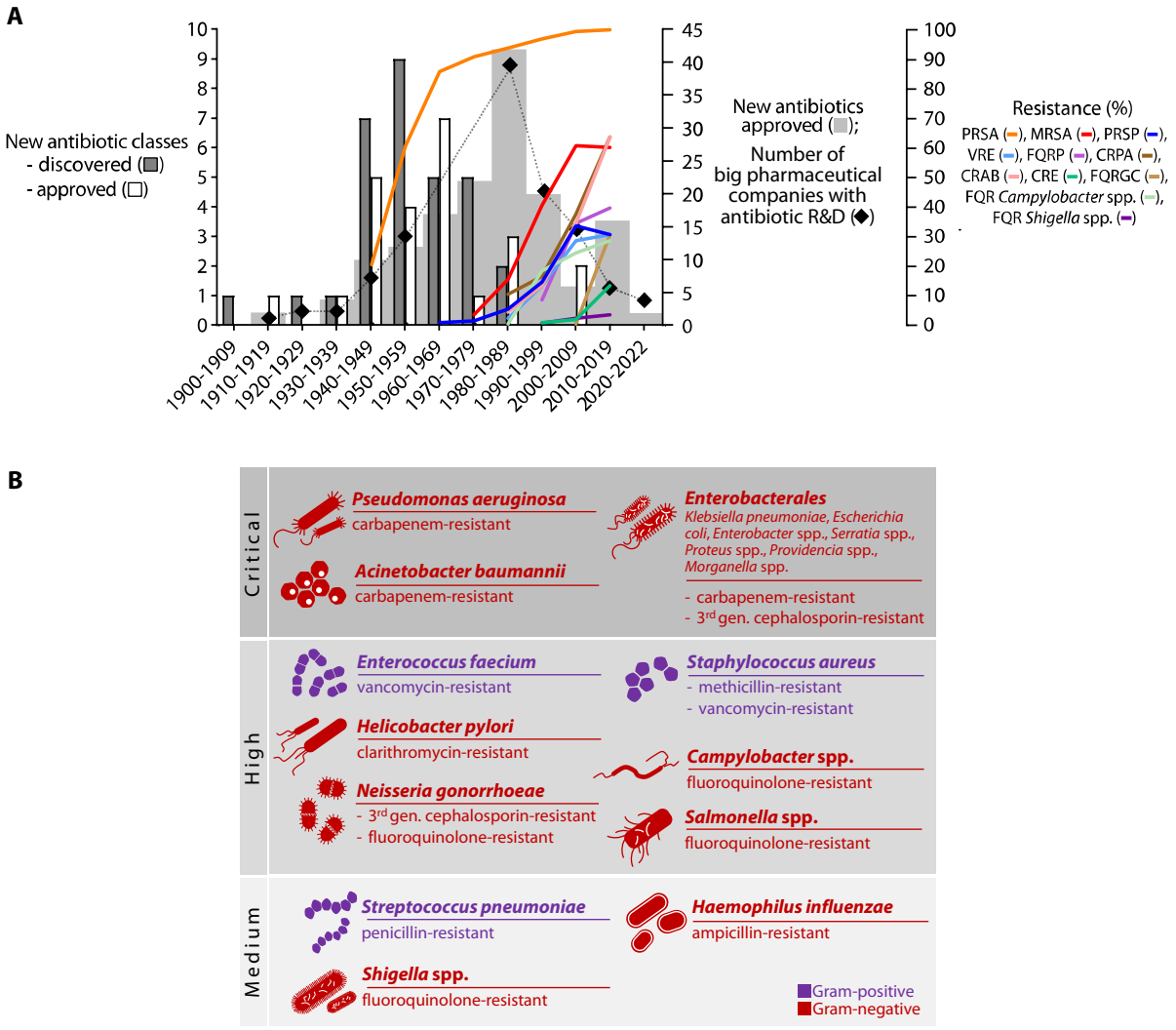

Figure 1. Antibiotic resistance at a glance. (A) The discovery of new antibiotic classes has lagged, accompanied by the retreat of Big Pharma from antibiotic research and development (R&D) and increasing occurrence of antibiotic-resistant pathogens. The discovery of a new antibiotic class is only included if at least one commercial product entered the market. Approval years of new antibiotic classes refer to FDA and EMA approvals, depending on which institution first approved the respective drug. Remaining Big Pharma with antibiotic R&D: Merck, Roche, GlaxoSmithKline, Pfizer. Relative resistance refers to average global resistance. Relative resistance within a shown decade refers to the mean of all years of the decade. Abbreviations: PRSA, penicillin-resistant *S. aureus*; MRSA, methicillin-resistant *S. aureus*; PRSP, pencillin-resistant *S. pneumoniae*; VRE, vancomycin-resistant enterococci; FQRP, fluoroquinolone-resistant *P. aeruginosa*; CRPA, carbapenem-resistant *P. aeruginosa*; CRAB, carbapenem-resistant *A. baumannii*; CRE, carbapenem-resistant *Enterobacterales*; FQRGC, fluoroquinolone-resistant *N. gonorrhoeae*, FQR, fluoroquinolone-resistant. **(B)** WHO global pathogens priority list adapted from WHO, 2017.

Figure 1A was created with data obtained from various sources: Pew Charitable Trusts; ClinicalTrials.gov; U.S. Food and Drug Administration (FDA); European Medicines Agency (EMA); European Centre for Disease Prevention and Control (ECDC); Central Asian and Eastern European Surveillance of Antimicrobial Resistance (CAESAR); European Antimicrobial Resistance Surveillance Network (EARS-Net); Global Antimicrobial Resistance Surveillance System (GLASS); Centers for Disease Control and Prevention (CDC); ResistanceMap Surveillance Network, Center for Disease Dynamics, Economics & Policy (CDDEP); John Rex, AMR Solutions; Lynn Silver, LL Silver Consulting; Wellcome Trust; CARB-X; Infectious Diseases Society of America (IDSA) report "Bad bugs, no drugs", 2004; Ammerlaan *et al.*, 2013; Asensio *et al.*, 2011; Boucher *et al.*, 2009; Butler *et al.*, 2022; Cassini *et al.*, 2019; Chambers, 2001; Deak *et al.*, 2016; Gould *et al.*, 2010; van Hecke *et al.*, 2017; Lewis, 2020; Livermore, 2004; McDonald, 2006; McKenna, 2020; Monnet, 2005; von Nussbaum *et al.*, 2006; OECD *et al.*, 2017; Rice, 2008; Silver, 2011; Simonsen, 2018; Spellberg *et al.*, 2004; Stewardson *et al.*, 2016, 2019; Tacconelli *et al.*, 2018; U.S. Committee on the Judiciary, 1961; U.S. Federal Trade Commission, 1958; Ventola, 2015; Wenzel and Bandow, 2011; Wright, 2010.

The bacterial cell wall as a target for antibiotics

Most successful antibiotics interfere with biosynthesis pathways of major cellular macromolecules, including cell wall (and cell divisome components), nucleic acids (i.e. DNA and RNA), proteins and folic acids. Moreover, membrane disintegration often occurs as side-effect owing to hydrophobic parts of an antibiotic that interact with membrane lipids.

Historically, cell wall biosynthesis was the first pathway attacked by antibiotic treatment and remains the most prominent target for antibacterial therapies. Approximately 50% of the overall antibiotic prescriptions, and more than 70% of intravenous clinical applications rely on cell wall biosynthesis inhibitors (Kresse *et al.*, 2007).

The bacterial cell wall and its biosynthetic machinery are highly conserved and unique among bacteria without structural homologs in mammals. It forms a complex multilayered surface structure, that confers cells their characteristic shape, provides mechanical stability, and protects the cells from lysis of the high internal osmotic pressure and from external environment (Höltje, 1998). The maintained cellular integrity plays a pivotal role for cell viability. During growth, the cell wall is dynamically synthesized and hydrolyzed in a highly balanced fashion.

Gram-negative bacteria are surrounded by 1-3 layers (10 nm total thickness) of the major sugar-peptide polymer component peptidoglycan (PGN), which itself is additionally covered by an asymmetric outer membrane (Ushijima, 1967) containing lipopolysaccharides (LPS), lipoproteins and porins. The outer membrane of some pathogenic *Enterobacterales* is composed of the so-called enterobacterial common antigen (ECA; Kunin *et al.*, 1962). In contrast, Gram-positive bacteria have about 40 layers (20-80 nm total thickness) of PGN and lack an outer membrane. Gram-positive PGN is densely decorated with secondary glycopolymers such as anionic wall teichoic acids (WTA), lipoteichoic acids (LTA), and surface proteins (Figure 2).

The mycobacterial cell envelope is composed of thin PGN layers, to which arabinogalactan (AG) is covalently linked. AGs are esterified at β-hydroxylated long-chain (C_{60}-C_{90}) mycolic acids, in which glycolipids are non-covalently embedded, forming the so-called mycomembrane. In addition, the membrane contains porins and is crossed by lipoglycans such as lipomannan (LM) and lipoarabinomannans (LAM; Figure 2; Dulberger *et al.*, 2020; Jackson, 2014). The complex structure of the mycobacterial cell wall plays a key role in instrinsic resistance to antibiotics as it limits permeability, which makes it even harder to find efficient antimycobacterial drugs (Batt *et al.*, 2020).

Cell envelopes of invasive pathogens can be further surrounded by capsular polysaccharides (CP), which contribute to virulence via preventing phagocytosis and desiccation, accompanied by enhanced adherence to surfaces in the bloodstream of infected hosts, which increases persistence (Nilsson *et al.*, 1997; Thakker *et al.*, 1998; see **"Bacterial capsule"**).

Overall, the bacterial cell envelope is negatively charged owing to the anionic character of phospholipids, teichoic acids (TA) and CP. Remarkably, the cell surface of Gram-positive bacteria is more negatively charged than eukaryotic cell membranes, in which anionic lipids are predominantly exposed to the inner membrane leaflet (Epand, 2019). This surface property renders the bacterial cell

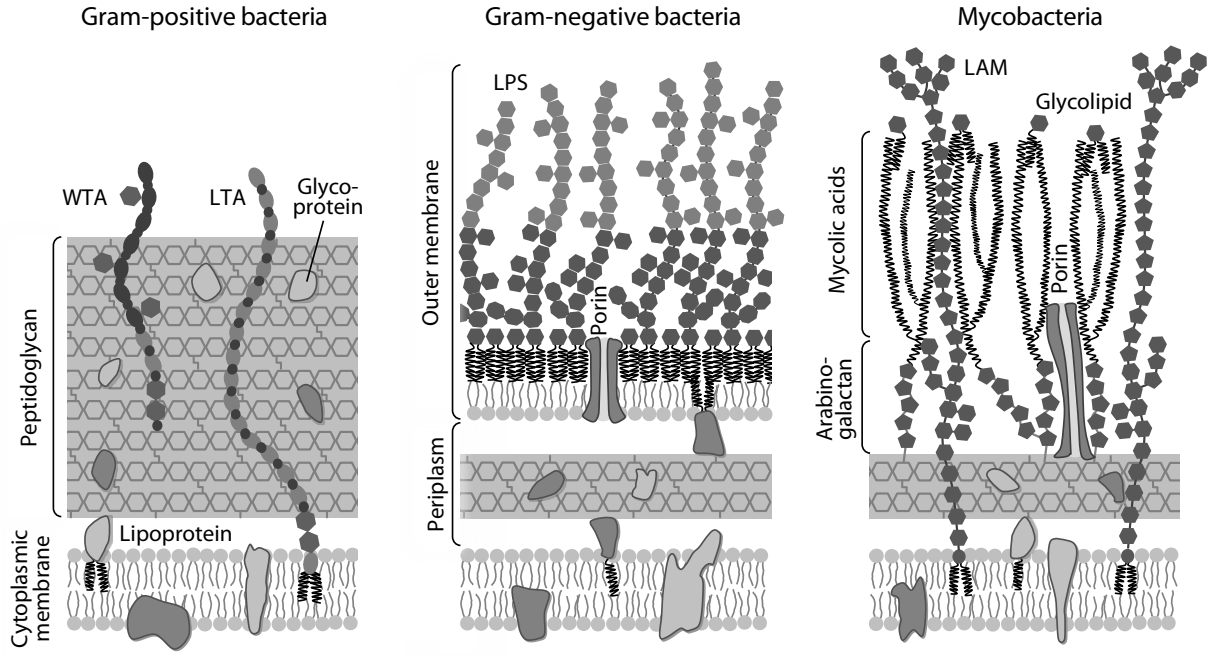

Figure 2. Schematic comparison of Gram-positive, Gram-negative and mycobacterial cell envelopes. Gram-positive bacteria have of a thick layer of PGN decorated with WTA. LTA are anchored to the cytoplasmic membrane through diglucosyl-diacylgylcerol. The cell wall of Gram-negative bacteria consists of a thin layer of PGN within the periplasmic space between the inner cytoplasmic membrane and an asymmetric outer membrane. The surface-exposed side of the outer membrane is composed of LPS. Transport of mainly hydrophilic molecules with a molecular weight less than 600 Da is facilitated through porins. The cell wall of mycobacteria consists of thin layers of PGN and AG, a thick layer of mycolic acids, and porins. Glycolipids such as LAMs, are anchored to the cell wall via diacylglycerol. PGN of all species is decorated with glycoproteins, and phospholipid membranes of all species are mostly decorated with lipoproteins.

envelope a "docking platform" promoting electrostatic interactions with the mostly positively charged amphipathic antibacterial compounds, also referred to as cationic antimicrobial peptides (cAMPs) (Ciumac *et al.*, 2019; Epand *et al.*, 2016).

The complex and dynamical biosyntheses of PGN, WTA, CP, AG, the LPS O-antigen and the ECA are tethered to the cytoplasmic membrane and consist of highly conserved multi-enzyme machineries that act in parallel (Lennarz and Scher, 1972). In addition, they share the common membrane lipid carrier undecaprenyl phosphate (C_{55}-P) as well as the UDP-*N*-acetylglucosamine (UDP-GlcNAc) substrate (Birch *et al.*, 2008; Hanson and Neely, 2012; Rai and Mitchell, 2020; Sachla and Helmann, 2021; Touzé *et al.*, 2008; Whitfield *et al.*, 2020). The biosynthetic complexes are based on fine-tuned protein-protein and enzyme-substrate interactions, and require a specific lipid environment (van den Brink-van der Laan *et al.*, 2003; Henrich *et al.*, 2016). Cell wall biosynthesis is intricately interlinked to bacterial cell division (Figure 3). This cell biosynthetic/divisome mega-complex requires a fine-tuned temporally and spatially coordination during septal growth (Lee *et al.*, 2014; Monteiro *et al.*, 2018; Pinho and Errington, 2003).

To ensure a well-orchestrated coordination between PGN biosynthesis and degradation during growth, a tightly regulated expression of autolysins (also referred to as PGN hydrolases) is required. Autolysins cleave glycosidic (glucosamidases, muramidases, lysozymes, lytic transglycosidases) or amide (carboxypeptidases, endopeptidases, amidases) bonds (Alcorlo *et al.*, 2017; Antignac *et al.*, 2007;

Do *et al.*, 2020b, 2020a; Egan *et al.*, 2017; and references herein). In *S. aureus* autolysin expression is primarily regulated by the WalKR two-component system (TCS; Dubrac *et al.*, 2007).

Consequently, it seems that imbalance of this tightly synced system, by either interfering with individual enzymes or substrates, is accompanied by irreversible disturbance of the functional integrity of the entire machinery, subsequently leading to cell death.

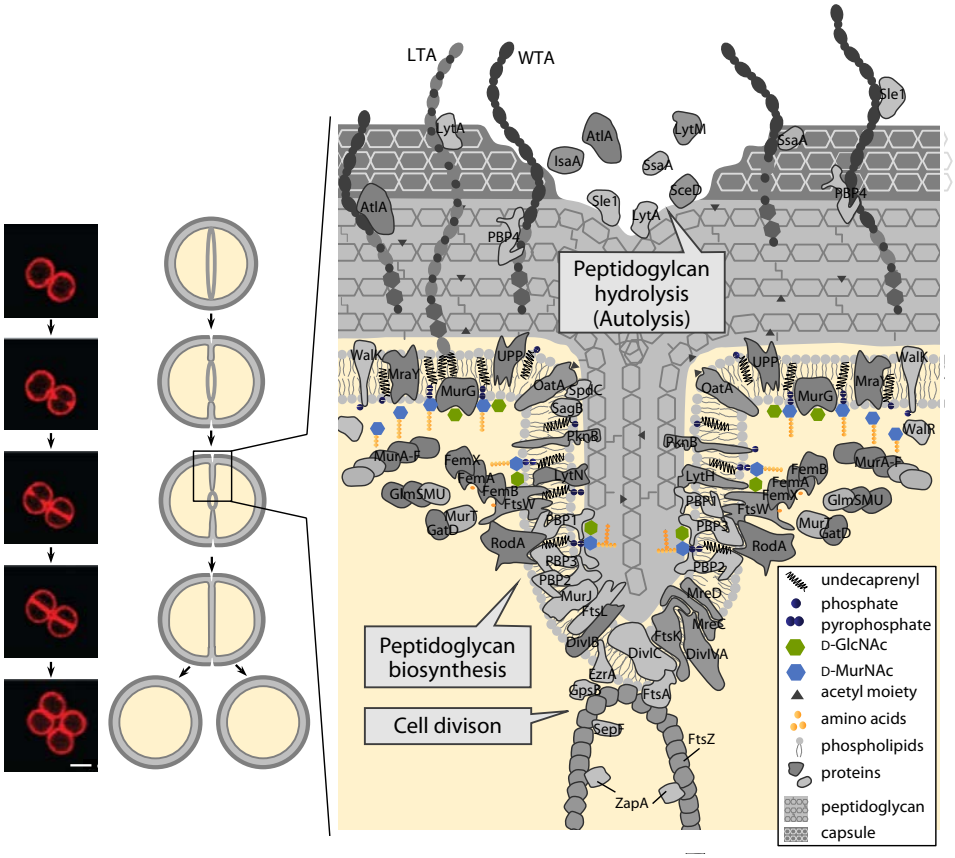

Figure 3. Schematic representation of the functional assembly of the spatial-temporally coordinated PGN biosynthetic/ cell division mega-complex machineries at the cell divison site of a growing *S. aureus* cell. Besides PGN biosynthesis, cell growth is accompanied by PGN degradation initiated by regulated expression of autolysins. WTA and LTA localize autolysins and the carboxypeptidase PBP4, thus playing an important role in balancing PGN turnover. Fluorescence microscopy images showing nile red-stained exponential-phase *S. aureus* cells are reproduced from Monteiro *et al.*, 2015. Scale bar = 1 µm. Abbreviations: WTA, wall teichoic acid; LTA, lipoteichoic acid; GlcNAc, *N*-acetylglucosamine; MurNAc, *N*-acetylmuramic acid.

Peptidoglycan biosynthesis

Peptidoglycan (PGN) consists of linear glycan chains of alternating units of β-1,4-linked *N*-acetyl-glucosamine (GlcNAc) and *N*-acetylmuramic acid (MurNAc), cross-linked by short peptides (Tipper and Strominger, 1966). Gram-positive PGN represents more than 20% of the cell dry weight (Reith and Mayer, 2011). These stem peptides, consisting of L-alanine (L-Ala), D-glutamic acid (D-Glu), L-lysine (L-Lys), and D-alanine (D-Ala) are linked to the D-lactyl moiety of the MurNAc units. Whereas incorporation of L-Lys in third position of the stem peptide is specific for most Gram-positive bacteria including *S. aureus*, the addition of *meso*-diaminopimelic acid (*m*DAP) is specific for Gram-negative species, mycobacteria and most bacilli (Schleifer and Kandler, 1972; Vollmer *et al.*, 2008). Likewise, cross-linking of adjacent stem peptides varies species-specifically and evolves under selective pressure

of antibiotics (Mainardi *et al.*, 2008; Vollmer *et al.*, 2008). Compared to other species, *S. aureus* is characterized by a highly cross-linked PGN structure (74-92% of total PGN), conferring increased mechanical stability (Labischinski, 1992; Vollmer and Seligman, 2010). The ε-amino group of L-Lys is modified with five glycine residues forming an interpeptide bridge to a neighboring D-Ala in fourth position (Figure 4A). Pentaglycine crossbridge formation is essential for the integrity of *S. aureus* PGN (Monteiro *et al.*, 2019).

PGN biosynthesis occurs in three distinct cellular compartments, starting with the formation of the ultimate soluble precursor UDP-MurNAc-pentapeptide (UDP-MurNAc-5p) in the cytoplasm (Figure 4B). UDP-MurNAc-5p is assembled from UDP-GlcNAc, consecutively synthesized by the enzymes GlmSMU out of fructose-6-phosphate (Badet *et al.*, 1987; Mengin-Lecreulx and van Heijenoort, 1994, 1996), followed by stepwise attachment of the stem peptide (L-Ala-D-Glu-L-Lys-D-Ala-D-Ala), catalyzed by the ligases MurA-F (Benson *et al.*, 1993; Patin *et al.*, 2010; Strominger, 1958). The undecaprenyl-coupled PGN precursors are synthesized by membrane-bound enzymes: The integral membrane protein MraY transfers UDP-MurNAc-5p to the membrane-anchored lipid carrier undecaprenyl phosphate (C_{55}-P) to yield lipid I (undecaprenyl-pyrophosphoryl-MurNAc-pentapeptide) (Anderson and Strominger, 1965; Anderson *et al.*, 1967; Neuhaus, 1971; Pless and Neuhaus, 1973), and the subsequent addition of GlcNAc catalyzed by the glycosyltransferase MurG yields the ultimate PGN precursor lipid II (undecaprenyl-pyrophosphoryl-MurNAc-pentapeptide-GlcNAc, Figure 4A; Higashi *et al.*, 1967, 1970). In *S. aureus*, further modification of lipid II with the pentaglycine bridge is consecutively catalyzed by the peptidyltransferases FemXAB (Schneider *et al.*, 2004). Amidation of D-Glu to D-iso-glutamine (D-iso-Gln), and thus reduction of negative charge, is mediated by the bi-enzyme complex MurT-GatD, consisting of a Mur ligase and a glutamine amidotransferase (Münch *et al.*, 2012). This modification is suggested to be relevant for efficient cross-linking (Siewert and Strominger, 1968; Zapun *et al.*, 2013).

Lipid II is then translocated from the cytoplasmic side to the outer surface of the membrane bilayer by the essential multidrug/oligosaccharidyl-lipid/polysaccharide (MOP) flippase MurJ (Sham *et al.*, 2014). The membrane-anchored PGN building block is bound in an internal cavity of the intregral membrane protein and gets transported through the conformational transition from a V-shaped inward-open to an outward-open form (Kohga *et al.*, 2022; Rubino *et al.*, 2020). Recently, it was proposed that PGN biosynthesis is driven by affinity gradients of different PGN precursor lipids from MraY to MurJ (Oluwole *et al.*, 2022).

Once lipid II is flipped across the membrane, it becomes substrate of transglycosylation (connection of growing glycan strands onto lipid II) and transpeptidation reactions (cross-linking of the glycan chains through short peptides) to yield polymerized PGN. In *S. aureus*, transglycosylation is achieved by the essential bifunctional penicillin-binding protein (also termed aPBP), PBP2 (Łeski and Tomasz, 2005). Moreover, transglycosylation is catalyzed by novel types of glycosyltransferase-transpeptidase pairs, including SEDS (shape, elongation, division, and sporulation) proteins and monofunctional PBPs (termed bPBPs; Cho *et al.*, 2016; Emami *et al.*, 2017; Meeske *et al.*, 2016; Taguchi *et al.*, 2019). In *S. aureus* these pairs constitute RodA-PBP3 and FtsW-PBP1. Although transpeptidase activity of the

FtsW-PBP1 pair is not essential, its function in maintaining the divisome at the midcell is of crucial importance. The RodA-PBP3 pair was shown to be required for slight cell elongation (Reichmann *et al.*, 2019). These enzymatic pairings further reflect the tight connection of cell wall biosynthesis and cell division, which have to be highly coordinated in space and time. The *S. aureus* PGN machinery is assembled at the division septum, initiated by treadmilling of the cell divisome tubulin homologue FtsZ followed by MurJ recruitment to the septum, which is mediated by the DivIB–DivIC–FtsL sub-complex. Subsequently, MurJ-catalyzed translocation of lipid II leads to midcell recruitment of PBP2, which recognizes the lipid II substrate (Monteiro *et al.*, 2018; Pinho and Errington, 2005).

The non-essential low molecular weight PBP4 possesses additional DD-carboxypeptidase activity and removes the terminal D-alanine of pentapeptides from already polymerized PGN. Thus, PBP4 prevents uncontrolled transpeptidase activity at these sites, resulting in highly cross-linked PGN (Atilano *et al.*, 2010; Egan *et al.*, 2017; Loskill *et al.*, 2014; Srisuknimit *et al.*, 2017; Wyke *et al.*, 1981). Besides PBPs, *S. aureus* harbors two monofunctional glycosyltransferases: Mgt (also referred to as SgtB) and SgtA, whose function in PGN biosynthesis is unclear (Karinou *et al.*, 2019; Reed *et al.*, 2011; Wang *et al.*, 2001).

The membrane anchor undecaprenyl phosphate (C_{55}-P) represents a crucial ferry for synthesis and translocation of PGN building blocks and is available at limited numbers in a bacterial cell. Despite *de novo* synthesis, recycling of the lipid carrier is important to maintain cell wall biosynthesis. During lipid II transglycosylation, undecaprenyl pyrophosphate (C_{55}-PP) is released and dephosporylated to sustain C_{55}-P pool levels. Different undecaprenyl pyrophosphate phosphatases (UPPs), including UppP/BacA and the phosphatidic acid phosphatases of type 2 (PAP2)-domain proteins PgpB, YbjG, and LpxT catalyze this reaction (Workman and Strynadka, 2020). Subsequently, C_{55}-P is translocated to the inner leaflet of the cytoplasmic membrane to provide C_{55}-P for another synthesis cycle (Manat *et al.*, 2014; Workman and Strynadka, 2020). The C_{55}-P flippase activity was proposed to be achieved by UppP/BacA (El Ghachi *et al.*, 2018; Workman *et al.*, 2018) and more recently reported to involve DUF368-containing proteins that interact with putative transporters of the DedA family (Sit *et al.*, 2022; Roney and Rudner 2022; Figure 4B).

The total number of C_{55}-P(P) carrier lipids in *S. aureus* is estimated about 1.5×10^5 copies per cell and a whole cycle (starting with coupling C_{55}-P to UDP-MurNAc-5p and ending in C_{55}-P retranslocation to the cytosolic leaflet) takes approximately 90 seconds (Barreteau *et al.*, 2009; Piepenbreier *et al.*, 2019), emphasizing the critical importance of this highly coordinated process in preventing imbalance of nascent cell envelope formation (Jorgenson *et al.*, 2019).

Glycan strands are further modified (about 35-90% in *S. aureus*) by covalent attachment of surface polymers such as WTA and CP via phosphodiester bonds to the C6-OH group of the MurNAc residues (Clarke and Dupont, 1992; Vollmer, 2008). Lipid intermediates of WTA and CP pathways are analogously synthesized on the lipid carrier C_{55}-P. The attachment is catalyzed by a yet elusive mechanism involving members of the LCP (LytR-CpsA-Psr) protein family. Recently, LCP proteins were shown to release the lipid carrier C_{55}-P, which then enters new synthesis cycles of PGN, WTA and CP biosynthesis pathways (Rausch *et al.*, 2019; Schaefer *et al.*, 2017; see **"WTA and CP biosyntheses"**).

Further modifications of the glycan strands include *N*-deacetylation of both MurNAc and GlcNAc, and *O*-acetylation of MurNAc and *N*-acetyl fucosamine (FucNAc), involved in CP biosynthesis (Bhasin *et al.*, 1998; Ghuysen and Strominger, 1963; Snowden *et al.*, 1989).

More recently, it was demonstrated that the *S. aureus* glucosaminidase-membrane protein complex SagB-SpdC cleaves newly polymerized but still membrane-anchored PGN strands to their physical length in order to release them for PGN integration into the cell wall (Schaefer *et al.*, 2021; Willing *et al.*, 2021; Figure 4B). *S. aureus* is composed of short glycan strands with approximately six disacchride units that make up 85-90% of the total PGN (Vollmer and Seligman, 2010).

PGN of Gram-positive bacteria is recycled within the stationary growth phase, however, with only 5-10% MurNAc recovered, due to a loss of degraded PGN to the surrounding environment. The process was shown to be catalyzed by the MurNAc-6-phosphate etherase MurQ and is not essential for growth, but crucial for long-term survival (Borisova *et al.*, 2016).

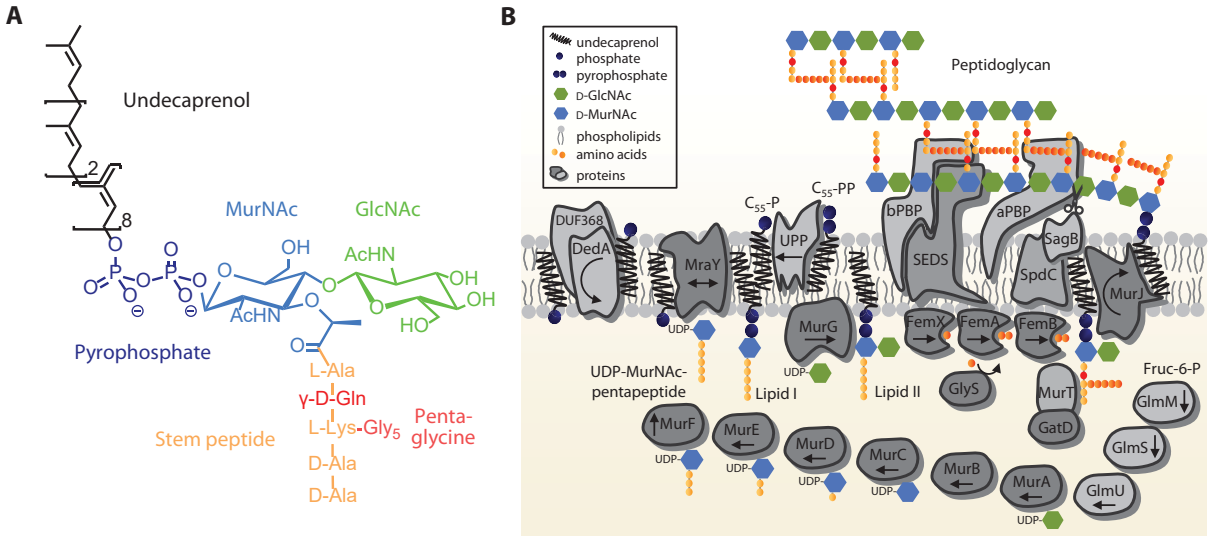

Figure 4. PGN biosynthesis is *S. aureus*. (A) Chemical structure of the PGN precursor lipid II (undecaprenyl-pyrophosphoryl-MurNAc-pentapeptide-GlcNAc). The structure includes the *S. aureus*-specific modifications such as the amidation at the second position, and an attached pentaglycine bridge at the third position of the stem peptide. **(B)** PGN biosynthesis starts in the cytosol with the formation of the ultimate soluble PGN precursor UDP-MurNAc-pentapeptide, catalyzed by the sequential activity of Mur ligases using nucleotide-linked precursors. The glycosyltransferase MraY then catalyzes the transfer of UDP-MurNAc-pentapeptide to the lipid carrier undecaprenyl phosphate (C_{55}-P) to yield lipid I. Another glycosyltransferase, MurG, adds GlcNAc to lipid I to form lipid II. In *S. aureus*, lipid II is further modified by amidation catalyzed by the MurT-GatD-bi-enzyme complex and the sequential attachment of five glycine residues to the stem peptide catalyzed by the peptidyltransferases FemXAB. Lipid II is translocated across the cytoplasmic membrane by the MurJ flippase and becomes subject to glycosyltransferases (aPBPs and SEDS proteins) that form glycan strands, and transpeptidases (aPBPs and bPBPs) that catalyze the cross-linking between adjacent stem peptides. During this process the cell wall hydrolase SagB and the membrane protein SpdC form a complex to release glycan strands from the membrane. Recycling of C_{55}-P is achieved by dephosphorylation of C_{55}-PP via undecaprenyl pyrophosphate phosphatases (UPPs) on the extracellular site and subsequent flipping by an elusive flippase proposed to involve DUF368-containing proteins interacting with putative transporters of the DedA family. Abbreviations: GlcNAc, *N*-acetylglucosamine; MurNAc, *N*-acetylmuramic acid; Fruc, fructose; UDP, uridine diphosphate; P, phosphate; SEDS, shape, elongation, division, and sporulation.

The clinically most relevant PGN biosynthesis inhibitors are the PBP-inhibiting β-lactams, which block transpeptidation, and subsequently lead to cell lysis (Bush and Bradford, 2016). Other cell wall enzyme inhibitors in clinical use are the MurA ligase inhibitor fosfomycin (introduced in 1996), as well as the DdlA ligase and Alr racemase inhibitor D-cycloserine (1964).

Clinically approved antibiotics that bind to cell wall intermediates of Gram-positive bacteria comprise the lipid II-sequestering glycopeptide vancomycin (1958), and the (semi-synthetic) lipoglycopeptides teicoplanin (1987), telavancin (2009), dalbavancin, and oritavancin (both 2014) as well as the C_{55}-PP-binding antibiotic bacitracin (1948). However, intravenous administration of the latter was soon replaced by a topical application due to severe nephrotoxic side effects (Michie and Zintel, 1949). The mechanism of action of the lipopeptide daptomycin (2003) remained unsolved for decades and is not entirely understood down to the last detail (Baltz *et al.*, 2005). Like the (lipo-) glycopeptides, daptomycin is used as an agent of last-resort for treatment of life-threatening infections caused by MRSA and enterococci. In addition to cell wall inhibitors in clinical use, the mechanisms of action of many more promising natural and synthetic compounds have been characterized so far.

Teichoic acids

S. aureus and most Gram-positive bacteria produce teichoic acids (TA), which are either covalently linked to PGN (wall teichoic acids, WTA) or anchored to the cytoplasmic membrane through a glycolipid anchor (lipoteichoic acids, LTA). TA are of zwitterionic character owing to negatively charged phosphate and positively charged amino groups. They protect Gram-positive bacteria from harmful molecules that could easily penetrate the PGN layer (Weidenmaier and Peschel, 2008). WTA and LTA of Gram-positive bacteria account for up to 60% and 9% of the cell wall mass, respectively (Ellwood, 1970; Fischer, 1994).

S. aureus WTA and LTA have been implicated in the correct localization of cell wall enzymes such as autolysins, or PBP4, thus regulating cell wall homeostasis and cross-linking (Atilano *et al.*, 2010; Bierbaum and Sahl, 1985; Flores-Kim *et al.*, 2019; Schlag *et al.*, 2010). Notably, TAs bind protons and divalent cations and are proposed to be important for cation homeostasis and to provide a reservoir of ions required for activity of enzymes localized close to the cell surface (Baddiley, 1970). TA alanylation and glycosylation (see **"WTA and capsule biosyntheses"**) play a crucial role in resistance to cAMPs and β-lactams, respectively (Brown *et al.*, 2012; Peschel *et al.*, 1999, 2000). Moreover, TA serve as binding scaffolds for biomaterials and are proposed to mediate biofilm formation (Gross *et al.*, 2001).

In particular, WTA of *S. aureus* serve as phage receptors (Chatterjee, 1969). Vice versa, *S. aureus* WTA were shown to adhere to host cells (Weidenmaier *et al.*, 2004, 2008). WTA are virulence determinants affecting antibiotic susceptibility e.g. in MRSA or streptococci, and thus represent potential antibiotic and anti-virulent targets (Campbell *et al.*, 2011; Farha *et al.*, 2013; Lee *et al.*, 2016a; Swoboda *et al.*, 2009; Wang *et al.*, 2013; Weidenmaier *et al.*, 2004). In addition, WTA were shown to mediate resistance to lysozyme, heat stress and low osmolarity (Bera *et al.*, 2007; Hoover and Gray, 1977; Oku *et al.*, 2009).

Bacterial capsule

Bacterial capsules are tightly packed, mostly anionic polysaccharide layers that are often covalently attached to the cell surface. Capsules were found in Gram-positive (e.g. *S. aureus*, *S. epidermidis, Streptococcus pneumoniae, S. pyogenes, S. agalactiae, Bacillus cereus, B. anthracis*) and Gram-negative pathogens (*Neisseria meningitidis*, *H. influenzae*, *Escherichia coli, K. pneumoniae, Salmonella enterica* subsp. *enterica* serovar Typhimurium*, P. aeruginosa, Campylobacter jejuni, Pasteurella multocida*), as well as for *M. tuberculosis*. Capsular polysaccharides (CP) are highly diverse, with e.g. more than 80 and 98 distinct capsule serotypes in *E. coli* and *S. pneumoniae*, respectively (Bentley *et al.*, 2006; Geno *et al.*, 2015, 2017; Orskov *et al.*, 1977; Yother, 2011). *S. aureus* comprises 13 capsular serotypes with the predominant serotype 5 and 8 among clinical isolates (Arbeit *et al.*, 1984; von Eiff *et al.*, 2007; Nilsson *et al.*, 1997; Thakker *et al.*, 1998).

CP are non-essential, but play an important role as major virulence factors by preventing desiccation and constituting a permeability barrier for phages and most hydrophobic substances, including cAMPs (Llobet *et al.*, 2008). Electrostatic and hydrophobic interactions of cAMPs with CP are suggested to induce structural changes resulting in a sequestration of cAMPs that prevent them from reaching membrane-associated targets (Fleeman *et al.*, 2020). Most notably, CP downregulate an effective host immune response through protection against antibody opsonization of surface antigens enabling phagocytotic uptake, and by mimicking host molecule structures (King and Wilkinson, 1981; Taylor and Roberts, 2004). Moreover, CP can act as immune invasion factors promoting adhesion to host cells and biofilm formation, thus enabling persistence in bloodstream of infected hosts (Deighton and Balkau, 1990; Hammerschmidt *et al.*, 2005; Horwitz and Silverstein, 1980; McKenney *et al.*, 1998; Nanra *et al.*, 2013).

Based on to their ability to elicit a type-specific immune response, CP are attractive antigens for vaccine development, with some vaccines already approved (Bogaert *et al.*, 2004; Ezzell and Welkos, 1999; Geno *et al.*, 2015; Joshi *et al.*, 2009; Pier, 2003; Weintraub, 2003; WHO, 2021).

WTA and capsule biosyntheses

The biosynthetic machineries of PGN, WTA and CP are tightly interlinked in order to build a vital cell wall. These pathways share the same limited precursor pools, including the lipid carrier C_{55}-P and UDP-GlcNAc (Figure 5).

Synthesis of WTA in *S. aureus* starts at the intracellular side of the cytoplasmic membrane with the assembly of lipid III_{WTA} (undecaprenyl-pyrophosphoryl-GlcNAc) catalyzed by the glycosyltransferase TarO transferring GlcNAc from UDP-GlcNAc to the lipid anchor C_{55}-P (Soldo *et al.*, 2002a). Next, *N*-acetylmannosamine (ManNAc) is added from UDP-ManNAc to lipid III_{WTA} catalyzed by the glycosyltransferase TarA to yield lipid IV_{WTA} (undecaprenyl-pyrophosphoryl-GlcNAc-ManNAc; Ginsberg *et al.*, 2006). UDP-ManNAc is a conversion product of the UDP-GlcNAc epimerase MnaA (Soldo *et al.*, 2002b).

Subsequently, two glycerol phosphate units are added by the phosphotransferases TarB and TarF, followed by a TarL polymerase and/or TarK primase-mediated addition (with TarL as the predominant

enzyme in *S. aureus*) of up to 40 ribitol phosphate units (Ginsberg *et al.*, 2006; Ishimoto and Strominger, 1966; Lovering *et al.*, 2010; Meredith *et al.*, 2008). Whereas TarD provides CDP-glycerol phosphate, the bi-enzyme complex TarIJ provides CDP-ribitol phosphate (Badurina *et al.*, 2003; Pereira and Brown, 2004). TA can become subject to tailoring modifications with D-alanine or GlcNAc (Fischer, 1988). D-alanylation of both WTA and LTA is catalyzed by the gene products of the *dltABCD* operon in *S. aureus*. WTA glycosylation with α- and/or β-GlcNAc is catalyzed via the cytoplasmic enzymes TarM and/or TarS, respectively (Brown *et al.*, 2012; Guo *et al.*, 2021; Xia *et al.*, 2010).

Translocation of the WTA polymers to the outer membrane leaflet is mediated by the ABC transporter TarGH (Chen *et al.*, 2020). The transfer of WTA from C_{55}-P to the C6-OH group of MurNAc within the PGN meshwork is catalyzed by members of the LytR-CpsA-Psr (LCP) family (Chan *et al.*, 2013; Dengler *et al.*, 2012; Hübscher *et al.*, 2009; Kawai *et al.*, 2011; Li *et al.*, 2020; Over *et al.*, 2011; Schaefer *et al.*, 2017).

Remarkably, the late enzyme reactions of WTA biosynthesis (TarB-H) were shown to be essential in contrast to the early steps catalyzed by TarO and TarA, referred to as the "essential gene paradox" (D'Elia *et al.*, 2006a, 2006b). It is suggested that an interference with the late WTA biosynthesis steps leads to the accumulation of C_{55}-P-linked dead-end intermediates, resulting in a critical depletion of C_{55}-P, thus impedeing PGN biosynthesis followed by cell death. Additionally, late-stage WTA inhibiton leads to a downregulation of CP biosynthetic genes to conserve C_{55}-P for PGN biosynthesis (Campbell *et al.*, 2012).

CP biosynthesis genes are arranged in gene clusters and encode for glycosyltransferases and enzymes involved in CP export and polymerization, or in biosynthesis of nucleotide-coupled sugars. Moreover, CP gene clusters encode for enzymes involved in regulation of CP biosynthesis (Reeves *et al.*, 1996).

CP biosynthesis starts at the inner face of the cytoplasmic membrane with the glycosyltransferase-catalyzed synthesis of CP repeating units attached to C_{55}-P (Figure 5). Subsequently, the lipid-coupled oligosaccharides become subject of one of three export-assembly strategies: the synthase-dependent, the ABC transporter-dependent or the Wzx/Wzy-dependent strategy, whereas the latter is widely distributed for polymerization and export of nearly all Gram-positive and most Gram-negative bacteria (Cuthbertson *et al.*, 2010). Wzx is assumed to flip the CP building blocks to the outer surface of the cytoplasmic membrane, being polymerized by Wzy in a non-processive manner (Woodward *et al.*, 2010). In Gram-positive bacteria CP are mainly attached to PGN or the cytoplasmic membrane (Yother, 2011).

Staphylococcal CP serotype 5 consists of trisaccharide repeating units of *N*-acetyl-D-fucosamine (D-FucNAc), *N*-acetyl-L-fucosamine (L-FucNAc), and *N*-acetyl-D-mannosaminuronic acid (D-ManNAcA). The building blocks derive from conversion of UDP-GlcNAc into the respective nucleotide-coupled sugars by three different reactions occurring in the cytoplasm. The synthesis of the first nucleotide-coupled subunit UDP-D-FucNAc is catalyzed in a two-step reaction via UDP-2-acetamido-2,6-dideoxy-D-*xylo*-4-hexulose by the dehydratase CapD and the reductase CapN (Li *et al.*, 2014; Rausch *et al.*, 2019). Generation of the second nucleotide-activated sugar UDP-L-FucNAc is achieved by a reaction cascade involving the epimerases CapEFG (Kneidinger *et al.*, 2003; Miyafusa *et al.*, 2013).

Synthesis of the third precursor UDP-D-ManNAcA is catalyzed by the epimerase CapP and the dehydrogenase CapO (Kiser *et al.*, 1999; Portolés *et al.*, 2001).

Membrane-associated CP bioynthesis steps are initiated by the glycosyltransferase CapM catalyzing transfer of UDP-D-FucNAc to the lipid anchor C_{55}-P, yielding lipid I_{cap} (undecaprenyl-pyrophosphoryl-D-FucNAc; Rausch *et al.*, 2019). Subsequently, glycosyltransferase CapL catalyzes the addition of L-FucNAc to lipid I_{cap}, yielding lipid II_{cap} (undecaprenyl-pyrophosphoryl-D-FucNAc-L-FucNAc) to which D-ManNAcA is added by CapI, yielding lipid III_{cap}. The L-FucNAc C3 residue of the final CP precursor is assumed to be partially *O*-acetylated by CapH (Bhasin *et al.*, 1998; Jones, 2005) and to be flipped to the outer surface with the putative flippase CapK and the polymerase CapJ involved. CP synthesis is further regulated by CapABC (Rausch *et al.*, 2019).

The attachment of WTA and CP precursors to the C6-OH MurNAc residue of PGN is achieved by LCP proteins by a yet unknown mechanism (Figure 5). *S. aureus* has three structurally similar LCP proteins, LcpA, LcpB and LcpC (Chan *et al.*, 2014; Hübscher *et al.*, 2009). LcpA and LcpB are important for WTA attachment, whereas LcpC is the key enzyme for CP attachment (Chan *et al.*, 2014; Rausch *et al.*, 2019; Schaefer *et al.*, 2017). The nature of the acceptor substrate of the LCP reaction is supposed to be the PGN precursor lipid II, nascent PGN, or cross-linked PGN (Kawai *et al.*, 2011; Rausch *et al.*,

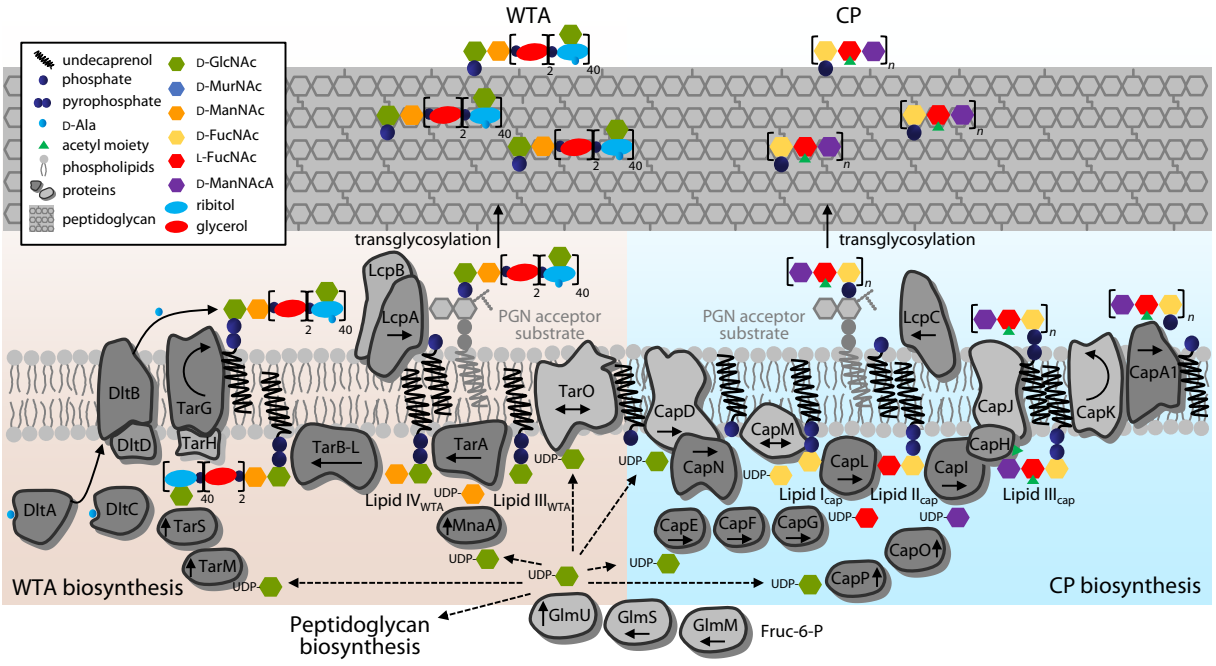

Figure 5. Biosynthesis and attachment of WTA and CP in *S. aureus*. The biosynthetic machineries of WTA (left) and CP (right) pathways are tightly interlinked. The shared precursors UDP-GlcNAc and undecaprenyl phosphate (C_{55}-P) are preferably channeled into PGN and WTA biosynthesis pathways (exponential phase), while CP biosynthesis is low (late-exponential to stationary phase). WTA biosynthesis is achieved by the Tar enzymes catalyzing glycosylation and flipping across the cytoplasmic membrane. The DltABCD machinery is responsible for D-alanylation of teichoic acids. CP biosynthesis (serotype 5) is performed by Cap enzymes catalyzing glycosylation and transport across the cytoplasmic membrane. The attachment of WTA and CP is achieved by LCP proteins that transfer the WTA precursor onto the C6-OH MurNAc residue of a lipid-bound PGN acceptor substrate, such as lipid II, accompanied by C_{55}-P release. Subsequently, glycosyltransferases catalyze the PGN polymerization. Abbreviations: GlcNAc, *N*-acetylglucosamine; MurNAc, *N*-acetylmuramic acid; ManNAc, *N*-acetylmannosamine; FucNAc, *N*-acetlyfucosamine, ManNAcA, *N*-acetylmannosaminuronic acid; Fruc, fructose; UDP, uridine diphosphate; P, phosphate.

2019; Schaefer *et al.*, 2017). The covalent linkage between CP or WTA and PGN is proposed to involve a phosphodiester bond or a glycosidic bond. Importantly, LcpC-mediated cleavage of the CP lipid precursor and phosphosugar transfer were enhanced in the presence of the phosphodiesterase CapA1 (Rausch *et al.*, 2019). The release of C_{55}-P during that reaction is suggested to represent a rescue mechanism to prevent depletion of C_{55}-P. Moreover, it indicates a phosphodiester linkage between CP and PGN.

Lipid II – the bacterial Achilles heel for antibiotic attack

Lipid II is a most relevant antibiotic target molecule in nature and a variety of structurally diverse compounds is known to interact with the PGN precursor. Besides the clinically relevant glycopeptides, lipid II-binding antibiotics can be found in different stages of (pre-)clinical development, particularly active against Gram-positive pathogens (Malin and De Leeuw, 2019).

The comparably small lipid II molecule is an excellent antibiotic target as it is accessible on the outside of the cell, highly conserved among bacteria, has no eukaryotic homologs, and is less prone to resistance development because modification is difficult. In particular, the polyprenyl chain and the pyrophosphate-sugar linkage are hard to modify and thus considered immutable (Müller *et al.*, 2017). Due to the fast lipid II turnover, and thus, very limited amount of only a few thousand molecules per cell (van Heijenoort *et al.*, 1992) in combination with the requirement of recycled C_{55}-P molecules for a new synthesis cycle, lipid II biosynthesis is highly susceptible to disturbance (Piepenbreier *et al.*, 2019). By forming a complex with the essential PGN building block, many antibiotics render lipid II unavailable as a substrate for transglycosylation and transpeptidation reactions, thereby blocking PGN biosynthesis.

Syntheses of the cell wall polymers PGN, WTA and CP, occur across the leading edge of the developing division septum (Lund *et al.*, 2018; Scheffers and Pinho, 2005), which contains numerous C_{55}-P-coupled cell wall precursors including lipid II (Cooper and Hsieh, 1988; Woldringh *et al.*, 1987). These septal and polar membranes are supposed to be enriched in anionic phospholipids, e.g. phosphatidylglycerol (PG) and cardiolipin (CL), affecting enzymatic functions (Barák *et al.*, 2008; Ben-Yehuda and Losick, 2002; Bolla *et al.*, 2018; Lin and Weibel, 2016; Mileykovskaya and Dowhan, 2005; Oliver *et al.*, 2014). That renders the divison septum a particular "landing terrain" for lipid II-binding antibiotics and cell wall-targeting antibiotics in general, as they mostly share cAMP-like features, such as amphiphilicity and a positive net charge (Chugunov *et al.*, 2013). Compounds with a negative or neutral net charge can involve divalent cations to promote binding to the anionic target.

Presently, lipid II-binding antibiotics of at least five chemical classes are known, comprising non-ribosomal (NRPs), ribosomally synthesized and post-translationally modified (RiPPs), and even unmodified peptides (Montalbán-López *et al.*, 2021; Süssmuth and Mainz, 2017; Wilmes *et al.*, 2011). They are produced by organisms from all domains of life in order to constitute host defense strategies (Baltzer and Brown, 2011; Grein *et al.*, 2019). Lipid II binders can be found among glycopeptides (e.g. vancomycin), lantibiotics (e.g. nisin), defensins (e.g. plectasin), lipopeptides (e.g. empedopeptin) and depsipeptides (e.g. teixobactin; Grein *et al.*, 2019; Medeiros-Silva *et al.*, 2019; Müller *et al.*, 2017). They vary substantially in sequences, secondary stuctures, sizes and antibiotic activities, that depend on

the compound's physiochemical properties such as hydrophobicity and charge, and in particular the binding site on lipid II.

Whereas the glycopeptide prototype **vancomycin** interacts with lipid II by binding to the D-Ala-D-Ala dipeptide terminus via formation of five hydrogen bonds (Reynolds, 1989), the binding affinity of the further developed lipoglycopeptide **oritavancin** (featuring an additional hydrophobic 4'-chlorobiphenyl methyl side chain and an 4-epi-vancosamine substituent) additionally involves the pentaglycine crossbridge and the D-iso-Gln in position 2 of the lipid II stem peptide as crucial binding sites (Kim *et al.*, 2008, 2017; Münch *et al.*, 2015). The additional binding sites account for an increased binding to modified lipid II ending in D-Ala-D-Lac, which is a common substitution of the resistance mechanism to vancomycin. In addition to vancomycin, oritavancin affects the membrane integrity (Belley *et al.*, 2010).

Resistance development to antibiotics that interact with the pyrophosphate moiety (a structural conserved motif among cell wall intermediates from different pathways, i.e. PGN, WTA and CP) is less readily achieved, as modification of this highly conserved structure has not been observed (Egan *et al.*, 2020). Strinkingly, antibiotics that recognize the pyrophosphate moiety vary substantially in their modes of action.

The most extensively studied lantibiotic **nisin** operates by a dual mode of action: firstly, nisin binds to lipid II and secondly forms lethal pores that span the cytoplasmic membrane (Medeiros-Silva *et al.*, 2018; Wiedemann *et al.*, 2001). The structure of the nisin-lipid II complex revealed a "pyrophosphate cage", in which the positively charged amides of thioether rings A and B of nisin interact with the lipid II pyrophosphate group via intermolecular hydrogen bonds (Hsu *et al.*, 2004). In addition, the MurNAc sugar moiety is supposed to be required for high-affinity interaction of nisin to lipid II (T'Hart *et al.*, 2016).

High-affinity lipid II binding of the fungal defensin **plectasin** relies on the formation of four hydrogen bonds to the pyrophosphate moiety and involves a salt bridge between the His_{18} residue and the free *N*-terminus of the compound with iso-D-Glu in position 2 of the lipid II stem peptide. To this end, amidation of iso-D-Glu_2 decreases bacterial susceptibility towards plectasin (Münch *et al.*, 2012; Schneider *et al.*, 2010).

Pyrophosphate binding of the recently discovered depsipeptide **teixobactin** appears to potentiate its antibiotic activity, as it simultaneously blocks additional pathways besides PGN biosynthesis, such as WTA biosynthesis (see **"Teixobactin-like depsipeptides"**). Binding of teixobactin to WTA precursors is suggested to contribute to rapid cell lysis, due to the uncontrolled liberation of autolysins (Homma *et al.*, 2016; Ling *et al.*, 2015).

These examples emphasize the high variability in binding modes among lipid II targeting antibiotics and their impact for antibiotic activity suggesting a variety of distinct consequences triggered within the bacterial cell. Apart from rendering lipid II unavailable for PGN biosynthesis, these may include disintegration of the cell wall biosynthetic/divisome machinery (leading to cell divison defects), disturbance of the cytoplasmic membrane integrity, missent regulation, and uncontrolled autolysis. Currently, less is known about antibiotic triggered effects and their interdependencies that cause the ultimate cell death (Baquero and Levin, 2021).

Lasso peptides

Lasso peptides constitute a structurally unique and particularly intriguing family of RiPPs. They are found among the bacterial domain and confer diverse bioactivities and mechanisms of action (Cao *et al.*, 2021; Montalbán-López *et al.*, 2021). Lasso peptides are characterized by adaptation of a specific knotted topology, the "lasso fold", in which the peptidic tail is trapped and locked into a ring. Since the discovery of the first lasso peptide, anantin, in 1991, more than 1,400 prospective lasso peptides have been identified by genome mining, of which 47 were studied in more detail with only a relatively small number that has been investigated at the molecular level. The majority of lasso peptides is produced by Proteobacteria and Actinobacteria, and less frequently by Firmicutes, Cyanobacteria, Bacteroidetes and Euryarchaeota (Tietz *et al.*, 2017).

Lasso peptides are typically comprised of 15-26 amino acids and have molecular weights in the range of 1.5-2.5 kDa. The characteristic structure results from an isopeptide bond between the *N*-terminal amino group and a carboxylic acid side chain of an aspartate or a glutamate residue, forming a macrolactam of 7-9 residues (Figure 6). The *C*-terminal tail is threaded through the lactam ring and sterically trapped by bulky side chains or disulfide bonds. The resulting lasso topology creates an extraordinary high stability and is remarkably resistant to proteases, denaturing agents, and heat (Hegemann, 2020). Lasso peptides comprise a large and chemically diverse group of peptides and can be subdivided into four classes (Figure 6): Class I lasso peptides contain two disulfide bridges, class II lasso peptides lack disulfides, and class III and IV contain a single disulfide bond, in which either ring and tail are linked (class III) or the disulfide bridge links the tail itself (class IV; Hegemann, 2020).

The biological activities of lasso peptides include antimicrobial, antiviral, and antimetastatic functions (Knappe *et al.*, 2008; Maksimov *et al.*, 2012; Um *et al.*, 2013). Notably, antimicrobial activity of lasso peptides has been demonstrated against both, Gram-positive and Gram-negative pathogens, including *B. anthracis*, *S. aureus*, *E. faecalis*, *M. tuberculosis*, *Listeria monocytogenes*, *E. coli*, *P. aeruginosa*, *K. pneumoniae*, *Burkholderia* sp., and *H. pylori* (Tan *et al.*, 2019; Yamamoto *et al.*, 2016).

Prior to the research carried out in this work, the molecular targets and antagonists of only six lasso peptides have been revealed, although some reported mechanisms of action remain questionable. Molecular targets and antagonists include the atrial natriuretic factor, a glucagon receptor, an endothelial type-B receptors, a calmodulin-activated myosin light chain kinase, a prolyl endopeptidase, a RNA polymerase, and the $ClpC_1$ subunit of the Clp protease (Hegemann *et al.*, 2015).

The lasso peptides streptomonomicin, arcumycin and siamycin-I were proposed to inhibit cell wall biosynthesis (Daniel-Ivad *et al.*, 2017; Metelev *et al.*, 2015; Stariha and McCafferty, 2021). The 21-amino acid membered class II lasso peptide **streptomonomicin** is produced by the halophilic actinomycete *Strepromonospora alba* (Li *et al.*, 2003). The compound was specificially active against *B. anthracis*. Though the molecular target of streptomonomicin is yet unknown, streptomonomicin-resistant mutants of *B. anthracis* mapped mutations in the gene encoding for the response regulator WalR of the WalKR TCS, regulating cell wall homeostasis via control of autolysin expression and cell division through *ftsAZ* expression (Dubrac and Msadek, 2004; Fukuchi *et al.*, 2000; Salzberg *et al.*, 2013). Notably, mutations in *walKR* are frequently found in vancomycin-intermediate *S. aureus* (VISA) strains (Howden *et al.*, 2011). Interestingly, streptomonomicin-resistant mutants displayed chaining

phenotypes, indicative of a defective cell separation as observed for autolysin-deficient bacilli (Hashimoto *et al.*, 2012). In addition, streptomonomicin-treatment upregulated the LiaRS (TCS cell wall stress regulon genes *liaI* and *liaH* in *B. anthracis* (Domínguez-Escobar *et al.*, 2014; Wolf *et al.*, 2010), which are known to be induced by antibiotics that interfere with the lipid II biosynthesis cycle (Mascher *et al.*, 2004; Radeck *et al.*, 2016).

The 21-amino acid membered class I lasso peptide **siamycin-I** produced by *Streptomyces* spp. shares structural features with the streptomonomicin core sequence, but has an overall amphiphlic character (Tsunakawa *et al.*, 1995). Besides displaying antibacterial activity against Gram-positive bacteria, including MRSA and VRE, siamycin-I exerts low cytotoxicity (Chokekijchai *et al.*, 1995; Daniel-Ivad *et al.*, 2017; Tsunakawa *et al.*, 1995; Yano *et al.*, 1996). Diverse types of bioactivity have been oberserved for siamycin-I, including the inhibition of an alternative menaquinone biosynthesis pathway in *H. pylori* (Yamamoto *et al.*, 2016), the attenuation of the quorum sensing mechanism in *E. faecalis* (Ma *et al.*, 2011; Nakayama *et al.*, 2007), the inhibition of ATP-dependent kinases (Ma *et al.*, 2011; Nakayama *et al.*, 2007; Yano *et al.*, 1996) and HIV (Chokekijchai *et al.*, 1995; Lin *et al.*, 1996; Tsunakawa *et al.*, 1995).

Daniel-Ivad *et al.* first demonstrated, that siamycin-I interferes with cell wall integrity of *B. subtilis*, as shown by the formation of severe cell shape-deformations of siamycin-I-treated *B. subtilis* cells (Daniel-Ivad *et al.*, 2017). Moreover, siamycin-I induced the LiaRS response. Later, work conducted in the course of this thesis identified lipid II as the molecular target of siamycin-I. A comprehensive analysis on the mode of action of siamycin-I is provided in **chapter 1**.

More recently, another class I lasso peptide, **arcumycin**, a 20-amino acid membered peptide produced by *Streptomyces* spp. was shown to interfere with cell wall biosynthetic reactions (Stariha and McCafferty, 2021). Arcumycin exhibits antibacterial activity against Gram-positive bacteria, including *B. subtilis*, *S. aureus*, but not against enterococci or Gram-negative bacteria. As observed for siamycin-I and streptomonomicin, arcumycin induced the *B. subtilis* cell wall stress response. However, detailed investigations on a specific molecular target are lacking so far.

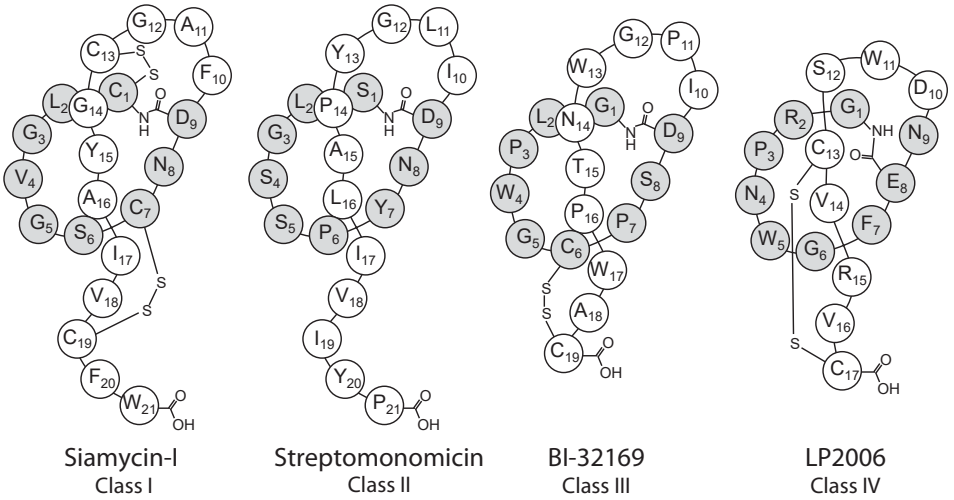

Figure 6. Lasso peptides. Representative structures for the four lasso peptide classes. Structures were adapted from Metelev *et al.*, 2015, Nar *et al.*, 2010, Tietz *et al.*, 2017, and Tsunakawa *et al.*, 1995.

Daptomycin

The lipocyclodepsipeptide daptomycin was first discovered by Eli Lily in 1983 and gained approval as cubicin by Cubist Pharmaceuticals in 2003, used for treatment of skin infections caused by Gram-positive bacteria, including MRSA, glycopeptide-intermediate *S. aureus* (GISA), methicillin-resistant *S. epidermidis* (MRSE), VRE and PRSP, and later in 2006 for bacteremia infections (Sauermann *et al.*, 2008). Daptomycin-resistant strains occurred two years after its approval in clinical settings (Clatworthy *et al.*, 2007). Daptomycin is a component of the A21978C mixture produced by the soil bacterium *Streptomyces roseosporus*, which shows the highest bioactivity (Debono *et al.*, 1987). The lipopeptides of the A21978C family are composed of a three exocylic amino acids linked to a 10-membred depsipeptide core containing the unusual non-proteinogenic amino acids L-kynurenine (L-Kyn), D-asparagine (D-Asn), L-ornithine (L-Orn), D-serine (D-Ser), and 3-methyl-L-glutamic acid (L-MeGlu). The exocyclic amino acids are interlinked with a fatty acid side chain, that differs between the A21978C members (Figure 7). The core of daptomycin is linked to a decanoyl fatty acid side chain (Debono *et al.*, 1988), which was shown to be essential for membrane anchoring (Epand, 1997; Mak *et al.*, 2003). Daptomycin has a negative net charge (–3) at physiological pH. After addition of Ca^{2+}, daptomycin builds up 14- to 16-mer micelles and displays rapid bactericidal activity (Ball *et al.*, 2004; Jung *et al.*, 2004, 2008). Ca^{2+} is suggested to both, neutralize the anionic charges of daptomycin and to facilitate its interaction with anionic membrane phospholipids (Ho *et al.*, 2008; Rotondi and Gierasch, 2005; Straus and Hancock, 2006). In addition, Ca^{2+} renders daptomycin an overall amphiphlic character, conferring typical cAMP features.

The mode of action of daptomycin remained enigmatic for decades and is still not fully understood in all its details. Since the 1980's the results of several studies have been controversially discussed, in parts referable to an unidentified molecular target. The identification of a specific target was further complicated by the pleiotropic and partially overlapping cellular effects induced by daptomycin, particularly affecting the cell envelope. Early studies suggested that daptomycin inhibits cell wall biosynthesis as accumulation of UDP-MurNAc-5p, a decrease in the intracellular UDP-GlcNAc pools, and a specific interference with UDP-GlcNAc incorporation into PGN were observed (Allen *et al.*, 1987; Eliopoulos *et al.*, 1985; Mengin-Lecreulx *et al.*, 1990). Later, LTA biosynthesis was proposed as the target site and "daptomycin-binding proteins" were identified (Boaretti and Canepari, 1995; Boaretti *et al.*, 1993; Canepari *et al.*, 1990). However, LTA binding as a mechanism of action was disproven soon (Laganas *et al.*, 2003). Moreover, potassium leakage, dissipation of the membrane potential, pore formation, membrane blebbing, and aberrant membrane curvature resulting in misplaced septum formation were observed upon daptomycin treatment and were closely correlated to the strong bactericidal effect of daptomycin, but also controversially discussed in literature (Alborn *et al.*, 1991; Allen *et al.*, 1991; Jung *et al.*, 2004; Silverman *et al.*, 2003; Wale *et al.*, 1989). Recently, insertion of daptomycin into artificial PG membranes and formation of toroidal pores was visualized by high-speed atomic force microscopy (Zuttion *et al.*, 2020). Transcriptomic analyses revealed upregulation of genes responsive to cell wall stress and membrane depolarization (Muthaiyan *et al.*, 2008). Notably, daptomycin-resistant mutants, encountered both *in vitro* and *in vivo*, did not reveal a common pattern of mutations pointing to a unique, defined molecular target.

The mode of action model proposed by Hancock and co-workers suggests that daptomycin adopts cAMP-like features in the presence of Ca^{2+} and forms oligomers, which upon close proximity to the cytoplasmic membrane trigger membrane binding, in particular facilitated by interaction with PG, followed by rearrangement into a pore-like structure. Finally, membrane perturbation leads to leakage of intracellular ions and membrane depolarization, followed by rapid cell death (Straus and Hancock, 2006). Importantly, involvement of PG was shown to favor deeper membrane insertion (Jung *et al.*, 2004; Muraih *et al.*, 2011).

Another study showed that daptomycin inserts to specific membrane microdomains containing mostly fluid lipids, and enriched with PG, which led to an overall decreased membrane fluidity triggering the detachment of essential membrane-associated enzymes involved in cell wall biosynthesis and cell divison (Müller *et al.*, 2016). Corroborating, daptomycin-mediated delocalization of essential cell division proteins leading to aberrant septation and cell wall morphology was also oberserved in other studies (Pogliano *et al.*, 2012).

Interestingly, synthetic daptomycin enantiomers completely lost bioactivity, which indicates for an interaction of daptomycin with a specific, chiral biomolecular target rather than only disrupting the cytoplasmic membrane (T'Hart *et al.*, 2014). Candidates for such a chiral target were proposed to be membrane proteins or chiral phospholipids (Kotsogianni *et al.*, 2021; Moreira and Taylor, 2022). **Chapter 2** describes the identification of the molecular target and elucidation of the mode of action of daptomycin.

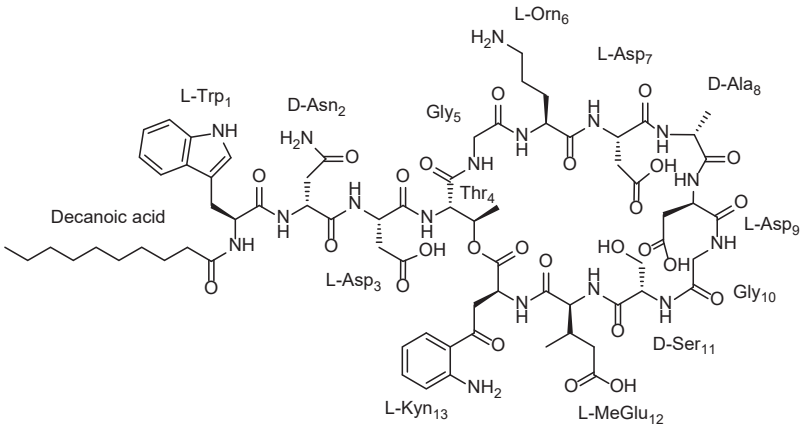

Figure 7: Chemical structure of the lipopeptide daptomycin.

Teixobactin-like depsipeptides

The recently discovered non-ribosomally synthesized undecadepsipeptide **teixobactin**, produced by the Gram-negative β-proteobacterium *Eleftheria terrae* represents a promising new class of lipid II-binding antibiotics with a unqiue chemical scaffold (Ling *et al.*, 2015). Teixobactin is composed of an aliphatic linear 7-residue *N*-terminus and a cyclotetradespi-peptide core. The structure includes five D-amino acids and the unusual non-proteinogenic amino acid L-*allo*-enduracidinine at the *C*-terminus (Figure 8A).

The previously uncultured producing strain of teixobactin was isolated using a miniaturized multichannel device for high-throughput cultivation, known as the iChip (isolation chip), which was developed to grow and isolate previously uncultured bacteria in their natural environment (Kaeberlein *et al.*, 2002; Nichols *et al.*, 2010).

Teixobactin was shown to be highly potent against a variety of Gram-positive pathogens, including *M. tuberculosis*, *C. difficile*, *Bacillus anthracis,* antibiotic-resistant *S. aureus, S. pneumoniae* and enterococci strains (MRSA, VISA, DAP^R, LRSA, VRSA, PRSP, and VRE). It demonstrated excellent bactericidal activity against MSSA and VISA strains and was superior to vancomycin in killing late-exponential phase cells. Also, teixobactin exhibited beneficial PK/PD, low toxicity, and showed good *in vivo* efficacy in three distinct murine models of infection using MRSA and *S. pneumoniae,* as well as in a rabbit model of anthrax infection (Lawrence *et al.*, 2020; Ling *et al.*, 2015). Currently, teixobactin is in preclinical development, being optimized to overcome limitations in intravenous administration as the peptide aggregates to form insoluble gels under physiological conditions (Cadete Pires *et al.*, 2019; Zhang *et al.*, 2021; Zong *et al.*, 2018).

Importantly, *S. aureus* and *M. tuberculosis* both failed to develop teixobactin-resistance *in vitro* and teixobactin was equally active against strains with resistance towards other lipid II-binding antibiotics (Ling *et al.*, 2015). Teixobactin is less prone to resistance development due to its unique mode of action which is based on high-affinity binding to different highly conserved target molecules. Besides the PGN precursor lipid II, teixobactin interacts with WTA precursors (such as lipid III_{WTA}) and C_{55}-PP. Binding to the targets primarily relies on the interaction with the pyrophosphate moiety, which is highly conserved among these cell wall lipid intermediates. This concomitant targeting of multiple cell wall biosynthetic pathways confers an "intrinsic synergy" and is suggested to trigger subsequent detrimental cellular effects that could explain teixobactin's potent activity. One of these effects is the rapid bacteriolytic activity that is suggested to be the result of an uncontrolled liberation of the WTA-anchored autolysins (Homma *et al.*, 2016). Besides PGN and WTA biosyntheses, teixobactin secondarily impacts on fundamental metabolic pathways including phospholipid and fatty acid biosyntheses, accompanied by a decrease of amino- and nucleotide-sugars levels, the perturbation of the histidine and arginine metabolism, the tricarboxylic acid cycle, as well as pantthenate and coenzyme A biosyntheses (Hussein *et al.*, 2020).

Very recently, Weingarth and co-workers studied the teixobactin-lipid II complex interface and topology in membranes using solid-state NMR spectroscopy (Shukla *et al.*, 2020, 2022). The data revealed that the alternating L- and D-amino acids are strategically positioned to align teixobactin into antiparallel β-sheets upon lipid II binding (Figure 8B), a structure that fosters the irreversible formation

of oligomeric teixobactin fibrils (Öster *et al.*, 2018; Shukla *et al.*, 2022; Yang *et al.*, 2018). These fibrils were suggested to thin the membrane by displacing phospholipids and concentrating the C_{55}-P tails (Figure 8D; Shukla *et al.*, 2022).

Structural analysis of the complex revealed that the pyrophosphate group of lipid II is coordinated by the depsi-cycle amino protons and the *N*-terminus of an adjacent teixobactin molecule, which contributes to an improved stability of the interface. In addition, the *C*-terminal enduracididine amino acid coordinates the MurNAc sugar (Figure 8B). The hydrophobic side chains of the exocyclic amino acids Ile_2, D-*allo*-Ile_5, and L-Ile_6 serve as membrane anchors, and the water-exposed hydrophilic amino acid residues L-Ser_3, D-Arg_4, and D-Ser_7 contribute to aggregation of further teixobactin molecules, resulting in a supramolecular fibrillar structure (Figure 8C; Shukla *et al.*, 2020, 2022). In addition, structure-activity relationship (SAR) studies of chemically-synthesized teixobactin analogues showed that a change in the order of polar and apolar or of D- and L-amino acids in the linear *N*-terminal portion cause a complete loss of activity (Abdel Monaim *et al.*, 2016; Chen *et al.*, 2017b; Parmar *et al.*, 2017).

To date, 64,000 microbial isolates and extracts were collected using the iChip culturing method, revealing more than 30 newly discovered antibiotics. Among these compounds, another teixobactin-like peptide, **hypeptin**, was discovered, sharing similar structural features, i.e. a despi-cycle of the same size and a comparable number of D- and L-amino acids, including a guanidine amino acid and β-hydroxy amino acids. Compared to teixobactin, hypeptin has a shorter exocylic linear peptide chain.

Hypeptin was isolated from *Lysobacter* sp. K5869. A comparison with the natural product database pointed towards a compound that was previously isolated from *Pseudomonas* sp. PB-6269 in 1989. The strongly β-hydroxylated octapeptide, eponymous for its designation hypeptin (Figure 8A), displays potent antibacterial activity against Gram-positive bacteria (Shoji *et al.*, 1989). The biosynthesis and the mechanism of action of hypeptin are described in **chapter 3**.

Very recently, another teixobactin-like depsipeptide named **clovibactin** was isolated from a subspecies of the teixobactin producer, *E. terrae* ssp. *carolina*, that was isolated from sandy soil in North Carolina. The octapeptide is composed of three D-amino acids and an uncommon β-OH-asparagine. Compared to teixobactin it shares a depsi-cycle, but has a shorter *N*-terminus with three less amino acids (Figure 8A). The discovery, the biosynthesis and the mode of action of clovibactin are described in **chapter 4**.

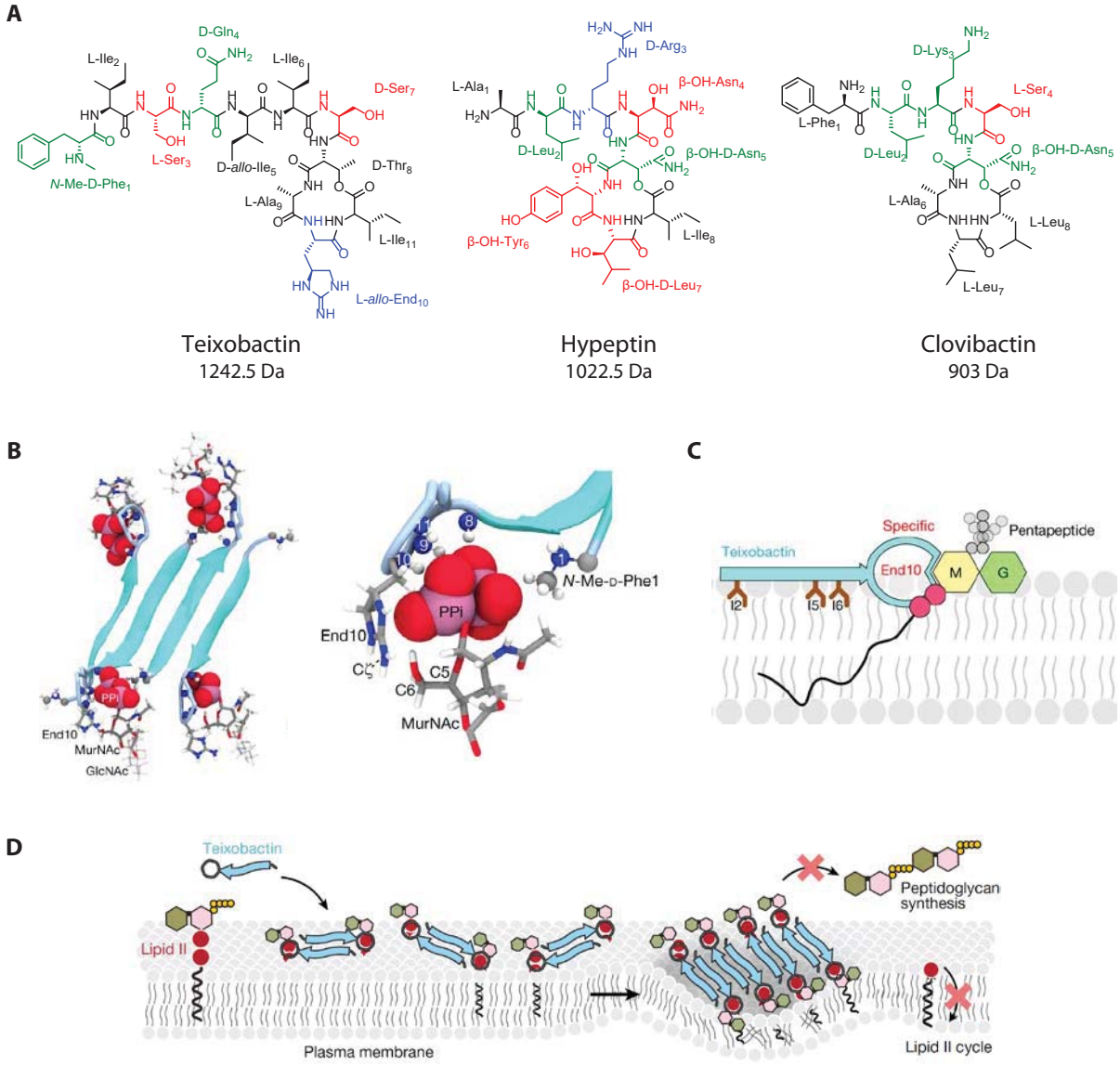

Figure 8. Teixobactin and structurally-related depsipeptides. (A) Structural comparison of teixobactin, hypeptin and clovibactin chemical structures. The compounds contain guanidine amino acids (blue), β-hydroxy amino acids (red), D-configurated amino acids (green), and branched aliphatic amino acids. **(B)** Teixobactin molecules that bind to lipid II align with each other into antiparallel fiber-like β-sheets (cyan). **(C)** *C*-terminal enduracididine (End_{10}) binds specificially to the pyrophosphate group and the MurNAc sugar. The hydrophobic residues of L-Ile_2, D-*allo*-Ile_5, and L-Ile_6 are exposed to the water-membrane interface. **(D)** Proposed mode of action of teixobactin according to Shukla *et al.*, 2022: Teixobactin forms fiber-like β-sheets upon lipid II binding followed by oligomerization into fibrils, thus blocking PGN biosynthesis and thinning the membrane. Figures B, C and D reproduced from Shukla *et al.*, 2022.

Cell envelope-targeting small molecule inhibitors

Permeation of the protective outer membrane of Gram-negative bacteria or the mycobacterial cell envelope is mainly achieved by small molecules with a molecular size of less than 600 Da. Therefore, the identification of synthetic small molecule antibiotics is of great interest. Notably, production costs of small molecules are low and the non-peptidic character is of importance rendering high stability and favorable PK/PD, as well as oral bioavailability (Arranz-Trullén *et al.*, 2017; Craik *et al.*, 2013).

Moreover, the compounds have to meet the physicochemical requirements for evasion of efflux pumps and to penetrate the hydrophobic outer lipid membranes (LPS layer, mycomembrane) by either diffusing through these restrictive barriers or by passing through hydrophilic porins (Acosta-Gutiérrez *et al.*, 2021; Nikaido, 2003; Nikaido and Vaara, 1985). A few groups are currently establishing rules of outer membrane permeation (Muñoz and Hergenrother, 2021; El Zahed *et al.*, 2021).

Besides the clinically used β-lactams, fosfomycin, and D-cycloserine, small molecule inhibitors targeting the bacterial cell envelope mainly comprise membrane-active agents, comprising synthetic proton-ionophores or peptidomimetics, mostly constituted of positively charged amino groups and often collectively active against Gram-positive, Gram-negative and mycobacteria, particularly in the form of dormant cells in biofilms (Chen *et al.*, 2018; Gänzle, 2004; Ghosh and Haldar, 2015; Kim *et al.*, 2016, 2019; Martin *et al.*, 2020; Su *et al.*, 2017; Wang *et al.*, 2016a; and references herein).

As a strategy to combat MRSA infections, small molecules are often used as combination agents to restore efficacy of β-lactam antibiotics (Kant *et al.*, 2017; Koyama *et al.*, 2012; Mann *et al.*, 2013; Nair *et al.*, 2017; Roemer *et al.*, 2013; Swoboda *et al.*, 2009; and references herein). From diverse HTS, inhibitors of cell wall biosynthetic enzymes, such as the mycolic acid transporter in *M. tuberculosis* (Sacksteder *et al.*, 2012; Tahlan *et al.*, 2012), the sortase SrtB of *Clostridioides difficile* (Donahue *et al.*, 2014), the C_{55}-PP synthase UppS of *Bacillus*, *S. aureus*, and *E. coli* (Czarny and Brown, 2016; Farha *et al.*, 2015; Inokoshi *et al.*, 2013, 2016; Peukert *et al.*, 2008; Sinko *et al.*, 2014; Wang *et al.*, 2016b; Zhu *et al.*, 2013), the *S. aureus* enzymes DltA and DltB involved in D-alanylation (Matano *et al.*, 2016; Pasquina *et al.*, 2016), the *S. aureus* O-actyltransferase OatA (Brott *et al.*, 2019), the *S. aureus* cell wall homeostasis regulon WalKR (Igarashi *et al.*, 2013; Qin *et al.*, 2006; Watanabe *et al.*, 2003) the *S. aureus* WTA transporter subunit TarG (Sewell and Brown, 2014; Wang *et al.*, 2013; and references herein), the *S. aureus* WTA glycosyltransferase TarO (Farha *et al.*, 2013; Suzuki *et al.*, 2012; Swoboda *et al.*, 2009), distinct *S. aureus* capsule biosynthethic enzymes (Li *et al.*, 2014), the *S. aureus* PGN peptidyltransferase FemA (Koyama *et al.*, 2012), the *S. aureus* PGN glycosyltransferase MurG (Hu *et al.*, 2004; Mann *et al.*, 2013), the lipid II flippase MurJ (Huber *et al.*, 2009; Mott *et al.*, 2008), and other inhibitors of the Mur ligases A-F (Sangshetti *et al.*, 2017; Silver, 2003) were identified.

Previously, small molecules have been demonstrated to interact with a shortened water-soluble lipid II variant, including pyrylium-, tryptamine-, indole- and indolene-containing compounds and derivatives thereof (Chauhan *et al.*, 2016; Derouaux *et al.*, 2011; Fletcher *et al.*, 2015; de Leeuw, 2014). The positively charged pyrylium moiety of the defensin mimetic lead compound **BAS00127538** with a molecular weight of 517 Da interacts with the anionic pyrophosphate group of lipid II, whereas the indolene and two phenyl rings were predicted to interact with the polyprenyl and the MurNAc moiety, respectively (Varney *et al.*, 2013). The small molecules BAS00127538 and 6Jc48-1a are currently in

preclinical development (Malin and De Leeuw, 2019). However, proof for an interaction with the natural full-length lipid II molecule is missing so far. Furthermore, the compounds did not specificially target cell wall biosynthesis, but also lipid, DNA and protein biosyntheses and antibacterial activity strongly correlated with cytotoxicity.

Very recently, a pneumococcal autolysis-based whole-cell screening for bacterial cell wall biosynthesis inhibitors identified a hit class of synthetic small molecules with a 1-amino substituted tetrahydro-carbazole (**THCz**) scaffold (Figure 9A). The antimicrobial activity and the mechanism of action of THCz are further characterized in **chapter 5**. Dependent on their scaffold, related THCz analogs were previously demonstrated to exhibit antimicrobial acitivity against Gram-positive and Gram-negative bacteria, mycobacteria as well as against pathogenic fungi (Akalaeva *et al.*, 1990; Bublitz *et al.*, 2018; Su *et al.*, 2019). Potent activity of THCz analogs is also described against human papilloma viruses (HPV; Gudmundsson *et al.*, 2009). Bublitz *et al.* identified a fungal P-type ATPase as the target of THCz analogs. A co-crystal structure with a mammalian Ca^{2+}-ATPase revealed a region above the ion inlet channel as the binding site (Bublitz *et al.*, 2018). Remarkably, THCz were also found to exhibit neuroprotective features for treatment of Alzheimer's disease (Honarnejad *et al.*, 2014).

The molecular target and the precise mode of action of another small molecule inhibitor with a chlorine-substituted carbazole scaffold, 2-((3-(3,6-dichloro-9*H*-carbazol-9-yl)-2-hydroxypropyl)-amino)-2-(hydroxymethyl)propane-1,3-diol (**DCAP**, Figure 9B), was elucidated in **chapter 6**. DCAP was previously proposed to target the bacterial membrane and to dissipate membrane potential (Eun *et al.*, 2012; Hurley *et al.*, 2015).

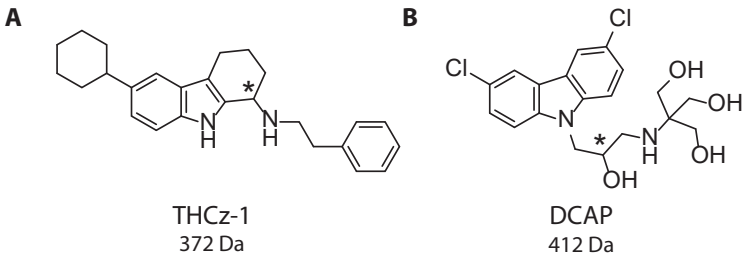

Figure 9. Chemical structures of synthetic small molecule inhibitors of cell wall biosynthesis. (A) Lead compound THCz-1 of a 1-amino substituted tetrahydrocarbazole (THCz) hit class. **(B)** 2-((3-(3,6-dichloro-9H-carbazol-9-yl)-2-hydroxypropyl)amino)-2-(hydroxymethyl)-propane-1,3-diol (DCAP). *, stereogenic center.

III. Aim of the thesis

The central peptidoglycan building block lipid II is a most relevant antibiotic target structure. Several reasons convene that make lipid II such a favorable target: **(i.)** Lipid II is highly conserved in prokaryotes, while eukaryotic counterparts are lacking, reducing adverse side and toxic effects. **(ii.)** The peptidoglycan precursor is not directly encoded by genes, as protein targets are, and thus resistance development is limited. **(iii.)** Most importantly, the membrane-bound lipid II serves various functions within the bacterial cell that go far beyond being a mere cell wall building block. Thus, binding to lipid II can induce a coalescence of antibiotic effects that may all contribute to bacterial killing.

It is intriguing that, despite binding to the same target molecule, lipid II-targeting antibiotics, even structurally closely related compounds, trigger differential cellular effects, affecting potency and the propensity to develop resistance. The aim of this thesis was the analysis of different antibiotics that target cell wall biosynthesis, to elucidate their mode of action and to identify the molecular targets. As all antibiotics were shown to bind to lipid II, a comparative evaluation was envisioned to dissect differences in the mechanisms of action and binding modes, and to illuminate the resulting cellular consequences. A particular focus was on the teixobactin-like compounds hypeptin and clovibactin.

IV. Publications and manuscripts included in this thesis

1. Tan S, **Ludwig KC**, Müller A, Schneider T, Nodwell JR. (2019) The Lasso Peptide Siamycin-I Targets Lipid II at the Gram-Positive Cell Surface. *ACS Chem. Biol.*, 14 (5), 966–974.
   https://doi.org/10.1021/acschembio.9b00157

2. Grein F*, Müller A*, Scherer KM*, Liu X, **Ludwig KC**, Klöckner A, Strach M, Sahl HG, Kubitscheck U, Schneider T. (2020) Ca^{2+}-Daptomycin Targets Cell Wall Biosynthesis by Forming a Tripartite Complex with Undecaprenyl-Coupled Intermediates and Membrane Lipids. *Nat. Commun.*, 11 (1), 1455.
   https://doi.org/10.1038/s41467-020-15257-1

3. Wirtz DA*, **Ludwig KC***, Arts M, Marx CE, Krannich S, Barac P, Kehraus S, Josten M, Henrichfreise B, Müller A, König GM, Peoples AJ, Nitti A, Spoering AL, Ling LL, Lewis K, Crüsemann M, Schneider T. (2021) Biosynthesis and Mechanism of Action of the Cell Wall Targeting Antibiotic Hypeptin. *Angew. Chem. Int. Ed.*, 60, 13579–13586.
   https://doi.org/10.1002/anie.202102224

4. Shukla R*, Peoples AJ*, **Ludwig KC**, Maity S, Derks MGN, De Benedetti S, Krueger AM Vermeulen BJA, Lavore F, Honorato RV, Grein F, Bonvin A, Kubitscheck U, Breukink E, Achorn C, Nitti A, Schwalen CJ, Spoering AL, Ling LL, Hughes D, Lelli M, Roos WH, Lewis K, Schneider T, Weingarth M. (2022) A new Antibiotic from an Uncultured Bacterium binds to an Immutable Target. *Under Review.*

5. Reithuber E*, Wixe T*, **Ludwig KC***, Müller A, Uvell H, Grein F, Lindgren AEG, Muschiol S, Nannapaneni P, Eriksson A, Schneider T, Normark S, Henriques-Normark B, Almqvist F, Mellroth P. (2021) THCz: Small Molecules with Antimicrobial Activity That Block Cell Wall Lipid Intermediates. *Proc. Natl. Acad. Sci.*, 118 (47), e2108244118.
   https://doi.org/10.1002/anie.202102224

6. **Ludwig KC***, Puls, JS*, Matos de Opitz CL, Bornikoel J, Arts M, Krannich S, Straetener J, Brajtenbach D, Henrichfreise B, Sass P, Müller A, Brötz-Oesterhelt H, Kubitscheck U, Grein F, Schneider T. The Dual Mode of Antibacterial Action of the Synthetic Small Molecule DCAP Involves Lipid II Binding. *To be submitted.*

* These authors contributed equally.

Chapter 1

The lasso peptide siamycin-I targets lipid II at the Gram-positive cell surface

Lasso peptides represent a class of ribosomally synthesized post-translationally modified peptides (RiPPs) that exert diverse biological activities. The 21-membered lasso peptide antibiotic siamycin-I displays good antmicrobial activity against multi-resistant Gram-positive bacteria, including clinically-relevant methicillin-resistant *Staphylococcus aureus* and vancomycin-resistant enterococci. Besides exhibiting anti-HIV activity, siamycin-I was proposed to inhibit quorum sensing and ATP-dependend enzymes and more recent studies indicated interference of bacterial cell wall biosynthesis (Daniel-Ivad *et al.*, 2017). The aim of this study was to obtain detailed knowledge on the mode of action of siamycin-I and to identify the molecular target.

Fluorescence microscopy revealed that the molecular target of siamycin-I is exposed at the divison site, since fluorescein-linked siamycin-I specificially localized to the divison septum of *S. aureus* and *Bacillus subtilis* cells. Moreover, delocalization of the bifunctional transglycosylase, penicillin-binding protein 2 (PBP2), pointed towards cell wall biosynthesis as the specific target pathway and the peptidoglycan precursor lipid II as the molecular target of siamycin-I.

Thus, the impact of siamycin-I on the *S. aureus* lipid II biosynthesis cycle was investigated *in vitro* using a cell wall biosynthesis reaction setup with purified, recombinant biosynthetic enzymes and substrates. The lasso peptide inhibited individual reactions with lipid I and lipid II as substrate, but not the conversion of undecaprenyl phosphate (C_{55}-P). Additionally, inhibition of undecaprenyl pyrophosphate (C_{55}-PP) dephosphorylation suggested the lipid-coupled pyrophosphate as the minimal binding motif. Corroborating, the siamycin-I-induced cell wall stress response in *B. subtilis* monitored by LiaI induction was antagonized by external addition of C_{55}-PP-containing lipid intermediates.

Interestingly, serial passage-derived siamycin-I-resistant *S. aureus* isolates were characterized by a thickened cell wall and exhibited cross-resistance to the lipid II-binding antibiotics vancomycin and nisin. Mutations that conferred siamycin-I resistance primarily affected genes encoding for the essential two-component system (TCS) WalKR, regulating the interplay between peptidoglycan biosynthesis and hydrolysis through control of autolysin expression.

Siamycin-I is the first lasso peptide that has been shown to inhibit cell wall biosynthesis by binding to lipid II. Among RiPPs, only lanthipeptides such as nisin are known to bind to lipid II. Siamycin-I shares the immutable C_{55}-PP binding motif with teixobactin, a potent antibiotic that targets multiple cell wall biosynthesis pathways (such as wall teichoic acid biosynthesis). Multi-targeting was not investigated but is most likely for the lasso peptide as well. Unlike siamycin-I, teixobactin's ability to target multiple cell envelope intermediates is suggested to trigger the antibiotic's strong bacteriolytic properties due to altered autolysin expression and to account for the lack of resistance (Ling *et al.*, 2015).

K.C.L. performed mechanism of action studies and identified the molecular targets (i.e. fluorescence microscopy, antagonization assays, *in vitro* enzyme assays including purification of enzymes and substrates, susceptibility testing of *guaA* insertion mutant), analyzed the data and contributed to writing of the manuscript. The publication is also included as part of the doctoral thesis of Dr. Stephanie Tan (Tan, 2022).

ACS chemical biology

Articles

Cite This: *ACS Chem. Biol.* 2019, 14, 966–974

pubs.acs.org/acschemicalbiology

The Lasso Peptide Siamycin-I Targets Lipid II at the Gram-Positive Cell Surface

Stephanie Tan,[†] Kevin C. Ludwig,[‡] Anna Müller,[‡,§] Tanja Schneider,[‡,§] and Justin R. Nodwell*[,†]

[†]Department of Biochemistry, MaRS Discovery District, University of Toronto, 661 University Avenue, Toronto, Ontario, Canada M5G 1M1

[‡]Institute for Pharmaceutical Microbiology, University of Bonn, Meckenheimer Allee 168, 53115 Bonn, Germany

[§]German Centre for Infection Research (DZIF), partner site Bonn-Cologne, Bonn, Germany

Supporting Information

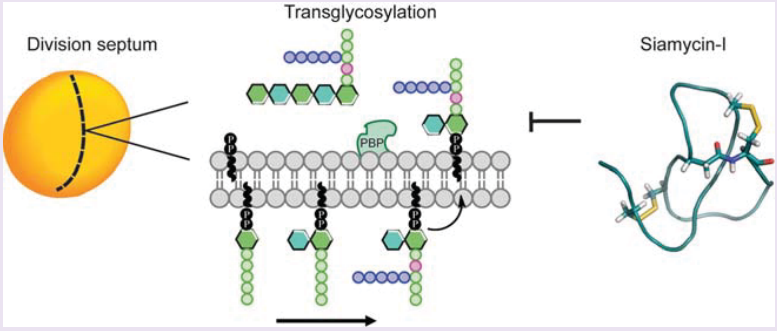

ABSTRACT: Ribosomally synthesized post-translationally modified peptides (RiPPs) are a diverse class of biologically active molecules produced by many environmental bacteria. While thousands of these compounds have been identified, mostly through genome mining, a relatively small number has been investigated at the molecular level. One less understood class of RiPPs is the lasso peptides. These are 20−25 amino acid residue compounds bearing an N-terminal macrocyclic ring and a C-terminal tail that is threaded through the ring. We have carried out a detailed investigation on the mechanism of action of the siamycin-I lasso peptide. We demonstrate that siamycin-I interacts with lipid II, the central building block of the major cell wall component peptidoglycan, which is readily accessible on the outside of the cell. This interaction compromises cell wall biosynthesis in a manner that activates the *liaI* stress response. Additionally, resistance to siamycin-I can be brought about by mutations in the essential WalKR two-component system that causes thickening of the cell wall. Siamycin-I is the first lasso peptide that has been shown to inhibit cell wall biosynthesis.

Methicillin-resistant *Staphylococcus aureus* (MRSA) and vancomycin-resistant *Enterococci* (VRE) are leading causes of Gram-positive bacterial infections. These nosocomial pathogens have largely supplanted sensitive strains and reflect more than 50% of clinical isolates throughout the world.[1,2] Despite the number of available therapeutics for infectious diseases, we are at our last lines of defense. There is a pressing need to find new antimicrobials—compounds having novel targets and mechanisms of action would be well suited as resistance breaking drugs.

The cell wall is a key determinant of cell integrity. It modulates osmotic pressure, cell size, and cell shape and protects the cytoplasm from harmful agents.[3−5] Moreover, cell wall synthesis requires a tight coordination with cell division. The cell wall is composed of peptidoglycan, a polymer of repeating disaccharide units composed of N-acetyl-glucosamine (GlcNAc) and N-acetyl-muramic acid (MurNAc) cross-linked via short peptides. The biosynthesis of peptidoglycan is an intricate process governed by diverse biosynthetic enzymes located in different cellular compartments. The first steps to peptidoglycan biosynthesis occur in the cytoplasm, whereas the key precursor, lipid II, is synthesized at the membrane. Lipid II is flipped to the outside of the cell where the GlcNAc-MurNAc disaccharide is polymerized into a matrix of linear glycan chains and cross-linked together at the pentapeptide chain (Figure 1).[6]

Many antibiotics target cell wall biosynthesis (Figure 1). Glycopeptide antibiotics like vancomycin, β-lactams such as ampicillin, and a more recent discovery, the cyclodepsipeptide antibiotic teixobactin, are a few among known inhibitors of peptidoglycan biosynthesis. Vancomycin interacts with lipid II by binding to the terminal dipeptide, D-Ala-D-Ala, on the pentapeptide chain to prevent polymerization by the penicillin-binding proteins (PBP).[7] β-Lactam antibiotics bind to PBPs

Received: February 26, 2019
Accepted: April 26, 2019
Published: April 26, 2019

DOI: 10.1021/acschembio.9b00157
ACS Chem. Biol. 2019, 14, 966–974

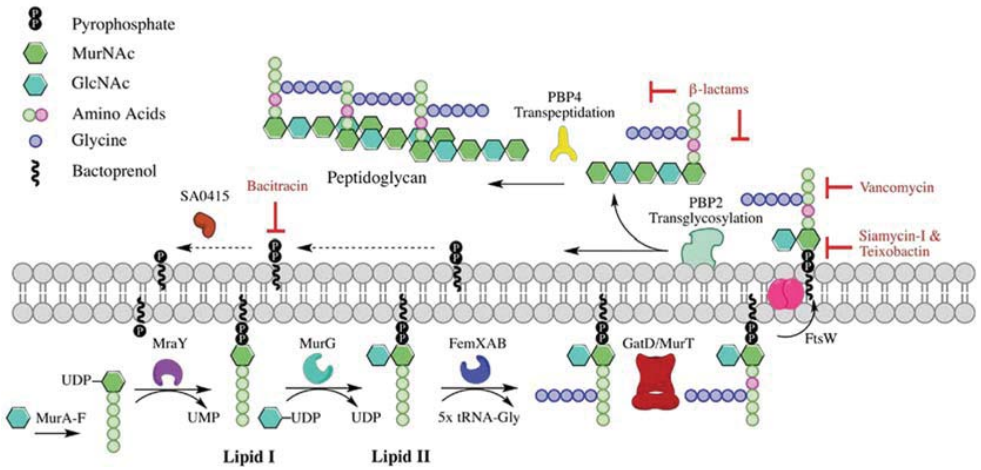

Figure 1. Inhibition of peptidoglycan biosynthesis. Peptidoglycan biosynthesis begins inside the cell to form the precursor, lipid II. Flipping of lipid II to the outside face of the membrane allows lipid II to be polymerized by PBPs into the peptidoglycan network. Inhibitors of peptidoglycan biosynthesis are shown (red). Siamycin-I binds to lipid II and pyrophosphate-containing lipid intermediates.

via irreversible acylation of the active site, consequently interfering with transpeptidation.[8] Teixobactin is an unusual antibiotic that targets multiple polyprenyl-coupled cell envelope precursors, including lipid II. It binds to the pyrophosphate-sugar moiety of lipid II, thereby inhibiting its incorporation into peptidoglycan.[9,10]

Ribosomally synthesized post-translationally modified peptides (RiPPs) are a diverse class of biologically active molecules. To date, 22 subclasses of RiPPs have been described based on their biosynthetic machinery and compound structure. The most well studied RiPPs include the lanthipeptides, thiopeptides, and cyanobactins, whereas new subclasses of RiPPs, such as the streptides, remain underexplored.[11] The various subclasses have provided a large platform of new compounds with varying biological activity and therapeutic potential.

The lasso peptides are an attractive RiPP subclass with an assortment of inhibitory activities.[12] These molecules have several important characteristics: they are resistant to proteases and denaturing agents, highly stable, and unique in topology.[11] Genome mining tools specific for RiPPs have found >1300 potential lasso peptides encoded in bacterial genomes,[13−15] and yet only a few have been extensively characterized. These include microcin J25, an inhibitor of RNA polymerase,[16−19] and lassomycin, an inhibitor of the ClpC1 ATPase involved in proteolysis by the ClpC1P1P2 complex.[20]

Siamycin-I is a 21 amino acid peptide derived from *Streptomyces* sp., in which two disulfide bonds and an N-terminal macrolactam stabilize the tricyclic lasso structure. The amphipathic lasso peptide has been previously reported to inhibit ATP-dependent enzymes *in vitro*, a quorum sensing system in *Enterococcus faecalis*, and human immunodeficiency virus growth in tissue culture cells.[21,22] We identified siamycin-I as a cryptic natural product with antibiotic activity against Gram-positive bacteria; importantly, this included both MRSA and VRE. Preliminary work, in particular its activation of the *liaI* stress response, suggested that siamycin-I might target the cell wall.[23] Given the rising interest in lasso peptides and need for new antibiotics, we set out to ascertain siamycin-I's mode of action in greater detail and identify the molecular target.

In this work, we show that siamycin-I targets the Gram-positive cell wall by binding to lipid II. Siamycin-I recognizes the pyrophosphate lipid anchor as part of its minimal binding site. This interaction appears to occur on the extracellular face of the membrane and primarily at the division septum. This is the first report of such a targeting mechanism for a lasso peptide and adds another antibiotic class to the portfolio of lipid II binding compounds.

RESULTS AND DISCUSSION

Siamycin-I Targets the Cell Wall. To determine how siamycin-I inhibits bacterial growth, we isolated siamycin-I resistant mutants (sia^R) in *Staphylococcus aureus* ATCC29213. We characterized six nonsibling mutants exhibiting resistance to 25 μM siamycin-I (versus minimum inhibitory concentration (MIC) = 3.7 μM against wildtype *S. aureus*). Interestingly, three of the six resistant mutants, sia^R-1, -2, and -5, also exhibited elevated MICs for vancomycin of 2 μM, compared to wildtype MIC = 1 μM. Furthermore, all of the mutants exhibited cross-resistance to the structurally unrelated lanthipeptide nisin. Whereas the MIC of nisin against the wildtype strain is 9 μM, the MICs for sia^R-1−3, -5, and -6, were at least 4-fold greater (38 μM), and that of sia^R-4 was 2-fold greater (18 μM; Figure 2a). We observed no cross-resistance to ciprofloxacin, rifampicin, or kanamycin, which are inhibitors of cytoplasmic targets involved in DNA, RNA, or protein synthesis, respectively. Vancomycin and nisin compromise peptidoglycan biosynthesis by binding lipid II,[7,24] so we surmised siamycin-I might similarly target a component of cell wall biosynthesis.

We sequenced the chromosomes of the six mutants and found that each harbors a single mutation in *walK* or *walR* which encode a two-component regulatory system (TCS); there were other mutations in some strains; however, none was shared by all of them (Supporting Information Table 1). In previous work, we isolated mutants in this background that were resistant to the unrelated antibiotic actinorhodin.[25] Two strains, ATCC29213 *walK* (G533S) and ATCC29213 *walR* (T101M), had mutations exclusively in the *walKR* operon. To rule out any effects of other sequence alterations, we tested these strains for resistance to siamycin-I and found that they

DOI: 10.1021/acschembio.9b00157
ACS Chem. Biol. 2019, 14, 966−974

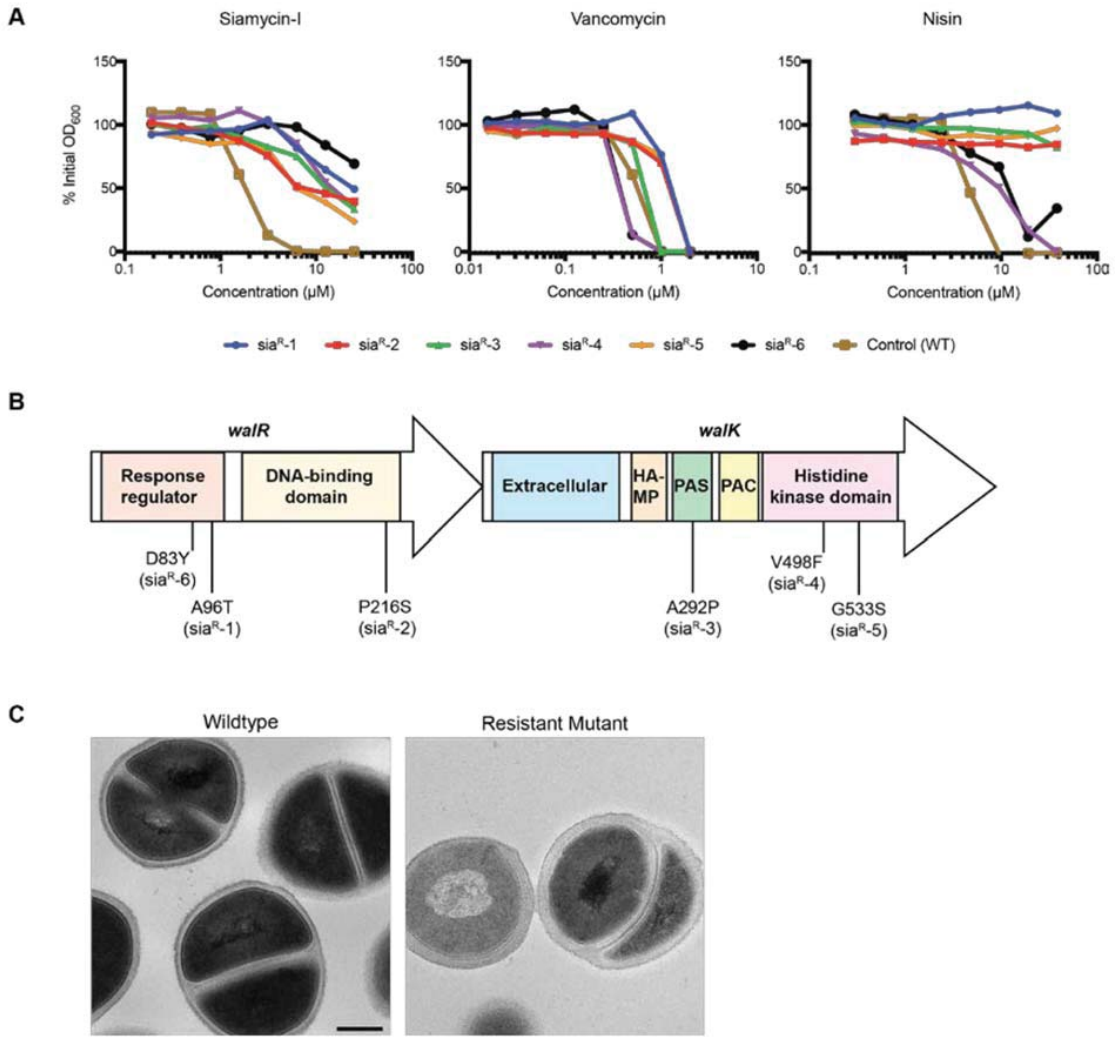

Figure 2. Siamycin-I resistant mutants showing resistance at the cell wall. (A) Cross resistance in siamycin-I resistant mutants was observed against vancomycin and nisin. (B) Single point mutations were found in siamycin-I resistant mutants in either *walK*, the histidine kinase, or *walR*, the respective response regulator. HAMP: **H**istidine kinases, **A**denylate cyclases, **M**ethyl accepting proteins, and **P**hosphatases. PAS: **P**er-**A**rnt-**S**im. PAC: C-terminal motif of PAS. (C) Transmission electron microscopy images of wildtype and mutant *S. aureus* cells. The cell wall thickness of the mutant was measured to 65 nm, and wildtype cells were 22 nm. Scale bar = 200 nm.

both exhibited resistance in comparison to the wildtype (Supporting Information Figure 1). Furthermore, we tested a strain with an insertion in *guaA*, the second most common mutation observed. We found that this strain is less susceptible in the absence of guanine (Supporting Information Table 2); however it was not pursued further at this time. We conclude that mutations in *walKR* confer resistance to siamycin-I.

WalKR regulates genes associated with cell wall metabolism including autolysis, cell division, the recycling of cell wall material, and cell wall maturation during growth.[26,27] WalK autophosphorylates at H192 and then transfers this phosphate to WalR, at D54. Sia^R-1, -2, and -6 each encoded a mutation in *walR*: one mutation fell in the DNA-binding domain (P216S), and two fell in the receiver domain (A96T and D83Y). Sia^R-3, -4, and -5 had mutations in *walK*: sia^R-3 mutation (A292P) was found in the putative signal sensing domain (also known as the PAS domain), whereas sia^R-4 (V498F) and sia^R-5 (G533S) mutations fell in the histidine kinase domain (Figure 2b). Mutations in either *walK* or *walR* have been previously reported and have been shown to play a role in resistance to vancomycin, which is consistent with our data.[28,29] Mutations conferring resistance to streptomonomicin, another lasso peptide, have recently been demonstrated in *walKR* in *Bacillus anthracis*; however, no further characterization on its mechanism of action has been reported.[30] Additionally, when we examined our sia^R mutants under electron microscopy, we found that they exhibited thickened cell walls, a feature of *walKR* mutants previously reported[28,31] (Figure 2c). This further supported the idea that siamycin-I targets a component in the cell wall.

Some antibiotics that target membrane-bound steps in peptidoglycan biosynthesis cause the cytoplasmic accumulation of the cell wall precursor UDP-MurNAc-pentapeptide.[32] To determine whether this is the case for siamycin-I, we carried

DOI: 10.1021/acschembio.9b00157
ACS Chem. Biol. 2019, 14, 966–974

out a precursor accumulation assay using liquid-chromatography mass-spectrometry (LC-MS). As expected, the antibiotics vancomycin, bacitracin, and ampicillin all caused the accumulation of the soluble precursor ($[M + H]^+$ = 1150.39). In contrast, siamycin-I did not trigger this accumulation (Figure 3), indicating that its action is distinct from these

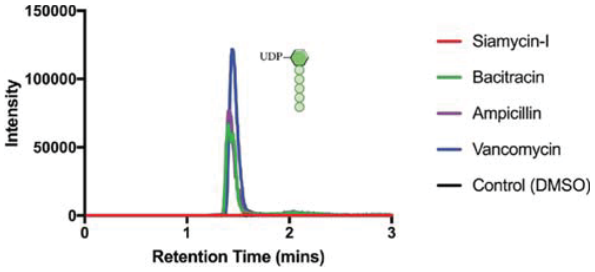

Figure 3. Accumulation of the soluble peptidoglycan precursor, UDP-MurNAc-pentapeptide, not triggered by siamycin-I. Cytoplasmic accumulation of the peptidoglycan precursor, UDP-MurNAc-pentapeptide, after treatment with an antibiotic was detected by LC-MS. Accumulation of UDP-MurNAc-pentapeptide, $[M + H]^+$ = 1150.39, was observed after treatment with bacitracin, ampicillin, and vancomycin but not siamycin-I.

compounds in some way. One possibility was that, like nisin, siamycin-I might cause the formation of pores in the membrane, resulting in depolarization.[33] To determine whether this is the case with siamycin-I, we used a fluorescent dye assay to measure the integrity of the electrochemical gradient across the cell membrane. Siamycin-I did not induce cell depolarization (Supporting Information Figure 2) showing that its mechanism of action is distinct from nisin as well.

In previous work, we showed that siamycin-I activates the *liaI* cell wall stress response.[23] *liaI* expression is known to be induced in response to cell wall damage, in particular by antibiotics targeting lipid II.[34] To establish if cell wall precursors are involved in this activity, we carried out an experiment to determine whether lipid II, its precursor lipid I, or its lipid components, undecaprenyl phosphate ($C_{55}P$) or undecaprenyl pyrophosphate ($C_{55}PP$), can antagonize the activation of the *liaI* genes by siamycin-I. As a control, we treated *B. subtilis* cells harboring a *liaI–lux* reporter fusion with vancomycin (4 μg/mL) and, as expected, observed a strong luminescent signal. We found that addition of one molar ratio of lipid I or lipid II, which both have the D-Ala-D-Ala terminus, blocked the activation of *liaI* (Figure 4a). In contrast, a 1:10 molar ratio of vancomycin/$C_{55}P$ or $C_{55}PP$ had no effect. This is consistent with the fact that the monophosphate and diphosphate constituents of lipid I and II do not participate in target recognition by vancomycin.[7]

We then carried out the same experiment with siamycin-I (8 μg/mL) and again found that the antibiotic activated the *liaI-lux* signal, though to a lesser extent than vancomycin. When we added lipid I or lipid II at an equal molar ratio, the *liaI-lux* signal was dramatically reduced, again consistent with the recognition of this cell wall building block. Intriguingly, the addition of $C_{55}PP$ (1:1 molar ratio), though not $C_{55}P$ (1:10 molar ratio siamycin-I/$C_{55}P$), also had this effect, in contrast to vancomycin, where it did not. This suggests that siamycin-I can interact with lipid I and lipid II and that at least part of this interaction involves binding to the pyrophosphate that connects MurNAc to the lipid moiety (Figure 4b).

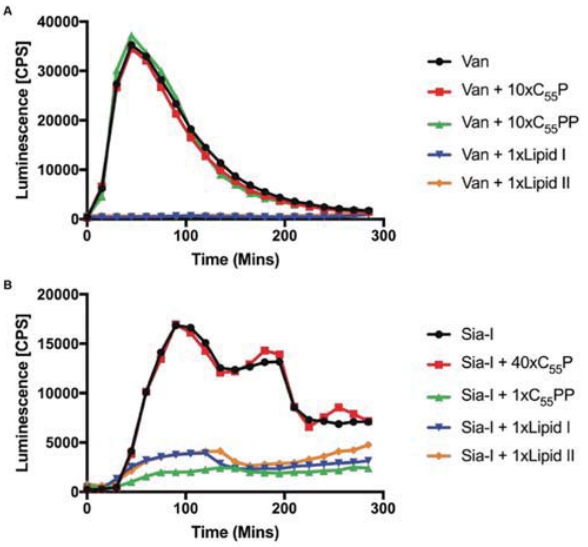

Figure 4. Cell wall stress response induced by siamycin-I antagonized by purified cell wall precursors. Induction of the cell wall stress response in *B. subtilis*, indicated by *liaI-lux* expression, was measured by luminescence (counts per second). (A) Vancomycin induced cell wall stress was suppressed when preincubated with lipid I or lipid II in a 1:1 molar ratio. Preincubation of vancomycin with $C_{55}P$ or $C_{55}PP$ (1:10 molar ratio) did not prevent activation of the cell wall stress response. (B) Siamycin-I activated the *liaI* response and was suppressed by lipid I, lipid II, and $C_{55}PP$ in a 1:1 molar ratio but not by $C_{55}P$.

These data are consistent with a target in cell wall biogenesis but do not distinguish whether the target is intracellular or extracellular. We therefore used a cellular uptake assay to determine whether siamycin-I is depleted from the growth medium when incubated with cells over time, or whether it associates with the extracellular surface. Over the first 15 min, siamycin-I was depleted slightly in the growth medium. After 15 min of treatment up to 4 h, siamycin-I remained constant in the growth media indicating that the lasso peptide was not being taken up into the cell (Supporting Information Figure 3). We conclude that siamycin-I interacts with (a) cell surface-associated molecule(s).

Siamycin-I Acts at the Cell Division Septum and Leads to PBP2 Delocalization. To identify the cellular target of siamycin-I, we created a semisynthetic adduct having a fluorescein analog conjugated to the lasso peptide's carboxy-terminus (Supporting Information Methods). We tested it for bioactivity and found that the fluorescein-labeled antibiotic had the same MIC as the unlabeled compound (3.7 μM). We used the commercially available BODIPY-FL vancomycin as a control.

We first treated *S. aureus* cells with a subinhibitory concentration of the vancomycin-fluorophore and the DNA stain DAPI. As expected, vancomycin bound to free D-Ala-D-Ala termini in the division septum and the peripheral cell wall (Figure 5a).[35,36] We carried out the same experiment with siamycin-I and found that the fluorophore accumulated in the division septum, but unlike with vancomycin, we did not observe accumulation in the peripheral cell wall (Figure 5b). This suggests that siamycin-I's interaction with the cell wall differs from that of vancomycin. We observed the same pattern in rod-shaped *B. subtilis* cells: vancomycin accumulated at the

DOI: 10.1021/acschembio.9b00157
ACS Chem. Biol. 2019, 14, 966–974

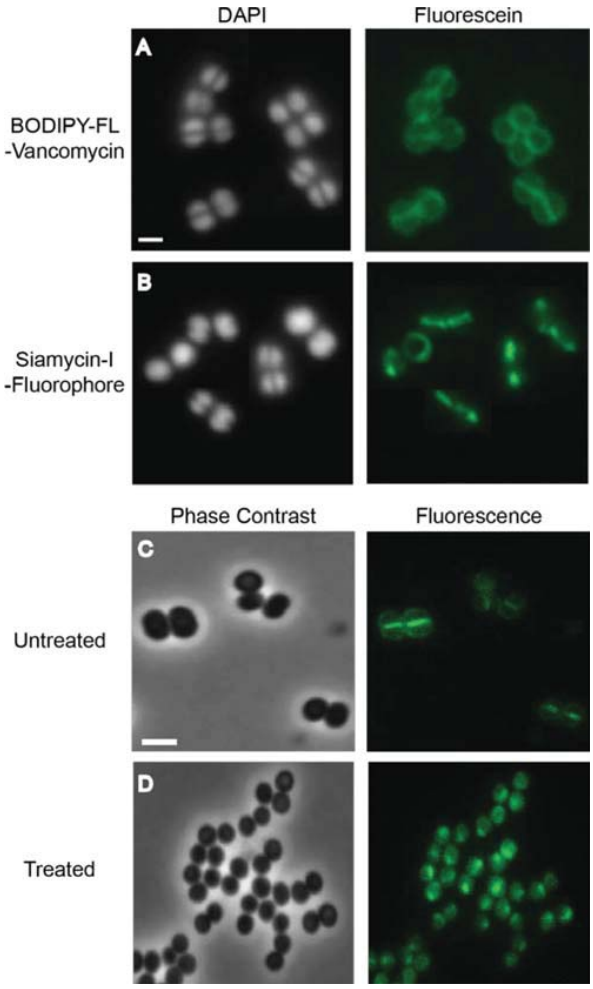

Figure 5. Siamycin-I only stains division septum and disrupts PBP2 localization. *S. aureus* was treated with (A) BODIPY-FL vancomycin or (B) siamycin-I-fluorescein at subinhibitory concentrations and visualized with fluorescence microscopy. Vancomycin treated cells show localization along the peripheral cell surface of *S. aureus* cells and at the division septum, whereas siamycin-I localizes to the division septum only. DAPI was used to stain DNA. Scale bar = 1 μm. *S. aureus* GFP-PBP2 localizes to the septum in untreated cells (C). Treatment with 10×MIC siamycin-I results in PBP2 delocalization (D). Scale bar = 2 μm.

septum and cell periphery, whereas siamycin-I accumulated preferentially at the division site (Supporting Information Figure 4). We interpret this as evidence that the specific siamycin-I binding motif is most exposed in the Gram-positive division plane.

A further question of interest was whether siamycin-I disrupted the cell wall biosynthetic machinery. To this end, we used a *S. aureus* strain expressing PBP2 fused to the green fluorescent protein. PBP2 is a bifunctional transglycosylase and transpeptidase that localizes specifically to the division plane in dependence of its substrate lipid II.[37] We visualized untreated cells and cells that had been treated with 10xMIC siamycin-I using fluorescent microscopy. We observed the expected pattern of PBP2 at the septum in untreated control cells, however in the presence of siamycin-I, PBP2 was delocalized and dispersed to other sites in the cell (Figure 5c,d). Thus, septal localization of PBP2 was compromised by siamycin-I, consistent with the targeting of lipid II as well as siamycin-I acting primarily at the division septum.

Siamycin-I Inhibits Enzymatic Reactions of the Lipid II Biosynthesis Cycle. As an orthogonal approach to the question of siamycin-I's molecular target, we explored its effect on individual biosynthetic reactions catalyzed by the intracellular enzymes MraY, MurG, and the GatD/MurT complex, as well as the extracellular enzymes PBP2, PBP4, and SA0415 (YbjG) *in vitro*. The position of each of these reactions in the lipid II cycle is shown in Figure 1.

We first tested whether siamycin-I blocks the biosynthesis of lipid I by MraY and found that it had no effect: the lipid I product was readily detectable on thin-layer chromatographs at levels that were indistinguishable from the control. In contrast, the addition of friulimicin B completely abolished lipid I production (Figure 6a).[32] This indicated that siamycin-I does not inhibit the formation of lipid I by MraY.

We next tested the effect of siamycin-I on two downstream steps catalyzed by MurG, which adds N-acetyl-glucosamine to lipid I to create lipid II, and GatD/MurT, which amidates glutamic acid of the lipid II stem peptide.[38,39] Siamycin-I inhibited the formation of lipid II by MurG; however it did not form an extraction-stable complex with lipid I as observed for the control antibiotic teixobactin. Compared to teixobactin, siamycin-I binding affinity appears low but sufficient to block enzymatic conversion of lipid I and lipid II. Similarly, lipid II was not amidated in the presence of siamycin-I but extracted from the reaction mixture, consistent with a weak interaction, unlike vancomycin which stably complexes with lipid II and is no longer detectable (Figure 6b,c). These results reveal specific binding of siamycin-I with lipid I and lipid II.

We then determined whether siamycin-I blocks the transglycosylation and carboxypeptidation reactions carried out by PBP2 and PBP4, respectively. We first tested the effect of siamycin-I on the transglycosylation reaction catalyzed by PBP2. Lipid II polymerization results in nonextractable glycan strands and release of detectable C_{55}PP as seen in the control reaction. Siamycin-I blocked the conversion such that the lipid II substrate was detectable by TLC, indicating that siamycin-I inhibits PBP2 like that of the vancomycin control (Figure 6d). We also investigated the carboxypeptidation function of PBP4 from *S. aureus*, which cleaves the terminal amino acid from the pentapeptide chain to create lipid II tetrapeptide, and thus alters migration behavior on TLC.[40] In contrast to vancomycin, siamycin-I did not inhibit the carboxypeptidation of lipid II (Figure 6e). We surmise that the interaction of siamycin-I with lipid II does not block the C-terminus of the pentapeptide such that it is free to be recognized and bound by PBP4.

To deduce the minimal binding motif, we determined the effect of siamycin-I on the reaction catalyzed by SA0415, an undecaprenyl pyrophosphate phosphatase that recycles C_{55}PP to C_{55}P, allowing the lipid to re-enter the peptidoglycan biosynthesis pathway.[41] When SA0415 was incubated with siamycin-I in the presence of C_{55}PP substrate, no monophosphorylated product was observed, suggesting that siamycin-I can inhibit the lipid recycling step, like that of the teixobactin control (Figure 6f). This is consistent with the finding that siamycin-I-mediated activation of *liaI* was antagonized by C_{55}PP. We conclude that siamycin-I requires

DOI: 10.1021/acschembio.9b00157
ACS Chem. Biol. 2019, 14, 966–974

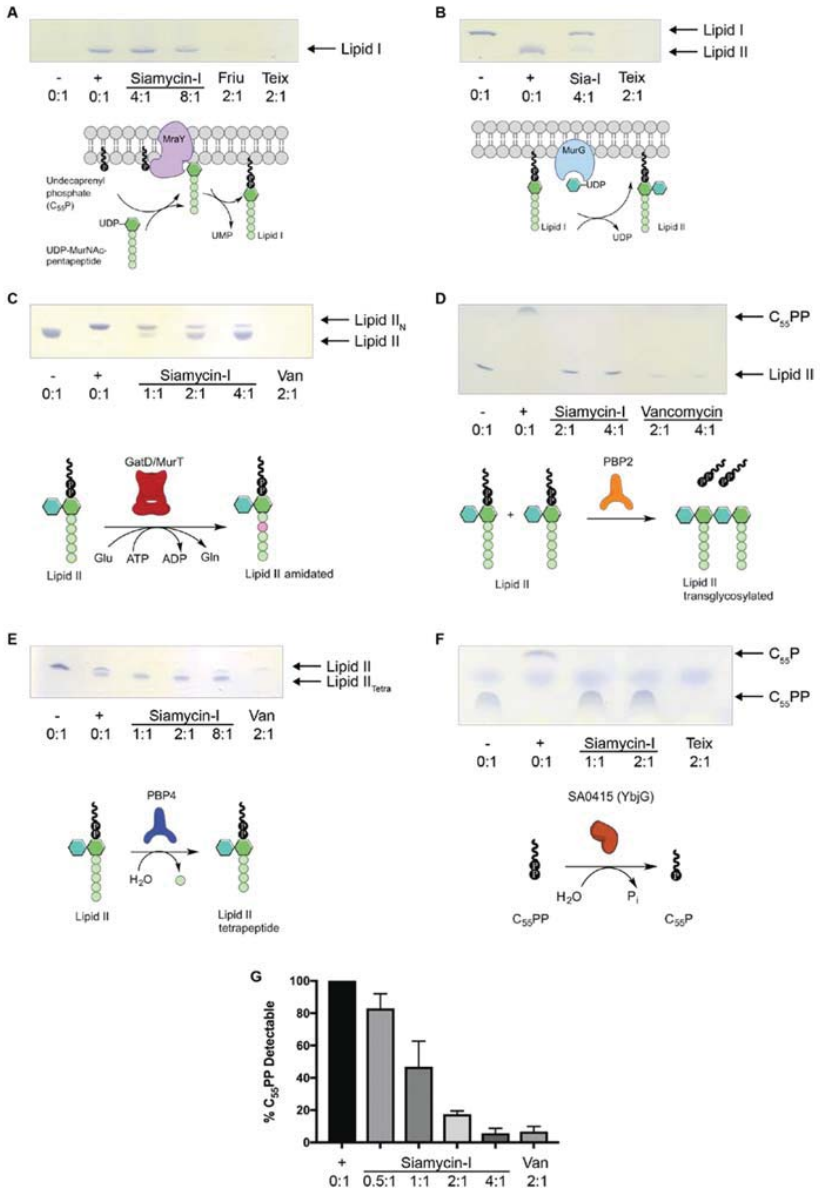

Figure 6. Interference of siamycin-I with individual peptidoglycan biosynthesis reactions. Siamycin-I inhibits individual peptidoglycan biosynthetic reactions by binding to substrates which comprise the minimal binding motif $C_{55}PP$. In contrast to the PBP2-catalyzed transglycosylation of lipid II, carboxypeptidation by PBP4 is unaffected reflecting that siamycin-I does not sterically hinder the C-terminus of the stem peptide. Siamycin-I was tested for inhibition of (A) lipid I formation by MraY, (B) lipid II formation by MurG, (C) amidation of lipid II by GatD/MurT, (D) lipid II transglycosylation by PBP2, (E) lipid II carboxypeptidation by PBP4, and (F) recycling of $C_{55}PP$ into $C_{55}P$ by SA0415. The − represents no enzyme control, and + represents no antibiotic control. Antibiotics were added in molar ratios of antibiotic/substrate with the substrate being (A and F) $C_{55}P$, (B) lipid I, (C−E) lipid II. (G) Inhibition of PBP2-catalyzed reaction by siamycin-I *in vitro* was quantified by the relative amount of $C_{55}PP$ released.

the pyrophosphate motif attached to the polyprenyl chain in lipid II for binding and represents the minimal binding motif.

We have demonstrated that siamycin-I directly interacts with cell wall intermediates. We note that while siamycin-I is able to inhibit the production of lipid II from lipid I *in vitro*, the fact that it appears to act outside the cell rules lipid I out as a biologically relevant target. Similarly, inhibition of the lipid II-consuming reaction catalyzed by GatD/MurT, while consistent with binding of lipid II, is not likely to be biologically significant. Rather, siamycin-I action appears to be restricted to binding lipid II on the cell surface, most likely compromising the incorporation of GlcNAc-MurNAc into the peptidoglycan polymer. This was measured by quantifying the relative amount of $C_{55}PP$ released after PBP2-mediated transglycosylation. Siamycin-I inhibited the formation of a transglycosylated lipid II polymer in a dose-dependent manner and almost completely inhibited formation of it at a 4:1 molar ratio of

DOI: 10.1021/acschembio.9b00157
ACS Chem. Biol. 2019, 14, 966–974

siamycin-I/lipid II (Figure 6g). This is the first report of the inhibition of cell wall biosynthesis by a lasso peptide.

The preferential localization of siamycin-I to the division septum is particularly intriguing. This likely reflects an enrichment of lipid II precursor at this site due to the *de novo* production of the septal cell wall. It is possible that there is some binding to the lateral wall but that, due to the apparently weak and/or transient binding of siamycin-I to its target, this binding is below the detection limit.

The structural diversity of the RiPPs is most intriguing as they share several commonalities in their biosynthetic machinery and yet are able to produce a myriad of post-translationally modified peptides.[11] Despite the commonalities among RiPPs, only members of the lanthipeptide group are known to bind to lipid II. The most prominent example is nisin, which targets lipid II through an interaction with the pyrophosphate lipid. However, nisin not only blocks cell wall biosynthesis but also forms a pore in the cytoplasmic membrane in a target-mediated manner, thus causing depolarization of the cell whereas siamycin-I does not.[24] As observed for other lipid II-binding antibiotics, such as teixobactin, the pyrophosphate-sugar motif which is exposed on the outside of Gram-positive bacteria comprises the minimal binding site.[6] Teixobactin targets multiple poly-prenyl-coupled cell envelope precursors, such as wall teichoic acid (WTA), which are also assembled on the membrane anchor $C_{55}P$. Its ability to target multiple essential pathways is what underlines teixobactin's potent efficacy, lytic properties, and lack of resistance, unlike siamycin-I.[9,10] Inhibition of WTA biosynthesis has not been investigated with siamycin-I; however, it may play a role in the activity as WTA are readily accessible outside. Additionally, teixobactin alters autolysin expression and causes liberation of the major autolysin Atl in *S. aureus*.[10,42] Autolysin expression is controlled by the TCS WalKR, to which mutations are mapped in siamycin-I resistant isolates.[27]

We infer that siamycin-I resistant mutants also have altered autolysin expression as the mutants are characterized by a thickened peptidoglycan layer as observed by electron microscopy.[28] Another compound that interacts with lipid II is vancomycin; however this compound binds the D-Ala-D-Ala terminus in the uncross-linked pentapeptide cross-bridge.[7] This interaction is chemically distinct from that of siamycin-I.

By binding to lipid II, it is likely that siamycin-I inhibits the incorporation of disaccharide units into the growing peptidoglycan network by PBP2. This interference in turn delocalizes PBP2. Delocalization of PBP2 is known to occur when the lipid II substrate is no longer accessible to the enzyme. This leads to disassembly of the peptidoglycan biosynthesis machinery and likely contributes to defective divisome assembly.[37]

METHODS

General Methods and Materials. *S. aureus* ATCC 29213 and *B. subtilis* 168 were maintained at 37 °C in LB-broth unless otherwise stated. Fluorescein-5-carboxamide cadaverine was purchased from AnaSpec. Siamycin-I was isolated and purified as previously described.[23] All other materials and compounds were purchased from Sigma-Aldrich.

Antimicrobial MIC Assays. Minimum inhibitory concentrations were determined as previously reported.[5] Experiments were performed in triplicate over three biological replicates.

Siamycin-I Resistant Mutant Studies. *S. aureus* was serial passaged by subculturing strains 1/1000 each day in media supplemented with siamycin-I or DMSO (vehicle control). Siamycin-I was added at 1/8th the wildtype's MIC and increased 2-fold each day up to 16× the MIC. Six nonsibling clones were isolated. Whole-genome sequencing of all six resistant mutants was performed as previously described,[23] except mutations were assembled and mapped to *S. aureus* ATCC29213 (GenBank accession: GCA_001879295.1). Coverages above 50× and a cutoff frequency of 75% were considered for the detection of mutations.

Transmission Electron Microscopy. Samples were applied to carbon-coated 300-mesh copper grids and stained with saturated uranyl acetate. EM images were acquired using a Hitachi H-7000 electron microscope at an operational voltage of 75 kV.

Accumulation of UDP-MurNAc-Pentapeptide Precursor. Cytoplasmic accumulation of the cell wall precursor UDP-MurNAc-pentapeptide after treatment of *S. aureus* with antibiotic was assessed as previously described.[32]

Antagonization of *lial-lux* Cell Wall Stress Response. *B. subtilis liaI-lux*[43] was grown in Mueller–Hinton broth with chloramphenicol (5 μg mL^{-1}) to OD_{600} = 0.6. Peptidoglycan precursors and shortened variants were added in molar ratios with respect to vancomycin (4 μg mL^{-1}) and siamycin-I (8 μg mL^{-1}). Antibiotics and antagonists in different molar ratios (1:1, 2:1, 5:1, 10:1, 20:1, 40:1) were preincubated for 10 min prior to addition of the reporter strain. Luciferase activities were measured using the Tecan Spark 10 M microplate reader for 5 h at 30 °C. At least three independent biological replicate experiments were conducted.

Fluorescent Microscopy. Cells were grown until growth reached an OD_{600} = 0.4. Cells were treated with vancomycin-fluorophore or siamycin-I-FL at 1 μg mL^{-1} and 8 μg mL^{-1}, respectively, for 15 min in the dark. Stained cells were centrifuged at 5000 rpm for 30 s and resuspended in sterile saline with 1 μg mL^{-1} DAPI and incubated for 10 min. Cells were centrifuged for 30 s at 5000 rpm and resuspended in 1/10th the original volume with saline. A total of 5 μL of concentrated cell suspension was mixed with 5 μL of 0.5% agarose. Fluorescent microscopy was performed using a Zeiss Imager M1 upright microscope (Zeiss). At least three field images, in at least two biological replicates, were captured under a 100× oil immersion objective using the ZEN imaging software.

PBP2-GFP Delocalization Studies. *S. aureus* RNpPBP2–31, a strain with a *gfp-pbp2* fusion under control of the P_{xyl} promoter, was grown in Mueller–Hinton broth to OD_{600} = 0.3.[31] Cells were treated with 10×MIC (80 μg mL^{-1}) of siamycin-I and incubated for 2 min at 37 °C. Untreated cells were used as a control. Samples were immobilized on microscope slides covered with 1% agarose and imaged immediately. Fluorescence microscopy was carried out using a Zeiss Axio Observer Z1 microscope equipped with an Axio Cam MR3 camera. Images were acquired with ZEN software and analyzed and postprocessed using ImageJ v.1.38.

***In Vitro* Reactions of Peptidoglycan Biosynthesis with Siamycin-I.** To determine the enzymatic activity of MraY-His_6, in 50 μL, 5 nmol of $C_{55}P$ were incubated with 25 nmol UDP-MurNAc-pentapeptide in 100 mM Tris-HCl, 10 mM $MgCl_2$, at pH 7.5, and 0.6% Triton X-100. The reaction was initiated by the addition of 2 μg of MraY and incubated for 1.5 h at 30 °C.

The MurG activity assay was performed in a 30 μL reaction containing 2.5 nmol of purified lipid I, 25 nmol of UDP-N-acetyl glucosamine (UDP-GlcNAc) in 200 mM Tris-HCl, 5.7 mM $MgCl_2$, at pH 7.5, and 0.8% Triton X-100 with 2 μg of purified, recombinant MurG-His_6 enzyme. Reaction mixtures were incubated for 30 min at 30 °C.

In vitro amidation was assayed by incubating 2.5 nmol of lipid II in 160 mM Tris-HCl, 40 mM $MgCl_2$, 30 mM KCl, at pH 7.5, 0.26% Triton X-100, 6 mM ATP, and 6.6 mM glutamine in 30 μL total volume. The reaction was initiated by the addition of 3 μg of the GatD-His_6/MurT complex and incubated for 2 h at 30 °C.

Enzymatic activity of *S. aureus* PBP2 and PBP4 was determined by incubating 2.5 nmol of lipid II in 20 mM MES, 2 mM $MgCl_2$, and 2 mM $CaCl_2$, at pH 5.5 in 50 μL. The reaction was initiated by the addition of 6 μg of PBP2-His_6 or PBP4-His_6 and incubated for 2 h at 30 °C.

DOI: 10.1021/acschembio.9b00157
ACS Chem. Biol. 2019, 14, 966–974

Dephosphorylation of C_{55}PP was carried out using purified *S. aureus* YbjG-His_6 enzyme. A total of 20 nmol of C_{55}PP was incubated with 3 μg of YbjG-His_6 in 20 mM Tris-HCl, at pH 7.5, 150 mM NaCl, and 0.8% Triton X-100 in 50 μL for 30 min at 37 °C.

In all *in vitro* assays, siamycin-I was added in molar ratios with regard to the respective substrate (C_{55}P, C_{55}PP, lipid I or lipid II). Friulimicin B, vancomycin, and teixobactin were used as control antibiotics. Peptidoglycan intermediates were purified as described previously.[44]

Polyprenyl containing products were extracted from the reaction mixture with an equal volume of n-butanol/pyridine acetate, at pH 4.2 (2:1; v/v), and analyzed by thin-layer chromatography (TLC) using chloroform/methanol/water/ammonia (88:48:10:1, v/v/v/v) as the solvent[45] and phosphomolybdic acid staining.[44] Quantification was carried out using ImageQuant TL software. Experiments were performed at least three times.

■ ASSOCIATED CONTENT

Supporting Information

The Supporting Information is available free of charge on the ACS Publications website at DOI: 10.1021/acschembio.9b00157.

Supporting experimental procedures, Supporting Tables 1 and 2, and Supporting Figures 1–5 (PDF)

■ AUTHOR INFORMATION

Corresponding Author

*E-mail: justin.nodwell@utoronto.ca.

ORCID

Anna Müller: 0000-0001-6420-3868

Justin R. Nodwell: 0000-0001-7909-1803

Notes

The authors declare no competing financial interest.

■ ACKNOWLEDGMENTS

The authors wish to thank the following for their assistance: E. Lai with fluorophore synthesis, S. Hossain with fluorescent microscopy, and S. Doyle with transmission electron microscopy. We thank T. Mascher and M. Pinho for providing strains and K. Lewis (Novobiotic) for providing teixobactin. Work in the Nodwell laboratory was funded by grants from the Canadian Institutes for Health Research and Cystic Fibrosis Canada. Stephanie Tan has been supported by scholarships from the Ontario Graduate Scholarship Fund and was funded by a CGS-M scholarship from Canadian Institutes for Health Research. Work in the Schneider laboratory was supported by the German Center for Infection Research (DZIF), TTU Novel Antibiotics.

■ REFERENCES

(1) Hassoun, A., Linden, P. K., and Friedman, B. (2017) Incidence, prevalence, and management of MRSA bacteremia across patient populations—a review of recent developments in MRSA management and treatment. *Crit. Care 21*, DOI: 10.1186/s13054-017-1801-3.

(2) Borg, M. A., de Kraker, M., Scicluna, E., van de Sande-bruinsma, N., Tiemersma, E., Monen, J., and Grundmann, H. (2007) Prevalence of methicillin-resistant Staphylococcus aureus (MRSA) in invasive isolates from southern and eastern Mediterranean countries. *J. Antimicrob. Chemother. 60*, 1310–1315.

(3) Young, K. D. (2010) Bacterial Shape: Two Dimensional Questions and Possibilities. *Annu. Rev. Microbiol. 64*, 223–240.

(4) Pinho, M. G., Kjos, M., and Veening, J. W. (2013) How to get (a)round: Mechanisms controlling growth and division of coccoid bacteria. *Nat. Rev. Microbiol. 11*, 601–614.

(5) Mcauley, S., Vadia, S., Jani, C., Huynh, A., Yang, Z., Levin, P. A., and Nodwell, J. R. (2019) A Chemical Inhibitor of Cell Growth Reduces Cell Size in Bacillus subtilis. *ACS Chem. Biol. 14*, 688.

(6) Müller, A., Klöckner, A., and Schneider, T. (2017) Targeting a cell wall biosynthesis hot spot. *Nat. Prod. Rep. 34*, 909–932.

(7) Williams, D. H., and Waltho, J. P. (1988) Molecular basis of the activity of antibiotics of the vancomycin group. *Biochem. Pharmacol. 37*, 133–141.

(8) Kozarich, J. W., and Strominger, J. L. (1978) A membrane enzyme from Staphylococcus aureus which catalyzes transpeptidase, carboxypeptidase, and penicillinase activities. *J. Biol. Chem. 253*, 1272–1278.

(9) Ling, L. L., Schneider, T., Peoples, A. J., Spoering, A. L., Engels, I., Conlon, B. P., Mueller, A., Schäberle, T. F., Hughes, D. E., Epstein, S., Jones, M., Lazarides, L., Steadman, V. A., Cohen, D. R., Felix, C. R., Fetterman, K. A., Millett, W. P., Nitti, A. G., Zullo, A. M., Chen, C., and Lewis, K. (2015) A new antibiotic kills pathogens without detectable resistance. *Nature 517*, 455–459.

(10) Homma, T., Nuxoll, A., Gandt, A. B., Ebner, P., Engels, I., Schneider, T., Götz, F., Lewis, K., and Conlon, B. P. (2016) Dual Targeting of Cell Wall Precursors by Teixobactin Leads to Cell. *Antimicrob. Agents Chemother. 60*, 6510–6517.

(11) Ortega, M. A., and van der Donk, W. A. (2016) New Insights into the Biosynthetic Logic of Ribosomally Synthesized and Post-translationally Modified Peptide Natural Products. *Cell Chem. Biol. Rev. 23*, 31–44.

(12) Hegemann, J. D., Zimmermann, M., Xie, X., and Marahiel, M. A. (2015) Lasso Peptides: An Intriguing Class of Bacterial Natural Products. *Acc. Chem. Res. 48*, 1909–1919.

(13) Tietz, J. I., Schwalen, C. J., Patel, P. S., Maxson, T., Blair, P. M., Tai, H. C., Zakai, U. I., and Mitchell, D. A. (2017) A new genome-mining tool redefines the lasso peptide biosynthetic landscape. *Nat. Chem. Biol. 13*, 470–478.

(14) Hegemann, J. D., Zimmermann, M., Zhu, S., Klug, D., and Marahiel, M. A. (2013) Lasso Peptides From Proteobacteria: Genome Mining Employing Heterologous Expression and Mass Spectrometry. *Biopolymers 100*, 527–542.

(15) Maksimov, M. O., Pelczer, I., and Link, A. J. (2012) Precursor-centric genome-mining approach for lasso peptide discovery. *Proc. Natl. Acad. Sci. U. S. A. 109*, 15223–15228.

(16) Wilson, K. A., Kalkum, M., Ottesen, J., Yuzenkova, J., Chait, B. T., Landick, R., Muir, T., Severinov, K., and Darst, S. A. (2003) Structure of Microcin J25, a Peptide Inhibitor of Bacterial RNA Polymerase, is a Lassoed Tail. *J. Am. Chem. Soc. 125*, 12475–12483.

(17) Mukhopadhyay, J., Sineva, E., Knight, J., Levy, R. M., and Ebright, R. H. (2004) Antibacterial Peptide Microcin J25 Inhibits Transcription by Binding within and Obstructing the RNA Polymerase Secondary Channel. *Mol. Cell 14*, 739–751.

(18) Mathavan, I., Zirah, S., Mehmood, S., Choudhury, H. G., Goulard, C., Li, Y., Robinson, C. V., Rebuffat, S., and Beis, K. (2014) Structural basis for hijacking siderophore receptors by antimicrobial lasso peptides. *Nat. Chem. Biol. 10*, 340–344.

(19) Braffman, N. R., Piscotta, F. J., Hauver, J., Campbell, E. A., Link, A. J., and Darst, S. A. (2019) Structural mechanism of transcription inhibition by lasso peptides microcin J25 and capistruin. *Proc. Natl. Acad. Sci. U. S. A. 116*, 1273–1278.

(20) Gavrish, E., Sit, C. S., Cao, S., Kandror, O., Spoering, A., Peoples, A., Ling, L., Fetterman, A., Hughes, D., Bissell, A., Torrey, H., Akopian, T., Mueller, A., Epstein, S., Goldberg, A., Clardy, J., and Lewis, K. (2014) Lassomycin, a ribosomally synthesized cyclic peptide, kills Mycobacterium tuberculosis by targeting the ATP-dependent protease ClpC1P1P2. *Chem. Biol. 21*, 509–518.

(21) Ma, P., Nishiguchi, K., Yuille, H. M., Davis, L. M., Nakayama, J., and Phillips-Jones, M. K. (2011) Anti-HIV siamycin I directly inhibits autophosphorylation activity of the bacterial FsrC quorum sensor and other ATP-dependent enzyme activities. *FEBS Lett. 585*, 2660–2664.

(22) Lin, P. F., Samanta, H., Bechtold, C. M., Deminie, C. A., Patick, A. K., Alam, M., Riccardi, K., Rose, R. E., White, R. J., and Colonno, R. J. (1996) Characterization of siamycin I, a human immunodefi-

DOI: 10.1021/acschembio.9b00157
ACS Chem. Biol. 2019, 14, 966–974

ciency virus fusion inhibitor. *Antimicrob. Agents Chemother. 40*, 133–138.
(23) Daniel-Ivad, M., Hameed, N., Tan, S., Dhanjal, R., Socko, D., Pak, P., Gverzdys, T., Elliot, M. A., and Nodwell, J. R. (2017) An Engineered Allele of afsQ1 Facilitates the Discovery and Investigation of Cryptic Natural Products. *ACS Chem. Biol. 12*, 628–634.
(24) Wiedemann, I., Breukink, E., van Kraaij, C., Kuipers, O. P., Bierbaum, G., de Kruijff, B., and Sahl, H. G. (2001) Specific Binding of Nisin to the Peptidoglycan Precursor Lipid II Combines Pore Formation and Inhibition of Cell Wall Biosynthesis for Potent Antibiotic Activity. *J. Biol. Chem. 276*, 1772–1779.
(25) Mak, S., and Nodwell, J. R. (2017) Actinorhodin is a redox-active antibiotic with a complex mode of action against Gram-positive cells. *Mol. Microbiol. 106*, 597–613.
(26) Dubrac, S., and Msadek, T. (2004) Identification of genes controlled by the essential YycG/YycF two-component system of Staphylococcus aureus. *J. Bacteriol. 186*, 1175–1181.
(27) Dubrac, S., Boneca, I. G., Poupel, O., and Msadek, T. (2007) New insights into the WalK/WalR (YycG/YycF) essential signal transduction pathway reveal a major role in controlling cell wall metabolism and biofilm formation in Staphylococcus aureus. *J. Bacteriol. 189*, 8257–8269.
(28) Howden, B. P., McEvoy, C. R. E., Allen, D. L., Chua, K., Gao, W., Harrison, P. F., Bell, J., Coombs, G., Bennett-Wood, V., Porter, J. L., Robins-Browne, R., Davies, J. K., Seemann, T., and Stinear, T. P. (2011) Evolution of multidrug resistance during Staphylococcus aureus infection involves mutation of the essential two component regulator WalKR. *PLoS Pathog. 7*, e1002359.
(29) Shoji, M., Cui, L., Iizuka, R., Komoto, A., Neoh, H. M., Watanabe, Y., Hishinuma, T., and Hiramatsu, K. (2011) walK and clpP mutations confer reduced vancomycin susceptibility in Staphylococcus aureus. *Antimicrob. Agents Chemother. 55*, 3870–3881.
(30) Metelev, M., Tietz, J. I., Melby, J. O., Blair, P. M., Zhu, L., Livnat, I., Severinov, K., and Mitchell, D. A. (2015) Structure, bioactivity, and resistance mechanism of streptomonomicin, an unusual lasso peptide from an understudied halophilic actinomycete. *Chem. Biol. 22*, 241–250.
(31) Cui, L., Murakami, H., Kuwahara-arai, K., Hanaki, H., and Hiramatsu, K. (2000) Contribution of a Thickened Cell Wall and Its Glutamine Nonamidated Component to the Vancomycin Resistance Expressed by Staphylococcus aureus Mu50. *Antimicrob. Agents Chemother. 44*, 2276–2285.
(32) Schneider, T., Gries, K., Josten, M., Wiedemann, I., Pelzer, S., Labischinski, H., and Sahl, H. G. (2009) The lipopeptide antibiotic friulimicin B inhibits cell wall biosynthesis through complex formation with bactoprenol phosphate. *Antimicrob. Agents Chemother. 53*, 1610–1618.
(33) Brotz, H., Josten, M., Wiedemann, I., Schneider, U., Gotz, F., Bierbaum, G., and Sahl, H. G. (1998) Role of lipid-bound peptidoglycan precursors in the formation of pores by nisin, epidermin and other lantibiotics. *Mol. Microbiol. 30*, 317–327.
(34) Mascher, T., Zimmer, S. L., Smith, T., and Helmann, J. D. (2004) Antibiotic-Inducible Promoter Regulated by the Cell Envelope Stress-Sensing Two-Component System LiaRS of Bacillus subtilis. *Antimicrob. Agents Chemother. 48*, 2888–2896.
(35) Pinho, M. G., and Errington, J. (2003) Dispersed mode of Staphylococcus aureus cell wall synthesis in the absence of the division machinery. *Mol. Microbiol. 50*, 871–881.
(36) Tiyanont, K., Doan, T., Lazarus, M. B., Fang, X., Rudner, D. Z., and Walker, S. (2006) Imaging peptidoglycan biosynthesis in Bacillus subtilis with fluorescent antibiotics. *Proc. Natl. Acad. Sci. U. S. A. 103*, 11033–11038.
(37) Pinho, M. G., and Errington, J. (2005) Recruitment of penicillin-binding protein PBP2 to the division site of Staphylococcus aureus is dependent on its transpeptidation substrates. *Mol. Microbiol. 55*, 799–807.
(38) van Heijenoort, J. (2001) Recent advances in the formation of the bacterial peptidoglycan monomer unit. *Nat. Prod. Rep. 18*, 503–519.
(39) Münch, D., Roemer, T., Lee, S. H., Engeser, M., Sahl, H. G., and Schneider, T. (2012) Identification and in vitro analysis of the GatD/MurT enzyme-complex catalyzing lipid II amidation in Staphylococcus aureus. *PLoS Pathog. 8*, e1002509.
(40) Sauvage, E., Kerff, F., Terrak, M., Ayala, J. A., and Charlier, P. (2008) The penicillin-binding proteins: Structure and role in peptidoglycan biosynthesis. *FEMS Microbiol. Rev. 32*, 234–258.
(41) Tatar, L. D., Marolda, C. L., Polischuk, A. N., van Leeuwen, D., and Valvano, M. A. (2007) An Escherichia coli undecaprenyl-pyrophosphate phosphatase implicated in undecaprenyl phosphate recycling. *Microbiology 153*, 2518–2529.
(42) Biswas, R., Voggu, L., Simon, U., Thumm, G., Hentschel, P., and Götz, F. (2006) Activity of the major staphylococcal autolysin Atl. *FEMS Microbiol. Lett. 259*, 260–268.
(43) Radeck, J., Gebhard, S., Orchard, P. S., Kirchner, M., Bauer, S., Mascher, T., and Fritz, G. (2016) Anatomy of the bacitracin resistance network in Bacillus subtilis. *Mol. Microbiol. 100*, 607–620.
(44) Schneider, T., Senn, M. M., Berger-Bächi, B., Tossi, A., Sahl, H. G., and Wiedemann, I. (2004) In vitro assembly of a complete, pentaglycine interpeptide bridge containing cell wall precursor (lipid II-Gly5) of Staphylococcus aureus. *Mol. Microbiol. 53*, 675–685.
(45) Rick, P. D., Hubbard, G. L., Kitaoka, M., Nagaki, H., Kinoshita, T., Dowd, S., Simplaceanu, V., and Ho, C. (1998) Characterization of the lipid-carrier involved in the synthesis of enterobacterial common antigen (ECA) and identification of a novel phosphoglyceride in a mutant of Salmonella typhimurium defective in ECA synthesis. *Glycobiology 8*, 557–567.

DOI: 10.1021/acschembio.9b00157
ACS Chem. Biol. 2019, 14, 966–974

SUPPORTING INFORMATION

The lasso peptide siamycin-I targets lipid II at the Gram-positive cell surface.

Stephanie Tan[1], Kevin C. Ludwig[2], Anna Müller[2,3], Tanja Schneider[2,3] and Justin R. Nodwell[1*]

1. Department of Biochemistry
MaRS Discovery District
University of Toronto
661 University Avenue
Toronto, Ontario
CANADA M5G 1M1

2. Institute for Pharmaceutical Microbiology
University of Bonn
Meckenheimer Allee 168
53115 Bonn
GERMANY

3. German Centre for Infection Research (DZIF), partner site Bonn-Cologne, Bonn, Germany.

*To whom correspondence should be addressed

Contents

Methods

Membrane disruption assay.

An overnight culture of *B. subtilis* 168 was diluted 1/100 in fresh LB media and incubated at 37°C until OD600 0.4. Cells were pelleted at 3000g for 10 minutes, the supernatant decanted, and washed twice in PBS+ (0.14 M NaCl, 2.7 mM KCl, 10 mM Na_2HPO_4, 1.8 mM KH_2PO_4 at pH 7.4 supplemented with 10 mM glucose and 0.5 mM $MgCl_2$). The pellet was then resuspended in PBS+ and diluted to an OD600 of 0.1. Concurrently, a blank PBS+ sample was also prepared without cells. Dyes were added into both the sample and control to a final concentration of 625 nM TO-PRO-3 iodide (λ_{ex} = 600 nm, λ_{em} = 650 nm) and 10 µM $DiOC_2(3)$ (λ_{ex} = 450 nm, λ_{em} = 510 nm). Both the culture and dye control solutions were added to 96-well plates and the test compounded were added to a final concentration of 5 µM and 20 µM. Each plate also contained treatment controls wells for $DiOC_23$ (10 µM CCCP) and TO-PRO-3 iodide (10 µg mL^{-1} nisin). Samples were incubated at room temperature in the dark for 5 minutes, then treated with the test compound. Fluorescence was read immediately following treatment using a BioTek Synergy H1 plate reader.

Cellular uptake assay.

S. aureus was grown to an OD_{600} 0.4 then treated with sub-MIC (8 µg mL^{-1}) antibiotic or DMSO (vehicle control) for 4 hours. Cells were collected at various time points, put on ice immediately and centrifuged at 4°C at 15,000 RPM for 3 minutes. The spent growth media was isolated. Cells were washed twice with cold 1X PBS pH 7.0 and each wash step was isolated. Cells were resuspended in 50 µL 1X PBS pH 7.0 and boiled for 15 minutes in a heat block. The lysed

supernatant was isolated. Each fraction was analyzed by UPLC-MS (Waters) for the antibiotic. Experiments were performed at least three times.

Siamycin-I fluorophore synthesis.

5 µmol of 5-FAM cadaverine, 5 µmol of siamycin-I and 15 µmol of PyBOP were dissolved in 500 µL anhydrous DMF. 30 µmol of N,N-Diisopropylethylamine was added. The reaction was mixed at room temperature for 3 hours and protected from light. The mixture was diluted into 20 mL of ether at -20°C and settled for 1 hour at -20°C. The precipitated siamycin-I-fluorophore was collected after centrifugation at 2000 x *g* for 10 minutes and purified by HPLC. The sample was purified by HPLC on an X-Select CSH C18, 5 µm, 4.6 mm x 150 mm column (Waters), column temperature: 35°C, with gradient of (A) H_2O + 0.1% formic acid and (B) MeCN + 0.1% formic acid: 0 min, %B = 5, 15 min, %B = 95, 20min, %B = 5. Sia-FL was collected and confirmed by UPLC-MS.

Supplementary Table 1) Mutations mapped in siamycin-I *S. aureus* resistant mutants

Mutant	Contig[a]	Gene	Annotation	NT Change	AA Change
sia^R-1	04	*guaA*	GMP synthase	- GAATTAGGTATT	- ELGI (378-381)
	46	*walR*	Transcriptional regulator	G → A	A96 T
sia^R-2	04	*guaA*	GMP synthase	A → G	H172R
	46	*walR*	Transcriptional regulator	C → T	P216S
sia^R-3	04	*guaA*	GMP synthase	- TTGAAA	- IE (209-210)
	11	*graS*	Histidine kinase	C → T	T283M
	46	*walK*	Histidine kinase	G → C	A292P
sia^R-4	14	*dltA*	D-alanine-poly(phosphoribitol) ligase	- A	Frameshift
	46	*walK*	Histidine kinase	G → T	V498F
	47	*sdrE*	Ser-Asp repeat containing protein E	- T	Frameshift
sia^R-5	46	*nsaS*	Nisin-susceptibility sensor associated histidine kinase	T → C	Y91C
	46	*walK*	Histidine kinase	G → A	G533S
sia^R-6	04	*guaA*	GMP synthase	- TACA	Frameshift
	46	*walR*	Transcriptional regulator	G → T	D83Y

[a] Contig is in reference to *S. aureus* ATCC29213 genome: GCA_001879295.1

Supplementary Table 2) Minimum inhibitory concentrations of siamycin-I in a *guaA* mutant

	Siamycin MIC [µg/ml] BHI + guanine (mM)			
Strain	0	0.25	0.5	1
HG001	32	32	32	32
HG001 *guaA*::IS*256-ermB*	64	64	32	32

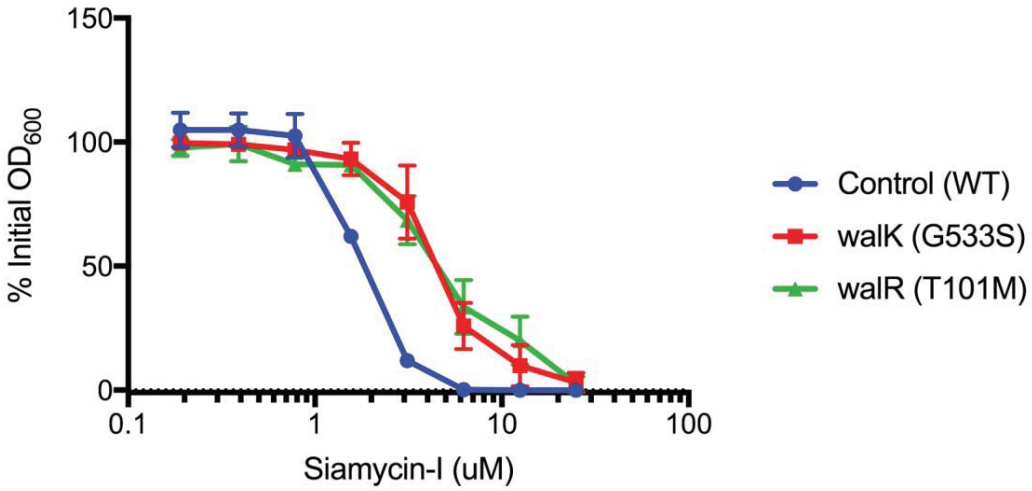

Supplementary Figure 1) Mutations in *walKR* confer resistance to siamycin-I.

S. aureus ATCC29213 strains harbouring either a single mutation in *walK* (G533S) or *walR* (T101M) have elevated resistance to siamycin-I compared to the wildtype background.

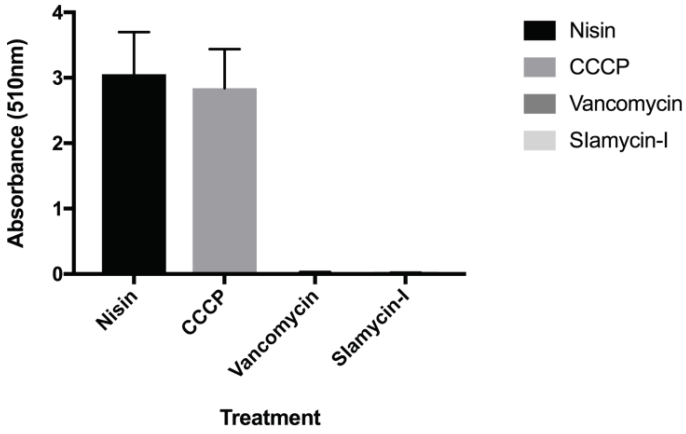

Supplementary Figure 2) Siamycin-I does not cause depolarization in *S. aureus*.

Membrane depolarization was determined after antibiotic treatment by measuring the fluorescence of $DIOC_2(3)$, a membrane potential probe, relative to the DMSO-control treated sample. Depolarization was observed in nisin and the ionophore, CCCP (carbonyl cyanide m-chlorophenyl hydrazone) treatment whereas vancomycin and siamycin-I did not disrupt the membrane potential.

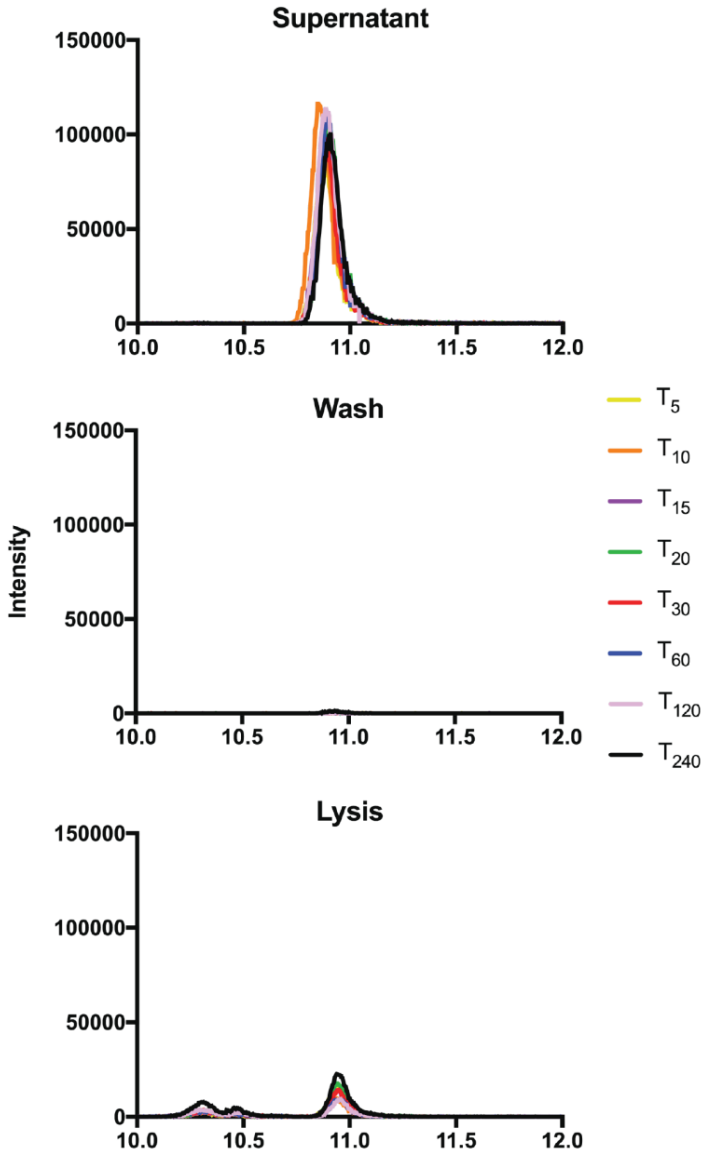

Supplementary Figure 3) Siamycin-I remains on the outside of the cell.

S. aureus cells were treated with sub-MIC of siamycin-I and aliquots were taken over 240 minutes. Siamycin-I levels were measured by LC-MS ($[M+2H]^{2+}$ = 1082.44) after each time point (T_{min}) in the supernatant and showed slight depletion of siamycin-I up until 15 minutes. Siamycin-I levels became saturated after 15 minutes. A constant level of siamycin-I is also detectable after lysing the cells. Experiment was performed over at least 3 replicates. One representative data set is shown here.

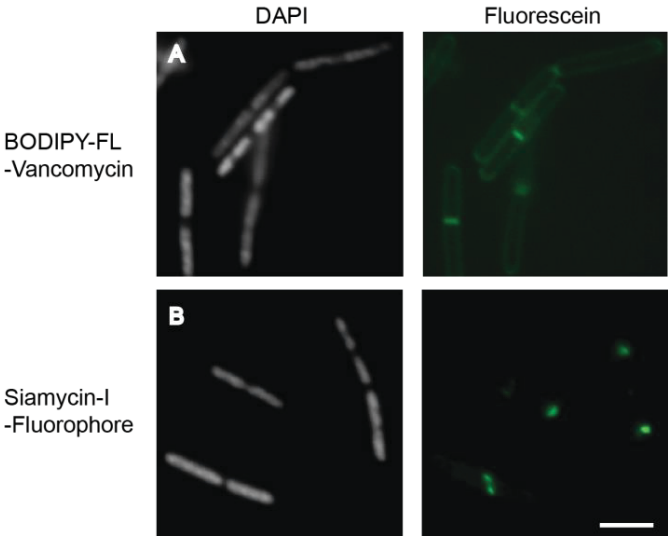

Supplementary Figure 4) Siamycin-I only stains the division septum in *B. subtilis* cells

B. subtilis 168 was treated with a (A) vancomycin-BODIPY FL or (B) siamycin-I fluorophore at sub-inhibitory concentrations and then visualized with fluorescent microscopy. Vancomycin treated cells show localization along the cell surface of a *B. subtilis* cell and at the division septum, whereas siamycin-I shows localization only at the division septum. DAPI was used to stain DNA. Scale bar = 5 µm.

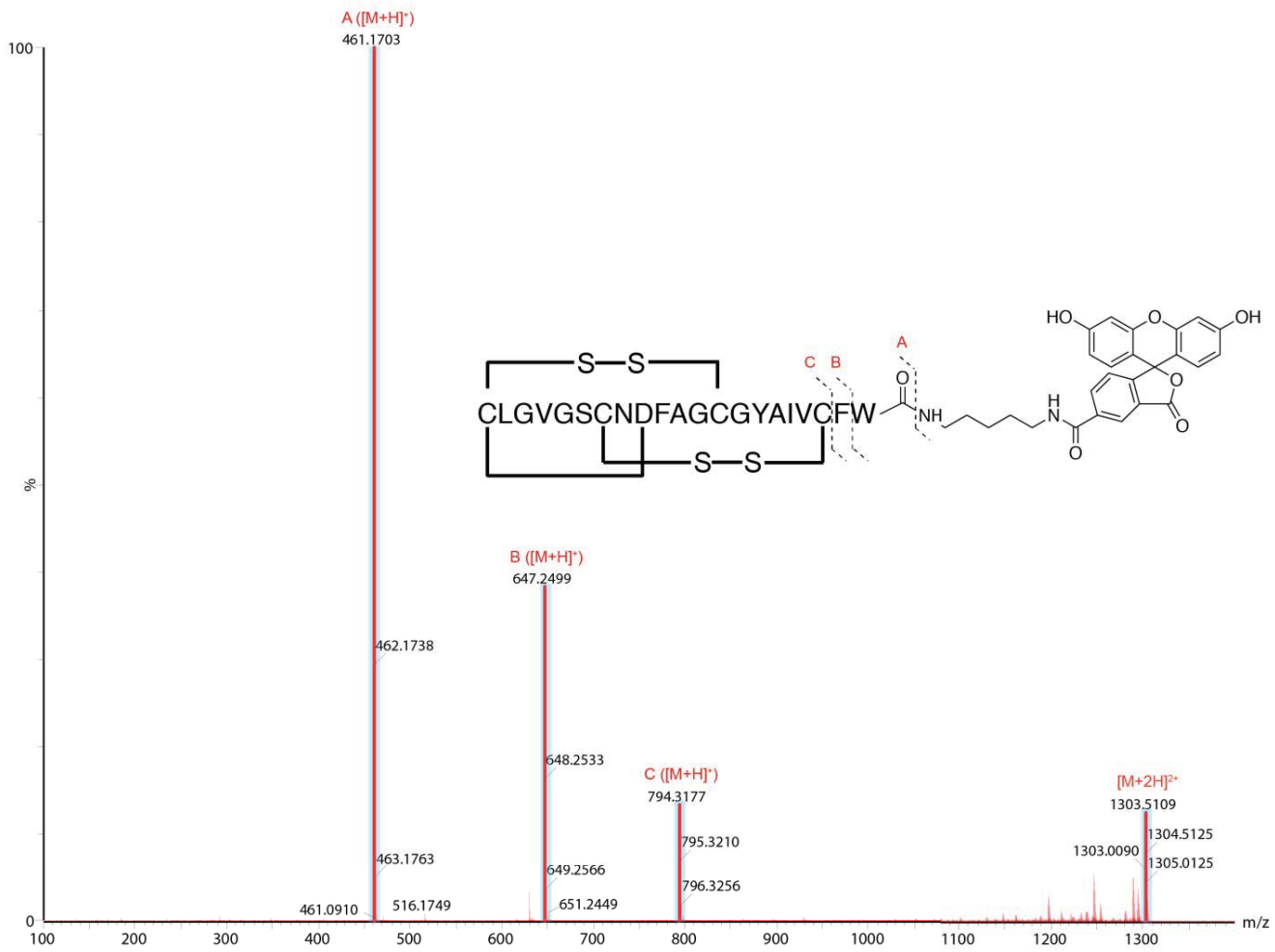

Supplementary Figure 5) Tandem MS/MS of siamycin-I-fluorophore.

Fragmentation pattern of modified siamycin-I with fluorescein-5-carboxamide (5-FAM) cadaverine. Siamycin-I-fluorophore ($[M+2H]^{2+}$) is fragmented to yield fragments A-C with a mass tolerance of <0.05Da.

Chapter 2

Ca^{2+}-daptomycin targets cell wall biosynthesis by forming a tripartite complex with undecaprenyl-coupled intermediates and membrane lipids

The lipopeptide daptomycin is a last-resort agent for the treatment of certain types of infections caused by Gram-positive pathogens, including methicllin-resistant *Staphylococcus aureus*, vancomycin-resistant enterocci, and penicillin-resistant *Streptococcus pneumoniae*. Its underlying mechanism of action was not completely understood, and a molecular target remained elusive for almost four decades. The aim of this study was to elucidate the precise mode of action and to identify the specific target of daptomycin.

The fact that daptomycin induced the LiaRS cell wall stress response in *Bacillus subtilis* in a Ca^{2+}- and dose-dependent manner suggested that the antibiotic interferes with a membrane-bound step of peptidoglycan biosynthesis. In line with this, fluorescently labeled daptomycin preferentially bound to the *S. aureus* division septum and led to delocalization of septal FtsW, supporting an interaction of the antibiotic with the peptidoglycan precursor lipid II. Notably, short pre-treatment of *S. aureus* cultures with lipid II-binding antibiotics such as teixobactin and oritavancin reduced daptomycin binding and delayed daptomycin-induced killing, emphasizing that daptomycin interacts with the same target.

Total internal reflection fluorescence (TIRF) microscopy of phosphatidylglycerol (PG)-containing model membranes individually doped with the putative target molecules, undecaprenyl phosphate (C_{55}-P), undecaprenyl pyrophosphate (C_{55}-PP), and lipid II, demonstrated an increased binding of daptomycin compared to PG-containing bilayers lacking the embedded precursor molecules. Corroborating the whole-cell binding experiments, pre-incubation with antibiotics that specificially bind to the tested precursors strongly decreased daptomycin binding efficiacy. In addition, antagonization of the LiaRS response was observed after addition of precursors and PG.

The formation of an extraction-stable daptomycin complex with lipid II was observed in the presence of PG, supporting the formation of a tripartite complex (daptomycin:PG:lipid II). Investigating the impact of daptomycin on individual cell wall biosynthesis reactions *in vitro* revealed inhibition of the MraY-catalyzed synthesis of lipid I (linking the first sugar building block to C_{55}-P) as well as inhibition of the penicillin-binding protein 2 (PBP2)-catalyzed transglycosylation of lipid II, both in a dose-dependent manner in the presence of PG. The *in vitro* reactions were fully blocked at a 10:1 molar ratio (daptomycin:lipid substrate), which is in line with daptomycin oligomerization (Kreutzberger *et al.*, 2017).

The study supports a new model for the mechanism of action, in which Ca^{2+}-daptomycin blocks cell wall biosynthesis via formation of a tripartite complex with PG and undecaprenyl-coupled lipid intermediates. Importantly, the study showed that PG and lipid II binding is the central event for promoting cell death as Ca^{2+}-daptomycin binds to the division septum within the first 15 min in contrast to membrane depolarization observed after 30 min of treatment (Silverman *et al.*, 2003). The latter is most likely a result of disintegrative membrane rearrangements following lipid II/PG complexation.

K.C.L. performed bioreporter and antagonization assays including purification of substrates, analyzed the data and contributed to writing of the manuscript.

nature COMMUNICATIONS

ARTICLE

https://doi.org/10.1038/s41467-020-15257-1 OPEN

Ca^{2+}-Daptomycin targets cell wall biosynthesis by forming a tripartite complex with undecaprenyl-coupled intermediates and membrane lipids

Fabian Grein[1,2,5], Anna Müller[1,5], Katharina M. Scherer[3,5], Xinliang Liu[3], Kevin C. Ludwig[1], Anna Klöckner[1,2], Manuel Strach[1], Hans-Georg Sahl[4], Ulrich Kubitscheck[3✉] & Tanja Schneider[1,2✉]

The lipopeptide daptomycin is used as an antibiotic to treat severe infections with gram-positive pathogens, such as methicillin resistant *Staphylococcus aureus* (MRSA) and drug-resistant enterococci. Its precise mechanism of action is incompletely understood, and a specific molecular target has not been identified. Here we show that Ca^{2+}-daptomycin specifically interacts with undecaprenyl-coupled cell envelope precursors in the presence of the anionic phospholipid phosphatidylglycerol, forming a tripartite complex. We use microbiological and biochemical assays, in combination with fluorescence and optical sectioning microscopy of intact staphylococcal cells and model membrane systems. Binding primarily occurs at the staphylococcal septum and interrupts cell wall biosynthesis. This is followed by delocalisation of components of the peptidoglycan biosynthesis machinery and massive membrane rearrangements, which may account for the pleiotropic cellular events previously reported. The identification of carrier-bound cell wall precursors as specific targets explains the specificity of daptomycin for bacterial cells. Our work reconciles apparently inconsistent previous results, and supports a concise model for the mode of action of daptomycin.

[1] Institute for Pharmaceutical Microbiology, University Hospital Bonn, University of Bonn, Bonn, Germany. [2] German Center for Infection Research (DZIF), partner site Bonn-Cologne, Bonn, Germany. [3] Institute for Physical and Theoretical Chemistry, University of Bonn, Bonn, Germany. [4] Institute of Medical Microbiology, Immunology and Parasitology, University Hospital Bonn, University of Bonn, Bonn, Germany. [5] These authors contributed equally: Fabian Grein, Anna Müller, Katharina M. Scherer. ✉email: u.kubitscheck@uni-bonn.de; tschneider@uni-bonn.de

Daptomycin (DAP) is an antibiotic with unprecedented biophysical properties and antibacterial activities. Being initially considered unsuitable for clinical application due to toxic myopathies, a revised once-daily administration scheme was approved by the US Food and Drug Administration (FDA) in 2003 for the treatment of complicated skin and soft-tissue infections caused by various Gram-positive pathogens, making it the first lipopeptide antibiotic in clinical use.

DAP (previously designated LY146032), produced by the soil bacterium *Streptomyces roseosporus*, is a depsipeptide with a 10-membered cyclic lactone core that contains a number of unusual non-proteinogenic and D-amino acids cyclized by an ester bond. Three exocyclic amino acids (Trp1, Asn2, Asp3) link the decapeptide core to a decanoyl fatty acid side chain[1,2]. Structurally, DAP resembles a group of acidic lipopeptides, including A54145, friulimicin, tsushimycin and amphomycin[3,4]. Apart from structural features these peptides share a strict requirement of Ca^{2+} ions for antimicrobial activity. Importantly, the complex formation with Ca^{2+} affects the physicochemical properties of DAP, masking the anionic nature and conferring an overall amphiphilic character. Since this is a typical feature of cationic antimicrobial peptides (cAMPs) it was suggested that DAP likewise would act as cAMPs, which primarily target negatively charged microbial membranes[5]. In line with an AMP-like mode of action, mechanisms of DAP resistance overlap with those observed for cAMPs, e.g. modulation of cell surface charge and membrane characteristics[6], suggesting that the main target of DAP is or is located within the cytoplasmic membrane. However, and despite considerable experimental studies, the mechanism of action is still not completely understood. In particular, a molecular target had not been identified so far.

DAP mechanism of action studies produced controversial results for several decades. The earliest reports suggested that DAP inhibits peptidoglycan biosynthesis, accompanied by potassium leakage from *S. aureus* cells[7]. Later, cell division and synthesis of secondary cell wall polymers (i.e. lipoteichoic acid) had been proposed as target sites of DAP action[8,9]. Diverse membrane perturbing mechanisms have been accounted for the bactericidal effect of DAP, including induction of altered membrane curvature, membrane depolarisation and pore formation (e.g. Silverman et al.[10]). However, based on analysis of killing kinetics, it was also suggested that membrane leakage would be the result rather than the cause of cell death[11]. More recently, DAP was shown to interfere with fluid lipid microdomains in the membranes of susceptible bacteria, resulting in a drastic rearrangement of local membrane architecture, followed by the delocalisation of essential peripheral membrane proteins, such as the lipid II synthase MurG[12].

From various experiments, two currently prevailing hypotheses for the mechanism of action of DAP emerged. One model, originating from structural studies and the observed membrane depolarising effect, suggests that Ca^{2+}-DAP forms oligomeric aggregates, which upon contact with phosphatidylglycerol (PG) rearrange into a pore-like complex, leading to ion leakage and dissipation of membrane potential[5]. Generally, the presence of PG in membranes was shown in various studies to be a prerequisite for DAP activity (e.g. Jung et al. and Muraih et al.[11,13]). The second model suggests that DAP insertion at specific membrane domains, also enriched in PG, affects the physicochemical properties of the cytoplasmic membrane, triggering pleiotropic effects on essential cell wall biosynthesis and cell division processes[9,12].

Here, we report the identification of specific DAP targets, which allows to amalgamate controversially discussed results of previous mechanism of action studies. Using comprehensive in vivo and in vitro approaches in combination with fluorescence and optical sectioning microscopy, we show that DAP specifically interacts with undecaprenyl-coupled cell envelope precursors in the presence of PG by forming a tripartite complex.

Results

DAP interferes with the lipid II biosynthesis cycle. Previous studies described various DAP-mediated effects using different model organisms and various experimental approaches, which resulted in diverse mechanism of action models for DAP[5,10,12,14]. The differences in experimental approaches and conditions largely hampered direct and unrestricted data comparison. To consolidate previous findings with in vivo and in vitro approaches conducted in this study, we revised selected key experiments under consistent conditions.

Early investigations on the mechanism of action of DAP proposed peptidoglycan biosynthesis as the primary target pathway of the lipopeptide antibiotic[7,15]. Corroborating, macromolecular incorporation assays revealed a preferential inhibition of the incorporation of glucosamine into cell wall, while other major biosynthesis pathways remained almost unaffected[12].

DAP had previously been demonstrated to elicit the LiaRS stress response, supporting a specific inhibition of cell wall biosynthesis. The LiaRS two-component system (TCS) is known to respond to antibiotics that interfere with the lipid II biosynthesis cycle[16,17].

In search for a molecular target within the peptidoglycan biosynthesis pathway we here revisited the effect of DAP on the LiaRS response, but monitored P_{liaI}-*lux* induction over time and tested the impact of Ca^{2+}. Evaluating bioluminescence revealed a concentration-dependent induction by DAP (Fig. 1a, Supplementary Fig. 1) similar to teixobactin, which targets bactoprenyl-bound peptidoglycan precursors[18]. DAP promoted *lux* expression was only observed in the presence of 1.25 mM Ca^{2+}, indicating response specificity and suggesting that DAP impacts on the membrane-bound peptidoglycan biosynthesis machinery. The peptidoglycan biosynthesis machinery is predominantly localised at the division septum in staphylococci[19]. Accordingly, we found Bodipy-FL-labelled DAP to preferentially localise to this cellular site in *S. aureus* (Fig. 1b). Results from this experiment were validated by fluorescence microscopy of native DAP, taking advantage of the naturally fluorescent amino acid kynurenine, to rule out any disturbing effect of the fluorescence label (Fig. 1c).

Monitoring DAP binding over time showed, that binding is dynamic and occurs in two phases (Fig. 2). In phase I (0.5–15 min after DAP exposure) DAP septal localisation is prevailing. Prolonged incubation resulted in a progressive dispersion of DAP throughout the entire cytoplasmic membrane (phase II), finally resulting in membrane collapse and cell shrinkage (Fig. 2a). Importantly, initial septal DAP binding in phase I appears to correlate with killing (Fig.2b), indicating that cell death is the consequence of septal binding. In agreement, a subset of the cells in phase I were found to be dead as determined by sytox green staining (Supplementary Fig. 2).

To study the interaction of DAP with putative target molecules within the peptidoglycan biosynthesis pathway (Supplementary Fig. 3), we analysed the effect of various cell wall targeting antibiotics on the binding of DAP-FL to *S. aureus* cells. Short-term pre-incubation (2 min) of cells with antibiotics that bind to cell wall lipid intermediates, such as the ultimate peptidoglycan precursor lipid II, strongly diminished DAP binding, suggesting a blockage of target access (Fig. 3a, b). Both, teixobactin and oritavancin, known to interact with bactoprenyl-coupled cell wall intermediates, reduced DAP binding up to 50%, while pre-treatment with the β-lactam oxacillin did not have any detectable effect. Of note, pre-incubation with teixobactin partially protected

Material from: Grein, F., Müller, A., Scherer, K.M. et al., Ca2+-Daptomycin targets cell wall biosynthesis by forming a tripartite complex with undecaprenyl-coupled intermediates and membrane lipids. Nat Commun 11, 1455, published 2020, Springer Nature.

S. aureus from DAP and significantly delayed DAP-induced killing, indicating that both compounds interact with the same target (Fig. 3c).

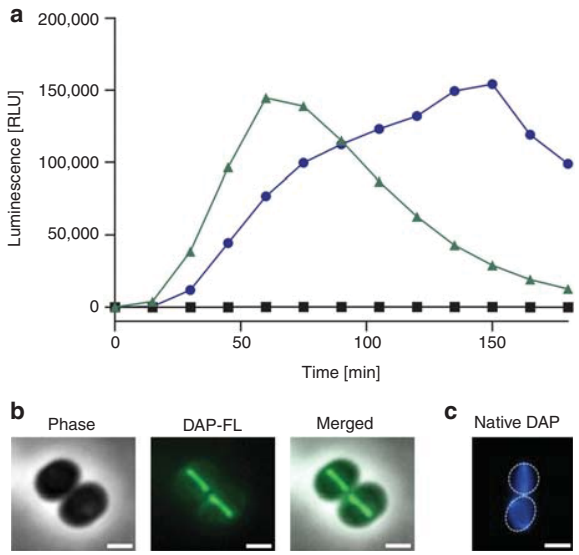

Fig. 1 DAP specifically induces the LiaRS stress response in the presence of Ca^{2+} and binds to the cell division site. a P_{liaI}-*lux* induction in *B. subtilis* was monitored upon addition of DAP (0.5 µg ml^{-1}) in the absence (black line) or presence (blue line) of 1.25 mM Ca^{2+} and teixobactin (0.5 µg ml^{-1}) (green line). Luciferase activity is presented as relative luminescence units (RLU). Representative graph of three independent experiments. **b**, **c** DAP localises to the septum of *S. aureus*. Cells were grown to mid-exponential phase (OD_{600} = 0.5) followed by the addition of Ca^{2+} and a mixture of labelled and unlabelled DAP (7 µg ml^{-1} DAP; 0.8 µg ml^{-1} DAP-FL) **b** or unlabelled DAP (7 µg ml^{-1}) **c**. Cells were washed and imaged by fluorescence microscopy; phase, phase contrast. Cell outlines in **c** are indicated by dashed lines. Scale bar: 1 µm. Representative images from five independent experiments are shown. Source data are provided as a Source Data file.

The cell wall precursor lipid II is synthesised on the cytoplasmic site of the bacterial membrane by a cascade of enzymatic reactions (Supplementary Fig. 3) before the bactoprenyl phosphate-linked disaccharide-pentapeptide is translocated to the outer leaflet, where lipid II is readily accessible to even large antibiotics[20]. Apart from its role as an essential cell wall building block, lipid II plays crucial roles as a functional scaffold coordinating cell wall biosynthesis and cell division. In this context, lipid II is discussed to contribute to the recruitment and assembly of these protein complexes[20–22].

To investigate the cellular effects triggered by DAP septum binding, we examined the co-localisation of DAP with the putative lipid II flippase FtsW. To this end *S. aureus* expressing a FtsW-GFP fusion protein was incubated with fluorescently labelled DAP (DAP-TMR) for 0.5 min (phase I). As revealed by dual-colour fluorescence microscopy using highly inclined and laminated optical (HILO) sheet illumination, FtsW-GFP and DAP-TMR co-localise to the division septum (Supplementary Fig. 4a, Supplementary Movie 1). In line with the observed dispersed distribution of DAP after prolonged incubation (20 min, phase II), FtsW-GFP was similarly delocalised from the division septum and found to accumulate in membrane spots together with DAP (Supplementary Fig. 4), further supporting a specific interaction with lipid II.

While the short-term exposure with lipid II-binding antibiotics blocked the interaction with the molecular target (Fig. 3a, b), we took advantage of the fact that the prolonged treatment of cells with sublethal concentrations of vancomycin results in an accumulation of lipid II[23]. Pre-incubation with vancomycin for 30 min resulted in strongly elevated cellular lipid II levels triggering hyperaccumulation of DAP (Supplementary Fig. 5a–c). In contrast, no such hyperaccumulation was observed in untreated or oxacillin-pre-treated control cells, in which lipid II levels were unchanged (Supplementary Fig. 5c). Corroborating, DAP-mediated killing was significantly accelerated in cells with increased lipid II content (Supplementary Fig. 5d).

DAP binding to supported bilayers doped with cell wall lipid intermediates. In vivo experiments clearly pointed to a specific interaction of DAP with bactoprenyl-coupled cell wall precursors.

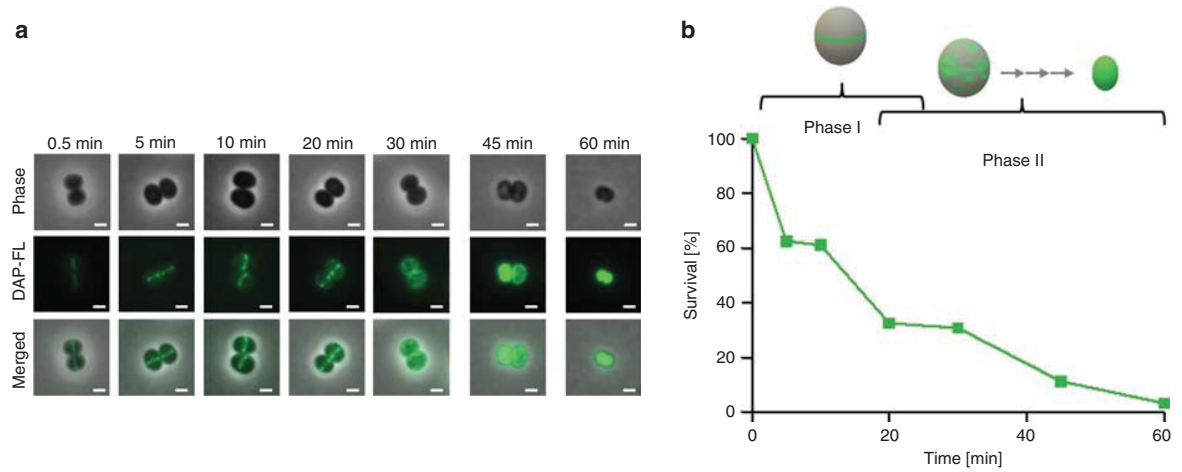

Fig. 2 DAP binds to *S. aureus* in a biphasic manner. a DAP-FL binding to *S. aureus* monitored over time (0–60 min). *S. aureus* HG003 was grown to mid-exponential phase (OD_{600} = 0.5) followed by the addition of Ca^{2+} and a mixture of labelled and unlabelled DAP (7 µg ml^{-1} DAP; 0.8 µg ml^{-1} DAP-FL). At different time points, samples were taken, washed and imaged by fluorescence microscopy. Representative pictures are shown from three independent experiments. Phase, phase contrast. Scale bar 1 µm. **b** Survival of cells from the experiment described in **a** and schematic depiction of DAP-FL-binding behaviour in two phases. Source data are provided as a Source Data file.

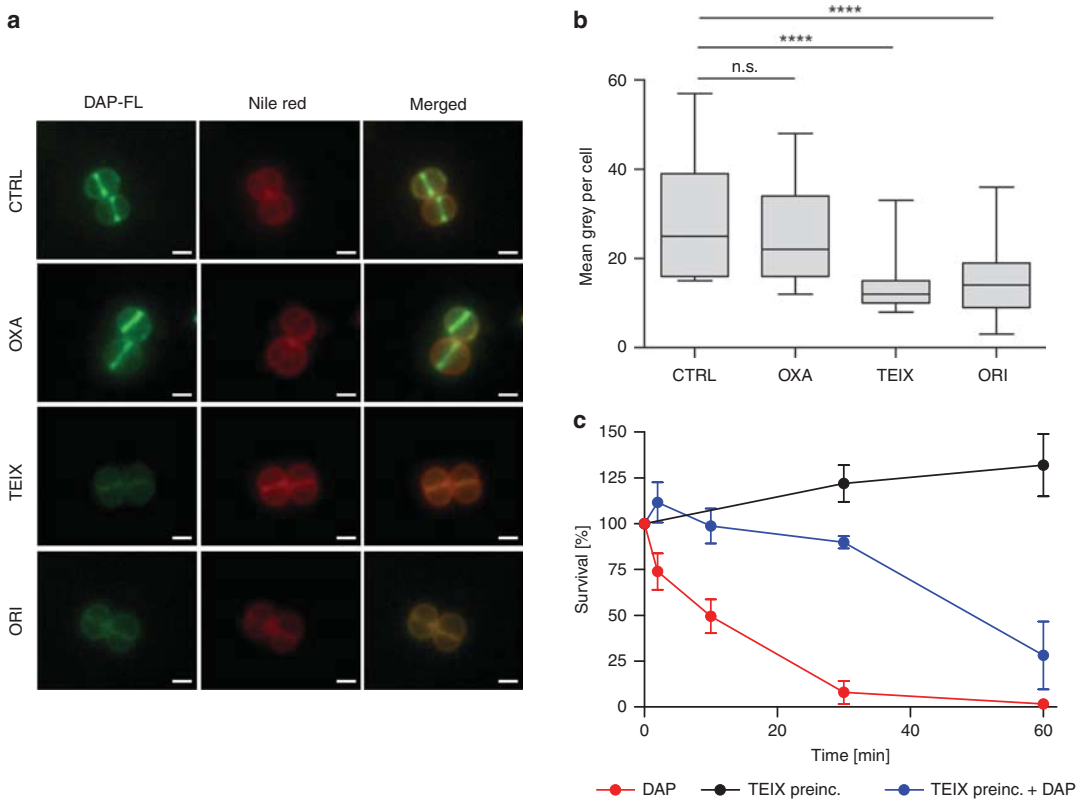

Fig. 3 Pre-incubation with lipid II-binding antibiotics prevents DAP binding to *S. aureus* and delays DAP-induced killing. a Binding of DAP-FL to *S. aureus* cells ($OD_{600} = 0.5$) pre-incubated with cell wall targeting antibiotics (oxacillin (OXA), teixobactin (TEIX) and oritavancin (ORI) (4-fold MIC)). After pre-incubation for 2 min, cells were washed and incubated with DAP-FL in the presence of Ca^{2+} for 10 min followed by washing and the addition of nile red membrane stain. Cells were washed again and subjected to fluorescence microscopy. In a control (CTRL) pre-incubuation with antibiotics was omitted. Scale bar 1 µm. Representative images are shown. **b** Quantification of DAP-FL binding measured in the experiment as described in **a**. Binding is expressed as mean grey value per cell. Box plots represent the interquartile range of the data. The black bar represents the mean and whiskers represent minimal and maximal values, respectively. At least $n = 350$ cells were evaluated for each condition from three biologically independent experiments. Significance was determined by unpaired Student's *t*-test with a 95% confidence interval. ****$p < 0.0001$, n.s., not significant ($p = 0.0835$). **c** Survival of *S. aureus* challenged with DAP (10 µg ml^{-1}) without (red line) or with (blue line) pre-incubation with TEIX as described in **a**. Bactericidal effects were not observed in cells only pre-treated with TEIX (black line). Data presented are mean values from $n = 3$ biologically independent experiments. Error bars represent the standard deviation (SD). Source data are provided as a Source Data file.

To test potential target molecules in a defined model system mimicking a more natural membrane environment, supported bilayers were individually loaded with $C_{55}P$, $C_{55}PP$ or lipid II (0.1 mol%) and DAP binding was monitored by total internal reflection fluorescence (TIRF) microscopy.

Basal binding of DAP to pure neutral phosphatidylcholine (PC) membranes was observed and only a moderate increase in binding was detected when bilayers were doped with individual cell wall precursors (Fig. 4a, left). In contrast, when the different bactoprenyl–lipid precursors were used in combination with PG (0.1 mol%), binding of DAP to the membrane was drastically increased (Fig. 4a, right and Supplementary Movie 2). Despite its essentiality for DAP antimicrobial activity, an equivalent increase in anionic PG (0.2 mol%) alone did not promote binding of the lipopeptide, compared to precursor containing PC-bilayers, revealing that binding does not solely rely on charge effects. As observed with whole cells, pre-incubation with antibiotics, that specifically bind peptidoglycan precursors $C_{55}P$ (friulimicin), $C_{55}PP$ (bacitracin) and lipid II (oritavancin), strongly decreased binding of DAP to the bilayer-embedded target molecules (Fig. 4b and Supplementary Movie 3).

These findings were further substantiated by the fact that antagonisation of the LiaRS response was only observed after addition of both, purified cell wall precursors and PG (Supplementary Fig. 6).

DAP forms a tripartite complex with lipid II and PG. To verify the formation of an antibiotic–target complex, purified lipid II was incubated with increasing concentrations of DAP in the absence and presence of PG, followed by extraction of the reaction mixture and subsequent thin layer chromatography (TLC) analysis. As expected, the formation of extraction-stable DAP complexes with lipid II was only observed in the presence of PG (Fig. 5a, left). Free PG, lipid II and DAP migrated to defined positions on the TLC. Increasing concentrations of DAP progressively diminished the amount of free, extractable lipid II as indicated by the respective band intensity compared to the control lacking DAP (Fig. 5a). In accordance with the formation of a tripartite complex, DAP and lipid II bands concurrently vanished from the TLC. DAP is known to aggregate and form oligomers of six or more molecules[14] and concordantly lipid II was almost

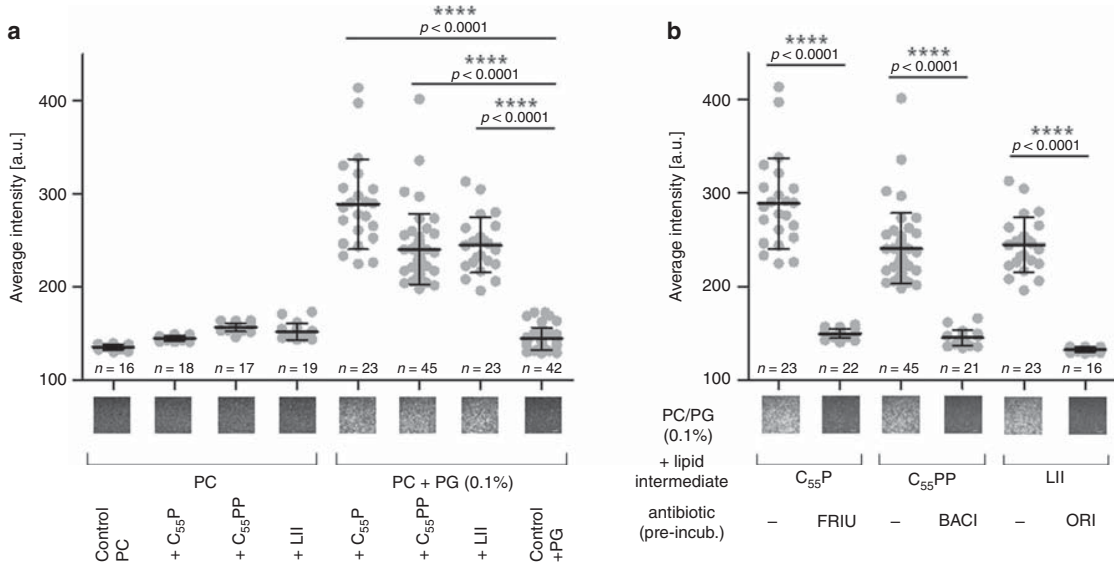

Fig. 4 DAP binding to supported bilayers doped with cell wall lipid intermediates. a Binding of DAP to supported bilayers is drastically increased in presence of bactoprenyl-coupled lipid intermediates and PG. Supported planar bilayers were prepared on coverslips using neutral DOPC lipids. Negatively charged PG lipids and bactoprenyl lipids were added, either 0.1 mol% bactoprenyl-coupled lipid intermediates or mixtures with PG (0.1 mol% each, 0.2 mol % PG served as a control). DAP was applied as a mixture of 1 µM native DAP and 50 nM DAP-FL. Movies with 100 frames were recorded at a frame rate of 60 Hz within 3 min after addition of DAP. The movies allowed to discern single binding events of DAP-FL. Exemplary fluorescence images are shown for each mixture. The field of view corresponds to $(32.5\ \mu m)^2$. **b** Inhibition of DAP-FL binding to supported planar bilayers (PC + 0.1% PG) by antibiotics that target specific bactoprenyl-coupled lipid intermediates. 300 nM of each antibiotic (FRIU, friulimicin; BACI, bacitracin and ORI, oritavancin) were incubated with the corresponding bactoprenyl-coupled lipid intermediate containing membranes for 5 min (antibiotic:lipid intermediates ratio 100:1). Excess of antibiotics was removed by buffer exchange followed by the addition of DAP as described in **a**. Exemplary movies are shown in Supporting Movies 2 and 3. Data were obtained from at least 20 movies for each experiment. We determined the mean values in a field of 160 μm^2 in the first image of each movie. Data in **a** and **b** are plotted as averages of these means and error bars represent the SD of all movies of a specific experiment. Significance was determined by unpaired Student's *t*-test with a 95% confidence interval, $^{****}p < 0.0001$. All experiments were independently repeated three times and yielded comparable results. Source data are provided as a Source Data file.

fully locked in an extraction-stable complex at a molar ratio of 1:10 with respect to DAP (Fig. 5a). In contrast, no change in band intensities was observed for lipid II and DAP in the absence of PG; even at the highest DAP concentration lipid II was uncomplexed (Fig. 5a, right). Complex formation was further not observed when lipid II and DAP were incubated in the presence of PC or the negatively charged cardiolipin (Supplementary Fig. 7), supporting specificity for PG to form a complex with DAP and lipid II.

Previous analyses showed only a minor impact of DAP on in vitro cell wall biosynthesis reactions, causing a 20% inhibition at a twofold molar excess of DAP[24,25]. However, these previous studies did not contain PG and did further not take into account that DAP oligomerises into multimers. In the presence of PG, the inhibitory effect of DAP on the MraY catalysed synthesis of lipid I was increased at a two-fold molar excess. MraY is the initial glycosyltransferase of peptidoglycan biosynthesis linking the first sugar building block to the lipid carrier $C_{55}P$ (Supplementary Fig. 3). The MraY catalysed reaction was almost completely blocked at a 10:1 molar ratio (Fig. 5b), in line with DAP oligomerisation. Similarly, the PBP2-catalysed transglycosylation of lipid II was inhibited in a dose-dependent manner (Fig. 5c).

Discussion

DAP has served as a life-saving antibiotic for almost two decades. However, fundamental aspects of its killing activity, in particular molecular details, such as the identification of a specific molecular target, remained elusive[14]. In contrast, downstream effects triggered by DAP were extensively described and revealed unique features of its activity on the cellular level[9,12]. It became clear that DAP primarily impairs cell wall biosynthesis by targeting fluid microdomains, causing massive membrane rearrangements and displacement of cell wall biosynthetic enzymes. Such activities are reminiscent of cAMPs[12,26] and indeed DAP, in complex with Ca^{2+}, has been proposed to act like cAMPs[5]. Typically, most cAMPs act without specific molecular targets and may have minimal inhibitory concentrations in the millimolar range. The potency of DAP, in contrast, is much higher and compares well with the activity of those cAMPs that combine membrane effects with specific target binding, such as plectasin-like defensins or nisin-like lantibiotics, which may have MICs in the nanomolar range[27,28]. Both groups of cAMPs are known to bind to bactoprenyl-coupled cell wall precursors, specifically the peptidoglycan precursor lipid II, and it was tempting to assume similar activities for DAP, particularly since DAP elicits the LiaRS-mediated response specific for antibiotics interfering with the lipid II biosynthesis cycle[29,30]. However, unlike with nisin, plectasin, teixobactin and several other lipid II-binding antibiotics[18,25,28], we were previously unable to demonstrate such activities for DAP.

DAP is structurally related to the lipopeptides friulimicin and amphomycin, both of which are characterised by an overall negative charge. A DXDG or EF-hand motif is likely involved in Ca^{2+} binding that is strictly required for antimicrobial activity of these antibiotics[4]. Despite such structural similarities, these true lipopeptides appear to significantly differ in their mechanism of action. Amphomycin and friulimicin bind to $C_{55}P$ and

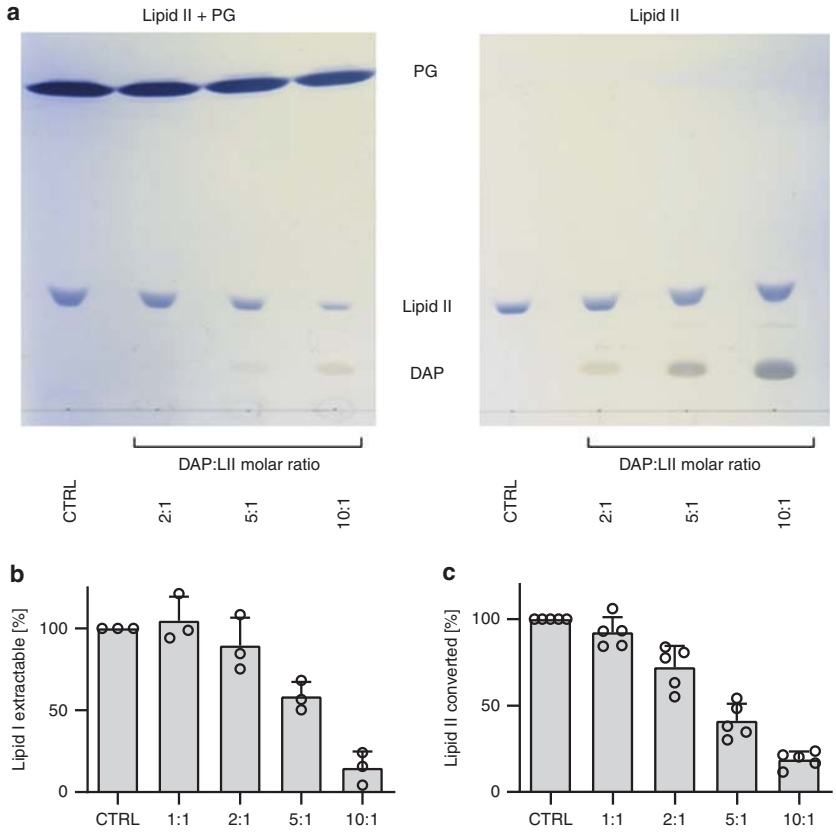

Fig. 5 DAP forms a tripartite complex with lipid II and PG and inhibits cell wall biosynthesis in vitro. a DAP was incubated with purified lipid II at increasing molar ratio in the presence (left TLC) and absence (right TLC) of PG. Reaction mixtures were extracted with BuOH and the upper solvent phase was spotted to TLC. Free PG, DAP and lipid II migrate to defined positions on the TLC, while components that are locked in complex are retained in the lower aqueous phase after extraction and as a result are diminished on the TLC. Representative images from five independent experiments are shown. **b** Impact of DAP on the MraY-catalysed synthesis of lipid I and **c** on the transglycosylation reaction catalysed by PBP2. DAP inhibits both reactions in a dose-dependent manner and almost completely blocks enzymatic activity when added in 10-fold molar excess. The enzymatic activity is expressed as synthesised lipid I (MraY) or converted lipid II (PBP2). The control reactions in the absence of antibiotics were set to 100%. DAP was added at molar ratios of 1:1 to 10:1 with respect to the lipid substrates as indicated. Data presented are means from three independent experiments and error bars represent the SD. Source data are provided as a Source Data file.

inhibit in vitro the formation of lipid I catalysed by the glycosyltransferase MraY at a two-fold molar ratio, corroborating the formation of active dimers[24,25]. Crystal structure analysis of another related calcium-dependent cyclic lipopeptide, tsushimycin, suggested that the biologically active form of the antibiotic is likely to be a dimer[31]. Dimerisation is dependent on the presence of Ca^{2+}, which results in a structure exhibiting a hydrophobic surface and a cleft-like tunnel, that is suitable for the accommodation of a target molecule such as $C_{55}P$.

Importantly, DAP has been reported to form oligomers[14] rather than dimers and was previously only tested at equimolar concentrations of $C_{55}P$ to DAP[25]. In addition, the detergent-based assays employed in the latter study lacked PG, which has been shown in numerous studies to be another prerequisite for DAP activity. We thus revisited bactoprenyl-coupled cell wall precursors as potential target molecules in a test system mimicking a more natural membrane environment and included higher DAP concentrations. Only in the presence of both Ca^{2+} and PG an extraction-stable complex with lipid II was formed. Furthermore, binding of DAP to supported bilayers doped with bactoprenyl-bound precursors was strongly enhanced in the presence of PG. Together these data reveal the formation of a tripartite Ca^{2+}-DAP complex with the anionic phospholipid and cell wall precursors.

It is well established that PG plays a key role in the mechanism of action of DAP, and PG levels have been associated with DAP susceptibility and resistance. It was recognised early that susceptible bacterial species, such as staphylococci are characterised by high membrane PG levels (up to 60%), while streptomycetes, including the DAP producer, have a reduced PG content[32]. DAP is active against Gram-positive bacteria and essentially lacks antimicrobial activity against Gram-negative species. Even in *E. coli* strains with a destroyed outer membrane barrier, no change in susceptibility was observed, which may well be linked to limited PG levels in these bacteria (about 15%)[33,34]. Numerous studies on clinical and laboratory daptomycin-resistant (DAP-R) strains, linked DAP non-susceptibility to the overall PG content[35–37]. Mutations in *mprF*, encoding for the bifunctional lysyl-phosphatidylglycerol (Lys-PG) synthase and flippase, are frequently found in DAP-R strains. Single nucleotide polymorphisms (SNPs) are often associated with increased conversion of PG to Lys-PG likely resulting in reduced DAP binding due to

Material from: Grein, F., Müller, A., Scherer, K.M. et al., Ca2+-Daptomycin targets cell wall biosynthesis by forming a tripartite complex with undecaprenyl-coupled intermediates and membrane lipids. Nat Commun 11, 1455, published 2020, Springer Nature.

charge repulsion[38]. A recent study hypothesised that mutations at the junction of synthase and flippase domain reduce intramolecular interactions proposed to result in an extended substrate spectrum of the flippase. Whether this directly affects translocation of the antibiotic or membrane-standing components crucial for activity remains to be elucidated[39].

Importantly, DAP exhibits limited toxicity in humans, correlating with the generally low abundance of PG in mammalian cells[40]. However, DAP was shown to be inactivated by pulmonary surfactant in vitro[41]. This effect is attributed to the relatively high PG content in lung surfactant (~10%), which excludes DAP as a therapeutic option in the treatment of pneumonia.

Our model membrane studies substantiate the proposed crucial role of PG for DAP membrane interaction, following structural transition and oligomerisation in the presence of Ca^{2+}[5,11,13]. Of note, an obviously defined stoichiometry in the binding of Ca^{2+}-DAP to PG of 1:1 or 1:2, depending on the model deployed, indicates a direct interaction, rather than PG-mediated modulating effects that may facilitate DAP membrane insertion indirectly[42,43]. In line, Ca^{2+}-DAP further induced the formation of extensive DAP/PG domains in giant unilamellar vesicles[44] and localised to membrane regions of increased fluidity (RIFs) in bacterial cells[12].

Anionic phospholipids, such as PG, are assumed to preferably localise to membrane domains in the septal and polar regions in bacterial cells, and to play important roles in biological processes. Phospholipids specifically interact with proteins and coordinate their spatial and temporal position and function, e.g. the positioning of the divisome complex at midcell, DNA replication, ATP synthesis and osmoregulation[45,46]. Furthermore, anionic phospholipids have been shown to be crucial for the enzymatic activity of membrane-bound and peripheral proteins, such as the initial glycosyltransferase MraY in peptidoglycan biosynthesis[47] and, thus, appear to impact on the organisation of cell wall biosynthetic machineries. In accordance, previous studies with *Bacillus* revealed that fluorescently labelled DAP preferentially localised at the division septum and in a helical pattern following the longitudinal axis of the cell, regions in the rod-shaped cells that are enriched in both anionic lipids, primarily PG, and C_{55}P-coupled cell wall precursors[9,29].

Moreover, association of phospholipids and bactoprenyl-bound cell wall precursors, like lipid II, has been reported[48]. Molecular dynamics simulations suggest that lipid II forms specific amphiphilic "island"-like regions on the membrane surface, in which the hydrophilic lipid II headgroup is central and surrounded by an extended and long-lived hydrophobic pattern. Importantly, the formation of this unique pattern induced by lipid II was observed only in membranes containing PG, but was absent in pure PC bilayers[48], creating an ideal "landing platform" for antibiotics.

DAP was shown to be bactericidal against both exponentially growing bacteria and *S. aureus* cells in stationary phase[49]. The authors at that time concluded that the bactericidal action of DAP likely does not require cell division or active metabolism. However, several lines of evidence showed that stationary-phase cells exhibit significant cell wall biosynthetic activity[50–52] and, thus, sufficient target availability. Reduced concentrations of cell wall precursors in stationary phase cells agree well with the increased concentrations (>100 μg ml^{-1}, 24 h) required to achieve comparable killing (three-fold log reduction) with regard to exponentially growing cells (2 μg ml^{-1}, 60 min). Moreover, due to its cationic nature, Ca^{2+}-DAP can bind to membranes even in the absence of molecular targets[42,43]. Likewise, the lantibiotic nisin also binds to membranes in the absence of lipid II[28]. This may also explain the fact that we found DAP-mediated killing is only delayed upon target blocking.

Membrane depolarisation has also been associated with the DAP killing mechanism, which is controversially discussed in literature[10,11,53]. Here, we show that initial binding of DAP to the septum correlates with antibiotic killing within the first 15 min of treatment (75% reduction in survival) and, thus, target binding appears the central event for promoting killing. In line with findings of Jung et al.[11] and the fact that pronounced depolarisation is observed only after 30 min of treatment[10], cell death is rather the consequence of lipid II binding, whereas depolarisation is most likely a result of disintegrative membrane rearrangements following PG and lipid II binding. The massive DAP clusters observed after prolonged incubation are highly reminiscent of the nisin:lipid II clusters reported by Hasper et al.[54].

Lipid II plays crucial roles in bacterial cell physiology that go beyond its role as a cell wall building block. In fact, lipid II appears to function as a crucial element in the organisation and coordination of enzymatic complexes, involved in peptidoglycan biosynthesis and cell division[21,22]. Thus, interfering with these membrane-bound machineries and biosynthetic networks by sequestration of lipid II can induce malfunctioning of a multitude of differential and overlapping cellular processes.

The identification of bactoprenyl-bound precursors as target molecules in this study sheds light on the unique requirements for DAP action. The interactions with these molecules and the cellular complexity arising from target binding can explain the pleiotropic cellular downstream effects of this unique antibiotic and reconcile the puzzling results from numerous studies on DAP resistance development (Fig. 6).

The identification of the molecular targets adds an important piece to the DAP MoA puzzle. However, since structural information (of comparatively simple complexes) on antibiotics in complex with full-length lipid II are scarce, the challenges of unravelling the structure and dynamics of the DAP tripartite complex will likely be much higher.

Methods

Chemicals. All chemicals were of analytical grade or better. Bodipy FL succinimidyl ester, 6-(tetramethylrhodamine-5-(and-6)-carboxamido) hexanoic acid (TMR) succinimidyl ester, Bodipy FL Vancomycin and nile red were purchased from Thermo Fisher Scientific, Waltham, USA. DAP was labelled with Bodipy FL succimidyl ester followed by ether precipitation, preparative TLC[55] and verification by MALDI-TOF spectrometry. The phospholipids 1,2-dioleoyl-sn-glycero-3-phosphocholine (DOPC), 1,2-dioleoyl-sn-glycero-3-phosphoglycerol (DOPG) and 1′,3′-bis[1,2-distearoyl-*sn*-glycero-3-phospho]-glycerol (DOCL, cardiolipin) were purchased from Avanti Polar Lipids (Alabaster, AL, USA) and used without further purification. Undecaprenyl phosphate (C_{55}P) and undecaprenyl diphosphate (C_{55}PP) were purchased from Larodan Fine Chemicals AB (Malmö, Sweden). DAP was purchased from Cubist Pharmaceuticals, Oritavancin was provided by The Medicines Company, Montreal, Canada and teixobactin was kindly provided by Kim Lewis, Northeastern University, Boston, USA. All other chemicals were from Sigma-Aldrich, Taufkirchen, Germany. Lipid II was enzymatically synthesised in vitro followed by n-butanol-pyridine acetate (pH 4.2) (2:1, v/v) extraction and purification via ion exchange chromatography[56].

Strains used in this study. *S. aureus* strains HG003[57] and RN4220[58] and *Bacillus subtilis* W168 *sacA*::pCHlux101 (P_{liaI}-*lux*)[17] were used. For cloning, *E. coli* DH5α (Invitrogen, Carlsbad, CA, USA) was used. To construct a strain expressing a FtsW-GFP fusion protein from the native FtsW promotor, the GFPmut2 coding sequence was amplified from plasmid pCQ11 (kindly provided by C. Quiblier and B. Berger-Bächi) using primers gfp-f (5′-AGTAACGCGTATGAGTAAAGGA GAAGAAC-3′) and gfp-r (5′-ATAGGCGCGAATTCTTTGTATAGTTCATCC-3′), the resulting fragment was restricted with *Eco*RI and *Mlu*I and ligated into pMAD[59], which has been cut with the same restriction enzymes giving plasmid pMAD-gfpmut2. A 506 bp fragment encoding the C-terminal part of *ftsW* and a 492 bp fragment downstream of *ftsW* were amplified using primers ftsW-up-f (5′-TACGCTAACAGATGGATCCCAATTCGAAT-3′), ftsW-up-r (5′-TGGCTAGTA TTTTTACGCGTAAATTGTCTTCT-3′) and ftsW-down-f (5′-GAAGACAATTT AATGAATTCAATACTAGCCAATA-3′) and ftsW-down-r (5′-TTTTATCTTAA AGATCTCTGTTTTGCTAT-3′), respectively, and the products cloned into pMAD-*gfpmut2* using *Bam*HI, *Mlu*I *Eco*RI and *Bgl*II. The final plasmid pMAD-*ftsW-gfpmut2* was electroporated into *S. aureus* RN4220 and a described protocol[59]

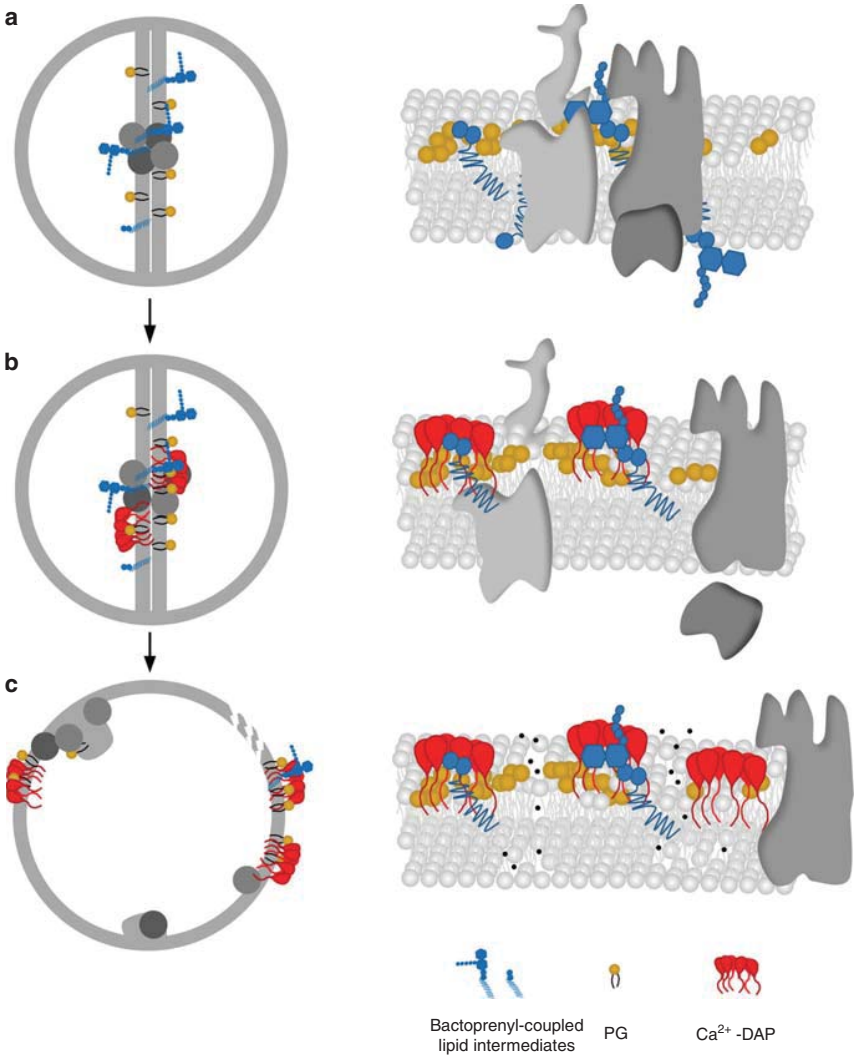

Fig. 6 Proposed model for the mechanism of action of DAP. a Orchestration of the cell wall biosynthesis machinery at the division septum of *S. aureus* in the absence of DAP. **b** Ca^{2+}-DAP oligomerises and preferentially localises at the division septum enriched in anionic lipids, primarily PG, and C_{55}P-coupled cell wall precursors. The formation of a tripartite complex of Ca^{2+}-DAP with PG and bactoprenyl-coupled lipid intermediates blocks cell wall synthesis and triggers the delocalisation of the cell wall biosynthetic machinery. **c** Prolonged treatment results in a progressive dispersion of DAP throughout the entire cytoplasmic membrane, followed by disintegration of the membrane bilayer finally resulting in membrane leakage and cell death.

was followed to achieve double homologous recombination of the plasmid insert into the genome.

Luciferase reporter assays. *B. subtilis* luciferase reporter assays were conducted as previously described[60]. Briefly, strains were grown in Mueller–Hinton broth at 30 °C containing 5 μg ml^{-1} chloramphenicol until they reached an OD_{600} of 0.5. Cells were added to 96-well white wall chimney plates containing antibiotics and luminescence measurements were performed at 30 °C in a microplate reader Spark 10M (Tecan). DAP and putative antagonists DOPG, C_{55}P and lipid II were pre-incubated for 10 min prior to addition of the reporter strain. At least three independent biological replicate experiments were conducted. Data analysis was performed using Graph Pad Prism 5.01.

Microscopy of bacteria. To study the localisation of DAP, *S. aureus* HG003 was grown in LB to the mid-exponential phase ($OD_{600} = 0.5$) followed by the addition of 1.25 mM $CaCl_2$ and either unlabelled DAP or a mixture of labelled and unlabelled DAP (7 μg ml^{-1} unlabelled/0.8 μg ml^{-1} DAP-FL). To visualise cell membranes, nile red was added to a final concentration of 1 μg ml^{-1}. Cells were washed twice in LB, re-suspended and analysed by fluorescence microscopy. Therefore, cells were spotted onto microscope slides covered with a thin film of 1% agarose in water. Microscopy was carried out at room temperature using a Zeiss Axio Observer Z1 microscope (Zeiss, Jena, Germany) equipped with HXP 120 V light source and an Axio Cam MR3 camera. Standard filter sets were used for Bodipy-FL (450–490 nm excitation and 500–500 nm emission), Marina blue (for native DAP visualisation, 335–383 nm excitation and 420–470 nm emission) and nile red (510–560 nm excitation and 590 nm long pass emission).

Image acquisition and analysis were performed with Zen 2 (Zeiss) and ImageJ v1.45s software (National Institutes of Health)[61]. For the quantification of fluorescence intensities, the mean grey values measured in the Bodipy-FL channel image of individual cells were summarised and divided by the total area of the cells measured in the phase contrast image. At least 350 cells were used for calculations for each condition.

Killing kinetics. To study the impact of short-term pre-incubation with teixobactin on *S. aureus* DAP susceptibility, cells were grown in LB to the mid-exponential phase ($OD_{600} = 0.5$) and the CFU ml^{-1} of the culture was determined and set as 100%. Two aliquots were taken from the culture that were either left untreated or pre-incubated with teixobactin (four-fold MIC) for 2 min. Cells were spun down and re-suspended in LB supplemented with 1.25 mM $CaCl_2$ and DAP (10 μg ml^{-1}) followed by incubation at 37 °C. To study the effect of lipid II accumulation,

Material from: Grein, F., Müller, A., Scherer, K.M. et al., Ca2+-Daptomycin targets cell wall biosynthesis by forming a tripartite complex with undecaprenyl-coupled intermediates and membrane lipids. Nat Commun 11, 1455, published 2020, Springer Nature.

vancomycin (5 μg ml^{-1}) was added to cells grown to the mid-exponential phase which were then incubated for 30 min. Cells were washed twice in LB supplemented with 1.25 mM $CaCl_2$, DAP (5 μg ml^{-1}) was added and the cells further incubated at 37 °C. Controls were performed without pre-incubation with vancomycin and/or without the addition of DAP. Aliquots were taken at the indicated time points and CFU ml^{-1} were determined. Therefore, cells were serially diluted in 0.9% NaCl solution and streaked on LB agar plates. Colony counts were determined after overnight incubation at 37 °C.

Bilayer preparation. In order to prepare planar bilayers on glass supports, very small unilamellar vesicles (VSUV) were prepared from detergent solution by addition of heptakis(2,6-di-O-methyl)-β-cyclodextrin (cyclodextrin) according to Roder et al.[62]. Neutral DOPC lipids were used to prepare fluid bilayers. Bactoprenyl-bound lipid intermediates and/or negatively charged DOPG were added with the amount of 0.1 or 0.2 mol%, respectively. For each mixture, 1.3 mM lipid solution was prepared in chloroform, and the chloroform was slowly removed in a nitrogen stream. The resulting lipid film was solubilized in HEPES buffer (20 mM HEPES, 150 mM NaCl, pH 7,4) supplemented with 20 mM Triton X-100. The lipid-detergent stock solution of 5 mM lipid was stored at −4 °C until use. A second stock solution contained 4 mM cyclodextrin in HEPES buffer and was also stored at −4 °C. A suspension of VSUV was prepared by first diluting the lipid-detergent stock solution 10-fold in HEPES buffer, followed by addition of an equal volume of cyclodextrin stock solution and immediate, thorough mixing by vortexing for 2 min. Vesicles were generally used within 1 h after preparation.

Coverslips (18 × 18 mm) were cleaned overnight in fresh Piranha solution (one part H_2O_2 30% and two parts concentrated H_2SO_4), rinsed thoroughly with milliQ water and dried in a nitrogen stream. Clean coverslips were placed into custom-built sample chambers with a Teflon O-ring as seal and two metal clips to fix the metal insert on top of the coverslip.

Bilayers were prepared immediately by adding 400 μl freshly made vesicle suspension filling the well of the sample chamber. Due to electrostatic interaction between the lipid headgroups and the highly hydrophilic glass surface, vesicles readily attached to the coverslip. The high surface tension led to fusion of VSUV and formation of homogeneous bilayers on the complete cover slip within 5 min. Residual, non-fused vesicles were removed by carefully washing three times with HEPES buffer. During the washing steps care was taken to not dry out the lipid bilayer. After washing, bilayers were kept in HEPES buffer.

Bilayer binding assay and dual colour HILO imaging. Successively, 1.25 mM $CaCl_2$ and DAP—in a mixture of 1 μM native DAP and 50 nM Bodipy FL-labelled daptomycin (DAP-FL)—in HEPES buffer were added to freshly prepared bilayers. For the binding inhibition test, 300 nM of the antibiotics friulimicin, bacitracin and oritavancin (specifically targeting C_{55}P, C_{55}PP and lipid II, respectively) were first incubated with the corresponding bactoprenyl lipid containing membranes for 5 min. Bacitracin was added together with 0.5 mM $ZnCl_2$ and oritavancin together with 0.002% Tween 80 (v/v). The peptide to lipid ratio was 100:1. Excess of antibiotics was removed by buffer exchange before $CaCl_2$ and DAP addition.

Images were acquired at a custom-built, single molecule sensitive, inverted microscope capable of TIRF microscopy with an EMCCD camera (iXon DU-897D; Andor Technology, Belfast, Northern Ireland)[63] using Andor Solis software. Lasers and acousto-optic tunable filter (AOTF, Gooch&Housego) were controlled by Labview 2012 software. Illumination with total internal reflection reduced fluorescence excitation to a thin region at the coverslip surface with the benefit of background suppression from fluorescence outside the illuminated region. The illumination beam angle was adjusted by tilting a collimated laser beam in the object focal plane of the imaging lens, which focused the beams in the back focal plane of the objective, until total reflection at the coverslip/medium interface was reached. Using a ×63 objective lens with a NA 1.45 (Zeiss), additional ×4 magnification and 2 × 2 binning during acquisition resulted in a pixel size of 127 nm. The imaged field of view with the extension (32.5 μm)^2 corresponded approximately to 1/4 of the total illuminated field. Thus, it can well be assumed that the observed field showed an isotropic fluorescence, and that there was no influx of putatively unbleached and no efflux of putatively bleached molecules. This assumption is corroborated by an evaluation of the movie data, which did not show any spatial fluorescence gradient occurring over the field of view as a function of time. DAP-FL was excited with laser light at 488 nm (Sapphire-100; Coherent, Santa Clara, CA) and fluorescence was detected by use of a standard fluorescein dichroic and a notch filter (NF03-488E-25, Semrock). Movies with 100 frames were recorded at a frame rate of 60 Hz immediately after addition of DAP within 5 min.

In each data acquisition session, all samples were measured during one day in order to guarantee optimal comparability among the samples. From each sample at least 20 movies at different locations of the bilayer on each cover slip were acquired. Intensity values over a cropped region of 100 × 100 pixels corresponding to 160 μm^2 within the first image of each movie were averaged in order to circumvent effects of possible photobleaching or molecular transport during movie data acquisition. Data analysis was performed using Origin 2019 software. The average background signal of the camera was subtracted and the intensity values were averaged for each experimental condition separately. The observation field was defined by the camera position and was constant, however, small deviations in the very sensitive TIRF excitation beam path resulted in absolute intensity variations from day to day. A Student's *t*-test was performed to demonstrate the significance of the intensity differences between respective samples from one session. All experiments were repeated three times and yielded comparable results.

The same instrument was employed for fluorescence microscopy based on HILO illumination[64] by reducing the incidence angle of the laser beam in the back focal plane of the objective lens compared to that for TIRF excitation[65]. Illumination using HILO reduced fluorescence excitation to a sheet-like axial section near the coverslip surface resulting in suppression of fluorescence outside the illuminated section. For dual-colour imaging of bacteria, an image splitter (OptoSplit II, Cairn Research, Faversham, UK) was inserted in the detection pathway in front of the camera. A dichroic mirror (FF509-FDi01-25 × 36, Semrock, Rochester, USA) and a band-pass emission filter (LP02-561RE-25, Semrock) were used to separate the emission channels. A motorised stage controlled by μManager[66] was used to acquire z-stacks with a step size of 50 nm. The stacks were then filtered and reconstructed in three-dimensions by the 3D Hybrid Median Filter function of ImageJ.

Complex formation of DAP with purified lipid II. Complex formation was analysed by incubating 3 nmol of purified lipid II in 50 mM Tris–HCl pH 7.5 and 1.25 mM $CaCl_2$ in presence or absence of 75 μg DOPG with increasing concentrations of DAP for 20 min at room temperature. Complex formation was further tested with 75 μg DOPC and DOCL. Free lipid II molecules were extracted with n-butanol–pyridine acetate (pH 4.2) (2:1, v/v) and analysed by TLC using chloroform/methanol/water/ammonia (88:48:10:1, v/v/v/v) as the solvent and phosphomolybdic acid (PMA) staining. The quantitative analysis of lipid II extracted to the butanol phase was carried out using ImageJ. Experiments were performed in triplicate.

Impact of DAP on peptidoglycan biosynthesis reactions in vitro. Peptidoglycan synthesis reactions were reconstituted in vitro using purified proteins and substrates. PBP2-His_6 and MraY-His_6 were produced in *E. coli* and purified via IMAC after solubilisation with 0.06% Triton and 18 mM n-dodecyl-β-D-maltoside, respectively[25]. Enzymatic activity of purified MraY-His_6 was assessed in a total volume of 50 μl containing 5 nmol C_{55}P and crude substrate in 0.08% Triton X-100, 37.5 μg DOPG, 100 mM Tris–HCl, 30 mM $MgCl_2$, pH 8.0, and 1.25 mM $CaCl_2$. The reaction was initiated by the addition of the recombinant enzyme and extracted after incubation for 90 min at 30 °C.

Transglycosylation by PBP2 was determined by incubating 3 nmol of lipid II in 0.04% Triton X-100, 20 mM MES, 2 mM $MgCl_2$, 2 mM $CaCl_2$ pH 5.5 in a total volume of 50 μl. The reaction was initiated by the addition of 8 μg of PBP2-His_6 and incubated for 2 h at 30 °C.

DAP was added in molar ratios ranging from 1 to 10 with respect to the respective substrate (C_{55}P or lipid II) in all in vitro assays and pre-incubated for 10 min prior to addition of the enzyme. Lipid intermediates were extracted from the reaction mixtures with n-butanol/pyridine acetate, pH 4.2 (2:1, v/v) and analysed by TLC as described above. Quantification was carried out by phosphorimaging in a StormTM imaging system (GE Healthcare) or PMA staining and analysis performed using ImageJ and Graph Pad Prism. Experiments were performed at least in triplicate.

Accumulation of lipid II. To verify accumulation of lipid II after vancomycin pre-treatment, cells were spun down and resuspended in phosphate buffered saline (PBS). Lipid extraction and TLC analysis were performed as described for the in vitro assays with the exception that the BuOH phase was washed twice with acidified H_2O.

Reporting summary. Further information on research design is available in the Nature Research Reporting Summary linked to this article.

Data availability

The authors declare that all data supporting the findings of this study are available within the Article and its Supplementary Information. The source data underlying Figs. 1a, 2b, 3b, c, 4a, b, 5a–c and Supplementary Figs. 1, 5a, c, d, 6a, b and 7 are provided as Source Data file.

Received: 15 July 2019; Accepted: 25 February 2020;
Published online: 19 March 2020

References

1. Debono, M. et al. A21978C, a complex of new acidic peptide antibiotics: isolation, chemistry, and mass spectral structure elucidation. *J. Antibiot.* **40**, 761–777 (1987).
2. Debono, M. et al. Enzymatic and chemical modifications of lipopeptide antibiotic A21978C: the synthesis and evaluation of daptomycin (LY146032). *J. Antibiot.* **41**, 1093–1105 (1988).

3. Wood, T. M. & Martin, N. I. The calcium-dependent lipopeptide antibiotics: structure, mechanism, & medicinal chemistry. *MedChemComm* **10**, 634–646 (2019).
4. Strieker, M. & Marahiel, M. A. The structural diversity of acidic lipopeptide antibiotics. *Chembiochem* **10**, 607–616 (2009).
5. Straus, S. K. & Hancock, R. E. W. Mode of action of the new antibiotic for Gram-positive pathogens daptomycin: comparison with cationic antimicrobial peptides and lipopeptides. *Biochim. Biophys. Acta* **1758**, 1215–1223 (2006).
6. Miller, W. R., Bayer, A. S. & Arias, C. A. Mechanism of action and resistance to daptomycin in *Staphylococcus aureus* and Enterococci. *Cold Spring Harb. Perspect. Med.* **6**, https://doi.org/10.1101/cshperspect.a026997 (2016).
7. Allen, N. E., Hobbs, J. N. & Alborn, W. E. Inhibition of peptidoglycan biosynthesis in Gram-positive bacteria by LY146032. *Antimicrob. Agents Chemother.* **31**, 1093–1099 (1987).
8. Canepari, P. & Boaretti, M. Lipoteichoic acid as a target for antimicrobial action. *Microb. Drug Resist.* **2**, 85–89 (1996).
9. Pogliano, J., Pogliano, N. & Silverman, J. A. Daptomycin-mediated reorganization of membrane architecture causes mislocalization of essential cell division proteins. *J. Bacteriol.* **194**, 4494–4504 (2012).
10. Silverman, J. A., Perlmutter, N. G. & Shapiro, H. M. Correlation of daptomycin bactericidal activity and membrane depolarization in *Staphylococcus aureus*. *Antimicrob. Agents Chemother.* **47**, 2538–2544 (2003).
11. Jung, D., Rozek, A., Okon, M. & Hancock, R. E. W. Structural transitions as determinants of the action of the calcium-dependent antibiotic daptomycin. *Chem. Biol.* **11**, 949–957 (2004).
12. Müller, A. et al. Daptomycin inhibits cell envelope synthesis by interfering with fluid membrane microdomains. *Proc. Natl Acad. Sci. USA* **113**, E7077–E7086 (2016).
13. Muraih, J. K., Pearson, A., Silverman, J. & Palmer, M. Oligomerization of daptomycin on membranes. *Biochim. Biophys. Acta* **1808**, 1154–1160 (2011).
14. Taylor, S. D. & Palmer, M. The action mechanism of daptomycin. *Bioorg. Med. Chem.* **24**, 6253–6268 (2016).
15. Mengin-Lecreulx, D., Allen, N. E., Hobbs, J. N. & van Heijenoort, J. Inhibition of peptidoglycan biosynthesis in *Bacillus megaterium* by daptomycin. *FEMS Microbiol. Lett.* **57**, 245–248 (1990).
16. Mascher, T., Zimmer, S. L., Smith, T.-A. & Helmann, J. D. Antibiotic-inducible promoter regulated by the cell envelope stress-sensing two-component system LiaRS of *Bacillus subtilis*. *Antimicrob. Agents Chemother.* **48**, 2888–2896 (2004).
17. Radeck, J. et al. Anatomy of the bacitracin resistance network in *Bacillus subtilis*. *Mol. Microbiol.* **100**, 607–620 (2016).
18. Ling, L. L. et al. A new antibiotic kills pathogens without detectable resistance. *Nature* **517**, 455–459 (2015).
19. Monteiro, J. M. et al. Cell shape dynamics during the staphylococcal cell cycle. *Nat. Commun.* **6**, 8055 (2015).
20. Müller, A., Klöckner, A. & Schneider, T. Targeting a cell wall biosynthesis hot spot. *Nat. Prod. Rep.* **34**, 909–932 (2017).
21. Henrichfreise, B. et al. Functional conservation of the lipid II biosynthesis pathway in the cell wall-less bacteria Chlamydia and Wolbachia: why is lipid II needed? *Mol. Microbiol.* **73**, 913–923 (2009).
22. Schirner, K. et al. Lipid-linked cell wall precursors regulate membrane association of bacterial actin MreB. *Nat. Chem. Biol.* **11**, 38–45 (2015).
23. Qiao, Y. et al. Lipid II overproduction allows direct assay of transpeptidase inhibition by β-lactams. *Nat. Chem. Biol.* **13**, 793–798 (2017).
24. Rubinchik, E. et al. Mechanism of action and limited cross-resistance of new lipopeptide MX-2401. *Antimicrob. Agents Chemother.* **55**, 2743–2754 (2011).
25. Schneider, T. et al. The lipopeptide antibiotic Friulimicin B inhibits cell wall biosynthesis through complex formation with bactoprenol phosphate. *Antimicrob. Agents Chemother.* **53**, 1610–1618 (2009).
26. Sass, V. et al. Human beta-defensin 3 inhibits cell wall biosynthesis in Staphylococci. *Infect. Immun.* **78**, 2793–2800 (2010).
27. Schneider, T. et al. Plectasin, a fungal defensin, targets the bacterial cell wall precursor Lipid II. *Science* **328**, 1168–1172 (2010).
28. Breukink, E. et al. Use of the cell wall precursor lipid II by a pore-forming peptide antibiotic. *Science* **286**, 2361–2364 (1999).
29. Hachmann, A.-B., Angert, E. R. & Helmann, J. D. Genetic analysis of factors affecting susceptibility of *Bacillus subtilis* to daptomycin. *Antimicrob. Agents Chemother.* **53**, 1598–1609 (2009).
30. Wolf, D. et al. In-depth profiling of the LiaR response of *Bacillus subtilis*. *J. Bacteriol.* **192**, 4680–4693 (2010).
31. Bunkóczi, G., Vértesy, L. & Sheldrick, G. M. Structure of the lipopeptide antibiotic tsushimycin. *Acta Crystallogr. D* **61**, 1160–1164 (2005).
32. Sandoval-Calderón, M. et al. Plasticity of *Streptomyces coelicolor* membrane composition under different growth conditions and during development. *Front. Microbiol.* **6**, 1465 (2015).
33. Randall, C. P., Mariner, K. R., Chopra, I. & O'Neill, A. J. The target of daptomycin is absent from *Escherichia coli* and other Gram-negative pathogens. *Antimicrob. Agents Chemother.* **57**, 637–639 (2013).
34. Epand, R. F., Savage, P. B. & Epand, R. M. Bacterial lipid composition and the antimicrobial efficacy of cationic steroid compounds (Ceragenins). *Biochim. Biophys. Acta* **1768**, 2500–2509 (2007).
35. Jones, T. et al. Failures in clinical treatment of *Staphylococcus aureus* Infection with daptomycin are associated with alterations in surface charge, membrane phospholipid asymmetry, and drug binding. *Antimicrob. Agents Chemother.* **52**, 269–278 (2008).
36. Mishra, N. N. et al. Perturbations of phosphatidate cytidylyltransferase (CdsA) mediate daptomycin resistance in *Streptococcus mitis/oralis* by a novel mechanism. *Antimicrob. Agents Chemother.* **61**, https://doi.org/10.1128/AAC.02435-16 (2017).
37. Hachmann, A.-B. et al. Reduction in membrane phosphatidylglycerol content leads to daptomycin resistance in *Bacillus subtilis*. *Antimicrob. Agents Chemother.* **55**, 4326–4337 (2011).
38. Yang, S.-J., Mishra, N. N., Rubio, A. & Bayer, A. S. Causal role of single nucleotide polymorphisms within the mprF gene of *Staphylococcus aureus* in daptomycin resistance. *Antimicrob. Agents Chemother.* **57**, 5658–5664 (2013).
39. Ernst, C. M. et al. Gain-of-function mutations in the phospholipid flippase MprF confer specific Daptomycin resistance. *MBio* **9**, https://doi.org/10.1128/mBio.01659-18 (2018).
40. Stillwell, W. *An Introduction to Biological Membranes. Composition, Structure and Function*. (Academic Press is an imprint of Elsevier, London, 2016).
41. Silverman, J. A., Mortin, L. I., Vanpraagh, A. D. G., Li, T. & Alder, J. Inhibition of daptomycin by pulmonary surfactant: in vitro modeling and clinical impact. *J. Infect. Dis.* **191**, 2149–2152 (2005).
42. Muraih, J. K., Harris, J., Taylor, S. D. & Palmer, M. Characterization of daptomycin oligomerization with perylene excimer fluorescence: stoichiometric binding of phosphatidylglycerol triggers oligomer formation. *Biochim. Biophys. Acta* **1818**, 673–678 (2012).
43. Zhang, T. et al. Mutual inhibition through hybrid oligomer formation of daptomycin and the semisynthetic lipopeptide antibiotic CB-182,462. *Biochim. Biophys. Acta* **1828**, 302–308 (2013).
44. Kreutzberger, M. A., Pokorny, A. & Almeida, P. F. Daptomycin-phosphatidylglycerol domains in lipid membranes. *Langmuir* **33**, 13669–13679 (2017).
45. Kimura, T., Jennings, W. & Epand, R. M. Roles of specific lipid species in the cell and their molecular mechanism. *Prog. Lipid Res.* **62**, 75–92 (2016).
46. Lin, T.-Y. & Weibel, D. B. Organization and function of anionic phospholipids in bacteria. *Appl. Microbiol. Biotechnol.* **100**, 4255–4267 (2016).
47. Henrich, E. et al. Lipid requirements for the enzymatic activity of MraY translocases and in vitro reconstitution of the lipid ii synthesis pathway. *J. Biol. Chem.* **291**, 2535–2546 (2016).
48. Chugunov, A. et al. Lipid-II forms potential "landing terrain" for lantibiotics in simulated bacterial membrane. *Sci. Rep.* **3**, 1678 (2013).
49. Mascio, C. T. M., Alder, J. D. & Silverman, J. A. Bactericidal action of daptomycin against stationary-phase and nondividing *Staphylococcus aureus* cells. *Antimicrob. Agents Chemother.* **51**, 4255–4260 (2007).
50. Pisabarro, A. G., Pedro, M. Ade & Vázquez, D. Structural modifications in the peptidoglycan of *Escherichia coli* associated with changes in the state of growth of the culture. *J. Bacteriol.* **161**, 238–242 (1985).
51. Blasco, B., Pisabarro, A. G. & Pedro, M. Ade Peptidoglycan biosynthesis in stationary-phase cells of *Escherichia coli*. *J. Bacteriol.* **170**, 5224–5228 (1988).
52. Romaniuk, J. A. H. & Cegelski, L. Bacterial cell wall composition and the influence of antibiotics by cell-wall and whole-cell NMR. *Philos. Trans. R. Soc. Lond. B* **370**, https://doi.org/10.1098/rstb.2015.0024 (2015)
53. Muthaiyan, A., Silverman, J. A., Jayaswal, R. K. & Wilkinson, B. J. Transcriptional profiling reveals that daptomycin induces the *Staphylococcus aureus* cell wall stress stimulon and genes responsive to membrane depolarization. *Antimicrob. Agents Chemother.* **52**, 980–990 (2008).
54. Hasper, H. E. et al. An alternative bactericidal mechanism of action for lantibiotic peptides that target lipid II. *Science.* **313**, 1636–1637 (2006).
55. Müller, A. et al. Differential daptomycin resistance development in *Staphylococcus aureus* strains with active and mutated gra regulatory systems. *Int. J. Med. Microbiol.* **308**, 335–348 (2018).
56. Schneider, T. et al. In vitro assembly of a complete, pentaglycine interpeptide bridge containing cell wall precursor (lipid II-Gly5) of *Staphylococcus aureus*. *Mol. Microbiol.* **53**, 675–685 (2004).
57. Herbert, S. et al. Repair of global regulators in *Staphylococcus aureus* 8325 and comparative analysis with other clinical isolates. *Infect. Immun.* **78**, 2877–2889 (2010).
58. Kreiswirth, B. N. et al. The toxic shock syndrome exotoxin structural gene is not detectably transmitted by a prophage. *Nature* **305**, 709–712 (1983).
59. Arnaud, M., Chastanet, A. & Débarbouillé, M. New vector for efficient allelic replacement in naturally nontransformable, low-GC-content, Gram-positive bacteria†. *Appl. Environ. Microbiol.* **70**, 6887–6891 (2004).
60. Tan, S., Ludwig, K. C., Müller, A., Schneider, T. & Nodwell, J. R. The lasso peptide siamycin-I targets lipid II at the Gram-positive cell surface. *ACS Chem. Biol.* **14**, 966–974 (2019).

Material from: Grein, F., Müller, A., Scherer, K.M. et al., Ca2+-Daptomycin targets cell wall biosynthesis by forming a tripartite complex with undecaprenyl-coupled intermediates and membrane lipids. Nat Commun 11, 1455, published 2020, Springer Nature.

61. Schneider, C. A., Rasband, W. S. & Eliceiri, K. W. NIH image to ImageJ: 25 years of image analysis. *Nat. Methods* **9**, 671–675 (2012).
62. Roder, F. et al. Reconstitution of membrane proteins into polymer-supported membranes for probing diffusion and interactions by single molecule techniques. *Anal. Chem.* **83**, 6792–6799 (2011).
63. Speil, J. et al. Activated STAT1 transcription factors conduct distinct saltatory movements in the cell nucleus. *Biophys. J.* **101**, 2592–2600 (2011).
64. Tokunaga, M., Imamoto, N. & Sakata-Sogawa, K. Highly inclined thin illumination enables clear single-molecule imaging in cells. *Nat. Methods* **5**, 159–161 (2008).
65. Landvogt, L. et al. Observing and tracking single small ribosomal subunits in vivo. *Methods* **153**, 63–70 (2019).
66. Edelstein, A. D. et al. Advanced methods of microscope control using μManager software. *J Biol. Methods* **1**, https://doi.org/10.14440/jbm.2014.36 (2014).

Acknowledgements

Funding was provided by the Deutsche Forschungsgemeinschaft (DFG, German Research Foundation)—Project-ID 398967434—TRR 261 (to T.S., F.G., U.K.) and grant SCHN1284/2 (to T.S.), NIH (grant 5R01AI13262701 (to T.S. and F.G.)), and the German Center for Infection Research (DZIF) (to F.G.). K.M.S. was supported by a fellowship from the Cusanuswerk. We would like to thank Kim Lewis for providing teixobactin and Julia Deisinger for PBP2-His_6, Michaele Josten for mass spectrometry, and Thorsten Mascher for providing strain TMB1617 *B. subtilis* W168 *sacA*::pCHlux101 (P_{liaI}-*lux*). We thank Kenneth Pfarr for proofreading.

Author contributions

U.K. and T.S. designed and coordinated the overall study. The experiments were performed by F.G., A.M., K.M.S., X.L., K.C.L., A.K. and M.S.; F.G., A.M., K.M.S., U.K. and T.S. analysed the data. The manuscript was written by F.G., A.M., H.-G.S., U.K. and T.S. with input from all authors.

Competing interests

The authors declare no competing interests.

Additional information

Supplementary information is available for this paper at https://doi.org/10.1038/s41467-020-15257-1.

Correspondence and requests for materials should be addressed to U.K. or T.S.

Peer review information *Nature Communications* thanks Andreas Peschel and the other, anonymous, reviewer(s) for their contribution to the peer review of this work. Peer reviewer reports are available.

Reprints and permission information is available at http://www.nature.com/reprints

Publisher's note Springer Nature remains neutral with regard to jurisdictional claims in published maps and institutional affiliations.

Supplementary information

Ca^{2+}-Daptomycin targets cell wall biosynthesis by forming a tripartite complex with undecaprenyl-coupled intermediates and membrane lipids

Grein et al.

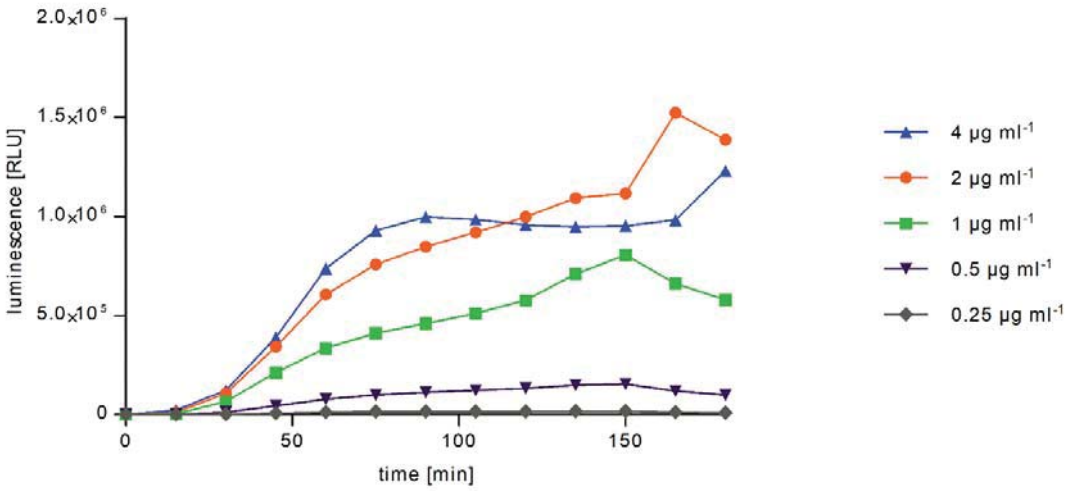

Supplementary Figure 1: DAP induces the LiaRS-mediated cell envelope stress response in *B. subtilis* in a dose-dependent manner. Induction of the LiaRS response in *B. subtilis* indicating interference with the lipid II biosynthesis cycle was examined by measuring P_{liaI}-*lux* expression over time. Treatment with DAP elicited cell envelope stress at concentrations ranging from 0.5 to 4 µg ml^{-1}. Luciferase activity is presented as relative luminescence units (RLU). Representative graph of three independent experiments with comparable results. Source data are provided as a Source Data file.

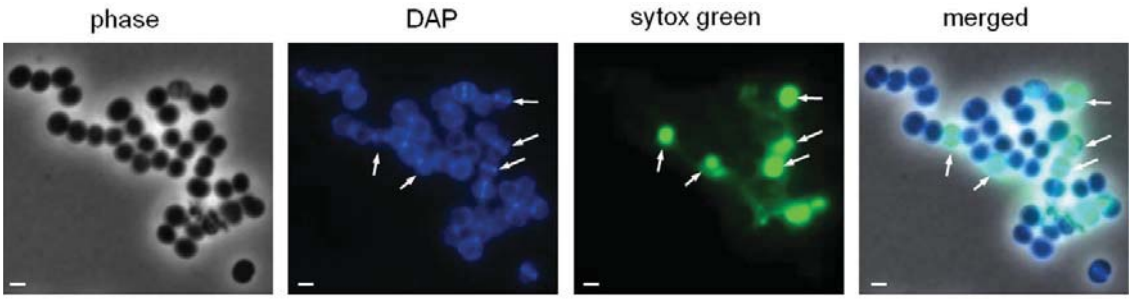

Supplementary Figure 2: Septal binding of DAP entails killing of *S. aureus* cells. An *S. aureus* culture was treated with DAP (7 µg ml^{-1}) in the presence of Ca^{2+} for 15 min followed by washing of the cells and incubation with sytox green. Cells were washed again and subjected to fluorescence microscopy. Arrows indicate cells with septal DAP localization that are intensively stained by sytox green. Phase, phase contrast. Scale bar 1 µm. Representative images from 3 independent experiments are shown.

Material from: Grein, F., Müller, A., Scherer, K.M. et al., Ca2+-Daptomycin targets cell wall biosynthesis by forming a tripartite complex with undecaprenyl-coupled intermediates and membrane lipids. Nat Commun 11, 1455, published 2020, Springer Nature.

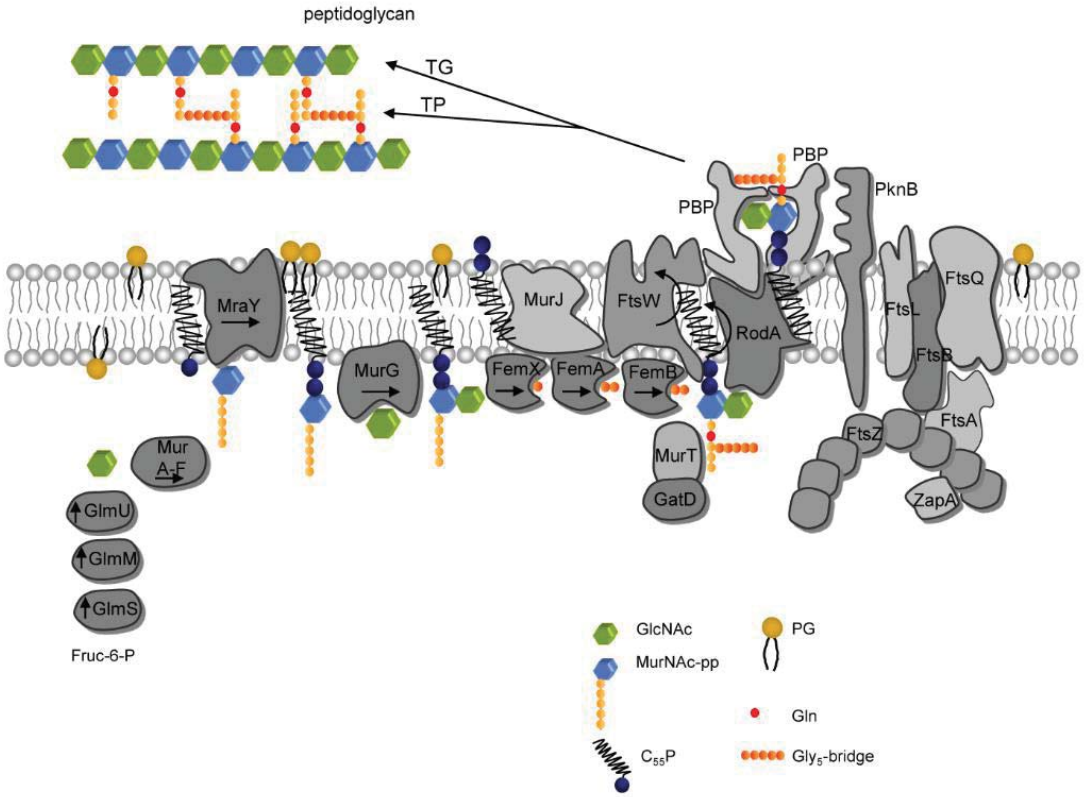

Supplementary Figure 3: Schematic depiction of peptidoglycan biosynthesis in *S. aureus*.
The ultimate soluble peptidoglycan precursor UDP-MurNAc-pentapeptide is synthesized in the cytoplasm by the sequential action of MurA to MurF enzymes starting from UDP-GlcNAc provided by GlmS, GlmM and GlmU. The glycosyltransferase MraY transfers the soluble sugar-peptide moiety in the first membrane-associated step to the lipid carrier $C_{55}P$ producing lipid I. MurG subsequently links a GlcNAc moiety to the muramoyl portion of lipid I converting it to lipid II. Lipid II is further species-specifically modified by the addition of five glycine residues catalysed by the peptidyltransferases FemXAB and by amidation of the glutamate residue in position 2 of the stem peptide catalysed by the hetero bi-enzyme complex MurT/GatD. Finally, lipid II is translocated across the cytoplasmic membrane by members of the SEDS or MOP families, and the peptidoglycan monomer is incorporated into the growing peptidoglycan network by transglycosylation and transpeptidation promoted by penicillin binding proteins. GlcNAc, N-acetyl-glucosamine; MurNAc-pp, N-acetyl-muramic acid pentapeptide; $C_{55}P$, undecaprenyl-phosphate; Gly5-bridge, pentaglycine interpeptide bridge; PG, phosphatidylglycerol; Gln, glutamine; TP, transpeptidase; TG, transglycosylase.

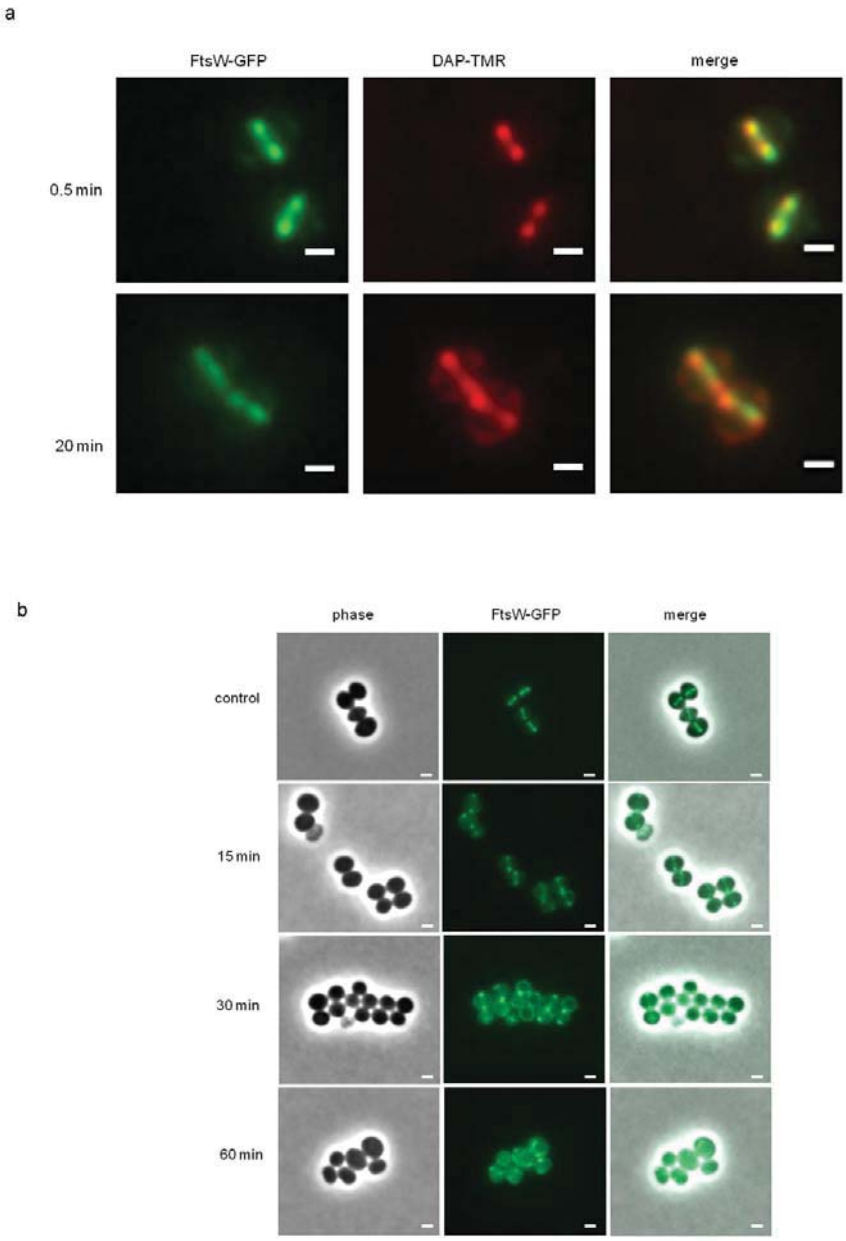

Supplementary Figure 4: Localization of the putative lipid II flippase FtsW under DAP treatment. (a) Co-localization of FtsW-GFP and DAP-TMR in *S. aureus* cells during phase I binding. *S. aureus* RN4220 FtsW-GFP was grown to mid-exponential phase (OD_{600} = 0.5) followed by addition of Ca^{2+} and a mixture of labelled and unlabelled DAP (1.6 µg ml^{-1} DAP; 0.16 µg ml^{-1} DAP-TMR). Excess DAP-TMR and non-labelled DAP was removed and cells imaged after 0.5 and 20 min by combining HILO microscopy with dual-color imaging using a dual-emission image splitter. Scale bar 1 µm. Representative images from 2 independent experiments are shown. (b) Sublethal concentrations of DAP lead to delocalization of the putative lipid II flippase FtsW. *S. aureus* cells expressing chromosomally encoded FtsW-GFP were treated with DAP (2 µg ml^{-1}) in the presence of Ca^{2+} and the cells subjected to fluorescence microscopy at the indicated time points. Phase, phase contrast. Scale bar 1 µm. Representative images from 3 independent experiments are shown.

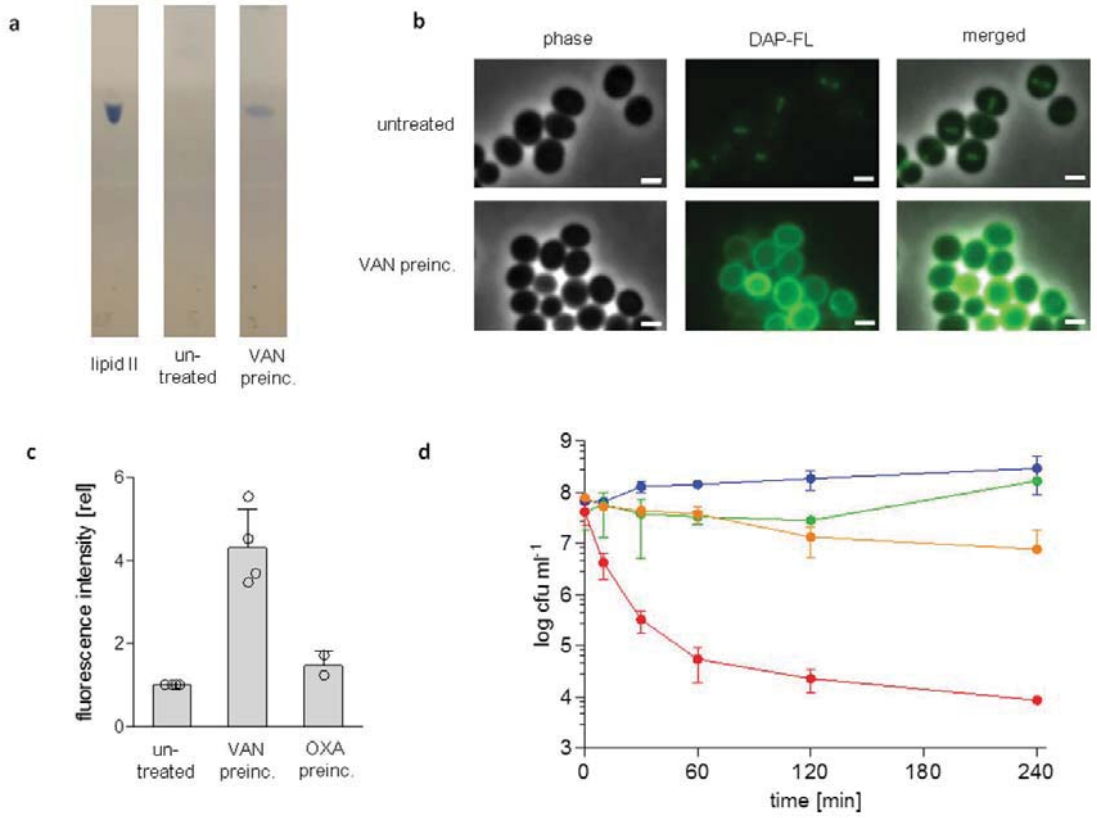

Supplementary Figure 5: Pre-treatment of *S. aureus* with VAN leads to increased lipid II levels and enhanced binding of DAP-FL. (a) TLC of lipids extracted from untreated cells (lane 2) or cells treated with VAN (5 µg ml^{-1}) (lane 3) for 30 min. Purified lipid II was applied in lane 1. Representative images from 3 independent experiments are shown. **(b)** DAP-FL binding to *S. aureus* cells treated with VAN (5 µg ml^{-1}) or oxacillin (5 µg ml^{-1}) for 30 min followed by washing the cells twice and incubation with DAP (mixture of DAP-FL and native DAP) for 10 min in the presence of Ca^{2+}. Lipid II is expected to be dispersed over the entire cell membrane, as a consequence of the strong accumulation. Scale bar 1 µm. Representative images from 3 independent experiments are shown. **(c)** Quantification of DAP-FL binding measured during the experiment described in (b). Fluorescence intensity of the untreated control cells was set as 1.Values are means from 4 (untreated, Vancomycin preincubated) or two (oxacillin treated) independent experiments. **(d)** Survival of *S. aureus* without treatment (blue line), after treatment with VAN (green line), treated with DAP (5 µg ml^{-1}) (yellow line) or treated with DAP (5 µg ml^{-1}) after pre-incubation with VAN (red line). Values are means from two independent experiments. Error bars in (c) and (d) represent the SD. Source data are provided as a Source Data file.

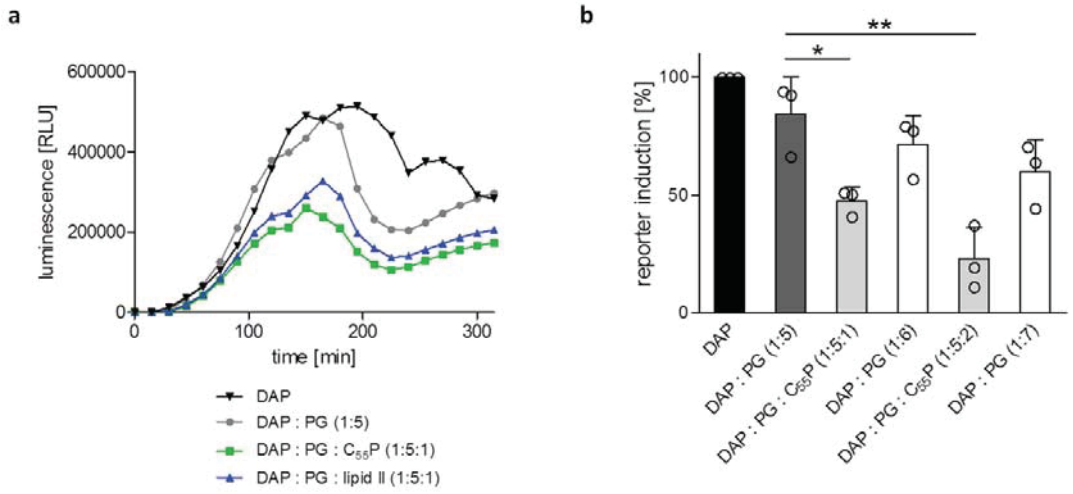

Supplementary Figure 6: LiaRS induction by DAP is antagonized by pre-incubation with purified cell wall precursors. (a) *liaI-lux* induction in *B. subtilis* is antagonized when DAP (1 µg ml^{-1}) is pre-incubated with $C_{55}P$ or lipid II in presence of PG in molar ratios as indicated. This effect is not observed when DAP is pre-incubated with PG alone. Representative graph of three independent experiments is shown. (b) To exclude unspecific charge effects, the amount of PG was adjusted (white bar) to equalize anionic charges of $C_{55}P$ (light grey bars). Maximal induction relative to the DAP control (black bar / set as 100 %) is shown as mean values from three independent experiments. Error bars represent the SD.Significance was determined by unpaired Student's t-test with a 95% confidence interval. *p = 0.0184, **p = 0.0065. Source data are provided as a Source Data file.

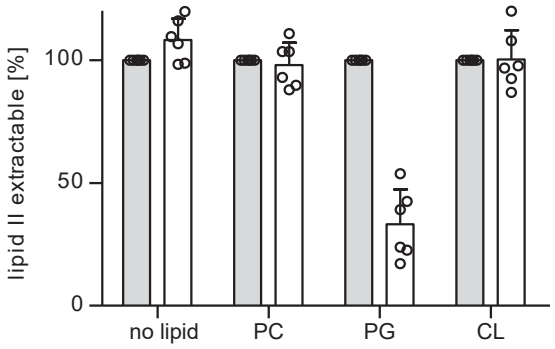

Supplementary Figure 7: DAP forms an extraction stable complex with lipid II only in the presence of PG. DAP was incubated with purified lipid II in a molar ratio of 10:1 in the presence of PC, PG or CL or in the absence of lipids (white bars). Controls (grey bars), to which DAP was added immediately prior to extraction, were set as 100%. Reaction mixtures were extracted with BuOH and the upper solvent phase was applied to TLC followed by staining and quantitative analysis of the lipid II band. Data presented are means from three independent experiments and error bars represent the SD. Source data are provided as a Source Data file.

Chapter 3

Biosynthesis and mechanism of action of the cell wall targeting antibiotic hypeptin

Hypeptin is a cyclodepsipeptide antibiotic, that was (re)discovered as a hit during a screen of uncultured bacteria using the iChip technology. The non-ribosomally synthesized octapeptide shares structural features with the recently discovered lipid II-binding antibiotic teixobactin and displayed potent antibacterial activity against Gram-positive pathogens, including drug-resistant staphylococci, such as methicillin-resistant, vancomycin-intermediate, and daptomycin-resistant *Staphylococcus aureus*, vancomycin-resistant enterococci and mycobacteria. Remarkably, hypeptin was not prone to resistance development *in vitro*. The aim of this study was to investigate the mode of action of hypeptin and to identify the molecular target.

A bioassay-guided HPLC-purification of culture supernatants of the producer-strain *Lysobacter* sp. K5869 yielded 6 mg hypeptin per liter. Mass spectrometry, NMR and other spectroscopic analyses confirmed an octadepsipeptide with three D-amino acids and half of the backbone being β-hydroxylated. Biochemical analysis of the hypeptin biosynthetic gene cluster (BGC), performed by Daniel Wirtz (co-first author of the study), identified two β-hydroxylases responsible for the stereoselective hydroxylation of four non-ribosomal peptide synthetase (NRPS) building blocks.

Despite its strongly lytic killing mechanism, that was found to be mediated by the major autolysin AtlA in *S. aureus*, hypeptin exhibited only moderate cytotoxic effects towards human epithelial cells and low hemolytic activity towards human red blood cells (RBCs).

Bioreporter screens, analysis of cell morphology and intracellular precursor pool levels of hypeptin-treated cells revealed that the antibiotic interferes with late-stage peptidoglycan biosynthesis reactions. Analyzing a set of individual peptidoglycan and wall teichoic acid biosynthetic reactions with purified, recombinant enzymes and substrates *in vitro* revealed that hypeptin blocks cell wall biosynthesis by binding to undecaprenyl pyrophosphate (C_{55}-PP)-containing lipid intermediates (lipid II, lipid III_{WTA}) and C_{55}-PP itself.

To systemically deduce the structural binding motif of hypeptin, whole-cell antagonization and complex formation assays were perfomed with purified cell wall precursors. Hypeptin formed stable complexes with C_{55}-PP-containing lipid precursors at a 2:1 molar ratio. Consistently, the antibacterial activity of hypeptin on growth of *S. aureus* was antagonized by external addition of these precursors. However, the WTA precursor lipid III_{WTA} and C_{55}-PP were bound with lower affinity compared to lipid II, pointing towards different binding modes, that appear to involve interactions with the first sugar moiety of lipid II.

Like for teixobactin, binding to multiple cell wall precursors that have the immutable C_{55}-PP-moiety in common, accompanied by a rapid autolysin-mediated cell lysis, might contribute to the lack of detectable resistance to hypeptin.

Results of this publication are partially included in the doctoral thesis of Dr. Carina E. Marx (Marx, 2018) and Dr. Daniel A. Wirtz (Wirtz, 2022). K.C.L. repeated and extended the mode of action studies with a revised production and purification of hypeptin, analyzed the data, and contributed to writing of the manuscript.

GDCh **Communications** Angewandte International Edition Chemie

Check for updates

How to cite: *Angew. Chem. Int. Ed.* **2021**, *60*, 13579–13586
International Edition: doi.org/10.1002/anie.202102224
German Edition: doi.org/10.1002/ange.202102224

Biochemistry

Biosynthesis and Mechanism of Action of the Cell Wall Targeting Antibiotic Hypeptin

Daniel A. Wirtz[+], Kevin C. Ludwig[+], Melina Arts, Carina E. Marx, Sebastian Krannich, Paul Barac, Stefan Kehraus, Michaele Josten, Beate Henrichfreise, Anna Müller, Gabriele M. König, Aaron J. Peoples, Anthony Nitti, Amy L. Spoering, Losee L. Ling, Kim Lewis, Max Crüsemann, and Tanja Schneider**

Abstract: *Hypeptin is a cyclodepsipeptide antibiotic produced by Lysobacter sp. K5869, isolated from an environmental sample by the iChip technology, dedicated to the cultivation of previously uncultured microorganisms. Hypeptin shares structural features with teixobactin and exhibits potent activity against a broad spectrum of gram-positive pathogens. Using comprehensive in vivo and in vitro analyses, we show that hypeptin blocks bacterial cell wall biosynthesis by binding to multiple undecaprenyl pyrophosphate-containing biosynthesis intermediates, forming a stoichiometric 2:1 complex. Resistance to hypeptin did not readily develop in vitro. Analysis of the hypeptin biosynthetic gene cluster (BGC) supported a model for the synthesis of the octapeptide. Within the BGC, two hydroxylases were identified and characterized, responsible for the stereoselective β-hydroxylation of four building blocks when bound to peptidyl carrier proteins. In vitro hydroxylation assays corroborate the biosynthetic hypothesis and lead to the proposal of a refined structure for hypeptin.*

The rapid emergence and worldwide spread of infections caused by antibiotic resistant bacteria represents a serious health threat, while the identification and development of novel antibiotic classes is scarce. Particularly, the pressing need for resistance-breaking antibiotics reinforced the focus on natural products, though increasingly becoming harder to find. Overmining of this limited resource in the 1960s ended the golden era of antibiotic discovery and, despite intensive effort, synthetic approaches were unable to replace natural products.[1]

To access a greater diversity of antibiotic producing microorganisms, novel cultivation methods have been developed. The iChip (isolation chip) technology was designed for high-throughput in situ cultivation of previously "uncultured" bacteria.[2,3] The iChip device enables to simultaneously cultivate and isolate about 50% of soil bacteria, compared with only 1% of strains that grow under laboratory conditions. This method facilitated the discovery of teixobactin, representing an entirely novel antibiotic class, produced by the previously uncultured β-proteobacterium *Eleftheria terrae*.[3] Another extract from the same screen that led to the discovery of teixobactin showed potent activity against *Staphylococcus aureus*. Bioassay-guided fractionation of culture extracts, followed by MALDI-TOF analysis, identified the bioactive compound, as a peak with a $[M+H]^+$ ion at m/z 1022.489 (Figure S1). Comparison with natural product databases pointed towards the known compound hypeptin (**1**, Figure 1), previously isolated from *Pseudomonas* sp. PB-6269 by Shionogi & Co. in 1989.[4] The producing strain K5869, isolated by the iChip was then cultivated in larger scale and **1** was isolated as described in the Supporting Information (SI, page 3), yielding approximately 18 mg of **1** from a 3 L culture.

NMR and other spectroscopic analyses further confirmed the identity of **1** (Figures S2–S11, Table S2), being an octadepsipeptide with a four-residue macrocycle. A comparably high proportion of amino acids, comprising half of the

[*] D. A. Wirtz,[+] P. Barac, Dr. S. Kehraus, Prof. G. M. König, Dr. M. Crüsemann
Institute for Pharmaceutical Biology, University of Bonn
Nussallee 6, 53115 Bonn (Germany)
E-mail: mcruesem@uni-bonn.de

K. C. Ludwig,[+] M. Arts, Dr. C. E. Marx, S. Krannich, Dr. B. Henrichfreise, Dr. A. Müller, Prof. T. Schneider
Institute for Pharmaceutical Microbiology, University of Bonn, University Clinic Bonn
Meckenheimer Allee 168, 53115 Bonn (Germany)
E-mail: tschneider@uni-bonn.de

K. C. Ludwig,[+] M. Josten
DZIF, German Center for Infectious Research, partner site Bonn-Cologne (Germany)

M. Josten
Institute for Medical Microbiology, Immunology and Parasitology, University Hospital Bonn
Venusberg Campus 1, 53127 Bonn (Germany)

A. J. Peoples, A. Nitti, A. L. Spoering, Dr. L. L. Ling
NovoBiotic Pharmaceuticals
Cambridge, MA 02138 (USA)

Prof. K. Lewis
Department of Biology, Antimicrobial Discovery Center, Northeastern University
Boston, MA 02115 (USA)

[+] These authors contributed equally to this work.

Supporting information and the ORCID identification number(s) for the author(s) of this article can be found under: https://doi.org/10.1002/anie.202102224.

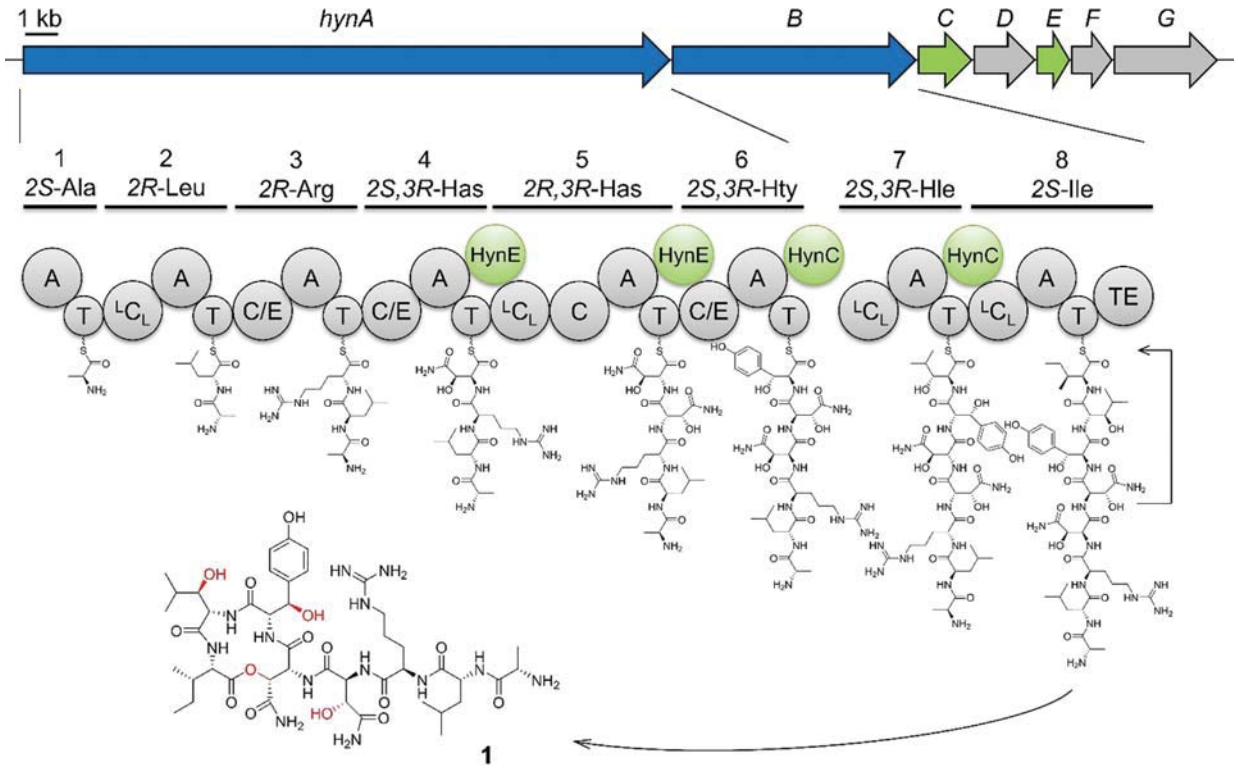

Figure 1. Gene organization of the *hyn* BGC and biosynthetic pathway of hypeptin (**1**). The NRPS HynAB assemble a linear octapeptide which is finally released and cyclized by $HynB_{TE}$. The tailoring hydroxylases HynC and HynE (green) modify the building blocks during assembly. Has: 3-Hydroxyasparagine Hty: 3-Hydroxytyrosine Hle: 3-Hydroxyleucine.

peptide backbone, are β-hydroxylated, which gave the compound the name hypeptin.[4] Determination of the absolute stereoconfiguration of **1** had revealed three amino acids to be D-configurated and three out of four amino acids to contain *R*-configuration at the β-carbon (2*S*,3*R*)-3-OH-Asn_4 (Has), (2*R*,3*R*)-3-OH-Asn_5, (2*S*,3*S*)-3-OH-Tyr_6 (Hty), and (2*S*,3*R*)-OH-Leu_7 (Hle). The configuration of Hty had not been experimentally determined due to degradation during hydrolysis, and NMR spectra were not provided in the original publication.[4]

We next sequenced the genome of the newly isolated producing strain K5869. 16S rDNA analysis revealed the organism to belong to the genus *Lysobacter*, γ-proteobacteria known to produce a range of secondary metabolites including compounds with antibacterial and antifungal bioactivities.[5] The overall structure of **1** suggested a nonribosomal origin. Nonribosomal peptide synthetases (NRPS) are multimodular megaenzymes that assemble peptides in a thiotemplated manner. A minimal NRPS elongation module, known to recruit specific amino acid building blocks and extend the growing peptide chain, consists of condensation (C), adenylation (A), and thiolation (T) domains, also named peptidyl carrier proteins.[6] Some A domains are dependent on the interaction with a small MbtH-like protein (MLP) to maintain their correct conformation and/or catalytic activity.[7] To analyze the biosynthesis of **1**, the genome sequence was searched for candidate NRPS biosynthetic gene clusters (BGC). AntiSMASH[8] analysis revealed a BGC with two NRPS genes (Table S3), that we termed *hynA* (19.4 kb) and *hynB* (7.3 kb), encoding six and two modules, respectively (Figure 1). The number of modules and predicted A domain specificities, as well as C domain functions, were consistent with the overall structure of **1**. Module 5 harbors a scarce additional C domain, that clusters together with known C_β epimerases in phylogenetic analysis (Figure S12, Table S4).[9,10] Interestingly, the active site of the C domain contains a HRxxxDR sequence, which would render the domain inactive by the bulky side chains of the arginines. The identical C_β configuration of Has_4 and Has_5 in the final peptide strongly supports this theory. BLAST analysis of the genes *hynAB* revealed an identical BGC in the genome of *Lysobacter psychrotolerans ZS60* (NZ_RIBS01000005.1), which helped to manually determine the borders of the BGC.

Despite extensive bioinformatic searches with BLAST and BigFAM,[11] no further related BGCs were identified in the databases. In addition to the two NRPS genes *hynAB*, bioinformatic analysis revealed two putative hydroxylases to be encoded in the BGC: HynC is a non-heme diiron monooxygenase (NHDM), a barely studied enzyme family, so far only described in the biosyntheses of chloramphenicol, teicoplanin, and FR900359,[12–14] while HynE is annotated as an α-ketoglutarate-dependent oxygenase (αKG).[15] Additional genes (*hynDFG*) likely represent transporter-related genes. The *hyn* BGC, comprising a 35.6 kb region, is located

in the 5′-end of a giant cluster with four other BGCs. The 3′-end of this region encodes a stand-alone MLP (*hynMLP*) that was assumed to be involved in the biosynthesis of **1**.

The different stereoconfiguration of the β-hydroxyl groups in **1** raised questions about the hydroxylation reactions in hypeptin biosynthesis. We thus focused on the characterization of the two different hydroxylases HynC and HynE, for which the nature of substrates is unclear. β-hydroxyl moieties in amino acids can be introduced by different mechanisms, either on the free amino acid or on the aminoacylated T domain during NRPS assembly. Comparable examples of NHDM and αKG were shown to hydroxylate their substrate amino acid when covalently bound to the cognate T domain.[14,15] Interestingly, all characterized NHDM are known to hydroxylate their substrate L-amino acids in *syn*-configuration,[10,12–14] whereas for αKG, hydroxylation of products in both configurations is reported.[16] Therefore, we hypothesized, that the αKG HynE might hydroxylate either free or T domain-bound Asn_4, Asn_5 and Tyr_6 prior to further modification, while the NHDM HynC would act on Leucinyl-T_7. We aimed at analyzing β-hydroxylation reactions in vitro to determine the substrate specificity of HynC and HynE. To this end, modules 4, 5, 6, and 7 were cloned and expressed in *E. coli* for in vitro reconstitution. As NRPS multidomain proteins frequently show difficulties to express heterologously in a soluble and active form,[13] we cloned different constructs of each module: AT, CAT, ATC or $C_{acc}ATC_{don}$, the latter two designed after the recently introduced XU- and XUC-exchange modules.[17] These were developed as exchange modules for NRPS engineering, but we also found them effective to define appropriate borders for successful in vitro reconstitution. Most of the attempted constructs yielded truncated or insoluble proteins, even when co-expressed with chaperones. The enzymatic activity of the A domains within the constructs was verified with the $\gamma^{18}O_4$-ATP exchange assay.[18] Finally, we obtained the soluble and functional enzymes $HynA_4C_{acc}ATC_{don}$, $HynA_5CAT$, $HynA_6CAT$, and $HynB_7AT$. $HynA_5CAT$ and $HynA_6CAT$ needed to be co-expressed with HynMLP, which is located ≈300 000 bp downstream of the *hyn* genes, to exhibit adenylating activity towards their preferred substrates L-Asn and L-Tyr. HynE was efficiently expressed in *E. coli* BL21(DE3), whereas HynC had to be co-expressed with each of the four different NRPS modules to be soluble and stable in vitro (Figure S13).

With all enzymes in hand, we performed hydroxylation assays for HynC and HynE, each with all four purified NRPS modules. For HynE, we could detect the mass of the hydroxylated amino acids in the assays with $HynA_4C_{acc}ATC_{don}$ and $HynA_5CAT$ after hydrolysis from the NRPS, but not with $HynA_6CAT$ and $HynB_7AT$. On the other hand, the masses of Hty and Hle were detected in HynC assays with $HynA_6CAT$ and $HynB_7AT$, respectively (Figure 2). We also detected Hle in the negative control of the assay with $HynB_7AT$, which was probably caused by in vivo hydroxylation during co-expression. To circumvent this, we generated the inactive mutant HynC E375D. An analogous mutation in the active site of the prototype NHDM, CmlA, was reported to lack oxygen regulation and thereby impaired hydroxylation activity, without any structural changes.[19] Indeed, when using co-expressed HynC E375D as negative control in the hydroxylation assay, the signal of Hle diminished almost completely (Figure 2).

We speculated, that the synthetase utilizes the two hydroxylases to obtain hydroxylated amino acids in different stereoconfiguration. Our in vitro hydroxylation assays unambiguously demonstrate, that HynE targets the T domain-bound L-Asn_4 and L-Asn_5, whereas the NHDM HynC hydroxylates the T domain-bound L-Tyr_6 and L-Leu_7. These results contradict the published configuration of Hty in **1** that was reported as (2*S*,3*S*) (*anti*), but, according to our in vitro data, should be (2*S*,3*R*) (*syn*). We were not able to verify the absolute configuration of Hty in the final peptide due to fast degradation of the amino acid during hydrolysis of **1** as observed previously.[4] Nevertheless, the observed high coupling constant between H_2Hty and H_3Hty of 7.2 Hz (Table S2) strongly indicates *syn* configuration in accordance with a published study on a Hty-containing peptide.[20] According to the results of our $\gamma^{18}O_4$-ATP exchange assay, the preferred substrate of the A_6 domain is (2*S*)-Tyr and the module does not contain any epimerase domain. In the light of these data, we propose to reassign the absolute configuration of the Hty residue in **1** to (2*S*,3*R*)-OH-Tyr. Analysis of ROESY correlations supports this configuration (Figure S14).

1 shows striking similarity with teixobactin, including a macrolactam ring of the same size, a comparable number of D- and L-amino acids, the presence of a guanidine amino acid, and β-hydroxy amino acids, suggesting a common mechanism of action for both compounds.[21] As observed for teixobactin, **1** exhibited potent antibacterial activity against gram-positive pathogens (Table 1), including drug-resistant staphylococci, such as methicillin-resistant, vancomycin intermediate resistant and daptomycin-resistant *Staphylococcus aureus* (MRSA, VISA and DAPR), with minimal inhibitory concentrations (MIC) in the ng mL^{-1} range. **1** further showed very good activity against mycobacteria and vancomycin-resistant enterococci (VRE) (Table 1), but was lacking activity against gram-negative species, most likely owing to the outer membrane permeability barrier, preventing penetration of the rather large compound. This is supported by the decreased MIC of *E. coli* strain MB5746 with a defective outer membrane.[22]

Killing kinetics of *S. aureus* exposed to **1** showed excellent bactericidal activity, even superior to vancomycin and teixobactin in killing late exponential phase cultures at 5-fold lower compound concentration (Figure 3 A, B). **1** had a strong lytic effect even at a concentration corresponding to 2 × MIC and showed enhanced lysis compared to vancomycin (Figure 3 C). Despite the pronounced lytic activity, **1** exhibits specificity for bacterial cells, indicating a favorable therapeutic window, as only moderate cytotoxic effects towards HEp-2 cells and low hemolytic activity toward red blood cells (RBCs) were observed at the highest concentration tested (128 μg mL^{-1}) (Figure S15).

To identify the antibiotic target pathway of **1**, we employed pathway-selective gram-positive bioreporter strains. **1** specifically induced the *B. subtilis* P_{yptA}-*lacZ* reporter strain indicative for interference with cell wall biosynthesis, while all other major biosyntheses (DNA,

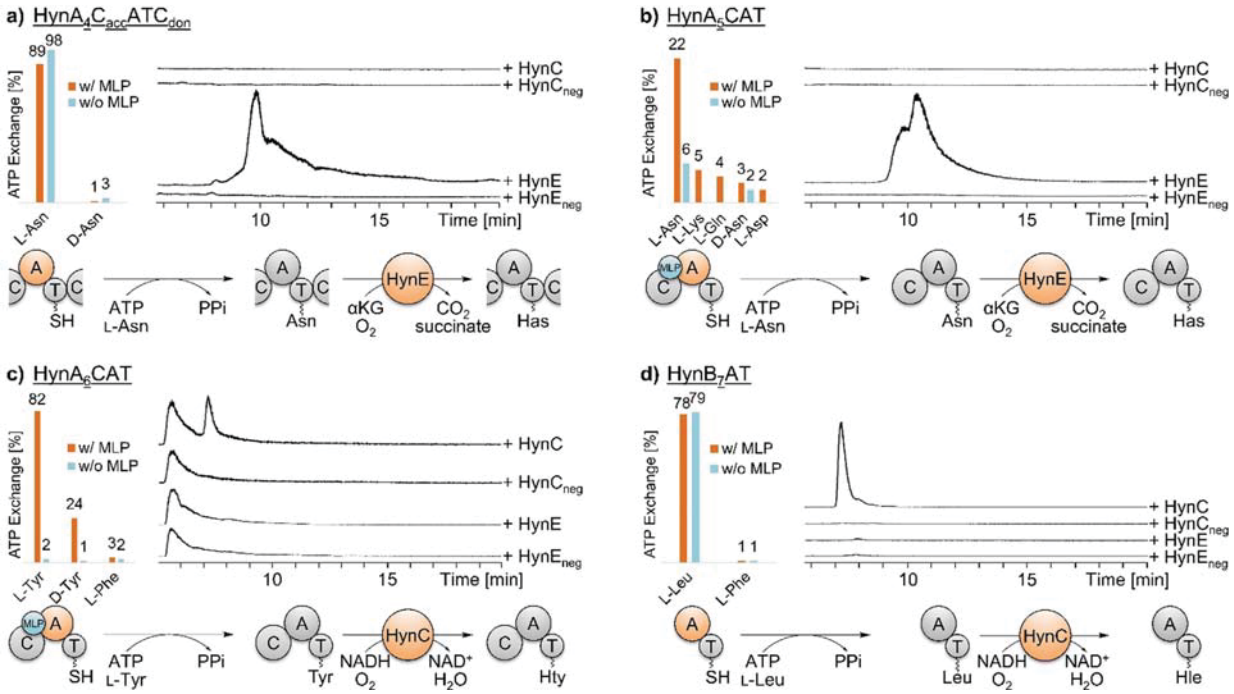

Figure 2. Results of in vitro assays to test NRPS and hydroxylase activities. On the left, the A domain specificity towards the substrate amino acid and the dependency of the MbtH-like protein (MLP) HynMLP was examined for each module via $\gamma^{18}O_4$-ATP exchange assay. On the right, extracted LC-MS traces of the hydroxylation assays of the module construct with HynC and HynE show formation of hydroxylated amino acids in comparison with the respective negative controls. At the bottom, the formation of the hydroxylated amino acid is summarized. a) The A domain of module 4 activates L-Asn and is independent of HynMLP. HynE then hydroxylates the bound amino acid, leading to the formation of 3-hydroxyasparagine (Has) ($m/z = 147.0$). b) The A domain in module 5 activates L-Asn only in presence of HynMLP. HynE then hydroxylates the bound amino acid, leading to the formation of 3-hydroxyasparagine (Has) ($m/z = 147.0$). c) The A domain of module 6 activates L-Tyr in the presence of HynMLP. Subsequently, HynC hydroxylates the amino acid ($m/z = 196.1$). d) The A domain of module 7 activates L-Leu independently of HynMLP. HynC then hydroxylates the amino acid ($m/z = 146.1$).

Table 1: Minimum inhibitory concentrations (MIC) of **1** against selected strains and pathogenic bacteria.

Organism	MIC [μg mL^{-1}]
Bacillus subtilis 168	0.0625
S. simulans 22	0.125
S. aureus SG 511	0.0625
S. aureus SG 511 (DAP^R)	0.0625
S. aureus LT-1334 (MRSA)	0.25
S. aureus 137/93G (VISA)	0.5
Enterococcus faecium I-11054 (VRE)	2
Mycobacterium bovis BGG	0.25
E. coli MB5746	4
E. coli O-19592	16
Pseudomonas aeruginosa PAO1	>64

RNA, protein) remained unaffected (Figure 4A). Substantiating inhibition of cell wall biosynthesis, treatment with **1** strongly inhibited incorporation of radiolabeled glucosamine, an essential precursor of cell wall biosynthetic reactions (Figure S16). Furthermore, treatment of *B. subtilis* with **1** induced severe cell-shape deformations as visualized by phase-contrast microscopy (Figure 4C). The formation of membrane bulges and blebs is characteristically induced by

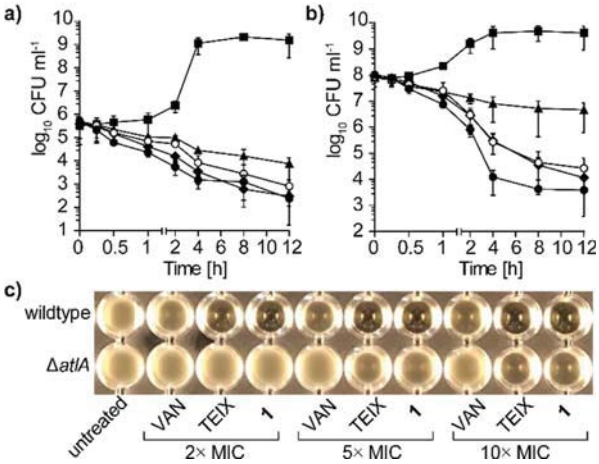

Figure 3. **1** shows excellent bactericidal activity against *S. aureus*. Time-dependent killing of early-exponential (a) and late-exponential phase-grown (b) cells treated with **1** at 1× (*open circles*) and 2× MIC (*circles*), with teixobactin (*diamonds*) and vancomycin (*triangles*) both at 10× MIC. Cells left untreated are shown with *squares*. Data are representative of three independent experiments. c) **1**-induced lysis is mediated by the major autolysin AtlA in *S. aureus*. Deletion of *atlA* results in markedly reduced autolysis after treatment with **1** and TEIX.

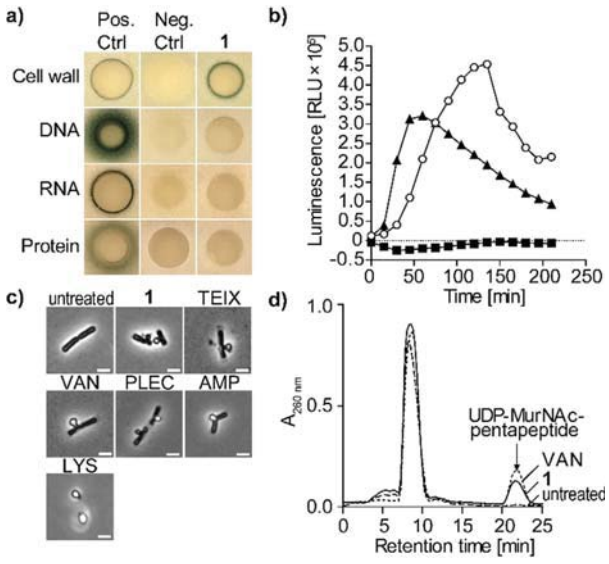

Figure 4. **1** targets bacterial cell wall biosynthesis. a) *B. subtilis* bioreporter strains with selected promotor-*lacZ* gene fusions were used to identify interference with major biosynthesis pathways including cell wall (P_{ypuA}), DNA (P_{yorB}), RNA (P_{ywgS}), and protein (P_{yhel}). A blue halo at the edge of the inhibition zone demonstrates induction of a specific stress response by β-galactosidase expression. Antibiotics vancomycin (VAN), ciprofloxacin, rifampicin, and clindamycin were used as positive controls. b) Treatment with **1** (1 × MIC, *open circles*) strongly induced P_{lial} as observed by expression of the *lux* operon from *Photorhabdus luminescens* in *B. subtilis* P_{lial}-*lux*. VAN (*triangles*) and clindamycin (CLI, *squares*) were used as control antibiotics. c) Phase-contrast microscopy of *B. subtilis* confirmed impairment of cell wall integrity as severe cell-shape deformations and characteristic blebbing were observed following **1** treatment. Cell wall active antibiotics teixobactin (TEIX), VAN, plectasin (PLEC), ampicillin (AMP), and lysozyme (LYS) were used as controls. Scale bar = 2 μm. d) Intracellular accumulation of the cell wall precursor UDP-MurNAc-pentapeptide after treatment of *S. aureus* with **1** (5 × MIC). Untreated and VAN-treated (5 × MIC) cells were used as controls. Experiments are representative of 3 independent experiments each.

many cell wall-acting antibiotics and was similarly observed with teixobactin and plectasin (Figure 4C).[23]

Despite the membrane alterations observed, **1** did not trigger pore formation or membrane disintegration. In contrast to the lantibiotic nisin, no rapid pore formation was observed (Figure S17 A). Furthermore, the membrane potential of **1**-treated *S. simulans* 22 cells remained unaffected even at higher concentrations (5× MIC) (Figure S17 B), as quantified by intra- and extracellular concentrations of the tritium-labeled lipophilic cation TPP^+. In line with these observations, **1** did not impact the cellular localization of the cell division inhibitor MinD of *B. subtilis*. MinD is bound to the membrane via a C-terminal amphipathic helix and requires the presence of the membrane potential for its specific cellular localization pattern. In growing cells, MinD accumulates at the newly formed cell poles to direct FtsZ to mid-cell division site and specific FtsZ positioning to guide division septum placement.[17,24] While treatment with CCCP resulted in a rapid delocalization and irregular dispersion of GFP-MinD within 2 min, localization of the fusion protein was unchanged in **1**-treated cells and only slightly affected with prolonged incubation time (30 min) (Figure S17 C).

In search of the molecular target within the peptidoglycan (PGN) biosynthesis pathway, we investigated the effect of **1** on the LiaRS stress response in *B. subtilis*. LiaRS is a two-component system (TCS), which is known to respond to antibiotics that interfere with the lipid II biosynthesis cycle.[25] Monitoring bioluminescence of reporter cells treated with **1** over time revealed a strong induction of P_{lial}-*lux*, even exceeding induction levels observed with the lipid II-binding antibiotic vancomycin, indicating interference of **1** with the lipid II biosynthesis cycle (Figure 4B). Mechanism of action studies revealed that the structurally-related teixobactin impairs cell wall biosynthesis by blocking several cell envelope precursors containing an undecaprenyl-pyrophosphate linkage unit including the ultimate PGN building block lipid II.[26]

PGN biosynthesis takes place in three different cellular compartments of a bacterial cell. Synthesis starts in the cytoplasm with the formation of the ultimate soluble precursor uridine diphosphate-*N*-acetylmuramic acid-pentapeptide (UDP-MurNAc-pentapeptide), which is then transferred to the membrane-anchor undecaprenyl phosphate ($C_{55}P$) to yield lipid I (undecaprenyl-pyrophosphoryl-MurNAc-pentapeptide). Subsequently, the addition of *N*-acetylglucosamine (UDP-GlcNAc) yields lipid II (undecaprenyl-pyrophosphoryl-MurNAc-pentapeptide-GlcNAc), which can further be species-specifically modified. Modified lipid II is translocated to the outer surface of the membrane and incorporated into the PGN polymer (Figure S18).

Antibiotics that interfere with late stages of PGN synthesis, such as vancomycin, trigger the accumulation of UDP-MurNAc-pentapeptide in the cytoplasm. To distinguish whether **1** interferes with the early cytoplasmic or the late membrane-associated steps of PGN synthesis, we determined the cytoplasmic levels of UDP-MurNAc-pentapeptide of *S. aureus* cells treated with **1**. Treatment with **1** led to the intracellular accumulation of UDP-MurNAc-pentapeptide similar to the vancomycin control (Figure 4D), suggesting that one of the later membrane-associated or extracellular biosynthesis steps is targeted. Taken together, results from whole cell experiments strongly supported the hypothesis that **1** and teixobactin, in accordance with their structural resemblance, share the same mechanism of action.

Based on this, we analyzed the impact of **1** on the membrane-associated steps of PGN biosynthesis in vitro to identify the molecular target of **1**. The first membrane-linked step of PGN synthesis is catalyzed by MraY, which transfers UDP-MurNAc-pentapeptide to the lipid carrier $C_{55}P$ yielding lipid I.[27] Subsequently, the glycosyltransferase MurG adds UDP-activated GlcNAc to the muramyl moiety of lipid I, yielding lipid II.[28] Membrane preparations of *M. luteus* possess the enzymatic activity of MraY and MurG to synthesize lipid II from the substrates UDP-MurNAc-pentapeptide, [^{14}C]-UDP-GlcNAc and $C_{55}P$.[29] Testing the reactions in the presence of increasing concentrations of **1** resulted in a dose-dependent inhibition of overall lipid II synthesis. Full inhibition was observed at a twofold molar excess of **1** with

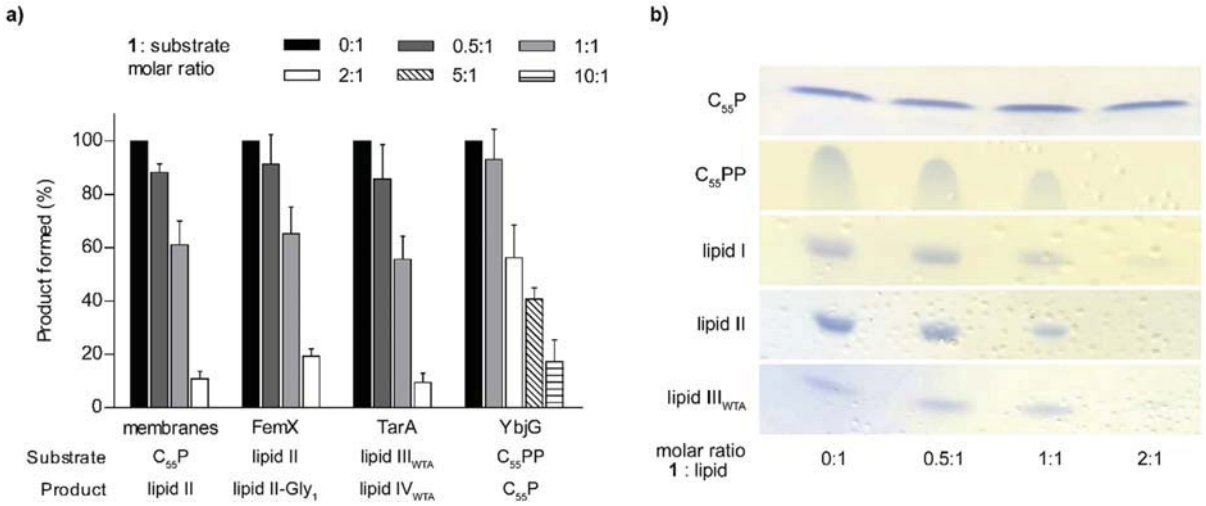

Figure 5. **1** binds to undecaprenyl pyrophosphate-containing cell wall precursors. a) **1** interferes with membrane-associated steps of PGN and WTA synthesis in vitro. The antibiotic was added in molar ratios from 0.5 to 10 with respect to the amount of the lipid substrate $C_{55}P$, $C_{55}PP$, lipid II, or lipid III_{WTA} used in the individual test system. The amount of reaction product synthesized in the absence of **1** was taken as 100%. Mean values from three independent experiments are shown. Error bars represent standard deviation. b) **1** forms extraction-stable complexes with $C_{55}PP$-containing purified cell wall precursors including the PGN precursors lipid I and lipid II, the WTA intermediate lipid III_{WTA} and $C_{55}PP$. Cell wall intermediates are fully locked in a complex at a twofold molar excess of **1**. No complex formation was observed with $C_{55}P$. Binding of **1** is indicated by a reduction of the amount of free lipid intermediates visible on the TLC. The chromatograms are representative of two independent experiments.

regard to the substrate $C_{55}P$ (Figure 5A). In staphylococci, lipid II is modified by the addition of five glycine residues, catalyzed by FemXAB peptidyltransferases.[30] Testing the impact of **1** on the FemX-catalyzed addition of a glycine residue to lipid II revealed, that the reaction was fully blocked at a 2:1 stoichiometry (antibiotic:lipid II), indicating the formation of a complex with the substrate rather than inhibition of the enzyme (Figure 5A), as observed for teixobactin.[3] In addition, **1** inhibited the YbjG-catalyzed dephosphorylation of $C_{55}PP$ to $C_{55}P$, although higher concentrations (10:1) were required for complete inhibition. This indicates that the pyrophosphate moiety is crucial for antibiotic interaction, but the first sugar attached to the lipid carrier contributes to high binding affinity. However, the nature of the sugar appears less important, as **1** further efficiently inhibited the synthesis of the wall teichoic acid (WTA) precursor lipid IV_{WTA} (undecaprenyl-pyrophosphoryl-GlcNAc-ManNAc) (Figure 5A, Figure S18).

Consistently, **1** efficiently trapped lipid intermediates containing a $C_{55}PP$ moiety in a stable complex that prevented extraction of the lipid intermediate from the reaction mixture when added in a twofold molar excess, indicating to the formation of a 2:1 stoichiometric complex. Complex formation was not observed with $C_{55}P$, confirming the lipid pyrophosphate moiety to be the minimal binding motif (Figure 5B). The inability of **1** to bind to $C_{55}P$ further shows that inhibition of the in vitro lipid II synthesis using membrane preparations (Figure 5A), relies on binding to the reaction products, lipid I and lipid II, rather than the $C_{55}P$ substrate.

To validate that the antimicrobial activity of **1** relies on complex formation with cell wall lipid intermediates, antagonization assays with selected purified precursors were performed. In line with the in vitro analyses, the addition of $C_{55}PP$-containing lipid intermediates counteracted **1** from inhibiting growth of *S. aureus* similar to teixobactin (Table S5). However, compared to lipid I and lipid II, the addition of lipid III_{WTA} or $C_{55}PP$ was less effective, since 4-fold higher concentrations were required to fully antagonize the antimicrobial activity of **1**, pointing to differences in the binding modes, that may involve interactions with the first sugar in lipid II. As expected, $C_{55}P$ and the anionic phospholipid 1,2-dioleoyl-sn-glycero-3-phosphoglycerol (DOPG) had no antagonistic effect.

Binding of **1** to lipid II blocks PGN biosynthesis resulting in a defective cell wall ultimately leading to cell death. In contrast to PGN, WTAs are not essential *per se*, but blocking WTA biosynthesis can result in the lethal accumulation of toxic intermediates and indirectly effect PGN biosynthesis, as the molecular machineries of both pathways are tightly interlinked.[31] In addition, WTAs anchor autolysins and thereby prevent uncontrolled hydrolysis of PGN,[32] suggesting that inhibition of WTA biosynthesis by binding WTA lipid intermediates helps to liberate autolysins. In agreement, **1**-induced lysis was markedly reduced in a Δ*atlA* mutant, compared to wildtype *S. aureus* cells (Figure 3C), confirming that lysis induced by **1** is dependent on the major autolysin AtlA in *S. aureus.* Our results further show that co-targeting of lipid II and WTA lipid intermediates by **1** cause synergistic effects by weakening the PGN structure and liberation of autolysins, which synergistically lead to cell lysis and death. In addition, multiple-targeting strongly reduced the propensity to develop resistance, as we could not generate resistant

mutants of *S. aureus* by serial passaging on incrementing concentrations of **1**.

Novel antibiotics with resistance breaking mechanisms of action are urgently needed to counteract the continuing spread of drug resistant pathogens. Hypeptin (**1**) is a cyclodepsipeptide that shares structural similarity with teixobactin (Figure S19).

1 contains four β-hydroxylated amino acids with different stereoconfiguration. We investigated the substrate specificity and stereoselectivity of the two tailoring hydroxylases HynC and HynE in vitro, which revealed specific interactions of both hydroxylases with their cognate domains. A transient hydrophobic interaction with a cognate T domain was characterized for the skyllamycin CYP450 β-hydroxylase, but the reason for specific recognition could not be determined.[33] Understanding and predicting domain interaction specificity of NRPS tailoring enzymes is a hallmark for future engineering attempts, a feature we are currently investigating. The structure revision of **1** based on bioinformatics, biochemical assays and extensive NMR analyses highlights the value of integrating these approaches for complex natural product structure elucidation.

Elucidation of the mechanism of action revealed, that **1** inhibits cell wall biosynthesis by binding to C_{55}PP-containing lipid intermediates within PGN, WTA, and capsule biosynthesis. Binding to multiple of these non-protein target structures within different biosynthesis pathways explains the potent activity towards a broad range of gram-positive pathogens, including drug resistant and difficult to treat strains, suggesting that the concomitant targeting of these precursors confers "intrinsic synergy". Besides the mere blocking of cell wall biosynthesis, binding to WTA precursors further triggered deregulation of autolysis resulting in rapid and uncontrolled lysis and impressive bactericidal activity.

The exact knowledge of the mode of action and molecular target, together with a deeper understanding of the structure–activity relationships (SAR) will support rational design of synthetic analogs of **1**. Synthetically generated teixobactin variants with modified N-terminus, by either replacing the linear chain by a lipophilic moiety[34] or the attachment of hydrophobic residues to *N*-Me-D-Phe_1,[35] have been reported to exhibit potent anti-microbial activity. Likewise, the semi-synthetic attachment of hydrophobic moieties to the N-terminal D-Ala_1 may increase membrane interaction and target binding of **1**. Notably, **1** was most refractory to resistance development in vitro, suggesting that the combined cellular activities, triggered by targeting different cell wall precursors, account for the reduced propensity to develop resistance, making this antibiotic class a favorable scaffold for development.

Acknowledgements

Funding was provided by the Deutsche Forschungsgemeinschaft (DFG, German Research Foundation)—Project-ID 398967434—TRR 261, the German Center for Infection Research (DZIF) (TTU Novel Antibiotics) and the Infect-Control2020 initiative (BMBF project TFP-TV10). M.C. acknowledges the DFG (grant No. CR464/7-1) for funding. Funding was provided by NIH grant AI091224 to ALS. Open access funding enabled and organized by Projekt DEAL.

Conflict of interest

The authors declare no conflict of interest.

Keywords: antibiotic · cell wall · cyclodepsipeptide · hydroxylase · lipid II

[1] K. Lewis, *Nature* **2012**, *485*, 439–440.
[2] D. Nichols, N. Cahoon, E. M. Trakhtenberg, L. Pham, A. Mehta, A. Belanger, T. Kanigan, K. Lewis, S. S. Epstein, *Appl. Environ. Microbiol.* **2010**, *76*, 2445–2450.
[3] L. L. Ling, T. Schneider, A. J. Peoples, A. L. Spoering, I. Engels, B. P. Conlon, A. Mueller, T. F. Schäberle, D. E. Hughes, S. Epstein, et al., *Nature* **2015**, *517*, 455–459.
[4] J. Shoji, H. Hinoo, T. Hattori, K. Hirooka, Y. Kimura, T. Yoshida, *J. Antibiot.* **1989**, *42*, 1460–1464.
[5] Y. Xie, S. Wright, Y. Shen, L. Du, *Nat. Prod. Rep.* **2012**, *29*, 1277–1284.
[6] R. D. Süssmuth, A. Mainz, *Angew. Chem. Int. Ed.* **2017**, *56*, 3770–3821; *Angew. Chem.* **2017**, *129*, 3824–3878.
[7] B. R. Miller, E. J. Drake, C. Shi, C. C. Aldrich, A. M. Gulick, *J. Biol. Chem.* **2016**, *291*, 22559–22571.
[8] K. Blin, S. Shaw, K. Steinke, R. Villebro, N. Ziemert, S. Y. Lee, M. H. Medema, T. Weber, *Nucleic Acids Res.* **2019**, *47*, W81–W87.
[9] K. Graupner, K. Scherlach, T. Bretschneider, G. Lackner, M. Roth, H. Gross, C. Hertweck, *Angew. Chem. Int. Ed.* **2012**, *51*, 13173–13177; *Angew. Chem.* **2012**, *124*, 13350–13354.
[10] J. Hou, L. Robbel, M. A. Marahiel, *Chem. Biol.* **2011**, *18*, 655–664.
[11] S. A. Kautsar, K. Blin, S. Shaw, T. Weber, M. H. Medema, *Nucleic Acids Res.* **2021**, *49*, D490–D497.
[12] C. Hermes, R. Richarz, D. A. Wirtz, J. Patt, W. Hanke, S. Kehraus, J. H. Voß, J. Küppers, T. Ohbayashi, V. Namasivayam, et al., *Nat. Commun.* **2021**, *12*, 144.
[13] M. Kaniusaite, R. J. A. Goode, R. B. Schittenhelm, T. M. Makris, M. J. Cryle, *ACS Chem. Biol.* **2019**, *14*, 2932–2941.
[14] T. M. Makris, M. Chakrabarti, E. Münck, J. D. Lipscomb, *Proc. Natl. Acad. Sci. USA* **2010**, *107*, 15391–15396.
[15] G. M. Singh, P. D. Fortin, A. Koglin, C. T. Walsh, *Biochemistry* **2008**, *47*, 11310–11320.
[16] a) Z. L. Reitz, C. D. Hardy, J. Suk, J. Bouvet, A. Butler, *Proc. Natl. Acad. Sci. USA* **2019**, *116*, 19805–19814; b) M. Strieker, E. M. Nolan, C. T. Walsh, M. A. Marahiel, *J. Am. Chem. Soc.* **2009**, *131*, 13523–13530.
[17] K. A. J. Bozhüyük, F. Fleischhacker, A. Linck, F. Wesche, A. Tietze, C.-P. Niesert, H. B. Bode, *Nat. Chem.* **2018**, *10*, 275–281.
[18] V. V. Phelan, Y. Du, J. A. McLean, B. O. Bachmann, *Chem. Biol.* **2009**, *16*, 473–478.
[19] A. J. Jasniewski, C. J. Knoot, J. D. Lipscomb, L. Que, *Biochemistry* **2016**, *55*, 5818–5831.
[20] Z. Lin, J. O. Falkinham, K. A. Tawfik, P. Jeffs, B. Bray, G. Dubay, J. E. Cox, E. W. Schmidt, *J. Nat. Prod.* **2012**, *75*, 1518–1523.
[21] F. von Nussbaum, R. D. Süssmuth, *Angew. Chem. Int. Ed.* **2015**, *54*, 6684–6686; *Angew. Chem.* **2015**, *127*, 6784–6786.
[22] S. Kodali, A. Galgoci, K. Young, R. Painter, L. L. Silver, K. B. Herath, S. B. Singh, D. Cully, J. F. Barrett, D. Schmatz, et al., *J. Biol. Chem.* **2005**, *280*, 1669–1677.

[23] T. Schneider, T. Kruse, R. Wimmer, I. Wiedemann, V. Sass, U. Pag, A. Jansen, A. K. Nielsen, P. H. Mygind, D. S. Raventós, et al., *Science* **2010**, *328*, 1168 – 1172.
[24] H. Strahl, L. W. Hamoen, *Proc. Natl. Acad. Sci. USA* **2010**, *107*, 12281 – 12286.
[25] a) J. Radeck, S. Gebhard, P. S. Orchard, M. Kirchner, S. Bauer, T. Mascher, G. Fritz, *Mol. Microbiol.* **2016**, *100*, 607 – 620; b) T. Mascher, S. L. Zimmer, T.-A. Smith, J. D. Helmann, *Antimicrob. Agents Chemother.* **2004**, *48*, 2888 – 2896.
[26] A. Müller, A. Klöckner, T. Schneider, *Nat. Prod. Rep.* **2017**, *34*, 909 – 932.
[27] M. Ikeda, M. Wachi, H. K. Jung, F. Ishino, M. Matsuhashi, *J. Bacteriol.* **1991**, *173*, 1021 – 1026.
[28] S. Ha, B. Gross, S. Walker, *Curr. Drug Targets Infect. Disord.* **2001**, *1*, 201 – 213.
[29] Y. van Heijenoort, M. Derrien, J. van Heijenoort, *FEBS Lett.* **1978**, *89*, 141 – 144.
[30] a) T. Schneider, M. M. Senn, B. Berger-Bächi, A. Tossi, H.-G. Sahl, I. Wiedemann, *Mol. Microbiol.* **2004**, *53*, 675 – 685; b) J. M. Monteiro, G. Covas, D. Rausch, S. R. Filipe, T. Schneider, H.-G. Sahl, M. G. Pinho, *Sci. Rep.* **2019**, *9*, 5010.
[31] T. Roemer, T. Schneider, M. G. Pinho, *Curr. Opin. Microbiol.* **2013**, *16*, 538 – 548.
[32] R. Biswas, R. E. Martinez, N. Göhring, M. Schlag, M. Josten, G. Xia, F. Hegler, C. Gekeler, A.-K. Gleske, F. Götz, et al., *PLoS One* **2012**, *7*, e41415.
[33] K. Haslinger, C. Brieke, S. Uhlmann, L. Sieverling, R. D. Süssmuth, M. J. Cryle, *Angew. Chem. Int. Ed.* **2014**, *53*, 8518 – 8522; *Angew. Chem.* **2014**, *126*, 8658 – 8662.
[34] H. Yang, K. H. Chen, J. S. Nowick, *ACS Chem. Biol.* **2016**, *11*, 1823 – 1826.
[35] Y. Zong, F. Fang, K. J. Meyer, L. Wang, Z. Ni, H. Gao, K. Lewis, J. Zhang, Y. Rao, *Nat. Commun.* **2019**, *10*, 3268.

Manuscript received: February 12, 2021
Revised manuscript received: March 19, 2021
Accepted manuscript online: March 26, 2021
Version of record online: May 7, 2021

Angewandte Chemie
Eine Zeitschrift der Gesellschaft Deutscher Chemiker

Supporting Information

Biosynthesis and Mechanism of Action of the Cell Wall Targeting Antibiotic Hypeptin

Daniel A. Wirtz[+], Kevin C. Ludwig[+], Melina Arts, Carina E. Marx, Sebastian Krannich, Paul Barac, Stefan Kehraus, Michaele Josten, Beate Henrichfreise, Anna Müller, Gabriele M. König, Aaron J. Peoples, Anthony Nitti, Amy L. Spoering, Losee L. Ling, Kim Lewis, Max Crüsemann, and Tanja Schneider**

anie_202102224_sm_miscellaneous_information.pdf

WILEY-VCH

SUPPORTING INFORMATION

Table of Contents

WILEY-VCH

SUPPORTING INFORMATION

Experimental Procedures

Purification and isolation of 1

Lysobacter sp. K5869 was grown on 2 % SMS agar containing 10 % R4 broth[1] for 5 days at room temperature. Homogenized colonies of strain K5869 were used to inoculate 250 mL R4 broth supplemented with trace elements. The seed culture was incubated for 5 days at 28°C on a rotary shaker (200 rpm), prior to 5 % (v/v) inoculation of 3 L of fresh medium. Cultures were grown at 28 °C with shaking at 120 rpm for 5 days and screened daily for antibiotic production by using 5 µl of sterile filtered broth supernatant in agar diffusion assays using the cell envelope stress bioreporter *B. subtilis* 168 *amyE*::pAC6 (P_{ypuA}-*lacZ*).[2] At day 3, 60 g of Sepabeads® SP-207 (Sigma-Aldrich) were added to the culture and separated by filtration at day 5. Sepabead-immobilized peptides were extracted with 300 ml of acetone by overnight shaking. The extract was evaporated to dryness and reconstituted in 0.1 % (v/v) aqueous trifluoroacetic acid (TFA). The sample was subjected to reversed-phase high performance liquid chromatography (RP-HPLC) using a preparative MultoKrom® 100-10 C_{18} column (250 × 26 mm, SFD GmbH) eluting with a linear gradient of water and acetonitrile (0-80) + 0.1% (v/v) TFA over 40 min at 10 ml min^{-1} flow rate and UV monitoring at 280 nm. MALDI-TOF profiling indicated the pseudomolecular ion $[M+H]^+$ peaks at 1022.489 *m/z*, indicative of **1** in the 30 - 50 % acetonitrile fractions, which showed bioactivity in agar diffusion assays.
Rechromatography of peak fractions with semipure **1** was carried out by RP-HPLC using three linear gradients of water and acetonitrile with 0 to 30% acetonitrile over a period of 5 min, 30 to 60% acetonitrile over 25 min, and 60 to 80% over 10 min (10 ml min^{-1} flow rate). Rechromatographed fractions were finally lyophilized and resulted in 18.2 mg of pure **1**, leaving a white powder.

WILEY-VCH

SUPPORTING INFORMATION

Cloning, expression and characterization of enzymes

DNA isolation and genome sequencing

Genomic DNA of *Lysobacter sp.* K5869 was prepared from 2 mL freshly grown culture with the GenElute Bacterial Genomic DNA kit (Sigma Aldrich). Sequencing was carried out by Eurofins Genomics (Ebersberg, Germany) with the PAC-BIO SMRT cell technology. After assembly, a single, circular scaffold consisting of 5,968,034 bp was obtained. The location of the chromosomal gene encoding for the replicator protein dnaA of *Lysobacter* was determined and its end position was set to be adjacent to start position 1. The modified scaffold consists out of 5,950,758 bp.

Sequential cloning

Oligonucleotide primers were synthesized by Eurofins Genomics. Primers used for amplification of the different modules of *hynA, hynB*, the genes *hynC*, *hynE*, and *hynMLP* from the genomic DNA of *Lysobacter sp.* K5869 are listed in Table S1. The resulting DNA fragments were cloned into restricted pET28a (*hynABE*) or pCDFDuet-1 (*hynC, hynMLP*) via sequential ligation cloning and transformed into *E. coli* alpha-select silver. The resulting constructs were isolated, analyzed via restriction digest and verified by Sanger DNA sequencing. The final plasmids were then transformed into *E. coli* BL21(DE3) or, when containing a NRPS T domain, into *E. coli* BAP1 for heterologous expression of the His-tagged protein.

Table S1. Primers used for cloning and mutagenesis of enzymes and enzymatic domains of the *hyn* BGC. Restriction sites are bold. Annealing sequences are given in upper case. Mutated nucleotides are underlined.

Name	Sequence (5'→3')
HynA4_Cacc_NdeI_for	tatcatatgGTGAGTGCGCAAGAGCAC
HynA5_Cdon_HindIII_rev	tagaagcttaCAGGCAGCGTCGTTGCCA
HynA5_C2_NdeI_for	tgccatatgGCCTTGTTCGAACCGGCG
HynA5_T_XhoI_rev	tatactcgagttaGCCGTTGGCCGGAACGAC
HynA6_C_NdeI_for	tatcatatgCAGATCGAACGCATCGTC
HynA6_T_HindIII_rev	tagaagcttaCTGACAGTCGACGATGGC
HynB7_A_NcoI_for	tgtccatgggaCGCGAGCAAGTCCTG
HynB7_T_HindIII_rev	tataagcttCTGCCCGACCCGCGCTGCGAA
HynC_BamHI_for	agcggatccATGACCCAGAAGAACTTCAAG
HynC_HindIII_rev	tataagcttTCACAGCAGCAGTTCCCT
HynC_EcoRI_pCDF_for	cacgggaattcgACCCAGAAGAACTTCAA
HynC_HindIII_pCDF_rev	gagaagcttTCACAGCAGCAGTTCCCT
Gib_HynC_E376D_for	tacggcgacCACGCCGATCTCGACAT
Gib_HynC_E376D_rev	cggcgtggTCGCCGTAGAACGGC
HynE_NdeI_for	gcgcatatgATGAGCATGTTCAATCAGCTT
HynE_HindIII_rev	gataagcttCTGGCCCATGCCGACCAG
HynMLP_NdeI_pCDF_for	gcgcatATGAGCAATCCCTTCGACGAC
HynMLP_PacI_pCDF_rev	aatttaattaattAGGCGCCGGGCCGGGC

Site-directed mutagenesis

Gibson assembly[3] was used to introduce specific mutations into the expression plasmids. Primers were designed with an annealing sequence of 18 bp prior to the mutated codon and 10 non-mutated bp to overlap in the assembly (Table S1). Mutated educt fragments were generated from the non-mutated plasmid as template *via* Q5-PCR (NEB). The template DNA was then eradicated by restriction hydrolysis with *dam*$^+$/*dcm*$^+$-methylation sensitive *Dpn*I. 5 µL of the linear PCR products were mixed with 15 µL assembly mixture (5 % PEG-8000, 100 mM Tris-HCl pH 7.5, 10 mM $MgCl_2$, 10 mM DTT, 0.25 mM each of the 4 dNTPs, 1 mM NAD, 0.08 U T5 exonuclease, 0.5 U Phusion polymerase) and incubated at 50 °C for 60 min. After incubation, the whole mixture was used for chemical transformation into *E. coli* alpha-select silver.

SUPPORTING INFORMATION

Protein expression

If the protein of interest included a T domain, the protein expression was conducted in *E. coli* BAP1 to ensure *in vivo* phosphopantetheinylation of the conserved serine residue. All other constructs were expressed in *E. coli* BL21(DE3). Media were supplemented with the appropriate antibiotic, dependent on the respective plasmids in the strain. For the expression of HynC, TB media was additionally supplemented with 25 µM $(NH_4)Fe(III)$-citrate. For the preculture, few mL of LB-broth were inoculated from a cryopreserved culture and incubated overnight (220 rpm, 37 °C). The densely grown preculture was then used in a ratio of 1:100 to inoculate the TB-medium in a baffled Erlenmeyer flask. This expression culture was grown (37 °C, 220 rpm) until OD_{600} = 0.8 and chilled on ice prior to induction with 400 µM isopropyl-β-D-thiogalactopyranoside (IPTG). The cultures were then further incubated at 16 °C and 220 rpm for additional 16 h.
For protein purification, the cells were harvested via centrifugation (10,000 *x g*, 4 °C, 2 min). The pellet was resuspended in 5 mL lysis buffer (50 mM NaH_2PO_4, 300 mM NaCl, pH 8.0) per g pellet and cells were lysed in ice by sonification in 10-seconds intervals. The lysate was centrifuged (12,000 *x g*, 4 °C, 10 min) and the clear supernatant mixed with 1 mL NiNTA agarose per 10 mL supernatant. The suspension was incubated on ice in slight movement. After 1 h, the suspension was filtered with a propylene column (Qiagen, 1 mL or 4 mL). The remaining NiNTA agarose matrix was washed with 4-8 mL 20 mM imidazole buffer and 0-4 mL 35 mM imidazole buffer, depending on the binding affinity of the desired protein. Proteins were eluted with 2.5 mL 250 mM imidazole buffer. The buffer of the elution fraction was exchanged with PD10 columns (Cytiva), following the gravity protocol. If necessary, proteins were concentrated with Amicon® Ultra 4 mL centrifugal filters (Merck) with a molecular weight cut off (MWCO) of at least half the proteins size.

$\gamma^{18}O_4$-ATP exchange assay

Two stock solutions were prepared for the assay. Substrate solution 1: 3 mM of the respective amino acid, 15 mM pyrophosphate in 20 mM Tris pH 7.5; Substrate solution 2: 3 mM $\gamma^{18}O_4$-ATP, 15 mM $MgCl_2$ in 20 mM Tris pH 7.5. 2 µL of each solution were mixed with 2 µL A domain containing protein concentrated to 5 µM in 5 % glycerol, 20 mM Tris pH 7.5 and incubated at 22 °C for 1.5 h. The reaction was stopped by addition of 6 µL 9-aminoacridine in acetone (10 mg/mL). Precipitated proteins were removed via centrifugation. 1 µL of each sample was spotted on the sample carrier and subsequently recrystallized by addition of 0.5 µL acetone. The samples were then analyzed with MALDI-TOF-MS (Bruker AutoFlex III) in negative mode. Absolute substrate conversion in [%] was calculated by dividing the peak area at *m/z* 506 through the combined peak areas at *m/z* 508, 510, 512, and 514, divided by 83.33 for the molar ratio of labelled against unlabeled pyrophosphate in the assay.[4]

In vitro hydroxylation assay with HynE

The phosphopantetheinylated NRPS modules $HynA_4C_{acc}ATC_{don}$, $HynA_5CAT$, $HynA_6CAT$ or $HynB_7AT$ were purified from *E. coli* BAP1 as described above and buffered in 50 mM Tris pH 7.5, 150 mM NaCl, 10 mM $MgCl_2$ using PD-10 columns. The assay was performed in a 500 µL one-pot-reaction: 50 µM HynE and 50 µM NRPS module were supplemented with 1 mM ATP, 1 mM of the respective amino acid, 5 mM DTT and 0.5 mM of each $(NH_4)_2Fe(SO_4)$, α-ketoglutarate and ascorbate. The reaction was incubated with slight movement for 3 h at 20 °C. Afterwards, the reaction was quenched by adding 50 µL 100 % (w/v) TCA and incubated for 30 min on ice. The precipitated proteins were washed twice with buffer after careful centrifugation (9000 *x g*, 5 min). Alkaline thioester cleavage was conducted with 200 µL KOH (0.1 M) at 70 °C for 20 min. The solution was lyophilized and the pellet dissolved in a minimal volume of ddH_2O for LC-MS analysis. As a negative control, HynE was heat-inactivated at 80 °C for 10 min prior to addition of the NRPS module and the substrates.
Analysis of the amino acids was performed on a Waters e2695 separation module, coupled to an Acquity QDa and 2998 PDA detector with a NUCLEODUR® HILIC 250x4.6 column as stationary phase. Elution was conducted with an isocratic gradient of Acetonitrile:5 mM aminoacetate pH 7.4 70:30 at a flow of 0.7 mL/min over 20 min. Amino acids were detected in negative mode.

In vitro hydroxylation assay with HynC

Heterologously expressed HynC was only stable, when co-expressed and purified with the respective NRPS module. The enzymes were purified from *E. coli* BAP1 and buffered in 50 mM Tris pH 7.5, 150 mM NaCl, 10 mM $MgCl_2$ using PD-10 columns. Afterwards, the protein mass was roughly determined by measuring the absorption at λ=280 nm. 500 µL of the solution with 5.0 mg/mL protein were supplemented with 1 mM ATP, 1 mM of the respective amino acid, 10 µM methylviologen and 1 mM NADH and incubated with slight movement at 20 °C overnight. Alkaline thioester cleavage, further processing, and analysis of the sample were conducted as described above.

WILEY-VCH

SUPPORTING INFORMATION

Bioinformatic analysis of $HynA_5C_2$

For phylogenetic analysis of the condensation domain superfamily, the datasets from Rausch et al.[5] and Reitz et al.[6] together with homologues of $HynA_5C_2$ were imported to MEGA-X.[7] Multiple sequence alignment was performed using the MUSCLE-algorithm. The maximum-likelihood tree was constructed using the Dayoff matrix based model. The tree with the highest log likelihood (-36592.07) is shown in Figure S3. The Initial tree for the heuristic search was obtained automatically by applying Neighbor-Join and BioNJ algorithms to a matrix of pairwise distances estimated using a JTT model, and then selecting the topology with superior log likelihood value. A discrete Gamma distribution was used to model evolutionary rate differences among sites (5 categories (+G, parameter = 2.1883)). The tree is drawn to scale, with branch lengths measured in the number of substitutions per site. All positions with less than 95 % site coverage were eliminated. Branch support was assessed by bootstrapping with 100 replicons.

WILEY-VCH

SUPPORTING INFORMATION

Bioactivity of 1

Antibiotic susceptibility testing

MIC was determined by broth microdilution according to CLSI guidelines, in polypropylene microtiter plates (Nunc brand) using cation-adjusted Mueller-Hinton broth (MHB, Oxoid).

Killing kinetics

S. aureus SA113 was grown in MHB at 37 °C to exponential phase (OD_{600} = 0.5) or stationary phase (OD_{600} = 1). Bacteria were challenged with **1** at 1× and 2× MIC. Vancomycin and teixobactin (both 10× MIC) served as positive controls. At defined time points aliquots were taken, centrifuged at 10,000 × *g* for 1 min, and resuspended in sterile phosphate buffered saline (PBS). Tenfold serially diluted suspensions were spotted as triplicates on Mueller Hinton agar (MHA) plates. CFU ml^{-1} were determined after overnight incubation at 37 °C.
For visual analysis of lysis in microtiter plates, stationary phase cells (OD_{600} = 1) cells of *S. aureus* SA113 and the AtlA-deficient mutant *S. aureus* SA113 Δ*altA* (supplemented with 150 µg ml^{-1} spectinomycin) were treated with **1**, teixobactin, and vancomycin at concentrations of 2×, 5× and 10× the MIC and were photographed after 24 h. Experiments were performed with three biological replicates.

β-galactosidase reporter assays

B. subtilis β-galactosidase reporter assays were performed as previously described.[2] In short, reporter strains were grown in MHB containing 5 µg/ml chloramphenicol at 30 °C to an OD_{600} of 0.5. Subsequently, cells were poured at 1 × 10^7 CFU ml^{-1} in MHA plates supplemented with 5 µg/ml chloramphenicol, 75 µg/ml (cell wall reporter), 125 µg/ml (DNA reporter), and 250 µg/ml (RNA and protein reporters) X-gal, respectively. After solidification of the plates, 5 µg of **1** and control antibiotics inducing the promotors were spotted (6 µg vancomycin for cell wall, 0.3 µg ciprofloxacin for DNA, 6 µg rifampicin for RNA, 3 µg clindamycin for protein). Results were documented after incubation overnight at 30 °C.

Luciferase reporter assays

B. subtilis luciferase reporter assays were conducted as previously described.[8] Briefly, *B. subtilis* P_{lial}-*lux* was grown in MHB containing 5 µg/ml chloramphenicol at 30 °C to an OD600 of 0.5. Cells were added to 96-well white wall chimney plates containing serially diluted antibiotics. Luminescence measurements were performed at 30 °C in a microplate reader Spark 10M (Tecan). At least three independent biological replicate experiments were conducted.

[^{3}H]-glucosamine incorporation studies

The effect of **1** on cell wall synthesis was studied by monitoring the incorporation of [^{3}H]*N*-acetyl-glucosamine (GlcNAc); 0.02 MBq ml^{-1} into the acid-precipitable cell fractions as previously described.[9] MHB-grown cultures of *S. simulans* 22 were treated with **1** at 1× MIC, and with vancomycin at 10× MIC.

Bacterial cell wall integrity assay

Bacterial cell wall integrity assays were adapted from previous work.[10] *B. subtilis* 168 cultures were grown in MHB at 30 °C to an OD_{600} of 0.3. Subsequently, cells were treated with 0.625 µg/ml **1**, 0.2 µg/ml teixobactin, 2 µg/ml vancomycin, 4 µg/ml plectasin, 256 µg/ml ampicillin, and further incubated at 30 °C for 90 min. Lysozyme-treated (128 µg/ml) cells were incubated for 10 min. Cells were immediately fixed with in a 1 ml 1:3 (v:v) mixture of acetic acid and methanol, and immobilized on thin 1 % w/v agarose slides. Imaging was performed by phase contrast microscopy on a Zeiss Axio Observer Z1 microscope (Zeiss, Jena, Germany) equipped with HXP 120 V light source and an Axio Cam MR3 camera. Images were acquired with ZEN 2 software (Zeiss) and analyzed and postprocessed using ImageJ v1.45s software (National Institutes of Health).[11]

SUPPORTING INFORMATION

MinD delocalization studies

B. subtilis 1981 *erm spc minD*::*ermC amyE*::P_{xyl}-*gfp-minD*, a strain with a *gfp-minD* fusion under control of the P_{xyl} promotor,[12] was grown in MHB supplemented with 0.1 % w/v xylose and 50 µg/ml spectinomycin at 30 °C to an OD_{600} of 0.6. Imaging was carried out within 2, 30, and 120 min after addition of **1** at 2× and 10× MIC. The proton ionophore carbonyl cyanide *m*-chlorophenylhydrazone (CCCP, 100 µM) was used as positive control and imaging was carried out within 2 min. Samples were immobilized on microscope slides covered with 1 % w/v agarose. Fluorescence microscopy and analysis was performed using the same microscope and software as described for phase contrast microscopy.

Determination of the membrane potential

The membrane potential was determined as previously described,[13] using the lipophilic cation tetraphenylphosphonium (TPP^+), which diffuses across the bacterial membrane in response to a trans-negative membrane potential (ΔΨ). 1 µCi/ml [^{3}H]TPP+ (26 Ci/mmol) was added to a culture of *S. simulans* 22 with an OD_{600} of 0.7 in half-concentrated MHB at 37 °C. The culture was treated with **1** at 1×, 2× and 5× MIC or with 500 µM of CCCP as positive control. Samples of 100 µl were filtered through 0.2 µm cellulose acetate filters and washed twice with 5 ml of 200 mM potassium phosphate buffer. Filters were dried and counted. For calculation of ΔΨ, cell-associated versus free TPP^+ concentrations were applied to the Nernst equation $\Delta\Psi = (-2.3 \times R \times T/F) \times \log(TPP^+_{in}/TPP^+_{out})$ where T is absolute temperature, R is the universal gas constant, and F is the Faraday constant. Mean ΔΨ values were calculated from three independent determinations.

Potassium release from whole cells

The potassium release assays were adapted as previously described.[10] Briefly, tryptic soy broth (TSB)-grown *S. simulans* 22 cells were harvested at an OD_{600} of 1.0 to 1.5, washed with cold choline buffer (300 mM choline chloride, 30 mM MES, 20 mM Tris, pH 6.5), and resuspended to an OD_{600} of 30. The concentrated cell suspension was kept on ice and used within 30 min. For each measurement, the potassium electrode (Mettler Toledo) was calibrated with potassium chloride. Cells were diluted in choline buffer at RT to an OD_{600} of 3, and the peptide-induced potassium release was monitored in 15 sec intervals for 5 min at RT. **1** was added in a concentration corresponding to 1× MIC. Potassium concentrations were calculated from the measured voltage according to Orlov *et al.*[14] and plotted relative to the total amount of potassium released after the addition of 1 µM of the pore-forming lantibiotic nisin (set 100 % efflux). Results show mean values of three independent experiments.

Quantification of intracellular UDP-N-acetylmuramic acid-pentapeptide (UDP-MurNAc-pp)

To analyze the cytoplasmic nucleotide pool we adapted the protocol of Kohlrausch and Höltje.[15] *S. aureus* SG511 was grown in 15 ml MHB at 37°C to an OD_{600} of 0.6 and incubated with 130 µg/ml chloramphenicol for 15 min. **1** was added at 1×, 2.5×, and 5× MIC and incubated for another 30 min. Lipid II-complexing vancomycin (5× MIC) was used as positive control. Extraction of nucleotide-linked PGN precursors and their analysis was performed by HPLC as described previously.[16] Corresponding fractions were confirmed by mass spectrometry.

Synthesis and purification of lipid intermediates

Large scale synthesis and purification of the PGN precursors lipid I, lipid II, and the wall teichoic acid precursor lipid III_{WTA} were performed as previously described.[17] UDP-*N*-acetyl-muramic acid pentapeptide (UDP-MurNAc-pp) was purified according to the protocol elaborated by Kohlrausch and Höltje.[15] Geranylgeranyl phosphate ($C_{20}P$), undecaprenyl phosphate ($C_{55}P$), geranylgeranyl diphosphate ($C_{20}PP$), and undecaprenyl diphosphate ($C_{55}PP$) were purchased from Larodan Fine Chemicals AB (Malmö, Sweden), 1,2-dioleoyl-sn-glycero-3-phosphoglycerol (DOPG) was purchased from Avanti Polar Lipids (Alabaster, AL, USA) The concentration of purified PGN and wall teichoic acid precursors was quantified on the basis of their phosphate content as described.[18]

WILEY-VCH

SUPPORTING INFORMATION

In vitro lipid II synthesis with isolated membranes

In vitro lipid II synthesis was performed using membranes of *M. luteus* as previously described.[19] Briefly, synthesis was assayed by incubating membrane preparations (200 µg protein) with 5 nmol $C_{55}P$, 50 nmol UDP-MurNAc-pp, 50 nmol UDP-*N*-acetylglucosamine (UDP-GlcNAc), and 0.5 nmol [^{14}C]UDP-GlcNAc in 60 mM Tris-HCl, 5 mM $MgCl_2$, and 0.5 % Triton X-100, at pH 7.5 in a total volume of 50 µl at 30 °C for 1 h. $C_{55}P$-containing products were extracted with an equal volume of *n*-butanol/pyridine acetate, pH 4.2 (2:1, v/v) and analyzed by TLC using chloroform/methanol/water/ammonia (88:48:10:1, v/v/v/v) as the solvent[20] and phosphomolybdic acid staining.[21] The quantitative analysis of lipids extracted to the butanol phase was carried out by phosphorimaging in a StormTM imaging system (GE Healthcare) or PMA staining and analysis performed using Image Quant TL. **1** was added in molar ratios of 0.5 to 2 with regard to $C_{55}P$.

In vitro PGN synthesis reactions using purified proteins and substrates

The synthesis of lipid II-Gly_1 catalyzed by FemX was performed in a 100 µl reaction containing 1 nmol lipid II, 2 mM ATP, 25 µg tRNA, 0.1 mM glycine, 50 nmol [^{14}C]glycine in 100 mM Tris-HCl, 20 mM $MgCl_2$, 0.8 % Triton X-100, at pH 7.5 with 2.7 µg FemX and 10 µg GlyS. The reaction mixtures were incubated for 30 min at 30°C.
The lipid IV_{WTA} synthesis reaction was determined by incubating 2 nmol of lipid III_{WTA} in 200 mM Tris-HCl, 0.2 % Triton X-100, 100 mM NaCl, and 1 mM UDP-GlcNAc, at pH 7.5 in 50 µL. The reaction was initiated by the addition of 3 µg of TarA-His_6 and 1 µg MnaA-His_6 and incubated for 4 h at 30 °C.
Dephosphorylation of $C_{55}PP$ was determined using purified *S. aureus* YbjG-His_6 enzyme. 20 nmol of $C_{55}PP$ were incubated with 3 µg of YbjG-His_6 in 20 mM Tris-HCl, 150 mM NaCl, and 0.8 % Triton X-100 at pH 7.5 in 50 µL for 30 min at 37 °C.
In all *in vitro* assays, **1** was added in molar ratios from 0.5 to 2 with respect to the respective substrate. $C_{55}P$-containing products were extracted, analyzed by TLC and quantified as described above. Experiments were performed at least three times.

*Complex formation of **1***

Binding of **1** to $C_{55}P$, $C_{55}PP$, lipid I, lipid II, and lipid III_{WTA} was analyzed by incubating 2 nmol (5 nmol for $C_{20}PP$ and $C_{55}PP$) of each cell wall precursor with 1 to 4 nmol (2.5 to 10 nmol) of **1** in 50 mM Tris-HCl, at pH 7.5 for 30 min at RT. Complex formation was analyzed by extracting unbound precursors from the reaction mixture followed by TLC analysis as described above. Experiments were performed with biological replicates.

Antagonization assays

Antagonization of the antibiotic activity of **1** and teixobactin by potential target molecules was performed by an MIC-based setup in microtiter plates. Both antibiotics (4× MIC) were mixed with HPLC-purified antagonists ($C_{20}P$, $C_{55}P$, $C_{20}PP$, $C_{55}PP$, lipid I, lipid II, lipid III_{WTA}, and DOPG) in 0.00156 to 16-fold molar excess with respect to the antibiotic. *S. aureus* SG511 (5×10^5 CFU ml^{-1}) was added and samples were examined for visible bacterial growth after incubation overnight. Experiments were performed with biological replicates.

Mammalian cytotoxicity

Cytotoxicity of **1** on human epithelial type 2 (HEp-2) cells (ATCC® CCL-23™) was measured by using the non-fluorescent resazurin-based alamarBlue™ cell viability reagent (Invitrogen) which is converted into fluorescent resorufin by living cells. HEp-2 cells were seeded at a density of 5×10^4 cells per well in 96-well flat base TC plates (Sarstedt), and incubated in Dulbecco's modified Eagle's medium (DMEM, Gibco) supplemented with 1× MEM non-essential amino acids (Gibco) and 1× MEM vitamin solution (Gibco) in an atmosphere of 5 % CO_2 at 37 °C. After 48 h, the culture was treated with **1** at serially diluted concentrations ranging from 1 to 128 µg/ml. After another incubation for 30 h, medium was removed and the cell monolayer was washed twice with Hank's balanced salt solution (HBSS, Gibco). To indicate cell viability, alamarBlue™ reagent was added to a final concentration of 10 % (v/v) and cells were incubated for 1 h at 37 °C and 5 % CO_2. Fluorescence measurements (570 nm excitation and 585 nm emission) were performed in black F-bottom microplates (FLUOTRAC, Greiner) with a microplate reader Spark 10M (Tecan). Relative cell viability was calculated as the percentage of untreated cells (set 100 %).

SUPPORTING INFORMATION

Red blood cell lysis assay

1 and teixobactin were serially diluted in phosphate buffered saline (PBS) in 96-well U-shaped plates (Greiner) at concentrations ranging from 1 to 128 µg/ml. Human red blood cells (RBCs) were washed three times with PBS immediately prior to addition of RBCs to the wells at a final concentration of 2.5 % RBC per well. After 6, 17, or 30 h of incubation in an atmosphere of 5 % CO_2 at 37°C, RBCs were pelleted by centrifugation (1500 × *g* for 10 min). Supernatants were diluted 5-fold in PBS in a new 96-well plate, and absorbance of the heme was measured at 405 nm in a microplate reader Spark 10M (Tecan). Relative hemolysis was calculated as the percentage of RBCs treated with 1 % (v/v) Triton X-100 (set 100 %).

Serial passaging

S. aureus SG511 was serially passaged in the presence of sub-MIC concentrations of **1** over a period of 30 days. Cells were incubated at 37 °C with agitation and passaged at 24 h intervals in the presence of **1** at subinhibitory concentration. The well containing bacterial suspension at the **1** concentration corresponding to 0.5× MIC was used as the inoculum for the second passage. For each passage, MICs were determined as described for *Antibiotic susceptibility testing*.

WILEY-VCH

SUPPORTING INFORMATION

Results and Discussion

Structural analysis of 1

Hypeptin (1): white, solid; $[\alpha]^{25}_{D}$ −14.5 (*c* 0.2, MeOH); UV (MeOH) λ_{max} (ε) 227 (8170), 289 (1800), 303 (1590) nm; IR (ATR) ν_{max} 3279, 1660, 1651, 1519, 1454, 1199, 1135, 839, 799, 721 cm^{-1}; ^{1}H NMR and ^{13}C NMR data, see Table S2; MALDIMS *m*/*z* 1022.489 $[M+H]^{+}$ (calcd for $C_{44}H_{72}N_{13}O_{15}$, 1022.527).

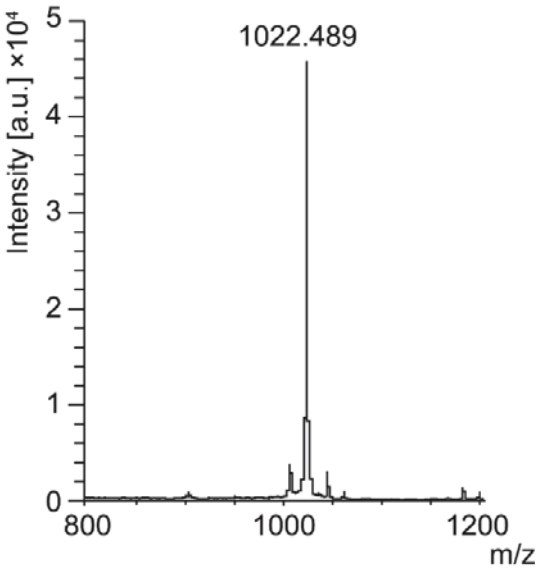

Figure S1. MALDI MS spectrum of **1**.

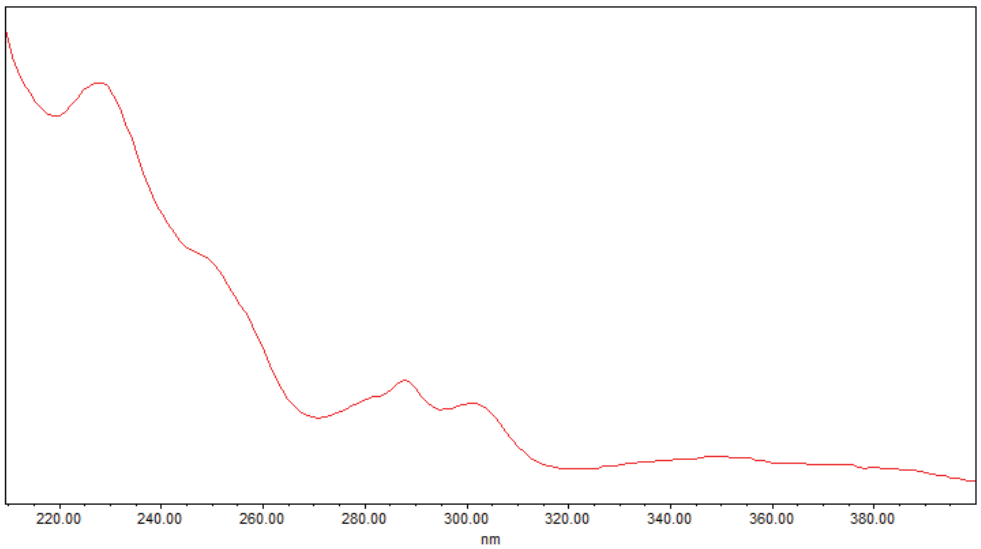

Figure S2. UV spectrum of **1** in MeOH.

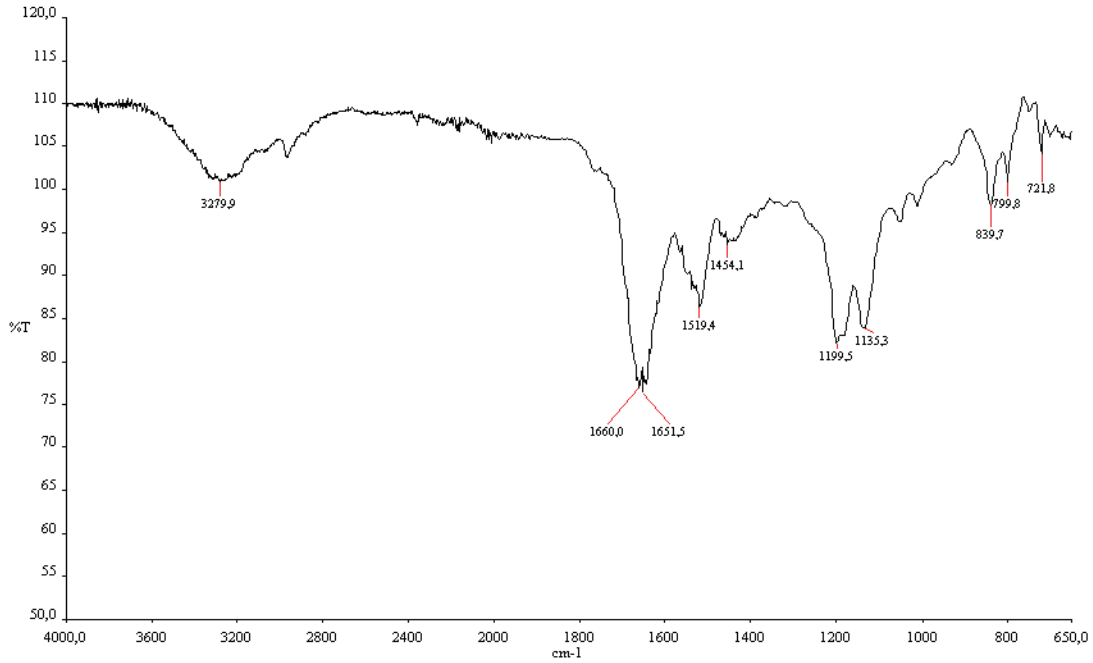

Figure S3. FT-IR spectrum of **1**.

SUPPORTING INFORMATION

Table S2. ^{1}H and ^{13}C NMR spectroscopic data of **1** (see Supplementary Figures S4-S11) in DMSO-d_6 at 40 °C (^{1}H: 600 MHz; ^{13}C: 150 MHz).

	C/H no.	δ_H (*J* in Hz)[a]	δ_C[a]	HMBC	ROESY
Ala	1		169.4, C		
	2	3.99, m	48.6, CH		3, NH_2-2, NH-5
	3	1.41, d (7.1)	16.9, CH_3		2, NH_2-2, NH-5
	NH_2-2	8.10, m		1	2, 3
Leu	4		171.1, C		
	5	4.40, m	51.3, CH	1, 4	6a/b, 8, NH-5, NH-11
	6	a: 1.55, m	40.3, CH_2		
		b: 1.69, m			
	7	1.63, m	24.4, CH		
	8	0.89, d (6.4)	20.8, CH_3		
	9	0.92, d (6.4)	23.0, CH_3		
	NH-5	8.67, d (8.0)		1	2, 3, 5, NH-11, NH-17
Arg	10	-	171.2, C		
	11	4.44, q (7.6)	55.2, CH	4, 10	12a/b, 13, 14, NH-11
	12	a: 1.70, m	28.9, CH_2		
		b: 1.93, m			
	13	1.55, m	24.5, CH_2		
	14	3.11, m	40.2, CH_2		13, NH-15
	15		156.7, C		
	NH-11	8.11, m		4	5, 12a, 13, NH-5
	NH-15	7.61, brs			
Has	16	-	169.0, C		
	17	4.82, dd (3.5, 10.0)	56.3, CH	10, 16, 19	18, NH-17
	18	4.36, m	72.3, CH	16, 19	17
	19	-	173.5, C		
	OH-18	6.25, brs			
	NH-17	8.16, d (10.0)			11, 17
	NH_2-19	a: 7.37, brs			NH-19b
		b: 7.62, brs			NH-19a
Has	20	-	167.6, C		
	21	5,13, dd (2.5, 10.0)	53.6, CH	16, 20	22, NH-21, NH_2-23, NH-37
	22	5.40, d (2.5)	72.7, CH	20, 23, 24	21, NH-21, NH_2-23
	23	-	168.6, C		
	NH-21	8.15, d (10.0)		16	21, NH-37
	NH_2-23	a: 7.18, brs			NH-23b
		b: 7.69, brs			NH-23a
Ile	24	-	168.7, C		
	25	4.14, t (9.6)	56.6, CH	24, 30	26, 27a/b, 28, 29, NH-25
	26	1.95, m	36.0, CH		
	27	a: 1.18, m	24.4, CH_2		
		b: 1.55, m			
	28	0.80, t (7.5)	10.0, CH_3		25, 26
	29	0.89, d (6.7)	14.9, CH_3		25, 26
	NH-25	8.02, d (9.6)		30	25, 26, 32, NH-31
Hle	30		169.6, C		
	31	4.34, dd (6.4, 10.4)	57.7, CH	30, 36	32,33,34,35, NH-25, NH-31
	32	3.58, m	75.1, CH		31, 33, 34, 35
	33	1.60, m	30.4, CH		
	34	0.71, d (6.7)	19.3, CH_3		31, 32, 33, 35
	35	0.92, d (6.4)	17.1, CH_3		31, 32, 34
	OH-32	5.77, brs			
	NH-31	8.33, brs		36	31, 32, 33, 38, NH-25
Hty	36	-	168.8, C		
	37	4.23, t (7.2)	63.3, CH	20, 36	38, 40, NH-37
	38	4.80, d (7.2)	71.6, CH	36	33, 35, 37, 40, 44
	39		130.8, C		
	40	7.12, d (8.2)	127.8, CH		33, 34, 35, 37, 38, 41
	41	6.63, d (8.2)	114.4, CH		34, 40
	42		156.5, C		
	43	6.63, d (8.2)	114.4, CH		44
	44	7.12, d (8.2)	127.8, CH		43
	OH-38	6.25, brs			
	OH-42	9.20, brs			
	NH-37	8.32, d (7.2)		20	21, 37, 38, 44, NH-21

[a] assignments are based on extensive 1D and 2D NMR measurements (HMBC, HSQC, COSY)

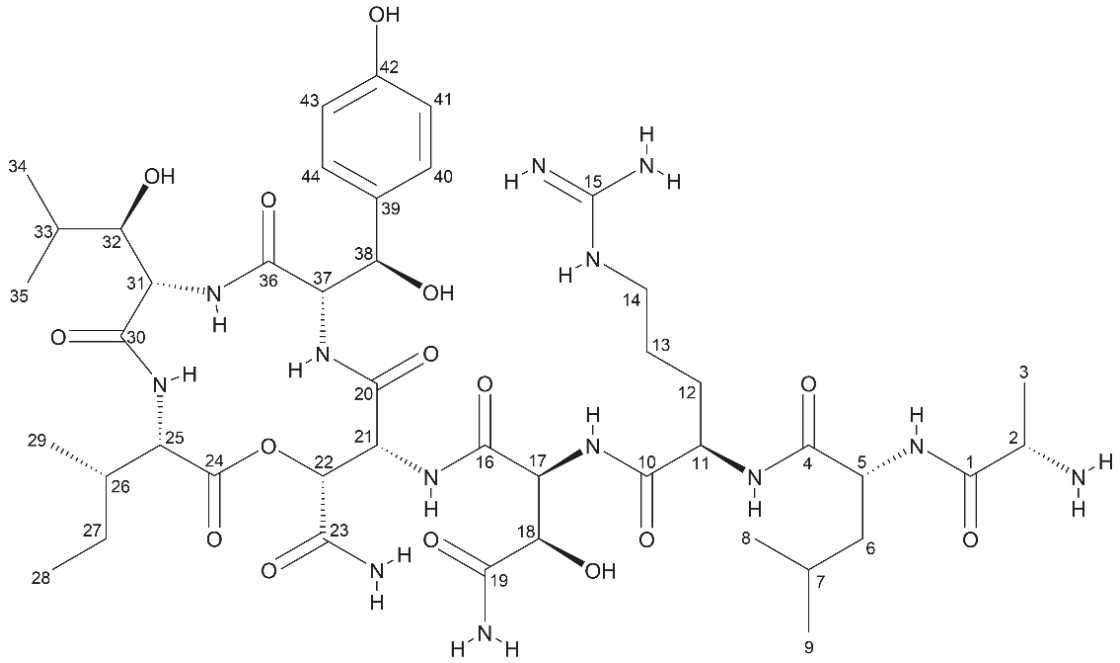

Figure S4. Chemical structure of **1**. Carbon atoms are numbered.

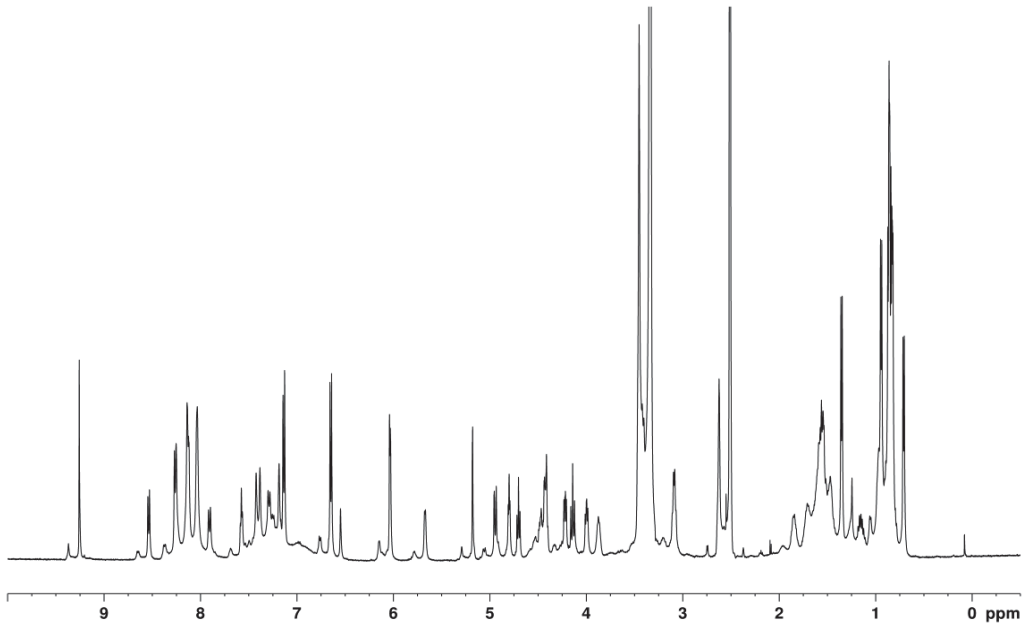

Figure S5. ^{1}H NMR spectrum of **1** in DMSO-d_6 (700 MHz).

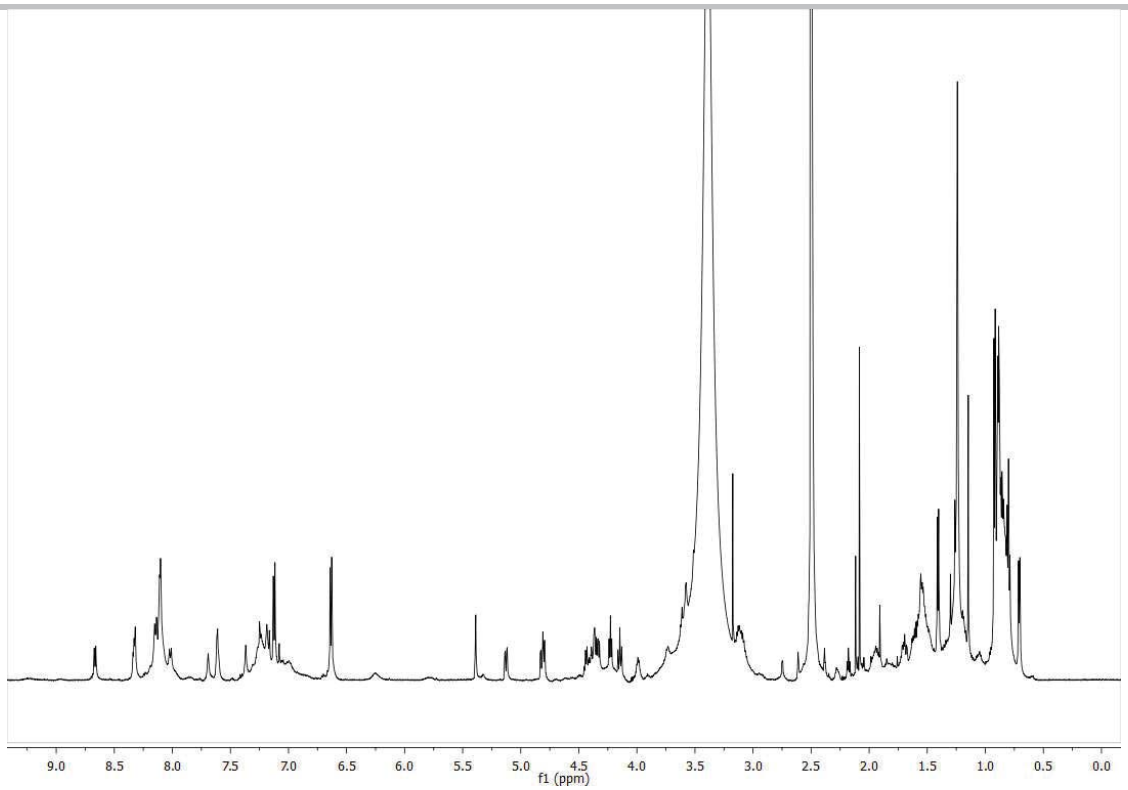

Figure S6. ^{1}H NMR spectrum of **1** in DMSO-d_6 (600 MHz, 40 °C).

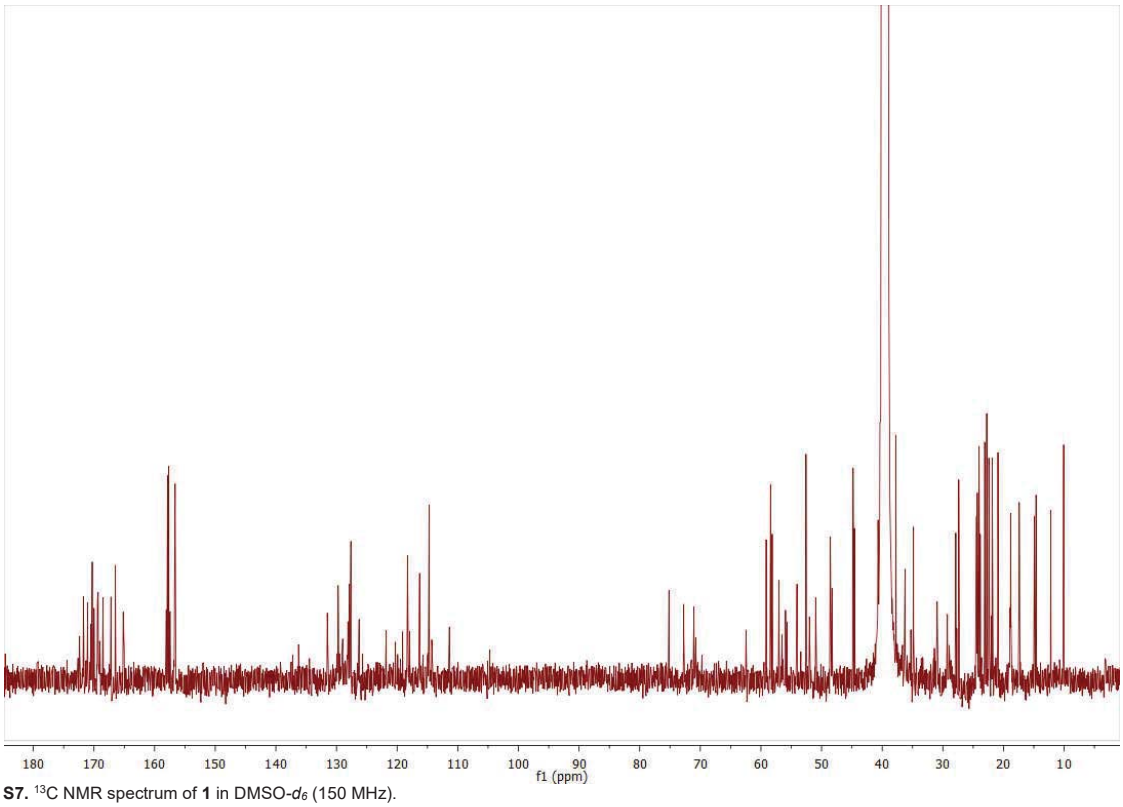

Figure S7. ^{13}C NMR spectrum of **1** in DMSO-d_6 (150 MHz).

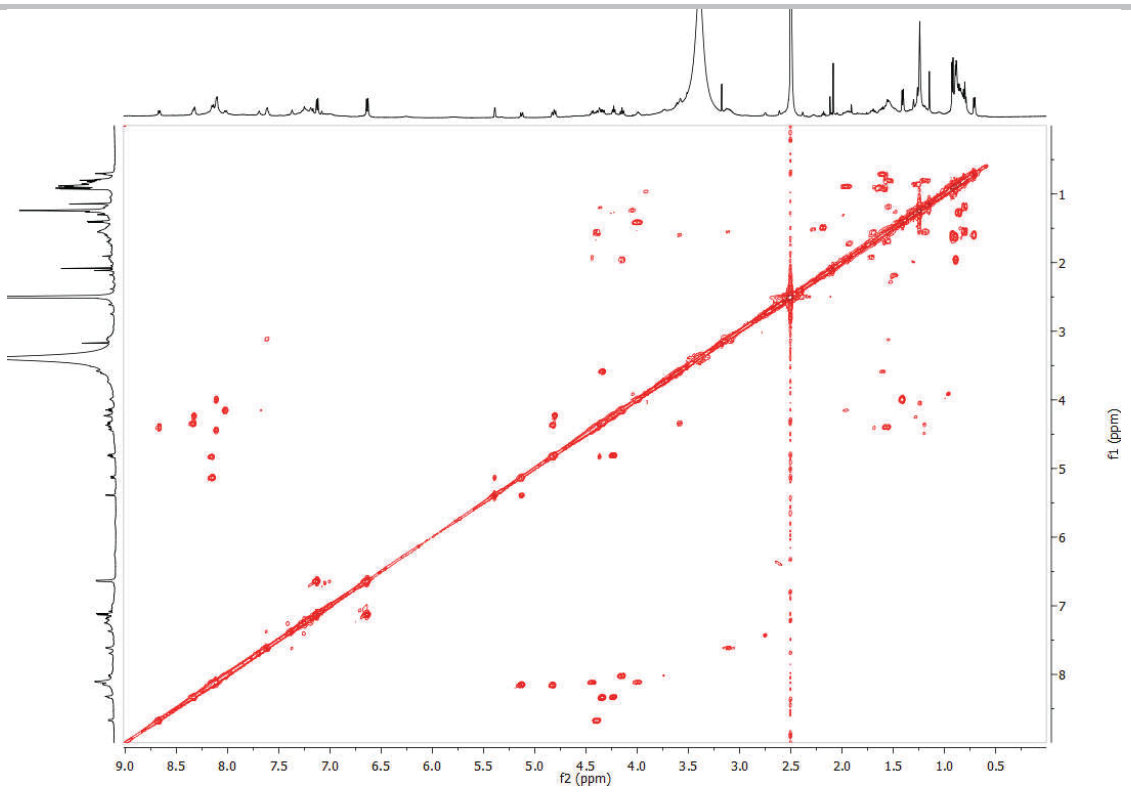

Figure S8. ^{1}H-^{1}H COSY spectrum of **1** in DMSO-d_6 (600 MHz).

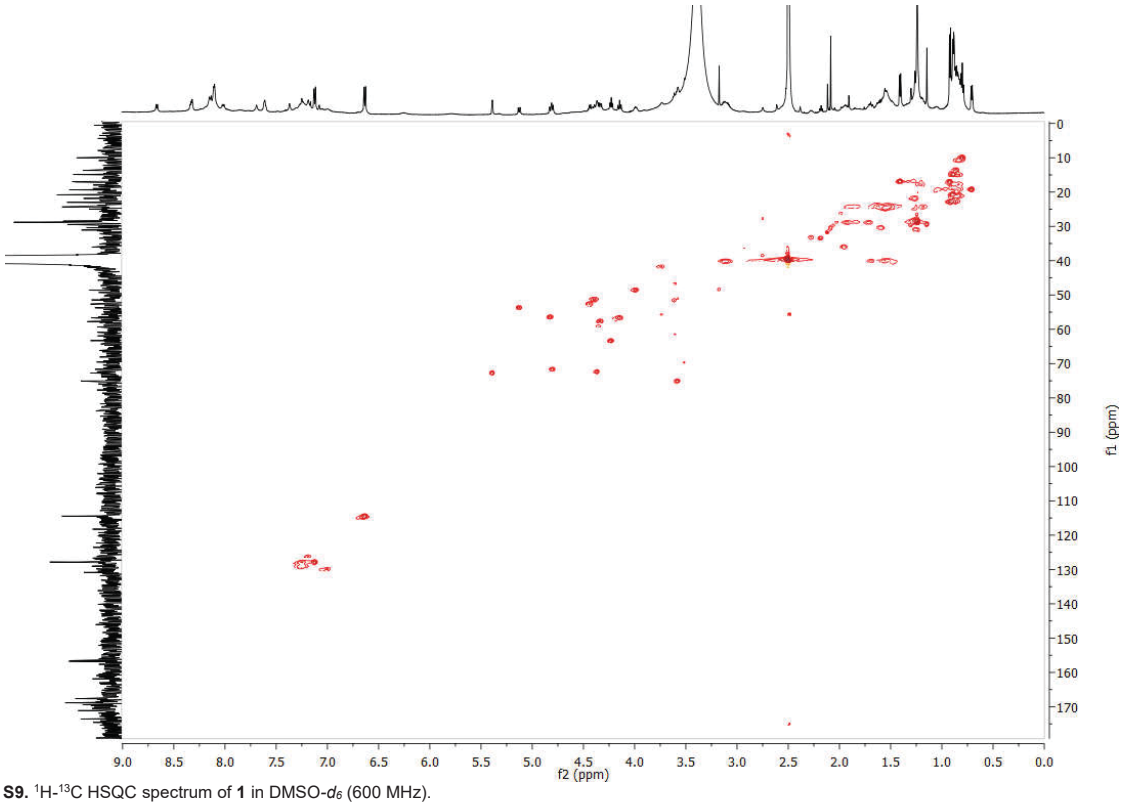

Figure S9. ^{1}H-^{13}C HSQC spectrum of **1** in DMSO-d_6 (600 MHz).

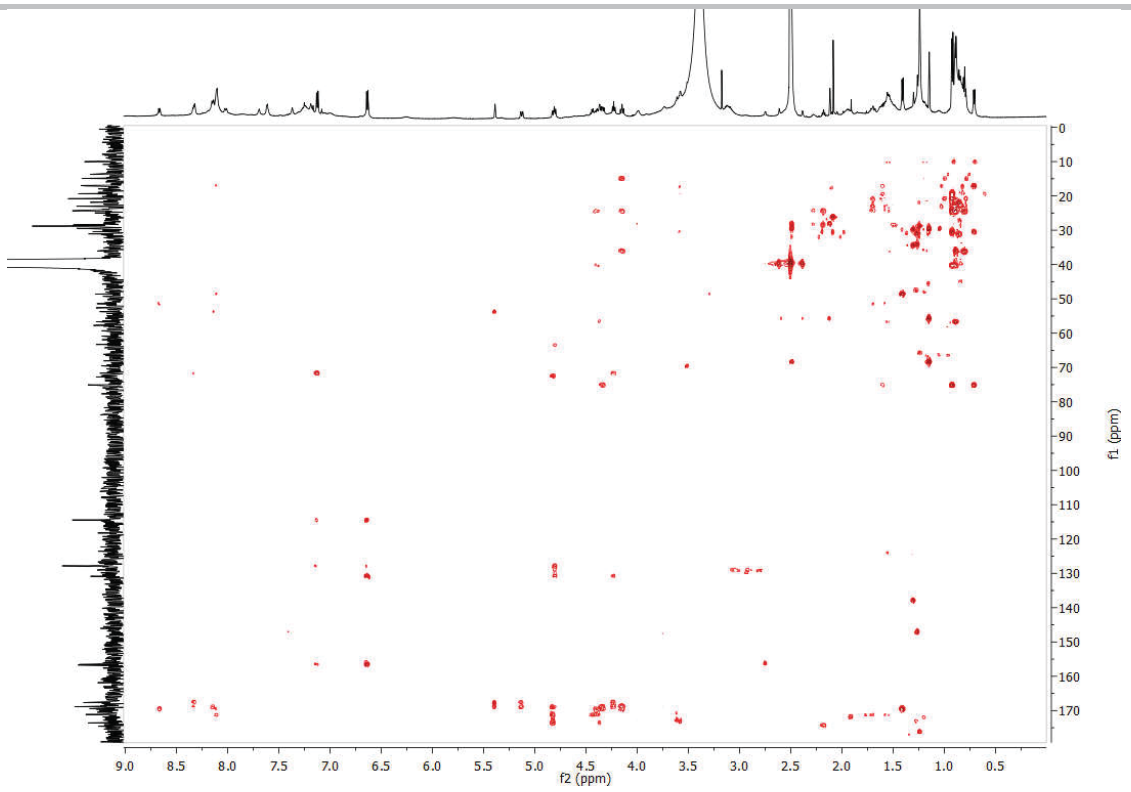

Figure S10. ^{1}H-^{13}C HMBC spectrum of **1** in DMSO-d_6 (600 MHz).

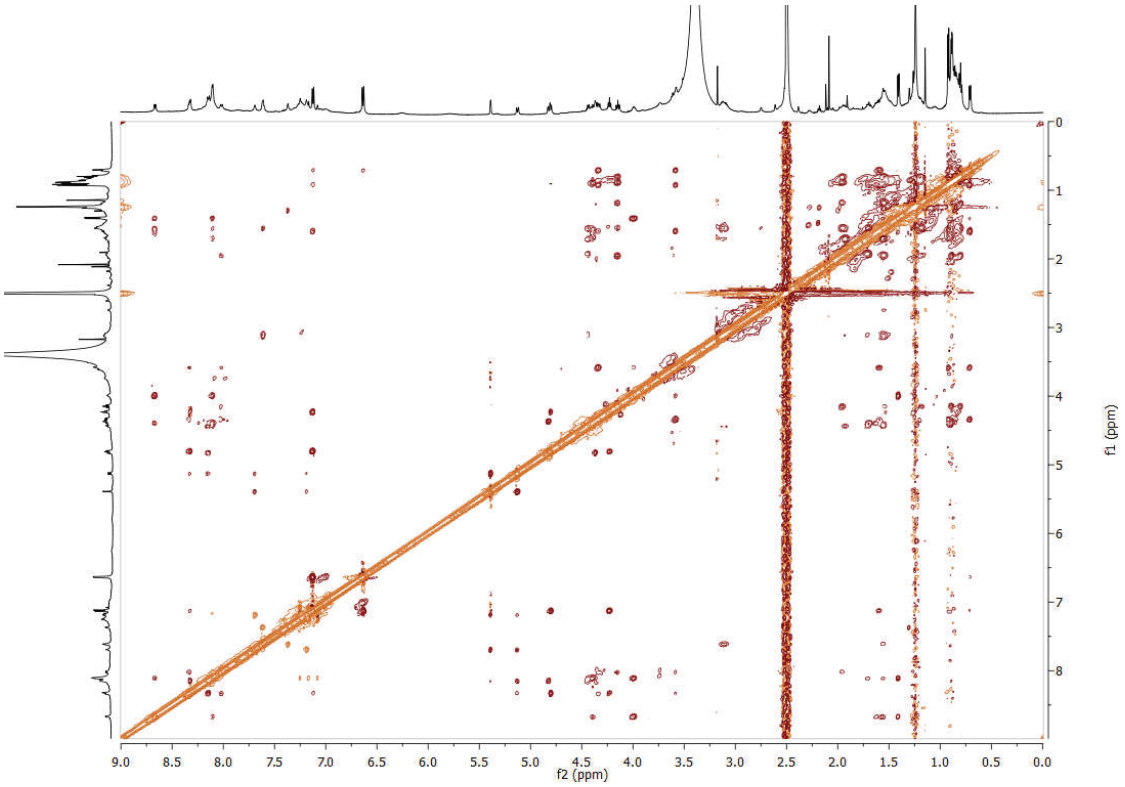

Figure S11. ^{1}H-^{1}H ROESY spectrum of **1** in DMSO-d_6 (600 MHz).

SUPPORTING INFORMATION

Biosynthesis of 1

Table S3. Top BLAST hits of the single genes of the *hyn* BGC (NCBI Accession Number BankIt2428365 MW759775).

Name	Size (aa)	Annotated function	Closest homologue (identity [%])	Accession No. of the homologue
HynA	6491	NRPS	Amino acid adenylation domain-containing protein [*Lysobacter psychrotolerans. ZS60*] (80)	WP_123088455.1
HynB	2447	NRPS	Non-ribosomal peptide synthetase [*Lysobacter psychrotolerans ZS60*] (82)	WP_123088454.1
HynC	531	Non-heme diiron monooxygenase	MBL fold metallo hydrolase [*Lysobacter psychrotolerans ZS60*] (92)	WP_123088453.1
HynD	608	ABC-transporter related protein	ATP-binding cassette domain-containing protein [*Lysobacter psychrotolerans ZS60*] (81)	WP_148041022.1
HynE	302	α-ketoglutarate dependent oxygenase	TauD/TfdA family dioxygenase [*Lysobacter psychrotolerans ZS60*] (83)	WP_123088451.1
HynF	401	RND family efflux transporter MFP subunit	Efflux RND transporter periplasmic adaptor subunit [*Lysobacter psychrotolerans ZS60*] (72)	WP_123088450.1
HynG	1028	AcrB/AcrD/AcrF family protein	Efflux RND permease subunit [*Lysobacter psychrotolerans ZS60*] (80)	WP_123088449.1

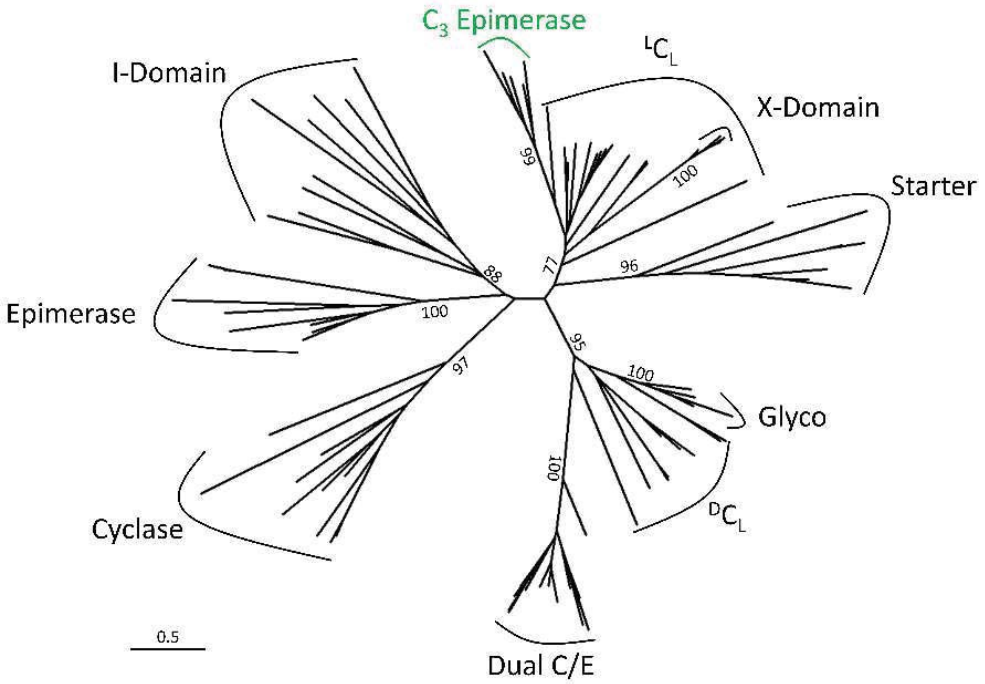

Figure S12. Phylogenetic tree of C domains from different datasets. The domains cluster depending on the specified function. $HynA_5C_2$ and homologues thereof form a new, distinct clade within the $^{L}C_L$ domains and probably catalyse C_3-epimerization (green). Bootstrap values indicate the distinctness of clades. The scale bar represents 50 substitutions per 100 amino acids.

SUPPORTING INFORMATION

Table S4. Accession numbers and source organisms of protein sequences used for phylogenetic analysis of C domains (Figure S12). If possible, accession numbers from Rausch et al.[5] were updated to NCBI nonredundant RefSeq (WP_).

Accession	Organism	Domain family	Ref.
WP_010924520.1	*Mycobacterium tuberculosis*	Cyclase	[5]
WP_010935625.1	*Corynebacterium diphtheriae*	Cyclase	[5]
WP_010949506.1	*Mycobacterium avium*	Cyclase	[5]
WP_002211388.1	*Yersinia pestis* CO92	Cyclase	[5]
WP_126987576.1	*Nostoc sp.* PCC 7120 = FACHB-418	Cyclase	[5]
CUV45544.1	*Ralstonia solanacearum*	Cyclase	[5]
WP_011030913.1	*Streptomyces coelicolor* A3(2)	Cyclase	[5]
AAN80883.1	*Escherichia coli* CFT073	Cyclase	[5]
WP_011146562.1	*Photorhabdus laumondii subsp. laumondii*	Cyclase	[5]
WP_011168195.1	*Pseudomonas savastanoi pv. phaseolicola*	Cyclase	[5]
WP_010895613.1	*Pseudomonas aeruginosa*	$^{D}C_{L}$	[5]
WP_010949130.1	*Mycobacterium avium subsp. paratuberculosis*	$^{D}C_{L}$	[5]
WP_011198677.1	*Bacillus cereus* E33L	$^{D}C_{L}$	[5]
WP_010949191.1	*Mycobacterium avium subsp. paratuberculosis*	$^{D}C_{L}$	[5]
WP_010954996.1	*Pseudomonas putida*	$^{D}C_{L}$	[5]
WP_011062374.1	*Pseudomonas protegens*	$^{D}C_{L}$	[5]
WP_011103865.1	*Pseudomonas syringae pv. tomato*	$^{D}C_{L}$	[5]
AAP09419	*Bacillus cereus* ATCC 14579	$^{D}C_{L}$	[5]
AAZ34524.1	*Pseudomonas savastanoi pv. phaseolicola* 1448A	$^{D}C_{L}$	[5]
CAD17793.1	*Ralstonia solanacearum* GMI1000	Dual C/E	[5]
WP_011060446.1	*Pseudomonas protegens*	Dual C/E	[5]
AND87649.1	*Bradyrhizobium diazoefficiens* USDA 110	Dual C/E	[5]
WP_011093070.1	*Pectobacterium atrosepticum* SCRI1043	Dual C/E	[5]
WP_011105127.1	*Pseudomonas syringae pv. tomato*	Dual C/E	[5]
WP_011136349.1	*Chromobacterium violaceum*	Dual C/E	[5]
WP_011146892.1	*Photorhabdus laumondii subsp. laumondii*	Dual C/E	[5]
WP_011204623.1	*Burkholderia mallei*	Dual C/E	[5]
WP_011205654.1	*Burkholderia pseudomallei* K96243	Dual C/E	[5]
WP_011104220.1	*Pseudomonas syringae pv. tomato*	Dual C/E	[5]
$HynA_3C$	*Lysobacter sp.* K5869	Dual C/E	[5]
$HynA_4C$	*Lysobacter sp.* K5869	Dual C/E	[5]
$HynA_6C$	*Lysobacter sp.* K5869	Dual C/E	[5]
WP_003916032.1	*Mycobacterium tuberculosis*	Epimerase	[5]
WP_010895613.1	*Pseudomonas aeruginosa*	Epimerase	[5]
WP_003412267.1	*Mycobacterium tuberculosis*	Epimerase	[5]
WP_010949130.1	*Mycobacterium avium subsp. paratuberculosis*	Epimerase	[5]
WP_010950704.1	*Mycobacterium tuberculosis variant bovis*	Epimerase	[5]
WP_010954975.1	*Pseudomonas putida*	Epimerase	[5]
NP_534179.1	*Agrobacterium tumefaciens* C58	Epimerase	[5]
WP_011062374.1	*Pseudomonas protegens*	Epimerase	[5]
AAP09415.1	*Bacillus cereus* ATCC 14579	Epimerase	[5]
AAQ59905.1	*Chromobacterium violaceum* ATCC 12472	Epimerase	[5]
AAM80537.1	*Streptomyces toyocaensis*	Glyco $^{L}C_{L}$	[5]
Q93N88	*Streptomyces lavendulae*	Glyco $^{L}C_{L}$	[5]
Q93N87	*Streptomyces lavendulae*	Glyco $^{L}C_{L}$	[5]
Q8KLL4	*Streptomyces toyocaensis*	Glyco $^{L}C_{L}$	[5]
AJF34464.1	*Eleftheria terrae*	C_3-epimerase	[17]
AEH59100.1	*Lysobacter sp.* ATCC 53042	C_3-epimerase	[22]
PRX87872.1	*Pseudomonas sp.* NFACC11-2	C_3-epimerase	[23]
CCJ67648.1	*Janthinobacterium agaricidamnosum*	C_3-epimerase	[24]
$HynA_5C_2$	*Lysobacter sp.* K5869	C_3-epimerase	This work
CAQ71827.1	*Cupriavidus taiwanensis* LMG 19424	I domain	[6]
CAJ96471.1	*Cupriavidus necator* H16	I domain	[6]
WP_063365585.1	*Pseudoalteromonas luteoviolacae*	I domain	[6]
WP_063365570.1	*Pseudoalteromonas luteoviolacae*	I domain	[6]
WP_082236112.1	*Cupriavidus necator*	I domain	[6]
WP_052269209.1	*Alcanivorax pacificus*	I domain	[6]
WP_029293154.1	*Pseudomonas sp.* 06C 126	I domain	[6]
WP_053122086.1	*Pseudomonas thivervalensis*	I domain	[6]
WP_053122092.1	*Pseudomonas thivervalensis*	I domain	[6]
AJW67534.1	*Pseudomonas taiwanensis*	I domain	[6]
WP_011534377.1	*Pseudomonas entomophila*	I domain	[6]
WP_003400794.1	*Mycobacterium tuberculosis*	$^{L}C_{L}$	[5]
WP_010895611.1	*Pseudomonas aeruginosa*	$^{L}C_{L}$	[5]
WP_000605281.1	*Staphylococcus aureus subsp. aureus*	$^{L}C_{L}$	[5]
WP_010949130.1	*Mycobacterium avium subsp. paratuberculosis*	$^{L}C_{L}$	[5]
WP_010954974.1	*Pseudomonas putida*	$^{L}C_{L}$	[5]
WP_000605273.1	*Staphylococcus aureus subsp. aureus*	$^{L}C_{L}$	[5]
BAC70870.1	*Streptomyces avermitilis* MA-4680 = NBRC 14893	$^{L}C_{L}$	[5]
WP_010996798.1	*Nostoc sp.* PCC 7120 = FACHB-418	$^{L}C_{L}$	[5]
CAD17793.1	*Ralstonia solanacearum* GMI1000	$^{L}C_{L}$	[5]
WP_010973240.1	*Agrobacterium fabrum*	$^{L}C_{L}$	[5]
$HynA_2C$	*Lysobacter sp.* K5869	$^{L}C_{L}$	[5]
$HynA_5C_1$	*Lysobacter sp.* K5869	$^{L}C_{L}$	[5]
$HynB_7C$	*Lysobacter sp.* K5869	$^{L}C_{L}$	[5]
$HynB_8C$	*Lysobacter sp.* K5869	$^{L}C_{L}$	[5]

SUPPORTING INFORMATION

Table S4 (continuation). Accession numbers and source organisms of protein sequences used for phylogenetic analysis of C domains. If possible, accession numbers from Rausch et al.[5] were updated to NCBI nonredundant RefSeq (WP_).

Accession	Organism	Domain family	Ref.
WP_000077805.1	*Escherichia coli* K12	Starter	[5]
AAD56240.1	*Bacillus subtilis*	Starter	[5]
WP_003113143.1	*Pseudomonas aeruginosa*	Starter	[5]
WP_010949130.1	*Mycobacterium avium subsp. paratuberculosis*	Starter	[5]
BAC68313.1	*Streptomyces avermitilis* MA-4680 = NBRC 14893	Starter	[5]
WP_000194139.1	*Salmonella typhimurium*	Starter	[5]
WP_001133934.1	*Bacillus cereus*	Starter	[5]
AEI58867.1	*Amycolatopsis orientalis* HCCB10007	X domain	[25]
CAC48362.1	*Amycolatopsis balhimycina* DSM 5908	X domain	[25]
CAG15012.1	*Actinoplanes teichomyceticus*	X domain	[25]
CAD91211.1	*Nonomuraea gerenanesis*	X domain	[25]

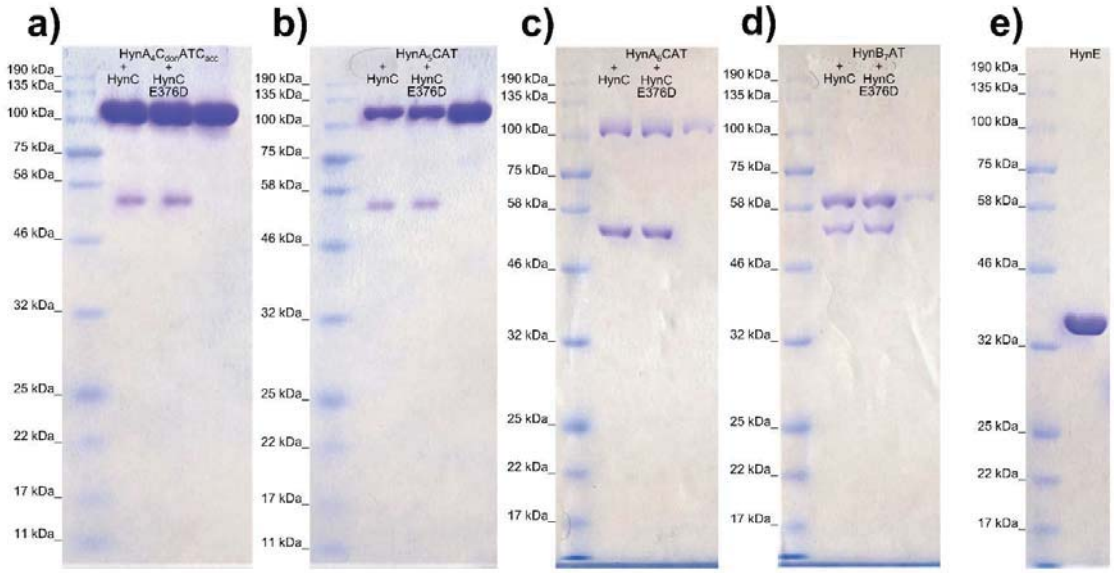

Figure S13. SDS-PAGEs of heterologously expressed enzymes. a) $HynA_4C_{acc}ATC_{don}$ (117.7 kDa) co-expressed with HynC (63.2 kDa), HynC E376D (63.7 kDa) and alone. b) $HynA_5CAT$ (122. kDa) co-expressed with HynC, HynC E376D and alone. c) $HynA_6CAT$ (117.5 kDa) co-expressed with HynC, HynC E376D and alone. d) $HynB_7AT$ (66.9 kDa) co-expressed with HynC, HynC E376D and alone. e) HynE (38.8 kDa).

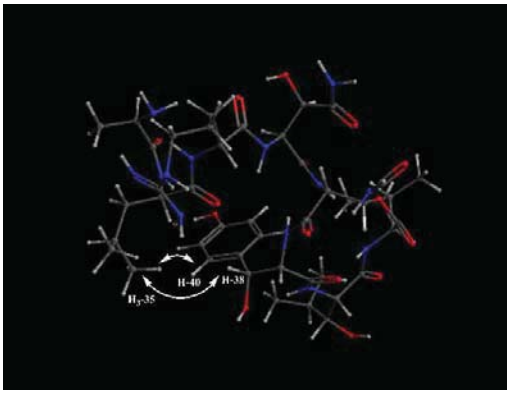

Figure S14. Conformation of **1**; white arrows indicate key ROESY correlations, supporting the (2*S*,3*R*) configuration of 3-Hydroxytyrosine, instead of (2*S*,3S).

Bioactivity of 1

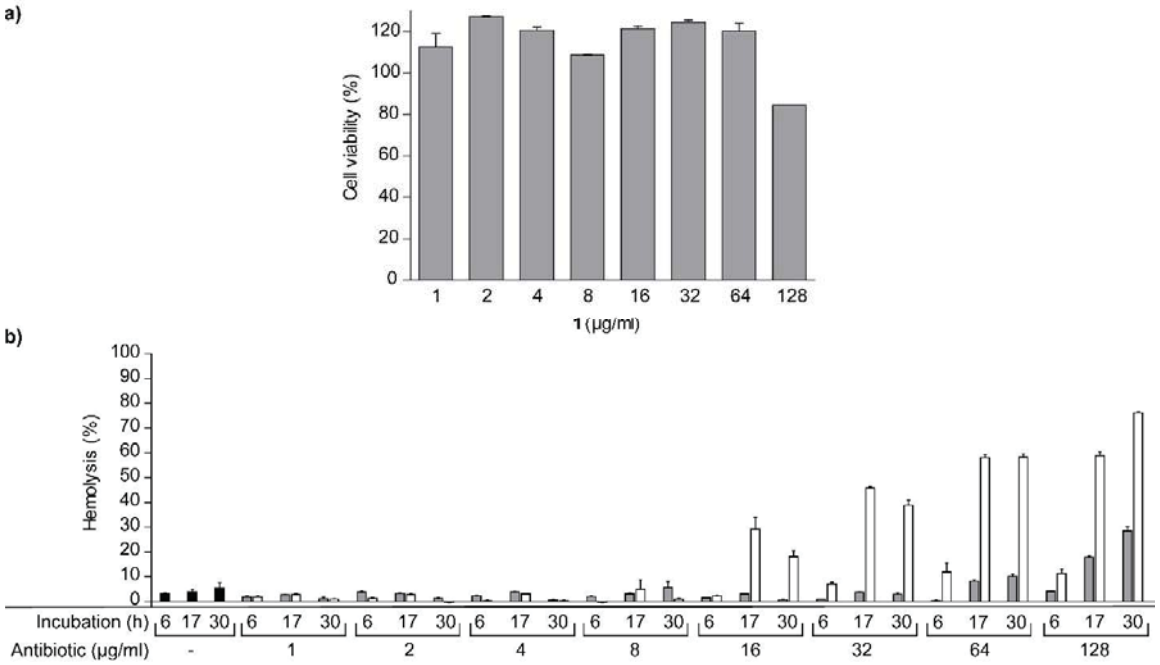

Figure S15. Cytotoxicity and hemolysis. a) Cytotoxicity of **1** against HEp-2 cells. HEp-2 cells were incubated with serially diluted concentrations of **1** for 30 h. Metabolically active cells reduced resazurin to resorufin and absorbance was measured. **1** did not show cytotoxic effects up to 64 µg/mL. b) Human RBC hemolysis following treatment with **1** (*grey bars*) and teixobactin (*white bars*) expressed relative to Triton X-100-induced RBC lysis (set 100 %). Cells left untreated are shown with *black bars*. RBCs were challenged with serially diluted concentrations of antibiotics for 6, 17, and 30 h, respectively. **1** exhibited low hemolytic activity towards RBCs and was inferior to teixobactin within the tested range up to 128 µg/ml. Error bars indicate ±standard deviation (*n* = 3).

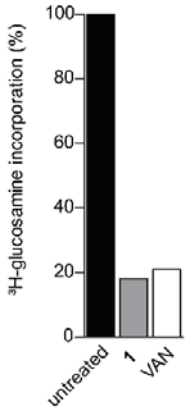

Figure S16. 1 (1× MIC, *grey bar*) inhibits incorporation of ^{3}H-glucosamine into the cell wall of *S. aureus* cells. Vancomycin (10× MIC) was used as control (*white bar*). The untreated control is shown as *black bar*.

WILEY-VCH

SUPPORTING INFORMATION

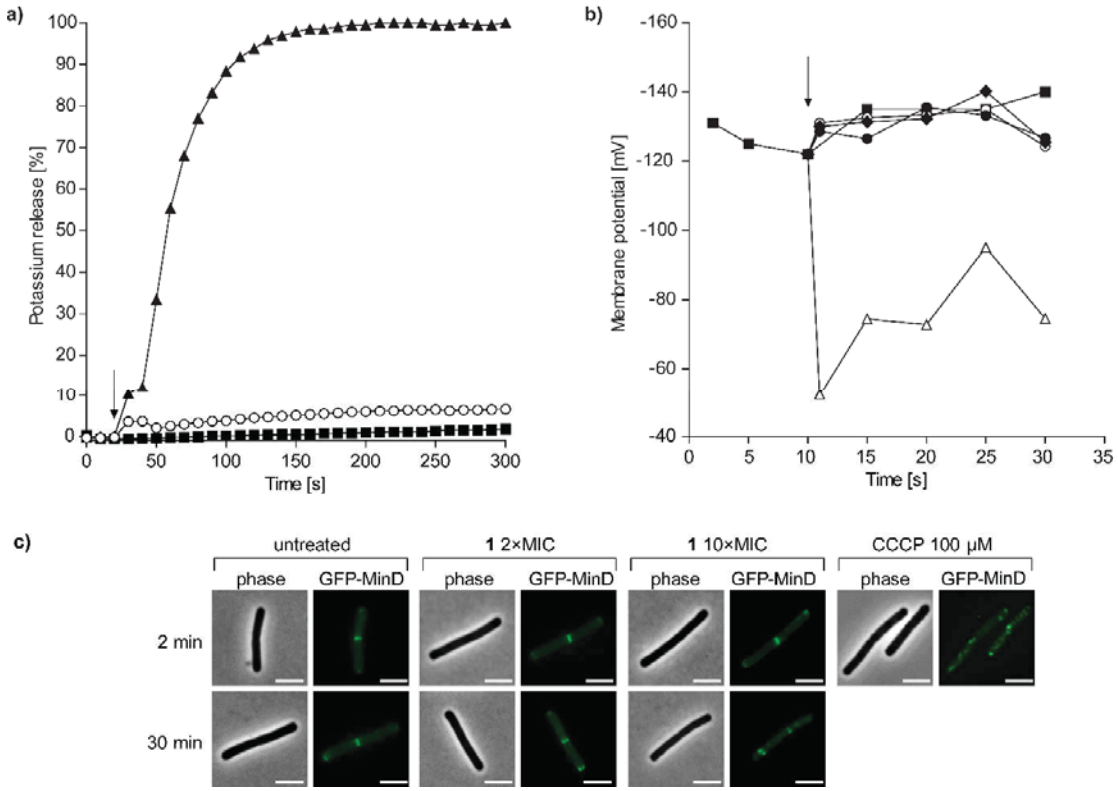

Figure S17. Impact of **1** on membrane potential a) **1** (1× MIC, *open circles*) is unable to form pores in the cytoplasmic membrane of *S. simulans* 22. Potassium efflux from living cells was monitored with a potassium-sensitive electrode. Ion leakage is expressed relative to the total amount of potassium released after addition of 1 µM pore-forming lantibiotic nisin (100 %, *triangles*). b) **1** does not affect membrane integrity or membrane potential. **1** shows no influence on the membrane potential of *S. simulans* 22 compared to the ionophore carbonyl cyanide *m*-chlorophenylhydrazone (CCCP, *open triangles*). The membrane potential was calculated from the distribution of the lipophilic cation TPP^+ inside and outside the cells. **1** was added at 1× MIC (*open circles*), 2× MIC (*circles*), and 5× MIC (*diamonds*). Untreated cells (*squares*). Arrows indicate the time of antibiotic or CCCP addition, respectively. c) Fluorescence microscopy revealed that **1** does not induce delocalization of membrane-potential driven GFP-MinD in early exponential phase cultures of *B. subtilis*. The ionophore CCCP was used as positive control. Scale bar = 5 µm.

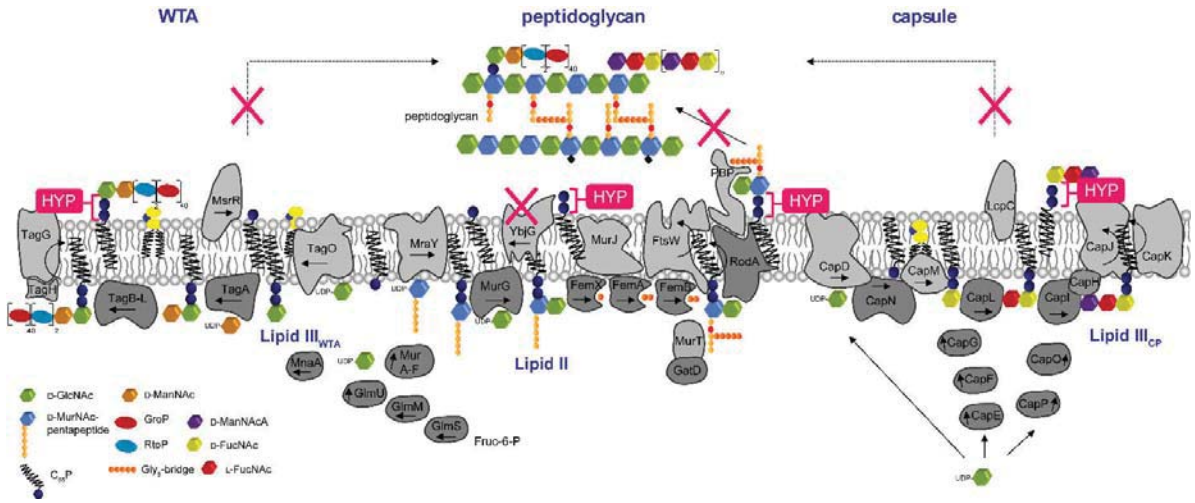

Figure S18. Cell wall biosynthesis network of *S. aureus*. Building up a vital cell wall requires the precise spatio-temporal coordination of multienzyme machineries of peptidoglycan, wall teichoic acid (WTA) and capsule biosynthesis, that consume intimately shared precursors, such as $C_{55}P$. Hypeptin (pink) interferes with these processes by binding to $C_{55}PP$-containing precursors. HYP, hypeptin; WTA, wall teichoic acid; CP, capsular polysaccharide; GlcNAc, *N*-acetyl-glucosamine; MurNAc, *N*-acetyl-muramic acid; ManNAc, *N*-acetyl-mannosamine; ManNAcA, *N*-acetyl-mannosaminuronic acid; FucNAc, *N*-acetyl-fucosamine; GroP, glycerol phosphate; RtoP, ribitol phosphate; Gly_5, pentaglycine; UDP, uridine-5'-diphosphate; Fruc-6-P, fructose-6-phosphate.

WILEY-VCH

SUPPORTING INFORMATION

Table S5. Antagonization of the antimicrobial activity of **1** and teixobactin by cell wall precursors. *S. aureus* was incubated with **1**, TEIX and VAN at 8× MIC in nutrient broth in microtiter plates, and growth was measured after a 24 h incubation at 37 °C. Putative HPLC-purified antagonists (undecaprenyl-phosphate [$C_{55}P$], geranylgeranyl-phosphate [$C_{20}P$], geranylgeranyl-pyrophosphate [$C_{20}PP$], undecaprenyl-pyrophosphate [$C_{55}PP$], lipid I, lipid II, and lipid III_{WTA}) and 1,2-dioleoyl-sn-glycero-3-phospho-glycerol (DOPG) were added in a fivefold molar excess with respect to the antibiotic. Experiments were performed with biological replicates. + antagonization; - no antagonization.

	Molar ratio lipid : antibiotic		
Lipid	**1**	**TEIX**	**VAN**
$C_{20}P$	–	–	–
$C_{55}P$	–	–	–
$C_{20}PP$	+ (4:1)	+ (4:1)	–
$C_{55}PP$	+ (4:1)	+ (4:1)	–
lipid I	+ (1:1)	+ (1:1)	+ (1:1)
lipid II	+ (1:1)	+ (1:1)	+ (1:1)
lipid III_{WTA}	+ (1:1)	+ (1:1)	–
DOPG	–	–	–

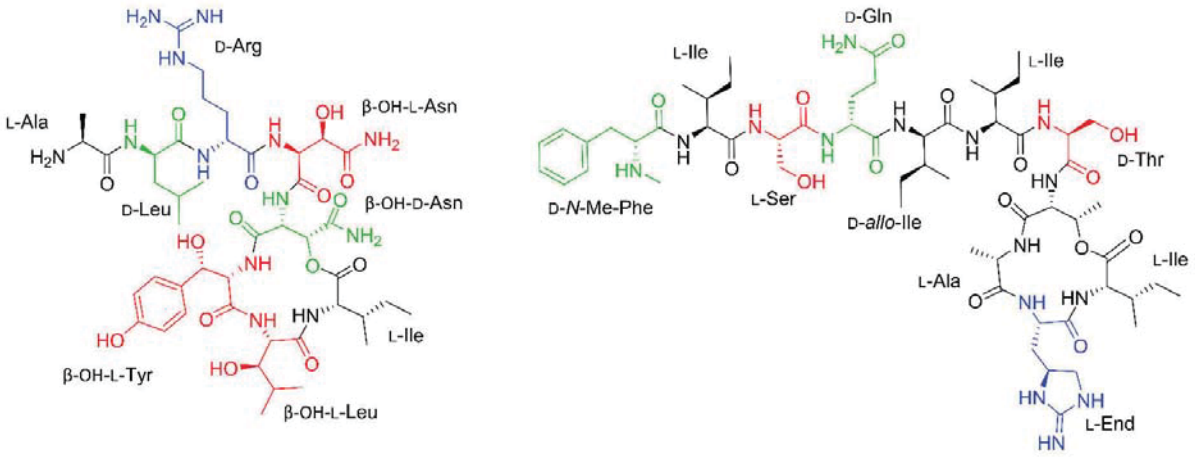

Figure S19. Structural comparison of **1** (left) with teixobactin (right). Both antibiotics are cyclodepsipeptides, consisting of guanidine amino acids (blue), β-hydroxy amino acids (red), D-configurated amino acids (green), and branched aliphatic amino acids. Adapted from Nussbaum and Süssmuth.[26]

SUPPORTING INFORMATION

References

[1] E. Gavrish, C. S. Sit, S. Cao, O. Kandror, A. Spoering, A. Peoples, L. Ling, A. Fetterman, D. Hughes, A. Bissell et al., *Chem Biol.* **2014**, *21*, 509.
[2] H. Harms, A. Klöckner, J. Schrör, M. Josten, S. Kehraus, M. Crüsemann, W. Hanke, T. Schneider, T. F. Schäberle, G. M. König, *Planta Med.* **2018**, *84*, 1363.
[3] D. G. Gibson, L. Young, R.-Y. Chuang, J. C. Venter, C. A. Hutchison, H. O. Smith, *Nat Methods.* **2009**, *6*, 343.
[4] V. V. Phelan, Y. Du, J. A. McLean, B. O. Bachmann, *Chem Biol.* **2009**, *16*, 473.
[5] C. Rausch, I. Hoof, T. Weber, W. Wohlleben, D. H. Huson, *BMC Evol. Biol.* **2007**, *7*, 78.
[6] Z. L. Reitz, C. D. Hardy, J. Suk, J. Bouvet, A. Butler, *Proc Natl Acad Sci U S A.* **2019**, *116*, 19805.
[7] S. Kumar, G. Stecher, M. Li, C. Knyaz, K. Tamura, *Mol Biol Evol.* **2018**, *35*, 1547.
[8] S. Tan, K. C. Ludwig, A. Müller, T. Schneider, J. R. Nodwell, *ACS Chem Biol* **2019**, *14*, 966.
[9] C. Freiberg, N. A. Brunner, G. Schiffer, T. Lampe, J. Pohlmann, M. Brands, M. Raabe, D. Häbich, K. Ziegelbauer, *J Biol Chem.* **2004**, *279*, 26066.
[10] T. Schneider, T. Kruse, R. Wimmer, I. Wiedemann, V. Sass, U. Pag, A. Jansen, A. K. Nielsen, P. H. Mygind, D. S. Raventós et al., *Science* **2010**, *328*, 1168.
[11] C. A. Schneider, W. S. Rasband, K. W. Eliceiri, *Nat Methods* **2012**, *9*, 671.
[12] a) A. Müller, M. Wenzel, H. Strahl, F. Grein, T. N. V. Saaki, B. Kohl, T. Siersma, J. E. Bandow, H.-G. Sahl, T. Schneider et al., *Proc Natl Acad Sci U S A.* **2016**, *113*, E7077-E7086; b) H. Strahl, L. W. Hamoen, *Proc Natl Acad Sci U S A.* **2010**, *107*, 12281.
[13] E. Ruhr, H. G. Sahl, *Antimicrob Agents Chemother.* **1985**, *27*, 841.
[14] D. S. Orlov, T. Nguyen, R. I. Lehrer, *J Microbiol Methods.* **2002**, *49*, 325.
[15] U. Kohlrausch, J. V. Höltje, *J Bacteriol.* **1991**, *173*, 3425.
[16] T. Schneider, K. Gries, M. Josten, I. Wiedemann, S. Pelzer, H. Labischinski, H.-G. Sahl, *Antimicrob. Agents Chemother.* **2009**, *53*, 1610.
[17] a) L. L. Ling, T. Schneider, A. J. Peoples, A. L. Spoering, I. Engels, B. P. Conlon, A. Mueller, T. F. Schäberle, D. E. Hughes, S. Epstein et al., *Nature.* **2015**, *517*, 455; b) A. Müller, H. Ulm, K. Reder-Christ, H.-G. Sahl, T. Schneider, *Microb Drug Resist.* **2012**, *18*, 261.
[18] G. Rouser, S. Fkeischer, A. Yamamoto, *Lipids.* **1970**, *5*, 494.
[19] a) J. N. Umbreit, J. L. Strominger, *J Bacteriol.* **1972**, *112*, 1306; b) H. Brötz, G. Bierbaum, K. Leopold, P. E. Reynolds, H. G. Sahl, *Antimicrob Agents Chemother.* **1998**, *42*, 154.
[20] P. D. Rick, G. L. Hubbard, M. Kitaoka, H. Nagaki, T. Kinoshita, S. Dowd, V. Simplaceanu, C. Ho, *Glycobiology.* **1998**, *8*, 557.
[21] T. Schneider, M. M. Senn, B. Berger-Bächi, A. Tossi, H.-G. Sahl, I. Wiedemann, *Mol Microbiol.* **2004**, *53*, 675.
[22] J. Hou, L. Robbel, M. A. Marahiel, *Chem Biol.* **2011**, *18*, 655.
[23] B. K. Scholz-Schroeder, J. D. Soule, D. C. Gross, *Mol Plant Microbe Interact.* **2003**, *16*, 271.
[24] K. Graupner, K. Scherlach, T. Bretschneider, G. Lackner, M. Roth, H. Gross, C. Hertweck, *Angew Chemie Int Ed. Engl.* **2012**, *51*, 13173.
[25] K. Haslinger, M. Peschke, C. Brieke, E. Maximowitsch, M. J. Cryle, *Nature.* **2015**, *521*, 105.
[26] F. von Nussbaum, R. D. Süssmuth, *Angew. Chem. Int Ed. Engl.* **2015**, *54*, 6684-6686.

Author Contributions

L.L.L., A.L.S, A.J.P, A.N. and K.L. isolated *Lysobacter sp.* K5869 and **1**;
D.A.W. performed all BCG cloning, in vitro experiments, and bioinformatic analyses under supervision of M.C.;
D.A.W. and P.B. assembled and analyzed the genome of *Lysobacter sp.* K5869.;
M.A., C.E.M. and M.J. optimized growth conditions and purified **1** under supervision of T.S., K.L., A.J.P. and L.L.L.;
P.B. characterized **1** under supervision of G.M.K.;
S.Ke. and D.A.W. elucidated the structure of **1**;
K.C.L., M.A., C.E.M. and A.M. performed mode of action analysis under supervision of T.S.;
S.Kr. performed cytotoxicity assays under supervision of B.H.;
The manuscript was written by T.S. and M.C. with contributions by all authors.

Chapter 4

A new antibiotic from an uncultured bacterium binds to an immutable target

Clovibactin is a teixobactin-like cyclodepsipeptide antibiotic with a shorter *N*-terminus, that was discovered from the previously unculturable soil-bacterium *Eleftheria terrae* ssp. *carolina*. The non-ribosomally synthesized octapeptide exhibits potent antibacterial activity against Gram-positive pathogens, including drug-resistant staphylococci, such as methicillin-resistant, vancomycin-intermediate, glycopeptide-intermediate, daptomycin-resistant and linezolid-resistant *Staphylococcus aureus*, as well as penicillin-resistant pneumococci, vancomycin-resistant enterococci, *Bacillus anthracis* and mycobacteria. The depsipeptide displayed low cytotoxicity and was efficious in a mouse infection model of *S. aureus*. Importantly, no resistant mutants of *S. aureus* could be generated *in vitro*.

Compared to teixobactin, clovibactin induced stronger lysis without any membrane disturbance involved. In search of a molecular target, whole-cell screens suggested that clovibactin interferes with late-stage peptidoglycan biosynthesis reactions. Corroborating, fluorescently labeled clovibactin preferentially bound to the *S. aureus* division septum, which is enriched with the peptidoglycan precursor lipid II. Short pre-treatment with lipid II-binding teixobactin drastically reduced septal clovibactin localization, highlighting that clovibactin interacts with the same target.

The dose-dependent inhibition of individual *in vitro* enzyme assays with purified enzymes and undecaprenyl pyrophosphate (C_{55}-PP)-containing lipid substrates (lipid I, lipid II, lipid III_{WTA}) and C_{55}-PP itself suggested interaction of clovibactin with the pyrophosphate moiety. In line with this, the addition of these substrates antagonized the antibacterial activity of clovibactin. Using solid-state NMR to study co-assembly of clovibactin and lipid II at the membrane surface demonstrated the formation of a well-defined complex in which the hydrophobic residues of clovibactin's depsi-cycle enclose the C_{55}-PP-moiety and parts of the first sugar of lipid II.

Moreover, high-speed atomic force microscopy (HS-AFM) showed that lipid II binding drives the self-assembly of a supramolecular complex that oligomerizes into an irreversible fibrillar structure on top of the membrane. This is enabled by an antiparallel alignment of clovibactin molecules. In contrast to teixobactin, fibril formation did not disturb the membrane integrity (Shukla *et al.*, 2022).

The study unmasks a counter-intuitive mechanism of action, in which high-affinity lipid II binding is achieved by clovibactin's depsi-cycle forming a hydrophobic cage that encloses the polar C_{55}-PP-moiety and in which target binding involves the formation of an irreversible supramolecular structure on the bacterial membrane surface. The formation of this higher-order fibrillar structure is suggested to exhibit favorable *in vivo* efficiacy as it specificially and permanently concentrates onto bacterial surfaces.

K.C.L. performed mechanism of action studies, identified the molecular targets, analyzed the data and contributed to writing of the manuscript.

A new antibiotic from an uncultured bacterium binds to an immutable target

Rhythm Shukla[1,2,#], Aaron J. Peoples[3,#], Kevin C. Ludwig[4], Sourav Maity[5], Maik G.N. Derks[1,2], Stefania de Benedetti[4], Annika M Krueger[6], Bram J.A. Vermeulen[1], Francesca Lavore[1], Rodrigo V. Honorato[1], Fabian Grein[4,7], Alexandre Bonvin[1], Ulrich Kubitscheck[6], Eefjan Breukink[2], Catherine Achorn[3], Anthony Nitti[3], Christopher J. Schwalen[8], Amy L. Spoering[3], Losee Lucy Ling[3], Dallas Hughes[3], Moreno Lelli[9,10], Wouter H. Roos[5], Kim Lewis[11], Tanja Schneider[4,*], Markus Weingarth[1,*]

[1]NMR Spectroscopy, Department of Chemistry, Utrecht University, Padualaan 8, 3584 CH Utrecht, The Netherlands
[2]Membrane Biochemistry and Biophysics, Department of Chemistry, Utrecht University, Padualaan 8, 3584 CH, Utrecht, The Netherlands
[3]NovoBiotic Pharmaceuticals, Cambridge, Massachusetts 02138, USA
[4]Institute for Pharmaceutical Microbiology, University Hospital Bonn, University of Bonn, Bonn, Germany
[5]Moleculaire Biofysica, Zernike Instituut, Rijksuniversiteit Groningen, Nijenborgh 4, 9747 AG Groningen, The Netherlands
[6]Institute for Physical and Theoretical Chemistry, University of Bonn, Bonn, Germany
[7]German Center for Infection Research (DZIF), partner site Bonn-Cologne, Bonn, Germany
[8]Novartis Institutes for Biomedical Research, Cambridge, MA 02139, USA
[9]Magnetic Resonance Center (CERM) and Department of Chemistry "Ugo Schiff", University of Florence, via Sacconi 6, Sesto Fiorentino, 50019 Italy
[10]Consorzio Interuniversitario Risonanze Magnetiche MetalloProteine (CIRMMP), via Sacconi 6, Sesto Fiorentino, 50019 Italy

[11]Antimicrobial Discovery Center, Northeastern University, Department of Biology, Boston, Massachusetts 02115, USA

[#]equal contributions

**corresponding authors: m.h.weingarth@uu.nl, tschneider@uni-bonn.de*

Summary
Antimicrobial resistance is a leading mortality factor worldwide. Here we report the discovery of clovibactin, a new antibiotic, isolated from uncultured soil bacteria. Clovibactin efficiently kills drug-resistant bacterial pathogens without detectable resistance. Using biochemical assays, solid-state NMR, and atomic force microscopy, we dissect its mode of action. Clovibactin blocks cell wall synthesis by targeting pyrophosphate of multiple essential peptidoglycan precursors (C_{55}PP, Lipid II, Lipid III_{WTA}). Clovibactin uses an unusual hydrophobic interface to tightly wrap around pyrophosphate, but bypasses the variable structural elements of precursors, accounting for the lack of resistance. Selective and efficient target binding is achieved by the irreversible sequestration of precursors into supramolecular fibrils that only form on bacterial membranes that contain lipid-anchored pyrophosphate groups. Uncultured bacteria offer a rich reservoir of antibiotics with new mechanisms of action that could replenish the antimicrobial discovery pipeline.

Keywords
Antibiotics, uncultured bacteria, peptidoglycan, cell wall, lipid II, mechanism of action, solid state NMR, atomic force microscopy, antibiotic resistance, infection, animal models

Introduction

The introduction of antibiotics has revolutionized medicine, providing effective treatment for infectious diseases that were once fatal, and enabling modern medicine such as surgery and organ transplantation. Widespread resistance development thwarts the effectiveness and lifespan of antibiotics, calling for the discovery of new drugs in the perpetual standoff against human pathogens (Brown and Wright, 2016; Cook and Wright, 2022; Miethke et al., 2021; Mordoch et al., 1999).

Most antibiotics used in the clinic originate from natural product scaffolds that were discovered by screening soil dwelling bacteria (Lewis, 2020). This approach, ushered in by the 'Waksman platform', was vastly successful in the 1940s to 1960s, considered the Golden Age of antibiotics discovery, and eventually led to the introduction of compounds such as streptomycin, vancomycin, or tetracycline. However, to date, traditional screening sources seem overmined as they tend to yield previously-known compounds. As the drug discovery pipeline has considerably thinned, it is prudent to search for new antibiotics with unprecedented mechanism of action among untapped groups of bacterial producers.

Uncultured bacteria represent a vast (~99% of all species), unexploited source of new natural product scaffolds (Lewis, 2013; Wilson et al., 2014). Recently, the development of the iChip technique (Nichols et al., 2010) provided access to a broad diversity of uncultured bacterial species, leading to the discovery of teixobactin (Ling et al., 2015), isolated from the soil bacterium *Eleftheria terrae*. Teixobactin shows excellent antibacterial activity and has a unique chemical structure. Teixobactin blocks cell wall biosynthesis by specific binding to highly conserved lipid precursors (Ling et al., 2015), leading to the formation of supramolecular structures that perturb membrane stability (Shukla et al., 2022b). Additional antibiotics with novel modes of action that came out of screening uncultured bacteria are lassomycin, an inhibitor of the ClpP1P2C1 protease and amycobactin, an inhibitor of the SecY protein exporter, both acting selectively against mycobacteria (Gavrish et al., 2014; Quigley et al., 2020). Uncultured bacteria hence appear to offer a rich source of compounds with new chemical and mechanistic characteristics, which bodes well for the sustained discovery of effective leads to develop next-generation antibiotics.

Here we report the discovery and mode of action of clovibactin, a new antibiotic without detectable resistance, identified from a screen of uncultured bacteria.

Results

Discovery of clovibactin

Some environmental bacteria, as well as spores, may require a prolonged incubation to initiate growth in vitro (Buerger et al., 2012a, b). This allows access to microorganisms that would be missed by standard cultivation techniques. To favor growth of spore-forming actinomycetes, we first incubated soil at 65°C for 30 minutes, then diluted it to extinction into a growth medium in microtiter plates to achieve ≤1 cell per well. Some non-spore formers can grow after this mild heating as well. Growth was followed by observing the wells under a dissecting microscope (50X magnification) at 1, 2, 4, 8, 12, and 16 weeks. Colonies were then sub-cultured and screened for antimicrobial activity on nutrient agar plates overlaid with *Staphylococcus aureus*. One of the producers was detected at 12 weeks of incubation and based on 16s rDNA sequence, is 99% identical to *Eleftheria terrae*. We refer to this isolate as *E. terrae ssp. carolina*; the sandy soil it was isolated from comes from North Carolina. The genus *Eleftheria* belongs to β-proteobacteria, is very rare, and the original *E. terrae* we isolated several years ago by growth in situ is the producer of teixobactin (Ling et al., 2015). We therefore decided to identify the antimicrobial compound produced by *E. terrae* ssp. *carolina*.

The first antibiotic identified from the producing organism was kalimantacin. However, extracts of the fermented broth showed activity against *B. subtilis*, while kalimantacin is not active against this species (Fage et al., 2020). Upon an initial separation of the crude extract by HPLC, we identified another fraction of the extract that showed activity against both *B. subtilis* and *S. aureus*. In an attempt to increase metabolic flux to novel compound production and simplify isolation, we set out to disrupt genes responsible for kalimantacin production.

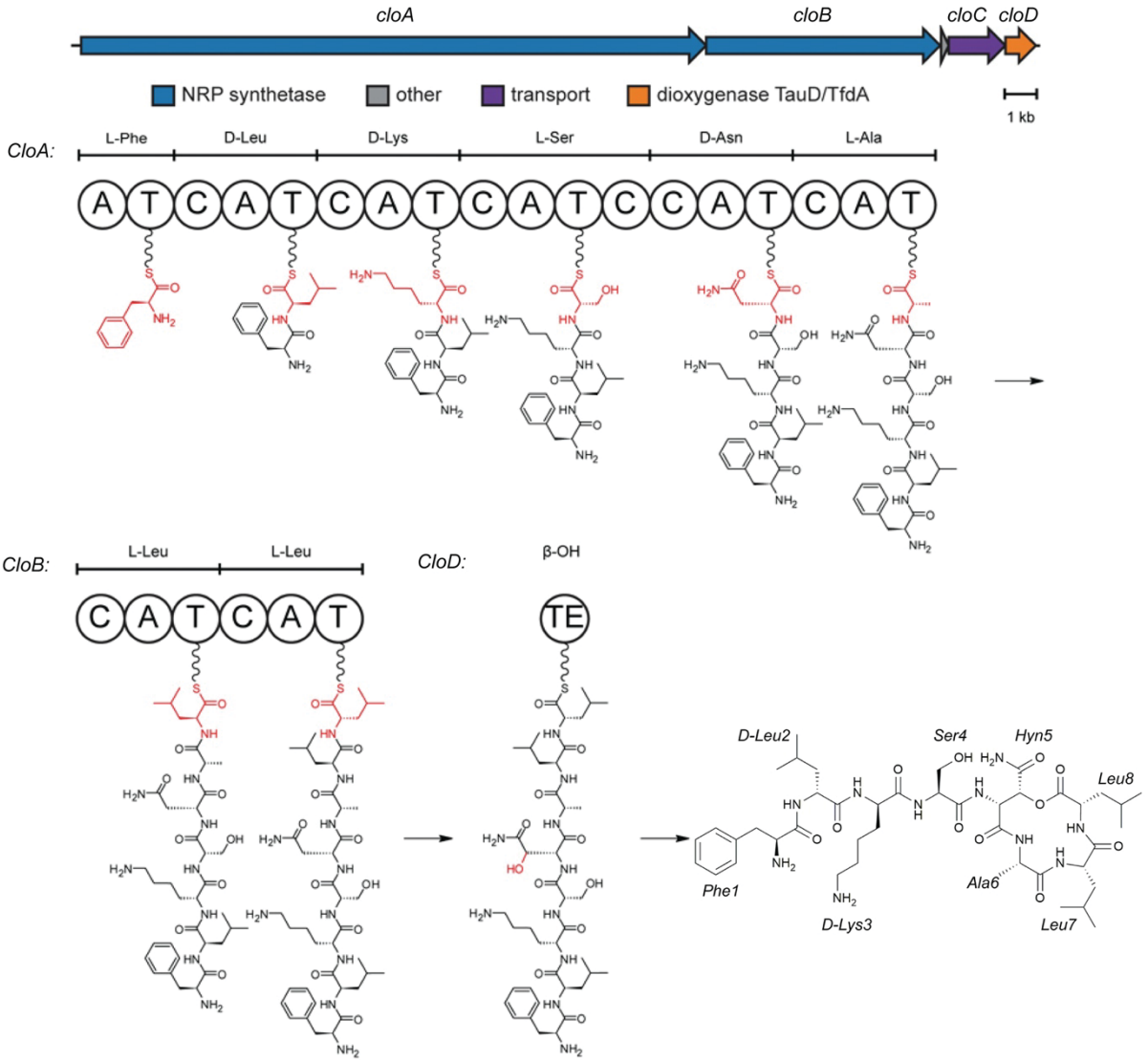

Figure 1. Biosynthetic gene cluster and proposed biosynthesis of clovibactin. The gene cluster associated with the biosynthesis of clovibactin was identified via whole genome sequencing and contained two nonribosomal peptide synthetases (NRPS) genes (*cloA* and *cloB*), a transporter gene (*cloC*) and a tailoring enzyme (*cloD*). Proposed biosynthetic pathway of clovibactin involves the assembly-line condensation of 8 canonical amino acids with 3 epimerizations carried out by dual-function condensation domains and a β-hydroxylation on Asn5 by the CloD, a TauD/TfdA dioxygenase. This hydroxylation provides the cyclization point for release from the NRPS and formation of the macrocyclic lactone.

Whole genome sequencing led to the identification of a biosynthetic gene cluster (BGC) with 55% identity to the kalimantacin/batumin operon (Mattheus et al., 2010). Production of kalimantacin was reduced below detectable levels by interrupting the first gene in the operon, bat1, using homologous recombination of a suicide vector (Fernández-Martínez and Bibb, 2014).

Fermentation broth of *E. terrae* ssp. *carolina* Δ*bat1* was separated by HPLC, and bioassay-guided isolation produced a fraction with a compound having a unique mass of 903.5291 $[M+H]^+$ as analysed by Antibase. According to Antibase, this mass is unique. A combination of mass spectrometry and solution NMR resolved the structure of this compound, which is a novel depsipeptide that we named clovibactin **(Figure 1 and Supplementary Tables 1 and 2)**. Stereochemistry was confirmed by Marfey's analysis.

Table 1. Antimicrobial activity of clovibactin. Minimal inhibitory concentrations (MIC) of clovibactin were determined by broth microdilution against selected strains and pathogenic bacteria. GISA, glycopeptide intermediate resistant *S. aureus*; MSSA, methicillin-sensitive *S. aureus*; MRSA, methicillin-resistant *S. aureus*; VISA, vancomycin intermediate resistant *S. aureus*; VRE, vancomycin-resistant enterococci.

Strain	**MIC (μg/mL)**
Staphylococcus aureus	
NCTC 8325-4 (MSSA)	0.5-1
ATCC 29213 (MSSA)	0.5-1
ATCC 700699 (GISA)	1-2
NRS71 (Epidemic MRSA)	1
NRS108 (MRSA, also synercid^{R})	1
ATCC 33591 (MRSA)	1-2
Mu50 (VISA)	2
SG511	0.125
HG001	2
Staphylococcus epidermidis	
ATCC 35982 (*mecA* positive)	0.5
NRS8 (*mecA* positive)	0.5
Staphylococcus haemolyticus	
NRS9 (*mecA* positive)	1
NRS69 (*mecA* positive)	0.5
Other Gram-positive	
Enterococcus faecium BM4147 (VRE) *(aac(6')-Ie-aph-(2'))*	0.5-1
E. faecalis ATCC 51299 (VRE)	0.5-2
Bacillus subtilis 1A1	1-2
B. subtilis 168 DSM 23778	2
B. anthracis Sterne	0.25
Streptococcus pneumoniae ATCC10813	0.25-0.5
S. pyogenes ATCC19615	0.25-0.5
S. warneri NRS138	1
Mycobacterium smegmatis MC^2 155	2
M. tuberculosis MC^2 6020	0.5-1
Gram-negative	
Haemophilus influenzae SJ7	2
Escherichia coli K12	64
E. coli WO153 (AB1157*:asmB1 ΔtolC:kan*)	1-2
Pseudomonas aeruginosa PAO1	>128

Clovibactin features two D-amino acids in its linear N-terminus and an uncommon residue D-3-hydroxyasparagine in the depsi-cycle. The compound's molecular scaffold bears some resemblance to the depsi-peptide teixobactin, as reflected by a Tanimoto coefficient of 0.8761. However, clovibactin has a considerably shorter linear N-terminus (4 residues in clovibactin, 7 residues in teixobactin) that harbors the two positive charges present in the compound. Additionally, teixobactin contains one of its two positively charged amino acids in the macrolactone that is further represented by the presence of the unusual enduracididine residue, missing in clovibactin.

The genome of *E. terrae ssp. carolina* was sequenced using PacBio. *E. terrae ssp. carolina* contains 19 predicted BGCs overall, of which 14 have NRPS-like elements (either pure NRPS or NRPS/PKS hybrid). The gene cluster associated with the biosynthesis of clovibactin was identified by antiSMASH (Hsu et al., 2004) version 5.1.1. It contains two NRPS genes (*cloA* and *cloB*), a transporter gene (*cloC*) and a tailoring enzyme (*cloD*). The proposed biosynthetic pathway of clovibactin is shown in **Figure 1**.

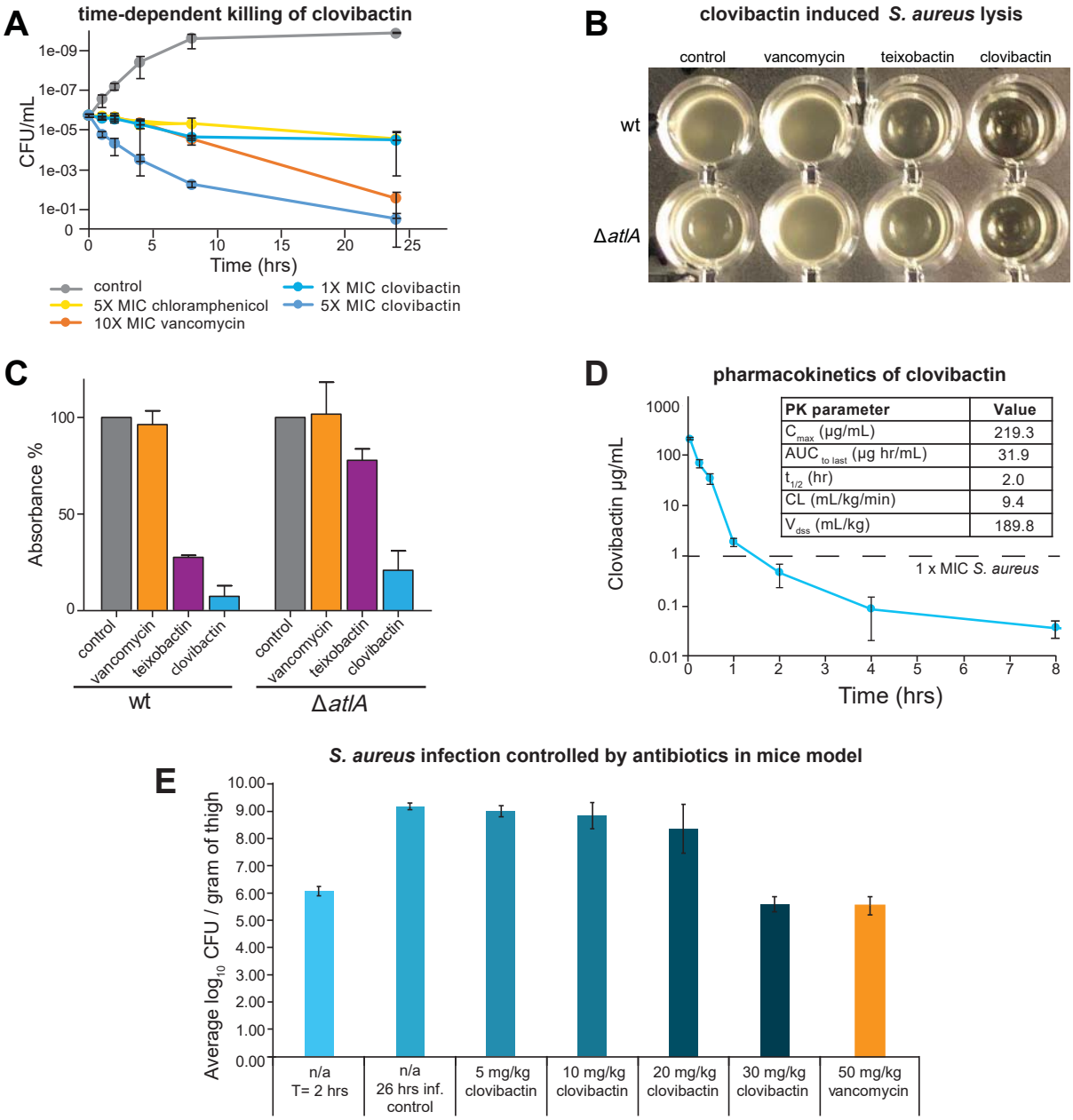

Figure 2. Clovibactin kills *S. aureus in vitro* and *in vivo*. (A) time-dependent killing of *S. aureus* (clovibactin (1xMIC), clovibactin (5xMIC), vancomycin (10xMIC) and chloramphenicol (5xMIC). **(B,C)** Clovibactin-induced lysis in *S. aureus*. Cells of *S. aureus* SA113 and a Δ*altA* mutant were incubated with each compound at 2xMIC for 24 hours as indicated. Mean values from three independent experiments are shown. Error bars represent standard deviation. **(D)** Pharmacokinetic parameters of clovibactin in mice model determined using Watson LIMS software. **(E)** The bacterial load from the thigh infection model prior to dosing and 24 hours after treatment. The infection controls demonstrated a bioload of 6.07 log10 CFUs/ gram of thigh at the time of treatment (2 hours). Clovibactin was delivered as two IV doses (2 and 4 hours post infection) of 5, 10, 20 and 30 mg/kg. Vancomycin was delivered as a single IV dose at 50 mg/kg.

When comparing the clovibactin and teixobactin BGCs, the identity is 72% by BLASTN alignment **(Figure 1)**.

Clovibactin exhibited antibacterial activity against a broad range of Gram-positive pathogens, including methicillin-resistant *S. aureus* (MRSA), daptomycin-resistant as well as vancomycin-intermediate resistant (VISA) strains, and difficult to treat vancomycin-resistant *Enterococcus faecalis* (Lebreton et al., 2017) and *E. faecium* (VRE) **(Table 1, Supplementary**

Table 3). *Escherichia coli* was only marginally affected compared to an outer membrane deficient *E. coli* WO153 strain, probably reflecting insufficient penetration of the compound.

Clovibactin is bactericidal, with *S. aureus* MBC (minimal bactericidal activity) of 2xMIC. We then examined the time-dependent killing in more detail **(Figure 2A)**. Clovibactin was more effective in killing *S. aureus* as compared to vancomycin, the first line of defense antibiotic. We noticed that clovibactin produced unusually strong lysis of the cell culture, and quantified this effect **(Figure 2B,C)**. Teixobactin was previously demonstrated to be rapidly bactericidal and to induce lysis mediated by AtlA (Ling et al., 2015), the major cell wall autolysin of *S. aureus* (Homma et al., 2016). To investigate the contribution of AtlA to the activity of clovibactin, the antibacterial activity against an Δ*atlA* deletion mutant was examined and compared to wild-type *S. aureus*. Clovibactin (2xMIC) induced strong lysis, more pronounced than teixobactin **(Figure 2B,C)**. Strikingly, lytic events were only slightly affected in the Δ*atlA* mutant, suggesting that clovibactin-induced lysis does not primarily rely on AtlA activity. Such pronounced lysis is typically observed with detergent-like compounds that rapidly destroy the cell membrane. However, lysis induced by clovibactin is not the result of rapid pore formation or membrane disruption, as evidenced by the absence of potassium efflux from staphylococcal cells in contrast to the pore-forming lantibiotic nisin **(Supplementary Figure 1)**. Similarly, clovibactin treatment did not lead to rapid membrane depolarization as determined using the membrane potential sensitive dye DisC2(5) or enable penetration of Sytox. This contrasts with the action of teixobactin that thins and depolarizes bacterial membranes (Shukla et al., 2022b). In agreement with this, clovibactin did not affect the cellular localization of the cell division protein MinD in *B. subtilis* **(Supplementary Figure 1)**. MinD is normally localized to cell poles and division sites and becomes delocalized upon dissipation of the membrane potential.

Clovibactin did not show any cytotoxicity against mammalian NIH/3T3 and HepG2 cells at 100 µg/mL (highest concentration tested). Given the strong antimicrobial activity of clovibactin and low cytotoxicity, we next examined the action of this antibiotic *in vivo*. We first performed a pharmacokinetic study to evaluate the systemic exposure and blood residence time of the compound. A single dose of clovibactin was administered to mice at 20 mg/kg intravenously and was well tolerated. Blood was drawn at different times and clovibactin plasma levels were determined by LC-MSMS, and PK parameters were determined using the software package Watson LIMS **(Figure 2D)**.

Next, clovibactin was evaluated in a neutropenic mouse thigh infection model with *S. aureus*. In this model, mice are treated with cyclophosphamide to disable the immune response. Antibiotics are then evaluated for their ability to control infection without the assistance of the immune system. Clovibactin was comparable to vancomycin in diminishing the bacterial burden **(Figure 2E)**.

Target identification

Given the novelty of the structure and the promising properties of this compound as a developmental lead, we sought to identify the molecular target of clovibactin. First, we determined the frequency of resistance, which is essential to know for advancing a compound. From a drug development standpoint, a desirable frequency of resistance is $<10^{-8}$ (Silver, 2007) - low enough to provide extended lifetime in the clinic. The added benefit of this determination is target identification by whole-genome sequencing of resistant mutants. However, plating *S. aureus* on media containing clovibactin even at a low concentration (4xMIC) produced no resistant mutants. We therefore estimate the frequency of resistance to be $<10^{-10}$. We then sought to determine a possible biosynthetic pathway that clovibactin might inhibit. For this, we followed the incorporation of labelled precursors into the major biosynthetic pathways of *S. aureus* – DNA, RNA, protein, and peptidoglycan. Clovibactin specifically interfered with the incorporation of radiolabeled GlcNAc into the cell wall, whereas DNA, RNA and protein biosynthesis remained unaffected **(Figure 3A)**. In a parallel approach, we

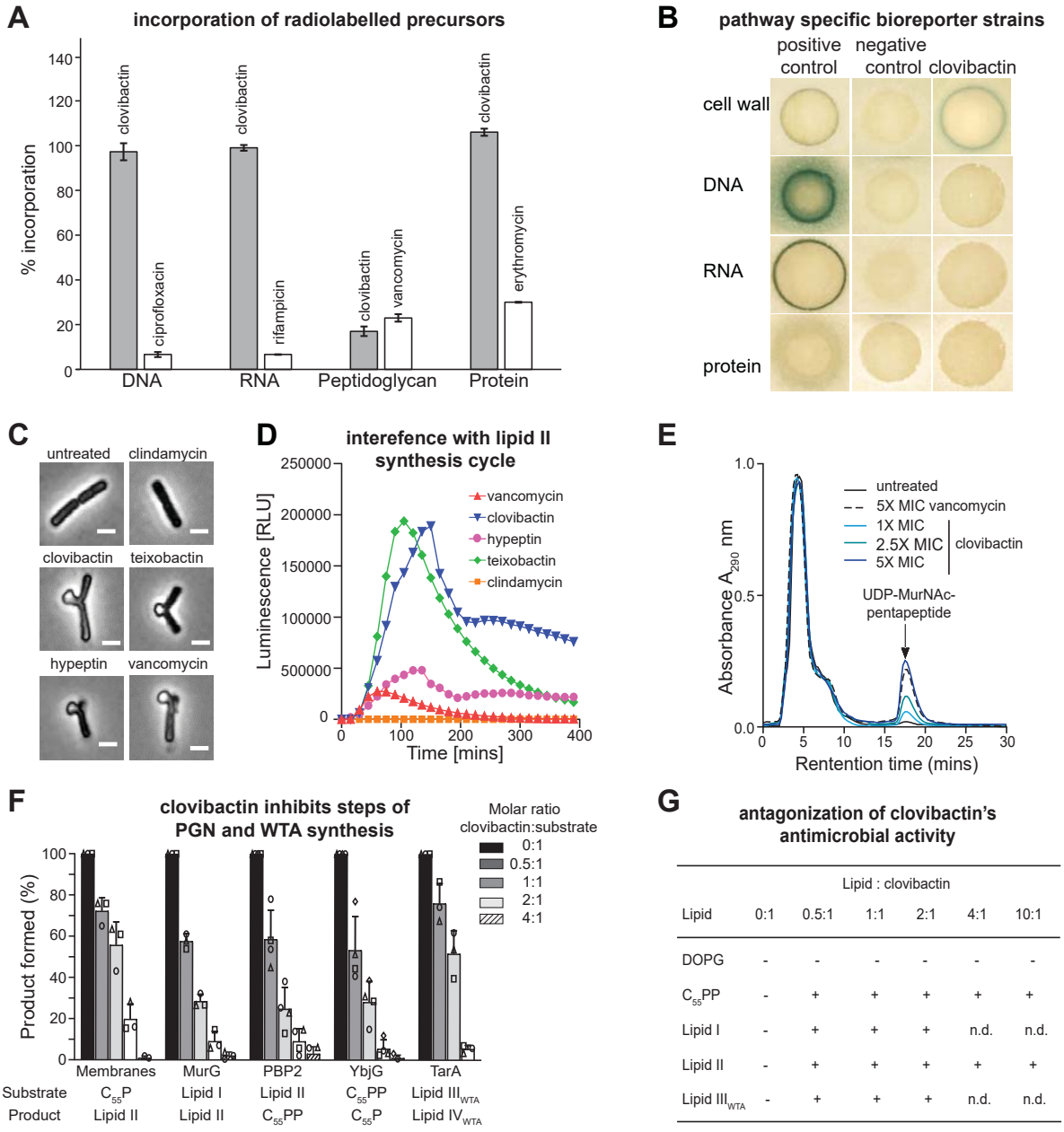

Lipid	Lipid : clovibactin 0:1	0.5:1	1:1	2:1	4:1	10:1
DOPG	-	-	-	-	-	-
$C_{55}PP$	-	+	+	+	+	+
Lipid I	-	+	+	+	n.d.	n.d.
Lipid II	-	+	+	+	+	+
Lipid III_{WTA}	-	+	+	+	n.d.	n.d.

Figure 3. Clovibactin targets cell wall biosynthesis. (A) Effect of clovibactin on macromolecular biosyntheses in *S. aureus*. Incorporation of ^{3}H-thymidine (DNA), ^{3}H-uridine (RNA), ^{3}H-leucine (protein), and ^{3}H-glucosamine (peptidoglycan) was determined in cells treated with clovibactin at 2xMIC (grey bars). Ciprofloxacin (8xMIC), rifampicin (4xMIC), vancomycin (2xMIC) and erythromycin (2xMIC) were used as positive controls (white bars). Data are averages of two independent experiments. **(B)** *B. subtilis* bioreporter strains with selected promotor-*lacZ* fusions were used to identify interference with major biosynthesis pathways. β-galactosidase (*lacZ*) is fused to promotors P_{ypuA} (cell wall), P_{yorB} (DNA), P_{yvgS} (RNA), and P_{yhel} (protein) and induction of a specific stress response is visualized by a blue halo at the edge of the inhibition zone. Antibiotics vancomycin, ciprofloxacin, rifampicin, and clindamycin were used as positive controls. **(C)** Clovibactin treatment results in cell-shape deformations and characteristic blebbing as observed by phase-contrast microscopy of *B. subtilis*. Cell wall active antibiotics teixobactin, hypeptin, vancomycin and protein synthesis inhibitor clindamycin were used as controls. Scale bar = 2 µm. **(D)** Clovibactin (1xMIC, blue) strongly induced P_{lial} as observed by expression of the lux operon in *B. subtilis* P_{lial}-*lux*. Teixobactin, hypeptin, vancomycin and clindamycin were used as control antibiotics. **(E)** Intracellular accumulation of the soluble cell wall precursor UDP-MurNAc-pentapeptide after treatment of *S. aureus* with different concentrations of clovibactin. Untreated and VAN-treated (5xMIC) cells were used as controls. Experiments are representatives of 3 independent experimxts. **(F)** Clovibactin inhibits membrane-associated

steps of PGN and WTA synthesis *in vitro*. The antibiotic was added in molar ratios from 0.5 to 4 with respect to the amount of the lipid substrate $C_{55}P$, $C_{55}PP$, lipid II, or lipid III_{WTA} used in the individual test systems. Reaction product synthesized in the absence of antibiotic was taken as 100%. Mean values from three independent experiments are shown. Error bars represent standard deviation. **(G)** Antagonization of the antimicrobial activity of clovibactin by cell wall precursors. *S. aureus* was incubated with clovibactin (8×MIC) in nutrient broth in microtiter plates, and growth was measured after a 24 h incubation at 37 °C. Putative HPLC-purified antagonists (undecaprenyl-pyrophosphate [$C_{55}PP$], lipid I, lipid II, and lipid III_{WTA}) and 1,2-dioleoyl-sn-glycero-3-phospho-glycerol (DOPG) were added in at molar ratios with respect to the antibiotic. Experiments were performed with biological replicates. + antagonization; - no antagonization; n.d. not determined.

used pathway-selective bioreporter strains of *Bacillus subtilis* treated with clovibactin (Harms et al., 2018). Expression of LacZ was specifically induced by clovibactin in *B. subtilis* P_{ypuA}-*lacZ,* indicative of interference with cell wall biosynthesis **(Figure 3B)**. Treatment of *B. subtilis* with clovibactin induced cell-shape deformations as visualized by phase-contrast microscopy. This blebbing phenotype is characteristically induced by many cell-wall acting antibiotics and was similarly observed with teixobactin (Ling et al., 2015), hypeptin (Wirtz et al., 2021), or vancomycin, but not the protein synthesis inhibitor clindamycin used as a control **(Figure 3C)**, further supporting direct interference with cell wall biosynthesis. To narrow down the molecular target within the cell wall biosynthesis pathway, *lial*-*lux* induction was monitored over time. LiaRS is a two-component system, known to respond to antibiotics that interfere with lipid II biosynthesis. Clovibactin strongly induced P_{lial}-*lux*, suggesting that it may directly interact with lipid II **(Figure 3D)**.

Synthesis of the peptidoglycan precursor lipid II occurs in two different compartments of the bacterial cell. In the cytoplasm, the soluble sugar building blocks UDP-*N*-acetylmuramic acid pentapeptide (UDP-MurNAc-pp) and UDP-N-acetylglucosamine (UDP-GlcNAc) are synthesized and transferred to the lipid carrier undecaprenyl phosphate ($C_{55}P$) to build lipid II that is flipped across the membrane to the exterior of the cell and incorporated into the growing peptidoglycan network **(Supplementary Figure 2)**. Antibiotics that block late stages of peptidoglycan biosynthesis, such as vancomycin, are known to trigger the intracellular accumulation of the last soluble peptidoglycan precursor UDP-MurNAc-pp. As observed for vancomycin, treatment of *S. aureus* with clovibactin at increasing concentrations led to an accumulation of UDP-MurNAc-pp in the cytoplasm **(Figure 3E)**. A fluorescent clovibactin-Bodipy-FL derivative bound preferentially to the septum of dividing staphylococcal cells, a site enriched in lipid II **(Supplementary Figure 3)**. Preincubation of cells with teixobactin almost completely blocked clovibactin-FL binding, suggesting that both compounds interact with the same targets **(Supplementary Figure 3)**.

Based on the results obtained with whole cells, the impact of clovibactin on the late steps of cell wall biosynthesis was analyzed *in vitro* to identify the molecular target – clovibactin was thus tested in individual biosynthesis assays using purified enzymes and substrates **(Figure 3F)**. Clovibactin inhibited all cell wall biosynthesis reactions that consume lipid I, lipid II, lipid III_{WTA} or undecaprenyl-pyrophosphate ($C_{55}PP$) as a substrate in a dose-dependent fashion, suggesting binding to these lipid intermediates, rather than inhibiting enzyme function. Corroborating this result, the addition of purified cell wall lipid intermediates antagonized the antimicrobial activity of clovibactin and restored growth of *S. aureus* **(Figure 3G).** Interestingly, similar molar concentrations of $C_{55}PP$ and lipid II were required to fully antagonize clovibactin activity, while antagonization of teixobactin activity required a 10-fold higher concentration of $C_{55}PP$ compared to lipid II, suggesting differences in the binding mode. In agreement with this, higher concentrations of teixobactin (Ling et al., 2015) were needed to completely block the YbjG-catalyzed dephosphorylation compared to clovibactin **(Figure 3F)**.

Oligomerization upon target binding

Next, we studied the interaction between clovibactin and lipid II in lipid bilayers using solid-state nuclear magnetic resonance (ssNMR), which allows the investigation of molecular

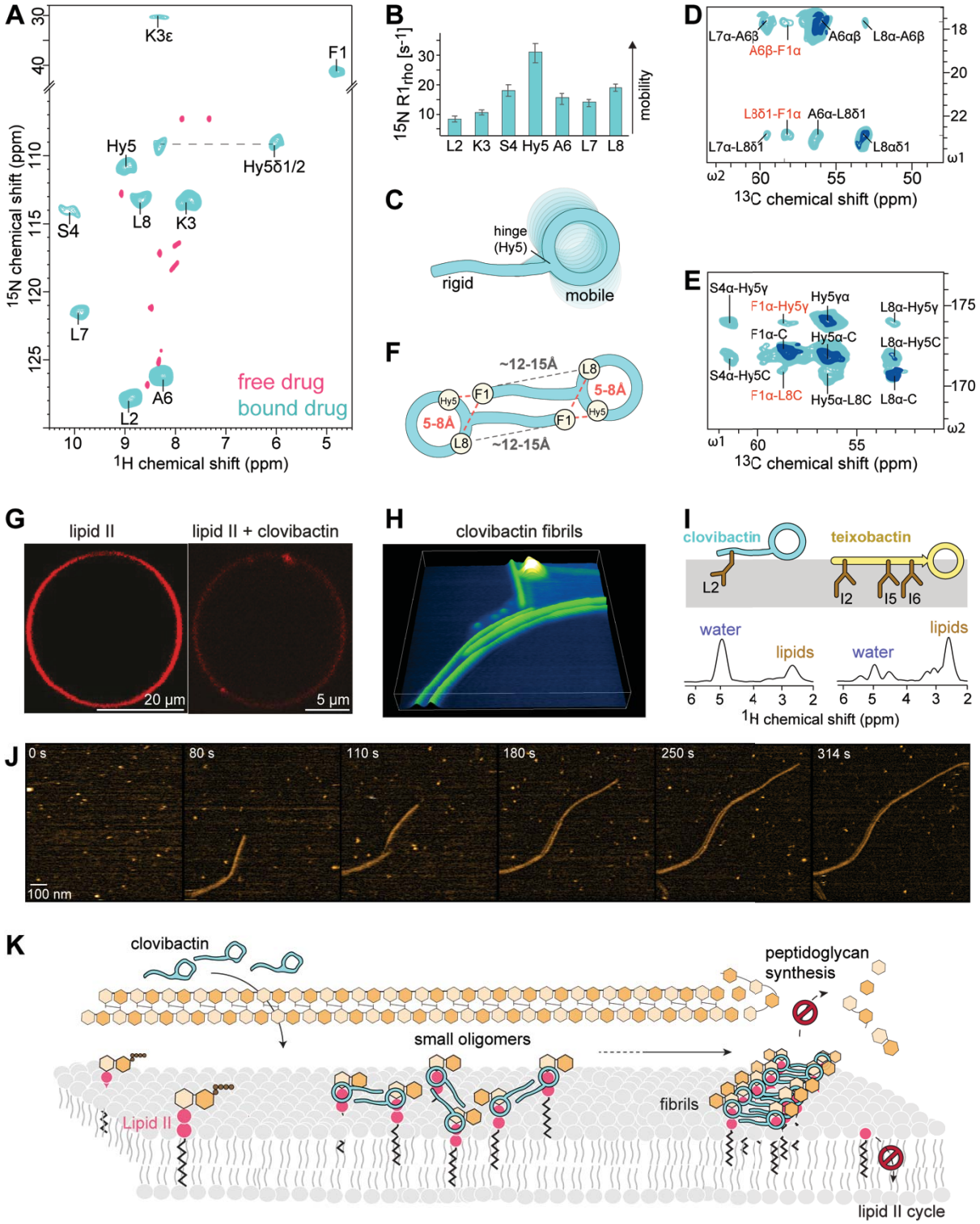

Figure 4: High-resolution ssNMR structure and oligomerization of the clovibactin/lipid II complex in membranes. (A) 2D NH ssNMR spectrum of lipid II bound clovibactin in membranes (cyan), superimposed on free clovibactin in aqueous solution (rose). **(B)** Site-resolved ^{15}N R_{1rho} dynamics of lipid II bound teixobactin and clovibactin in DOPC membranes. **(C)** Illustration of the NMR-derived dynamics. While clovibactin's N-terminus is rigid, the depsi-cycle shows elevated dynamics. **(D, E)** Zooms into a 2D CC spectrum of the complex show head-to-tail contacts in clovibactin, suggesting a dimeric (supramolecular) arrangement of clovibactin in the complex. Data acquired at 1200 MHz magnetic field using 50 (cyan) and 250 ms (dark blue) CC mixing time. **(F)** Schematic illustration of the head-to-tail contacts between Phe1-Hyn5 and Phe1-Leu8 seen in **(D, E)** a dimeric model. **(G)** Confocal microscopy of DOPC GUVs doped with Atto-labelled lipid II and treated with clovibactin show domain/cluster formation. **(H)** 3D rendered high-speed AFM image show the formation of clovibactin –

lipid II supramolecular fibrils after 10 minutes of interactions. **(I)** left: Mobility-edited (Doherty and Hong, 2009) ssNMR experiments show that clovibactin is much more water-accessible than teixobactin in the lipid II-bound state. right: ssNMR-derived topology and membrane insertion of clovibactin. **(J)** Snapshots of a timelapse HS-AFM video (Supplementary Video 1) following the assembly of clovibactin–lipid II fibrils. Images were obtained on a supported lipid bilayer containing 4% (mol) lipid II in the presence of 5 μM clovibactin, added at 0 s. Image acquisition rate of 0.5 frames per second. **(K)** Model of the mode of action of clovibactin. At the membrane surface, clovibactin binds lipid II and forms small oligomers that serve as nuclei for the formation of fibrils. Fibril formation enables a stable binding of lipid II and other cell wall precursors, blocking cell wall biosynthesis.

mechanism of antibiotics binding to membrane targets under near-native conditions (Hong, 2006; Medeiros-Silva et al., 2018; Shukla et al., 2022b). To make the drug amenable to a comprehensive ssNMR characterization, we produced uniformly ^{13}C,^{15}N-labelled clovibactin by fermentation of *E. terrrae spp. carolina* Δ*bat* in ^{13}C,^{15}N-enriched media (see Methods section). Co-assembly of clovibactin and lipid II in membranes resulted in high-quality 2D ssNMR correlation spectra that demonstrate the formation of a well-defined complex. We fully assigned the chemical shifts of clovibactin in the complex using 2D CC, CN, and NH spectra **(Supplementary Figure 4)**. Large signal shifts of the backbone amide protons show that clovibactin undergoes a major conformational change upon lipid II binding **(Figure 4A)**. An analysis of the ^{13}C chemical shifts (Wang, 2002), suggests that the short linear N-terminus of clovibactin does not does not adopt a classical secondary structure

but seems to contain elements of β-structuring. **(Supplementary Figure 4)**. Subsequently, we investigated the site-resolved dynamics of clovibactin in the lipid II bound state using ssNMR relaxation measurements (Lewandowski et al., 2011) **(Figure 4B,C)**. Globally, clovibactin is immobilised in the complex, indicative of the formation of a larger supramolecular structure. Strikingly, the N-terminus (Leu2 and Lys3) strongly rigidifies upon complex formation, which is reminiscent of the antimicrobial action of teixobactin, whose N-terminus drives the self-assembly into large clusters upon target binding (Shukla et al., 2022b; Shukla et al., 2020).

We used confocal microscopy to probe the assembly of the complex on the surface of giant unilamellar vesicles (GUVs) doped with Atto-tagged lipid II. Microscopy images clearly show the formation of large clovibactin – lipid II patches, while such accumulation was not observed without clovibactin **(Figure 4G)**. These data confirm the formation of large supramolecular clovibactin – lipid II domains.

Next, we investigated at high-resolution how clovibactin molecules arrange in the supramolecular assemblies. We acquired 2D ssNMR PARISxy (Weingarth et al., 2010) CC spectra of the complex, in which we observed numerous clear head-to-tail contacts between N-terminal (Phe1) and C-terminal (Hyn5 and Leu8) clovibactin residues. In agreement with the formation of a supramolecular structure, these are likely intermolecular contacts between clovibactin molecules, as the intramolecular distances between N-terminal and C-terminal residues appear too far for CC magnetization transfer with a distance threshold of approximately 8 Å **(Figure 4D,E, Supplementary Figure 5)**. The contacts that we observe are consistent with an antiparallel dimeric organization of clovibactin molecules **(Figure 4F, Supplementary Figure 5)**.

Flexible fibrils

To examine the supramolecular nature and the membrane interactions of clovibactin – lipid II complex in more detail, we first used high-speed atomic force microscopy (HS-AFM), a dynamic technique that provides biomolecular-scale structural resolution in real time (Kodera et al., 2010; Maity et al., 2020). Within minutes after the addition of 5 μM of clovibactin to membranes doped with lipid II, HS-AFM data show the formation of fibrils on the membrane surface **(Figure 4H, J and Supplementary Figure 6A)**. These fibrils only formed in the presence of both clovibactin and lipid II **(Supplementary Figure 6B)**. The observed fibrils showed a limited extend of lateral nucleation, forming thin, flat strings of associated fibrils.

The clovibactin concentrations required to observe supramolecular structures by HS-AFM requirements are comparable to the MIC, suggesting the oligomerization upon target binding is important or even critical for the mode of action of clovibactin **(Table 1 and Supplementary Table 3)**. The differential nature of the supramolecular structures of clovibactin and teixobactin (Shukla et al., 2022) is also in line with mobility measurements in supported bilayers using single-molecule tracking. These measurements agree with higher concentration requirements for the formation of clovibactin fibrils and show that lipid II remains more mobile in assemblies formed by clovibactin **(Supplementary Figure 8C)**.

To better understand the nature of clovibactin – lipid II assemblies, we next looked at its membrane topology at high-resolution using ssNMR experiments that monitor the exposure of the antibiotic to water and phospholipid phases (Doherty and Hong, 2009) **(Figure 4I and Supplementary Figure 7)**. ssNMR data show that lipid II-bound clovibactin localizes close to membrane/water interface and is in contact with both the water and lipid phases. Since the exposure to the water phase is much more pronounced, the data imply that the supra-structure formed by clovibactin lies on top of the membrane surface **(Figure 4K)**, sharply contrasting with teixobactin-supra structures, which show very strong interactions with the phospholipid tails and embeds deeply into the membrane. The differential membrane insertion can be rationalized by the presence of three long hydrophobic anchors (Ile2, Ile5, Ile6) in the N-terminus of teixobactin, while the much shorter N-terminus of clovibactin features only a single hydrophobic anchor (Leu2). The shallow membrane insertion of the clovibactin supramolecular structure is in agreement with the high localization of the fibrils above the membrane surface observed by HS-AFM (1.2 ± 0.2 nm above the membrane surface for clovibactin fibrils, 0.8 ± 0.1 nm above the membrane surface for teixobactin fibrils) **(Supplementary Figure 6A)**, and also appears in line with the increased mobility of lipid II in clovibactin assemblies **(Supplementary Fig 6C)**. Given that samples of the clovibactin complex yielded similar ssNMR spectra after weeks of storage at 278 K, the supra-structures apparently form irreversibly on biological timescales.

The complex interface

Next, we sought to determine precisely how clovibactin targets lipid II, a complex lipid with a conserved pyrophosphate (PPi) group, a headgroup composed of the sugars MurNAc and GlcNAc and a pentapeptide whose variation confers resistance to antibiotics such as vancomycin (Münch and Sahl, 2015) **(Figure 5A)**.

First, we investigated how clovibactin targets the PPi group. Upon addition of clovibactin, 1D ^{31}P ssNMR data showed marked changes in the pyrophosphate signals of lipid II, suggesting a direct coordination **(Figure 5B and Supplementary Figure 8)**. A similar signal shift was observed for lipid I (which lacks the GlcNAc sugar). Furthermore, the emergence of intense sidebands in 1D ^{31}P ssNMR data demonstrate that clovibactin also binds and immobilises C_{55}PP (which lacks the sugars and the pentapeptide), in line with our biochemical binding analysis. Together, these data confirm that clovibactin is a multi-targeting antibiotic that blocks cell wall biosynthesis at several distinct, indispensable stages. To pinpoint the role of the lipid II PPi group in complex formation, we acquired a 2D ^{31}P^{1}H ssNMR spectrum which monitors magnetization transfer from amino protons of clovibactin to PPi **(Figure 5B)**. These data demonstrate that the backbone amino-protons of clovibactin directly coordinate the PPi group with the amino protons of the depsi-cycle (Hyn5, Ala6, Leu8). Furthermore, a weaker, but clearly discernible, signal shows that Ser4 of the N-terminus-depsi-cycle junction is in proximity close to the PPi group. These direct contacts with the PPi group agree with the stark signal changes observed upon addition of the drug.

Subsequently, to resolve the role of the lipid II sugars and the pentapeptide for target binding, we prepared a complex of ^{13}C,^{15}N-clovibactin and ^{13}C,^{15}N-lipid II to measure a series of 2D PARISxy (Weingarth et al., 2010) ^{13}C^{13}C spectra at ultra-high magnetic fields of 950 and 1200 MHz **(Figure 5C and Supplementary Figure 9A)**. We observed a total of 12 unambiguous interfacial contacts between clovibactin and the lipid II sugars, 10 of which relate to Ala6 and Leu8 **(Figure 5D)**, confirming that the depsi-cycle directly interacts with the lipid II

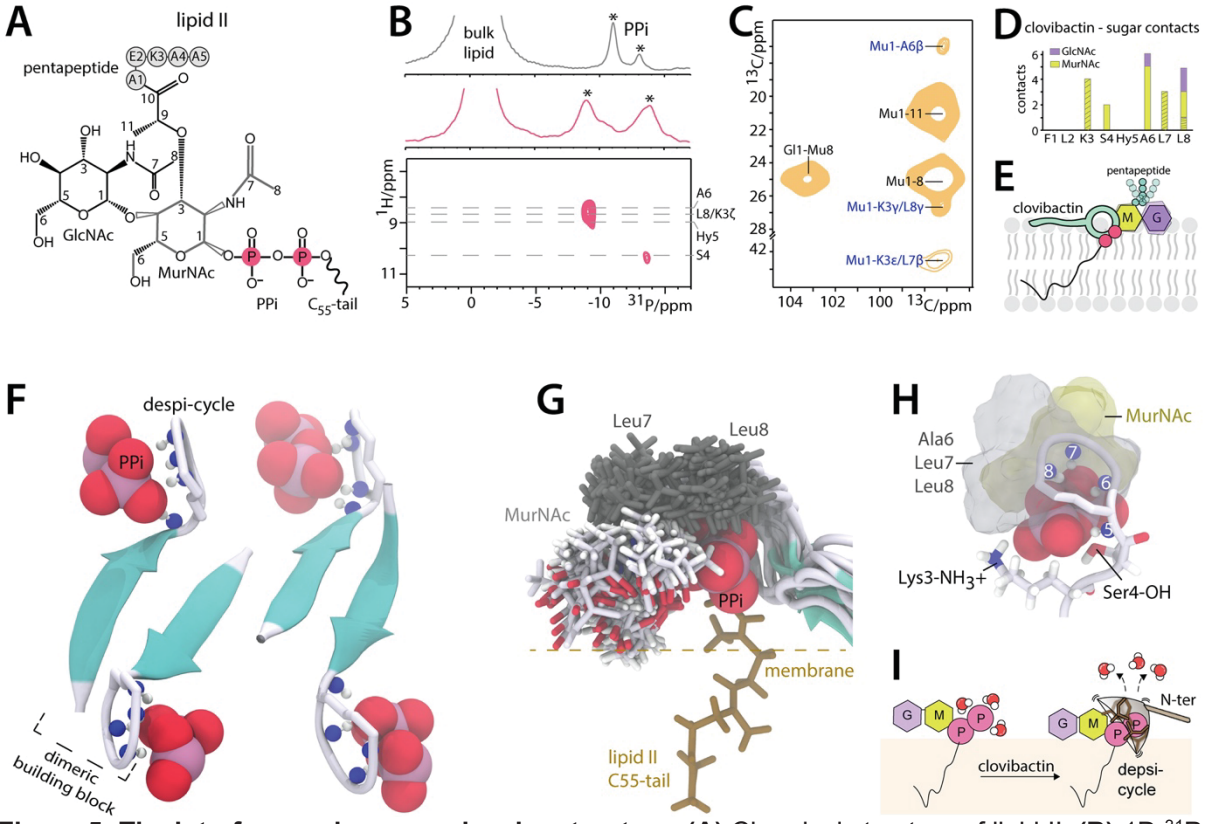

Figure 5: The interface and supramolecular structure. (A) Chemical structure of lipid II. **(B)** 1D ^{31}P ssNMR data in liposomes show marked changes of the lipid II PPi signal upon addition of clovibactin. 2D ^{1}H^{31}P ssNMR spectrum establishes direct interactions between the backbone of the depsi-cycle and PPi. **(C)** 2D CC ssNMR data of the ^{13}C,^{15}N-clovibactin – ^{13}C,^{15}N-lipid II complex in liposomes show interfacial contacts with the MurNAc sugar and the hydrophobic sidechains of the depsi-cycle. Interfacial contacts in blue. Data acquired at 950 MHz using 300 ms CC mixing time. **(D)** Sum of interfacial contacts with the sugars of lipid II. Shaded bars show ambiguous contacts of MurNAc with either K3 or L7. **(E)** Illustration of the interface: PPi and MurNAc are in direct proximity, GlcNAc is distal, the pentapeptide is flexible and not involved in the interface. **(F)** ssNMR-derived structural model of the clovibactin – lipid II complex. **(G)** Calculated interfaces of ssNMR structures superimpose very well and show that the hydrophobic depsi-cycle sidechains (Ala6, Leu7, Leu8) wrap like a glove around lipid II-PPi group, interacting with the hydrophobic side of MurNAc. **(H)** The cationic K3 and the polar S4 sidechains favorably interact with the lipid II PPi group**. (I)** Hydrophobic residues of clovibactin embrace the PPi-group like a glove, which appears entropically favourable by the release of boundary water.

headgroup. This is also in line with additional ambiguous interfacial contacts that we observed between Leu7 and the sugars. Together, our data show that all hydrophobic residues of the depsi-cycle are in direct proximity to the lipid II sugars. Almost all interfacial contacts are with MurNAc, the sugar that is covalently attached to the pyrophosphate, while we observed only three weak contacts with the GlcNAc sugar. This means that MurNAc is directly present at the interface with clovibactin, while the GlcNAc sugar is distal to this interface.

Strikingly, most residues of the lipid II pentapeptide were not observable in dipolar-based 2D CC spectra, in which we could only detect the first two residues (Ala*1 and γGlu*2). Since only rigid residues are observable in dipolar ssNMR spectra, our data strongly suggest that the pentapeptide is mobile and not part of the complex interface. This was confirmed with a complimentary scalar spectrum (Baldus and Meier, 1996), which gives a read-out on the mobile residues, in which we exclusively detected the last four residues (γGlu2*, Lys*3, Ala*4, Ala*5) of the pentapeptide **(Figure 5E and Supplementary Figure 10B)**.

Structural model of the complex

We next calculated a structural model of the complex using HADDOCK (van Zundert et al., 2016). While the dimeric (2 x 2) clovibactin is likely the minimal binding arrangement to stably

bind lipid II, we calculated a (4 x 4) arrangement to get a better idea about the supramolecular structure. The structure calculations were based on intermolecular clovibactin – clovibactin distance restraints and interfacial clovibactin – lipid II distance restraints. Hydrogen bonding restraints were applied among and between the dimeric units **(Supplementary Figure 11)**.

The obtained structures superimposed well (2.50±0.85 Å average backbone RMSD for clovibactin in the complex) **(Figure 5F and Supplementary Figure 12)** and show antiparallel dimeric units of clovibactin that could elongate to fibre-like supramolecular structures, in agreement with supramolecular structures observed by HS-AFM. A secondary structure analysis (Heinig and Frishman, 2004) shows about 60-70% β-strand propensity for clovibactin's short N-terminus, an unusual molecular conformation that could foster oligomerization and fibril formation **(Supplementary Figure 12)**. Enabled by the sequence of alternating D- and L-amino acids, hydrophobic (Leu2) and hydrophilic (Lys3, Ser4) sidechains are divided below and above the sheet-like arrangement, positioned to face lipid and water phases, respectively **(Supplementary Figure 12).**

The clovibactin – lipid II interface is well defined by several unambiguous distance restraints (1.47±0.40 Å interfacial RMSD defined by residues Ala6, Leu7, Leu8 of clovibactin, PPi and MurNAc of lipid II) and shows that the backbone amino-protons of the depsi-cycle directly coordinate the PPi group of lipid II. Strikingly, the hydrophobic residues of the despi-cycle (Ala6, Leu7, Leu8) neatly wrap around the PPi-moiety, reminiscent of a hydrophobic glove structure, in agreement with ssNMR distance measurements **(Figure 5G)**. In this configuration, the hydrophobic depsi-cycle sidechains of clovibactin do not form specific interactions with the sugars. Instead, they form a plastic, adjustable interface with the hydrophobic side of the MurNAc sugar, in agreement with unambiguous contacts between Leu8δ1 – MurNAcC3, Ala6Cβ - MurNAcC11, or ambiguous contacts between Leu7Cβ - MurNAcC3 that are all within the hydrophobic patch of MurNAc. The lack of specific interactions with the MurNAc sugar also matches well with the increased dynamics of clovibactin's depsi-cycle in the complex observed by ssNMR relaxation data, and the relatively weak interfacial clovibactin - sugar contacts observed in 2D CC ssNMR spectra. Residue 5 (3-hydroxyasparagine) that attaches the depsi-cycle to the linear N-terminus, shows by far the strongest dynamics, and hence acts as a sort of hinge that uncouples the dynamics of the PPi-binding depsi-cycle from the N-terminal oligomerization domain **(Figure 4B,C)**.

The structures consistently show favourable closer-distance interactions between the anionic lipid II PPi group and the cationic (Lys3) and the polar (Ser4) sidechains of the N-terminus **(Figure 5H)**. This agrees with clear interfacial ssNMR distance restraints Ser4Cβ - MurNAcC1 and Ser4Cβ - MurNAcC3 that show that Ser4-hydroxyl group is in proximity of the lipid II headgroup, and it matches well with the high rigidity of the Lys3 sidechain that is observable in dipolar 2D NH spectra **(Figure 4A and Supplementary Figure 4)**. 2D NH spectra also show that the protons of the cationic N-terminal amino-group of Phe1 are in fast exchange with water, which implies that they are not bound in a tight interaction.

The absence of specific interactions with the hydrophobic depsi-cycle sidechains (Ala6, Leu7, Leu8) is one of the reasons why clovibactin is able to efficiently (K_d for lipid II = 0.086 +/- 0.007 μM) bind a broad spectrum of cell wall precursors with a PPi group (C_{55}PP, lipid I, lipid II) **(Figure 3E, 3F, and Supplementary Figure 13)**. The lack of specific interactions is likely compensated by favourable entropic contributions of the hydrophobic cage, which remains flexible but strips off boundary water molecules that coordinate the PPi group (**Figure 5I**). Critically, we did not observe binding of clovibactin to soluble PPi (Na-pyrophosphate) in isothermal titration calorimetry (ITC) experiments **(Supplementary Figure 13)**, demonstrating that clovibactin selectively binds lipid-anchored pyrophosphate groups. This suggests that settling on the membrane surface and the irreversible formation of supramolecular structures contribute to the effective binding of precursors.

Discussion

Traditional screening platforms have failed to introduce new antibiotics in the last decades, in part due to overmining of Actinomycetes, the traditional source of antibiotics. Novel antibiotics

are likely to be discovered by accessing silent operons, uncovering compounds masked by abundantly produced antimicrobials, and by growing previously uncultured bacteria (Cook and Wright, 2022; Lewis, 2020).

Clovibactin was isolated from an uncultured soil Gram-negative β-proteobacterium *E. terrae ssp. carolina*. It is a new cell wall acting antibiotic with an unusual structure and mode of action. The extract from the producing organism was active against *S. aureus* but isolating the major compound responsible for this activity led to kalimantacin, a known antibiotic (Fage et al., 2020). Kalimantacin is produced by *Pseudomonas* and *Alcaligenes* and inhibits the FabI enoyl-acyl carrier protein reductase of the fatty acid biosynthesis. Kalimantacin is inactive against *B. subtilis* carrying a different biosynthetic enzyme, but the extract was active against *B. subtilis* as well. Upon further examination of the extract, we isolated clovibactin, which was a relatively low abundant compound relative to kalamantacin. In order to simplify the isolation of clovibactin, we inactivated the kalimantacin operon. Inactivating the biosynthesis of abundant compounds to help detect and isolate minor compounds from extracts of interesting producers should be generally applicable to antibiotic discovery. In a similar approach, we recently reported isolation of a novel prodrug antibiotic aminodeoxyguanosine from a silent operon of *Photorhabdus luminescens* by first fractionating and concentrating an extract, and then screening (Shahsavari et al., 2022).

Clovibactin binds to the pyrophosphate moiety of multiple essential cell wall precursors $C_{55}PP$, lipid II and lipid III_{WTA}, from different cell wall biosynthetic pathways. Clovibactin binds to the PPi moiety of these precursors. In general, PPi seems as an unsuitable target for an antibiotic, since it will be released from dead cells together with PPi-containing nucleoside phosphates, and commonly present in the environment. At the same time, pyrophosphate is both an essential and immutable moiety of cell wall lipid intermediates, unlike other portions of the molecules, such as the pentapeptide of lipid II or sugars that can be modified in, e.g., mycobacteria (Mahapatra et al., 2005) or mutated. Moreover, a D-Ala-D-Lac substitution in the lipid II pentapeptide is a common mechanism of resistance to vancomycin that binds to the terminal D-Ala-D-Ala motif. Binding to immutable PPi would explain the lack of detectable resistance to this compound. How clovibactin manages to bind PPi of the central peptidoglycan precursor lipid II tightly *and* selectively is a fascinating question that we address in this study by performing a detailed structural analysis.

From the external medium, clovibactin settles at the membrane surface where it binds cell wall precursors. The leucine sidechain on the N-terminus helps partition clovibactin into the membrane at the site of its targets. Backbone amino-protons of clovibactin's depsi-cycle directly coordinate the PPi, while the hydrophobic depsi-cycle sidechains (Ala6, Leu7, Leu8) surround the PPi group like an adjustable glove, an unusual interaction which is presumably entropically favorable by replacing boundary water, and which enables efficient binding to distinct, indispensable cell wall precursors. Attacking a highly polar target (PPi) with a hydrophobic warhead is a striking, counter-intuitive mode of action. Selective binding to the PPi moiety of lipid precursors is achieved by the formation of a supramolecular complex and subsequent oligomerization into an irreversible higher-order fibrillar assembly of interacting clovibactin molecules bound to the targets on the surface of the membrane. This is presumably enabled by an antiparallel arrangement of clovibactin molecules, in which the short N-terminus acts as oligomerization domain. The comparable concentrations for antibacterial action and for the formation of clovibactin fibrils suggests that supra-structures are an important or even essential part of the killing mechanism. The unique presence of readily accessible PPi-carrying molecules on bacterial membranes enables the formation of this structure and accounts for the lack of clovibactin toxicity against mammalian cells. A surprising feature of clovibactin is its superior ability to cause cell lysis. An intriguing possibility is that clovibactin fibrils, floating on top of the membrane, have an additional function of displacing autolysins from wall teichoic acids, resulting in lysis. The formation of an irreversible supramolecular structure will have

favorable consequences for the in vivo activity of this compound, concentrating it onto bacterial surfaces where it belongs, and continuing to act long after the soluble compound has been cleared from the body. Clovibactin's action against the PPi of cell wall precursors, a simple immutable target, expands our understanding of antibiotics evolved to avoid resistance, and points the way to rationally designing compounds with a long clinically useful life.

Acknowledgements
This work was funded by the Netherlands Organisation for Scientific Research (NWO, grant numbers 723.014.003 & 711.018.001 to MW, and 718.015.001 to AMJJB). This project has received funding from the European Union's Horizon Europe grant and innovation programme under grant agreement No. 101045485 (to MW). Funding for TS, KCL, FG, SDB was provided by the Deutsche Forschungsgemeinschaft (DFG, German Research Foundation), Project-ID 398967434 - TRR 261, and the German Center for Infection Research (DZIF). KL is supported by NIH grants P01AI118687 and RO1AI170962. Funding was also provided by NIH grant AI136137 to L.L.L., and NIH grant AI091224 to A.L.S. NMR experiments at the 950 and 1200 MHz instruments were supported by uNMR-NL, an NWO-funded Roadmap NMR Facility (no. 184.032.207). Support by Instruct-ERIC (to ML and MW) is acknowledged. This work has been supported BioExcel, grant numbers 675728 and 823830, funded by the Horizon 2020 program of the European Commission. The NRS strains were provided by the Network on Antimicrobial Resistance in *Staphylococcus aureus* (NARSA) for distribution by BEI Resources, NIAID, NIH. The authors also wish to acknowledge the help and expertise of the University of Maryland Core Genome Sequencing Facility, Micromyx LLC, Kalamazoo MI, NeoSome Life Sciences, Billerica MA. We would like to thank the following scientists for their work on clovibactin at NovoBiotic Pharmaceuticals, LLC Alysha Desrosiers, William Millett, Kelly Demeo, Ashley Zullo, and Cintia Felix. The plasmid pIJ12738 was a gift from the John Innes Centre.

Author contributions
KL, TS, DH, LLL and MW designed the study. RS, AJP, MGN, AN, ML, and MW did NMR experiments. AN isolated clovibactin. KCL and SDB did mode of action studies. RS and FG did fluorescence microscopy. AMK and UK did single molecule mobility measurements in supported bilayers. SM and WHR did HS-AFM studies. ALS performed the fermentations, gene knockout work, and isolated the DNA for sequencing. CA performed susceptibility and cytotoxicity assays. CJS sequenced and annotated the genome. RS did calorimetric studies. RS, MGND, and EB prepared ssNMR samples and Lipid II. FL, BJAV, RVH, AMJJB, and MW did structure calculations. All authors contributed to data analysis. RS, KL, TS, and MW wrote the manuscript with input from all authors.

Competing Interests
The following authors, A. J. Peoples, C. Achorn, A. Nitti, A. L. Spoering, L. L. Ling, D. E. Hughes, and K. Lewis, declare competing financial interests as they are employees and consultants of NovoBiotic Pharmaceuticals. A patent US 11,203,616 B2 was issued 12/21/2021 and describes the use of clovibactin (Novo29) and as an antibiotic, as well as the pharmaceutical composition and antibiotic use of derivatives. The other authors have no competing interests.

Data availability
The NMR assignments of unbound clovibactin and the clovibactin – Lipid II complex have been deposited in the BMRB database (accession numbers 51629 and 51630). Experimental solid-state NMR raw data have been deposited in an open repository (DOI: 10.5281/zenodo.7075976).

Material & Methods

Isolation of strain producing clovibactin

The isolate producing clovibactin, P9846, was isolated from a sandy soil collected in North Carolina using techniques previously described (Buerger et al., 2012a, b). Briefly, 1 gram of heat-treated soil (dry heat at 65° C for 30 minutes) was mixed with 9 mL of sterile water, vortexed, and then diluted into molten SMS agar (0.125 g casein, 0.1 g potato starch, 1 g casamino acids, 20 g bacto-agar in 1 L of water). This mixture was then dispensed in 100 µL aliquots per well of a flat bottom 96-well plate. The 96-well plates were incubated for 16 weeks at room temperature in a humidified chamber and observations of growth were made over time. The isolate P9846 grew to a size detectable under a dissecting microscope (50X magnification) at week 12 of the incubation.

Isolates from long-term incubation experiments were sub-cultured from their original incubation plates to individual plates of SMSR4 (0.125 g casein, 0.1 g potato starch, 1.5 g casamino acids, 1 g glucose, 0.1 g yeast extract, 0.3 g proline, 1 g $MgCl_2$-6H2O, 0.4 g $CaCl_2$-$2H_2O$, 0.02 g K_2SO_4, 0.56 g TES free acid (2-[[1,3-dihydroxy-2-(hydroxymethyl) propan-2-yl]amino]ethanesulfonic acid) and 20 g bacto-agar in 1 L of water agar). Monocultures of isolates were grown in a seed medium (15 g glucose, 10 g malt extract, 10 g soluble starch, 2.5 g yeast extract, 5 g casamino acids, and 0.2 g $CaCl_2$-$2H_2O$ per 1 litre of deionized H_2O, pH 7.0) to promote biomass production. Grown cultures were diluted 1:20 into 4 different fermentation broths. After 11 days of agitation at 28°C, the fermentations were dried and resuspended in an equal volume of 100% DMSO. Then 5 µL of extracts were spotted onto a lawn of growing *S. aureus* NCTC8325-4 cells in Mueller Hinton agar (MHA) plates. After 20 hours of incubation at 37°C, visible clearing zones indicated antibacterial activity. The extract from P9846 produced a large clearing zone. Although it produced antibacterial activity under several fermentation media, the best activity (that is, largest clearing zone) was seen with R4 fermentation broth (10 g glucose, 1 g yeast extract, 0.1 g casamino acids, 3 g proline, 10 g $MgCl_2$-$6H_2O$, 4 g $CaCl_2$-$2H_2O$, 0.2 g K_2SO_4, 5.6 g TES free acid (2-[[1,3-dihydroxy-2-(hydroxymethyl) propan-2-yl]amino]ethanesulfonic acid) per 1 litre of deionized H_2O, pH adjusted to 7.0 using KOH).

Clovibactin Isolation Procedure

n-Butanol (0.5V) was added to fermentation broth. The mixture was shaken vigorously, then left over night at room temperature until 2 distinct phases developed. The butanol phase was dried to completeness on a Buchi rotary evaporator. The resulting residue was reconstituted in a solution of 25% acetonitrile in water with 0.1% trifluoroacetic acid (~240 mL). This concentrated extract was centrifuged, and the supernatant decanted to remove any undissolved material. The supernatant was divided into 6 equal portions (~40 mL each) and successively purified on a preconditioned C18 flash chromatography column (Biotage, Sfar C18 60g, gradient of 25% - 100% acetonitrile in water (w/0.1% TFA), 50 mL/min). The compound of interest (clovibactin) was found at an adequate level of purity in two fractions as verified by mass spectrometry. The fractions containing clovibactin were concentrated under reduced pressure and lyophilized to yield approximately 125 mg from 6L of fermentation.

Clovibactin Mass Spectrometry

Clovibactin was obtained as a white amorphous powder and its molecular formula ($C_{43}H_{70}N_{10}O_{11}$) was determined by LC-MS (*m/z* of 903.5291 $[M+H]^+$, calculated 903.5298). This is consistent with ^1H and ^{13}C NMR data. Furthermore, ^{13}C and ^{15}N labeled clovibactin had an observed mass of 956.6472 $[M+H]^+$ (calculated 956.6460).

Clovibactin 1D and 2D solution NMR Experiments
About 10 mg of Clovibactin was dissolved in ~600 µL of DMSO-*d*6. The following NMR experiments were performed on this sample: ^{1}H, ^{13}C, ^{1}H-^{1}H COSY, ^{1}H-^{1}H COSY, ^{1}H-^{1}H NOESY, ^{1}H-^{1}H TOCSY, ^{1}H-^{13}C HSQC, ^{1}H-^{13}C HMBC, ^{1}H-^{15}N HSQC.

Whole genome sequencing of P9846
Isolated gDNA was sequenced on a multiplexed PacBio Sequel II SMRT Cell 8M (Pacific Biosciences) using Sequel II 2.0 chemistry at the University of Maryland Core Genome Sequencing Facility yielding 836,139 total reads for this sample with a mean read length of 11,416 bp. Reads were assembled with SMRT8.0.0_HGAP4 (N50 = 5,455,962). The completed genome for P9846 contained a single circular chromosome and 3 extrachromosomal contigs (5.5 Mb chromosome, 7.0 Mb total) with 69% GC content.

Biosynthetic analysis of P9846 genome
Assembled contigs were concatenated into a single nucleotide FASTA file and analyzed by AntiSMASH (https://antismash.secondarymetabolites.org/#!/start) version 5.1.1 using relaxed detection strictness and all extra features enabled. 10 putative biosynthetic gene clusters (BGCs) were identified on the chromosome, as well as 4 and 5 on two of the three extrachromosomal contigs for a total of 19 BGCs. Of these, two were found to have high similarity to known compounds in the Minimum Information about a Biosynthetic Gene cluster (MIBiG) database, the PKS compounds SGR-polycyclic tetramate macrolactam and malleilactone.

Annotation of clovibactin biosynthetic gene cluster
The BGC responsible for cyclic peptide clovibactin was identified in the extrachromosomal genetic material where the majority of the NRPS BGCs are located. Eight complete NRPS modules corresponding to the amino acids found in the compound were identified and predictions of adenylation domain specificity from AntiSMASH were checked against Non-Ribosomal Peptide Synthase Substrate Predictor (NRPSsp, http://www.nrpssp.com/). Presence of dual-function condensation domains were used to identify sites of epimerization. Dioxygenase function was assigned based on homology to *cucE* from cupriachelin biosynthesis (MIBiG BGC0000330). The annotated sequence for clovibactin has been deposited into the MIBiG repository under the accession number #####.

Determination of MICs
MIC values were determined using a broth microdilution method as recommended by the CLSI. The test medium for most species was cation-adjusted Mueller-Hinton broth (MHB). The same test medium was supplemented with 3% lysed horse blood (Cleveland Scientific, Bath, OH.) for growing Streptococci. *Haemophilus* Test Medium was used for *H. influenzae* (Teknova, Hollister, CA, or HTM; Remel; Lot No. 903401), Middlebrook 7H9 broth (Difco) was used for mycobacteria. For *N. gonorrhoeae*, a modified broth medium described by the ATCC was used. The medium contained 15 g Oxoid Special Peptone (Oxoid, Hampshire, UK; Lot No. 1280296), 1 g corn starch (Ward's Science; Rochester, NY; Lot No. AD-13344-14), 5 g NaCl (VWR, Radnor, PA; Lot No. 57897), 4 g K_2HPO_4 (Sigma, St. Louis, MO; Lot No. 052K0147), and 1 g KH_2PO_4 (Sigma; Lot No. SLBC1921V). After autoclaving, the medium was centrifuged at 5,000 x g for 10 min, the supernatant was passed through a 0.45 µm filter, and IsoVitaleX supplement (BD; Lot No. 6309687) was added at 1% (v/v).

All test media were supplemented with 0.002% polysorbate (Tween) 80 to prevent drug binding to plastic surfaces, and cell concentration was adjusted to approximately $5x10^5$ cells/mL. After 20 hours of incubation at 37ºC (2 days for *M. smegmatis,* 7 days for *M. tuberculosis*), the MIC was defined as the lowest concentration of antibiotic with no visible growth.

Fetal bovine serum (ATCC) was added to MHB (1:10) to test the effect of serum for *S. aureus* NCTC8325-4 and *S. aureus* ATCC29213. Experiments were performed with three biological replicates.

Mammalian cytotoxicity.
The CellTiter 96® AQueous One Solution Cell Proliferation Assay (Promega) was used to determine the cytotoxicity of clovibactin on NIH 3T3 mouse embryonic fibroblast (ATCC CRL-1658, in Dulbecco's Modified Eagle's medium supplemented with 10% bovine calf serum), and HepG2 cells (ATCC HB-8065^{TM}, in Dulbecco's Modified Eagle's medium supplemented with 10% fetal calf serum). Exponentially growing cells were seeded into a 96-well flat bottom plate, and incubated at 37°C. After 24 hours, the medium was replaced with fresh medium containing test compounds (0.5 µL of a two-fold serial dilution in DMSO to 99.5 µL of media, tested up to 100 µg/mL clovibactin). After 72 hours of incubation at 37°C, reporter solution was added to the cells and after 2 hours, the OD_{490} was measured using a Spectramax Plus Spectrophotometer. Experiments were performed with three biological replicates.

Minimum bactericidal concentration (MBC) .
Cells from the wells from an MIC microbroth plate for *S. aureus* NCTC8325-4 and *S. aureus* ATCC29213 that had been incubated for 20 hours at 37°C were pelleted. An aliquot of the initial inoculum for the MIC plate was similarly processed. The cells were resuspended in fresh media, plated onto MHA, and the colonies enumerated after incubating for 24 hours at 37°C. The MBC is defined as the first drug dilution which resulted in a 99.9% decrease from the initial bacterial titer of the starting inoculum. Experiments were performed with three biological replicates.

Time-kill curves
Macrobroth MIC was determined for S. aureus ATCC 29213 in MHB II supplemented with 0.002% polysorbate 80 as 1 mL culture in polystyrene culture tubes after 20 hours of incubation at 37°C with aeration at 225 rpm. The MIC was 16 µg/mL for chloramphenicol, 1 µg/mL for vancomycin and 2 µg/mL for clovibactin under these conditions. To conduct time dependent killing, exponentially growing *S. aureus* ATCC 29213 cells were challenged with antibiotics at 37°C with aeration at 225 rpm -chloramphenicol (5X MIC, 80 µg/mL), vancomycin (10X MIC, 10 µg/mL), clovibactin (1XMIC, 2 µg/mL) or clovibactin (5X MIC, 10 µg/mL) in culture tubes at 37°C and 225 rpm. At intervals, 100 µL aliquots were removed, and 100 µL of ten-fold serially diluted suspensions were plated on MHA plates. Colonies were counted after 20 hours of incubation at 37°C, and CFU/mL was calculated. Experiments were performed with three biological replicates.

Macromolecular synthesis assay
S. aureus NCTC8325-4 cells were cultured in minimal medium (0.02 M Hepes, 0.002 M $MgSO_4$, 0.0001 M $CaCl_2$, 0.4% succinic acid, 0.043 M NaCl, 0.5% $(NH_4)_2 SO_4$) supplemented with 5% Tryptic Soy Broth (TSB). Cells were pelleted and resuspended into fresh minimal medium supplemented with 5% TSB containing test compounds and radioactive precursors to a density of 10^8 cells/mL. The radioactive precursors were glucosamine hydrochloride, D-[6-3H(N)] (1 mCi/mL), leucine, L-[3,4,5-3H(N)] (1 mCi/mL), uridine, [5-3H] (1 mCi/mL), or thymidine, [methyl-3H] (0.25 mCi/mL) to measure cell wall, protein, RNA, and DNA synthesis, respectively. After 20 minutes of incubation at 37°C, aliquots were removed, added to ice cold 25% trichloroacetic acid (TCA), and filtered using Multiscreen Filter plates (Millipore Cat. MSDVN6B50). The filters were washed twice with ice cold 25% TCA, twice with ice cold water, dried and counted with scintillation fluid using Perkin Elmer MicroBeta TriLux Microplate Scintillation and Luminescence counter. Experiments were performed with two biological replicates.

Resistance studies

No spontaneous resistant mutants of *S. aureus* ATCC 29213 were obtained when plating $1.2X10^{10}$ cells on agar media with 4xMIC clovibactin. No colonies grew up after 3 days of incubation at 37°C.

Single dose PK in mice.

Clovibactin was tested in a PK study to evaluate the systemic exposure and blood residence time of the compound. CD-1 female mice (n=3 per timepoint) were administered a single dose of compound at 20 mg/kg IV bolus. Blood was drawn at different times and clovibactin plasma levels determined by LC-MSMS. PK parameters were determined using the software package Watson LIMS.

Neutropenic mouse thigh infection study

Clovibactin was evaluated in a neutropenic mouse thigh infection model. Female CD-1 mice (n=4 per group) received two doses of cyclophosphamide 4 days (150mg/kg), and 1 day (100 mg/kg) prior to infection. S*. aureus* ATCC 33591 (MRSA) was injected into the thighs. The infection controls demonstrated a bioload of 6.07 $\log_{10}$ CFUs/ gram of thigh at the time of treatment (2 hours). Clovibactin was delivered as two IV doses (2 and 4 hours post infection).

Producing ^{13}C -^{15}N labeled clovibactin

P9846 makes multiple antibacterial compounds. Under the typical fermentation conditions (R4 broth) clovibactin is made in sufficient quantities. However, under labelling conditions we found that a known antibiotic, kalimantacin (Kamigiri et al., 1996), was produced in large amounts and interfered with clovibactin purification. Using the whole genome sequence, we identified the BGC with 55% identity to the kalimantacin gene(Mattheus et al., 2010). Production of kalimantacin was reduced below detectable levels by interrupting the bat genes and generating the strain P9846m01. The bat genes were interrupted using homologous recombination previously described (Fernández-Martínez and Bibb, 2014). Following procedures from Martinez et al. ~500 bp fragments from upstream and downstream of the P9846 bat1 gene were made by pcr using primers in supplemental table 2. Fragments were digested with XbaI or KpnI and BamHI (New England Biolabs) and cloned into plasmid pIJ12738 digested with XbaI and KpnI. This created a 4605 bp plasmid, pBat1ko. pBat1ko was transformed into mobilization strain ET12567. Using conjugation conditions, the pIJ12738 was transferred into P9846 and selected with 50 ug/ml apramycin on SMSR4 agar. The insertion in mutant, P9846m01 was confirmed using pcr with primers bat1downstream and bat1upstream (supplemental table 2). Disruption was further confirmed by fermentation in R4 medium and subsequent loss of kalimantacin derived active zones against a lawn of *S. aureus* followed by a lack of detectable kalimantacin by LC-MS in the appropriate fraction.

To label clovibactin, P9846m01 was grown from a frozen stock on SMSR4 agar supplemented with 50 ug/ml apramycin for 48 hours at room temperature. Biomass was scraped into 20ml flask of Celtone-R4 broth (10 g D-glucose; Cambridge Isotope Laboratories (CLM) #CLM-1396-5, 1 g Celtone base powder; CLM #CGM-1030P-CN-1, 0.5 g L-proline; CLM #CNLM-436-H-0.5, 10 g MgCl2-6H2O, 4 g CaCl2- 2H2O, 0.2 g K2SO4, 5.6 g TES free acid (2-[[1,3-dihydroxy-2-(hydroxymethyl) propan-2-yl]amino]ethanesulfonic acid) per 1 liter of deionized H2O, pH 7 C). After 3 days of incubation with shaking at 28°C the culture was split between 2 flasks of 500ml Celtone-R4 broth. This culture was incubated with shaking at 28°C for 6 days. ^{13}C and ^{15}N labeled clovibactin was isolated in a similar manner as above, yielding 5.7 mg of $^{13}C^{15}N$ - labeled clovibactin from a 1 L fermentation.

β-galactosidase reporter assays

B. subtilis β-galactosidase reporter assays were performed as previously described (Harms et al., 2018). In short, reporter strains were grown in MHB containing 5 µg/ml chloramphenicol at 30 °C to an OD_{600} of 0.5. Subsequently, cells were poured at 1×10^7 CFU/ml in MHA plates supplemented with 5 µg/ml chloramphenicol, 75 µg/ml (cell wall reporter), 125 µg/ml (DNA reporter), and 250 µg/ml (RNA and protein reporters) X-gal, respectively. After solidification of the plates, 6 µg of clovibactin and control antibiotics

selectively inducing the promotors were spotted (6 µg vancomycin for cell wall, 0.3 µg ciprofloxacin for DNA, 6 µg rifampicin for RNA, 3 µg clindamycin for protein). Results were documented after incubation overnight at 30°C.

Quantification of intracellular UDP-*N*-acetylmuramic acid-pentapeptide

To analyze the cytoplasmic nucleotide pool we adapted the protocol of Kohlrausch and Höltje (Kohlrausch and Höltje, 1991). *S. aureus* SG511 was grown in 20 ml MHB at 37°C to an OD_{600} of 0.6 and incubated with 130 µg/ml chloramphenicol for 15 min. Clovibactin was added at 0.5×, 1×, 2.5×, and 5×MIC and incubated for another 30 min. Vancomycin (5× MIC) was used as positive control. Extraction and analysis of nucleotide-linked peptidoglycan precursors was performed as described previously (Schneider et al., 2009). Corresponding fractions were confirmed by mass spectrometry.

Luciferase reporter antagonization assays

B. subtilis luciferase reporter assays were conducted as previously described (Tan et al., 2019; Umbreit and Strominger, 1972). Briefly, luciferase reporters were grown in MHB containing 5 µg/ml chloramphenicol at 30°C to an OD_{600} of 0.5. Cells were added to 96-well white wall chimney plates containing serially diluted antibiotics. For antagonization assays, purified cell wall lipid intermediates (C_{55}PP, lipid I, lipid II, lipid III_{WTA}) and phospholipids (phosphatidylglycerol [PG], phosphatidylcholine [PC], cardiolipin [CL]) were added in 0.5 to 4-fold molar excess with respect to clovibactin (0.5× MIC) and were pre-incubated for 10 min prior to addition of the reporter strain. Luminescence measurements were performed at 30 °C in a microplate reader Spark 10M (Tecan). At least three independent biological replicate experiments were conducted.

Bacterial cell wall integrity assay

Bacterial cell wall integrity assays were adapted from previous work (Schneider et al., 2010). *B. subtilis* 168 cultures were grown in MHB at 30°C to an OD_{600} of 0.3. Subsequently, cells were treated with 0.5 µg/ml clovibactin, 1 µg/ml vancomycin, 32 µg/ml clindamycin, or DMSO for 30 min. Cells were immediately fixed in a 1 ml 1:3 (v:v) mixture of acetic acid and methanol and immobilized on thin 1% w/v agarose slides. Imaging was performed by phase contrast microscopy on a Zeiss AxioObserver Z1 equipped with an HXP 120 C lamp, an αPlan-APOCHROMAT 100×/1.46 oil objective and an AxioCam MRm camera and further processed with Zen 2 (Zeiss) and analyzed and postprocessed using ImageJ v1.52p (Schneider et al., 2012).

MIC-type antagonization assays

Antagonization of the antibiotic activity of clovibactin by potential target molecules was performed by an MIC-based setup in microtiter plates. Clovibactin (8× MIC) was mixed with HPLC-purified antagonists (C_{55}PP, lipid I, lipid II, lipid III_{WTA} and DOPG) in 0.5 to 4-fold molar excess with respect to the antibiotic. *S. aureus* SG511 (5×10^5 CFU/ml) was added and samples were examined for visible bacterial growth after incubation at 37°C overnight. Experiments were performed with at least three biological replicates.

Synthesis and purification of lipid intermediates

Large scale synthesis and purification of the PGN precursors lipid I and lipid II were performed as previously described (Ling et al., 2015). UDP-*N*-acetyl-muramic acid pentapeptide (UDP-MurNAc-pp) was purified according to the protocol elaborated by Kohlrausch and Höltje (Kohlrausch and Höltje, 1991). Undecaprenyl phosphate (C_{55}P) and undecaprenyl diphosphate (C_{55}PP) were purchased from Larodan Fine Chemicals AB (Malmö, Sweden). The phospholipids 1,2-dioleoyl-*sn*-glycero-3- phosphocholine (DOPC), 1,2-dioleoyl-*sn*-glycero-3-phosphoglycerol (DOPG) and 1′,3′-bis[1,2-distearoyl-*sn*-glycero-3-phospho]-glycerol (DOCL, cardiolipin) were purchased from Avanti Polar Lipids (Alabaster, AL, USA). The concentration of purified PGN and wall teichoic acid precursors was quantified on the basis of their phosphate content as described (Rouser et al., 1970).

In vitro lipid II synthesis with isolated membranes

In vitro lipid II synthesis was performed using membranes of *M. luteus* as previously described (Brötz et al., 1998) (Umbreit and Strominger, 1972). Briefly, synthesis was assayed by incubating membrane preparations (200 µg protein) with 5 nmol $C_{55}P$, 50 nmol UDP-MurNAc-pentapeptide, 50 nmol UDP-*N*-acetylglucosamine (UDP-GlcNAc) in 60 mM Tris-HCl, 5 mM $MgCl_2$, and 0.5 % Triton X-100, at pH 7.5 in a total volume of 50 µl at 30°C for 1 h. $C_{55}P$-containing products were extracted with an equal volume of *n*-butanol/pyridine acetate, pH 4.2 (2:1, v/v) and analyzed by TLC using chloroform/methanol/water/ammonia (88:48:10:1, v/v/v/v) as the solvent(Rick et al., 1998) and phosphomolybdic acid staining (Schneider et al., 2004). The quantitative analysis of lipids extracted to the butanol phase was carried out by phosphorimaging in a StormTM imaging system (GE Healthcare) or PMA staining and analysis performed using Image Quant TL. Clovibactin was added in molar ratios of 0.5 to 4 with regard to $C_{55}P$.

In vitro PGN synthesis reactions using purified proteins and substrates

To determine the enzymatic activity of MraY-His_6 the assay was carried out in a total volume of 50 µl containing 5 nmol $C_{55}P$, 25 nmol of UDP-MurNAc-pp in 100 mM Tris-HCl, 10 mM $MgCl_2$, at pH 7.5, and 0.6% Triton X-100. The reaction was initiated by the addition of 2 µg of MraY-His_6 and incubated for 1.5 hours at 30°C.

The *in vitro* MurG reaction was performed in a 30 µL reaction containing 2 nmol of purified lipid I and 25 nmol of UDP-*N*-acetyl glucosamine (UDP-GlcNAc) in 200 mM Tris-HCl, 5.7 mM $MgCl_2$, at pH 7.5, and 0.8% Triton X-100 with 2 µg of purified, recombinant MurG-His_6 enzyme. Reaction mixtures were incubated for 30 min at 30°C.

The PBP2 activity assay was performed in a 50 µL reaction containing 2 nmol of purified lipid II, in 20 mM MES, 2 mM $MgCl_2$, and 2 mM $CaCl_2$, at pH 5.5 with 2 µg of purified, recombinant PBP2-His_6 enzyme. Reaction mixtures were incubated for 2 h at 30 °C.

Dephosphorylation of $C_{55}PP$ was determined using purified YbjG-His_6 enzyme (SA0415). A total of 20 nmol of $C_{55}PP$ was incubated with 3 µg of YbjG-His_6 in 20 mM Tris-HCl, 150 mM NaCl, and 0.8% Triton X-100 at pH 7.5 in 50 µL for 30 min at 30°C.

In all *in vitro* assays, clovibactin was added in molar ratios from 0.5 to 2 (and to 4 for MraY and MurG) with respect to the respective substrate. $C_{55}P$-containing products were extracted, analyzed by TLC and quantified as described above. The quantitative analysis of lipids extracted to the *n*-butanol phase was carried out using ImageJ v1.53p software (National Institutes of Health) (Schneider et al., 2012). Experiments were performed at least in triplicates.

Complex formation clovibactin

Binding of clovibactin to $C_{55}PP$, lipid I, lipid II, lipid III_{WTA} and DOPG was analyzed by incubating 2 nmol (lipid I, lipid II, lipid III_{WTA}) or 5 nmol ($C_{55}PP$ and DOPG) with 8-fold molar excess of clovibactin in 50 mM Tris-HCl, at pH 7.5 for 30 min at room temperature. Complex formation was analyzed by extracting unbound precursors from the reaction mixture followed by TLC analysis as described above. Experiments were performed with biological replicates.

Lysis assay

Visual analysis of lysis was conducted in microtiter plates, exponential and stationary phase cells (OD_{600} 0.5 and 1, respectively) cells of *S. aureus* SA113 and the AtlA-deficient mutant *S. aureus* SA113 Δ*altA* (supplemented with 150 µg/ml spectinomycin) were treated with clovibactin and vancomycin at concentrations of 0.5×, 1× and 2× the MIC and were photographed after 24 hours. Experiments were performed with three biological replicates.

Bacterial cell wall integrity "blebbing" *assay*

Bacterial cell wall integrity assays were performed as described previously (Schneider et al., 2010). *B. subtilis* 168 cultures were grown in MHB at 30°C to an OD_{600} of 0.3. Subsequently, cells were treated with clovibactin, teixobactin, hypeptin and vancomycin (0.25 x MIC each), 256 µg/ml ampicillin, and further incubated at 30°C for 90 min. Cells were immediately fixed

with in a 1 ml 1:3 (v:v) mixture of acetic acid and methanol and immobilized on thin 1 % w/v agarose slides. Imaging was performed by phase contrast microscopy on a Zeiss Axio Observer Z1 microscope (Zeiss, Jena, Germany) equipped with HXP 120 V light source and an Axio Cam MR3 camera. Images were acquired with ZEN 2 software (Zeiss) and analyzed and postprocessed using ImageJ v1.45s software (National Institutes of Health).

Potassium efflux

The potassium release assay was performed as described previously. Briefly, tryptic soy broth (TSB)-grown *S. simulans* 22 cells were harvested at an OD_{600} of 1.0 to 1.5, washed with cold choline buffer (300 mM choline chloride, 30 mM MES, 20 mM Tris, pH 6.5), and resuspended to an OD_{600} of 30. The concentrated cell suspension was kept on ice and used within 30 min. For each measurement, the potassium electrode (Mettler Toledo) was calibrated with potassium chloride. Cells were diluted in choline buffer at RT to an OD_{600} of 3, and antibiotic-induced potassium release was monitored in 15 sec intervals for 5 min at RT. Clovibactin was added in a concentration corresponding to 1 and 5× MIC. Potassium concentrations were calculated from the measured voltage according to (Orlov et al., 2002) and plotted relative to the total amount of potassium released after the addition of 1 µM of the pore-forming lantibiotic nisin (set 100 % efflux). Results show mean values of three independent experiments.

MinD delocalization studies

B. subtilis 1981 *erm spc minD*:*ermC amyE*::P_{xyl}-*gfp-minD*, a strain with a *gfp-minD* fusion under control of the P_{xyl} promotor, was grown in MHB supplemented with 0.1 % w/v xylose and 50 µg/ml spectinomycin at 30 °C to an OD_{600} of 0.6. Imaging was carried out within 2, 5, and 30 min after addition of antibiotic at 2× and 10× MIC. The proton ionophore carbonyl cyanide *m*-chlorophenylhydrazone (CCCP, 100 µM) was used as positive control and imaging was carried out within 2 min. Samples were immobilized on microscope slides covered with 1 % w/v agarose. Fluorescence microscopy and analysis was performed using the same microscope and software as described for phase contrast microscopy.

Fluorescence labeling and fluorescence microscopy

Clovibactin was dissolved in anhydrous DMF (5 mg/ml) and BODIPY™ FL succimidyl ester (Invitrogen) was dissolved in DMSO (10 mg/ml). For labeling, 1 vol of BODIPY™ FL was added to 0.5 vols of DIPEA and 5 vols clovibactin solution and incubated at room temperature with gentle agitation. After 2 hours, ice-cold diethylether was added to the reaction mixture leading to precipitation of clovibactin. After centrifugation, the supernatant was carefully aspirated, and the pellet was dissolved in anhydrous DMF. Separation of labeled and non-labeled clovibactin was achieved by HPLC purification on a Poroshell 120 EC-C18, 2.7 µm, 3 × 150 mm column (Agilent), column temperature 50 °C, with gradient of (A) 79.9% H_2O + 20% acetonitrile (MeCN) + 0.1% trifluoroacetic (TFA) and (B) 49,9% H_2O + 50% MeCN + 0.1% TFA: 0 min, %B = 0, 10 min, %B = 60, 34 min, %B = 80. Clovibactin-FL was collected and confirmed by LC-MS.

To study localization of clovibactin, cultures were grown in MHB at 37°C until an OD_{600} of 0.5 and were pre-incubated for 10 min with teixobactin (2× MIC) or the corresponding amount of DMSO. Cells were then washed four times with MHB prior to 10 min incubation with a 1:3 mixture of unlabeled and labelled clovibactin (2× MIC) and Tween 80 at a final concentration of 0.002%. To visualize cell membranes, nile red was added to a final concentration of 1 µg/ml. Subsequently, cells were washed four times in phosphate-buffered saline (PBS) and mounted on microscope slides covered with a thin film of 1% v/v agarose. Images were acquired using a Zeiss AxioObserver Z1 equipped with an HXP 120 C lamp, an αPlan-APOCHROMAT 100×/1.46 oil objective and an AxioCam MRm camera. Standard filter sets were used for BODIPY™ FL (450–490 nm excitation and 500–500 nm emission). Images were further processed with Zen 2 (Zeiss) and analyzed and postprocessed using ImageJ v1.52p (Schneider et al., 2012).

Analysis of single molecule mobility in supported lipid bilayers

Lipid II-Atto565 was obtained by labeling of lipid II with a 10-fold excess of Atto565-NHS ester (Sigma-Aldrich, Taufkirchen, Germany) in presence of 0.6 vol% diisopropylethylamine (Sigma-Aldrich, Taufkirchen, Germany). The reaction was carried out in water-free chloroform for 2 hours at room temperature. Lipid II-Atto565 was purified via thin layer chromatography.Supported bilayers were formed by DOPC 0.2 mol% lipid II/lipid II-Atto565. The required lipid composition was prepared in chloroform to reach a lipid concentration of 1.3 mM. Then, chloroform was removed in a nitrogen stream and the dried lipid film was solved in HEPES/Triton buffer (20 mM HEPES, 150 mM NaCl, 20 mM Triton X-100, pH 7,4) in order to reach a lipid concentration of 5 mM. The stock solution was divided into 20 µL aliquots and stored at -20°C. To enable the preparation of planar lipid bilayers on coverslips, a suspension containing very small unilamellar vesicles (VSUV) was prepared by addition of 200 µL HEPES buffer (20 mM HEPES, 150 mM NaCl) and 200 µL of a 4 mM heptakis(2,6-di-O-methyl)-ß-cyclodextrin to each of the aliquoted lipid-detergent solutions. Finally, the vial was vortexed for 2 minutes.

In order to increase the hydrophilicity of the glass support, coverslips with a diameter of 18 mm were placed for at least 1 hour in freshly prepared Piranha-solution (one-part H_2O_2 30% and three parts H_2SO_4). Then, the coverslips were washed with milliQ water, dried in a nitrogen stream and inserted into custom-built sample chambers. The VSUV suspension resulting from one aliquot was immediately added on top of the cleaned coverslip. After an incubation time of 6 minutes, unfused vesicles were removed by washing of the coverslip with HEPES buffer. During the washing steps care was taken to not dry out the lipid bilayer. Bilayers were kept in HEPES buffer and the respective amounts of teixobactin and clovibactin were added from stock solutions in DMSO to freshly prepared bilayers.

After an incubation time of 30 minutes the samples were imaged using a custom-built setup enabling single-molecule microscopy (Ruland et al., 2021). An α-plan-apochromat 63x/1.46 objective (Zeiss) and a sCMOS camera (Prime BSI, Teledyne Photometrics, Tucson, AZ, USA) were used for data acquisition resulting in a pixel size of 103.2 nm. Images were acquired with a field of view of 30.96 µm x 30.96 µm and a single frame integration time of 10 ms. Excitation of Atto565 was performed using a DPL 561 nm laser (Hübner Photonics GmbH, Kassel, Germany). For every sample 27 movies consisting of 1000 frames were acquired at different sample locations. For every experimental condition three independently prepared samples were measured. Single-particle tracking was performed with the ImageJ 1.52p (Schindelin et al., 2012) (Schindelin et al., 2012) plugin TrackMate (Tinevez et al., 2017) after background subtraction using a rolling ball radius of 50. For spot detection, the LoG-based detector was used, the parameter “estimated blob diameter” was set to 0.75 µm, the threshold was set to 2.2. Tracking was performed by the “Simple LAP Tracker”. Gap-closing was allowed with a maximum closing distance of 1 µm and a maximum frame gap of two frames. A maximum linking distance of 1 µm was chosen. From the resulting tracking data, the mean square displacement as function of time was determined and plotted with the Software OriginPro 2021b (OriginLab Co., Northhampton, MA, USA). A linear fit was performed and according to the Einstein equation for two-dimensional diffusion, the diffusion coefficient of lipid II-Atto565 molecules was determined by dividing the slope of the linear fit by 4.

Synthesis and purification of isotopically labelled Lipid II

Lipid II was produced according to published methods(Breukink et al., 2003) based on enzymatic lipid reconstitution using the Lipid II precursors UDP-GlcNAc, UDP-MurNAc-pentapeptide and polyisoprenolphosphate as substrates.(Breukink et al., 2003) Lysine-form UDP-MurNAc-pentapeptide was extracted from *Staphylococcus simulans* 22. ^{13}C,^{15}N-labelled UDP-GlcNAc and UDP-MurNAc-pentapeptide (lysine form) were extracted from *S. simulans* 22 grown in [^{13}C/^{15}N]-labelled rich medium (Silantes) and supplemented with [U-^{13}C]-D-glucose and [^{15}N]-NH_4Cl. Polyisoprenolphosphate was synthesized via phosphorylation of polyisoprenol obtained from *Laurus nobilis*(Danilov et al., 1989). The head-group precursors were extracted from bacteria and polyisoprenol was extracted from leaves as described

(Kohlrausch, 1991). After synthesis, Lipid II was extracted with 2:1 BuOH:(Pyr/Acetate, 6 M) and then purified with a DEAE cellulose resin using a salt gradient of 0 - 600 mM NH_4HCO_3 with 2:3:1 $CHCl_3$:MeOH:[H_2O+salt]. Fractions containing pure Lipid II were pooled, dried, and dissolved in 2:1 chloroform/methanol. Lipid II concentration was estimated through an inorganic phosphate determination(Rouser et al., 1970).

Solid-State NMR sample preparation

Multi-lamellar vesicles (MLVs) of DOPC doped with 4 mol% Lysine-Lipid II in buffer (30mM Citrate, 300mM NaCl, pH 5.5) were collected by centrifugation (60,000×*g*) and loaded into ssNMR rotors. For 3.2 mm rotors, we used 800 nmol of clovibactin with unlabelled Lipid II, while we used 400 nmol with labelled Lipid II. For 1.3 mm rotors, samples contained 200 nmol of antibiotic for unlabelled Lipid II.

Solid-state NMR spectroscopy

^{1}H-detected ssNMR experiments were performed at 60 kHz magic angle spinning (MAS) using magnetic fields of 700, 950, and 1200 MHz (^{1}H frequency) with dipolar transfer steps and using low-power PISSARRO (Weingarth et al., 2009a) decoupling in all dimensions. ^{1}H-detected ^{15}N T_{1rho} relaxation experiments (Lewandowski et al., 2011) were acquired with a ^{15}N spin lock-field of 18 kHz and spin-lock durations of 0, 10, 20, 40, 70, and 100 ms. T_{1rho} trajectories were fit to single exponentials. 2D CC experiments were acquired with PARIS (Weingarth et al., 2009b) PARISxy (Weingarth et al., 2010) recoupling (m=1) at 950 and 1200 MHz magnetic field and 15 to 18 kHz MAS. To probe interfacial contacts between ^{13}C,^{15}N-clovibactin and ^{13}C,^{15}N-Lipid II, we used CC magnetization transfer times of 50, 150, and 300 ms. 2D CaN and CON experiment were acquired at 800 MHz, 15 kHz MAS, and 5 to 7 ms N to C cross-polarization transfer time. To characterize Lipid II-bound teixobactin, we used CC magnetization transfer times of 50 and 300 ms. The scalar 2D CC TOBSY (Baldus and Meier, 1996) experiment was acquired at 700 MHz using 8 kHz MAS with 6 ms CC mixing time. The mobility edited(Doherty and Hong, 2009) H(H)C experiment was measured at 1200 MHz with 16.5 kHz MAS at 300 K temperature using a T_2 relaxation filter of 2.5 ms. 1D MAS ^{31}P experiments were acquired at 500 MHz magnetic field and 12 kHz MAS. 2D HP experiments were acquired at 800 MHz and 60 kHz MAS using 1 and 2 ms ^{1}H to ^{31}P cross-polarization contact time.

Fluorescence Microscopy

GUVs preparation: We used a self-assembled GUV cell, aligned with two titanium electrodes in a closed Teflon chamber (volume = 500 mL). 1 mL of 0.5 mM DOPC doped with Atto 550-labelled Lipid II (0.1 mol%) was brushed on the titanium electrodes. The GUV cell was dried under vacuum. Next, the chamber was filled with 350 mL 0.1M sucrose solution, the electrodes dipped in and connected to a power supply of a sine wave (2.5V; 10 Hz; 90 minutes). Each microscopy slide (m-slide 8 well, Ibidi) was incubated with 350 mL BSA solution (1 mg/mL) for 1 hour. To detach the GUVs, the power supply was changed to square wave (2V; 2Hz; 15 minutes). The slides were washed once with water and 0.1M glucose solution. The slides were immersed in 300 mL of 0.1M glucose solution to which 50mL of GUVs were added. These were incubated for 3 hours with 1 mM clovibactin and later observed under confocal microscope Zeiss LSM 880. GUVs were imaged using Zeiss LSM 880 with 63x/1.2NA glycerol and 100x/1.2NA oil objective lenses. The Atto 550 label appeared red upon excitation by the 560 nm laser. The brightfield was used for detection and location of the GUVs and to observe their shape. ImageJ software(Schindelin et al., 2012) was used for the analysis of the images.

Isothermal Titration Calorimetry

For ITC measurements LUVs (Large unilamellar vesicles) containing Lys-Lipid II were prepared by incorporating 2 mol% of Lys-Lipid II in DOPC from the stock solution. The lipids were dried under a nitrogen stream and hydrated with buffer (30mM Citrate, 300mM NaCl, pH 5.5) to a lipid-phosphate concentration of 20mM determined by Rouser's method(Rouser et al., 1970). Finally, unilamellar vesicles were obtained after 10 rounds of extrusion through 200 nm membrane filters (Whatman Nuclepore, Track-Etch Membranes). ITC experiments were performed with the Affinity ITC (TA Instruments-Waters LLC, New Castle, DE, USA) to determine interaction between LUVs and clovibactin. Clovibactin was diluted in the buffer, to a final concentration of 30 mM. The samples were degassed before use. The chamber was filled with 177 mL of clovibactin, and the LUVs were titrated into the chamber at a rate of 1.96 mL/150 seconds with a constant syringe stirring rate of 125 rpm. Number of injections = 21. Experiments were performed at 37°C and analyzed using the Nano Analyze Software (TA instruments – Water LLC). All experiments were performed in triplicates. Control experiments were performed with Lipid II-free DOPC LUVs. The independent model was used to determine the interaction between clovibactin and lipid II. ITC data for teixobactin was recently published(Shukla et al., 2022a).

High Speed-Atomic Force Microscopy (HS-AFM) Imaging

The HS-AFM images were acquired in amplitude modulation tapping mode in liquid using a high-speed atomic force microscope (RIBM, Japan). Short cantilevers (~7 μm) with a nominal spring constant of 0.15 N/m were used (USC-F1.2-k0.15, NanoWorld, Switzerland). A minimal imaging force was applied by using a small set-point amplitude of 0.8 nm (for a 1 nm free amplitude). The HS-AFM results showing the assembly of clovibactin filaments were obtained from imaging of supported lipid bilayers on mica. The lipid bilayer was obtained by incubating LUVs containing 0.5 mg/ml of DOPC and 4 mol% Lipid II (prepared as mentioned above) mixture (or 0.5 mg/ml DOPC without lipid II) on top of a freshly cleaved mica for 20-30 minutes. After the incubation period, the mica was cleaned gently using recording buffer (10 mM Tris-Cl, 100 mM NaCl, pH 8.0). Imaging was started on the lipid bilayer surface in recording buffer. Next, a concentrated clovibactin solution was added and pipetted to reach the desired final concentration in the AFM liquid chamber of 40 μl. Images were primarily processed using built-in scripts (RIBM, Japan) in Igor Pro (Wavemetrics, Lake Oswego, OR, USA) and analyzed using ImageJ software. The images/movies were corrected minimally for tilt, drift, and contrast. Unless otherwise mentioned, the times reported in AFM images are relative to clovibactin addition into the imaging chamber. Reported image acquisition rate is 0.5 frames/second, and the line rate is 150 lines/second. Stated errors are standard deviation.

Permeabilization assay

The bacterial cultures were grown overnight at 37ºC in LB media for *B. subtilis*. Secondary cultures were grown for 3 hours until the OD_{600} = 0.5 was reached. The bacterial cells were then centrifuged at 1500 x g for 10 minutes at 4ºC and washed twice with 10 mL of buffer (10 mM Tris, 100 mM NaCl, 1 mM $MgCl_2$, 0.5% glucose, pH=7.2). The bacterial cells were resuspended to an OD_{600} = 10 in the buffer and used for the experiment. All permeability experiments were performed with a Cary Eclipse (FL0904M005) fluorometer. All samples 1.0 mL) were continuously stirred in a 10 × 4-mm quartz cuvette and kept at 20°C. For the assay, 1 mL of the bacterial suspension was added to 1 mL of buffer. For ion leakage assays, 1 mL of the DISC-2 probe from a 1 mM stock was added to the cuvette and the fluorescence was measured between 650 nm to 670 nm wavelength (bandwidth = 5 mm) for 2 minutes before the addition of the antibiotic and 6 minutes after. For Sytox green leakage assays, 1 mL of the Sytox green probe from a 0.25 mM stock was added to the cuvette and the fluorescence was measured between 500 nm to 520 nm wavelength (bandwidth = 5 mm) for 2 minutes before the addition of the antibiotic and 6 minutes after. All experiments were performed in triplicates. The concentrations of antibiotics used are 10 nM nisin (1 x MIC) and 2 mM clovibactin (1 x MIC) and 0.2 mM teixobactin (10 x MIC) for *B. subtilis*.

Structure Calculations

Parametrization of Clovibactin

Clovibactin parametrization was started from a linear peptide topology of L-amino acids. D-amino acids were generated by inverting relevant dihedral and improper torsion angles and hydroxyasparagine (Hyn) topology was based on asparagine, where -OH group parameters were derived from threonine -OH group parameters. Depsi-cycle formation between Hyn5 and Leu8 was performed as previously described for [R4,L10]-teixobactin (Shukla et al., 2020). Parameters for lipid II were taken from ref. (Hsu et al., 2004).

Structure calculation protocol

We used HADDOCK version 2.4 (van Zundert et al., 2016) for the structure calculations. An eight-body docking (four lipid II and four clovibactin molecules) was performed using ssNMR-derived distance and dihedral restraints. Five thousand models were generated in the rigid-body docking stage of HADDOCK, of which the best-scoring 500 were subjected to the flexible refinement protocol of HADDOCK. The resulting models were energy minimized. Default HADDOCK settings were used except for doubling the weight of the distance restraints during all stages of the structure calculation. The final models were further filtered based on the topological requirements (that is, the lipid tails of all lipid II molecules must point in the same direction as the membrane-exposed hydrophobic residue Leu2). This resulted in a final ensemble of 22 structure models. See Supporting Information for detailed analysis of the calculated structure models.

References

Baldus, M., and Meier, B.H. (1996). Total Correlation Spectroscopy in the Solid State. The Use of Scalar Couplings to Determine the Through-Bond Connectivity. Journal of Magnetic Resonance, Series A 121, 65-69.

Breukink, E., van Heusden, H.E., Vollmerhaus, P.J., Swiezewska, E., Brunner, L., Walker, S., Heck, A.J.R., and de Kruijff, B. (2003). Lipid II is an intrinsic component of the pore induced by nisin in bacterial membranes. J Biol Chem 278, 19898-19903.

Brötz, H., Bierbaum, G., Leopold, K., Reynolds, P.E., and Sahl, H.-G. (1998). The Lantibiotic Mersacidin Inhibits Peptidoglycan Synthesis by Targeting Lipid II. Antimicrobial Agents and Chemotherapy 42, 154-160.

Brown, E.D., and Wright, G.D. (2016). Antibacterial drug discovery in the resistance era. Nature 529, 336-343. Buerger, S., Spoering, A., Gavrish, E., Leslin, C., Ling, L., and Epstein, S.S. (2012a). Microbial Scout Hypothesis and Microbial Discovery. Applied and Environmental Microbiology 78, 3229-3233.

Buerger, S., Spoering, A., Gavrish, E., Leslin, C., Ling, L., and Epstein, S.S. (2012b). Microbial Scout Hypothesis, Stochastic Exit from Dormancy, and the Nature of Slow Growers. Applied and Environmental Microbiology 78, 3221-3228.

Cook, M.A., and Wright, G.D. (2022). The past, present, and future of antibiotics. Science Translational Medicine 14.

Danilov, L.L., Druzhinina, T.N., Kalinchuk, N.A., Maltsev, S.D., and Shibaev, V.N. (1989). Polyprenyl phosphates: synthesis and structure-activity relationship for a biosynthetic system of Salmonella anatum O-specific polysaccharide. Chemistry and Physics of Lipids 51, 191-203.

Doherty, T., and Hong, M. (2009). 2D 1H–31P solid-state NMR studies of the dependence of inter-bilayer water dynamics on lipid headgroup structure and membrane peptides. Journal of Magnetic Resonance 196, 39-47. Fage, C.D., Lathouwers, T., Vanmeert, M., Gao, L.J., Vrancken, K., Lammens, E.M., Weir, A.N.M., Degroote, R., Cuppens, H., Kosol, S., et al. (2020). The Kalimantacin Polyketide Antibiotics Inhibit Fatty Acid Biosynthesis in Staphylococcus aureus by Targeting the Enoyl-Acyl Carrier Protein Binding Site of FabI. Angewandte Chemie International Edition 59, 10549-10556.

Fernández-Martínez, L.T., and Bibb, M.J. (2014). Use of the Meganuclease I-SceI of Saccharomycescerevisiae to select for gene deletions in actinomycetes. Scientific Reports 4.

Gavrish, E., Sit, C.S., Cao, S., Kandror, O., Spoering, A., Peoples, A., Ling, L., Fetterman, A., Hughes, D., Bissell, A., et al. (2014). Lassomycin, a ribosomally synthesized cyclic peptide, kills Mycobacterium tuberculosis by targeting the ATP-dependent protease ClpC1P1P2. Chem Biol 21, 509-518.

Harms, H., Klöckner, A., Schrör, J., Josten, M., Kehraus, S., Crüsemann, M., Hanke, W., Schneider, T., Schäberle, T., and König, G. (2018). Antimicrobial Dialkylresorcins from Marine-Derived Microorganisms: Insights into Their Mode of Action and Putative Ecological Relevance. Planta Medica *84*, 1363-1371.
Heinig, M., and Frishman, D. (2004). STRIDE: a web server for secondary structure assignment from known atomic coordinates of proteins. Nucleic Acids Research *32*, W500-W502.
Homma, T., Nuxoll, A., Gandt, A.B., Ebner, P., Engels, I., Schneider, T., Götz, F., Lewis, K., and Conlon, B.P. (2016). Dual Targeting of Cell Wall Precursors by Teixobactin Leads to Cell Lysis. Antimicrobial Agents and Chemotherapy *60*, 6510-6517.
Hong, M. (2006). Solid-State NMR Studies of the Structure, Dynamics, and Assembly of β-Sheet Membrane Peptides and α-Helical Membrane Proteins with Antibiotic Activities. Accounts of Chemical Research *39*, 176-183.
Hsu, S.-T.D., Breukink, E., Tischenko, E., Lutters, M.A.G., de Kruijff, B., Kaptein, R., Bonvin, A.M.J.J., and van Nuland, N.A.J. (2004). The nisin–lipid II complex reveals a pyrophosphate cage that provides a blueprint for novel antibiotics. Nature Structural & Molecular Biology *11*, 963-967.
Kamigiri, K., Suzuki, Y., Shibazaki, M., Morioka, M., Suzuki, K.-I., Tokunaga, T., Setiawan, B., and Rantiatmodjo, R.M. (1996). Kalimantacins A, B and C, Novel Antibiotics fromAlealigenes sp. YL-02632S. I. Taxonomy, Fermentation, Isolation and Biological Propertie. The Journal of Antibiotics *49*, 136-139.
Kodera, N., Yamamoto, D., Ishikawa, R., and Ando, T. (2010). Video imaging of walking myosin V by high-speed atomic force microscopy. Nature *468*, 72-76.
Kohlrausch, U. (1991). One-step purification procedure for UDP-N-acetylmuramyl-peptide murein precursors from Bacillus cereus. FEMS Microbiology Letters *78*, 253-257.
Kohlrausch, U., and Höltje, J.V. (1991). Analysis of murein and murein precursors during antibiotic-induced lysis of Escherichia coli. Journal of Bacteriology *173*, 3425-3431.
Lebreton, F., Manson, A.L., Saavedra, J.T., Straub, T.J., Earl, A.M., and Gilmore, M.S. (2017). Tracing the Enterococci from Paleozoic Origins to the Hospital. Cell *169*, 849-861 e813.
Lewandowski, J.R., Sass, H.J., Grzesiek, S., Blackledge, M., and Emsley, L. (2011). Site-Specific Measurement of Slow Motions in Proteins. Journal of the American Chemical Society *133*, 16762-16765.
Lewis, K. (2013). Platforms for antibiotic discovery. Nature Reviews Drug Discovery *12*, 371-387.
Lewis, K. (2020). The Science of Antibiotic Discovery. Cell *181*, 29-45.
Ling, L.L., Schneider, T., Peoples, A.J., Spoering, A.L., Engels, I., Conlon, B.P., Mueller, A., Schäberle, T.F., Hughes,D.E., Epstein, S., et al. (2015). A new antibiotic kills pathogens without detectable resistance. Nature 517, 455-459.
Mahapatra, S., Scherman, H., Brennan, P.J., and Crick, D.C. (2005). N Glycolylation of the Nucleotide Precursors of Peptidoglycan Biosynthesis of Mycobacterium
spp. Is Altered by Drug Treatment. Journal of Bacteriology 187, 2341-2347.
Maity, S., Ottelé, J., Santiago, G.M., Frederix, P.W.J.M., Kroon, P., Markovitch, O., Stuart, M.C.A., Marrink, S.J., Otto, S., and Roos, W.H. (2020). Caught in the Act: Mechanistic Insight into Supramolecular Polymerization-Driven Self-Replication from Real-Time Visualization. Journal of the American Chemical Society 142, 13709-13717.
Mattheus, W., Gao, L.-J., Herdewijn, P., Landuyt, B., Verhaegen, J., Masschelein, J., Volckaert, G., and Lavigne, R.(2010). Isolation and Purification of a New Kalimantacin/Batumin-Related Polyketide Antibiotic and Elucidation of Its Biosynthesis Gene Cluster. Chemistry & Biology 17, 149-159.
Medeiros-Silva, J., Jekhmane, S., Paioni, A.L., Gawarecka, K., Baldus, M., Swiezewska, E., Breukink, E., and Weingarth, M. (2018). High-resolution NMR studies of antibiotics in cellular membranes. Nature Communications 9.
Miethke, M., Pieroni, M., Weber, T., Brönstrup, M., Hammann, P., Halby, L., Arimondo, P.B., Glaser, P., Aigle, B., Bode, H.B., et al. (2021). Towards the sustainable discovery and development of new antibiotics. Nature Reviews Chemistry 5, 726-749.
Mordoch, S.S., Granot, D., Lebendiker, M., and Schuldiner, S. (1999). Scanning cysteine accessibility of EmrE, an H+-coupled multidrug transporter from Escherichia coli, reveals a hydrophobic pathway for solutes. J Biol Chem 274, 19480-19486.
Münch, D., and Sahl, H.-G. (2015). Structural variations of the cell wall precursor lipid II in Gram-positive bacteria— Impact on binding and efficacy of antimicrobial peptides. Biochimica et Biophysica Acta (BBA) - Biomembranes 1848, 3062-3071.

Nichols, D., Cahoon, N., Trakhtenberg, E.M., Pham, L., Mehta, A., Belanger, A., Kanigan, T., Lewis, K., and Epstein, S.S. (2010). Use of ichip for high-throughput in situ cultivation of "uncultivable" microbial species. Appl Environ Microbiol *76*, 2445-2450.
Orlov, D.S., Nguyen, T., and Lehrer, R.I. (2002). Potassium release, a useful tool for studying antimicrobial peptides. Journal of Microbiological Methods *49*, 325-328.
Quigley, J., Peoples, A., Sarybaeva, A., Hughes, D., Ghiglieri, M., Achorn, C., Desrosiers, A., Felix, C., Liang, L., Malveira, S*., et al.* (2020). Novel Antimicrobials from Uncultured Bacteria Acting against Mycobacterium tuberculosis. mBio *11*.
Rick, P.D., Hubbard, G.L., Kitaoka, M., Nagaki, H., Kinoshita, T., Dowd, S., Simplaceanu, V., and Ho, C. (1998). Characterization of the lipid-carrier involved in the synthesis of enterobacterial common antigen (ECA) and identification of a novel phosphoglyceride in a mutant of Salmonella typhimurium defective in ECA synthesis. Glycobiology *8*, 557-567.
Rouser, G., Fleischer, S., and Yamamoto, A. (1970). Two dimensional thin layer chromatographic separation of polar lipids and determination of phospholipids by phosphorus analysis of spots. Lipids *5*, 494-496.
Ruland, J.A., Krüger, A.M., Dörner, K., Bhatia, R., Wirths, S., Poetes, D., Kutay, U., Siebrasse, J.P., and Kubitscheck, U. (2021). Nuclear export of the pre-60S ribosomal subunit through single nuclear pores observed in real time. Nature Communications *12*.
Schindelin, J., Arganda-Carreras, I., Frise, E., Kaynig, V., Longair, M., Pietzsch, T., Preibisch, S., Rueden, C., Saalfeld, S., Schmid, B*., et al.* (2012). Fiji: an open-source platform for biological-image analysis. Nature Methods *9*, 676-682.
Schneider, C.A., Rasband, W.S., and Eliceiri, K.W. (2012). NIH Image to ImageJ: 25 years of image analysis. Nature Methods *9*, 671-675.
Schneider, T., Gries, K., Josten, M., Wiedemann, I., Pelzer, S., Labischinski, H., and Sahl, H.G. (2009). The Lipopeptide Antibiotic Friulimicin B Inhibits Cell Wall Biosynthesis through Complex Formation with Bactoprenol Phosphate. Antimicrobial Agents and Chemotherapy *53*, 1610-1618.
Schneider, T., Kruse, T., Wimmer, R., Wiedemann, I., Sass, V., Pag, U., Jansen, A., Nielsen, A.K., Mygind, P.H., Raventós, D.S*., et al.* (2010). Plectasin, a Fungal Defensin, Targets the Bacterial Cell Wall Precursor Lipid II. Science *328*, 1168-1172.
Shahsavari, N., Wang, B., Imai, Y., Mori, M., Son, S., Liang, L., Böhringer, N., Manuse, S., Gates, M.F., Morrissette, M*., et al.* (2022). A Silent Operon of Photorhabdus luminescens Encodes a Prodrug Mimic of GTP. mBio *13*. Shukla, R., Lavore, F., Maity, S., Derks, M.G.N., Jones, C.R., Vermeulen, B.J.A., Melcrová, A., Morris, M.A., Becker, L.M., Wang, X*., et al.* (2022a). Teixobactin kills bacteria by a two-pronged attack on the cell envelope. Nature *608*, 390-396.
Shukla, R., Lavore, F., Maity, S., Derks, M.G.N., Jones, C.R., Vermeulen, B.J.A., Melcrová, A., Morris, M.A., Becker, L.M., Wang, X*., et al.* (2022b). Teixobactin kills bacteria by a two-pronged attack on the cell envelope. Nature. Shukla, R., Medeiros-Silva, J., Parmar, A., Vermeulen, B.J.A., Das, S., Paioni, A.L., Jekhmane, S., Lorent, J., Bonvin, A.M.J.J., Baldus, M*., et al.* (2020). Mode of action of teixobactins in cellular membranes. Nature Communications *11*.
Silver, L.L. (2007). Multi-targeting by monotherapeutic antibacterials. Nature Reviews Drug Discovery *6*, 41-55. Tan, S., Ludwig, K.C., Müller, A., Schneider, T., and Nodwell, J.R. (2019). The Lasso Peptide Siamycin-I Targets Lipid II at the Gram-Positive Cell Surface. ACS Chemical Biology *14*, 966-974.
Tinevez, J.-Y., Perry, N., Schindelin, J., Hoopes, G.M., Reynolds, G.D., Laplantine, E., Bednarek, S.Y., Shorte, S.L., and Eliceiri, K.W. (2017). TrackMate: An open and extensible platform for single-particle tracking. Methods *115*,80-90.
Umbreit, J.N., and Strominger, J.L. (1972). Isolation of the Lipid Intermediate in Peptidoglycan Biosynthesis from Escherichia coli. Journal of Bacteriology 112, 1306-1309.
van Zundert, G.C.P., Rodrigues, J.P.G.L.M., Trellet, M., Schmitz, C., Kastritis, P.L., Karaca, E., Melquiond, A.S.J., van Dijk, M., de Vries, S.J., and Bonvin, A.M.J.J. (2016). The HADDOCK2.2 Web Server: User-Friendly Integrative Modeling of Biomolecular Complexes. Journal of Molecular Biology 428, 720-725.
Wang, Y. (2002). Probability-based protein secondary structure identification using combined NMR chemical-shift data. Protein Science 11, 852-861.
Weingarth, M., Bodenhausen, G., and Tekely, P. (2009a). Low-power decoupling at high spinning frequencies in high static fields. Journal of Magnetic Resonance 199, 238-241.
Weingarth, M., Bodenhausen, G., and Tekely, P. (2010). Broadband magnetization transfer using moderate radio-frequency fields for NMR with very high static fields and spinning speeds. Chemical Physics Letters 488, 10-16.

Weingarth, M., Demco, D.E., Bodenhausen, G., and Tekely, P. (2009b). Improved magnetization transfer in solid-state NMR with fast magic angle spinning. Chemical Physics Letters *469*, 342-348.
Wilson, M.C., Mori, T., Rückert, C., Uria, A.R., Helf, M.J., Takada, K., Gernert, C., Steffens, U.A.E., Heycke, N., Schmitt, S.*, et al.* (2014). An environmental bacterial taxon with a large and distinct metabolic repertoire. Nature *506*, 58-62.
Wirtz, D.A., Ludwig, K.C., Arts, M., Marx, C.E., Krannich, S., Barac, P., Kehraus, S., Josten, M., Henrichfreise, B., Müller, A.*, et al.* (2021). Biosynthesis and Mechanism of Action of the Cell Wall Targeting Antibiotic Hypeptin. Angewandte Chemie International Edition *60*, 13579-13586.

Supplementary Information

A new antibiotic from an uncultured bacterium binds to an immutable target

Rhythm Shukla[1,2,#], Aaron J. Peoples[3,#], Kevin C. Ludwig[4], Sourav Maity[5], Maik G.N. Derks[1,2], Stefania de Benedetti[4], Annika M Krueger[6], Bram J.A. Vermeulen[1], Francesca Lavore[1], Rodrigo V. Honorato[1], Fabian Grein[4,7], Alexandre Bonvin[1], Ulrich Kubischeck[6], Eefjan Breukink[2], Catherine Achorn[3], Anthony Nitti[3], Christopher J. Schwalen[8], Amy L. Spoering[3], Losee Lucy Ling[3], Dallas Hughes[3], Moreno Lelli[9,10], Wouter H. Roos[3], Kim Lewis[11], Tanja Schneider[4,*], Markus Weingarth[1,*]

[1]NMR Spectroscopy, Department of Chemistry, Utrecht University, Padualaan 8, 3584 CH Utrecht, The Netherlands
[2]Membrane Biochemistry and Biophysics, Department of Chemistry, Utrecht University, Padualaan 8, 3584 CH, Utrecht, The Netherlands
[3]NovoBiotic Pharmaceuticals, Cambridge, Massachusetts 02138, USA
[4]Institute for Pharmaceutical Microbiology, University Hospital Bonn, University of Bonn, Bonn, Germany
[5]Moleculaire Biofysica, Zernike Instituut, Rijksuniversiteit Groningen, Nijenborgh 4, 9747 AG Groningen, The Netherlands
[6]Institute for Physical and Theoretical Chemistry, University of Bonn, Bonn, Germany
[7]German Center for Infection Research (DZIF), partner site Bonn-Cologne, Bonn
[8]Novartis Institutes for Biomedical Research, Cambridge, MA 02139, USA
[9]Magnetic Resonance Center (CERM) and Department of Chemistry "Ugo Schiff", University of Florence, via Sacconi 6, Sesto Fiorentino, 50019 Italy
[10]Consorzio Interuniversitario Risonanze Magnetiche MetalloProteine (CIRMMP), via Sacconi 6, Sesto Fiorentino, 50019 Italy
[11]Antimicrobial Discovery Center, Northeastern University, Department of Biology, Boston, Massachusetts 02115, USA

[#]equal contributions
**corresponding authors: m.h.weingarth@uu.nl, tschneider@uni-bonn.de*

Supplementary Table 1: Primer DNA sequences used in the interruption of bat1 in P9846. Capitalized letters highlight the restriction enzyme cuts sites used in cloning fragments into pIJ12738.

Primer Name	Primer sequence 5'-3'
bat1kofrag2F	agactaGGATCCctgcgggtggaccccgt
bat1kofrag2R	acagtaTCTAGAgcgcacactccctactcggtc
bat1kofrag1F	agactaGGATCCgacgggccttacgcagg
bat1kofrag1R	agactGGTACCactccacagcagtgttgaaggt
Bat1downstream	gcgctggccctcggaaag
Bat2upstream	gcgccgcttggacacttat

Supplementary Table 2: ^{1}H and ^{13}C solution NMR data of clovibactin in DMSO-*d*6 (500 Hz, δ in ppm).

	HN	Hα	Hβ	Others
L-Phe (1)	8.21	4.11	3.01	$H\delta_{(1,2)}$: 7.27, $H\varepsilon_{(1,2)}$: 7.33, Hζ: 7.28
D-Leu (2)	8.62	4.30	1.34/1.52	Hγ: 1.21, $H\delta_1$: 0.75, $H\delta_2$: 0.79
D-Lys (3)	8.22	4.33	1.53/1.68	Hγ: 1.28/1.33, Hδ: 1.52, Hε: 2.74, Hζ: 7.78
L-Ser (4)	7.91	4.41	3.41/3.59	Hγ: N.A.
3-OH-Asn (5)	8.10	5.03	5.28	Hδ: 7.40/7.88
L-Ala (6)	8.32	3.99	1.34	-
L-Leu (7)	7.62	4.37	1.51	Hγ: N.A., $H\delta_1$: N.A., $H\delta_2$: N.A.
L-Leu (8)	7.76	4.35	1.51/1.66	Hγ: N.A., $H\delta_1$: N.A., $H\delta_2$: N.A.
	N	**Cα**	**Cβ**	**Others**
L-Phe (1)	39.20	53.63	37.52	Cγ:135.32, $C\delta_{(1,2)}$: 129.94, $C\varepsilon_{(1,2)}$: 128.98, Cζ: 127.63
D-Leu (2)	123.10	51.26	41.43	Cγ: 23.98, $C\delta_1$: 21.78, $C\delta_2$: 23.51
D-Lys (3)	118.00	52.54	31.45	Cγ: 22.57, Cδ: 26.77, Cε: 38.97, Nζ: 33.30
L-Ser (4)	113.30	56.14	61.71	-
3-OH-Asn (5)	109.60	53.46	73.74	Cγ: N.A., Nδ: 106.1
L-Ala (6)	123.00	52.31	17.06	-
L-Leu (7)	110.00	52.72	41.89	Cγ: N.A., $C\delta_1$: N.A., $C\delta_2$: N.A.
L-Leu (8)	113.60	50.96	40.32	Cγ: N.A., $C\delta_1$: N.A., $C\delta_2$: N.A.

N.A.: Not Assigned

Supplementary Table 3: Antibacterial activity of clovibactin and known drugs against contemporary clinical isolates. Susceptibility testing determined by broth microdilution in accordance with CLSI guidelines was conducted by Micromyx LLC, Kalamazoo, MI, USA. MSSA, methicillin-sensitive *S. aureus;* MRSA, methicillin-resistant *S. aureus;* VISA, vancomycin-intermediate *S. aureus;* DAP^{NS}, daptomycin non-susceptible; LZD^{R}, linezolid-resistant; MRSE, methicillin-resistant *S. epidermidis*; MRSH, methicillin-resistant *S. haemolyticus*; PSSP, penicillin-susceptible *S. pneumoniae*; PISP, penicillin-intermediate *S. pneumoniae*; PRSP, penicillin-resistant *S. pneumoniae*; VSE, vancomycin-sensitive enterococci; VRE, vancomycin-resistant enterococci, ESBL, extended spectrum β-lactamase positive; KPC, *Klebsiella pneumoniae* carbapenemase-positive

Organism (Gram-positives)	**# Isolates**	**Clovibactin MIC range (µg/mL)**	**Vancomycin MIC range (µg/mL)**
Staphylococcus aureus (MSSA)	3	1	0.5 - 1
Staphylococcus aureus (MRSA)	3	1	0.5 - 1
Staphylococcus aureus (VISA)	3	1 - 4	4
Staphylococcus aureus (DAP^{NS})	3	1 - 4	4 - 8
Staphylococcus aureus (LZD^{R})	3	0.5 - 2	0.5 - 1
Staphylococcus epidermidis (MSSE)	1	1	1
Staphylococcus epidermidis (MRSE)	2	0.5 - 1	1
Streptococcus pneumoniae (PSSP)	3	0.25 – 0.5	0.25
Streptococcus pneumoniae (PISP)	4	0.5 - 1	0.12 - 0.25
Streptococcus pneumoniae (PRSP)	3	0.25 – 0.5	0.25
Streptococcus pyogenes	4	0.5 - 1	0.25
Streptococcus agalactiae	3	1	0.25
Streptococcus anginosus	1	0.5	0.5
Streptococcus mutans	1	1	0.5
Streptococcus salivarius	1	0.25	0.25
Enterococcus faecium (VSE)	3	2	0.5 - 1
Enterococcus faecium (VanA VRE)	2	1 - 2	≥ 32
Enterococcus faecium (VanB VRE)	2	1 - 2	≥ 32
Enterococcus faecalis (VSE)	3	4 - 8	0.5 - 4
Enterococcus faecalis (VanA VRE)	2	2 - 4	> 32
Enterococcus faecalis (VanB VRE)	2	4	> 32
Organism (Gram-negatives)	**# Isolates**	**Clovibactin MIC range (µg/mL)**	**Ciprofloxacin MIC range (µg/mL)**
Escherichia coli ATCC 25922	1	> 64	0.008
Escherichia coli (ESBL)	1	> 64	> 32
Klebsiella pneumoniae	1	64	2
Klebsiella pneumoniae (KPC)	1	> 64	> 32
Proteus vulgaris	1	> 64	0.015
Proteus mirabilis	1	> 64	8
Enterobacter cloacae	2	≥ 64	0.008 – 0.015
Enterobacter aerogenes	2	> 64	0.03 – 0.06
Serratia marcescens	2	> 64	0.06
Pseudomonas aeruginosa	2	> 64	32
Acinetobacter baumannii	2	> 64	> 32
Haemophilus influenzae	3	>64	0.06 – 0.25
Moraxella catarrhalis	2	4 - 16	0.03
Neisseria gonorrhoeae	2	≥ 64	0.002 - 16

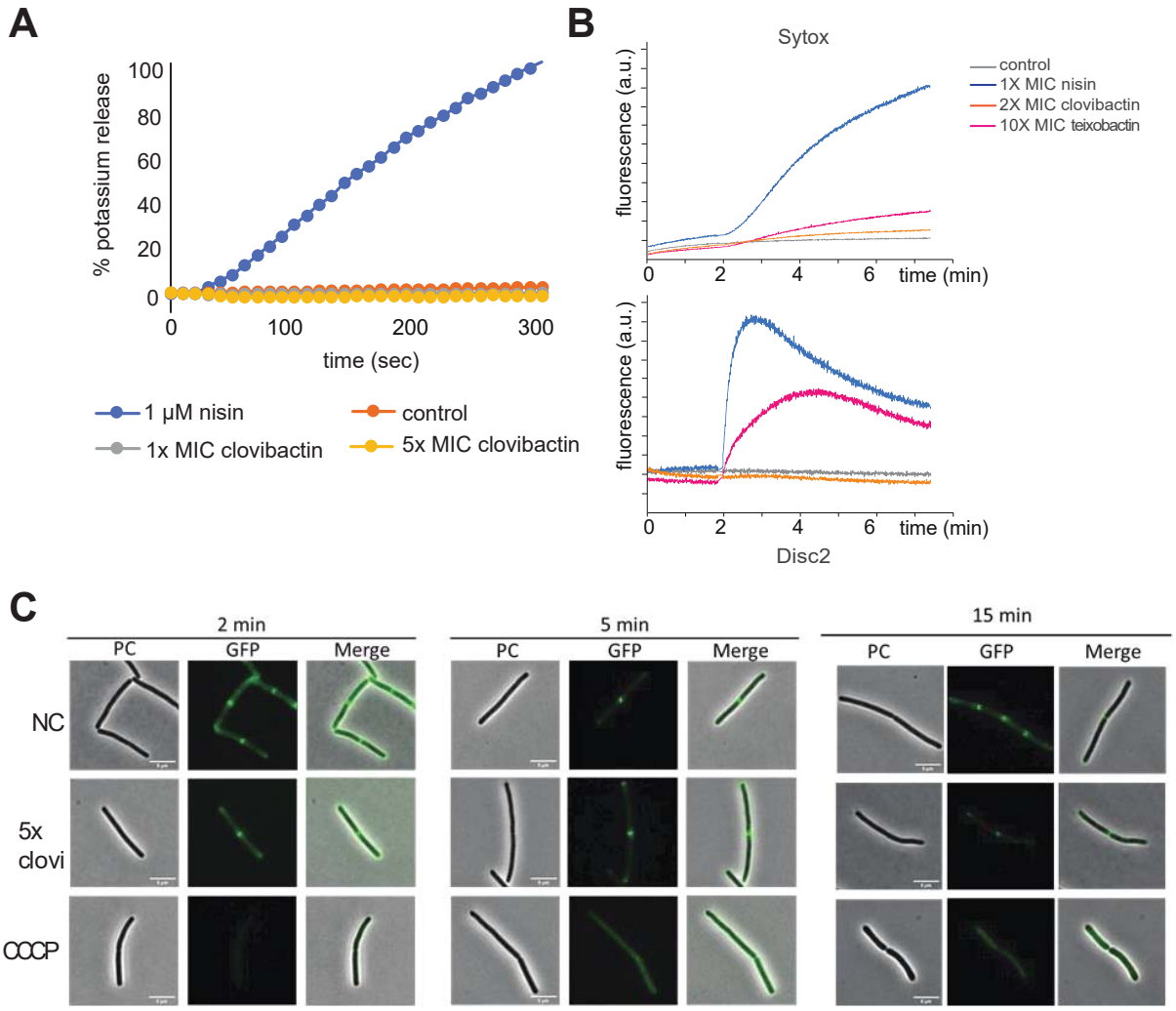

Supplementary Figure 1: Clovibactin does not disrupt the membrane. (A) Potassium efflux from living cells of *S. simulans* was monitored with a potassium-sensitive electrode. Ion leakage is expressed relative to the total amount of potassium released after addition of 1 μM pore-forming lantibiotic nisin (100%). (B) Permeabilization assay with DiSC(2) and Sytox reporter dye for *B. subtilis* with nisin, teixobactin, clovibactin and untreated cells. While nisin and teixobactin compromise the membrane integrity, clovibactin shows no permeabilizing activity for either of the two reporters. (C) GFP-MinD cells of *B. subtilis* were treated with clovibactin (5xMIC). The ionophore CCCP was used as a positive control. Scale bar = 5 μm.

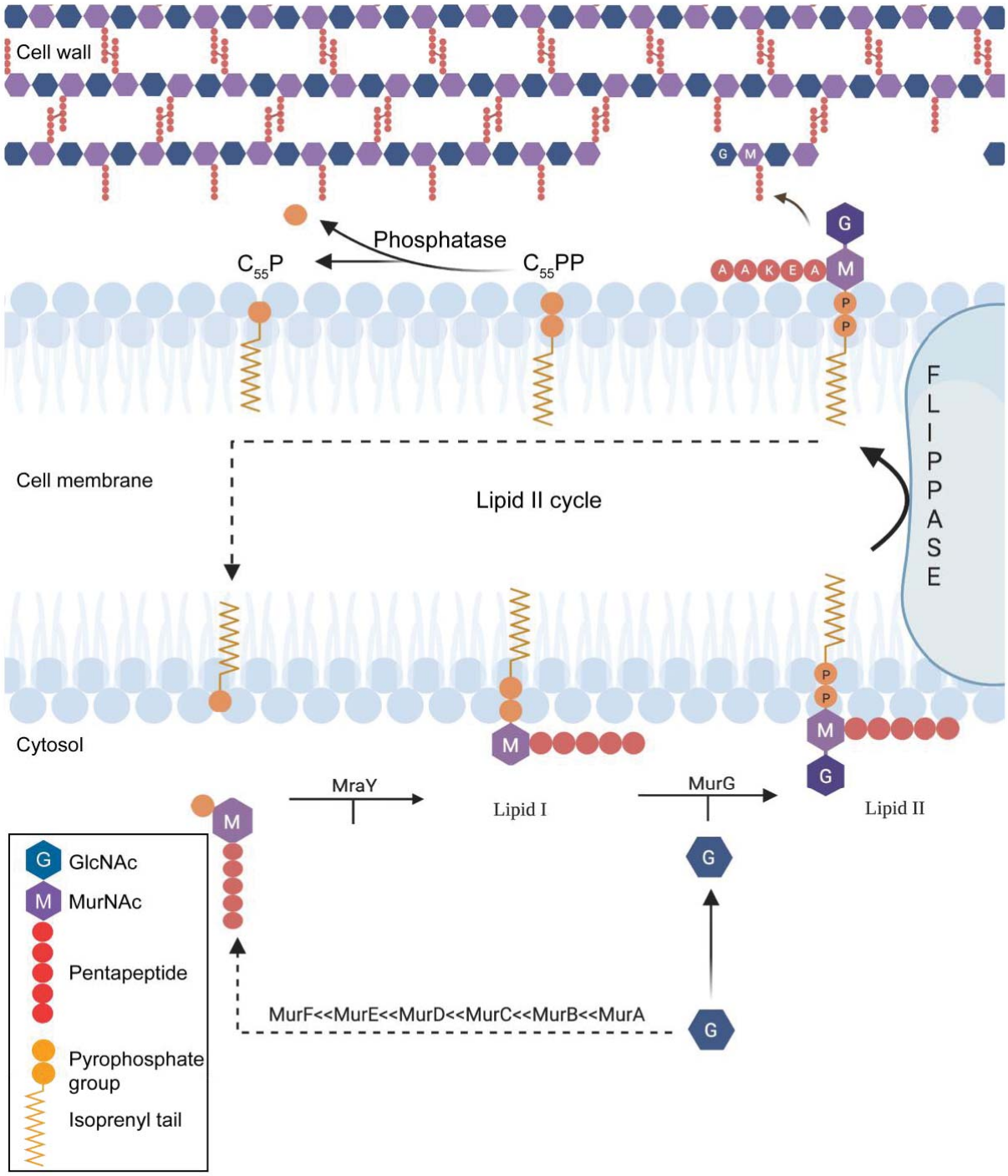

Supplementary Figure 2: Schematic of peptidoglycan synthesis. Peptidoglycan synthesis is dependent on the lipid II cycle which is shown in the illustration. It shows the organization of the lipid II molecule on the inner leaflet which is eventually flipped to the outer leaflet. When present in the outer leaflet lipid II deposits the disaccharide moiety (GlcNAc-MurNAc) and the attached pentapeptide to develop the peptidoglycan layer. The $C_{55}P$ moiety is then recycled to continue the cycle.

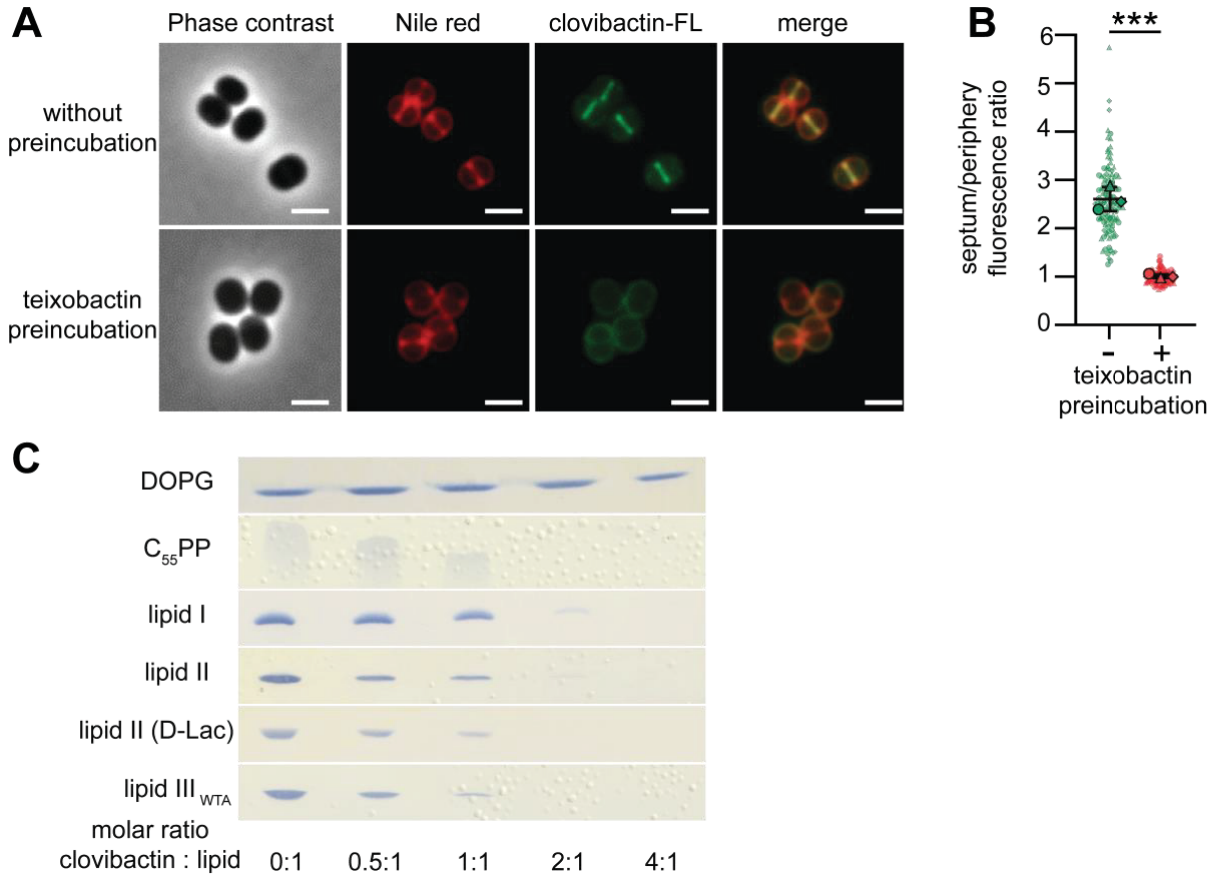

Supplementary Figure 3: BODIPY-FL-clovibactin localizes to the septum of *S. aureus* and forms extraction-stable complexes with undecaprenyl pyrophosphate-containing cell wall precursors. (A) In cells pre-incubated with teixobactin (2 min), septal localization of FL-clovibactin is diminished. Nile red was used for membrane staining. Scale bar 1 µm. (B) Images of individual cells were used to calculate the fluorescence ratio (FR) of the septal versus peripheral fluorescence signal for cells pre-treated with teixobactin and lacking pre-treatment. FR >2 indicates septal localization. At least $n = 30$ cells were evaluated for each condition from three biologically independent experiments. Significance was determined by unpaired Student's *t*-test with a 95% confidence interval. ****$p < 0.0004$. (C) Complex formation is indicated by a reduction of the amount of free lipid intermediates visible on the TLC. Cell wall intermediates are fully locked in a complex at a twofold molar excess of antibiotic. No complex formation was observed with the anionic phospholipid DOPG. Note that the molar clovibactin : lipid ratios are not representative for stoichiometries. The chromatograms are representative of three independent experiments.

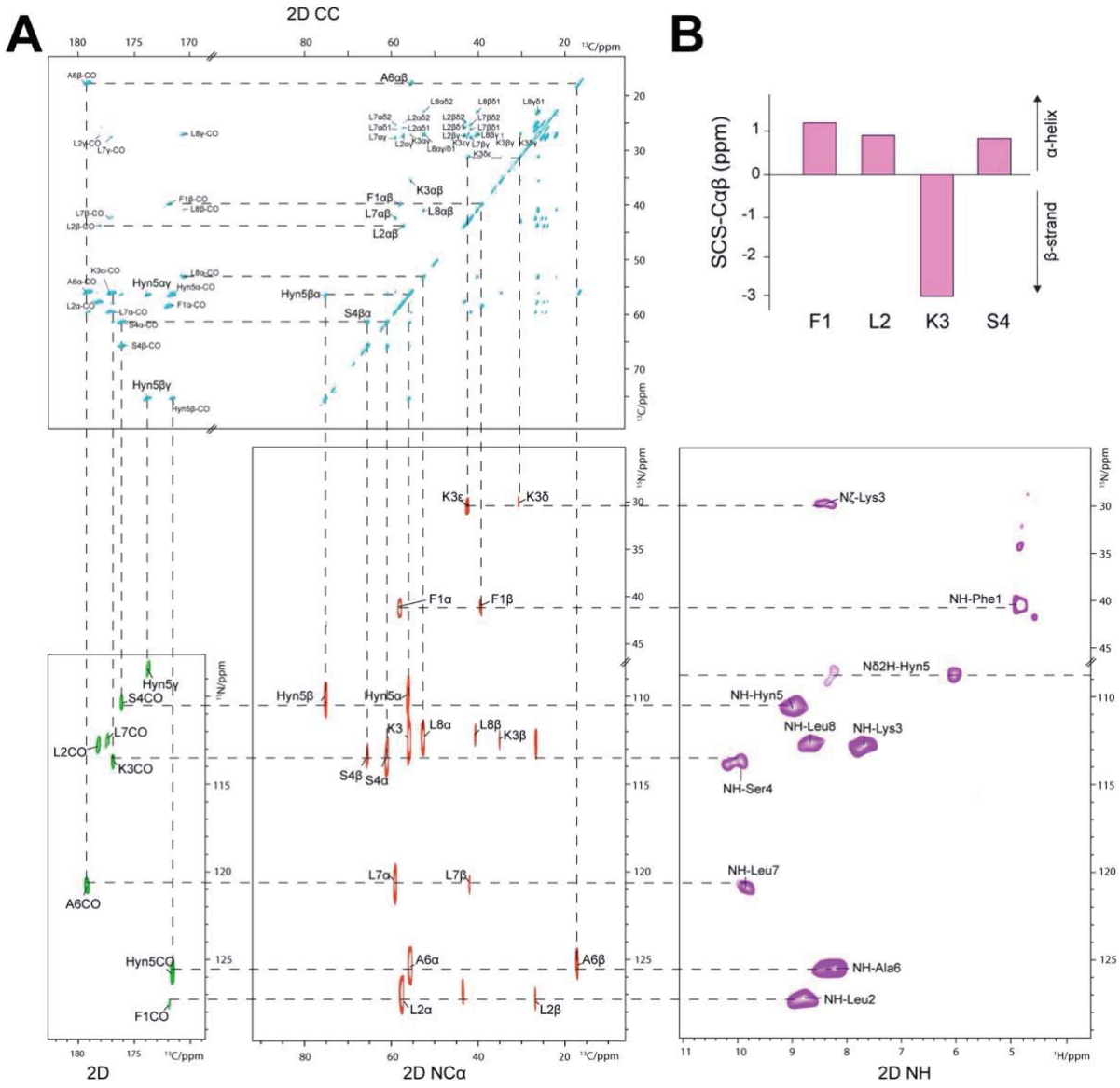

Supplementary Figure 4: ssNMR assignments of clovibactin in the lipid II-bound state in DOPC liposomes. Assignments were performed using a 2D PARIS CC experiments (in blue), 2D NCO(i-1) (in green), 2D NCA (in red), and 2D NH (in purple). 2D PARIS CC ssNMR experiment was recorded at 1200 MHz magnetic field at 18k Hz MAS. 2D NCO(i-1) and 2D NCA experiments were recorded at 800 MHz magnetic field at 15 kHz MAS. 2D NH experiment was recorded at 700 MHz magnetic field at 16.5 kHz MAS.
B) Cβα Secondary chemical shifts (SCS) do not show consistent β-structuring for the linear clovibactin N-terminus. We note that it is unclear to which standard chemical shift information (Wang, 2002) extent chemical shift information applies to the very short N-terminus with its unusual structure and non-canonical residues. We note that chemical shift of teixobactin (Shukla et al., 2022), residues D-N-Me-Phe1 and Ser7, i.e., the residue connected to the depsi-cycle, also did not indicate β-structuring.

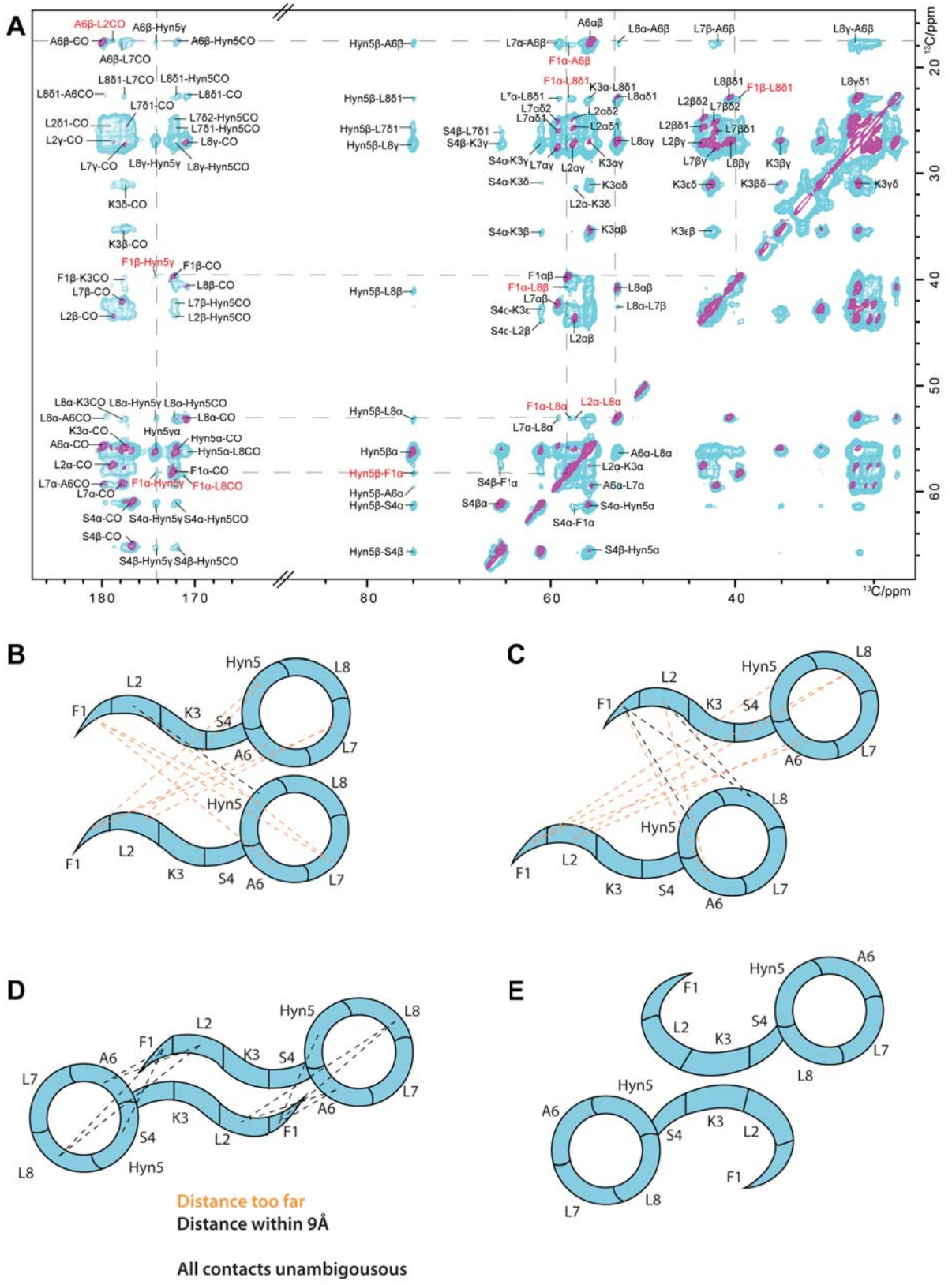

Supplementary Figure 5: Antiparallel arrangement of the clovibactin dimer. ssNMR, confocal microscopy, and AFM-data show that clovibactin assembled into fibrils upon lipid II

binding. From ssNMR data, the nature of the fibrils can be gauged. (A) Superposition of 2D PARIS CC spectra of clovibactin in the lipid II-bound state with 50 ms (magenta) and 300 ms (cyan) mixing times measured at 1200 MHz magnetic field and 18 kHz MAS. The contacts (in red) very likely arise from intermolecular interactions between adjacent clovibactin molecules as they are beyond the 8 Å range of such an experiment. The illustrations show how these contacts are consistent with be an antiparallel arrangement (D) of the neighbouring clovibactin molecules. The parallel (B) and out of register parallel (C) arrangements still contain many contacts that would not be satisfied by the distance limit of the experiment. In the antiparallel arrangement, the N- and C-terminal residues of adjacent clovibactin molecules come close enough to justify observing contacts such as F1α-L8α and F1α-A6β. E) Due to the small size of clovibactin, we note that the ssNMR restraints could potentially also be fulfilled by alternative supramolecular arrangements in which the N-terminus bends towards the C-terminal depsi-cycle. However, such an alternative arrangement appears difficult to align with the formation of fibrils observed by AFM.

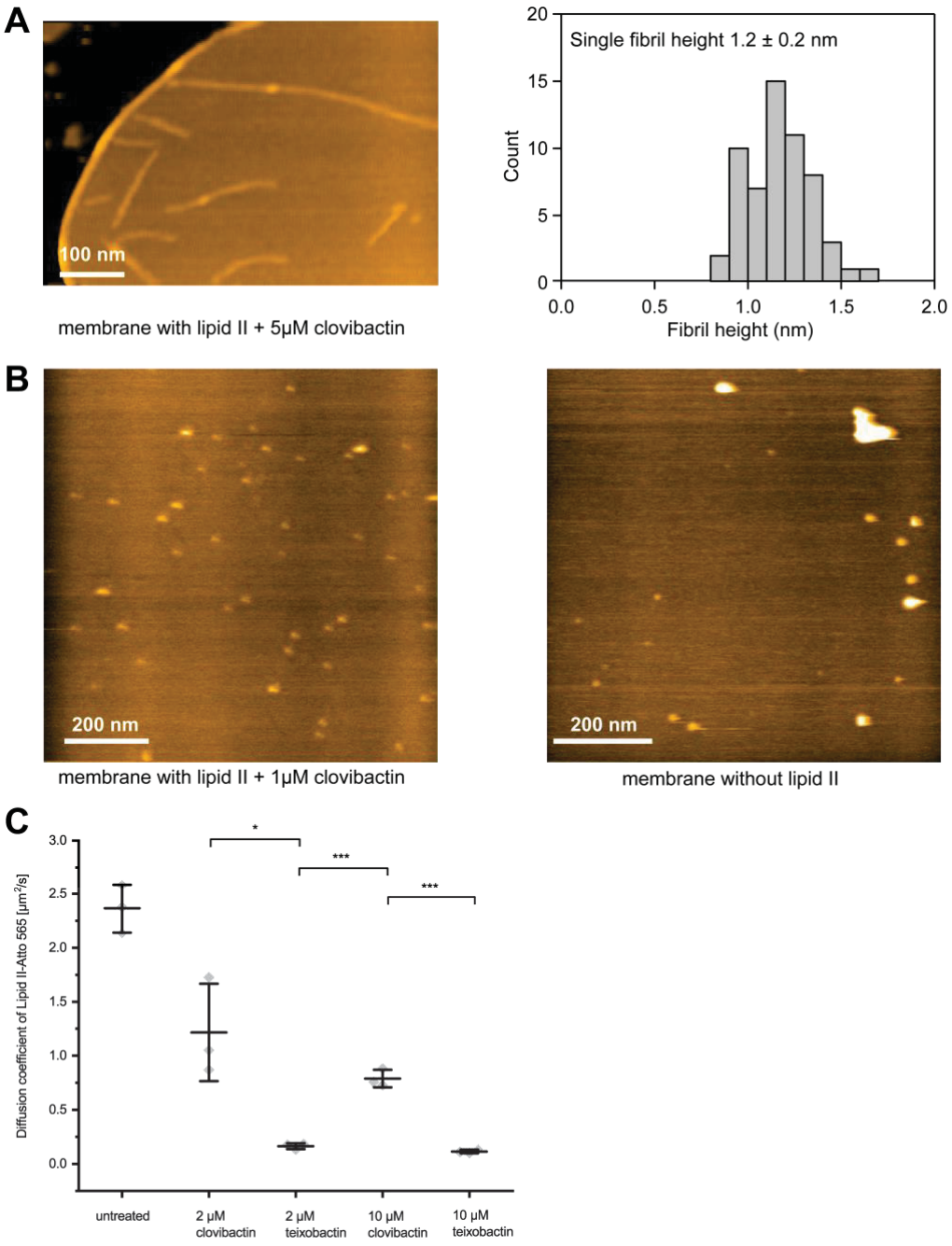

Supplementary Figure 6: HS-AFM demonstrating the fibrilization of clovibactin and lipid II. A) The HS-AFM experiments show the formation of the clovibactin fibrils only at high-concentrations of 5 μM and in the presence of lipid II. Also, the fibrils are loosely attached to the membrane and the average height of the fibrils is 1.2 ± 0.2 nm above the membrane. There was no visible membrane deformation, and this is in line with our permeabilization assays which also show no effect on bacterial membrane depolarization.

B) Control experiments with low clovibactin concentration (1 μM) at a membrane containing 4% lipid II (left image) and 5 μM clovibactin at a membrane containing no lipid II (right image) both show no fibrilization events.

C) Lipid II mobility was also monitored using single-molecule tracking microscopy experiments in supported lipid bilayers. These experiments also align with the requirement of higher clovibactin concentrations to immobilize lipid II in lipid bilayers. This contrasts with the low concentrations of teixobactin required for maximum lipid II immobilizations.

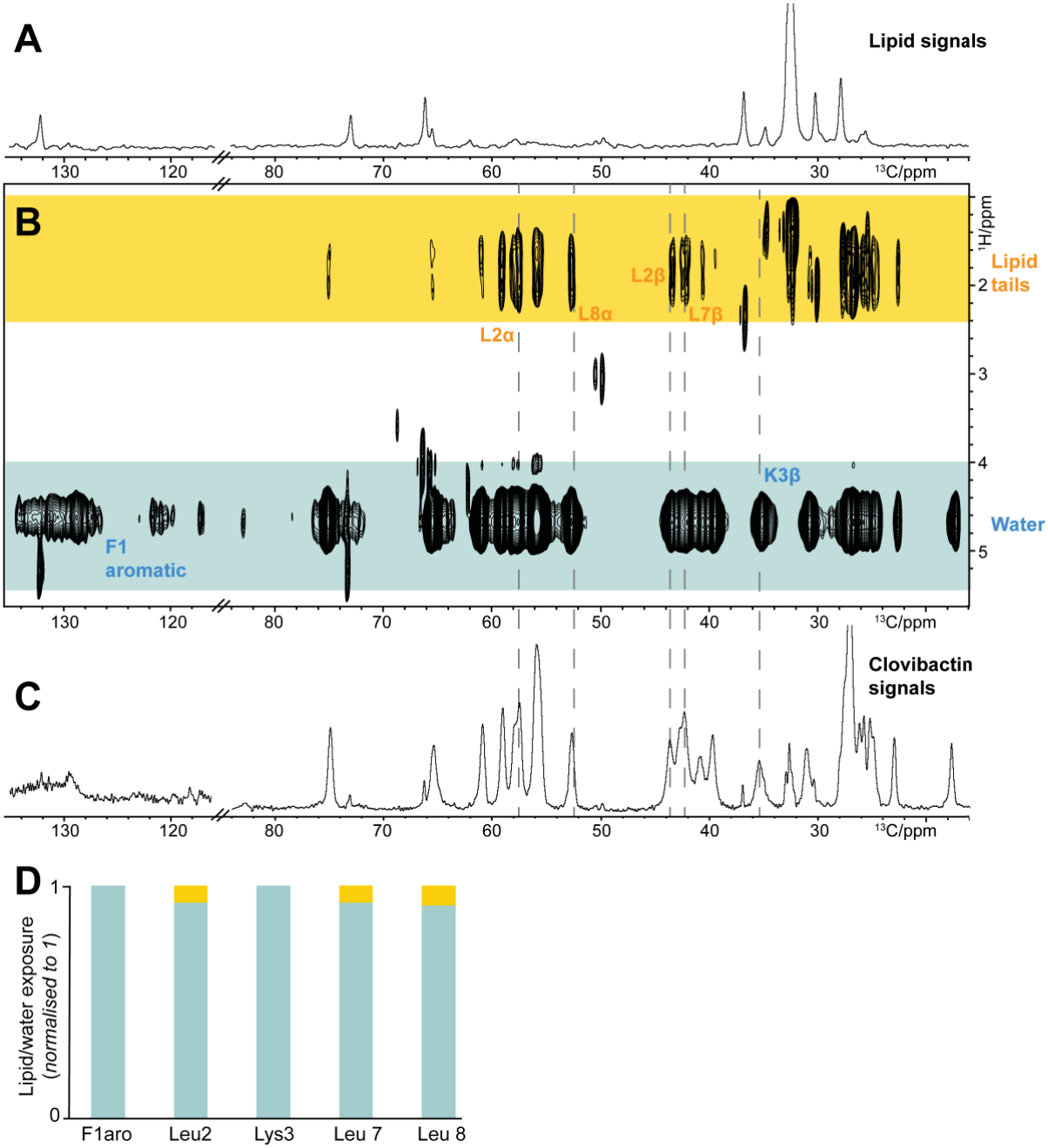

Supplementary Figure 7: The membrane topology of the complex. A) and B) show mobility-edited ('T_2-filtered') $^{1}H(^{1}H)^{13}C$ ssNMR experiments(Doherty and Hong, 2009) of $^{13}C,^{15}N$-clovibactin bound to Lipid II. Here, magnetization from mobile water and lipid molecules is transferred to the rigid clovibactin protons via ^{1}H-^{1}H mixing and eventually transferred to the ^{13}C nuclei of clovibactin via a short cross polarization step (200 µs). A 2D implementation of this experiment demonstrates that the sidechain of Leu2 is partially inserted in the membrane, whereas the sidechain of Lys3 points to the water phase. In general, as shown in Figure 4I of the main text, clovibactin fibrils do reside on the membrane surface and do not insert deeply into the membrane. Spectra were measured at 1200 MHz, 16.5 kHz MAS, and 300 K sample temperature. A) Control: 1D $^{1}H(^{1}H)^{13}C$ ssNMR spectrum (5120 scans) using a T_2-filter of 2.5 ms without transfer to clovibactin (0 ms ^{1}H-^{1}H mixing). All signals relate to lipids, demonstrating the effectiveness of the T_2-filter. B) 2D $^{1}H(^{1}H)^{13}C$ ssNMR spectrum using 2.5 ms T_2 filter (1792 scans) and 5 ms ^{1}H-^{1}H mixing. C) ^{13}C cross-polarization spectrum (200 µs contact time) of Lipid II-bound teixobactin. D) Normalized relative signal intensities (peak heights) of the correlations with water (blue) and lipid (brown) protons for several residues. See Supplementary Figure 12 for a structural representation of the topology.

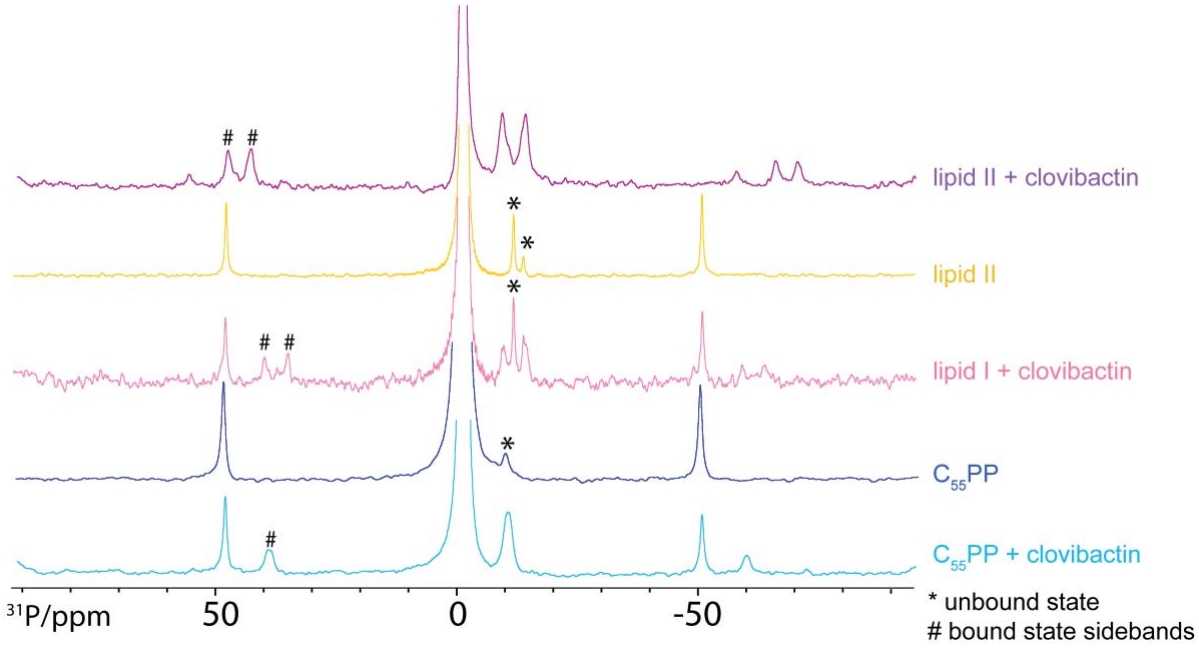

Supplementary Figure 8: ^{31}P magic angle spinning ssNMR of clovibactin with cell wall precursors in DOPC liposomes. Clovibactin binds to all cell wall precursors containing the C_{55}PP unit (C_{55}PP, lipid I, lipid II). Changes in the chemical shifts of the pyrophosphate groups of lipid II and lipid I upon addition of clovibactin show the direct binding to the site. Furthermore, the emergence of strong spinning sidebands around +45/-55 ppm show that clovibactin binds and immobilises C_{55}PP. Experiments were performed using MLV's containing 2 mol% of the cell wall precursor with and without the treatment with clovibactin at 500MHz and 10 kHz MAS (lipid II + clovibactin was performed at 12 kHz MAS).

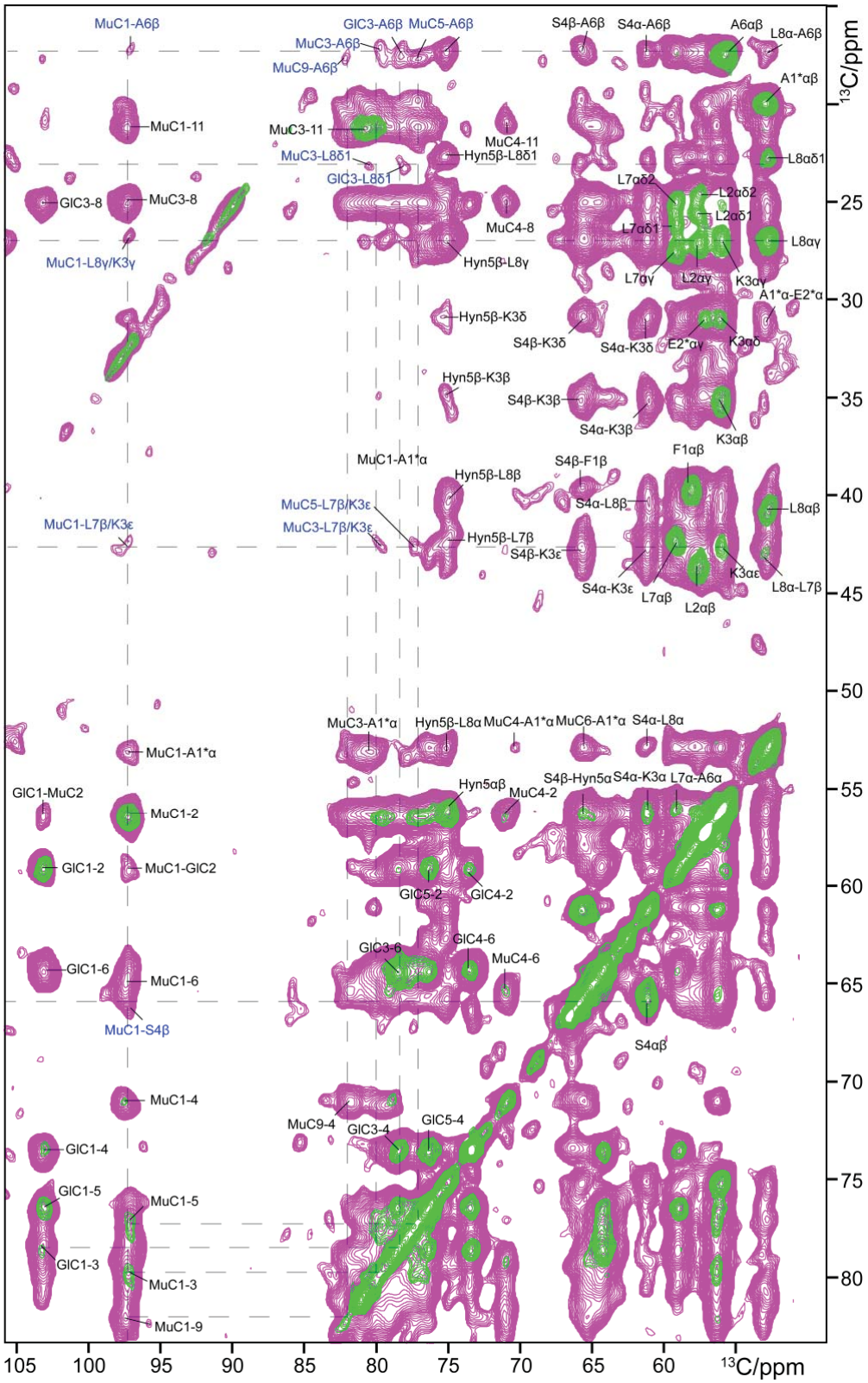

Supplementary Figure 9: The binding interface and absence of the pentapeptide in the binding. Spectrum showing multiple interfacial contacts illustrating the interaction between the depsi-cycle of clovibactin with the first sugar of lipid II. The experiments were performed at 950 MHz magnetic field with15.5 kHz MAS with a mixing time of 50 ms (green) and 300 ms (magenta).

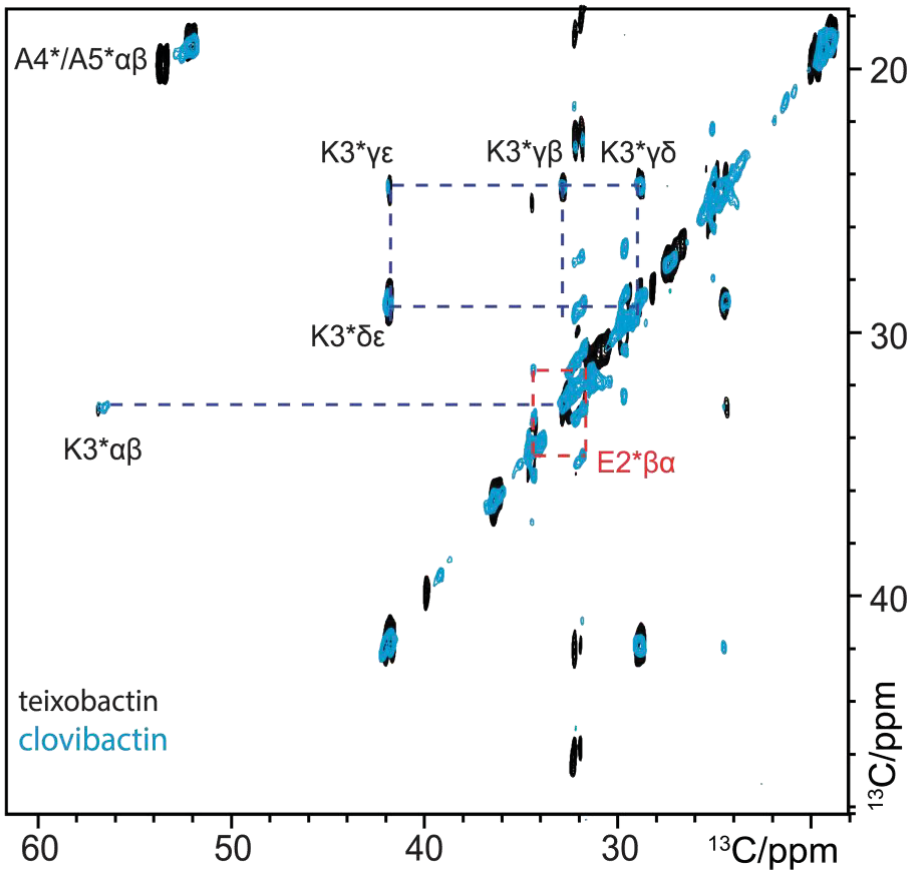

Supplementary Figure 10: The TOBSY spectrum shows that the lipid II pentapeptide is not involved in complex formation. The scalar based TOBSY spectrum only shows highly mobile residues in the complex. Here one can clearly see the presence of all the residues of the pentapeptide of lipid II, except for A1*. This indicates that the pentapeptide is highly mobile in the complex and not involved in the binding interface. The first A1* residue is linked to the first sugar (MurNAc) and therefore more rigid and in the dipolar based spectrum (Supp. Fig. 9). This contrasts with teixobactin's scalar spectrum (black) where residue E2 (in red) was not observed due to specific interactions of the MurNAc sugar with the enduracididine residue, leading to higher degree of rigidification of the pentapeptide.

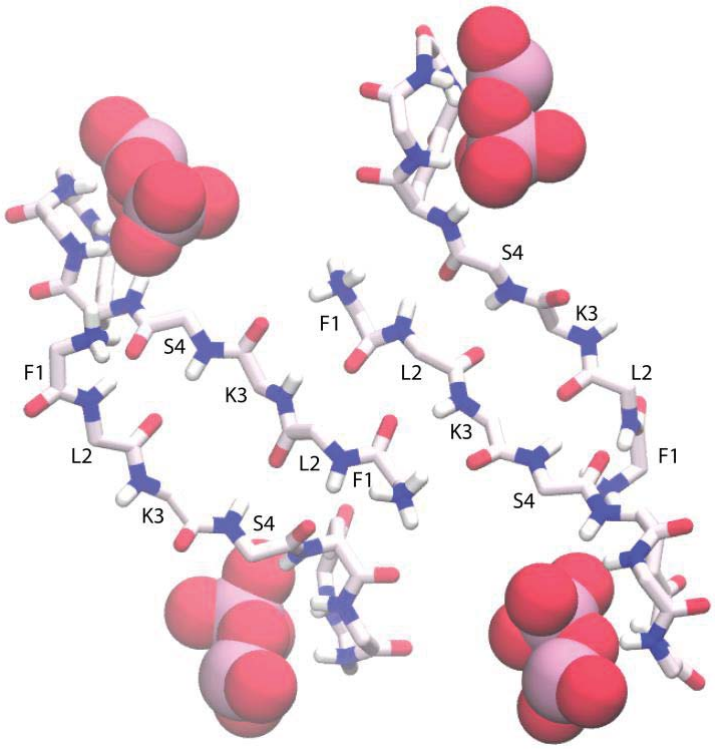

Supplementary Figure 11: Hydrogen bonding in the structural model. Atomic force microscopy, confocal microscopy, and ssNMR data demonstrate that clovibactin and Lipid II oligomerize into fibrils. ssNMR distance measurements are consistent with an antiparallel arrangement of clovibactin molecules, something that is also in line with the fibrils observed in AFM experiments.
Based on these experimental data, we applied hydrogen bonding restraints to foster an antiparallel arrangement in the structural model.

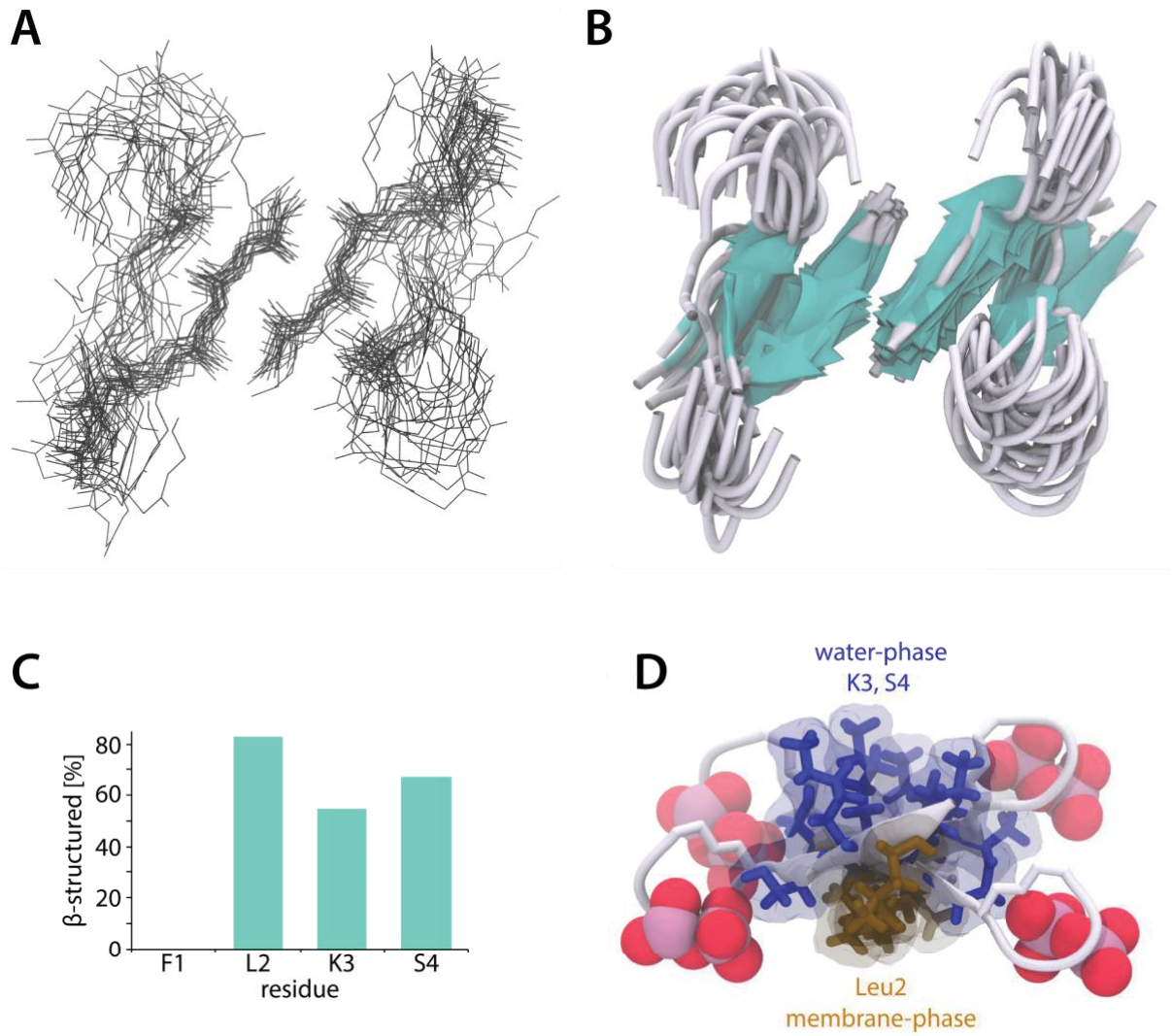

Supplementary Figure 12: RMSD, secondary structure, and membrane topology. (A, B) Superposition (2.50±0.85 Å average backbone RMSD for clovibactin in the complex) of 22 calculated structure models of the clovibactin – lipid II complex. Lipid II is not shown for clarity. (C) Quantification (Heinig and Frishman, 2004) of secondary structure elements of the very short linear N-terminus based on the calculated structural model. The N-terminus adopts a secondary structure that contains elements of β-structuring and an elongated loop. This is also reflected in the calculated ensemble (A, B) that does not show consistent β-structuring for the N-terminus. (D) Membrane-topology of clovibactin in the complex derived from ssNMR T2-edited H(H)C experiments (Doherty and Hong, 2009). The long-hydrophobic Leu2 sidechain (in brown) is embedded in the membrane, while the cationic (Lys3) and polar (Ser4) sidechains (in blue) of the N-terminus are water-exposed and, at the same time, favourably interact with the anionic PPi-group.

clovibactin - lipid II

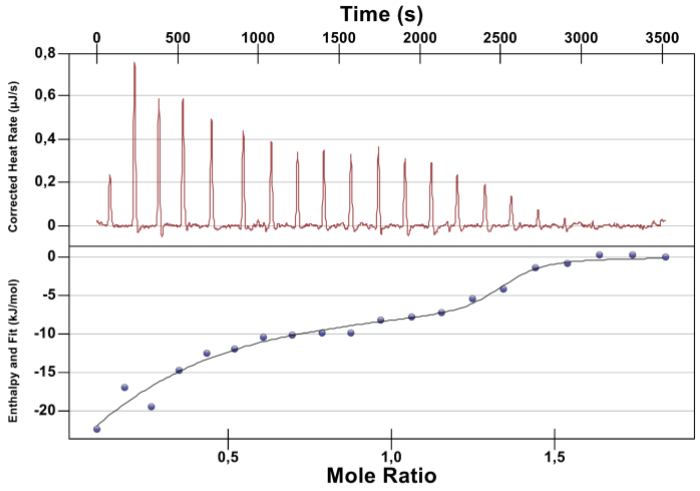

clovibactin - lipid I

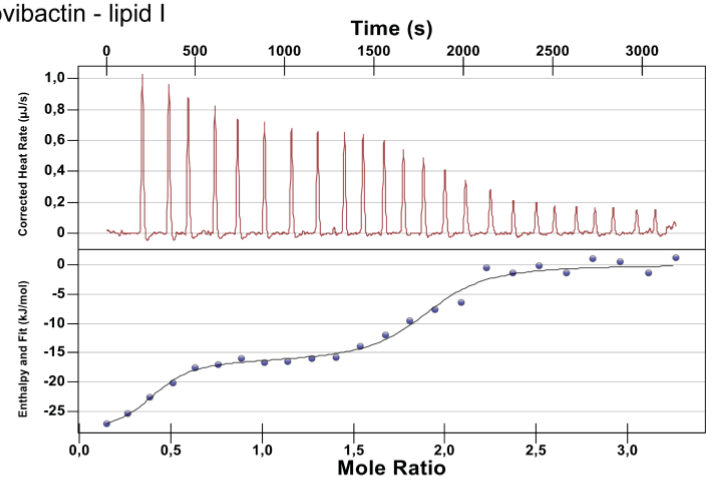

clovibactin - Na-pyrophosphate

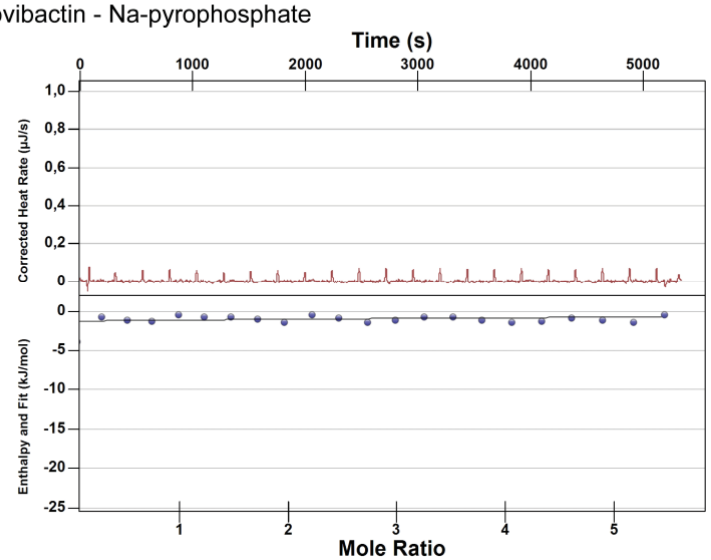

Antibiotic	lipid II K_d (µM)	lipid I K_d (µM)
Clovibactin	0.0862+/- 0.007	0.0807+/- 0.017
Teixobactin	0.0146 +/-0.002	0.0805+/- 0.007

Supplementary Figure 13: ITC data for clovibactin and teixobactin. The ITC data shows a binding isotherm for interaction between clovibactin and lipid II and lipid I. When compared to teixobactin, clovibactin has lower affinity for lipid II. This is in line with the less specific interaction of the clovibactin depsi-cycle with the first sugar of lipid II. There is no binding observed between clovibactin and soluble Na-pyrophosphate.

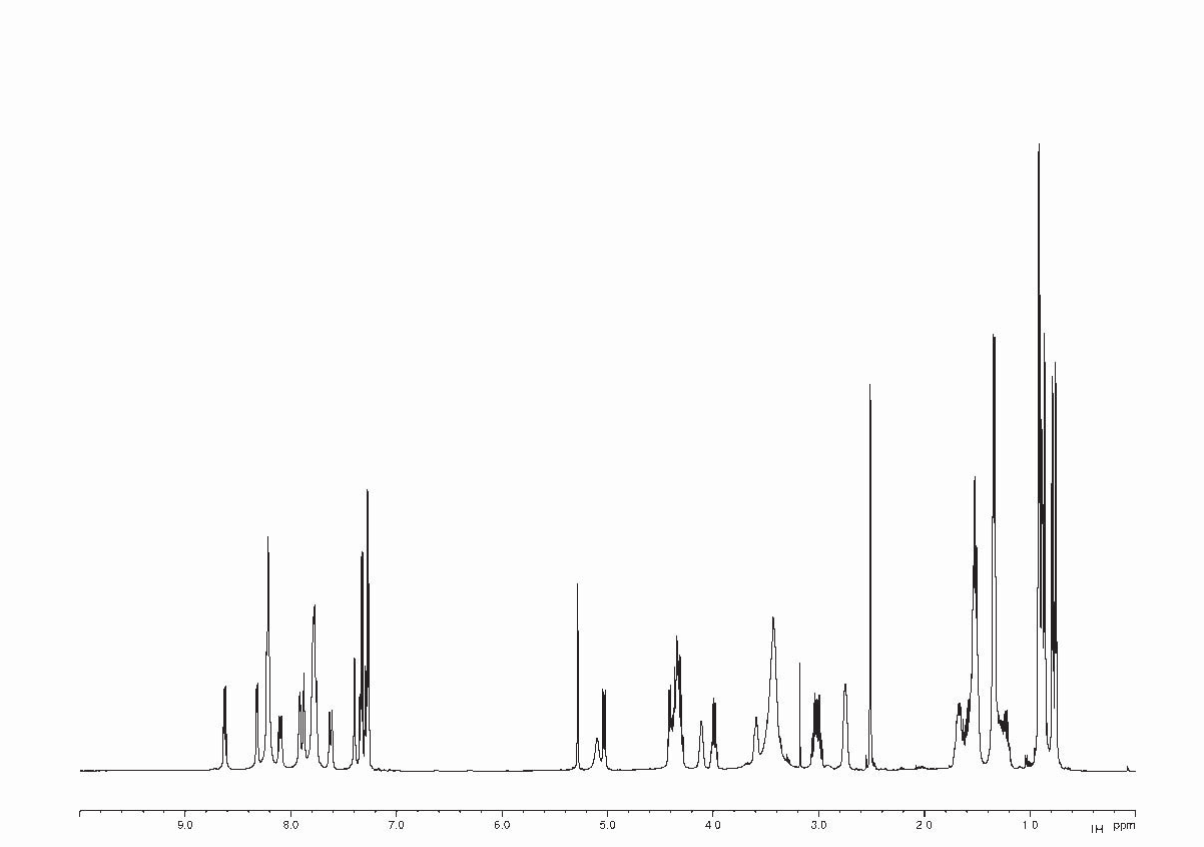

Supplementary Figure 15: ^{1}H NMR Spectrum of Clovibactin

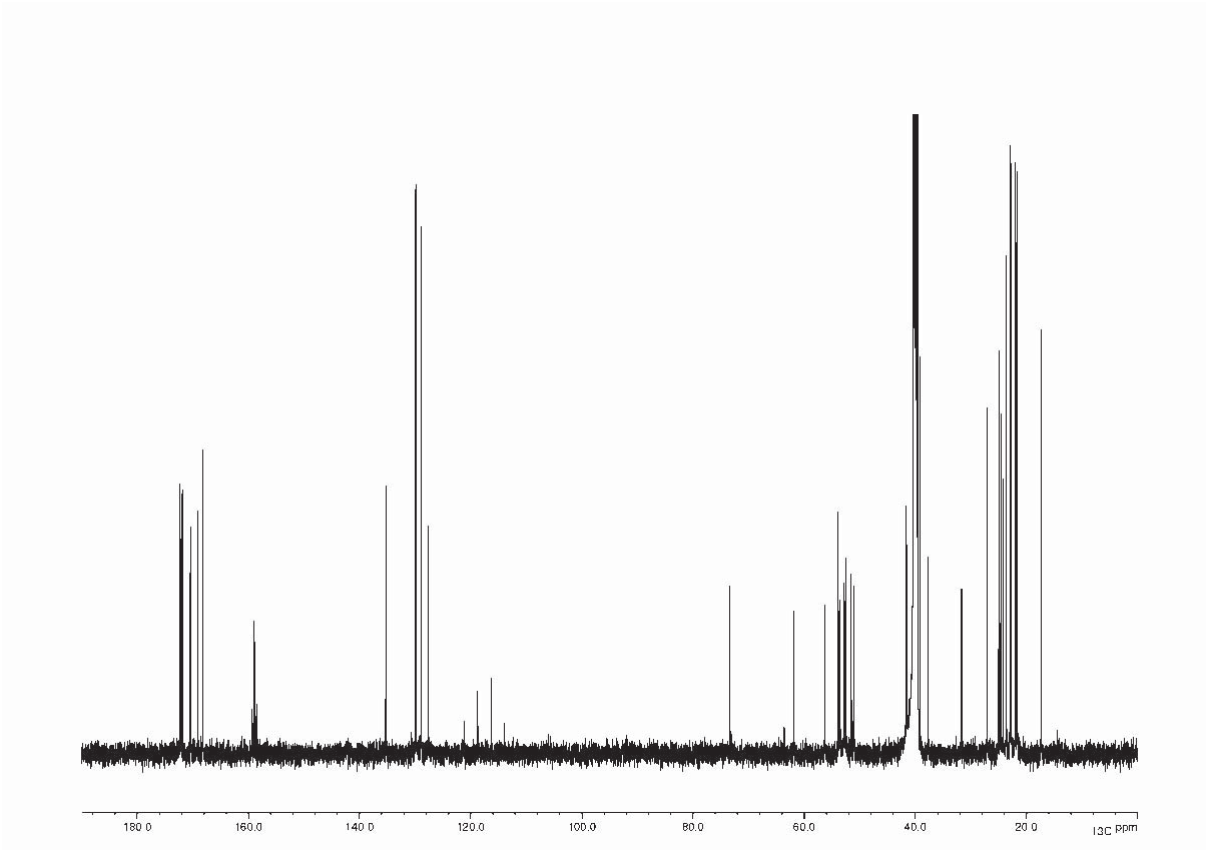

Supplementary Figure 16. ^{13}C solution NMR spectrum of clovibactin.

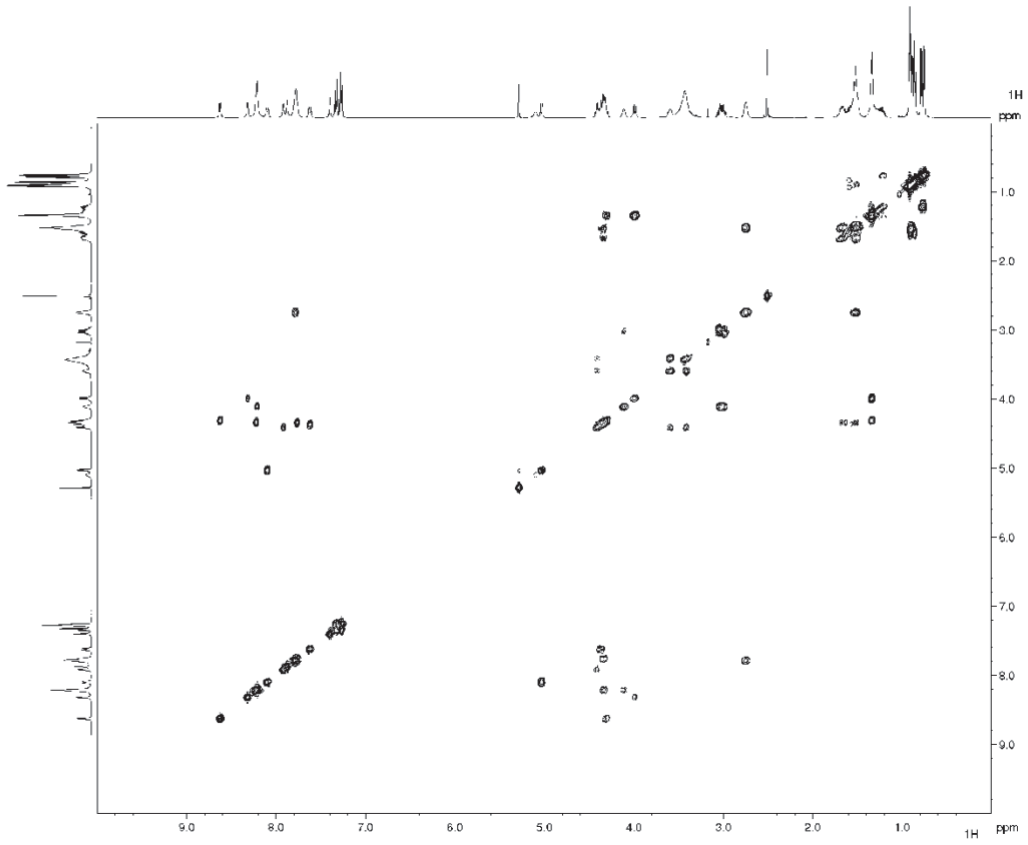

Supplementary Figure 17. ^{1}H-^{1}H COSY solution NMR Spectrum of clovibactin.

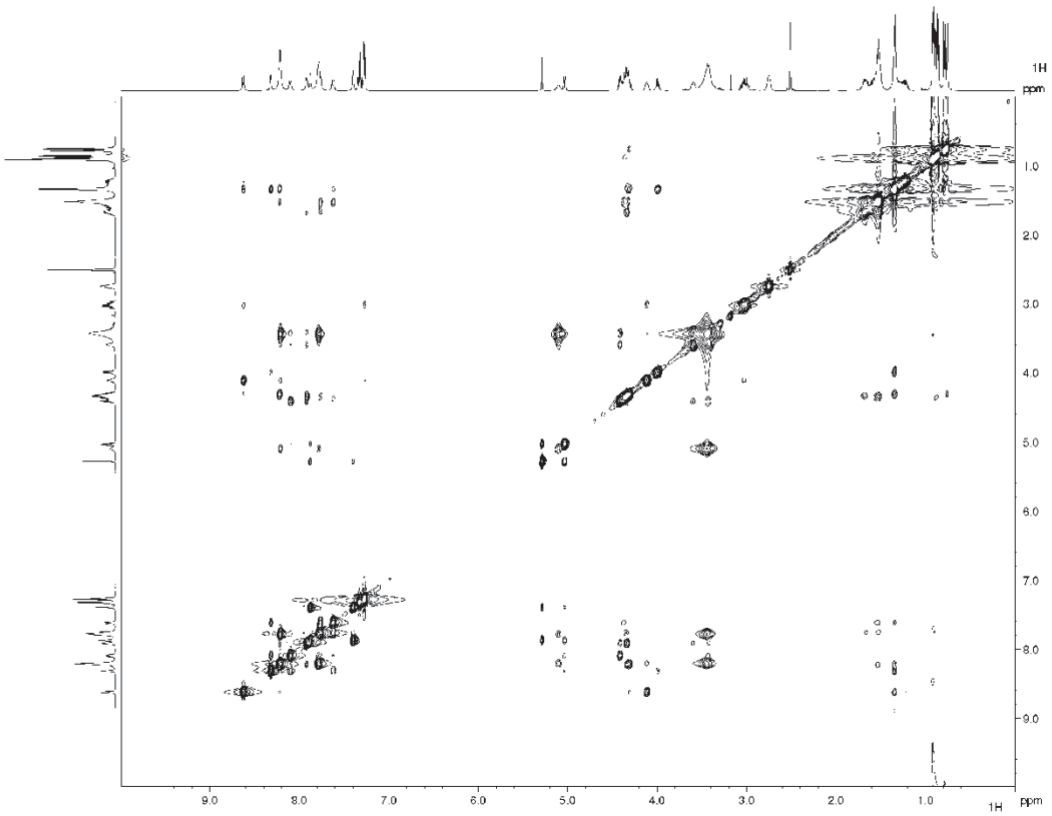

Supplementary Figure 18. ^{1}H-^{1}H NOESY solution NMR Spectrum of clovibactin.

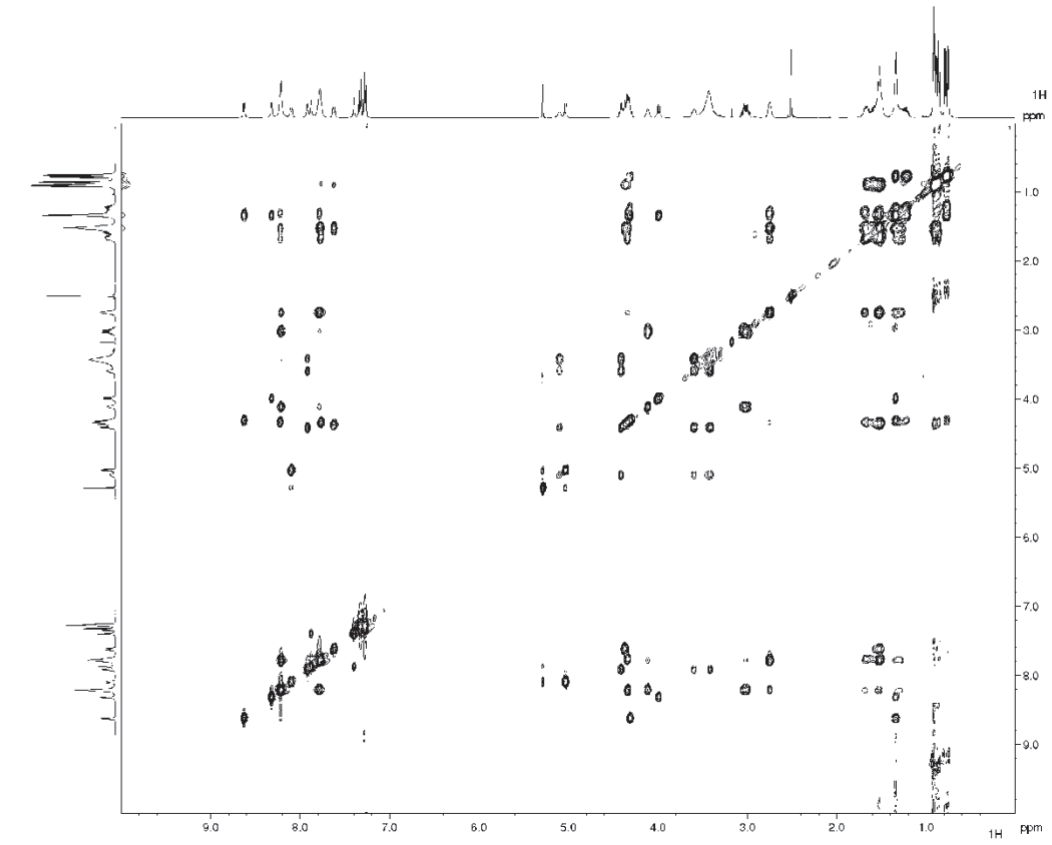

Supplementary Figure 19. ^{1}H-^{1}H TOCSY solution NMR spectrum of clovibactin.

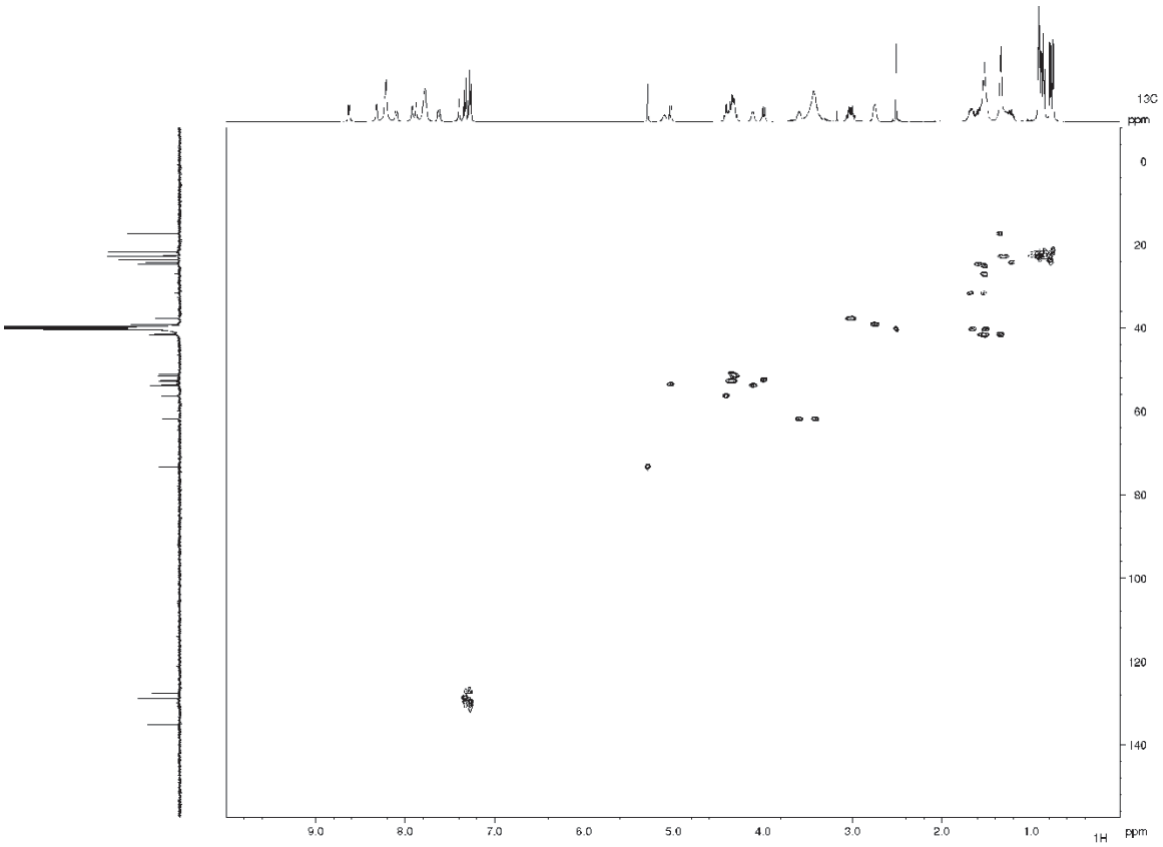

Supplementary Figure 20. ^{1}H-^{13}C HSQC solution NMR spectrum of clovibactin.

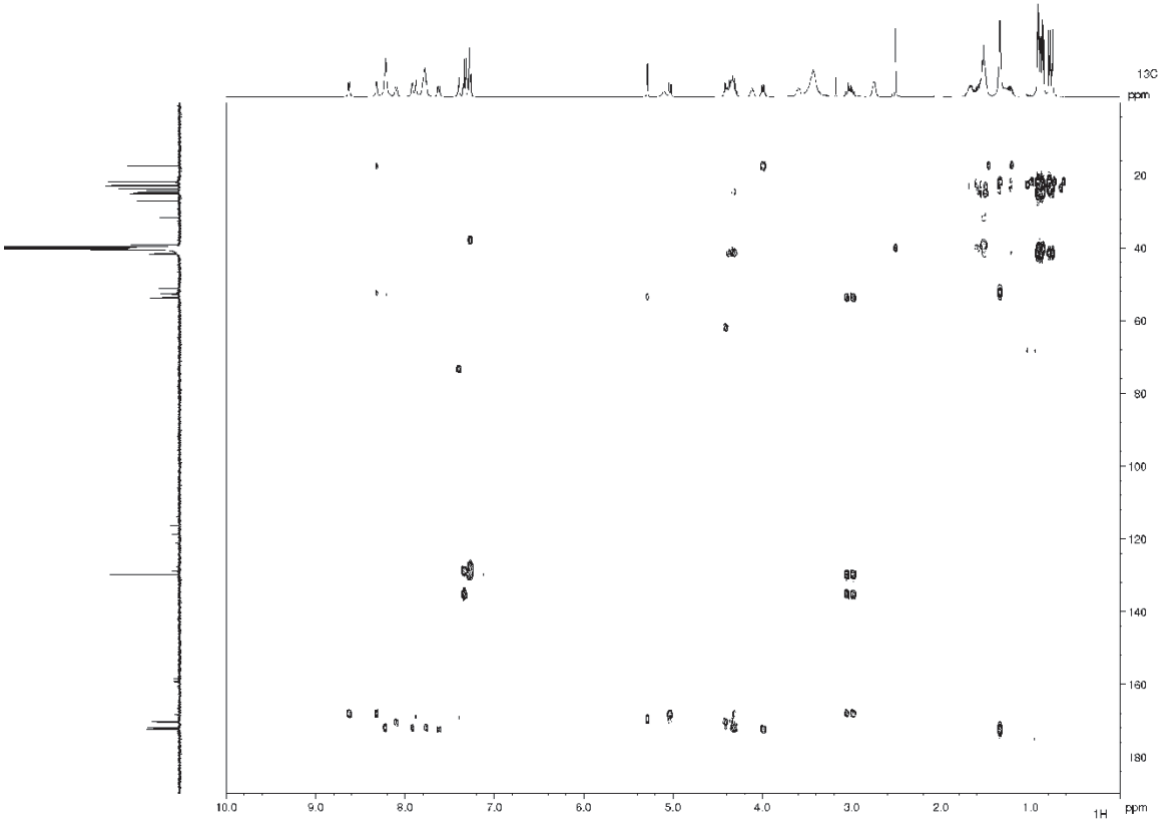

Supplementary Figure 21. ^{1}H-^{13}C HMBC solution NMR spectrum of clovibactin.

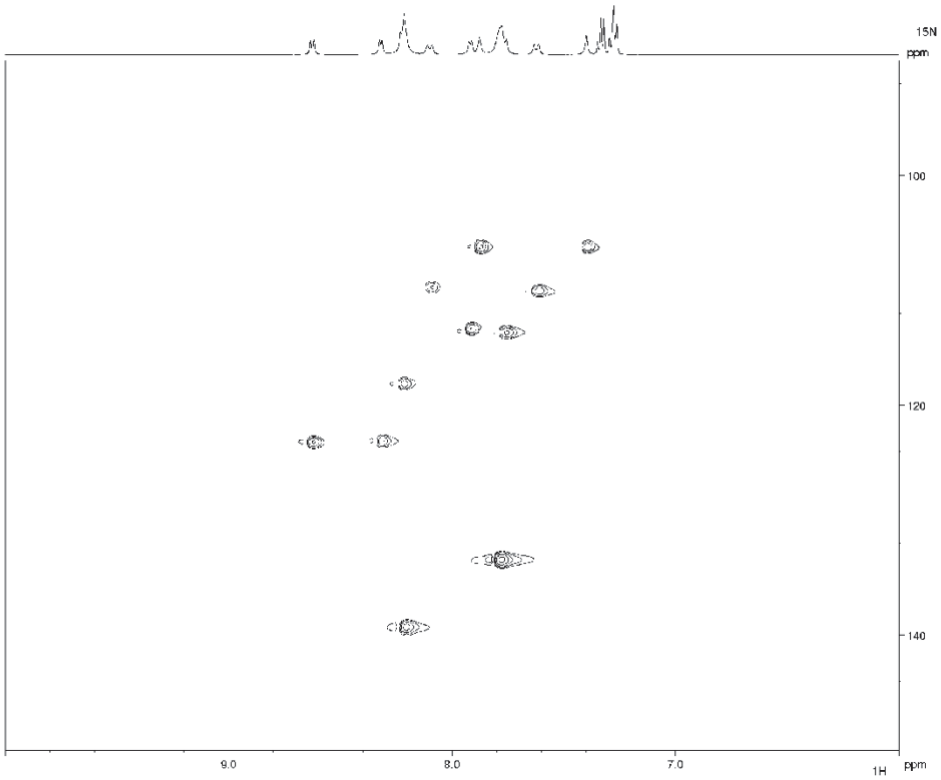

Supplementary Figure 22. ^{1}H-^{15}N HSQC solution NMR Spectrum of clovibactin.

Supplementary Table 4

^{13}C,^{15}N-labelled clovibactin in the unbound state, obtained from solution NMR measurements, acquired at 600 MHz ^{1}H-frequency in 30 mM Citrate buffer with 10% D2O, pH = 5.5. Assignments in ppm. Overlapping ^{13}C-signals are shown in the same colour.

Res	#	N	H(N)	Cα	Cβ	Nδ
Phe	1			57.3	39.1	
D-Leu	2	127.9	8.4	55.5	42.2	
D-Lys	3	121.8	8.3	56.2	32.8	
Ser	4	117.7	8.1	58.8	63.9	
Hyn	5	112.9	8.9	56.4	76.1	107.3
Ala	6	126.1	8.1	55.3	18.4	
Leu	7	117.0	7.8	56.0	42.3	
Leu	8	118.6	7.9	54.2	42.1	

Supplementary Table 5

^{13}C,^{15}N-labelled clovibactin in the lipid II bound state, obtained from ssNMR measurements in DOPC liposomes. Assignments in ppm. Overlapping ^{13}C-signals (also with ^{13}C,^{15}N-labelled lipid II) are colour coded.

Res	#	N	H(N)	CO	Cα	Cβ	Cγ	Cδ1	Cδ2	Cε1/2	Cζ	Nδ	Nζ	H(N)ζ	Hγ1+2
Phe	1	40.9		172	58.5	39.7	140.2	~132	~132	~132	~132				
D-Leu	2	127.7	8.8	178.6	57.7	43.7	27.4	25.7	24.7						
D-Lys	3	113.0	7.7	177.4	56.1	35.2	27.0	31.1		42.4			29.9	8.4	
Ser	4	113.8	9.9	176.6	61.3	65.9									
Hyn	5	110.7	9.0	171.7	56.3	75.3	174.1					108.8			8.4/6.1
Ala	6	125.9	8.2	179.6	55.9	17.4									
Leu	7	121.2	9.9	177.6	59.5	42.2	27.6	26.1	25.1						
Leu	8	112.9	8.7	171.2	53.1	40.9	27.0	22.9	27.0						

Supplementary Table 6

^{13}C,^{15}N-labelled lipid II in the bound state with clovibactin, obtained from ssNMR measurements in DOPC liposomes. Assignments in ppm. Overlapping ^{13}C-signals (also with ^{13}C,^{15}N-labelled clovibactin) are colour coded.

Sugars	#	C1	C2	C3	C4	C5	C6	C7	C8	C9	C10	C11
MurNAc		97.5	56.5	80.0	71.2	77.6	64.6	176.9	25.2	81.8	178.3	20.4
GlcNAc		103.3	59.3	78.6	73.7	76.5	64.5	175.6				
Pentapep		CO	Cα	Cβ	Cγ	Cδ	Cε					
L-Ala	1	176.9	53.5	20.0								
D-γ-Glu	2		34.4	30.9	57.4	180.7						
L-Lys	3		56.5	32.8	24.5	28.8	41.9					
D-Ala	4/5		52.2	19.2								

PPi		**P**										
Pi	**1**	- 8.4										
Pi	**2**	-13.0										

Analysis of calculated structure models

The average backbone RMSD (from the average structure) of the 22 clovibactin molecules in the complex was 2.50 ± 0.85 Å.

NMR restraints

Intermolecular distance restraints between clovibactin molecules

All restraints based on a series of 2D $^{13}C^{13}C$ PARIS experiments (up to 300 ms $^{13}C^{13}C$ transfer) using a target distance of 7.5 Å, and lower distance margin of 5.5 Å, and a higher distance margin of 2.0 Å; i.e., format (7.5 5.5 2.0). Note that in the arrangement of four clovibactin molecules, intermolecular clovibactin-clovibactin distance restraints for the *inner* clovibactin molecules were implemented so that a restraint could be with the clovibactin molecule on either side.

Detailed list of clovibactin – clovibactin restraints.

Supplementary Table T4:

Clovibactin-Clovibactin contacts
Unambiguous

#		^{13}C-CS (ppm)		^{13}C-CS (ppm)	Average shortest intramolecular distance (Å)	Average shortest intermolecular distance (Å)
1	Phe1Cα	58.5	Hyn5Cβ	75.3±	11.8 ± 0.6	6.3 ± 0.7
2	Phe1Cα	58.5	Hyn5Cγ	174.1	10.4 ± 0.7	6.5 ± 0.9
3	Phe1Cα	58.5	Ala6Cβ	17.4	15.3 ± 0.5	6.5 ± 1.0
4	Phe1Cα	58.5	Leu8Cα	53.1	13.4 ± 0.8	8.8 ± 1.0
5	Phe1Cα	58.5	Leu8CO	171.2	12.6 ± 0.8	8.2 ± 0.9
6	Phe1Cα	58.5	Leu8Cβ	40.9	12.6 ± 0.9	8.1 ± 1.3
7	Phe1Cα	58.5	Leu8Cδ1	22.9	13.6 ± 1.1	7.8 ± 1.6
8	Phe1Cβ	39.7	Hyn5Cβ	75.3	11.3 ± 0.9	5.4 ± 0.6
9	Phe1Cβ	39.7	Hyn5Cγ	174.1	9.9 ± 1.0	5.9 ± 0.7
10	Phe1Cβ	39.7	Ala6CO	179.6	15.4 ± 0.8	6.6 ± 0.9
11	Phe1Cβ	39.7	Leu8CO	171.2	12.1± 1.2	7.6 ± 0.6
12	Phe1Cβ	39.7	Leu8Cδ1	22.9	13.2 ± 1.6	8.1 ± 1.7
13	Phe1Cγ	140.2	Leu8Cα	53.1	13.5 ± 1.6	8.5 ± 0.7
14	Phe1Cγ	140.2	Leu8Cβ	40.9	12.7 ± 1.7	8.3 ± 1.2

15	Phe1Caro	~132	Leu8Cβ	40.9	13.5 ± 2.1	7.3 ± 1.3
16	Leu2Cα	57.7	Leu8Cα	53.1	11.2 ± 0.6	9.6 ± 1.0
17	Leu2Cβ	43.7	Leu8CO	171.2	10.9 ± 0.6	8.5 ±1.2
18	Leu2CO	178.6	Ala6Cβ	17.4	10.8 ± 0.5	8.6 ± 0.6
19	Leu2CO	178.6	Leu8Cδ1	22.9	10.7 ± 0.7	9.6 ± 1.0

Hydrogen bond restraints (intermolecular) between clovibactin molecules: Hydrogen bonding restraints in line with experimentally determined antiparallel clovibactin arrangements were applied. While two different register shifts are possible to form antiparallel teixobactin β-sheets (i.e., Ser4NH could interact with Leu2CO or Ser4CO), only the variant with Leu2CO agrees with the intermolecular ssNMR distance restraints. Hydrogen bonding distance restraints were defined accordingly with upper and lower limits of 2.3 and 1.5 Å, respectively, i.e., format (2.0 0.5 0.3).

*clovibactin **A** with clovibactin **B***
Leu2NH - Ser4CO
Leu2CO - Ser4NH
Ser4NH - Leu2CO
Ser4CO - Leu2NH

*clovibactin **C** with clovibactin **D***
Phe1NH - Lys3CO
Phe1CO - Lys3NH
Lys3NH - Phe1CO
Lys3CO - Phe1NH

*clovibactin **C** with clovibactin **D***
Similar as in ***A*** with ***B***

Intermolecular distance restraints between clovibactin and lipid II: *Restraints involving the pyrophosphate group:* Ambiguous distance restraints were applied between the backbone amino protons of the four depsi-cycle residues (Hyn5-Leu8) with either phosphate of the pyrophosphate group using upper and lower limits of 2.4 and 1.7 Å, respectively, i.e., format (2.0 0.3 0.4). Restraints based on a 2D $^{1}H^{31}P$ experiment (Fig. 5b of the manuscript).

Restraints involving the MurNAc/GlcNAc sugars: Restraints were based on a series of 2D $^{13}C^{13}C$ PARIS and PARISxy experiments with 50, 250, and 300 ms magnetization transfer. Due to the mobility of the depsi-cycle in the complex (Figure 4C,D of the main text), most interfacial restraints were weak. We therefore applied all interfacial CC restraints with wider boundaries (7.5 5.5 2.0), i.e., upper and lower boundaries of 9.5 and 2.0 Å, respectively. Notwithstanding the wider boundaries, the interface is well defined (1.47±0.40 Å interfacial RMSD defined by residues Ala6, Leu7, Leu8 of clovibactin, PPi and MurNAc of lipid II)

.

Supplementary Table T6:
Detailed list of clovibactin – lipid II restraints

		^{13}C-CS (ppm)		^{13}C-CS (ppm)	Average shortest interfacial distance (Å)
1	Ser4Cβ	65.9	Mu6C1	97.5	5.7 ± 0.9
2	Ser4Cβ	65.9	Mu6C3	80.0	7.4 ± 1.0
3	Ala6Cβ	17.4	Mu6C1	97.5	4.5 ± 0.6
4	Ala6Cβ	17.4	Mu6C3	80.0	6.4 ± 0.6
5	Ala6Cβ	17.4	Mu6C5	77.6	5.0 ± 0.9
6	Ala6Cβ	17.4	Mu6C9	81.8	7.6 ± 0.8
7	Ala6Cβ	17.4	Mu6C11	20.4	7.8 ± 1.1
8	Ala6Cβ	17.4	Gl7C3	78.6	7.2 ± 1.9
9	Leu7Cβ	42.2	Mu6C1	97.5	4.4 ± 0.6
	Lys3Cε	42.4	Mu6C1	97.5	8.1 ± 0.9
10	Leu7Cβ	42.2	Mu6C3	80.0	5.6 ± 0.5
	Lys3Cε	42.4	Mu6C3	80.0	8.5 ± 1.3
11	Leu7Cβ	42.2	Mu6C5	77.6	5.6 ± 1.0
	Lys3Cε	42.4	Mu6C5	77.6	9.2 ± 0.9
12	Leu8CO	171.2	Mu6C1	97.5	5.8 ± 0.8
13	Leu8Cδ1	81.7	Mu6C3	80.0	6.0 ± 1.1
14	Leu8Cδ1	81.3	Gl7C3	78.6	8.6 ± 1.1
15	Leu8Cδ1	81.7	Gl7C5	76.5	7.0 ± 0.7
16	Leu8Cγ	27.0	Mu6C1	27.0	5.7 ± 0.8
	Lys3Cγ	27.0	Mu6C1	27.0	7.9 ± 1.0

The shortest distances were averaged over the 22 structure models of the ensemble. The error shows the standard deviation.

Topological restraints: Eventually, a filtering strategy was applied to constrain the conformational space of the isoprenyl tails. Structure models were only accepted if all lipid II tails pointed into the direction of the membrane-exposed sidechain of Leu2, Ile5, and Ile6 (see Fig. 4I of the main text and Supplementary Fig. 7). Sorting of the lipid II tails was steered by imposing soft distance restraints between the sidechain of Leu2 and the lipid II isoprenyl-tail, and by imposing soft distance restraints between the isoprenyl-tails.

Supplementary Table T7:
Number and type of restraints used for the structure calculations. Intramolecular restraints are listed per monomers, while intermolecular/interfacial restraints are listed per pair of interacting molecules.

Number of Restraints		
Intermolecular	*Unambiguous*	*Ambiguous*
clovibactin - clovibactin		
Distance restraints	19	0
Hydrogen bonds**	4	0
Intermolecular clovibactin - lipid II	*Unambiguous*	*Ambiguous*
Distance restraints with sugars	12	4
Distance restraints with PPI***	0	4

*,**,*** See Methods (NMR Structure calculations) for details

Analysis of calculated structure models

Structural and violation statistics of the final 22 structure models are given below:

Structure ensemble precision:

- Average backbone RMSD (from the average structure) of the 22 clovibactin molecules in the complex: 2.50 +/- 0.85 Å.

Details of 2D ssNMR experiments

1. 2D CC PARIS experiment with $^{13}C,^{15}N$-clovibactin – $^{12}C,^{14}N$-lipid II

Magnetic field /MAS = 1200 MHz (^{1}H-frequency) / 18 kHz
Mixing time (CC) = 50 ms
t1 points / AQ = 452 / 5.00 ms
Recycle delay = 2.40 s
Co-added transients = 144
Experimental time = 1d 21h

2. 2D CC PARIS experiment with $^{13}C,^{15}N$-clovibactin – $^{12}C,^{14}N$-lipid II

Magnetic field /MAS = 1200 MHz (^{1}H-frequency) / 18 kHz
Mixing time (CC) = 300 ms
t1 points / AQ = 452 / 5.00 ms
Recycle delay = 2.40 s
Co-added transients = 224
Experimental time = 3d 5h

3. 2D CC PARISxy (m = 1) experiment with $^{13}C,^{15}N$-clovibactin – $^{13}C,^{15}N$-lipid II

Magnetic field /MAS = 950 MHz (^{1}H-frequency) / 15.5 kHz
Mixing time (CC) = 50 ms
t1 points / AQ = 316 / 4.40 ms
Recycle delay = 1.90 s
Co-added transients = 192
Experimental time = 1d 10h

4. 2D CC PARISxy (m = 1) experiment with $^{13}C,^{15}N$-clovibactin – $^{13}C,^{15}N$-lipid II

Magnetic field /MAS = 950 MHz (^{1}H-frequency) / 15.5 kHz

Mixing time (CC) = 300 ms
t1 points / AQ = 215 / 3.00 ms
Recycle delay = 1.84 s
Co-added transients = 1024
Experimental time = 5d 14h

5. 2D CC PARIS experiment with $^{13}C,^{15}N$-clovibactin – $^{13}C,^{15}N$-lipid II

Magnetic field /MAS	= 1200 MHz (^{1}H-frequency) / 18 kHz
Mixing time (CC)	= 50 ms
t1 points / AQ	= 452 / 5.00 ms
Recycle delay	= 2.40 s
Co-added transients	= 144
Experimental time	= 1d 21h

6. 2D CC PARIS experiment with $^{13}C,^{15}N$-clovibactin – $^{13}C,^{15}N$-lipid II

Magnetic field /MAS	= 1200 MHz (^{1}H-frequency) / 18 kHz
Mixing time (CC)	= 250 ms
t1 points / AQ	= 316 / 3.50 ms
Recycle delay	= 2.30 s
Co-added transients	= 752
Experimental time	= 7d 1h

7. 2D T2-edited H(H)C experiment with $^{13}C,^{15}N$-clovibactin – $^{12}C,^{14}N$-lipid II

Magnetic field /MAS	= 700 MHz (^{1}H-frequency) / 16.5 kHz
Mixing time (HH)	= 5 ms
T2 filter	= 2.5 ms
t1 points / AQ	= 60 / 2.08 ms
Recycle delay	= 2.15 s
Co-added transients	= 1972
Experimental time	= 2d 17h

8. 2D CC TOBSY experiment with $^{13}C,^{15}N$-clovibactin – $^{13}C,^{15}N$-lipid II

Magnetic field /MAS	= 950 MHz (^{1}H-frequency) / 8 kHz
Mixing time (HH)	= 6 ms
t1 points / AQ	= 265 / 5.38 ms
Recycle delay	= 1.61 s
Co-added transients	= 2304
Experimental time	= 11d 16h

9. 2D NCA experiment with $^{13}C,^{15}N$-clovibactin – $^{12}C,^{14}N$-lipid II

Magnetic field /MAS	= 800 MHz (^{1}H-frequency) / 15 kHz
Mixing time (NC)	= 5.5 ms
t1 points / AQ	= 17 / 3.6td ms
Recycle delay	= 1.82 s
Co-added transients	= 7168
Experimental time	= 2d 17h

9. 2D NCO experiment with $^{13}C,^{15}N$-clovibactin – $^{12}C,^{14}N$-lipid II

Magnetic field /MAS	= 800 MHz (^{1}H-frequency) / 15 kHz
Mixing time (NC)	= 7 ms
t1 points / AQ	= 25 / 4.4 ms
Recycle delay	= 1.9 s
Co-added transients	= 8192
Experimental time	= 4d 18h

10. 2D NH experiment with $^{13}C,^{15}N$-clovibactin – $^{12}C,^{14}N$-lipid II

Magnetic field /MAS	= 700 MHz (^{1}H-frequency) / 60 kHz
t1 points / AQ	= 87 / 5.6 ms
Recycle delay	= 0.72 s
Co-added transients	= 4096
Experimental time	= 5d 4h
Note	= high number of co-added transients was necessary to obtain good data for the sidechains of 3 and 5.

For all 2D experiments, sign discrimination in indirect dimensions was achieved with the TPPI (time-proportional phase incrementation) method.

Supplementary Video 1: Real-time observation of the growth of clovibactin fibrils on membrane captured by HS-AFM. Membrane containing 4 % lipid II and 5 μM of clovibactin is used. The imaging rate is 0.5 frames/second with line rate of 150 lines/second. Clovibactin is added at 0 sec.

References

Doherty, T., and Hong, M. (2009). 2D 1H–31P solid-state NMR studies of the dependence of inter-bilayer water dynamics on lipid headgroup structure and membrane peptides. Journal of Magnetic Resonance *196*, 39-47.

Heinig, M., and Frishman, D. (2004). STRIDE: a web server for secondary structure assignment from known atomic coordinates of proteins. Nucleic Acids Research *32*, W500-W502.

Wang, Y. (2002). Probability-based protein secondary structure identification using combined NMR chemical-shift data. Protein Science *11*, 852-861.

Chapter 5

THCz: Small molecules with antimicrobial activity that block cell wall lipid intermediates

In search for novel bacterial cell wall biosynthesis inhibitors, a whole-cell screen based on autolysis induction in pneumococci identified a hit class of synthetic small molecules with a 1-amino substituted tetrahydrocarbazole (THCz) scaffold. THCz displayed potent activity against a broad spectrum of Gram-positive, selected Gram-negative pathogens and mycobacteria. The objective of this study was to investigate the structure activity relationship (SAR) and the precise mode of action, including the elucidation of the molecular target, of a series of THCz analogs.

Whole-cell analyses confirmed that THCz target the cell wall biosynthesis pathway. Moreover, induction of the cell wall stress stimulon in *Bacillus subtilis* and intracellular accumulation of the soluble peptidoglycan precursor UDP-*N*-acetylmuramic acid pentapeptide after treatment with THCz pointed towards interference with one of the membrane-associated steps of the lipid II biosynthesis cycle. In search for the molecular target, THCz were found to inhibit both, the staphylococcal penicillin-binding protein 2 (PBP2)-catalyzed transglycosylation of lipid II and the YbjG-catalyzed dephosphorylation of undecaprenyl pyrophosphate (C_{55}-PP) to undecaprenyl phosphate (C_{55}-P) by binding to the lipid substrates at a 2:1 molar ratio. In line with the *in vitro* analyses, the addition of C_{55}-PP-containing lipid intermediates, including the peptidoglycan precursors lipid I and lipid II, the wall teichoic acid precursor lipid III_{WTA}, and the capsule precursor lipid I_{cap}, counteracted THCz from inhibiting growth of *Micrococcus luteus*. Interaction with the first sugar moiety of the lipid intermediates appeared to contribute to higher binding affinity, since two-fold higher concentrations of C_{55}-PP itself were required for full antagonization of THCz activity. SAR studies identified hydrophobic substituents and the two central amine groups of THCz as essential for potent antibacterial activity. Thus, the positively charged diamino motif of the small molecule inhibitors was proposed to electrostatically interact with the anionic pyrophosphate moiety of the cell wall precursors.

Remarkably, no THCz-resistant mutants of *Streptococcus pneumoniae* were obtained during passaging in broth with sub-lethal concentrations of the antibiotic. However, an isolate with reduced susceptibility was obtained from passaging on plates containing incrementing THCz concentrations. A point mutation in the *cpsE* gene, encoding for the initial glycosyltransferase of pneumococcal capsule biosynthesis (the main virulence factor of pneumocci), was found to confer decreased capsule production associated with reduced susceptibility towards THCz.

The majority of lipid II-binding antibiotics are bulky molecules. Importantly, the study highlights THCz to be the first small molecule inhibitors (<500 Da) targeting the bacterial cell wall by binding to C_{55}-PP-containing precursors of peptidoglycan, WTA and capsule biosyntheses. Thus, THCz represent an excellent scaffold for the future design of small molecule lipid II-binding antibiotics.

K.C.L. performed the determination of antimicrobial activity, mechanism of action studies, identified the molecular targets (all with a focus on staphylococci), analyzed the data and contributed to writing of the manuscript. A manuscript version of the publication is included as part of the doctoral thesis of Dr. Elisabeth Reithuber (Reithuber, 2021).

THCz: Small molecules with antimicrobial activity that block cell wall lipid intermediates

Elisabeth Reithuber[a,1], Torbjörn Wixe[b,1], Kevin C. Ludwig[c,1], Anna Müller[c], Hanna Uvell[b], Fabian Grein[c,d], Anders E. G. Lindgren[b,e], Sandra Muschiol[a,f], Priyanka Nannapaneni[a], Anna Eriksson[b], Tanja Schneider[c,2], Staffan Normark[a,2], Birgitta Henriques-Normark[a,f,2,3], Fredrik Almqvist[b,e,2,3], and Peter Mellroth[a,3]

[a]Department of Microbiology, Tumor and Cell Biology, Karolinska Institutet 171 77 Stockholm, Sweden; [b]Department of Chemistry, Umeå University, Umeå 90736, Sweden; [c]Institute for Pharmaceutical Microbiology, University Hospital Bonn, University of Bonn, Bonn 53115, Germany; [d]German Center for Infection Research (DZIF), partner site Bonn-Cologne, Bonn 53115, Germany; [e]Laboratories for Chemical Biology Umeå (LCBU), Umeå University, Umeå 90736, Sweden; and [f]Clinical Microbiology, Karolinska University Hospital Solna 171 76 Stockholm, Sweden

Contributed by Staffan Normark, October 1, 2021 (sent for review May 4, 2021; reviewed by Patrice Courvalin and Leiv Sigve Håvarstein)

Emerging antibiotic resistance demands identification of novel antibacterial compound classes. A bacterial whole-cell screen based on pneumococcal autolysin-mediated lysis induction was developed to identify potential bacterial cell wall synthesis inhibitors. A hit class comprising a 1-amino substituted tetrahydrocarbazole (THCz) scaffold, containing two essential amine groups, displayed bactericidal activity against a broad range of gram-positive and selected gram-negative pathogens in the low micromolar range. Mode of action studies revealed that THCz inhibit cell envelope synthesis by targeting undecaprenyl pyrophosphate–containing lipid intermediates and thus simultaneously inhibit peptidoglycan, teichoic acid, and polysaccharide capsule biosynthesis. Resistance did not readily develop in vitro, and the ease of synthesizing and modifying these small molecules, as compared to natural lipid II–binding antibiotics, makes THCz promising scaffolds for development of cell wall–targeting antimicrobials.

Streptococcus pneumoniae | antibiotic resistance | antimicrobials | cell wall biosynthesis | tetrahydrocarbazole

Since the discovery of penicillin by Alexander Fleming (1) in 1928, antibiotics have greatly improved the health quality and life expectancy of mankind. However, multidrug resistance among most microbial pathogens is reaching alarming levels, and the World Health Organization foresees a postantibiotic era where common bacterial infections may become life-threatening again due to the lack of adequate treatment regimens (2). Many of the most commonly used antibacterial drugs today, ∼50% of all antibiotic prescriptions, and over 70% of intravenous applications in clinical settings, rely on inhibitors of cell wall biosynthesis (3). The essentiality of the bacterial cell wall for structural integrity and growth, and the lack of a similar structure in mammalian cells, makes the cell wall biosynthesis machinery a most attractive antibiotic target. Inhibition of cell wall synthesis can be accomplished by two main mechanisms: either by inhibition of enzyme function, for example, by beta-lactam antibiotics targeting the penicillin-binding proteins (PBPs), or by binding and blocking access to essential cell wall precursors such as the ultimate peptidoglycan building block lipid II. While a wide range of beta-lactam derivatives of different classes are continuously optimized to bypass bacterial resistance development (4), the highly conserved lipid II molecule constitutes an attractive target, as resistance development is intrinsically limited (5, 6). Lipid II is a disaccharide pentapeptide peptidoglycan subunit linked to an undecaprenyl lipid vehicle via a pyrophosphate group. It is synthesized in the cytoplasm and flipped over to the outer leaflet of the plasma membrane to provide cell wall building blocks for PBPs (7). On the outside, the ultimate peptidoglycan precursor is readily accessible for antibiotics. Presently, lipid II–binding antibiotics of at least five chemical classes are known, comprising glycopeptides (e.g., vancomycin) (8), lantibiotics (e.g., nisin), defensins (e.g., plectasin), lipopeptides (e.g., empedopeptin), and depsipeptides (e.g., teixobactin) (9, 10). More recently, the last-resort antibiotic daptomycin was further shown to target undecaprenyl-containing lipid intermediates (11). In common for these agents is that binding to lipid II sequesters the molecule and makes it unavailable for peptidoglycan biosynthesis. However, antibiotic activities can vary substantially depending on the binding site on the lipid II molecule (6). Vancomycin, for example, binds to the terminal D-alanyl-D-alanine residue of the lipid II stem peptide, a part of the molecule that is altered in resistant strains. In contrast, resistance development to compounds that recognize the pyrophosphate moiety as minimal binding motif, which is present in several cell wall intermediates from different pathways (i.e., peptidoglycan, wall teichoic acid, and capsule biosynthesis), is strongly hampered. This structural feature is highly conserved among bacteria, and direct target modifications have not been observed (7).

The vast majority of lipid II–binding antibiotics described so far mainly act on gram-positive bacteria, since the outer membrane of gram-negative bacteria restricts target access mainly due to the large size of these compounds. Notably, no small-molecule inhibitor (< 500 Da) targeting lipid II has been identified so far.

Here, we developed a bacterial whole-cell screening platform aimed to identify small molecules with cell wall synthesis

Significance

Considering the alarming emergence of resistance to most antibiotics and the need for new antibiotics, the finding here of a small-molecule class, THCz, that displayed bactericidal activity against gram-positive and selected gram-negative bacteria, is of the greatest importance. We found that THCz target the cell envelope synthesis and can easily be synthesized and modified, and resistance did not readily develop in vitro. Thus, THCz are promising scaffolds for development of bacterial cell wall inhibitors.

Author contributions: E.R., T.S., S.N., B.H.-N., F.A., and P.M. designed research; E.R., T.W., K.C.L., A.M., H.U., F.G., A.E.G.L., S.M., P.N., and A.E. performed research; E.R., F.A., and P.M. contributed new reagents/analytic tools; E.R., T.W., K.C.L., A.M., H.U., F.G., A.E.G.L., S.M., P.N., A.E., T.S., S.N., B.H.-N., F.A., and P.M. analyzed data; and E.R., T.S., S.N., B.H.-N., F.A., and P.M. wrote the paper.

Reviewers: P.C., Institut Pasteur; and L.S.H., Norges miljo- og biovitenskapelige universitet.

The authors declare no competing interest.

[1]E.R., T.W., and K.C.L. contributed equally to this work.

[2]To whom correspondence may be addressed. Email: tschneider@uni-bonn.de, staffan.normark@ki.se, birgitta.henriques@ki.se, or fredrik.almqvist@umu.se.

[3]B.H.-N., F.A., and P.M. contributed equally to this work.

This article contains supporting information online at http://www.pnas.org/lookup/suppl/doi:10.1073/pnas.2108244118/-/DCSupplemental.

Published November 16, 2021.

inhibiting activity. The screen used the induction of autolysin-mediated lysis as a phenotypic readout for cell wall inhibition. It is well established that cell wall targeting agents, in addition to stalling cell wall synthesis, can also trigger activation of endogenous bacterial autolysins that facilitate cell wall degradation, leading to bacterial lysis (12). From the screen, a 1-amino substituted tetrahydrocarbazole (THCz) hit class was identified that was found to be bactericidal at low micromolar concentrations. Comprehensive structure–activity relationship (SAR) studies of a series of synthesized THCz analogs identified the two central amine groups as essential for antibacterial activity. Mode of action studies revealed that THCz simultaneously inhibit different cell envelope biosynthesis pathways by targeting lipid II (peptidoglycan), lipid III_{WTA} (wall teichoic acid), and lipid I_{cap} (capsule) as well as the central lipid carrier undecaprenyl pyrophosphate (C_{55}-PP). Compared to natural lipid II inhibitors, THCz are relatively easy to synthesize and modify, and thus represent promising scaffolds for antibiotic drug development.

Results

Screening for Cell Wall Inhibitors. A whole-cell high-throughput screening (HTS) procedure was developed using the major respiratory tract pathogen *Streptococcus pneumoniae* as the bacterial target organism. The screen utilized the induction of pneumococcal autolysis to score for compounds with potential cell wall synthesis inhibiting activity. The decrease in optical density (OD_{600nm}) following compound treatment was used as an indicator of bactericidal activity and provided an easy and powerful readout for hit selection. For the main screen, we used the nonencapsulated strain Tigr4R (T4R) that is generally more sensitive to most treatments than the encapsulated parental Tigr4 (T4) strain (Fig. 1*A*). Bacterial cultures in the early logarithmic growth phase were challenged with a compound library (50 μM per substance) comprising 17,500 substances (http://www.cbcs.se/), and the OD_{600nm} was measured at timed intervals. For 99.1% of the compounds, an increase in OD_{600nm} following compound addition was recorded, suggesting that no substantial growth inhibition occurred. Furthermore, no compound had a ΔOD_{600nm} value near zero at 120 min after challenge that would indicate bacteriostatic activity. Compounds yielding a negative ΔOD_{600nm} value at 120 min after treatment (156 compounds, 0.9%) were scored as hits. Out of these compounds, 71 also exhibited comparable activity against the encapsulated T4 strain and were validated on the LytA-deficient T4 derivative strain, resulting in a hit rate of 0.4% for the total screen (Fig. 1*A*).

Characterization of THCz Analogs. The present study characterizes three hit compounds from the screen (THCz-1, THCz-2, and THCz-3) (Fig. 1*A*) and related synthesized derivatives. These initial THCz screening hits shared a central tetrahydrocarbazole scaffold with a short 1-amino substituted linker (–NH–CH_2CH_2–) and had different substitutions in positions R^1 and R^2 (Fig. 1). The minimum inhibitory concentration (MIC) of the hit compounds against *S. pneumoniae* was determined to 1 μg/mL (Tables 1 and 2 and *SI Appendix*, Tables S1–S3). Clinical pneumococcal isolates from the Pneumococcal Molecular Epidemiology Network strain collection, resistant to one or several conventional antibiotics, were equally as sensitive to THCz-1 as the wild-type strain (*SI Appendix*, Table S4), showing that common acquired resistance mechanisms did not confer decreased sensitivity to THCz-1. Further testing of THCz-1 against a panel of clinically relevant pathogens (Table 1) revealed antimicrobial activity against a broad range of gram-positive bacteria,

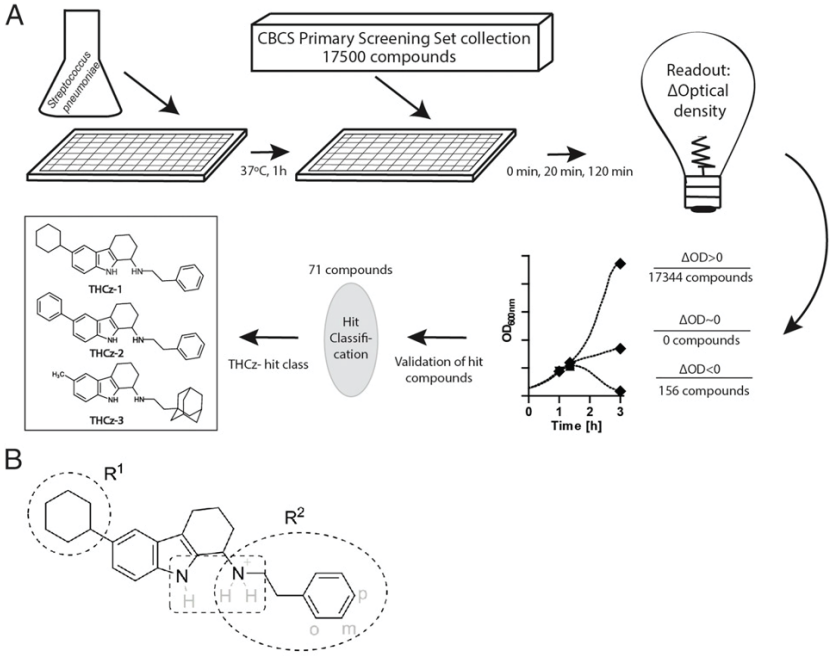

Fig. 1. Autolysin-mediated lysis screening identified THCz as an antibacterial hit class. (*A*) Schematic illustration of the autolysin-mediated lysis screen. Pneumococcal cultures grown in multiwell plates were challenged with the chemical compound library, and OD was recorded and used for evaluation of lysis induction and hit selection. Hit compounds were validated and classified. The three hit compounds from the tetrahydrocarbazole compound class (THCz-1, THCz-2, and THCz-3) are depicted. (*B*) Structure of THCz-1, where molecular moieties relevant for the structure activity and toxicity relationship investigations (R^1 and R^2) are highlighted with dashed lines. Also indicated is the central diamino motif that was identified as essential for activity shown in the protonation state likely encountered at physiological pH.

Table 1. Antibacterial spectrum of THCz-1

Species	Strain	MIC THCz-1, μg mL^{-1}
S. pneumoniae	T4	1*
		0.3†
Streptococcus parasanguinis	ATCC 903	5†
Streptococcus pyogenes	serotype M1T1 (45)	1†
B. subtilis	ATCC 6051	3†
	168	2
Staphylococcus simulans	22	2
Staphylococcus epidermidis	CLB26329 (MRSE)	2
S. aureus	ATCC 25923	5†
	ATCC 29213	2
	SG511	2
	USA300 JE2 (MRSA)	4
	SG511 DAP^R	2
	HG001	4
	HG001 DAP^R	4
	Mu50 (VISA)	2
	Vc40 (VISA)	4
	SA113	4
	SA113Δ*atlA*	4
	SA113Δ*tarO*	4
Enterococcus faecalis	JH2-2	2
E. faecium	BM4147 (VRE)	2
Micrococcus luteus	DSM1790	1
M. bovis	ATCC 35734	16‡
M. smegmatis	ATCC 70084	8‡
M. catarrhalis	ATCC 43617	1
E. coli	ATCC 11775	>41†
	O-19592	>128
	MB5746§	2
P. aeruginosa	ATCC 10145	>41†
N. gonorrhoeae		1 to 8¶

THCz-1 sensitivity was determined in cation-adjusted MHB. All strains are characterized in *SI Appendix,* Table S8.
*THCz-1 sensitivity was determined in supplemented C+Y medium.
†THCz-1 sensitivity was determined in THY medium.
‡THCz-1 sensitivity was determined in Tween80 supplemented cation-adjusted MHB.
§Outer membrane hyperpermeable and efflux deficient.
¶Depending on the medium.

including drug-resistant strains, such as methicillin-resistant *Staphylococcus aureus* (MRSA), vancomycin-intermediate *S. aureus* (VISA), and vancomycin-resistant *Enterococcus faecium* (VRE). Importantly, THCz-1 was also active against gram-negative pathogens such as *Neisseria gonorrhoeae* and *Moraxella catarrhalis,* with MIC values in the range of 1 μg/mL to 8 μg/mL, and against mycobacteria (*Mycobacterium bovis* and *Mycobacterium smegmatis*, 8 μg/mL to 16 μg/mL). Moreover, the substance displayed activity against an *Escherichia coli* strain with a defective outer membrane, but not against wild-type *E. coli* or *Pseudomonas aeruginosa,* indicating that the outer membrane of certain gram-negative species may provide protection against THCz-1. Interestingly, Su et al. (13) have previously recorded activity against an *E. coli* strain of a related THCz analog but with a 2,4-diaminopyrimidine substituent in position R^2.

As the hit compound THCz-1 was obtained from an HTS assay that employed pneumococcal autolysis as the readout, lysis and killing kinetics were compared to penicillin and tetracycline that inhibits peptidoglycan and protein synthesis, respectively. Treatment of pneumococci with THCz-1 induced a more rapid bacteriolytic effect than penicillin, and no viable colonies could be recorded 9 h after treatment (Fig. 2 *A* and *B* and *SI Appendix*, Fig. S1). The contribution of cell wall hydrolase activity to the lytic and bactericidal response was assayed using an isogenic pneumococcal strain deficient in the major autolysin LytA (T4Δ*lytA*) grown in an elevated (110 mM) concentration of choline chloride that causes cell wall dissociation and functional inactivation of other choline-binding cell wall hydrolases. In the absence of hydrolase activity, reduced lysis was observed following treatment of pneumococci with THCz-1 and penicillin (Fig. 2*C*), yet the bactericidal effect was retained, albeit with delay (Fig. 2 *B* and *D*). Tetracycline caused a growth-inhibitory phenotype without any prominent lysis and displayed a considerably slower killing curve that was not affected by the activity of cell wall hydrolases (Fig. 2 *A–D*). Transmission electron microscopy (TEM) of THCz-1–treated unencapsulated T4R cells confirmed that lysis was exerted through the action of choline-binding cell wall hydrolases, since bacteria remained intact in a strain lacking the major autolysin *lytA* (T4RΔ*lytA*) grown in elevated choline chloride concentration (Fig. 2 *E–H*). THCz-1–treated *S. pneumoniae* (T4R) displayed cell wall ruptures in close proximity to the equatorial plane (Fig. 2*F*) correlating to the site where nascent peptidoglycan, the putative substrate of LytA, has been suggested to be incorporated during cell wall synthesis (14, 15). Together, these data confirmed that THCz-1 treatment, as for penicillin, caused induction of autolysin-mediated lysis, although the bactericidal activity is not solely explained by autolysin activation.

SAR. We next explored the molecular context of the THCz compound class in relation to the antibacterial activity. For this, we developed a synthesis scheme for substituted THCz and oxygen analogs (*SI Appendix*, Figs. S2 and S3) that allowed an exploration of the SAR of THCz derivatives and the investigation of the impact on toxicity of different substitutions on cultured human cell lines. The following SAR description is supported by a more extensive analysis provided in *SI Appendix*, Tables S1–S3, Fig. S4, and *SI Text*. The central diamino motif (Fig. 1*B*) was found to have a major impact on the antibacterial activity (*SI Appendix*, Table S1). Thus, replacement of either of the two nitrogens with oxygens of otherwise similar analogs led to no, or much reduced, antibacterial activity (THCz-2 vs. THCz-6 and THCz-5 vs. THCz-19) (Table 2). However, also, the cytotoxic properties of THCz analogs were correlated to the presence of the diamino motif, as the 50% inhibitory concentration (IC_{50}) increased about sixfold for THCz-5 vs. THCz-19, and about sevenfold for THCz-6 vs. THCz-2 (Table 2).

Further investigation of the effect of substitutions in position R^1 and R^2 of the THCz scaffold was performed (Fig. 1*B* and *SI Appendix*, Tables S1–S3). Most substitutions in position R^1 had little or no effect on the antibacterial activity, and an unsubstituted analog (THCz-45) maintained activity. However, a carboxylate in R^1 (THCz-42) was found to have a marked negative effect on the antibacterial activity, suggesting that an anionic substituent in this position was not suitable. Sterically demanding substituents in R^1 (THCz-43 and THCz-44) did have an adverse effect on toxicity, leaving a methyl group (i.e., THCz-39 and THCz-40) or an unsubstituted R^1 (THCz-19 and THCz-45) the most favorable of the herein tested R^1 substitutions. In position R^2, it was important for antibacterial activity that a sterically demanding substituent, such as an adamantyl or a phenyl (i.e., THCz-3 and THCz-36 vs. THCz-24), was linked to the central scaffold by at least two carbons (THCz-36, THCz-37, and THCz-38 vs. THCz-35). Substitutions in the phenyl ring of R^2 were only favorable in the *para* position in the context of toxicity. A hydroxyl or bromo substituent (THCz-39 and THCz-40) caused a twofold to fourfold reduction in MIC and a corresponding increase in IC_{50} in comparison to the original screening hit THCz-1 (Table 2).

MICROBIOLOGY

Table 2. SAR and toxicity of a selection of THCz analogs

THCz-	R1*	X	R2*	MIC [μM (μg mL^{-1})]†	IC_{50} [μM(μg mL^{-1})] [n]‡
1§		NH	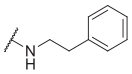	3.1 (1.3)	12.1 (4.9) ± 3.0 (1.2) [6]
2§		NH	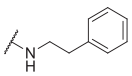	3.1 (1.1)	17.5 (7.1) ± 1.9 (0.8) [3]
5		NH	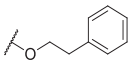	>100 (>29.1)	140.8 (41.0) ± 16.9 (4.9) [4]
6¶		O	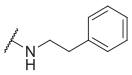	50 (18.4)	134.1 (49.3) ± 42.4 (15.6) [5]
19		NH	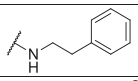	6.3 (1.9)	22.2 (6.8) ± 1.8 (0.6) [3]
39		NH	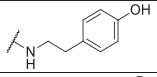	6.3 - 12.5 (2.0 - 4.0)	33.4 (10.7) ± 5.9 (1.9) [7]
40		NH	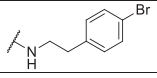	6.3 (2.4)	28.0 (10.7) ± 4.1 (1.6) [7]

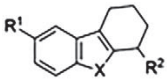

*Cy, cyclohexyl; Ph, phenyl; Me , methyl.
†Minimal inhibitory concentration of THCz analogs for *S. pneumoniae* T4 in supplemented C+Y medium. Most abundant MIC is given. An overview of the observed MIC distribution is given in *SI Appendix*, Fig. S4.
‡IC_{50} values of 10^5 A549 cells/mL challenged with a serial titration of the respective THCz analogs. Average ± SD are given, and the number of biological replicates is noted in brackets. In the presence of 10% fetal bovine serum, mimicking cell culture conditions, the plasma protein binding affinity of THCz analogs caused an overall fourfold increase in MIC (*SI Appendix, SI Text*).
§Original hit compounds from the screen; see also Fig. 1 for structures.
¶For simplicity, we refer to all compounds studied here as THCz, although this compound is an oxa-tetrahydrofluorene.

The THCz analogs contain a stereocenter (*SI Appendix*, Fig. S5 *A* and *B*), and the initial screen and the SAR were carried out with racemic mixtures of the two enantiomers. We therefore separated the enantiomers from a subset of THCz analogs (THCz-1, THCz-39, and THCz-40) (*SI Appendix*, Fig. S5 *C–I*) and tested their antibacterial activities separately. Our data showed that both the R and S forms displayed similar MIC (*SI Appendix*, Table S5) in comparison to each other and to the racemic mixture. Combined, the untargeted investigation on modifications of the THCz scaffold showed that the central diamino motif was essential, and sterically demanding substitutions on a not less than two-carbon chain linker in R^2 were required, while modifications in R^1 were dispensable for antibacterial activity.

Mode of Action Studies. As THCz analogs showed an autolysin-inducing bacteriolytic effect in the early logarithmic phase, a well-known feature for cell wall targeting agents, we reasoned that THCz might interfere with cell wall synthesis. To verify this hypothesis and to approach target identification, a set of pathway-specific *Bacillus subtilis* bioreporter strains (16, 17) was treated with selected active analogs, THCz-1, THCz-39, and THCz-40 and compared to the inactive derivative THCz-5 (Table 2 and *SI Appendix*, Table S5). Indeed, THCz-1, THCz-39, and THCz-40, but not THCz-5, specifically induced the cell wall responsive reporter strain, while reporter strains indicative for interference with DNA, RNA, and protein biosynthesis were not activated (Fig. 3*A*). Furthermore, treatment of *B. subtilis* with THCz-1, THCz-39, and THCz-40 induced characteristic cell shape deformations, as visualized through phase-contrast microscopy, revealing the formation of cell membrane blebbing, indicative of inhibition of peptidoglycan biosynthesis and autolysin activation. Membrane blebbing was also observed following control treatment with vancomycin, nisin, or bacitracin, but not with the inactive THCz-5 or with antibiotics having targets other than the cell wall, such as clindamycin, ciprofloxacin, and rifampicin (Fig. 3*B*). To narrow down the target within the peptidoglycan biosynthesis pathway, we investigated the effect of THCz analogs on the LiaRS stress response using a *B. subtilis* luciferase bioreporter. The LiaRS two-component system is known to be sensitively induced in response to antibiotics that target lipid II or C_{55}-PP, for example, vancomycin or bacitracin (18). Monitoring $P_{liaI\text{-}lux}$ bioluminescence over time revealed a strong induction for all THCz analogs tested, except for the inactive analog THCz-5 (Fig. 3*C*). Similar induction of the LiaRS reporter was also observed for the separated enantiomers of the active analogs, validating that the S and R forms have the same mode of action (*SI Appendix*, Fig. S6 *A–C*).

Corroborating interference with the lipid II biosynthesis cycle, treatment of *S. aureus* whole cells resulted in accumulation of the ultimate soluble peptidoglycan precursor UDP-MurNAc-pentapeptide (Fig. 3*D*), indicating that a late-stage membrane-associated peptidoglycan biosynthesis step was inhibited. Higher THCz concentrations (>5× MIC) impeded cytoplasmic accumulation due to increased lysis, as a result of induction of the autolytic system, or due to effects related to membrane interaction.

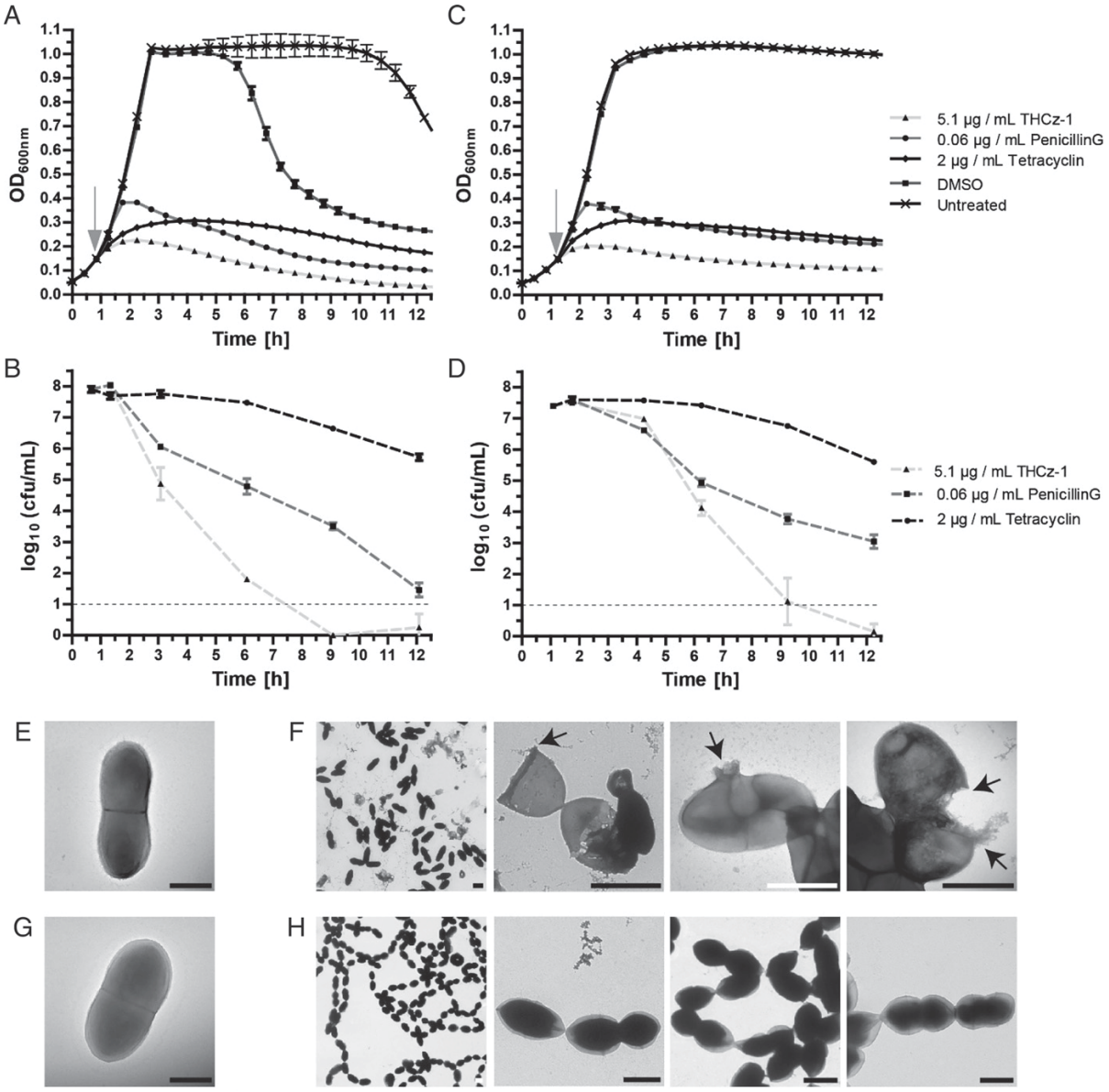

Fig. 2. Kinetics of pneumococcal lysis and viability following THCz-1 treatment. Treatment of (*A* and *B*) T4 wild type and (*C* and *D*) T4Δ*lytA* with THCz-1 (5.1 μg/mL, 12.5 μM, 4× MIC), penicillin G (0.06 μg/mL, 2× to 4× MIC), tetracycline (2 μg/mL, 8× to 16× MIC), or (in *A* and *C*) DMSO (1%). Bacteria were grown in C+Y media in the absence (*A* and *B*) or presence (*C* and *D*) of 110 mM choline chloride that inhibits cell wall association of autolysins and cell wall hydrolases of *S. pneumoniae*. Dotted black lines in *B* and *D* indicate the detection limit of the assay. Growth kinetics (*A* and *C*) are shown from one representative experiment as the average and SD of three technical replicates. Death kinetics (*B* and *D*) are summarized as the average and SD of three independent experiments. Short dashed black lines in *B* and *D* indicate the detection limit of the assay. (*E–H*) Electron micrographs of T4R (*E* and *F*) and T4RΔ*lytA* (*G* and *H*), fixed and imaged after treatment with THCz-1 (25 μM) (*F* and *H*) and as untreated controls (*E* and *G*). In *F* and *H*, representative overview images of cell populations are shown (*Left*) followed by three close-up images (*Right*). The use of unencapsulated mutants facilitated examination of the cell morphology. Pneumococcal chain formation in choline-treated autolysin-deficient T4RΔ*lytA* cells are attributable to the inhibition of LytB activity, required for separation of diplococcal cells (44). (Scale bars, 1 μm.)

THCz did not induce the formation of pores in comparison to the lantibiotic nisin which is an established pore former (*SI Appendix*, *Supplementary Materials and Methods* and Fig. S7)(9). However, THCz treatment resulted in the delocalization of GFP-MinD in *B. subtilis*, indicating membrane depolarization. The cell division inhibitor MinD is bound to the membrane via a C-terminal amphipathic helix and requires the presence of the membrane potential for its specific cellular localization pattern. MinD localizes to newly formed cell poles, thereby directing FtsZ to midcell guiding division septum placement (19). Compared to untreated control cells, GFP-MinD delocalized in cells treated with THCz, resulting in irregular dispersion of GFP-MinD within

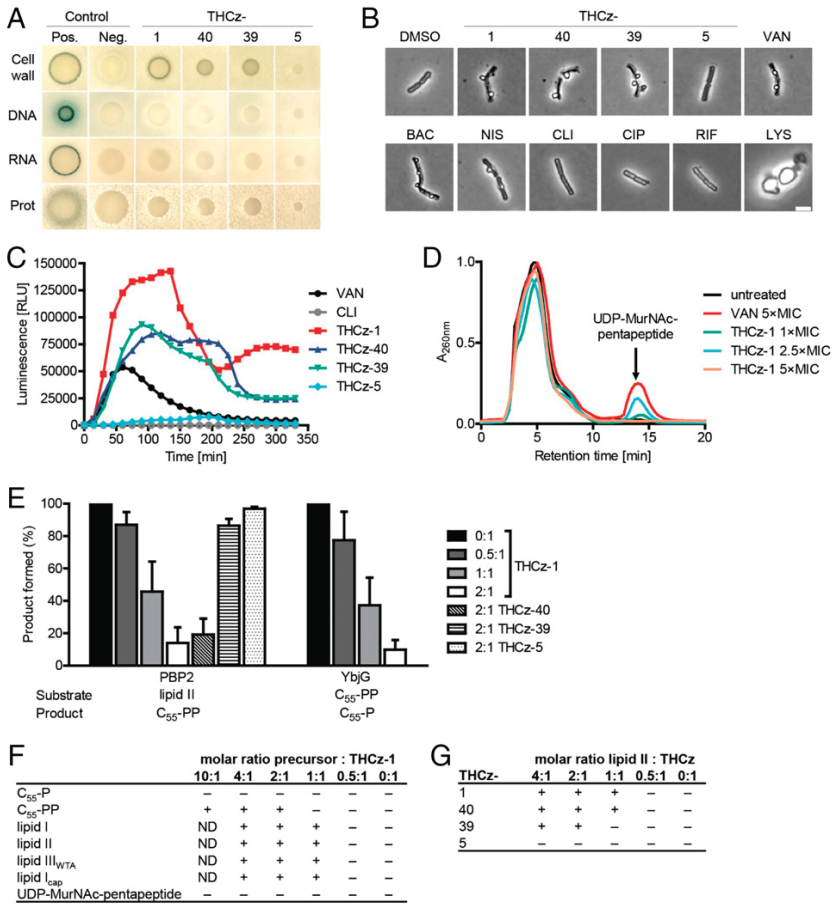

F

	molar ratio precursor : THCz-1					
	10:1	4:1	2:1	1:1	0.5:1	0:1
C_{55}-P	–	–	–	–	–	–
C_{55}-PP	+	+	+	–	–	–
lipid I	ND	+	+	+	–	–
lipid II	ND	+	+	+	–	–
lipid III_{WTA}	ND	+	+	+	–	–
lipid I_{cap}	ND	+	+	+	–	–
UDP-MurNAc-pentapeptide	–	–	–	–	–	–

G

	molar ratio lipid II : THCz				
THCz-	4:1	2:1	1:1	0.5:1	0:1
1	+	+	+	–	–
40	+	+	+	–	–
39	+	+	–	–	–
5	–	–	–	–	–

Fig. 3. THCz analogs with intact diamino motif interact with C_{55}-PP and C_{55}-PP–linked cell wall precursors. (*A*) Impact of THCz-1 and analogs (THCz-40, THCz-39, and THCz-5) on major biosynthesis pathways in *B. subtilis*. *B. subtilis* bioreporter strains with selected promotor-*lacZ* gene fusions were used to identify interference with DNA (P_{yorB}), RNA (P_{yvgS}), protein (P_{yheI}), and cell wall (P_{ypuA}) biosynthesis. Induction of a specific stress response results in expression of β-galactosidase indicated by a blue halo surrounding the inhibition zone. Antibiotics vancomycin, ciprofloxacin, clindamycin, and rifampicin were used as positive controls. (*B*) Treatment of *B. subtilis* with THCz induces severe cell shape deformations as visualized by phase-contrast microscopy. (Scale bar for all images: 2 μm.) (*C*) Induction of the LiaRS bioreporter by THCz compared to vancomycin, indicating interference with the lipid II biosynthesis cycle. (*D*) Intracellular accumulation of the ultimate soluble cell wall precursor UDP-MurNAc-pentapeptide in vancomycin-treated and THCz-1–treated cells of *S. aureus* as analyzed by means of reverse-phase HPLC. (*E*) Impact of THCz on individual peptidoglycan biosynthesis reactions. THCz inhibits the PBP2-catalyzed transglycosylation of lipid II and the YbjG-catalyzed dephosphorylation of C_{55}-PP. THCz were added in molar ratios of 0.5 to 2 with respect to the amount of the substrate lipid II or C_{55}-PP used in the individual test system. Inhibitions of PBP2- and YbjG-catalyzed reactions were quantified by the relative amount formed of C_{55}-PP and C_{55}-P, respectively. The error bars represent the SD from the triplicate runs. (*F* and *G*) Antagonistic effect of purified cell wall intermediates on antimicrobial activity of THCz. THCz compounds were exposed to selected purified cell wall precursors for 10 min at indicated molar ratios prior to incubation with *M. luteus* cells; +, antagonization of antimicrobial activity; –, no antagonization; ND, not determined. Results of three independent experiments are shown.

5 min. MinD delocalization was also observed for the inactive THCz-5 variant, suggesting that the induced membrane effects are not the primary cause of killing (*SI Appendix*, Fig. S8).

In search of the molecular target, we next investigated the impact of THCz-1 on peptidoglycan biosynthesis reactions in vitro using purified *S. aureus* enzymes and substrates. Quantitative analysis of PBP2-mediated transglycosylation of lipid II revealed a dose-dependent inhibition (Fig. 3*E*). Almost complete inhibition was observed at a twofold molar excess of THCz-1 with respect to lipid II, suggesting that THCz-1 forms a stoichiometric complex with the substrate rather than inhibiting the enzyme. Similarly, lipid II synthesis catalyzed by the MurG glycosyltransferase was inhibited (*SI Appendix*, Fig. S9). Furthermore, THCz-1 was also found to inhibit dephosphorylation of C_{55}-PP to C_{55}-P, a crucial step in the recycling of the lipid carrier conducted by undecaprenyl pyrophosphate phosphatase YbjG. A twofold molar excess of THCz-1 caused a full inhibition of YbjG-mediated dephosphorylation of C_{55}-PP (Fig. 3*E*). Corroborating, the addition of purified C_{55}-PP, lipid I and lipid II as well as the wall teichoic acid precursor lipid III_{WTA} (C_{55}-PP-GlcNAc) and the capsular precursor lipid I_{cap} (C_{55}-PP-glucose) all antagonized the antimicrobial activity of THCz-1, while C_{55}-P did not (Fig. 3*F*). These data thus clearly indicate that THCz-1 interacts with undecaprenyl pyrophosphate and C_{55}-PP–containing cell wall precursors. However, the interaction with the first sugar moiety attached to the lipid carrier appears to contribute to binding, since a higher concentration of C_{55}-PP than of lipids I, II, and III_{WTA} and lipid I_{cap} was required to fully antagonize THCz-1 activity (Fig. 3*F*). Furthermore, lipid II was found to antagonize THCz analogs

THCz-39 and THCz-40 that contained an intact diamino motif, in contrast to the inactive THCz-5 (Fig. 3*G*). In accordance with the in vitro data and the SAR profile, THCz-39 was less efficiently antagonized by lipid II compared to THCz-1 and THCz-40 (Fig. 3*G*), and fourfold higher concentrations of THCz-39 were required for full inhibition of the PBP2-catalyzed reaction (*SI Appendix*, Fig. S10). In agreement with the in vitro activity of the racemic mixture, both enantiomers of THCz-40 similarly inhibited lipid II transglycosylation (*SI Appendix*, Fig. S6 *D* and *E*). Combined, these data indicate that the pyrophosphate moiety represents the essential motif for target interaction, and that the diamino motif of THCz analogs is required for this interaction. In agreement, the MurT/GatD-catalyzed amidation of lipid II was unaffected in the presence of THCz-1, strongly suggesting that the stem peptide of lipid II is not involved in binding (*SI Appendix*, Fig. S11). Furthermore, THCz analogs did not interfere with the PBP4-mediated carboxypeptidation, releasing the terminal D-Ala residue from the pentapeptide stem (*SI Appendix*, Fig. S9*B*), suggesting that interactions with the lipid II stem peptide are less relevant and that THCz do not sterically hinder enzyme interaction with that region of the target molecule. Compared to natural lipid II binders, for example, vancomycin, THCz do not form extraction-stable complexes with lipid II (*SI Appendix*, Fig. S12), pointing to decreased binding affinity.

Together, these data reveal that THCz specifically binds to multiple undecaprenyl pyrophosphate–coupled cell wall precursors, and with C_{55}-PP as such, thereby simultaneously inhibiting several cell wall biosynthetic pathways, including the recycling of the C_{55}-P carrier utilized by all these pathways.

A recent study reported that fungal P-type ATPases can be inhibited by similar THCz analogs, and a complex with a THCz analog and a mammalian Ca^{2+} ATPase (SERCA) was shown in a cocrystal structure (20). However, in our study, neither single-deletion mutants of the four genes annotated as P-type ATPases in the *S. pneumoniae* T4 strain (*SP0729, SP1551, SP1623,* and *SP2101*) (*SI Appendix*, Tables S7 and S8) nor the quadruple mutant displayed decreased sensitivity to THCz-1, suggesting that P-type ATPases are not essential bacterial, or at least pneumococcal, THCz targets (*SI Appendix*, Table S6). The sequence similarity of these pneumococcal P-type ATPases with rabbit/human SERCA is only between 21% and 38% by identity, suggesting that the binding interfaces might be different.

THCz-1 Affects Capsule Production. More recently, dual targeting of similar cell wall precursors by teixobactin was correlated with a limited propensity to develop resistance (5). Resistance to THCz-1 also did not readily develop in vitro, as no resistant mutants were obtained when continuously subculturing *S. aureus* using a broth microdilution method with sublethal concentrations of THCz-1 (*SI Appendix*, *Supplementary Materials and Methods* and Fig. S13). However, through continuous cultivation of encapsulated *S. pneumoniae* T4 on THY plates containing small incremental concentrations of THCz-1, we could obtain an isolate (#22) with marginally decreased sensitivity to THCz-1 compared to control strains similarly passaged on THCz-1–free THY plates (BHN1368-9). Comparative sensitivity testing in THY liquid medium confirmed that, even though clone BHN1364 of the continuously THCz-1 exposed isolate #22 was affected by 2× MIC, it could still grow at this concentration, contrary to the unexposed clone BHN1368, which tolerated only 1× MIC (Fig. 4 *A* and *B*). Whole genome sequencing of four #22 derived clones (BHN1364-7) identified a set of point mutations that were absent in the control strains (*SI Appendix*, *Supplementary Materials and Methods* and Fig. S14). Thus, we constructed deletion mutants in the corresponding genes (*cpsE* (BHN1690), *aguA* (BHN1371), pneumolysin (*ply*) (BHN2043), and *SP1901* (BHN1693) (*SI Appendix*, *Supplementary Materials and Methods* and Tables S7 and S8). Only a deletion mutant of *cpsE* (BHN1690), as well as the strain with the reconstituted nonsynonymous mutation $cpsE^{G394C}$ (BHN1691), displayed a similar decrease in sensitivity. Pneumococcal *cpsE* encodes the glycosyltransferase that adds a sugar phosphate to the C_{55}-P lipid carrier to initiate capsule synthesis in the cytoplasm and is therefore essential for biosynthesis of the polysaccharide capsule, which is the main virulence factor for pneumococci (21, 22). Indeed, the $cpsE^{G394C}$ mutant was found to express lower amounts of capsular polysaccharide in comparison to wild-type T4 but was not deficient in capsule production, similar to the T4Δ*cpsE* strain (Fig. 4*C*). The influence of capsule expression on THCz-1 sensitivity was supported by the reduced THCz-1 sensitivity observed in the capsule-deficient T4R strain (*SI Appendix*, Table S8), that was found refractory to even 2.4× MIC THCz-1 (Fig. 4*D*). This increased sensitivity to THCz-1 mediated by pneumococcal capsular expression was already apparent after 1 h of exposure to a 2× MIC concentration of THCz-1, where the encapsulated T4 was killed more prominently than the unencapsulated T4R and marginally more than the less encapsulated T4$cpsE^{G394C}$-Erm (BHN1691) (Fig. 4*E*). Thus, decreased or abolished capsule production caused a marginal desensitization to THCz-1. Interestingly, a short passage of *S. pneumoniae* in sub-MIC concentrations of THCz-1 (*SI Appendix*, *Supplementary Materials and Methods*) led to a decrease in the phosphorylcholine amount compared to the untreated strains (*SI Appendix*, *Supplementary Materials and Methods* and Fig. S15)as well as a decrease in the sensitivity of T4Δ*lytA* to externally added LytA (*SI Appendix*, *Supplementary Materials and Methods* and Fig. S16), indicating that THCz-1 also targets teichoic acid synthesis.

Discussion

In the present study, we developed a screening procedure where small-molecular compounds were screened for their ability to trigger autolysin-mediated lysis of pneumococci in order to find potential cell wall inhibitors. Although discovered in the 1970s, the underlying molecular mechanisms behind how cell wall–targeting antibiotics trigger autolysin activation still remain elusive (12). It has been suggested that an active cell wall synthesis machinery would sequester a potential autolysin substrate and that autolysin misplacement on teichoic acids would be part of the triggering event (14, 23–27). Our screening procedure for pneumococcal autolysin activation provided an uncomplicated and powerful protocol for identification of potential cell wall inhibitors. The herein described THCz compound class was one of the most active identified in the screen. Related THCz analogs with antimicrobial activity have been reported, but few targets have been proposed (13, 20, 28). Our mode of action studies revealed that THCz analogs stalled cell wall biosynthesis by targeting lipid II and other undecaprenyl pyrophosphate–containing lipid precursors involved in teichoic acid and capsule synthesis. The interaction required the pyrophosphate moiety (C_{55}-PP) as minimal motif, and THCz relied on the diamino motif for potent antibacterial activity. It seems therefore likely that the two amino groups of THCz interact with the two negatively charged phosphate groups of the target. Supporting this, THCz analogs are expected to be positively charged at physiological pH, since the amino group in R^2 has a calculated pK_a of 9.8 (for THCz-1). Furthermore, the requirement of a $–NH–CH_2CH_2–$ linker-connected hydrophobic group in position R^2 supports a model for target interaction in which this group is inserted into the plasma membrane to facilitate the diamino–pyrophosphate interaction (Fig. 5). The comparable activities of the tested THCz enantiomers could possibly be understood by such a model. If the role of the hydrophobic part of R^2 is to anchor THCz into the plasma membrane, the relative stereo conformation would not be crucial for the

MICROBIOLOGY

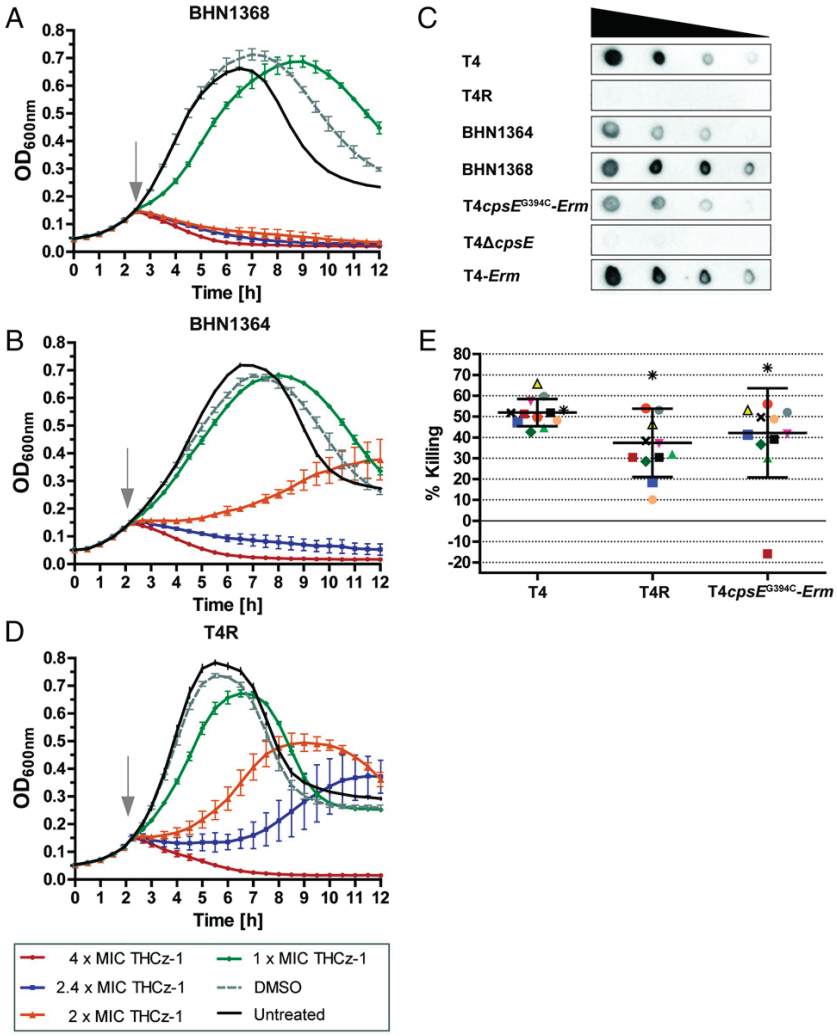

Fig. 4. Decreased capsular polysaccharide production confers reduced sensitivity to THCz. Growth curves of strains (*A*) BHN1368 and (*B*) BHN1364 in THY medium challenged with a titration series of THCz-1, solvent control (DMSO) in comparison to untreated growth control. (*C*) Quantification of the capsular polysaccharide amount of the wild-type T4 (BHN842), the unencapsulated T4R (BHN659), an isolate of T4 with reduced THCz-1 sensitivity (BHN1364), unexposed control strain of T4 with retained THCz-1 sensitivity (BHN1368), point mutant T4*cps4E*^{G394C}-erm (BHN1691) with an *erm* open reading frame (ORF) inserted in the capsular operon after *cps4E* ORF, the *cpsE* knockout strain (BHN1690), and the control wild-type strain T4-erm(BHN1692) with an *erm* ORF inserted in the capsular operon after *cps4E* ORF. (*D*) Growth curve and exposure to a serial dilution of THCz-1 of T4R. (*E*) Bacterial killing after 1 h of exposure to 2× MIC THCz-1 (1.5 μM, 0.6 μg/mL in THY medium) of wild-type T4 (BHN842), the unencapsulated T4R (BHN659), and the mutant T4*cpsE*^{G394C} (BHN1691). Paired experiments (each experiment was carried out in technical triplicates) are depicted with the same symbol. Average and SD are given.

diamino–pyrophosphate interaction. This would thus contrast many antibiotics where stereoisomers display stereoselectivity due to protein binding constraints (29).

THCz analogs displayed a broad antibacterial spectrum and were active against all gram-positive Firmicutes species tested as well as Actinobacteria, including mycobacterial species. Notably, they were also active against gram-negative *N. gonorrhoeae* and *M. catarrhalis*, possessing lipooligosaccharides instead of lipopolysaccharides, which provides higher permeability across the outer membrane (30, 31), as has been observed for cationic and amphiphilic antimicrobial peptides, for example, the defensin Plectasin and the lantibiotic nisin (32). This is probably attributable to their relatively small molecular mass that allows for translocation across the outer membrane of certain species. THCz did not exhibit antimicrobial activity against wild-type *E. coli*, while an *E. coli* mutant with a hyperpermeable outer membrane was shown to be susceptible, indicating that THCz, despite their small size, are unable to pass the water-filled porins of gram-negatives. In addition to the broad antimicrobial spectrum, the low propensity of resistance development and absence of cross-protective resistant phenotypes are attributable to the target. The ubiquitous and highly conserved undecaprenyl pyrophosphate constitutes a keystone lipid scaffold for the synthesis and subcellular translocation not only of peptidoglycan but also for teichoic acids and polysaccharide capsule precursors, and is therefore hard for bacteria to modify. In accordance, the slightly decreased THCz-1 sensitivity of the obtained spontaneous *cpsE* mutant with decreased capsule

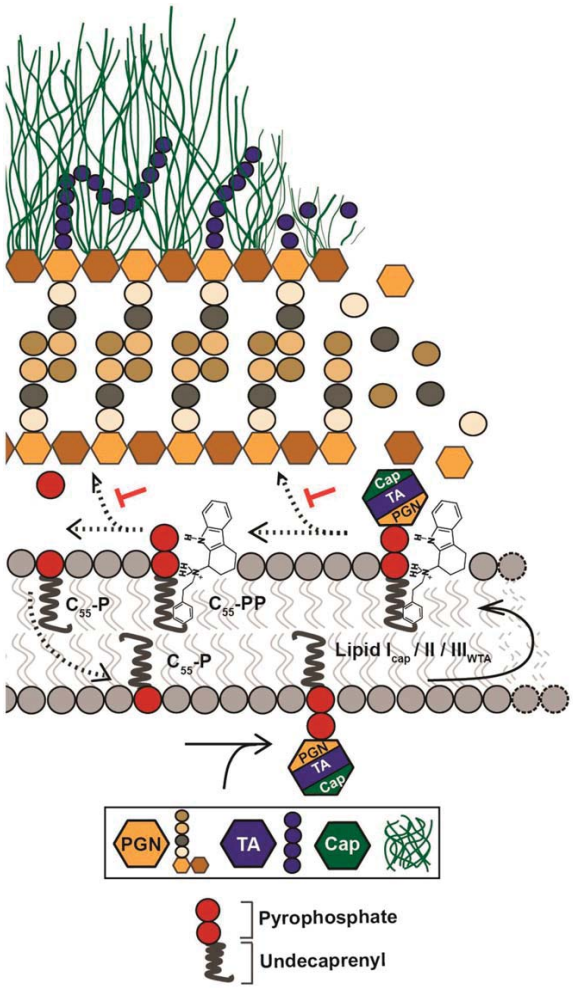

Fig. 5. Proposed model for the mechanism of bactericidal action of THCz. Cell wall polymer precursors (lipid II, lipidIII_{WTA}, and lipid I_{cap}) are synthesized in the cytoplasm onto C_{55}-P to form C_{55}-PP–linked substrates that are flipped over to the outer leaflet of the plasma membrane to provide building blocks for peptidoglycan (PGN), teichoic acid (TA), or capsular (CAP) biosynthesis. Our data suggest that the pyrophosphate is the essential binding motif of THCz, presumably by electrostatic interaction, thereby stalling all three branches of cell wall polymer formation as well as dephosphorylation and recycling of C_{55}-PP to C_{55}-P.

production might have a liberated C_{55}-P pool that could, instead, be available for peptidoglycan and teichoic acid production. As capsule production is required for pneumococcal virulence, such mutants are likely attenuated in virulence.

THCz analogs, similar to those described here, have been shown to exhibit antifungal properties by binding to and inhibiting P-type ATPases (20). Related mammalian P-type ATPases such as the Ca^{2+}-ATPase (SERCA) were also inhibited by THCz analogs, and a cocrystal structure of a THCz analog and SERCA revealed the binding site. The binding is stabilized by interactions with the diamino motif of THCz via two aspartic acids (D59 and D254) (20). This is also in line with our data showing that THCz diamino motif is involved in toxicity, suggesting inhibition of human P-type ATPases as a plausible reason for the toxicity. Bacteria also expresses P-type ATPases, but genetic inactivation of all four pneumococcal P-type ATPases did not affect sensitivity to THCz-1, arguing against these proteins as antibacterial targets. The low sequence similarity (< 39%) between the pneumococcal and mammalian orthologs indicates that the binding interface might be different. Thus, knowledge of the structural requirements for C_{55}-PP interaction of THCz and the constrains of mammalian P-type ATPases binding should facilitate further modifications of THCz analogs to reduce cytotoxicity without affecting the antibacterial activity. In conclusion, the presented THCz analogs represent a class of small (<500 Da) synthetic molecules that inhibit bacterial cell wall synthesis by binding to lipid II and other undecaprenyl pyrophosphate–containing lipid precursors, targets conserved and present in all bacteria. This bacterial target interaction is highly attractive, and the small size and relative ease by which tetrahydrocarbazoles can be synthesized and modified could constitute a molecular platform for development of novel bacterial cell wall inhibitors.

Materials and Methods

Chemicals. A subset of 17,500 compounds from the Chemical Biology Consortium Sweden Primary Screening Set collection were screened in the whole-cell HTS assay. These compounds are chemically diverse and have lead- to drug-like properties with respect to parameters such as molecular weight, hydrogen bond accepting and donating groups, lipophilicity, and polar surface area. Compounds THCz-1, THCz-2, THCz-3, THCz-24, and THCz-35 corresponding to ChemBridge ID nos. 5279631, 5272685, 5265433, 5279631, and 5277652, respectively, were purchased from ChemBridge. All other compounds were synthesized as described in *SI Appendix* for general chemistry and synthesis of THCz analogs. The separation of enantiomers, circular dichroism spectroscopy, and the synthesis of the stereoselective compound (+)-(R)-AL682 are also given in *SI Appendix*. THCz analogs were dissolved in anhydrous dimethyl sulfoxide (DMSO) (Invitrogen).

Bacterial Growth Conditions. Pneumococci were cultured overnight on blood agar plates at 37 °C with 5% CO_2. For pneumococcal suspension cultures, C+Y medium (*SI Appendix*) supplemented with 9% Glucose Bouillon (1% glucose added to 25 g/L Nutrient broth No. 2, Oxoid) and 1% horse serum (Håtunalab) or Todd Hewitt broth (Sigma-Aldrich-T1438) with 0.5% yeast extract (THY medium) were used as indicated. For experiments with T4Δ*lytA* (*SI Appendix*, Table S8), the growth medium was supplemented with 110 mM choline chloride (Sigma), to inhibit choline-binding cell wall hydrolases. Growth conditions for other bacterial species are specified in the respective sections.

HTS Procedure. The unencapsulated *S. pneumoniae* strain T4R (*SI Appendix*, Table S8), an isogenic T4-derived strain, was used for the primary antibiotic screen. *S. pneumoniae* was grown in C+Y medium to an optical density at 600 nm OD_{600nm} = 0.6 and sedimented by centrifugation (5 min, 5,000 rcf, 4 °C). The cells were resuspended in a 1:10 volume (thus 10-fold concentrated) in C+Y medium containing 20% glycerol and frozen at −80 °C. For screening, a 0.5-mL aliquot was thawed and diluted by mixing with 49.5 mL of prewarmed (37 °C) C+Y medium. The bacterial suspension was distributed into 96-well tissue culture plates (200 μL per well) and incubated for 1 h at 37 °C. Screening compounds dissolved in DMSO at a concentration of 5 mM were added by the assistance of a pipetting robot (Beckman Coulter, Biomek NX^P) to a final concentration of 50 μM. The OD_{600nm} was measured immediately after compound addition (t = 0), after 20 min (t = 20), and after 2 h (t = 120). All calculations were done correlated to the OD measurement at t = 0 to take into account any possible contribution to the optical density from the compounds. Challenge with penicillin G (1 μg/mL) was used as positive control treatment, and DMSO (1% vol/vol) was used as a negative control treatment. Positive hits were scored as compounds that caused a Δ-negative OD_{600nm} measurement after 120 min following treatment [$\Delta = OD_{600nm}(t = 0) - OD_{600nm}(t = 120)$]. Hits were validated on the encapsulated wild-type T4 and a T4 strain deficient in LytA (T4Δ*lytA*).

Lysis Kinetics. For comparative lysis kinetics precultures of T4 or T4Δ*lytA* grown in supplemented C+Y medium (with an additional 110 mM choline chloride for the autolysin mutant) to midlog phase [$OD_{600nm} \approx 0.5$ (~5 to 6 × 10^8 colony-forming units (cfu)/mL)] were diluted to OD_{600nm} = 0.05 in fresh media and distributed into wells (400 μL per well) of a Honeycomb plate (Oy Growth Curves AB Ltd). A Bioscreen C plate reader (Oy Growth Curves AB Ltd) was used to record the growth kinetics. Cultures were grown to early log-phase ($OD_{600nm} \approx 0.15$ (~1 to 2 × 10^8 cfu/mL), and treatments were added to a

MICROBIOLOGY

final concentration of 5.1 μg/mL (12.5 μM) THCz-1 (1% [vol/vol] DMSO), 0.06 μg/mL penicillin (dissolved in water) and 2 μg/mL tetracycline (1% [vol/vol] DMSO) or a twofold serial dilution (*SI Appendix*, Fig. S1). The compounds were administrated in 100× stock solutions in 4-μL volumes to each well followed by thorough mixing. One percent (vol/vol) DMSO-treated cells and untreated controls were included. Sterile media samples were used to blank the measurement values. Viability determination of T4 and T4Δ*lytA* was performed at 30 min, 3 h, 6 h, 9 h, and 12 h following challenge by serial dilutions and spreading on blood agar plates from which colonies were counted after overnight incubation at 37 °C at 5% CO_2. Where appropriate, 100 μL of the undiluted sample was plated, providing a detection limit of 10 cfu/mL.

TEM. Pneumococcal strains T4R and T4RΔ*lytA* (*SI Appendix*, Table S8) were prepared as for the lysis kinetic examination. Untreated cells and cells treated with 25 μM THCz-1 for 1 h were centrifuged at 6,500 × *g* for 2 min. Cell pellets were resuspended and fixed for 20 min with a 400-μL mixture of paraformaldehyde (2%) and glutaraldehyde (0.05%) in phosphate-buffered saline (PBS). Cells were then washed once with 1 mL of PBS and resuspended in 40 μL of PBS. Samples of 10 μL were placed for 2 min on carbon-coated grids (Oxford Instruments), and negative staining was performed with 2% uranyl acetate in water. Specimens were examined in a Tecnai 12 Spirit Bio TWIN TEM (FEI Company) operated at 100 kV. Digital images were recorded using a Veleta camera (Olympus Soft Imaging Solutions, GmbH).

Minimal Inhibitory Concentration Determinations. Determination of the minimal inhibitory concentration (MIC) was performed by the standardized microdilution procedure in accordance with the Performance Standards for Antimicrobial Susceptibility Testing from the Clinical and Laboratory Standards Institute (33) with the following modifications: For *S. pneumoniae* strains, the assay was done in supplemented C+Y medium and in THY medium for comparison with other bacterial species. MIC against mycobacteria were determined in cation-adjusted Mueller Hinton broth (MHB) (Oxoid) supplemented with 0.05% Tween80 (Sigma-Aldrich). *N. gonorrhoeae* was grown in tryptone soy broth (Merck) supplemented with IsoVitaleX (Becton Dickinson) according to the manufacturer's instructions. All other strains were tested using cation-adjusted MHB. Briefly, the inoculum was prepared from a liquid preculture grown to midlog phase and diluted to reach a concentration of ∼5×10^5 cfu/mL. Two microliters of the 100-fold concentrated serial dilutions of chemicals were added to the wells. The plates were incubated overnight at ambient atmosphere and 37 °C. For *S. aureus*, *P. aeruginosa*, and *B. subtilis* MIC determination in THY medium, the plates were incubated with shaking (∼200 rpm). The MICs were determined as the lowest concentrations where no visible growth was observed. For determination of the plasma protein binding capacity of the THCz-1 compounds, bacteria were grown in C+Y medium supplemented with 10% HyClone Fetal Bovine Serum (GE Healthcare).

Cytotoxicity Assay. Lung epithelial A549 cells (ATCC CCL-185) were grown in 1× RPMI medium 1640 (Gibco) with 9% HyClone Fetal Bovine Serum (GE Healthcare) and 1× Penicillin/Streptomycin solution (Gibco). Cells were trypsinized and seeded at 1×10^5 cells/mL for IC_{50} determination (Table 2) and 1×10^6 cells/mL for SAR/structure toxicity relationship (STR) investigation (*SI Appendix*, Tables S1–S3) in 100 μL of medium per well of 96-well flat bottom plates (Sarstedt) and incubated overnight at 37 °C with 5% CO_2. The antibiotic-containing medium was removed on the following day, and cells were washed with PBS. Subsequently, 100 μL of antibiotic-free medium containing the compounds in a serial dilution for IC_{50} determination (Table 2), and concentrations of 100, 50, 25, and 12.5 μM in 1% DMSO (final concentration) for SAR/STR investigation (*SI Appendix*, Tables S1–S3) were added to the wells. After 19 h, resazurin sodium salt (Sigma) (20 μL of 440 μM in H_2O) was added to each well, and cells were further incubated for 4 h. Samples (80 μL per well) were transferred to micro test plates for immunoanalytics (Sarstedt), and absorbance was measured at 590 nm (SpectraMAX plus, Molecular Devices). Absorbance values were blanked with resazurin-containing medium, and the percentage of viable cells was calculated in comparison to solvent-treated cells. The reciprocal number for nonviable cells is given in *SI Appendix*, Tables S1–S3 for the estimation of cytotoxicity. Negative toxicity values or toxicity values of more than 100% were set to zero or 100% respectively. IC_{50} calculation was performed using nonlinear fit $\log_{(inhibitor)}$ vs. response calculation with variable slope and constraints of 0% and 100% toxicity for top and bottom constraints respectively in GraphPad Prism 5.04.

β-Galactosidase Reporter Assays. *B. subtilis* 168 *amyE*::pAC6 cultures with the promotor fusions P_{ypuA}-*lacZ* (cell wall), P_{yorB}-*lacZ* (DNA), P_{yvgS}-*lacZ* (RNA), and P_{yheI}-*lacZ* (protein) (34) were grown in MHB containing 5 μg/mL chloramphenicol at 30 °C to an OD_{600nm} of 0.5. Subsequently, melted Mueller Hinton agar was inoculated with 1×10^7 cfu/mL of the respective reporter strain. The agar was further supplemented with 5 μg/mL chloramphenicol, and X-gal (5-Bromo-4-chloro-3-indolyl β-D-galactopyranoside) at final concentrations of 75 μg/mL (cell wall), 125 μg/mL (DNA), and 250 μg/mL (RNA and protein). After pouring and solidification of the inoculated agar, 10 μg of THCz-1, 20 μg of THCz-40, 80 μg of THCz-39, and 100 μg of THCz-5 were spotted. Three micrograms of clindamycin served as positive control for the protein reporter and as negative control for the cell wall, DNA, and RNA reporter; 6 μg of vancomycin were used as positive control for the cell wall reporter and as negative control for the protein reporter; 0.3 μg of ciprofloxacin served as positive control for the DNA reporter; and 6 μg of rifampicin were used as positive control for the RNA reporter. Results were documented after 20 h of incubation at 30 °C.

Luciferase Reporter Assays. *B. subtilis* luciferase reporter assays were conducted as previously described (35). Briefly, *B. subtilis* 168 *sacA*::pCHlux101 (P_{liaI}-*lux*) was grown in MHB containing 5 μg/mL chloramphenicol at 30 °C to an OD_{600nm} of 0.5. Cells were added to 96-well white wall chimney plates containing antibiotics (2 μg/mL THCz-1,128 μg/mL THCz-5, 8 μg/mL THCz-39, 4 μg/mL THCz-40, 4 μg/mL vancomycin), and luminescence measurements were performed at 30 °C in a microplate reader Spark 10M (Tecan). At least three independent biological replicate experiments were conducted.

Bacterial Cell Wall Integrity Assay. Bacterial cell wall integrity assays were adapted from previous work (36). *B. subtilis* 168 cultures were grown in MHB at 30 °C to an OD_{600nm} of 0.3. Subsequently, cells were treated with 1 μg/mL THCz-1, 2 μg/mL THCz-40, 8 μg/mL THCz-39, 256 μg/mL THCz-5, 2 μg/mL vancomycin, 2 μg/mL bacitracin, 0.5 μg/mL nisin, 128 μg/mL clindamycin, 128 μg/mL ciprofloxacin, 128 μg/mL rifampicin, 128 μg/mL lysozyme, or DMSO and incubated at 30 °C. After 30 min of antibiotic exposure (treatment with lysozyme was shortened to 10 min), 200-μL culture samples were fixed in 1 mL of a 1:3 mixture of acetic acid and methanol. Five microliters of fixed cells were immobilized on a thin film of 1% wt/vol agarose containing 0.9% (wt/vol) NaCl supported on a microscope slide. Imaging was performed by phase contrast microscopy on a Zeiss Axio Observer Z1 microscope (Zeiss) equipped with an HXP 120-V light source and an Axio Cam MR3 camera. Images were acquired with ZEN 2 software (Zeiss) and analyzed and postprocessed using ImageJ v1.45s software (NIH) (37).

Antagonization Assays. Antagonization assays were performed as previously described (5). Briefly, antagonizing the antibiotic activity of THCz by potential target molecules was conducted by an MIC-type assay setup in microtiter plates. THCz-1 (5× MIC) was mixed with potential antagonists (C_{55}-P, C_{55}-PP, UDP-*N*-acetylmuramic acid pentapeptide [UDP-MurNAc-pentapeptide], lipid I, lipid II, lipid III_{WTA}, and lipid I_{cap}) in 0.5- to 10-fold molar excess with respect to the antibiotic. *M. luteus* DSM1790 (5×10^5 cfu/mL) was added, and samples were examined for visible growth after 20-h incubation. Experiments were performed in triplicate.

Quantification of Intracellular UDP-MurNAc-pp. To analyze the cytoplasmic nucleotide pool, we adapted the protocol of Kohlrausch and Höltje (38). *S. aureus* SG511 was grown in 15 mL of MHB at 37 °C to an OD_{600nm} of 0.6 and incubated with 130 μg/mL chloramphenicol for 15 min. THCz-1 was added at 1×, 2.5×, and 5× MIC and incubated for another 30 min. Lipid II-complexing vancomycin (5× MIC) was used as positive control. Extraction of nucleotide-linked peptidoglycan precursors and their analysis was performed by high-pressure liquid chromatography (HPLC) as described previously (39).

Impact of THCz on Membrane-Bound Peptidoglycan Biosynthesis Reactions In Vitro. Peptidoglycan synthesis reactions were reconstituted using purified proteins and substrates in vitro. PBP2-His_6 and YbjG-His_6 were purified as described earlier (5, 39), except that PBP2 was solubilized with 0.06% Triton X-100, and additional immobilized metal ion affinity chromatography purification steps were performed.

Transglycosylation by PBP2 was determined by incubating 2 nmol of lipid II in 20 mM 2-(*N*-morpholino)ethanesulfonic acid, 2 mM $MgCl_2$, 2 mM $CaCl_2$, 0.04% Triton X-100, pH 5.5 in a total volume of 50 μL. The reaction was initiated by the addition of 8 μg of PBP2-His_6 and incubated for 2 h at 30 °C.

Dephosphorylation of C_{55}-PP was carried out using purified *S. aureus* YbjG-His_6 enzyme. Twenty nanomoles of C_{55}-PP was incubated with 1 μg of YbjG-His_6 in 20 mM Tris·HCl, 150 mM NaCl, 10 mM β-mercaptoethanol, 0.8% Triton X-100, pH 7.5 in a total volume of 50 μL for 30 min at 37 °C.

THCz were added in molar ratios ranging from 0.5 to 2 with respect to the respective substrate (C_{55}-PP or lipid II) in all in vitro assays, and samples were preincubated for 10 min prior to addition of the enzyme. Polyprenyl-containing products were extracted from the reaction mixtures with an equal volume of l-butanol/pyridine acetate, pH 4.2 (2:1, vol/vol), and analyzed by thin-layer chromatography using chloroform/methanol/water/ammonia

(88:48:10:1, vol/vol/vol/vol) as the solvent (40) and phosphomolybdic acid staining (41). Quantification was carried out using ImageJ v1.45s software (NIH) (37). Experiments were performed at least in triplicate.

Synthesis and Purification of Lipid Intermediates. Large-scale synthesis and purification of the peptidoglycan precursors lipid I and II and the wall teichoic acid precursor lipid III_{WTA} was performed as previously described (5, 41). Streptococcal lipid I_{cap} (undecaprenyl pyrophosphoryl glucose) was synthesized using 10 nmol of C_{55}-P and 100 nmol of UDP-glucose in the presence of 1.2 mg/mL 1,2-dioleoylphosphatidylglycerol, 50 mM Tris·HCl, and 10 mM $MgCl_2$. Reaction was initiated by the addition of recombinant His_6-CpsE, and samples were incubated for 16 h at 30 °C. Lipid I_{cap} was extracted from the reaction mixture and purified as described for staphylococcal capsule intermediates (42). UDP-MurNAc-pp was purified according to the protocol elaborated by Kohlrausch and Höltje (38). C_{55}-P and C_{55}-PP were purchased from Larodan Fine Chemicals AB. The concentration of purified precursors was quantified on the basis of their phosphate content as described (43).

Selection of Strains with Reduced THCz-1 Sensitivity. T4 wild-type was continuously cultured on THCz-1–containing THY agar plates which were prepared as follows: Prewarmed 2× concentrated THY medium was mixed in equal parts with autoclaved agar containing 18 g/L bacteriological agar for molecular biology (Sigma Aldrich) and 2 g/L corn starch (Maizena). Additionally, choline chloride dissolved in 2×THY was added to 10 μg/mL final concentration; 100-fold concentrated THCz-1 was mixed with 15 mL of nutrient agar in a 9-cm Petri dish and mixed thoroughly; 36 μL of freshly prepared sterile filtered catalase from bovine liver (Sigma Aldrich) dissolved to 5 mg/mL in 50 mM KPO_4 buffer were overlaid on the solidified agar to reach at least 24 U/mL medium. THCz-1 concentrations were increased in small incremental steps (1, 1.6, and 2 μM), and a wild-type strain was carried in parallel on chemical-free plates. Growth and lysis kinetics of pneumococci with reduced THCz-1 sensitivity originating from strain T4 (BHN1364-BHN1367) as well as knockouts (BHN1371, BHN1690, BHN1691, BHN1693, and BHN2043) in genes with point mutations (*SI Appendix*, Fig. S14)were examined in THY medium and carried out as described above, whereas THCz-1 was added in a narrow titration series of 4× MIC (3 μM, 1.2 μg/mL), 2.4× MIC (1.8 μM, 0.7 μg/mL), 2× MIC (1.5 μM, 0.6 μg/mL), and 1× MIC (0.8 μM, 0.3 μg/mL) THCz-1. T4 wild type, BHN1368, BHN1369, BHN1692, and the unencapsulated T4R were included as controls. Viability upon challenge with 2× MIC (1.5 μM, 0.6 μg/mL) THCz-1 was determined after 1 h and compared to the colony counts of the respective strain at the time of challenge for T4 wild type, T4R, and T4 *cps4E*^{G394C} (BHN1691). Pneumococcal mutant construction is described in *SI Appendix*, and used strains are described in *SI Appendix*, Table S8.

Determination of Capsular Polysaccharide Amount. *S. pneumoniae* strains were grown until midlog phase to a comparable OD and stored on ice to prevent further growth. One milliliter of the bacterial culture was lysed with 0.1% Triton X-100 (Sigma) and incubation at 37 °C for 5 min and thereafter stored on ice. Protein concentration was determined with the Pierce BCA Protein Assay Kit (Thermo Scientific) according to the manufacturer's instructions, and samples were adjusted to the same protein concentration. Four microliters of a serial dilution was blotted on an Amersham Hybond-P PVDF Western blotting membrane with 0.45-μm pore size (GE Healthcare), which was activated for 30 s in ethanol and incubated 10 min thereafter in PBS, after which it was allowed to air dry briefly. Samples were allowed to dry for 1 h at 37 °C, and then the membrane was blocked for 1 h with 5% BSA in PBS+0.1% Tween20 (Sigma). Pneumococcal type serum 4 (SSI Diagnostica) was incubated with T4R for 1 h at 37 °C with shaking, the bacteria were pelleted thereafter, and the supernatant was spun twice for 5 min at 13,000 rpm to remove residual bacteria. The blot was incubated with the purified antibody in PBS+0.1% Tween20 overnight in 4 °C. AMDEX Goat Anti Rabbit IgG Horseradish Peroxidase Conjugate (GE Healthcare) was applied for 2 h, and the blot was developed using the ECL Prime Western Blotting Detection Reagent (GE Healthcare).

Data Availability. All data are available in the main text or *SI Appendix*. Additional data for Fig. S14 are available from National Center for Biotechnology Information (PRJNA774187).

ACKNOWLEDGMENTS. We thank Dr. Sofia Essén, Lund University, for assistance with high resolution mass spectrometry measurements, and Dr. Andrew Gerard Cairns for valuable comments on the manuscript. We thank Laboratories for Chemical Biology Umeå for providing the compound library used for the HTS, Sebastian Krannich for performing cytotoxicity assays, and Dr. Pardeep Singh for chiral HPLC separation of enantiomers. Funding was provided by the Swedish Foundation for Strategic Research (F.A. and B.H.-N.), the Swedish Research Council (F.A. and B.H.-N.), the Knut and Alice Wallenberg Foundation (F.A. and B.H.-N.), the Stockholm City Council (B.H.-N.), the Göran Gustafsson Foundation (F.A.), the Deutsche Forschungsgemeinschaft Project-ID 398967434 – TRR261 (to T.S., F.G., and A.M.), and the German Center for Infection Research.

1. A. Fleming, On the antibacterial action of cultures of a penicillium, with special reference to their use in the isolation of *B. influenzae*. *Br. J. Exp. Pathol.* **10**, 226 (1929).
2. World Health Organization, *Antimicrobial Resistance: Global Report on Surveillance* (World Health Organization, 2014).
3. H. Kresse, M. J. Belsey, H. Rovini, The antibacterial drugs market. *Nat. Rev. Drug Discov.* **6**, 19–20 (2007).
4. K. Bush, P. A. Bradford, β-Lactams and β-lactamase inhibitors: An overview. *Cold Spring Harb. Perspect. Med.* **6**, a025247 (2016).
5. L. L. Ling *et al.*, A new antibiotic kills pathogens without detectable resistance. *Nature* **517**, 455–459 (2015).
6. A. Müller, A. Klöckner, T. Schneider, Targeting a cell wall biosynthesis hot spot. *Nat. Prod. Rep.* **34**, 909–932 (2017).
7. A. J. F. Egan, J. Errington, W. Vollmer, Regulation of peptidoglycan synthesis and remodelling. *Nat. Rev. Microbiol.* **18**, 446–460 (2020).
8. I. G. Boneca, G. Chiosis, Vancomycin resistance: Occurrence, mechanisms and strategies to combat it. *Expert Opin. Ther. Targets* **7**, 311–328 (2003).
9. F. Grein, T. Schneider, H. G. Sahl, Docking on lipid II-A widespread mechanism for potent bactericidal activities of antibiotic peptides. *J. Mol. Biol.* **431**, 3520–3530 (2019).
10. J. Medeiros-Silva, S. Jekhmane, E. Breukink, M. Weingarth, Towards the native binding modes of antibiotics that target lipid II. *ChemBioChem* **20**, 1731–1738 (2019).
11. F. Grein *et al.*, Ca^{2+}-Daptomycin targets cell wall biosynthesis by forming a tripartite complex with undecaprenyl-coupled intermediates and membrane lipids. *Nat. Commun.* **11**, 1455 (2020).
12. A. Tomasz, S. Waks, Mechanism of action of penicillin: Triggering of the pneumococcal autolytic enzyme by inhibitors of cell wall synthesis. *Proc. Natl. Acad. Sci. U.S.A.* **72**, 4162–4166 (1975).
13. L. Su *et al.*, Design, synthesis and evaluation of hybrid of tetrahydrocarbazole with 2,4-diaminopyrimidine scaffold as antibacterial agents. *Eur. J. Med. Chem.* **162**, 203–211 (2019).
14. P. Mellroth *et al.*, LytA, major autolysin of *Streptococcus pneumoniae*, requires access to nascent peptidoglycan. *J. Biol. Chem.* **287**, 11018–11029 (2012).
15. A. Typas, M. Banzhaf, C. A. Gross, W. Vollmer, From the regulation of peptidoglycan synthesis to bacterial growth and morphology. *Nat. Rev. Microbiol.* **10**, 123–136 (2011).
16. A. Urban *et al.*, Novel whole-cell antibiotic biosensors for compound discovery. *Appl. Environ. Microbiol.* **73**, 6436–6443 (2007).
17. D. A. Wirtz *et al.*, Biosynthesis and mechanism of action of the cell wall targeting antibiotic hypeptin. *Angew. Chem. Int. Ed. Engl.* **60**, 13579–13586 (2021).
18. T. Mascher, S. L. Zimmer, T. A. Smith, J. D. Helmann, Antibiotic-inducible promoter regulated by the cell envelope stress-sensing two-component system LiaRS of *Bacillus subtilis*. *Antimicrob. Agents Chemother.* **48**, 2888–2896 (2004).
19. H. Strahl, L. W. Hamoen, Membrane potential is important for bacterial cell division. *Proc. Natl. Acad. Sci. U.S.A.* **107**, 12281–12286 (2010).
20. M. Bublitz *et al.*, Tetrahydrocarbazoles are a novel class of potent P-type ATPase inhibitors with antifungal activity. *PLoS One* **13**, e0188620 (2018).
21. R. T. Cartee, W. T. Forsee, M. H. Bender, K. D. Ambrose, J. Yother, CpsE from type 2 *Streptococcus pneumoniae* catalyzes the reversible addition of glucose-1-phosphate to a polyprenyl phosphate acceptor, initiating type 2 capsule repeat unit formation. *J. Bacteriol.* **187**, 7425–7433 (2005).
22. J. C. Paton, C. Trappetti, *Streptococcus pneumoniae* capsular polysaccharide. *Microbiol. Spectr.*, 10.1128/microbiolspec.GPP3-0019-2018 (2019).
23. J. Flores-Kim, G. S. Dobihal, A. Fenton, D. Z. Rudner, T. G. Bernhardt, A switch in surface polymer biogenesis triggers growth-phase-dependent and antibiotic-induced bacteriolysis. *eLife* **8**, e44912 (2019).
24. T. Homma *et al.*, Dual targeting of cell wall precursors by teixobactin leads to cell lysis. *Antimicrob. Agents Chemother.* **60**, 6510–6517 (2016).
25. P. Mellroth *et al.*, Structural and functional insights into peptidoglycan access for the lytic amidase LytA of *Streptococcus pneumoniae*. *MBio* **5**, e01120–e13 (2014).
26. T. Sandalova *et al.*, The crystal structure of the major pneumococcal autolysin LytA in complex with a large peptidoglycan fragment reveals the pivotal role of glycans for lytic activity. *Mol. Microbiol.* **101**, 954–967 (2016).
27. M. Schlag *et al.*, Role of staphylococcal wall teichoic acid in targeting the major autolysin Atl. *Mol. Microbiol.* **75**, 864–873 (2010).
28. T. V. Akalaeva *et al.*, Antitubercular, antifungal, and antibacterial activity in vitro of 1-phenethylamino-1,2,3,4-tetrahydrocarbazoles. *Pharm. Chem. J.* **24**, 826–829 (1990).
29. A. J. Hutt, J. O'Grady, Drug chirality: A consideration of the significance of the stereochemistry of antimicrobial agents. *J. Antimicrob. Chemother.* **37**, 7–32 (1996).

30. P. Edebrink *et al.*, Structural studies of the O-polysaccharide from the lipopolysaccharide of *Moraxella (Branhamella) catarrhalis* serotype A (strain ATCC 25238). *Carbohydr. Res.* **257**, 269–284 (1994).
31. T. Schneider *et al.*, Plectasin, a fungal defensin, targets the bacterial cell wall precursor Lipid II. *Science* **328**, 1168–1172 (2010).
32. C. Brunati *et al.*, Expanding the potential of NAI-107 for treating serious ESKAPE pathogens: Synergistic combinations against Gram-negatives and bactericidal activity against non-dividing cells. *J. Antimicrob. Chemother.* **73**, 414–424 (2018).
33. Clinical Laboratory Standards Institute, *Methods for Dilution Antimicrobial Susceptibility Tests for Bacteria That Grow Aerobically; Approved Standard* (Clinical and Laboratory Standards Institute, Wayne, PA, ed. 9, 2012).
34. H. Harms *et al.*, Antimicrobial dialkylresorcins from marine-derived microorganisms: Insights into their mode of action and putative ecological relevance. *Planta Med.* **84**, 1363–1371 (2018).
35. S. Tan, K. C. Ludwig, A. Müller, T. Schneider, J. R. Nodwell, The lasso peptide siamycin-I targets lipid II at the Gram-positive cell surface. *ACS Chem. Biol.* **14**, 966–974 (2019).
36. M. Wenzel *et al.*, Proteomic response of *Bacillus subtilis* to lantibiotics reflects differences in interaction with the cytoplasmic membrane. *Antimicrob. Agents Chemother.* **56**, 5749–5757 (2012).
37. C. A. Schneider, W. S. Rasband, K. W. Eliceiri, NIH Image to ImageJ: 25 years of image analysis. *Nat. Methods* **9**, 671–675 (2012).
38. U. Kohlrausch, J. V. Höltje, Analysis of murein and murein precursors during antibiotic-induced lysis of *Escherichia coli*. *J. Bacteriol.* **173**, 3425–3431 (1991).
39. T. Schneider *et al.*, The lipopeptide antibiotic Friulimicin B inhibits cell wall biosynthesis through complex formation with bactoprenol phosphate. *Antimicrob. Agents Chemother.* **53**, 1610–1618 (2009).
40. P. D. Rick *et al.*, Characterization of the lipid-carrier involved in the synthesis of enterobacterial common antigen (ECA) and identification of a novel phosphoglyceride in a mutant of *Salmonella typhimurium* defective in ECA synthesis. *Glycobiology* **8**, 557–567 (1998).
41. T. Schneider *et al.*, In vitro assembly of a complete, pentaglycine interpeptide bridge containing cell wall precursor (lipid II-Gly5) of *Staphylococcus aureus*. *Mol. Microbiol.* **53**, 675–685 (2004).
42. M. Rausch *et al.*, Coordination of capsule assembly and cell wall biosynthesis in *Staphylococcus aureus*. *Nat. Commun.* **10**, 1404 (2019).
43. G. Rouser, S. Fkeischer, A. Yamamoto, Two dimensional then layer chromatographic separation of polar lipids and determination of phospholipids by phosphorus analysis of spots. *Lipids* **5**, 494–496 (1970).
44. P. García, M. P. González, E. García, R. López, J. L. García, LytB, a novel pneumococcal murein hydrolase essential for cell separation. *Mol. Microbiol.* **31**, 1275–1281 (1999).
45. R. G. Kansal, A. McGeer, D. E. Low, A. Norrby-Teglund, M. Kotb, Inverse relation between disease severity and expression of the streptococcal cysteine protease, SpeB, among clonal M1T1 isolates recovered from invasive group A streptococcal infection cases. *Infect. Immun.* **68**, 6362–6369 (2000).

Supplementary Materials for

THCz - Small molecules with antimicrobial activity that block cell wall lipid intermediates

Elisabeth Reithuber†, Torbjörn Wixe†, Kevin C. Ludwig†, Anna Müller, Hanna Uvell, Fabian Grein, Anders E.G. Lindgren, Sandra Muschiol, Priyanka Nannapaneni, Anna Eriksson, Tanja Schneider, Staffan Normark, Birgitta Henriques-Normark#, Fredrik Almqvist#, Peter Mellroth#,¤

Correspondence to: Birgitta Henriques-Normark, birgitta.henriques@ki.se,
Fredrik Almqvist, fredrik.almqvist@umu.se,
Tanja Schneider, Tanja Schneider, tschneider@uni-bonn.de

† E.R., T.W., and K.L. contributed equally to this work.
#B.H-N., F.A. and P.M., contributed equally to this work.
¤Did not participate in the final version of the manuscript

This PDF file includes:

Supplementary Materials and Methods

Supplementary Text

Supplementary Figures S1-S16

Supplementary Tables S1-S8

References 1-29

Supplementary Information

Materials and Methods

Composition of C+Y medium

5 g / L casamino acids, 1.1 g / L yeast extract, 1.2 g / L anhydrous sodium acetate, 5 mg / L L-tryptophan, 50 mg / L L-cysteine, 25 mg / L L-glutamine, 250 mg / L sodium pyruvate, 3 mM sodium hydroxide, 455 mg / L glucose, 56.9 mg / L sucrose, 113.8 mg / L magnesium chloride, 0.894 mg / L calcium chloride dihydrate, 4.55 g / L adenosine, 4.55 g / L uridine, 0.5 mg / L asparagine, 50 µg / L choline chloride, 6 µg / L niacin, 7 µg / L pyridoxine hydrochloride, 24 µg / L D-pantothenic acid hemicalcium salt, 6.4 µg / L thiamine hydrochloride, 280 µg / L riboflavin, 0.6 µg / L biotin, 1.25 µg / L ferrous sulfate heptahydrate, 1.25 µg / L copper(II) sulfate pentahydrate, 0.6 µg / L zinc chloride, 0.55 µg / L manganese(II)chloride tetrahydrate, 3.7 ppm hydrochloric acid, 281.3 mg / L potassium dihydrogen phosphate, 6.169 g / L dipotassium hydrogenphosphate.

Broth microdilution assay for resistant mutant selection in *S. aureus*

Continuous growth in sub-inhibitory concentrations of THCz-1 was performed to provide a milieu that would favor mutants with decreased sensitivity to the compound, as described by Ling et. al. (*1*). Shortly, *S. aureus* (ATCC25923) was inoculated in THY medium to a concentration of ~$2*10^5$ cfu / mL and challenged with THC-1 titrated in small incrementing steps in a range that covered the MIC concentration. Similar treatment with ofloxacin (Sigma) was used as control. Growth was assessed visually after incubation overnight at 37 ºC at ambient atmosphere with shaking. Sub-culturing of bacteria from wells treated below MIC concentration with good growth was performed by inoculating 1:100 diluted culture samples into wells with fresh THY medium. These cultures were re-challenged with a THCz-1 and ofloxacin titration as described above and the procedure was iterated for 15 or 22 consecutive days. Assessment of selected cultures that grew at a higher concentration than previously observed was done by plating a sample from the culture on blood plates and re-challenge those isolates with a titration of THCz-1.

DNA Isolation and Illumina sequencing/Bioinformatic data analysis

Chromosomal DNA from *Streptococcus pneumoniae* clones of both THCz-1 exposed (#22) and unexposed (#25) isolates was prepared from 10 mL of a mid-log phase liquid culture in a 10 µM choline chloride (Sigma) supplemented THY medium using the genomic DNA buffer set and Genomic-tip 100/G (Qiagen) by following the manufacturer's instructions with the following modifications. To facilitate efficient pneumococcal lysis purified recombinant LytA, instead of lysozyme, was added to the cell suspension to a final concentration of 10 µg / mL followed by a 30 min incubation at 37 ˚C after which Proteinase K (Qiagen) was added and incubation proceeded for an additional 20 min. Sequencing libraries were prepared using Illumina TruSeq PCR free kit and using MiSeq Reagent v3 kit. Adapters were removed from the demultiplexed reads, and reads were quality trimmed using Trimmomatic (*2*). The reads were aligned to the NCBI annotated reference genome (NC_003028.3) using BWA-MEM (*3*) and variants were identified using GATK tools (*4*).

Construction of pneumococcal mutant strains

Deletion mutants were made with allelic replacement in which the open reading frames (Orfs) of targeting genes were replaced with antibiotic Orfs or cassettes (consisting of a promoter and Orf) as indicated in table S8. Transformation constructs were generated by sequential overlap PCR. First, the ~700 bp up- and down-stream regions flanking the Orfs to be deleted were amplified with Phusion high-fidelity DNA polymerase (New England biolabs) using genomic DNA from *S. pneumoniae* T4 as the template, with primers given in table S7. Likewise, the antibiotic resistance Orfs (or cassettes) were amplified with specific primers also given in table S7. In this process the primers used to amplify the flanking regions contained ~20 bp overhang sequences that were complimentary to the corresponding resistance genes (Table S7). Next, the ~700 bp up-stream region were fused to the corresponding antibiotic cassette (or Orf) through thermal annealing of the complementary overhang sequences followed by overlap extension for six cycles (without adding primers) to join the fragments and then by 33 successive cycles in the presence primers annealing the 5' and 3' ends of the amplicon. In parallel and using the same methodology the antibiotic cassette was also joined with the downstream region. In the final step the fused up region/antibiotic cassette amplicon was joined with the fused antibiotic cassette/down region amplicon in a similar approach as in previous step using 6 cycles without primers followed by 33 cycles with primers annealing to the terminal ends of the +700 bp up-region and the -700 bp down region. The final PCR products that contained the joined (700 bp upstream region-antibiotic cassette/Orf-700 bp downstream region) were purified (PCR clean up kit (Qiagen)) and used to transform the T4 strain. Using this methodology PCR products were generated for replacing the four genes annotated to encode P-type ATPases (*SP0729*, *SP1551*, *SP1623* and *SP2101*), agmatine deiminase *aguA* (SP0921), sugar transferase *cpsE* (*SP0350*) and RNA methyltransferase (*SP1901*) with antibiotic resistance Orfs or cassettes as indicated in table S8. The same methodology was used to produce transformation construct for the pneumolysin (*ply*) mutant except that the frw and rev primers annealed ~1000 bp up- and –downstream of the *ply* (*SP1923*) Orf. To introduce a G394C point mutation into the T4 wild type strain the following strategy was employed. Using the same methodology as described above an *ermB* Orf was inserted immediately downstream of the *SP0350* stop codon to extend the capsular operon with one additional Orf. Thus, the 700 bp up- and down-stream flanking regions of the *SP0350* stop codon were PCR amplified and fused to the erm Orf by overlap extension PCR followed by primer-based amplification. For generating the *SP0350*-G394C mutation construct we used genomic DNA from the BHN1364 strain (carrying the mutation) as template for the PCR and to generate the control amplicon (without the mutation) the wildtype T4 genomic DNA was used as the PCR template.

For transformation, the T4 strain grown in C+Y medium to OD_{600nm} = 0.1 was diluted 10-fold into tryptic soy broth with 10 % glycerol and 0.01 % $CaCl_2$ and incubated at 30 °C for 15 min after which competence stimulating peptide 2 was added (1 µg / mL). Following 15 min incubation 500 ng of PCR product (described in previous section) was added (to a 500 µL reaction) and the cells were incubated for 60 min at 30 °C and then for 90 min at 37 °C before the cells were spread on blood agar plates containing the corresponding antibiotic agent. Resistant colonies were isolated and the mutation was validated by Sanger sequencing (Eurofins) of a PCR-amplified amplicon of the corresponding locus using primers that annealed ~800 bp (~1100 bp for *ply*) up- and down-stream of the cognate Orf (see table S7 for primer sequences). For the quadruple P-type ATPase mutant the same procedure was iterated four times using sequenced mutant isolates that had acquired the corresponding mutations. Strains produced are listed in table S8.

Potassium release from whole cells

The potassium release assays were adapted as previously described. Briefly, tryptic soy broth (TSB)-grown *S. simulans* 22 cells were harvested at an OD_{600nm} of 1.0 to 1.5, washed with cold choline buffer (300 mM choline chloride, 30 mM MES, 20 mM Tris, pH 6.5), and resuspended to an OD_{600nm} of 30. The concentrated cell suspension was kept on ice and used within 30 min. For each measurement, the potassium electrode (Mettler Toledo) was calibrated with potassium chloride. Cells were diluted in choline buffer at room temperature (RT) to an OD_{600nm} of 3, and the peptide-induced potassium release was monitored in 15 s intervals for 5 min at RT. THCz-1 was added in a concentration ranging from 0.25× to 5× MIC. The effect of THCz analogs THCz-5, THCz-39 and THCz-40 was compared to THCz-1 at 2.5× MIC. Potassium concentrations were calculated from the measured voltage according to Orlov *et al.* (5) and plotted relative to the total amount of potassium released after the addition of 1 µM of the pore-forming lantibiotic nisin (set 100 % efflux). Results show mean values of three independent experiments.

Additional *in vitro* peptidoglycan biosynthesis reactions

The *in vitro* MurG reaction was performed in a 30 µL reaction containing 2 nmol of purified lipid I and 25 nmol of UDP-N-acetyl glucosamine (UDP-GlcNAc) in 200 mM Tris-HCl, 5.7 mM $MgCl_2$, at pH 7.5, and 0.8% Triton X-100 with 2 µg of purified, recombinant *S. aureus* MurG-His_6 enzyme. Reaction mixtures were incubated for 30 min at 30 °C.

In vitro amidation was assayed in a 30 µL reaction containing 2 nmol lipid II in 160 mM Tris-HCl, 40 mM MgCl2, 30 mM KCl, at pH 7.5, 0.26 % Triton X-100, 6 mM ATP, and 6.6 mM glutamine with 3 µg of the GatD-His6/MurT complex. Reaction mixtures were incubated for 2 h at 30 °C.

The *S. aureus* PBP4 enzymatic activity was assayed using the same conditions as described for the PBP2 *in vitro* enzyme assay.

In all *in vitro* assays, THCz were added in molar ratios with regard to the respective substrate (lipid I or lipid II) and pre-incubated for 10 min prior to addition of the individual enzyme. Extraction and TLC analysis were performed as described for the PBP2 and YbjG *in vitro* enzyme assays.

Complex formation with lipid II

Binding of THCz-1 and vancomycin to lipid II was analyzed by incubating 2 nmol of the cell wall precursor with 0.5 to 16 nmol of the antibiotics in 50 mM Tris-HCl (pH 7.5) for 15 min at RT. Complex formation was analyzed by extracting unbound lipid II from the reaction mixture followed by TLC analysis as described for the PBP2 and YbjG *in vitro* enzyme assays. Experiments were performed with biological replicates.

Passaging of *S. pneumoniae* in sub-MIC concentration of THCz-1:

S. pneumoniae T4 and T4Δ*lytA* from a mid-log phase liquid culture were inoculated to a concentration of 10^5 cfu/mL in pre-warmed 5 mL of THY medium containing 1 % DMSO or 0.4 µM THCz-1 and incubated over night at 37 °C and ambient atmosphere. The cultures were then passaged with thousand-fold dilution into fresh 5 mL medium containing the respective chemicals and incubation was continued. On the following day a liquid culture in medium containing the respective chemicals was started from the passaged cultures and grown until mid-log phase to a synchronized OD.

Measurement of phosphorylcholine:
Three times 500 µL of the passaged bacterial culture was lysed with 0.1 % Triton X-100 (Sigma) and incubation at 37 ˚C for 5 min and thereafter stored on ice. Protein concentration was determined with the Pierce™ BCA Protein Assay Kit (Thermo scientific) according to the manufacturer's instructions and samples were adjusted to the same protein concentration. A serial dilution was blotted on an Amersham™ Hybond™ PVDF western blotting membrane with 0.45 µm pore size (GE Healthcare), which was activated 30 s in methanol and incubated 10 min thereafter in PBS after which it was allowed to air dry shortly. Samples were allowed to dry at 37 ˚C, then the membrane was blocked for 30 min with 5 % BSA in PBS+0.1 % Tween20 (Sigma). The blot was incubated with IgA, Kappa from murine myeloma, clone TEPC 15 (Sigma) in PBS+0.1 % Tween20 overnight at 4 ºC. Anti-mouse immunoglobulins HRP (Dako) were applied for 2 h and the blot was developed using the ECL™ Prime Western Blotting Detection Reagent (GE Healthcare). The experiment was repeated with three biological replicates in technical triplicates. Relative quantification of the dots was performed using Image Lab Version 6.1.9 (Bio-Rad Laboratories, Inc.).

Sensitivity determination of THCz-1 passaged pneumococci to externally added LytA:
T4Δ*lytA* passaged in sub-MIC concentrations of THCz-1 and 1 % DMSO was challenged with 3 µM THCz-1 in mid-log phase and OD_{600nm} was monitored in the Bioscreen C plate reader as described above. The culture medium contained 1 µg/mL or 10 µg/mL recombinant LytA which was produced as described previously (*6*). The slope of the decrease in OD_{600nm} was determined in technical triplicates and at least five biological replicates.

MinD delocalization studies
B. subtilis 1981 *erm spc minD*::*ermC amyE*::P_{xyl}-*gfp-minD*, a strain with a *gfp-minD* fusion under control of the P_{xyl} promotor (*7*), was grown in MHB supplemented with 0.1 % w/v xylose and 50 µg/ml spectinomycin at 30 °C to an OD_{600} of 0.3. Imaging was carried out within 5 min after addition of THCz at 0.5× to 4× MIC. The proton ionophore carbonyl cyanide *m*-chlorophenylhydrazone (CCCP, 100 µM) was used as positive control. Samples were immobilized on microscope slides covered with 1 % w/v agarose. Fluorescence microscopy was performed using a Zeiss Axio Observer Z1 microscope (Zeiss, Jena, Germany) equipped with HXP 120 V light source and an Axio Cam MR3 camera. Images were acquired with ZEN 2 software (Zeiss) and analyzed and postprocessed using ImageJ v1.53e software (National Institutes of Health)(*8*).

General chemistry and synthesis of THCz analogs
All chemicals were used as received from commercial suppliers, unless otherwise stated. All moisture sensitive reactions were carried out under an atmosphere of dry nitrogen using oven-dried glassware. MeOH was dried by activated 3Å MS, CH_2Cl_2, $CHCl_3$ and benzene (PhH) were dried with activated 4 Å MS, added 24-72 h prior to use. Pyridine and Et_3N were distilled under N_2(g) from CaH_2 and used directly. Microwave reactions were run in sealed vials in a Biotage Initiator (SW version 2.2). Column chromatography was performed on Matrex (25-70 µm) silica gel or by the Biotage Isolera One flash purification system on Biotage SNAP KP-Sil cartridges. The eluent is given in parenthesis as (eluent). Reversed phase preparative HPLC was performed by Gilson HPLC system (Gilson 333/334 Prep-Scale HPLC pumps, the UV/Vis 151 detector and GX-271 liquid handler) on a C18 reversed phase column (25 cm x 21.2 mm, 5 µm). Samples were dissolved in DMSO and eluted by MeCN:H_2O (20:80-100:0) with 0.75% formic acid as additive at 18 mL /

min. Pure fractions were concentrated *in vacuo* and freeze dried from MeCN:H_2O (1:3 or 1:4 v/v) to afford the compound as the formate salt. Analytical HPLC was performed by Agilent 1290 Infinity Quaternary LC System equipped with the 6150 Quadruple LC/MS. TLC analyses (Merck 60 F254 sheets) were visualized under UV light (254 or 366 nm) or by impregnation with Seebach solution. An Electrothermal IA9000 SERIES Digital Melting Point Apparatus recorded melting points using open capillary tubes. ^{1}H and ^{13}C NMR spectra were recorded at 298 K on a Bruker AVIII400 or AVIIIHD600 spectrometer. The spectra were recorded in $CDCl_3$, DMSO-d_6, MeOH-d_4 or acetone-d_6 and the residual solvent signals (7.26/77.16, 2.50/39.52, 3.31/49.00, 2.05/29.84 ppm, respectively) were used as references. ^{19}F NMR resonances are reported without reference. Typically, the secondary amine ^{1}H resonances broadened out under the conditions used. Assignments of new compounds were accomplished by coupling constants and integrals, as well as 2D correlation experiments. HRMS were determined by KILU-CAS MS facility, Lund University. All compounds used for biological testing were ≥95 % pure as estimated by analytical HPLC and ^{1}H NMR.

Synthesis and purification of compounds depicted in Fig. S2

2-Phenyl-1-(2,3,4,9-tetrahydro-1*H*-carbazol-1-yloxy)ethane (**THCz-5**). NBS (1.09 g, 6.13 mmol) and a few grains of benzoylperoxide were added to a solution of 2,3,4,9-tetrahydro-1*H*-carbazole (1.0 g, 5.8 mmol) and dry pyridine (1.20 mL, 14.9 mmol) in dry PhH (20 mL). The mixture was stirred at RT for 24 h and the formed suspension was let to sediment. The top layer of benzene was removed leaving a brown, oily residue that was dissolved in a mixture of Et_2O:Phenylethanol (1:3, v/v%, 5 mL) that had been dried for 24 h by activated 3 Å molecular sieves. This is solution A. Sodium (200 mg, 8.7 mmol) was dissolved in dry Et_2O:Phenylethanol mixture (1:3, v/v%, 2 mL) to get solution B. Solution B was then added to solution A and stirred at RT for 2 days. NH_4Cl (sat. aq. 3 mL) was added to the reaction mixture. The phases were separated and the aqueous phase was extracted with Et_2O (2x10 mL), and the combined organic phases were washed with H_2O, brine and dried over Na_2SO_4. Removal of the solvent *in vacuo* gave 3.01 g brown oil. Purification by column chromatography (Heptane: EtOAc, 9:1) yielded 215 mg (13%) of **THCz-5** as clear yellow oil, which crystallised upon standing. R_f: (0.22% Heptane:EtOAc, 9:1); mp: 97 °C; ^{1}H NMR (400 MHz, DMSO-d_6): δ = 10.78 (s, 1H), 7.39 (d, 1H, *J* = 7.6 Hz), 7.32-7.25 (m, 5H), 7.21-7.17 (m, 1H), 7.07 (m, 1H), 6.96-6.92 (m, 1H), 4.58 (t, 1H, *J* = 4.0 Hz), 3.82-3.77 (m, 2H), 2.86 (t, 2H, *J* = 7.2 Hz), 2.70 (m, 1H), 2.57-2.51 (m, 1H), 1.94-1.70 (m, 4H) ppm; ^{13}C NMR (100 MHz, $CDCl_3$): δ = 139.0, 136.0, 133.9, 128.9, 128.2, 126.3, 126.0, 121.2, 118.2, 111.2, 110.5, 70.1, 69.2, 36.2, 29.1, 20.6, 19.2 ppm; HRMS (ESI): *m/z* calcd for $C_{20}H_{21}NONa^+$: 314.1515 [*M* + Na^+], found: 314.1495.

(Phenethyl)(6-phenyl-9-oxa-1,2,3,4-tetrahydrofluoren-1-yl)amine (**THCz-6**). To a solution of **THCz-18** (105 mg, 0.400 mmol) in dichloroethane (4 mL) was added $NaBH(OAc)_3$ (509 mg, 2.40 mmol), HOAc (137 µL, 2.40 mmol) and phenylethylamine (300 µL mL, 290 mg, 2.40 mmol). The mixture was stirred at RT for 46 h before addition of $NaHCO_3$ (sat. aq., 2 mL). Extracted with CH_2Cl_2 (2x5 mL), drying over Na_2SO_4, filtration and removal of the solvent in vacuo afforded 233 mg of clear, brown oil that after purification by column chromatography (30-50% EtOAc in Heptane) yielded 84 mg (57 %) of **THCz-6** as a clear yellow oil. R_f: 0.11 (Heptane: EtOAc; 1:1); ^{1}H NMR (400 MHz, $CDCl_3$): δ = 7.63-7.61 (m, 3H), 7.48-7.42 (m, 4H), 7.35-7.29 (m, 3H), 7.27-7.20 (m, 3H, overlap with solvent peak), 3.99 (t, 1H, *J* = 4.8 Hz), 3.18-3.04 (m, 2H), 2.91-2.86 (m, 2H), 2.72-2.60 (m, 2H), 2.11-2.05 (m, 1H), 2.0-1.78 (m, 3H) ppm; ^{13}C NMR (100 MHz, $CDCl_3$): δ = 155.6, 154.3, 142.0, 140.1, 136.2, 128.92, 128.90, 128.84, 128.61, 127.6, 126.9, 126.3, 123.5,

117.8, 115.1, 111.4, 51.7, 48.9, 36.9, 30.1, 20.8, 20.3 ppm; HRMS (ESI): *m/z* calcd for $C_{26}H_{26}NO$: 368.2008 [$M + H^+$], found: 368.2014.

6-Bromo-2,3,4,9-tetrahydrocarbazol-1-ol (**THCz-10**). Dry MeOH (1.0 mL) was added rapidly, at RT, to a suspension of **THCz-9**, (*9*) (264 mg, 1.00 mmol) and $NaBH_4$ (113 mg, 2.99 mmol) in dry CH_2Cl_2 (10 mL). The formed clear, orange, solution was stirred at RT for 2.5 h before TLC showed full conversion. NH_4Cl (sat. aq. 0.5 mL) was added and the phases were separated. Approximately 90 % of the solvent was removed in vacuo. The remaining slurry was directly purified by column chromatography (Heptane: EtOAc 1:1) to afford 217 mg (82 %) of **THCz-10** as a yellow solid. ^{1}H NMR (400 MHz, MeOH-d_4): δ = 7.52 (d, 1H, J = 1.2 Hz), 7.22 (d, 1H, 1.2 Hz), 7.14 (dd, 1H, J = 1.2, 6.0 Hz), 4.86-4.84 (m, 1H, overlap with H_2O residue), 2.73-2.67 (m, 1H), 2.62-2.57 (m, 1H), 2.12-2.02 (m, 2H), 1.92-1.78 (m, 2H) ppm; NMR ^{13}C (100 MHz, MeOH-d_4): δ = 138.3, 136.6, 130.1, 125.0, 121.8, 113.6, 112.5, 111.8, 64.5, 34.4, 21.8, 21.1 ppm.

6-Bromo-2,3,4,9-tetrahydro-1*H*-carbazol-1-yl phenylacetate (**THCz-11**). Phenylacetic acid anhydride, (*10*) (508 mg, 1.99 mmol) dissolved in dry CH_2Cl_2 (26 mL), was added to a solution of **THCz-10** (537 mg, 2.02 mmol), DMAP (25 mg, 0.20 mmol) and dry Et_3N (0.30 mL, 0.22 g, 2.1 mmol) in dry CH_2Cl_2 (65 mL). The solution was stirred at RT for 2 h. NH_4Cl (sat. aq. 1 mL) and H_2O (1 mL) was added and the phases were separated. The aqueous phase was extracted once with CH_2Cl_2 (40 mL). The combined organic phases were dried (Na_2SO_4), filtered and concentrated in vacuo to afford an orange/brown oil, that after purification by column chromatography (9:1; Heptane: EtOAc) afforded 598 mg (78%) of **THCz-11** as a pale yellow solid. R_f: 0.28 (8:2, Heptane: EtOAc); mp: 119-121 °C; ^{1}H NMR (600 MHz, $CDCl_3$): δ = 8.57 (s, 1H), 7.66 (s, 1H), 7.36-7.33 (m, 2H), 7.30-7.27 (m, 4H, partial overlap with residual $CHCl_3$), 7.16 (d, 1H, J = 8.4 Hz), 5.83 (s, 1H), 3.69, 3.64 (ABq, 2H, J_{AB} = 15.6 Hz), 2.85-2.82 (m, 1H), 2.64-2.59 (m, 1H), 2.20-2.16 (m, 1H), 2.07-2.03 (m, 3H) ppm; ^{13}C NMR (150 MHz, $CDCl_3$): δ = 173.8, 134.7, 133.8, 132.4, 129.5, 128.8, 128.2, 127.4, 125.7, 121.7, 114.1, 112.9, 112.6, 66.7, 41.4, 29.2, 20.8, 19.3 ppm; HRMS (ESI): *m/z* calcd for $C_{20}H_{17}{}^{79}BrNO_2$: 382.0443 [$M$ - H], found: 382.0439.

3-(4-Biphenylyloxy)cyclohexene (**THCz-15**). K_2CO_3 (4.15 g, 30.0 mmol) was added to a solution of 4-phenylphenol (**THCz-13**) (2.6 g, 15 mmol) and 3-bromocyclohexene (**THCz-14**) (technical grade, 90%, 1.93 mL, 15.0 mmol) in DMF (50 mL). The turbid mixture was stirred at RT for 22 h before concentrated in vacuo. The afforded white/brown residue was suspended in EtOAc (50 mL) and washed with H_2O (2x20 mL), brine and dried with Na_2SO_4. Filtration and removal of the solvent in vacuo afforded 3.29 g off-white solid that after purification by column chromatography (0-100% EtOAc in Heptane) yielded the 1.26 g (34%, 81% brsm) of **THCz-15** as a white solid. R_f: 0.64 (1:1, Heptane: EtOAc); mp: 49-50 °C; ^{1}H NMR (400 MHz, $CDCl_3$): δ = 7.58-7.52 (m, 4H), 7.43 (t, 2H, J = 7.6 Hz), 7.33-7.30 (m, 1H), 7.02 (d, 2H, J = 8.4 Hz), 6.03-5.99 (m, 1H), 5.94-5.91 (m, 1H), 4.86 (bs, 1H), 2.16-2.14 (m, 1H), 2.08-1.85 (m, 4H), 1.71-1.28 (m, 1H) ppm; ^{13}C NMR (100 MHz, $CDCl_3$): δ = 157.6, 141.0, 133.8, 132.4, 128.8, 128.3, 126.8, 126.7, 126.4, 116.2, 71.1, 28.4, 25.3, 19.1 ppm; HRMS (ESI): *m/z* calcd for $C_{18}H_{18}O$: 249.1279 [M - H], found: 249.1277.

3-(2-Cyclohexen-1-yl)-4-biphenylol (**THCz-16**). **THCz-15** (751 mg, 3.00 mmol) was dissolved in *N*,*N*-diethylaniline (6 mL) and heated at 195°C for 40 h. The mixture was cooled to RT and poured into HCl (6M, 30 mL). The aqueous phase was extracted with EtOAc (3x50 mL) and the combined organic phases dried with Na_2SO_4. Filtration and removal of the solvent in vacuo afforded 841 mg brown oil, that after purification by column chromatography (4x14 cm; 9:1 Heptane: EtOAc) yielded 710 mg (95%) of **THCz-16** as clear yellow oil. R_f: 0.38 (Heptane: EtOAc; 7:3); ^{1}H NMR (400 MHz, $CDCl_3$): δ = 7.57-7.54 (m, 2H), 7.44-7.40 (m, 2H), 7.37-7.35

(m, 2H), 7.32-7.28 (m, 1H), 6.90-6.87 (m, 1H), 6.11-6.07 (m, 1H), 5.90-5.87 (m, 1H), 3.67-3.64 (m, 1H), 2.16 (bs, 2H), 2.14-2.05 (m, 1H), 1.86-1.82 (m, 1H), 1.76-1.66 (m, 1H), 1.63-1.62 (m, 2H) ppm; ^{13}C NMR (100 MHz, $CDCl_3$): δ = 153.8, 141.2, 133.9, 131.4, 131.3, 129.7, 128.8, 128.5, 126.9, 126.7, 126.3, 116.7, 38.3, 30.2, 25.2, 21.6 ppm HRMS (ESI): *m/z* calcd for $C_{18}H_{18}O$: 249.1279 [*M* - H], found: 249.1274.

6-Phenyl-9-oxa-1,2,3,4,4a,9a-hexahydrofluoren-1-ol (**THCz-17**). mCPBA (621 mg, 2.77 mmol) was added to a solution of **THCz-16** (680 mg, 2.70 mmol) in benzene (20 mL). The solution was stirred at 90 °C in a sealed tube for 4 h, cooled to RT, washed with a 1:1 mix of H_2O:$NaHCO_3$ (sat. aq., 5x10 mL), H_2O (10 mL) and dried over Na_2SO_4. Filtration and removal of the solvent in vacuo afforded 670 mg yellow oil that after purification by column chromatography (4x15 cm; 7:3 Heptane: EtOAc) yielded 383 mg (53 %) of **THCz-17** as clear yellow oil. R_f: 0.17 (Heptane:EtOAc; 7:3); ^{1}H NMR (400 MHz, $CDCl_3$): δ = 7.55-7.53 (m, 2H), 7.43-7.35 (m, 3H), 7.32-7.28 (m, 2H), 6.90 (d, 1H, *J* = 8.4 Hz), 4.59-4.55 (m, 1H), 3.72 (bs, 2H), 2.30 (bs, 1H), 2.19-2.13 (m, 1H), 1.91-1.82 (m, 2H), 1.73-1.68 (m, 1H), 1.46-1.33 (m, 2H), ppm; ^{13}C NMR (100 MHz, $CDCl_3$): δ = 158.8, 141.4, 134.6, 131.5, 128.8, 127.3, 127.0, 126.8, 121.9, 110.7, 89.6, 71.2, 41.2, 30.1, 25.0, 19.8 ppm; HRMS (ESI): *m/z* calcd for $C_{18}H_{19}O_2$: 267.1380 [$M + H^+$], found: 267.1394.

6-Phenyl-9-oxa-3,4-dihydro-2*H*-fluoren-1-one (**THCz-18**). DDQ (840 mg, 3.70 mmol) was added to a pale yellow solution of **THCz-17** (325 mg, 1.22 mmol) in xylene (12 mL). The formed red solution was heated in a sealed tube at 150 °C for 20 h. The now dark brown solution, containing grey precipitation, was filtered through Celite and rinsed with EtOAc. Removal of the solvent in vacuo afforded 764 mg brown oil that after purification by column chromatography (4x18 cm; 30-50 % EtOAc in Heptane) yielded 245 mg (77 %) of **THCz-18** as a brown solid. R_f: 0.47 (Heptane: EtOAc; 1:1); mp: dec.>120 °C; ^{1}H NMR (400 MHz, $CDCl_3$): δ = 7.80 (d, 1H, *J* = 2.0 Hz), 7.71 (dd, 1H, *J* = 2.0, 8.0 Hz), 7.61-7.59 (m, 3H), 7.48-7.44 (m, 2H), 7.39-7.36 (m, 1H), 3.02 (t, 2H, *J* = 6.0 Hz), 2.71 (t, 2H, *J* = 6.0 HZ), 2.33-2.27 (m, 2H) ppm; ^{13}C NMR (100 MHz, $CDCl_3$): δ = 188.5, 155.5, 148.3, 140.8, 137.5, 134.9, 129.0 (2C), 127.5 (2C), 127.0, 120.1, 113.1, 38.7, 24.2, 21.5 ppm; HRMS (ESI): *m/z* calcd for $C_{18}H_{15}O_2$: 263.1067 [$M + H^+$], found: 263.1049.

Synthesis of tetrahydrocarbazole-1-amines - General Procedures as depicted in Fig. S3

Synthesis of 2,3,4,9-tetrahydrocarbazol-1-ylideneamines. Procedure A: *p*TsOH (0.05 eq.) was added to a solution of tetrahydrocarbaloze-1-one (1 eq.) and amine (1.1-3 eq.) in PhH or toluene (PhMe) (5-25 mL). The solution was refluxed 12-48 h while removing water with a Dean-Stark apparatus. The reaction mixture was allowed to cool to RT before equal amounts of $NaHCO_3$ (sat. aq.) and H_2O was added to the mixture. The phases were separated and the aqueous phase was extracted with EtOAc. The combined organic phases were dried (Na_2SO_4), filtered and concentrated in vacuo and purified.

Synthesis of 2,3,4,9-tetrahydro-1*H*-carbazol-1-ylamines. Procedure B: The imine afforded from procedure A, was dissolved in MeOH. $NaBH_4$ (1.2-2 eq.) was added at RT and the reaction was monitored with TLC. Sometimes, the imine and the formed amine had the same R_f-values on TLC (MeOH 2-5% in CH_2Cl_2). However, the imines are visualised at both 254 and 366 nm, but the amines are only visualised at 254 nm, why the conversion can be monitored by the disappearance of the spot visualised at 366 nm. Stirred for 10-120 min before quenched by addition of NH_4Cl (sat. aq.). The mixture was reduced in vacuo, and the afforded slurry was partitioned between EtOAc/H_2O. The phases were separated and the aqueous phase extracted with EtOAc, dried (Na_2SO_4), filtered, concentrated in vacuo and purified.

2,3,4,9-tetrahydro-1*H*-carbazol-1-ylamines. Procedure C: As procedure A and B described above. The difference is that the imine afforded from procedure A was neither fully characterised nor purified before the reduction with $NaBH_4$. Work up as procedure B.

Synthesis and purification of tetrahydrocarbazole-1-amines according to Fig. S3

(Phenethyl)-2,3,4,9-tetrahydro-1*H*-carbazol-1-ylamine (**THCz-19**). Procedure C: 2,3,4,9-tetrahydrocarbazol-1-one (56 mg, 0.30 mmol), 2-phenylethylamine (57 µL, 55 mg, 0.45 mmol), *p*TsOH (2.6 mg, 15 µmol) in PhH (15 mL), refluxed overnight. Usual workup gave 96 mg yellow oil that was dissolved in MeOH (10 mL). $NaBH_4$ (23 mg, 0.60 mmol) was added and stirred for 10 min. Usual workup afforded 75 mg brown/yellow solid. Purification by preparative HPLC afforded 35 mg (40 %) of **THCz-19** as a white solid. R_f: 0.34 (5 % MeOH in CH_2Cl_2); mp: dec. >140 °C; ^{1}H NMR (600 MHz, $CDCl_3$): δ = 10.24 (bs, 1H), 8.59 (s, 0.3H, HOOCH), 7.44 (d, 1H, *J* = 7.8 Hz), 7.34 (d, 1H, *J* = 8.4 Hz), 7.26-7.23 (m, 2H), 7.20-7.18 (m, 1H), 7.15-7.12 (m, 3H), 7.06-7.03 (m, 1H), 4.51 (t, 1H, *J* = 6.6 Hz) 3.16-3.08 (m, 3H), 3.04-3.00 (m, 1H), 2.74-2.65 (m, 2H), 2.27-2.22 (m, 1H), 2.09-2.02 (m, 2H), 1.76-1.71 (m, 1H) ppm; ^{13}C NMR (100 MHz, $CDCl_3$): δ = 169.0 (HOOCH), 136.7, 136.5, 129.0, 128.9, 127.3, 126.5, 126.4, 123.1, 119.6, 118.9, 116.0, 111.9, 51.7, 44.4, 33.1, 25.8, 21.4, 20.7 ppm; HRMS (ESI): *m/z* calcd for $C_{20}H_{23}N_2$: 291.1855 [$M + H^+$], found: 291.1866.

6-Cyclohexyl-2,3,4,9-tetrahydrocarbazol-1-one (**THCz-20a**). A solution of (*p*-Cyclohexylphenyl)hydrazine hydrochloride (*11*) (453.4 mg, 2.0 mmol) and 1,2-cyclohexanedione (224.2 mg, 2.0 mmol) in a mixture of concentrated HCl (4 mL) and glacial HOAc (16 mL) was heated by MWI at 120 °C for 15 min. The now dark brown solution was poured into ice-cooled NaOH (12.4 g in 100 mL) and the formed cloudy mixture was extracted with EtOAc (5x60 mL). The combined organic phases were dried ($MgSO_4$), filtered and concentrated in vacuo to afford 432 mg brown solid. The solid was dissolved in MeOH/CH_2Cl_2, evaporated onto Celite and passed through a pad of silica (10 % EtOAc in Heptane) to afford 296 mg of brown solid. ^{1}H NMR showed a mix of **THCz-20a** and 4-cyclohexylaniline. The solid was therefore triturated with a small portion of warm MeOH, washed with small portions of cooled MeOH and dried to afford 181 mg (34 %) of pure **THCz-20a** as beige solid. R_f: 0.69 (5 % MeOH in CH_2Cl_2); mp: 220-221 °C; ^{1}H NMR (400 MHz, DMSO-d_6): δ = 11.43 (s, 1H), 7.45 (s, 1H), 7.39 (d, 1H, *J* = 8.8 Hz), 7.20 (dd, 1H, *J* = 1.6, 8.4 Hz), 2.93 (t, 2H, *J* = 6.0 Hz), 2.56-2.52 (m, 3H, overlap with DMSO peak), 2.17-2.11 (m, 2H), 1.83-1.71 (m, 5H), 1.51-1.42 (m, 5H) ppm; ^{13}C NMR (100 MHz, DMSO-d_6): δ = 190.3, 139.1, 136.7, 131.3, 127.8, 126.2, 125.3, 117.8, 112.5, 43.9, 38.1, 34.5, 26.5, 25.7, 24.7, 20.9 ppm; HRMS (ESI): *m/z* calcd for $C_{18}H_{22}NO$: 268.1696 [$M + H^+$], found: 268.1668.

1,3-Bis|(*E*)-6-methyl-2,3,4,9-tetrahydrocarbazol-1-ylideneamino|propane (**THCz-23**). *p*TsOH (4.3 mg, 25 µmol) was added to a solution of 1,3-diaminopropane (41.8 µL, 37.1 mg, 0.50 mmol) and **THCz-20b** (204.2 mg, 1.02 mmol) in benzene (20 mL). The solution was refluxed for 23 h, while removing water using a Dean-Stark trap, and then cooled to RT. Upon cooling to RT, a precipitate started to form in the now orange solution. The formed precipitate was filtered off, washed with small portions of benzene, freeze dried from MeCN:H_2O (1:4) to afford 159 mg (73 %) of pure **THCz-23** as a white powder. R_f: 0.05 (5% MeOH in CH_2Cl_2); mp: 187-189 °C; ^{1}H NMR (400 MHz, DMSO-d_6): δ = 10.79 (bs, 2H), 7.27-7.24 (m, 4H), 6.96 (d, 2H, *J* = 8.0 Hz), 3.60 (t, 4H, *J* = 8.0 Hz), 2.77-2.74 (m, 4H), 2.58-2.55 (m, 4H), 2.35 (s, 6H), 2.06 (t, 2H, *J* = 8.0 H), 2.04-1.93 (m, 4H) ppm; ^{13}C NMR (100 MHz, DMSO-d_6): δ = 159.1, 135.4, 133.3, 127.0, 126.4, 124.9, 118.7, 117.7, 111.7, 47.8, 32.3, 26.6, 23.8, 21.2, 20.5 ppm; HRMS (ESI): *m/z* calcd for $C_{29}H_{32}N_4$: 437.2700 [$M + H^+$], found: 437.2703.

[2-(*o*-Methoxyphenyl)ethyl](*E*)-(6-methyl-2,3,4,9-tetrahydrocarbazol-1-ylidene)amine (**THCz-26**). Procedure A: **THCz-20b** (100 mg, 0.50 mmol), 2-(2methoxyphenyl)ethylamine (80.5 µL, 83.2 mg, 0.55 mmol), *p*TsOH (4.3 mg, 25 µmol) in PhH (10 mL), refluxed for 23 h. Usual workup gave 179 mg of brown sticky solid that after column chromatography (3-4% MeOH in CH_2Cl_2) afforded 112 mg (67 %) of **THCz-26** as a yellow solid. R_f: 0.28 (4 % MeOH in CH_2Cl_2); mp: 58-59 °C; ^{1}H NMR (400 MHz, $CDCl_3$): δ = 7.33-7.30 (m, 2H), 7.23-7.19 (m, 2H), 7.14-7.12 (m, 1H), 6.88-6.84 (m, 2H), 3.83 (s, 3H), 3.81-3.78 (m, 2H), 3.10-3.06 (m, 2H), 2.85-2.82 (m, 2H), 2.48-2.45 (m, 2H), 2.43 (s, 3H), 1.99-1.93 (m, 2H) ppm; ^{13}C NMR (100 MHz, MeOH-d_4): δ = 165.3, 159.1, 138.3, 131.8, 131.0, 130.4, 129.2, 128.3, 127.7, 126.7, 121.7, 120.6, 112.7, 111.5, 55.8, 50.0, 32.3, 24.3, 24.7, 21.9, 21.5 ppm; HRMS (ESI): *m/z* calcd for $C_{22}H_{24}N_2O$: 333.1961 [$M + H^+$], found: 333.1973.

[2-(*p*-Fluorophenyl)ethyl](*E*)-(6-methyl-2,3,4,9-tetrahydrocarbazol-1-ylidene)amine (**THCz-27**). Procedure A: **THCz-20b** (100 mg, 0.50 mmol), 4-fluorphenylethylamine (79 µL, 83.2 mg, 0.6 mmol), *p*TsOH (4.3 mg, 25 µmol) in PhH (10 mL), refluxed for 18 h. Usual workup gave 168 mg of brown sticky solid that after column chromatography (5 % MeOH in CH_2Cl_2) afforded 48 mg (30 %) of **THCz-27** as a yellow solid. R_f: 0.33 (5 % MeOH in CH_2Cl_2); mp: 46-49 °C; ^{1}H NMR (400 MHz, DMSO-d_6): δ = 10.88 (bs, 1H), 7.36-7.26 (m, 4H), 7.11-7.07 (m, 2H), 6.98 (d, 1H, J = 8.4 Hz), 3.72-3.69 (m, 2H), 2.95 (t, 2H, J = 7.2 Hz), 2.74 (t, 2H, J = 6.0 Hz), 2.47-2.44 (m, 2H), 2.35 (s, 3H), 1.90-1.87 (m, 2H) ppm; ^{13}C NMR (100 MHz, DMSO-d_6): δ = 160.8 (d, J_{CF} = 242 Hz), 159.9, 136.6, 135.5, 132.8, 130.6, (d, J_{CF} = 8 Hz) 127.2, 126.3, 125.3, 118.8, 118.4, 114.8 (d, J_{CF} = 21) Hz, 111.8, 51.4, 35.9, 26.5, 23.7, 21.1, 20.5 ppm; ^{19}F NMR (376 MHz, DMSO-d_6): δ = -117.2 ppm; HRMS (ESI): *m/z* calcd for $C_{21}H_{22}FN_2$: 321.1761 [$M + H^+$], found: 321.1740.

[2-(*o*-Methoxyphenyl)ethyl](6-methyl-2,3,4,9-tetrahydro-1*H*-carbazol-1-yl)amine (**THCz-29**). Procedure B: **THCz-26** (90 mg, 0.27 mmol) $NaBH_4$ (21 mg, 0.56 mmol) in MeOH (9 mL) and stirred for 10 min. Usual workup gave 90 mg pale yellow foamy solid that after column chromatography (1-3 % MeOH, 1 % Et_3N in CH_2Cl_2) afforded 80 mg (88 %) of **THCz-29** as an amorphous yellow solid. R_f: 0.31 (5 % MeOH in CH_2Cl_2); ^{1}H NMR (400 MHz, $CDCl_3$): δ = 8.08 (bs, 1H), 7.24-7.14 (m, 4H, partial overlap with solvent signal), 6.96-6.88 (m, 3H), 3.99-3.96 (m, 1H), 3.81 (s, 3H), 3.02-3.81 (m, 4H), 2.70-2.65 (m, 2H), 2.44 (s, 3H), 2.19-2.16 (m, 1H), 2.02-1.98 (m, 1H), 1.82-1.72 (m, 1H), 1.67-1.59 (m, 1H) ppm; ^{13}C NMR (100 MHz, $CDCl_3$): δ = 157.7, 136.5, 134.2, 130.6, 128.6, 128.2, 127.8, 127.6, 123.0, 120.6, 118.1, 110.8, 110.6, 110.5, 55.5, 52.3, 46.1, 31.5, 30.5, 21.9, 21.6, 21.1 ppm; HRMS (ESI): *m/z* calcd for $C_{22}H_{27}N_2O$: 335.2117 [$M + H^+$], found: 335.2128.

[2-(*p*-Fluorophenyl)ethyl](6-methyl-2,3,4,9-tetrahydro-1*H*-carbazol-1-yl)amine (**THCz-30**). Procedure C. **THCz-20b** (100 mg, 0.50 mmol), 4-fluorphenylethylamine (0.13, mL, 140 mg, 1.0 mmol), *p*TsOH (4.3 mg, 25 µmol) in PhH (20 mL), refluxed for 18 h. Usual workup gave 173 mg of brown sticky solid that was passed through a silica pad (3x8 cm; 3-5% MeOH in CH_2Cl_2) to afford 134 mg clear, dark yellow oil. The oil was dissolved in MeOH (20 mL) and $NaBH_4$ (38 mg, 1.0 mmol) was added. Stirred for 50 min. followed by usual workup to yield 133 mg pale brown solid that after purification by preparative HPLC afforded 108 mg (58 %) of **THCz-30** as a white powder. R_f: 0.26 (free base, 5 % MeOH in CH_2Cl_2); mp: 140-141 °C; ^{1}H NMR (400 MHz, $CDCl_3$): δ = 10.28 (bs, 1H), 8.67 (bs, 1H, HCOOH), 7.23-7.21 (m, 2H), 7.03-7.00 (m 2H), 6.96-6.88 (m, 3H), 4.46-4.43 (m, 1H), 3.00-2.85 (m, 4H), 2.68-2.65 (m, 2H), 2.40 (s, 3H), 2.22-2-17 (m, 1H), 2.02-1.95 (m, 2H), 1.78-1.73 (m, 1H) ppm; ^{13}C NMR (100 MHz, $CDCl_3$): δ = 169.1 (HCOOH), 162.0 (d, J_{CF} = 245 Hz), 135.1, 132.3, 132.2, 130.3 (d, J_{CF} = 8 Hz), 128.8, 126.7 (d, J_{CF} = 12 Hz), 124.7, 118.5, 115.7(d, J_{CF} = 22 Hz), 115.2, 111.5, 51.7, 44.3, 32.1, 25.8, 21.5, 21.4, 20.7 ppm; ^{19}F

NMR (376 MHz, $CDCl_3$): δ = -115.5 ppm; HRMS (ESI): *m/z* calcd for $C_{21}H_{24}FN_2$: 323.1918 [*M* + H^+], found: 323.1924.

1,3-Bis(6-methyl-2,3,4,9-tetrahydro-1*H*-carbazol-1-ylamino)propane (**THCz-31**). Procedure B: 23 (65.5 mg, 0.15 mmol), $NaBH_4$ (23 mg, 0.6 mmol), MeOH (10 mL). Stirred for 2 h. Usual workup gave 73 mg pale yellow solid that after column chromatography (4-6 % MeOH, 2 % Et_3N in CH_2Cl_2) afforded 52 mg (79 %) of **THCz-31** as a colourless solid. R_f: 0.05 (5 % MeOH in CH_2Cl_2); mp: slow dec. >120 °C; ^{1}H NMR (400 MHz, DMSO-d_6): δ = 10.45 (bs, 2H), 7.15-7.12 (m, 4H), 6.81 (d, 2H, *J* = 8 Hz), 3.84 (bs, 2H), 2.74-2.67 (m, 4H), 2.55 (bs, 4H), 2.34 (s, 6H), 2.00-1.90 (m, 4H), 1.73-1.61 (m, 6H) ppm; ^{13}C NMR (100 MHz, DMSO-d_6): δ = 136.8, 134.1, 127.0, 126.3, 122.0, 117.4, 110.7, 108.7, 51.6, 44.8, 44.7, 30.9, 29.4, 21.3, 20.8, 20.6 ppm; HRMS (ESI): *m/z* calcd for $C_{29}H_{37}N_4$: 441.3013 [*M* + H^+], found: 441.3015.

[(2-Pyridyl)methyl](*E*)-(6-methyl-2,3,4,9-tetrahydrocarbazol-1-ylidene)amine (**THCz-32**). Procedure A: **THCz-20b** (60 mg, 0.30 mmol), 2-(aminomethyl)pyridine (33.6 µL, 35.8 mg, 0.33 mmol), *p*TsOH (2.6 mg, 15 µmol) in PhH (10 mL), refluxed for 18 h. Usual workup gave 71 mg beige solid as a mixture of starting material and product. The mixture was again subjected to the reaction conditions and 80 µL of amine added. Refluxed for 14 h and cooled to RT. The formed precipitate was filtered off and washed with benzene (3x3 mL) and dried to afford 68 mg of white solid. The solid was dissolved in EtOAc and washed w. $NaHCO_3$ (sat. aq.), dried (Na_2SO_4) and evaporated to dryness to afford 55 mg (63 %) of **THCz-32** as a crème yellow solid. R_f: 0.15 (5 % MeOH in CH_2Cl_2); mp: dec. >240 °C; ^{1}H NMR (400 MHz, DMSO-d_6): δ = 10.94 (s, 1H), 8.54 (d, 2H, *J* = 6.0 Hz), 7.53 (d, 2H, *J* = 6.0 Hz), 7.31 (s, 1H), 7.27 (d, 1H, *J* = 8.4 Hz), 6.99 (dd, 1H, *J* = 1.6, 8.4 Hz), 4.71 (s, 2H), 2.81-2.78 (m, 2H), 2.67-2.63 (m, 2H), 2.37 (s, 3H), 2.05-1.99 (m, 2H) ppm; ^{13}C NMR (100 MHz, $DMSO_3$): δ = 160.7, 150.2, 149.4 (2C), 135.6, 133.0, 127.2, 126.3, 125.3, 123.0 (2C), 118.9, 118.6, 52.1, 27.1, 23.7, 21.2, 20.5 ppm; HRMS (ESI): *m/z* calcd for $C_{19}H_{20}N_3$: 290.1651 [*M* + H^+], found: 290.1642.

[(2-Pyridyl)methyl](6-methyl-2,3,4,9-tetrahydro-1*H*-carbazol-1-yl)amine (**THCz-33**). Procedure B: Imine **THCz-32** (40 mg, 0.14 mmol), $NaBH_4$ (10.5 mg, 0.28 mmol) in MeOH (4.7 mL). Stirred for 30 min. Usual workup gave 33 mg crème white solid that after column chromatography (4 % MeOH in CH_2Cl_2), afforded 28 mg (70 %) of **THCz-33** as a white solid. R_f: 0.18 (5 % MeOH in CH_2Cl_2); mp: 172-173 °C; ^{1}H NMR (400 MHz, $CDCl_3$): δ = 8.57 (d, 2H, *J* = 5.6 Hz), 8.21 (bs, 1H), 7.35 (d, 2H, *J* = 5.6 Hz), 7.27 (apparent s, 1H, overlap with solvent signal), 7. 22 (d, 1H, *J* = 8.4 Hz), 6.98 (d, 1H, *J* = 8.0 Hz), 4.02-3.98 (m, 2H), 3.88 (d, 1H, *J* = 14.8 Hz), 2.70-2.67 (m 2H), 2.44 (s, 3H), 2.32-2.27 (m, 1H), 2.09-2.04 (m, 1H), 1.82-1.75 (m, 1H), 1.71-1.63 (m, 2H) ppm; ^{13}C NMR (100 MHz, $CDCl_3$): δ = 150.0, 149.8, 135.7, 134.3, 128.5, 127.8, 123.4, 123.1, 118.2, 111.4, 110.6, 52.3, 49.0, 30.4, 21.9, 21.6, 21.1 ppm; HRMS (ESI): *m/z* calcd for $C_{19}H_{22}N_3$: 292.1808 [*M* + H^+], found: 292.1816.

[2-(2-Pyridyl)ethyl](6-methyl-2,3,4,9-tetrahydro-1*H*-carbazol-1-yl)amine (**THCz-34**). Procedure C: **THCz-20b** (100 mg, 0.50 mmol), 2-(2-aminoethyl)pyridine (90.2 µL, 92 mg, 0.75 mmol), *p*TsOH (4.3 mg, 25 µmol) in PhH (20 mL). Refluxed for 18 h. Usual workup gave 155 mg of orange, sticky solid that after column chromatography (4 % MeOH, 1% Et_3N in CH_2Cl_2) afforded 117 mg (77 %) of the intermediate imine as a yellow solid. R_f: 0.21 (6 % MeOH, 1.5 % Et_3N in CH_2Cl_2. The afforded imine (100 mg, 0.33 mmol) as dissolved in MeOH (11 mL), $NaBH_4$ (25 mg, 0.7 mmol) was added and stirred for 30 min. Usual workup gave 103 mg orange solid that after column chromatography (5-8 % MeOH in CH_2Cl_2) afforded 94 mg (93 %) of **THCz-34** as a pale yellow solid. R_f: 0.15 (3% MeOH in CH_2Cl_2); mp: 69-70 °C; ^{1}H NMR (400 MHz, $CDCl_3$): δ = 9.47, (bs, 1H), 8.55 (d, 1H, *J* = 4.8 Hz), 7.65-7.61 (m, 1H), 7.25 (s, 2H), 7.20-7.18 (m, 2H), 6.99-

6.96 (m, 1H), 4.20-4.18 (m, 1H), 3.27-3.05 (m, 4H), 2.70-2.67 (m, 2H), 2.43 (s, 3H), 2.22-2.16 (m, 1H), 2.04-2.01 (m, 1H), 1.87-1.73 (m, 2H) ppm; ^{13}C NMR (100 MHz, $CDCl_3$): δ = 160.0, 149.0, 137.0, 134.6, 134.0, 128.3, 127.5, 123.8, 123.5, 121.9, 118.1, 111.8, 111.0, 52.2, 45.3, 36.5, 29.5, 21.7, 21.6, 21.1 ppm; HRMS (ESI): *m/z* calcd for $C_{20}H_{24}N_3$: 306.1964 [M + H^+], found: 306.1971.

(Phenethyl)(6-methyl-2,3,4,9-tetrahydro-1*H*-carbazol-1-yl)amine (**THCz-36**). Procedure C: **THCz-20b** (50 mg, 0.25 mmol), 2-phenylethylamine (47.4 µL, 45.6 mg, 0.38 mmol), *p*TsOH (2.2 mg, 13 µmol) in PhH (10 mL), refluxed for 10. The crude afforded from usual workup was dissolved in MeOH (20 mL) and $NaBH_4$ (19 mg, 0.5 mmol) was added. Stirred for 10 min. before usual workup. The afforded residue was passed through a pad of silica (5 % MeOH in CH_2Cl_2) to afford 41 mg yellow sticky solid and subsequent purification by preparative HPLC gave 23 mg (30 %) of **THCz-36** as pale yellow solid. R_f: 0.33 (5 % MeOH in CH_2Cl_2); mp: 140-142 °C; ^{1}H NMR (600 MHz, $CDCl_3$): δ = 10.55 (s, 1H), 8.71 (bs, 1H, HCOOH), 7.30-7.27 (m, 4H), 7.24-7.21 (m, 1H), 7.13 (d, 2H), 7.01 (dd, 1H, J = 1.8, 8.4 Hz), 4.53 (t, 1H, J = 6.6 Hz), 3.10-2.97 (m, 4H), 2.72-2.70 (m, 2H), 2.45 (s, 3H), 2.26-2.24 (m, 1H), 2.08-2.04 (m, 2H), 1.81-1.75 (m, 1H) ppm; ^{13}C NMR (150 MHz, $CDCl_3$): δ = 169.2 (HCOOH), 136.8, 135.1, 128.9, 128.8, 128.6, 127.16, 127.15, 126.8, 124.5, 118.4, 114.9, 111.5, 51.6, 44.1, 33.1, 26.0, 21.61, 21.56, 20.7 ppm; HRMS (ESI): *m/z* calcd for $C_{21}H_{25}N_2$: 305.2021 [M + H^+], found: 305.2021.

(3-Phenylpropyl)(6-methyl-2,3,4,9-tetrahydro-1*H*-carbazol-1-yl)amine (*12*) (**THCz-37**). Procedure C: **THCz-20b** (50 mg, 0.25 mmol), 3-phenyl-1-propylamine (107 µL, 102 mg, 0.75 mmol) in PhH, refluxed for 23 h. Usual workup afforded a brown oil that was passed through a silica pad (4 % MeOH in CH_2Cl_2) to yield 52 mg of the intermediate imine as a yellow oil. The oil was dissolved in MeOH (15 mL), $NaBH_4$ (19 mg, 0.5 mmol) was added and stirred for 10 min. Usual workup and purification by column chromatography (4 % MeOH in CH_2Cl_2) afforded 37 mg (46%) **THCz-37** as a pale yellow amorphous solid. R_f: 0.31 (5 % MeOH in CH_2Cl_2; ^{1}H NMR (400 MHz, $CDCl_3$): δ = 8.42 (bs, 1H), 7.34-7.28 (m, 3H), 7.25-7.20 (m, 4H), 7.00 (dd, 1H, J = 1.6, 12 Hz), 4.01-3.98 (m, 1H), 2.90-2.83 (m, 1H), 2.78-2.66 (m, 5H), 2.47 (s, 3H), 2.42-2.19 (m, 1H), 2.06-2.00 (m, 1H), 1.95-1.86 (m, 2H), 1.81-1.75 (m, 1H), 1.70-1.64 (m, 1H) ppm; ^{13}C NMR (100 MHz, $CDCl_3$): δ = 141.9, 135.0, 134.3, 128.5, 128.4, 127.7, 126.0, 123.3, 118.2, 111.4, 110.7, 52.3, 45.3, 33.7, 31.7, 29.8, 21.8, 21.6, 21.0 ppm; HRMS (ESI): *m/z* calcd for $C_{22}H_{76}N_2$: 319.2168 [M + H^+], found: 319.2179.

(4-Phenylbutyl)(6-methyl-2,3,4,9-tetrahydro-1*H*-carbazol-1-yl)amine (**THCz-38**). Procedure C: **THCz-20b** (50 mg, 0.25 mmol), phenylbutylamine (59.5 µL, 56.2 mg, 0.38 mmol), *p*TsOH (2.2 mg, 13 µmol) in PhH (10 mL), refluxed for 10 h. The crude afforded from usual workup was dissolved in MeOH (20 mL), $NaBH_4$ (19 mg, 0.5 mmol) was added and stirred for 10 min. before usual workup. Purification by column chromatography (5 % MeOH in CH_2Cl_2) afforded 75 mg (90 %) of **THCz-38** as pale yellow amorphous solid. R_f: 0.28 (5 % MeOH in CH_2Cl_2); ^{1}H NMR (400 MHz, $CDCl_3$): δ = 8.84 (bs, 1H), 7.26-7.20 (m, 3H, overlap with solvent peak), 7.18-7.13 (m, 4H), 6.96 (dd, 1H, J = 1.6, 8.0 Hz), 4.63 (bs, 1H), 4.09-4.06 (m, 1H), 2.81-2.65 (m, 4H), 2.60-2.56 (m, 2H), 2.43 (s, 3H), 2.21-2.16 (m, 1H), 2.03-1.96 (m, 1H), 1.78-1.73 (m, 6H) ppm; ^{13}C NMR (100 MHz, $CDCl_3$): δ = 142.2, 134.4, 133.0, 128.46, 128.44, 128.43, 127.4, 125.9, 123.6, 118.2, 112.4, 110.9, 52.1, 45.1, 35.7, 29.14, 29.08, 28.8, 21.63, 21.57, 20.9 ppm; HRMS (ESI): *m/z* calcd for $C_{23}H_{29}N_2$: 333.2325 [M + H^+], found: 333.2335.

***p*-[2-(6-Methyl-2,3,4,9-tetrahydro-1*H*-carbazol-1-ylamino)ethyl]phenol** (**THCz-39**). Procedure C: **THCz-20b** (199.2 mg, 1.0 mmol), tyramine (151 mg, 1.1 mmol), *p*TsOH (8.6 mg, 50 µmol) in PhH (20 mL), refluxed for 20 h. Usual workup gave 274 mg of crude imine as yellow

solid. The crude was dissolved in MeOH (20 mL), $NaBH_4$ (76 mg, 2 mmol) was added and stirred for 90 min. before usual workup gave 245 mg pale orange solid. Column chromatography (5-10 % MeOH in CH_2Cl_2) afforded 99 mg (31 %) of **THCz-39** as a pale yellow foamy solid. R_f: 0.08 (5 % MeOH in CH_2Cl_2); mp: dec. > 70 °C ^{1}H NMR (600 MHz, $CDCl_3$): δ = 8.36 (s, 1H), 7.24 (s, 1H), 7.12 (d, 1H, *J* = 5.6 Hz), 7.03 (d, 2H, 5.6 Hz), 6.94 (d, 1H, *J* = 5.6 Hz), 6.73 (d, 2H, *J* = 5.6 Hz), 4.05-4.03 (m, 1H), 3.01-2.98 (m, 1H), 2.96-2.93 (m, 1H), 2.83-2.80 (m, 1H), 2.75-2.63 (m, 3H), 2.43 (s, 3H), 2.14-2.12 (m, 1H), 1.95-1.93 (m, 1H), 1.76-1.70 (m, 2H) ppm; ^{13}C NMR (150 MHz, $CDCl_3$): δ = 154.8, 134.9, 134.3, 131.1, 130.0, 128.4, 127.5, 123.3, 118.1, 116.0, 111.6, 110.7, 52.0, 46.7, 35.5, 29.6, 21.60, 21.59, 21.1 ppm; HRMS (ESI): *m/z* calcd for $C_{21}H_{25}N_2O$: 321.1961 [$M + H^+$], found: 321.1973.

***[2-(p*-Bromophenyl)ethyl](6-methyl-2,3,4,9-tetrahydro-1*H*-carbazol-1-yl)amine** (**THCz-40**). Procedure A: **THCz-20b** (200 mg, 1.00 mmol), 4-bromophenylethylamine (0.23 mL, 0.30 g, 1.50 mmol), *p*TsOH (8 mg, 50 µmol) in PhMe (30 mL) gave 487 mg red oil after usual work up. Purified by column chromatography (3 % MeOH in CH_2Cl_2) to afford 250 mg (65 %) of the imine as a red amorphous solid. R_f: 0.32 (5 % MeOH in CH_2Cl_2); ^{1}H NMR (400 MHz, $CDCl_3$): δ = 9.72 (bs, 1H), 7.41-7.37 (m, 2H), 7.35 (bs, 1H), 7.24 (d, 1H, *J* = 8.0 Hz), 7.13-7.09 (m, 3H), 3.78-3.75 (m, 2H), 3.01-2.98 (m, 2H), 2.58-2.82 (m, 2H), 2.48-2.45 (m, 5H), 2.04-1.98 (m, 2H) ppm; ^{13}C NMR (100 MHz, $CDCl_3$): δ = 161.3, 139.1, 136.0, 131.9, 131.5, 130.8, 129.0, 127.0, 126.9, 122.0, 120.1, 119.5, 111.5, 51.2, 36.6, 27.0, 24.0, 21.5, 21.0 ppm; HRMS (ESI): *m/z* calcd for $C_{21}H_{21}BrN_2$: 381.0961 [$M + H^+$], found: 381.0906. Procedure B: The afforded imine (186 mg, 0.49 mmol), $NaBH_4$ (37 mg, 0.98 mmol) in MeOH (20 mL). Stirred for 25 minutes. Usual workup gave 187 mg red/orange oil that after column chromatography (2% MeOH in CH_2Cl_2) afforded 171 mg (92 %) of **THCz-40** as red amorphous solid. R_f: 0.11 (3 % MeOH in CH_2Cl_2); ^{1}H NMR (400 MHz, DMSO-d_6): δ = 10.42 (s, 1H), 7.47-7.44 (m, 2H), 7.22-7.16 (m, 3H), 7.12 (s, 1H), 6.82 (dd, 1H, *J* = 1.6, 8.4 Hz), 3.86 (bs, 1H), 2.89-2.79 (m, 2H), 2.75.2-70 (m, 2H), 2.54 (bs, 2H), 2.34 (s, 3H), 1.95-1.92 (m, 2H), 1.68-1.66 (m, 2H) ppm; ^{13}C NMR (100 MHz, $CDCl_3$): δ = 161.3, 139.1, 136.0, 131.9, 131.5, 130.8, 129.0, 127.0, 126.9, 122.0, 120.1, 119.5, 111.5, 51.2, 36.6, 27.0, 24.0, 21.5, 21.0 ppm; HRMS (ESI): *m/z* calcd for $C_{21}H_{24}{}^{81}BrN_2$: 385.1096 [$M + H^+$], found: 385.1102.

[2-(*p*-Bromophenyl)ethyl](6-fluoro-2,3,4,9-tetrahydro-1*H*-carbazol-1-yl)amine (**THCz-41**). Procedure C: 6-Fluoro-2,3,4,9-tetrahydrocarbazol-1-one (*13*) (101.6 mg, 0.50 mmol), 4-bromophenylethylamine (116 µL, 150 mg, 0.75 mmol), *p*TsOH (4.3 mg, 25 µmol) in PhH (10 mL), refluxed overnight. Usual workup gave a yellow crude that was dissolved in MeOH (20 mL). $NaBH_4$ (37.8 mg, 1.0 mmol) was added and stirred for 10 min. Usual workup gave 197 mg pale brown solid, that was purified twice by column chromatography (2-3 % MeOH in CH_2Cl_2) to afford 147 mg (76 %) of **THCz-41** as a pale yellow amorphous solid. R_f: 0.35 (5 % MeOH in CH_2Cl_2); ^{1}H NMR (600 MHz, $CDCl_3$): δ = 8.01 (s, 1H), 7.44-7.42 (m, 2H), 7.16 (dd, 1H, *J* = 4.2, 7.2 Hz), 7.11-7.08 (m, 3H), 6.87 (dt, 1H, *J* = 1.2, 9.6 Hz), 3.96-3.94 (m, 1H), 3.00-2.91 (m, 2H), 2.83-2.72 (m, 1H), 2.69-2.63 (m, 3H), 2.21-2.17 (m, 1H), 2.02-2.01 (m, 1H), 1.80-1.76 (m, 1H), 1.61-1.57 (m, 1H) ppm; ^{13}C NMR (150 MHz, $CDCl_3$): δ = 157.7 (d, J_{CF} = 232 Hz), 139.3, 138.1, 132.2, 131.6, 130.7, 127.9 (d, J_{CF} = 10 Hz), 120.1, 111.5 (d, J_{CF} = 5 Hz), 111.3 (d, J_{CF} = 10 Hz), 109.5 (d, J_{CF} = 26 Hz), 103.3 (d, J_{CF} = 23 Hz), 52.6, 47.0, 36.6, 30.3, 21.9, 20.9 ppm; ^{19}F NMR (375 MHz, $CDCl_3$): -125.2 ppm; HRMS (ESI): *m/z* calcd for $C_{20}H_{21}{}^{81}BrFN_2$: 389.0846 [$M + H^+$], found: 389.0859.

1-[2-(*p*-Bromophenyl)ethylamino]-2,3,4,9-tetrahydro-1*H*-carbazole-6-carboxylic acid (**THCz-42**). I_2O_5 (1.86 g, 5.58 mmol) was added to a suspension of 6,7,8,9-tetrahydro-5*H*-carbazole-3-carboxylic acid (1.00 g, 4.65 mmol) in THF:H_2O (9.3 mL:37.2 mL). After stirring at

RT for 2 h, the reaction mixture was diluted with H_2O (150 mL) and extracted with EtOAc (5x100 mL). The combined organic phases were washed with $Na_2S_2O_3$ (5 % w/t aq.), dried ($MgSO_4$), filtered and concentrated to in vacuo to afford 982 mg (92 %) of 1-oxo-2,3,4,9-tetrahydrocarbazole-6-carboxylic acid as a brown/orange solid. ^{1}H NMR (400 MHz, DMSO-d_6): δ = 12.61 (bs, 1H), 11.95 (s, 1H), 8.35 (s, 1H), 7.88 (dd, 1H, *J* = 1.2, 6.0 Hz), 7.44 (d, 1H, *J* = 6.0 Hz), 3.01 (t, 2H, *J* = 4.0 Hz), 2.60-2.58 (m, 2H), 2.18-2.16 (m, 2H) ppm.

1-Oxo-2,3,4,9-tetrahydrocarbazole-6-carboxylic acid (115 mg, 0.50 mmol), 4-bromophenylethylamine (194 µL, 250 mg, 1.25 mmol), *p*TsOH (4.3 mg, 25 µmol) in PhH (10 mL), refluxed overnight. H_2O (5 mL) and EtOAc (10 mL) were added to the formed green/yellow suspension. The precipitate was filtered off and washed with EtOAc to afford 111 mg of crude imine. 100 mg was suspended in MeOH (20 mL) and $NaBH_4$ (37.8 mg, 1.0 mmol) was added. The suspension became a yellow solution within a few minutes and after 15 min NH_4Cl (sat aq.) was added and the volume was reduced in vacuo. The afforded solid had a low solubility and was suspended in H_2O and extracted with EtOAc (8x50 mL). The combined organic phases were dried ($MgSO_4$), filtered and concentrated *in vacuo* to afford 98 mg pale brown solid. Preparative HPLC and freeze drying from MeCN:H_2O (1:4) afforded 42 mg (20 %) of **THCz-42** as white solid. R_f: 0.10 (formate, 5 % MeOH in CH_2Cl_2); mp: 213-215 °C; ^{1}H NMR (400 MHz, DMSO-d_6): δ = 11.25 (s, 1H), 8.21 (s, 1H, HCOOH), 8.07 (s, 1H), 7.68 (dd, 1H, *J* = 1.6, 8.4 Hz), 7.48-7.46 (m, 2H), 7.36 (d, 1H, *J* = 8.4 Hz), 7.24-7.21 (m, 2H), 4.04 (bs, 1H), 3.01-2.88 (m, 2H), 2.85-2.74 (m, 2H), 2.67-2.64 (m, 2H), 2.07-1.96 (m, 2H), 1.83-1.69 (m, 2H) ppm; ^{13}C NMR (100 MHz, DMSO-d_6): δ = 168.5, 163.8 (HCOOH), 139.3, 138.5, 136.7, 131.2, 130.9, 126.2, 122.3, 120.8, 120.5, 119.1, 111.4, 110.8, 51.0, 47.4, 34.9, 28.6, 20.5, 20.1 ppm; HRMS (ESI): *m/z* calcd for $C_{21}H_{22}{}^{81}BrN_2O_2$: 415.0838 [$M + H^+$], found: 415.0850.

[2-(*p*-Bromophenyl)ethyl](6-cyclohexyl-2,3,4,9-tetrahydro-1*H*-carbazol-1-yl)amine (THCz-43). Procedure C: **THCz-20a** (65 mg, 0.24 mmol), 4-bromophenylethylamine (56.6 µL, 73 mg, 0.36 mmol), *p*TsOH (2.1 mg, 12 µmol) in benzene (10 mL), refluxed overnight. The crude afforded from usual workup was dissolved in MeOH (20 mL) and $NaBH_4$ (18 mg, 0.49 mmol) was added and stirred for 10 min. before usual workup afforded 56 mg pale brown solid. Purification by column chromatography (2 % MeOH in CH_2Cl_2) and subsequent preparative HPLC yielded 20 mg (16 %) of **THCz-43** as pale yellow solid. R_f: 0.30 (free base, 5 % MeOH in CH_2Cl_2); mp: 138-140 °C; ^{1}H NMR (600 MHz, DMSO-d_6): δ = 10.50 (s, 1H), 8.18 (s, 1H, HCOOH), 7.47-7.45 (m, 2H), 7.22-7.18 (m, 3H), 7.15 (s, 1H), 6.89 (dd, 1H, *J* = 1.8, 8.4 Hz), 3.93 (bs, 1H), 2.90-2.86 (m, 2H), 2.76-2.73 (m, 2H), 2.58-2.52 (m, 3H), 1.95-1.93 (m, 2H), 1.80-1.70 (m, 7H), 1.44-1.36 (m, 4H), 1.25-1.23 (m, 1H) ppm; ^{13}C NMR (150 MHz, DMSO-d_6): δ = 163.5 (HCOOH), 139.6, 137.5, 135.7, 134.5, 131.1, 130.9, 126.8, 120.2, 119.0, 115.0, 110.7, 109.5, 51.2, 47.5, 44.1, 40.1, 35.4, 34.9, 29.1, 26.6, 25.8, 20.8 ppm (two carbon resonances not resolved); HRMS (ESI): *m/z* calcd for $C_{26}H_{32}{}^{81}BrN_2$: 453.1723 [$M + H^+$], found: 453.1717.

[2-(*p*-Bromophenyl)ethyl](6-phenyl-2,3,4,9-tetrahydro-1*H*-carbazol-1-yl)amine (THCz-44). Procedure C. **THCz-12b** (80 mg, 0.31 mmol), 4-bromophenylethylamine (71.2 µL, 91.9 mg, 0.46 mmol), *p*TsOH (2.6 mg, 15 µmol) in PhH (15 mL), refluxed for 24 h before usual workup gave 174 mg apricot solid. The solid was dissolved in MeOH (20 mL), $NaBH_4$ (23 mg, 0.61 mmol) was added and stirred for 25 min. Usual workup gave 147 mg pink solid that after purification by preparative HPLC afforded 74 mg (54 %) of **THCz-44** as a crème white solid. R_f: 0.28 (free base, 5 % MeOH in CH_2Cl_2); mp: 164-165 °C; ^{1}H NMR (400 MHz, $CDCl_3$): δ = 10.57 (s, 1H), 8.67 (s, 1H, HCOOH), 7.61-7.57 (m, 3H), 7.44-7.38 (m, 4H), 7.34-7.28 (m, 3H), 6.93 (d, 2H, *J* = 8.4 Hz), 4.45 (t, 1H, *J* = 6.4 Hz), 3.06-2.80 (m, 4H), 2.72 (t, 2H, *J* = 5.6 Hz), 2.24-2.22 (m, 1H), 2.20-2.03

(m, 2H), 1.83-1.73 (m, 1H) ppm; ^{13}C NMR (100 MHz, $CDCl_3$): δ = 169.1 (HCOOH), 142.4, 136.3, 135.6, 133.1, 132.0, 130.5, 128.8, 127.6, 127.4, 127.1, 126.5, 122.8, 121.2, 117.3, 115.9, 112.0, 51.7, 44.3, 32.4, 25.9, 21.4, 20.72 ppm; HRMS (ESI): *m/z* calcd for $C_{26}H_{26}{}^{81}BrN_2$: 447.1253 [*M* + H^+], found: 447.1250.

[2-(*o*-Bromophenyl)ethyl](6-methyl-2,3,4,9-tetrahydro-1*H*-carbazol-1-yl)amine (**THCz-45**). Procedure C. 2,3,4,9-tetrahydrocarbazol-1-one (100 mg, 0.54 mmol), 4-bromophenylethylamine (126 µL, 162 mg, 0.81 mmol), *p*TsOH (4.7 mg, 27 µmol) in PhMe (20 mL), refluxed for 14 h. Usual workup gave 248 mg yellow sticky solid that was dissolved in MeOH (20 mL). $NaBH_4$ (40.8 mg, 1.1 mmol) was added and stirred for 20 min. Usual workup afforded 243 mg yellow oil. 80 mg of this oil was purified by preparative HPLC to afford 38 mg of **THCz-45** as a crème white solid. R_f: 0.29 (free base, 5 % MeOH in CH_2Cl_2); mp: 72-77 °C; ^{1}H NMR (400 MHz, $CDCl_3$): δ =10.44 (bs, 1H), 8.61 (s, 1H, HCOOH), 7.44 (d, 1H, *J* = 7.8 Hz), 7.36-7.33 (m, 3H), 7.16-7.12 (m, 1H), 7.07-7.03 (m, 1H), 6.96-6.94 (m, 2H), 4.49-4-46 (m, 1H), 3.06-2.83 (m, 4H), 2.70 (t, 2H, *J* = 6.0 Hz), 2.25-2.18 (m, 1H), 2.05-1.96 (m, 2H), 1.81-1.73 (m, 1H) ppm; ^{13}C NMR (100 MHz, DMSO-d_6): δ = 164.7 (HCOOH), 138.8, 136.0, 133.3, 131.2, 131.0, 126.5, 121.1, 119.3, 118.3, 118.0, 111.2, 110.7, 51.0, 46.8, 34.1, 28.0, 20.6, 20.0 ppm; HRMS (ESI): *m/z* calcd for $C_{20}H_{22}{}^{81}BrN_2$: 371.0940 [*M* + H^+], found: 371.0948.

[2-(*p*-Chlorophenyl)ethyl](6-methyl-2,3,4,9-tetrahydro-1*H*-carbazol-1-yl)amine (**THCz-46**). Procedure C: **THCz-20b** (50 mg, 0.25 mmol), 2-(4-chlorophenyl)ethylamine (52.7 µL, 58.6 mg, 0.38 mmol), *p*TsOH (2.2 mg, 13 µmol) in PhH (10 mL), refluxed for 14 h. The crude afforded from usual workup was dissolved in MeOH (15 mL), $NaBH_4$ (19 mg, 0.5 mmol) was added. Stirred for 25 min. before usual workup. The afforded residue was passed through a silica pad (5 % MeOH in CH_2Cl_2) to afford 33 mg pale yellow amorphous solid that after purification by preparative HPLC afforded 18 mg (21 %) of **THCz-46** as a pale yellow powder. R_f: 0.28 (free base, 5 % MeOH in CH_2Cl_2); mp: 138-139 °C; ^{1}H NMR (600 MHz, $CDCl_3$): δ = 10.26 (bs, 1H), 8.66 (s, 1H, HCOOH), 7.22-7.17 (m, 4H), 6.98-6.94 (m, 3H), 4.44-4.42 (m, 1H), 2.99-2.95 (m, 1H), 2.94-2.82 (m, 3H), 2.67-2.65 (m, 2H), 2.40 (s, 3H), 2.20-2.18 (m, 1H), 2.04-1.95 (m, 2H), 1.76-1.73 (m, 1H) ppm; ^{13}C NMR (150 MHz, $CDCl_3$): δ = 169.2 (HCOOH), 135.4, 135.0, 133.0, 130.1, 129.0, 128.7, 127.6, 126.8, 124.5, 118.4, 114.7, 111.4, 51.8, 44.3, 32.6, 26.2, 21.6, 21.5, 20.7 ppm; HRMS (ESI): *m/z* calcd for $C_{21}H_{24}ClN_2$: 339.1622 [*M* + H^+], found: 339.1619.

[2-(*p*-Tolyl)ethyl](6-methyl-2,3,4,9-tetrahydro-1*H*-carbazol-1-yl)amine (**THCz-47**). Procedure C: **THCz-20b** (50 mg, 0.25 mmol), 2-(p-tolyl)ethylamine (54.7 µL, 50.9 mg, 0.38 mmol), *p*TsOH (2.2 mg, 13 µmol) in PhH (10 mL), refluxed for 14 h. The crude afforded from usual workup was dissolved in MeOH (20 mL), $NaBH_4$ (19 mg, 0.5 mmol) was added and stirred for 10 min. before usual workup. The afforded residue was passed through a silica pad (5 % MeOH in CH_2Cl_2) to afford 36 mg pale yellow amorphous solid that after purification by preparative HPLC yielded 13 mg (16 %) of **THCz-47** as pale yellow powder. R_f: 0.25 (free base, 5 % MeOH in CH_2Cl_2); mp: 148-149 °C; ^{1}H NMR (600 MHz, $CDCl_3$): δ = 10.54 (bs, 1H), 8.66, (s, 1H, HCOOH), 7.25 (d, 1H, *J* = 8.4 Hz), 7.22 (s, 1H), 7.04-7.-03 (m, 2H), 6.98-6.96 (m, 3H), 4.50-4.47 (m, 1H), 3.02-2.99 (m, 1H), 2.97-2.88 (m, 3H), 2.67-2.66 (m, 2H), 2.41 (s, 3H), 2.26 (s, 3H), 2.21-2.18 (m, 1H), 2.03-1.97 (m, 2H), 1.75-1.72 (m, 1H) ppm; ^{13}C NMR (150 MHz, $CDCl_3$): δ = 169.2 (HCCOH), 136.8, 135.1, 133.7, 129.6, 128.64, 128.58, 127.3, 126.8, 124.4, 118.4, 114.8, 111.5, 51.6, 44.1, 32.7, 26.1, 21.64, 21.56, 21.1, 20.8 ppm; HRMS (ESI): *m/z* calcd for $C_{22}H_{27}N_2$: 319.2168 [*M* + H^+], found: 319.2182.

[2-(*p*-Methoxyphenyl)ethyl](6-methyl-2,3,4,9-tetrahydro-1*H*-carbazol-1-yl)amine (**THCz-48**). Procedure C: **THCz-20b** (100 mg, 0.50 mmol), 2-(4-methoxyphenyl)ethylamine (110 µL, 114

mg, 0.75 mmol), *p*TsOH (4.3 mg, 25 µmol) in PhMe (20 mL), refluxed for 14 h. The crude afforded from usual workup was dissolved in MeOH (20 mL) and $NaBH_4$ (19 mg, 0.5 mmol) was added. Stirred for 10 min. before usual workup afforded 228 mg brown oil. The oil was passed through a silica pad (elute with 5 % MeOH in CH_2Cl_2) to yield 91 mg clear brown/orange oil that after purification by preparative HPLC gave 71 mg (37 %) of **THCz-48** as pale yellow powder. R_f: 0.23 (5 % MeOH in CH_2Cl_2); mp: 145-146 °C; ^{1}H NMR (600 MHz, $CDCl_3$): δ = 10.59 (s, 1H), 8.67 (s, 1H, HCOOH), 7.25 (d, 1H, partial overlap with $CHCl_3$), 7.22 (s, 1H), 7.00-6.96 (m, 3H), 6.75 (d, 2H, *J* = 8.4 Hz), 4.89 (t, 1H, *J* = 7.2 Hz), 3.72 (s, 3H), 3.02-2.99 (m, 1H), 2.94-2.85 (m, 3H), 2.67 (bs, 2H), 2.41 (s, 3H), 2.22-2.19 (m, 1H), 2.02-1.97 (m, 2H), 1.76-1.73 (m, 1H) ppm; ^{13}C NMR (150 MHz, $CDCl_3$): δ = 169.2 (HCOOH), 158.8, 135.2, 129.8, 128.7, 128.6, 127.2, 126.8, 124.5, 118.4, 114.9, 114.3, 111.5, 55.4, 51.6, 44.2, 32.2, 26.0, 21.62, 21.56, 20.7 ppm; HRMS (ESI): *m/z* calcd for $C_{22}H_{27}N_2O$: 335.2117 [$M + H^+$], found: 335.2130.

[2-(*m*-Bromophenyl)ethyl](6-methyl-2,3,4,9-tetrahydro-1*H*-carbazol-1-yl)amine (**THCz-49**). Procedure C: **THCz-20b** (100 mg, 0.50 mmol), 3-bromophenylethylamine (107.2 µL, 150.7 mg, 0.75 mmol), *p*TsOH (4.3 mg, 25 µmol) in PhMe (15 mL). Refluxed for 24 h and usual workup gave red oil that was dissolved in MeOH (20 mL). $NaBH_4$ (37.8 mg, 1.0 mmol) was added, stirred for 55 min. and usual workup afforded a pale red solid that was passed through a silica pad (3x6 cm, 3 % MeOH in CH_2Cl_2) to yield 142 mg red oil. Subsequent purification by preparative HPLC afforded 108 mg (56 %) of **THCz-49** as a crème white solid. R_f: 0.27 (free base, 5 % MeOH in CH_2Cl_2); mp: 122-123 °C; ^{1}H NMR (400 MHz, $CDCl_3$): δ = 10.35 (s, 1H), 8.65 (s, 1H, HCOOH), 7.32 (d, 1H, *J* = 8 Hz), 7.24-7.20 (m, 3H), 7.08 (t, 1H, *J* = 8 Hz), 6.98-6.94 (m, 2H), 4.47-4.44 (m, 1H), 3.04-2.78 (m, 4H), 2.67 (t, 2H, *J* = 6 Hz), 2.38 (s, 3H), 2.22-2.17 (m, 1H), 2.06-1.96 (m, 2H), 1.81-1.73 (m, 1H) ppm; ^{13}C NMR (100 MHz, $CDCl_3$): δ = 164.3 (HCOOH), 142.6, 134.3, 134.1, 131.4, 130.5, 129.0, 127.8, 126.8, 126.6, 122.6, 121.7, 117.6, 110.9, 109.9, 51.1, 47.1, 34.6, 28.4, 21.2, 20.7, 20.1 ppm; HRMS (ESI): *m/z* calcd for $C_{21}H_{24}{}^{81}BrN_2$: 385.1096 [$M + H^+$], found: 385.1101.

[2-(*o*-Bromophenyl)ethyl](6-methyl-2,3,4,9-tetrahydro-1*H*-carbazol-1-yl)amine (**THCz-50**). Procedure C: **THCz-20b** (100 mg, 0.50 mmol), 2-bromophenylethylamine (107.9 µL, 150.7 mg, 0.75 mmol), *p*TsOH (4.3 mg, 25 µmol) in PhMe (15 mL), refluxed for 24 h. Usual workup gave 246 mg red/brown sticky solid that was suspended in MeOH (20 mL). $NaBH_4$ (37.8 mg, 1.0 mmol) was added and the suspension slowly turned into a yellow solution. Stirred for 25 min. before usual workup afforded 176 mg brown solid that was passed through a silica pad (3x6 cm, 3 % MeOH in CH_2Cl_2) to yield 134 mg red oil that in turn was purified by preparative HPLC to afford 117 mg (56 %) of **THCz-50** as a crème white solid. R_f: 0.26 (free base, 5 % MeOH in CH_2Cl_2); mp: 156-157 °C; ^{1}H NMR (400 MHz, DMSO-d_6): δ = 10.81 (s, 1H), 8.27 (s, 1H, HOOCH), 7.59 (dd, 1H, *J* = 1.2, 8.0 Hz), 7.40 (dd, 1H, *J* = 2.0, 7.6 Hz), 7.35-7.31 (m, 1H), 7.20-7-14 (m, 3H), 6.86 (dd, 1H, *J* = 2.0, 8.4 Hz), 4.10-4.08 (m, 1H), 2.99-2.90 (m, 4H), 2.61-2.54 (m, 2H), 2.35 (s, 3H), 2.02-1.96 (m 2H), 1.85-1.79 (m, 1H), 1.74-1-72 (m, 1H) ppm; ^{13}C NMR (100 MHz, DMSO-d_6): δ = 164.4 (HCOOH), 138.7, 134.3, 134.1, 132.5, 131.0, 128.4, 127.9, 126.8, 126.6, 123.8, 122.5, 117.6, 110.9, 109.9, 51.1, 45.7, 35.5, 28.5, 21.3, 20.7, 20.2 ppm; HRMS (ESI): *m/z* calcd for $C_{21}H_{24}{}^{81}BrN_2$: 385.1096 [$M + H^+$], found: 385.1109.

(+)-(R)-N-(4-bromophenethyl)-6-chloro-2,3,4,9-tetrahydro-1H-carbazol-1-amine (AL682). (R)-6-chloro-2,3,4,9-tetrahydro-1H-carbazol-1-amine (31 mg, 0.14 mmol, prepared according to reference (*14*) and 1-bromo-4-(2-bromoethyl)benzene (21 µl, 0.14 mmol) were dissolved in DMF (1.1 mL) and stirred at 60 °C for 3 days. The mixture was concentrated and purified using column chromatography on silica gel (3 % MeOH in CH_2Cl_2) to afford 12 mg (21 %) of AL682 as a brown

solid; $[\alpha]_D$ 28 (c, 1.00, MeOH); ^{1}H NMR (400 MHz, MeOH-*d4*): δ = 7.42 (d, 2H, *J*, = 8.2 Hz), 7.34 (d, 1H, *J* = 1.7 Hz), 7.23 (d, 1H, *J* = 8.7 Hz), 7.15 (d, 2H, *J* = 8.2 Hz), 7.00 (dd, 1H, *J* = 8.7, 1.7 Hz), 4.00-3.94 (m, 1H), 2.99-2.90 (m, 2H), 2.84-2.75 (m, 2H), 2.68-2.60 (m, 2H), 2.12-1.96 (m, 2H), 1.88-1.73 (m, 2H) ppm; ^{13}C NMR (100 MHz, MeOD-*d4*): δ = 139.0, 136.4, 134.7, 131.2, 130.3, 128.2, 123.9, 120.9, 119.6, 117.0, 111.6, 110.5, 51.4, 35.2, 29.0, 20.4, 20.4 ppm.

Separation of enantiomers

(-)-(S)-6-cyclohexyl-N-phenethyl-2,3,4,9-tetrahydro-1H-carbazol-1-amine ((-)-(S)-THCz-1) and **(+)-(R)-6-cyclohexyl-N-phenethyl-2,3,4,9-tetrahydro-1H-carbazol-1-amine ((+)-(R)-THCz-1)**.

The racemic compound (2.5 mg) was dissolved in hexane:isopropanol 95:5 (0.2 mL) and the enantiomers were separated using a CHIRALPAK IA column (particle size 5 µm, 10 mm x 250 mm, hexane:isopropanol 95:5, 4 mL / min). This was repeated until sufficient amounts of each enantiomer was obtained. ^{1}H NMR and ^{13}C NMR for both enantiomers identical to the racemic compound. Enantiomeric ratios were analysed using a CHIRACEL 0D-H column (hexane:isopropanol 95:5, 1 mL / min). **(-)-(S)-THCz-1** eluted after 10 min and **(+)-(R)-THCz-1** eluted after 14 min. **(-)-(S)-THCz-1**: $[\alpha]_D$ -15 (c, 0.60, MeOH); enantiomeric ratio better than 99:1. **(+)-(R)-THCz-1**: $[\alpha]_D$ +13 (c, 0.55, MeOH); enantiomeric ratio better than 99:1.

(-)-(S)-*p*-[2-(6-Methyl-2,3,4,9-tetrahydro-1*H*-carbazol-1-ylamino)ethyl]phenol ((-)-(S)-THCz-39) and **(+)-(R)-*p*-[2-(6-Methyl-2,3,4,9-tetrahydro-1*H*-carbazol-1-ylamino)ethyl]phenol ((+)-(R)-THCz-39).**

The racemic compound (2.5 mg) was dissolved in hexane:isopropanol 88:12 (0.2 mL) and the enantiomers were separated using a CHIRALPAK IA column (particle size 5 µm, 10 mm x 250 mm, hexane:isopropanol 88:12, 4 mL / min). This was repeated until sufficient amounts of each enantiomer was obtained. ^{1}H NMR and ^{13}C NMR for both enantiomers identical to the racemic compound. Enantiomeric ratios were analysed using a CHIRACEL 0D-H column (hexane:isopropanol 90:10, 1 mL / min). **(-)-(S)-THCz-39** eluted after 31 min and **(+)-(R)-THCz-39** eluted after 41 min. **(-)-(S)-THCz-39**: $[\alpha]_D$ -1 (c, 0.55, MeOH); enantiomeric ratio better than 99:1. **(+)-(R)-THCz-39**: $[\alpha]_D$ +1 (c, 0.53, MeOH); enantiomeric ratio better than 99:1.

(-)-(S)-*p*-Bromophenyl)ethyl](6-methyl-2,3,4,9-tetrahydro-1*H*-carbazol-1-yl)amine ((-)-(S)-THCz-40) and **(+)-(R)-*p*-Bromophenyl)ethyl](6-methyl-2,3,4,9-tetrahydro-1*H*-carbazol-1-yl)amine ((+)-(R)-THCz-40).**

The racemic compound (2.5 mg) was dissolved in hexane:isopropanol 95:5 (0.2 mL) and the enantiomers were separated using a CHIRALPAK IA column (particle size 5 µm, 10 mm x 250 mm, hexane:isopropanol 95:5, 4 mL / min). This was repeated until sufficient amounts of each enantiomer was obtained. ^{1}H NMR and ^{13}C NMR for both enantiomers identical to the racemic compound. Enantiomeric ratios were analysed using a CHIRACEL 0D-H column (hexane:isopropanol 95:5, 1 mL/min). **(-)-(S)-THCz-40** eluted after 18 min and **(+)-(R)-THCz-40** eluted after 26 min. **(-)-(S)-THCz-40**: $[\alpha]_D$ -13 (c, 0.51, MeOH); enantiomeric ratio better than 99:1. **(+)-(R)-THCz-40**: $[\alpha]_D$ +14 (c, 0.69, MeOH); enantiomeric ratio better than 99:1.

Circular dichroism spectroscopy for determination of absolute configuration

To determine the absolute optical rotation of the compounds, CD spectra were recorded in the near- and far-UV range between 195 nm – 400 nm using a Jasco J-720 Spectropolarimeter (Japan). The sample concentration for all experiments was ~0.1 mg / mL, using samples dissolved in pure methanol. Spectra were acquired at 20 °C using an average of three scans, a 0.1 cm quartz cuvette

and a bandwidth of 2 nm with a subtracted methanol background. The scanning speed was set to 50 nm / s. Our conclusion after comparing compounds to the stereoselectively prepared AL682 is that for all compounds the (+)-enantiomer corresponds to absolute configuration = R and the (-)-enantiomer corresponds to absolute configuration = S.

Supplementary Information to Tables S1-S3

Extended description of the Structure activity Relationship (SAR) investigation

Supplementary information to Table S1. Central core scaffold investigation

The first synthesized analogs aimed to investigate the influence of the central core scaffold, that was shared between the initial high throughput screen (HTS) hit compounds THCz-1, -2 and -3, which only differed in the substituents at R^1 and R^2 (Figure 1A and Table S1). No growth inhibitory activity (THCz-5, -10, -11, and -17), or only effects upon treatment with high micromolar concentrations (THCz-6) were recorded for analogs that lacked the diamino moiety by either a replacement of the nitrogen with an oxygen in position X or R^2 (Table S1). Compound THCz-6 enabled a direct comparison with the screening hit compound THCz-2 and the prominent reduction in activity indicated that the amine group in position X (Table 2) was crucial. Additionally, the comparison of the antibacterial activity of THCz-5 versus THCz-19 led to the conclusion that the replacement of an amine with an ether in position R2 rendered the compounds inactive. The imino analogs, THCz-26 and -27 (Table S1) were also only moderately active compared to the corresponding amino compounds THCz-29 and -30 (Table S1). Combined these observations revealed that the diamino moiety essentially affected the antibacterial activity.

Supplementary information to Table S2. Investigation of modifications in R^2

A sterically demanding substituent in position R^2 was vital for bactericidal activity since THCz-24 with an N-propyl group lacked such (Table S2). It was not possible to increase the anti-pneumococcal activity by introducing another 1-amino substituted THCz motive in R^2 (THCz-31) yet also for the corresponding inactive imino analog THCz-23 these modifications had unfavourable effects on toxicity.

Despite the presence of the diamino moiety derivate THCz-33 was similarly inactive as the corresponding imine THCz-32 (Table S2). The reduced activity could be attributable to the proximity of a pyridyl group to the amine in R^2 which may compete with the protonation of the central moiety. Alternatively, inclusion of a triad of basic nitrogen in proximity could convey new attributes for the molecule such as metal chelating properties. Indeed, THCz-34 with the pyridyl group one carbon further away from the central core as compared to THCz-33 displayed moderate activity. Also, THCz-35 with a phenyl in the same position as the pyridyl in THCz-33, displayed moderate activity (vs no activity of THCz-33) further demonstrating the negative impact of the pyridyl group on activity. Furthermore, a minimum chain length of two carbons in R^2 was required for activity, since reducing the chain length to one carbon (THCz-36 vs -35) had a negative effect on the MIC, while increasing the length (THCz-37 and -38 vs -36) did neither affect activity nor cytotoxicity.

Compared to the original screening hits the MIC of compounds THCz-36 to -38 increased 2-fold, which went in hand with a reduction in toxicity towards A549 cells. Similar observations were made for compounds THCz-30, -39 and -40 with substitutions on the para-position of the phenyl ring in R^2.

Supplementary information to Table S3. Extended investigation of modifications in R^1 and R^2

From the previous SAR evaluations (Tables S1-S2) we got the indication that also modifications in R^1 could influence activity and cytotoxicity of the THCz compounds. Compounds THCz-19 and -36 which shared the substituent in R^2 with the initial hit compound THCz-1 but differed in R^1 (where THCz-1 had a cyclohexyl group while THCz-19 was unsubstituted and THCz-36 had a methyl group) had a 2-fold increase in MIC and conveyed lower cytotoxicity compared to THCz-1. Therefore, the role of substituents in R^1 was further investigated using THCz-40 as the starting point and the evaluation of modifications within the phenyl group in R^2 was further expanded (Table S3).

Sterically demanding hydrophobic residues in R^1, exemplified by the phenyl and cyclohexyl group in THCz-43 and -44 were unfavourable since they resulted in similar bactericidal activity as THCz-40 but had an adverse effect on toxicity, which was comparable to the toxicity of the initial screening hit compounds. A fluorine substituent in R^1 as in THCz-41 increased the MIC 2-fold in comparison to THCz-40 but displayed comparable cytotoxic properties, whereas a carboxyl group (THCz-42) in R^1 abolished the bactericidal activity, which could indicate a negative impact on activity of an anionic group in this position. Overall, the investigated uncharged modifications in R^1 (THCz-19, -45) retained the antibacterial activity and cytotoxic characteristics of THCz-40 The higher activity and toxicity of the initial screening hit compound THCz-3, which has a methyl group in R^1 might therefore be accountable to the adamantly group in R^2.

From the preceding SAR investigations (Table S2) we observed though that a sterically demanding group in R^2 was required for antibacterial activity and continued therefore to investigate substitutions in the 2-phenylethylamine backbone. A fluorine (THCz-30), bromine (THCz-40) or a methyl group (THCz-47) substitution in the para-position of the phenyl ring in R^2 had similar antibacterial activity and cytotoxicity as an unsubstituted position (THCz-36), whereas chlorine (THCz-46) in the para-position resulted in retained antibacterial activity but elevated toxicity. A methoxy group (THCz-48) in the para-position however decreased the antibacterial activity, similarly as the substitution with a hydroxyl group in this position (THCz-39). Positioning the methoxy group in the ortho-position (THCz-29) did increase antibacterial activity in relation to the initial screening hit activity, but also resulted in increased cytotoxicity. Changing the bromo substituent from the para- (THCz-40) to the meta- (THCz-49) position of the phenyl ring in R^2 was unfavourable for cytotoxicity and did not increase antibacterial activity. Substituting the ortho-position with a bromine (THCz-50) did result in increased antibacterial activity and toxicity. Substitutions in the para-position are therefore preferred.

Due to the hydrophobic nature of the THCz-compounds we tested a subset of analogs (THCz-1,-29,-30,-36,-37,-38,-39,-40,-43,-44,-45,-46,-47,-48,-49; Tables S1-S3) for their antibacterial activity in presence of 10% fetal bovine serum (FBS) to mimic cell culture conditions, resulting in an overall 4x increase of the MIC. We could therefore exclude that varying plasma protein binding tendencies were accountable for differences in cytotoxicity of the investigated THCz derivates.

Supplementary Figures

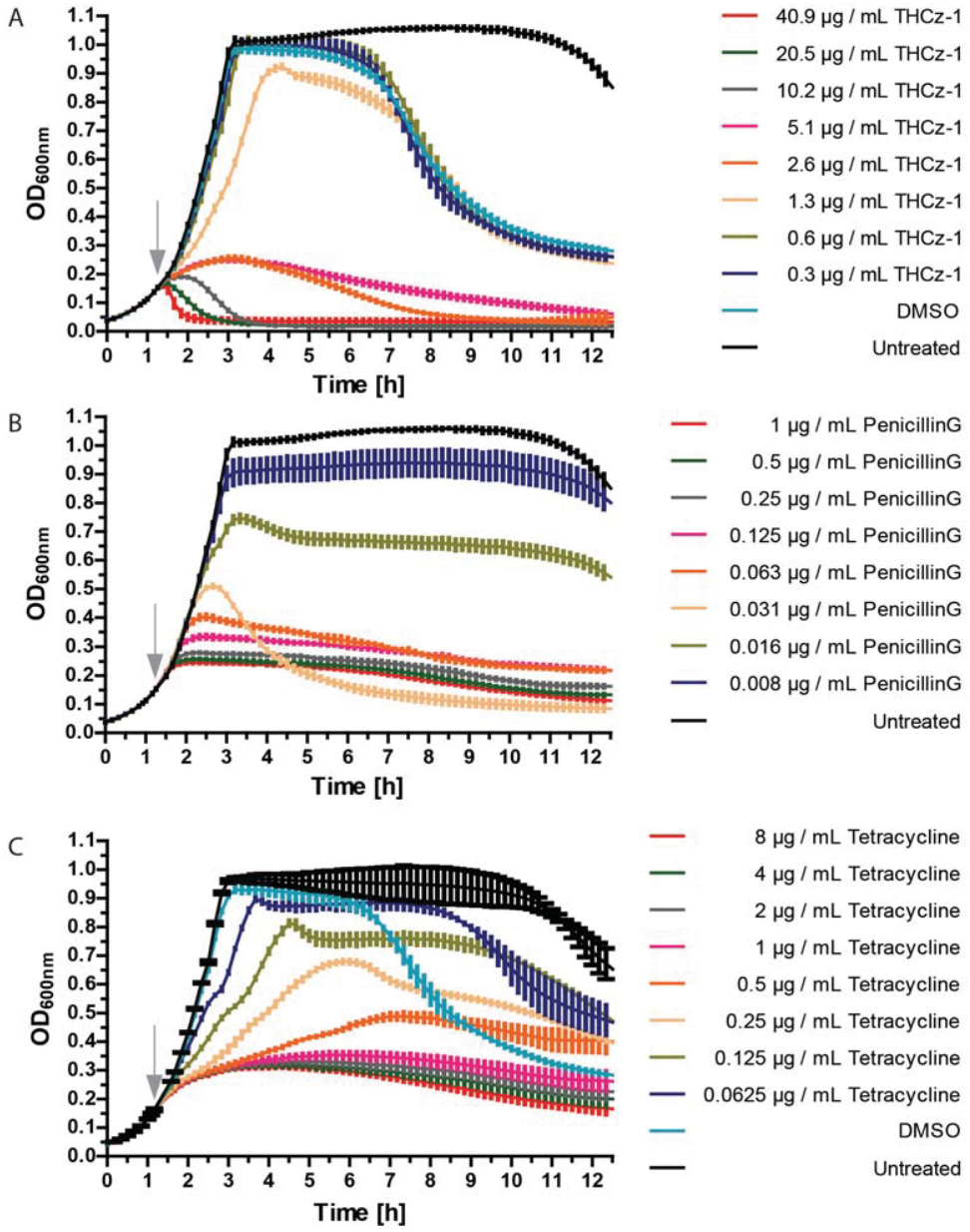

Figure S1. Dose-response curves of THCz-1 treated log-phase grown *S. pneumoniae*. *S. pneumoniae* T4 wild type challenged in early log phase with a titration of **(A)** THCz-1, **(B)** penicillin G and **(C)** tetracycline. Average values are plotted, and error bars display standard deviations of triplicate treatments in one experiment that are repeatable in an independent experiment.

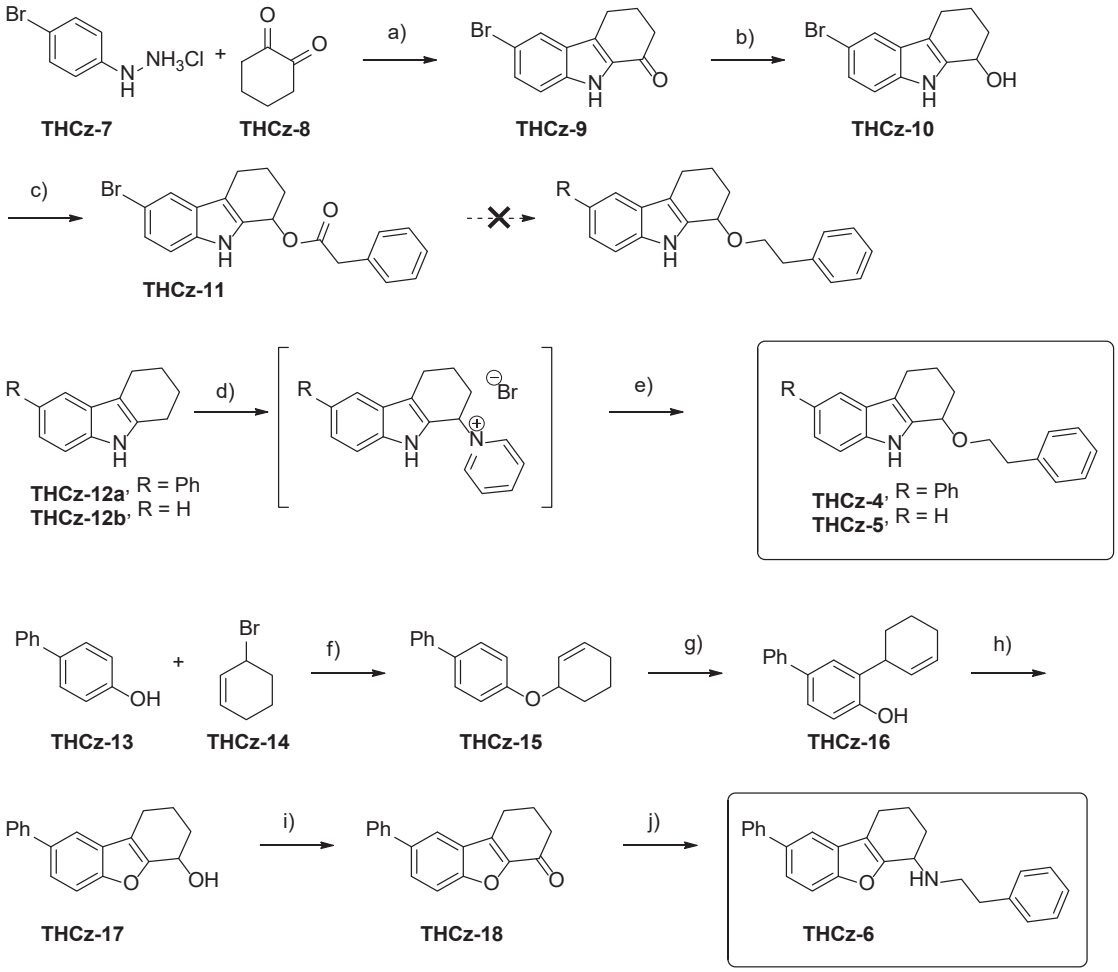

Figure S2. Graphic overview of the scheme for the synthesis of substituted tetrahydrocarbazole and its oxygen analogs Reagents and conditions **(a)** HCl/HOAc, MeOH, 60 °C, 58%, **(b)** $NaBH_4$/MeOH, CH_2Cl_2, RT, 82%, **(c)** $(PhCH_2CH_2O)_2O$, DMAP, Et_3N, CH_2Cl_2, RT, 78%, **(d)** NBS, Pyridine, PhH, RT, **(e)** $Ph(CH_2)_2ONa$, Et_2O, RT, 13%, **(f)** K_2CO_3, DMF, RT, 34%, **(g)** *N*, *N*-Diethylaniline, 195 °C, 40 h, 95%, **(h)** mCPBA, PhH, 90 °C, 4h, 53% **(i)** DDQ, xylene, 150 °C, 20 h, 77%, **(j)** $NaBH(OAc)_3$, HOAc, $Ph(CH_2)_2NH_2$, DCE, 57%. The compound numbers in the figure correspond to the respective THCz-analog numbers. Note that also the oxygen analogs are given THCz-numbers for simplicity.

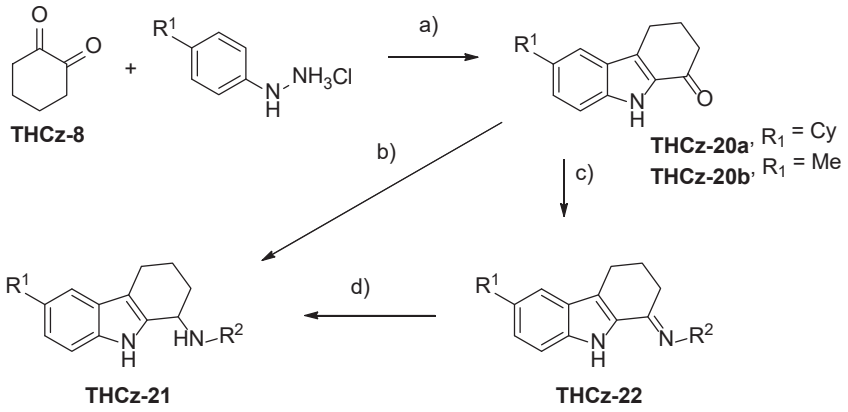

Figure S3. Graphic overview of the scheme for the synthesis of tetrahydrocarbazole-1-amines Reagents and conditions **(a)** HCl:HOAc (1:4), MeOH, reflux **(b)** NH2-R2, NaBH(OAc)3, HOAc, DCE, **(c)** pTsOH, NH2-R2, toluene or benzene, Dean-Stark, **(d)** NaBH4, MeOH, RT.

THCz-	MIC									n	Sparkline
	0.8 µM	1.6 µM	3.1 µM	6.3 µM	12.5 µM	25 µM	50 µM	100 µM	>100 µM		
1		10	34	11		3				58	
2			14							14	
3			14							14	
5									6	6	
6							12	3		15	
10									6	6	
11									6	6	
17									6	6	
19			2	6						8	
23								8		8	
24								10		10	
26						6				6	
27							6	3		9	
29			17	5						22	
30				16						16	
31		7	8							15	
32									6	6	
33									6	6	
34						6				6	
35					2		6			8	
36				21						21	
37				16						16	
38				16						16	
39				10	11					21	
40				32	4					36	
41					11	1				12	
42									6	6	
43			4	16						20	
44			1	21	5					27	
45				19						19	
46				19						19	
47			5	17						22	
48			2		23	1				26	
49				23	1					24	
50			10							10	

Figure S4. Overview of Minimal Inhibitory Concentration (MIC) values for the respective THCz-derivates, recorded in in individual technical replicates in supplemented C+Y medium. Most abundant MIC values are summarized in Tables S1-S3.

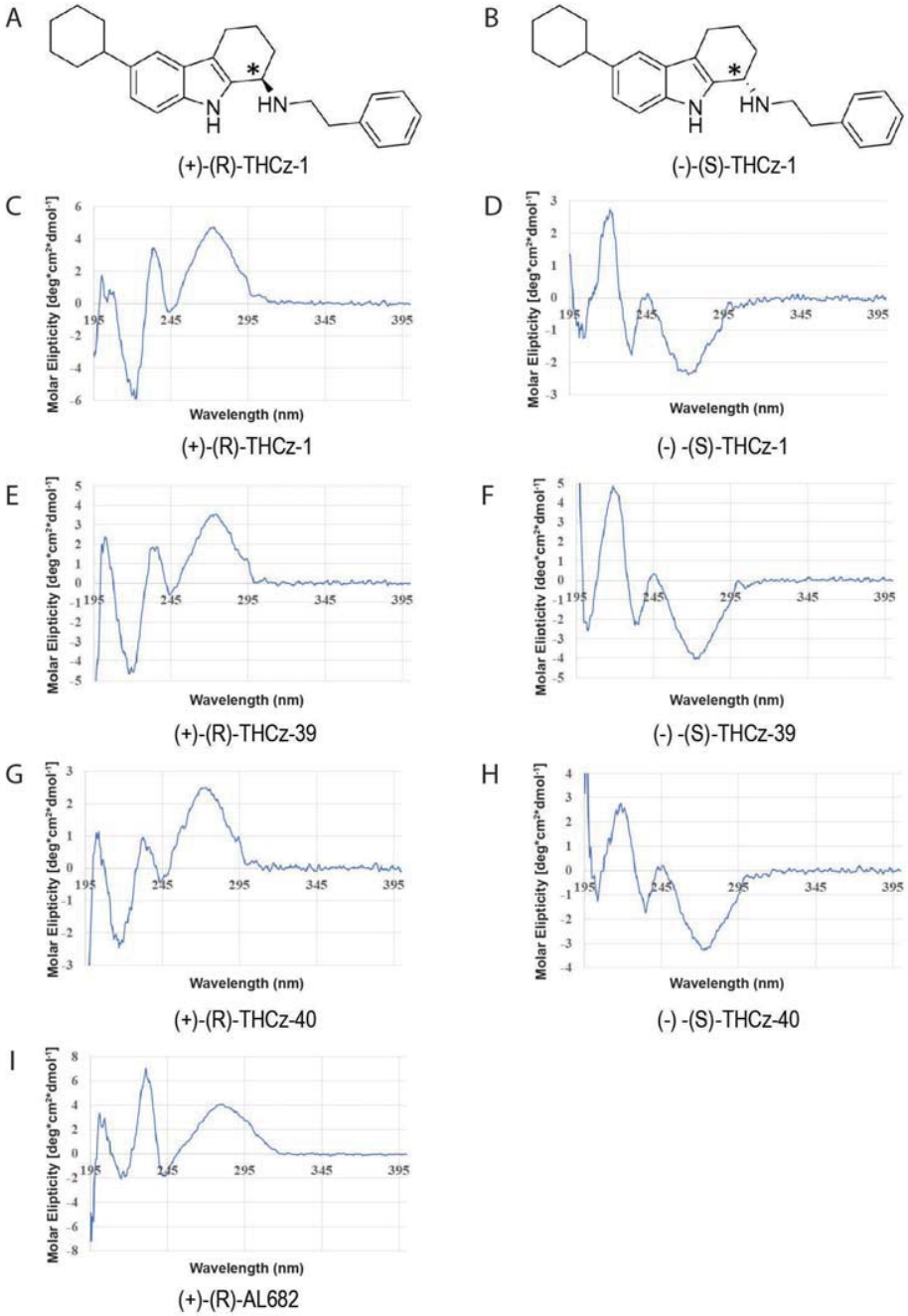

Figure S5. THCz enantiomers. (**A**) R (+) and the (**B**) S (-) structures of the THCz-1 enantiomers with the stereocenter indicated with a star (*). **(C-I)** Circular dichroismspectra in the near- and far-UV range between 195 nm – 400 nm for **(C)** (+)-(R)-THCz-1, **(D)** (-)-(S)-THCz-1, **(E)** (+)-(R)-THCz-39, **(F)** (-)-(S)-THCz-39, **(G)** (+)-(R)-THCz-40, **(H)** (-)-(S)-THCz-40 and **(I)** the stereoselectively synthesized reference compound (+)-(R)-AL682.

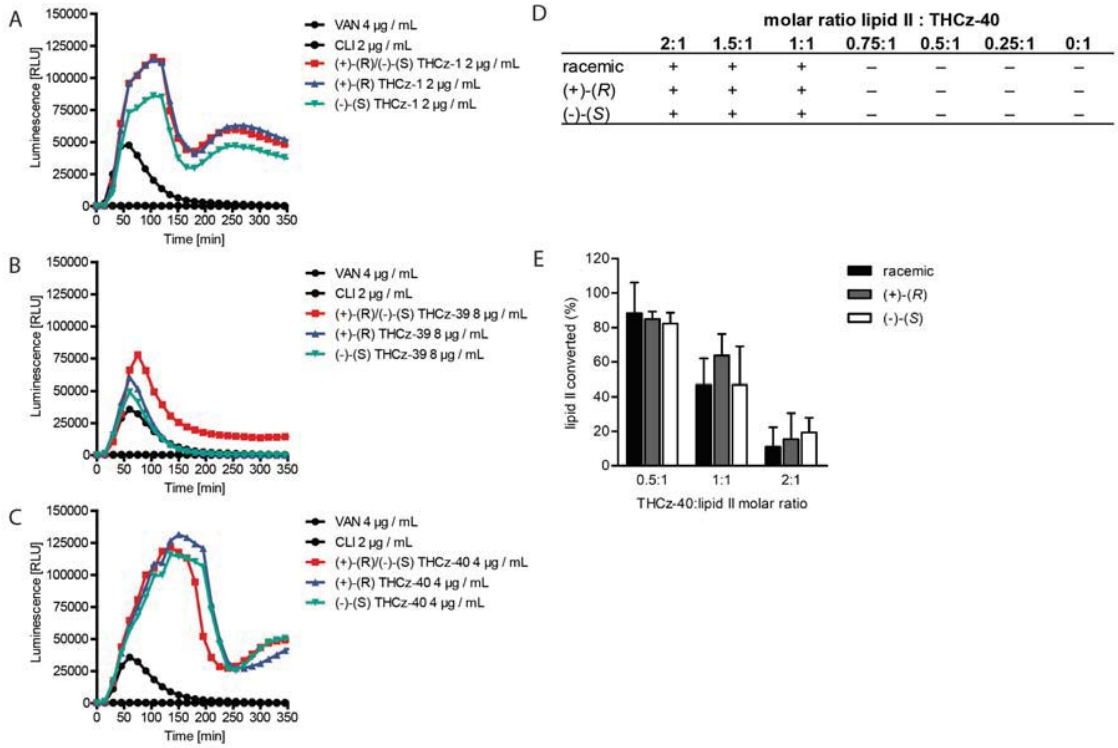

Figure S6. **Impact of THCz stereochemistry on cell wall biosynthesis. (A-C)** Induction of the LiaRS bioreporter by both enantiomer forms and racemic of (**A**) THCz-1, (**B**) THC-39 and (**C**) THCz-40 compared to vancomycin (positive control) and clindamycin (negative control), indicating that interference with the lipid II biosynthesis cycle is independent of stereochemistry of THCz. (**D**) Antagonistic effect of purified lipid II on antimicrobial activity of enantiomers and racemic of THCz-40. The compounds were exposed to lipid II for 10 min at indicated molar ratios prior to incubation with *M. luteus* cells. +, antagonization of antimicrobial activity; –, no antagonization. Results of three independent experiments are shown. (**E**) Both enantiomer forms of THCz-40 inhibit the PBP2-catalyzed transglycosylation reaction of lipid II *in vitro* in a dose-dependent manner and block enzymatic activity when added at a molar ratio of 2:1 with respect to lipid II. The enzymatic activity is expressed as converted lipid II and was set 100 % in the absence THCz-40. The error bars represent the standard deviation from three independent experiments.

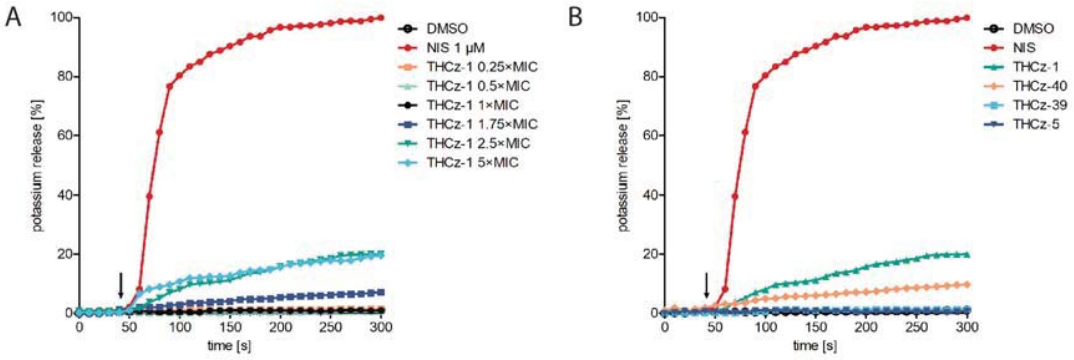

Figure S7. THCz do not form pores. (A, B) Potassium release of THCz-treated S. simulans. Potassium efflux from living cells was monitored with a potassium-sensitive electrode. Ion leakage is expressed relative to the total amount of potassium released after addition of 1 µM of the pore-forming lantibiotic nisin (set 100 %). The compound solvent DMSO was used as negative control. **(A)** Serial dilution of THCz-1 and **(B)** a comparison of THCz-analogs THCz-5, THCz-39 and THCz-40 at 2.5× MIC, showing that THCz do not cause a prominent K^+ release compared to nisin. Arrows indicate the time of compound addition.

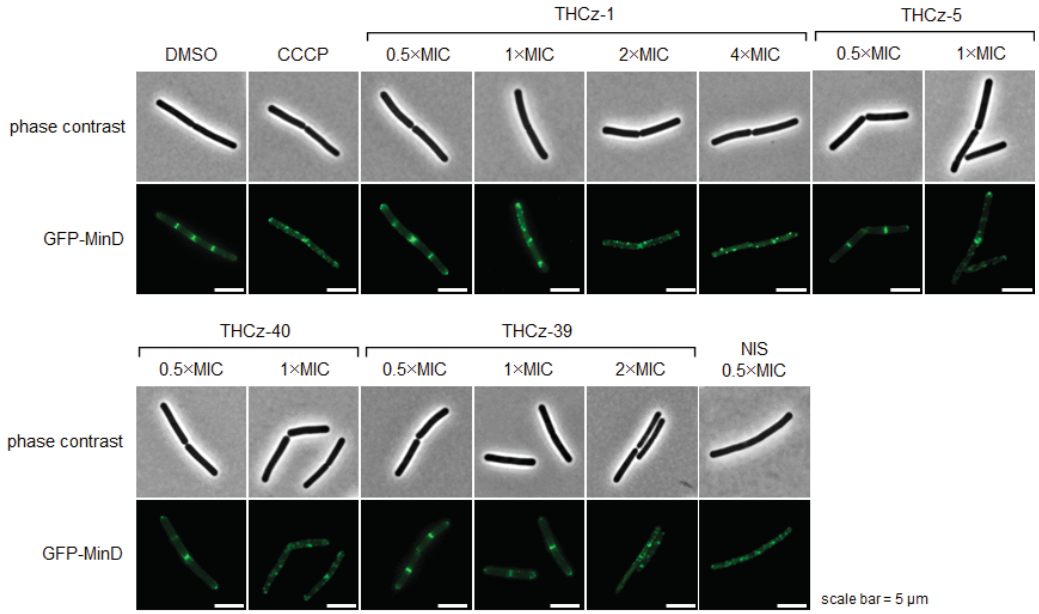

Figure S8. THCz analogs affect the cellular localisation of GFP-MinD in *B. subtilis*.

Reithuber, Wixe, Ludwig *et al.* (2021)
Proc. Natl. Acad. Sci., 118 (47), e2108244118

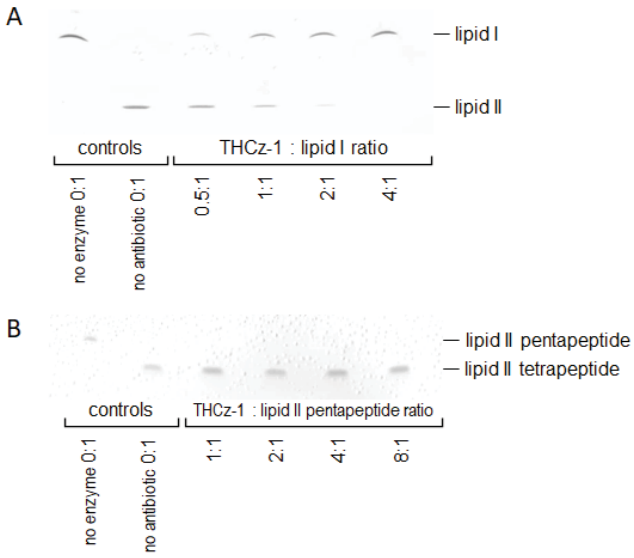

Figure S9. Impact of THCz-1 on individual peptidoglycan biosynthesis reactions. THCz-1 inhibits the MurG catalyzed synthesis of lipid II **(A)** and does not affect PBP4-catalyzed carboxypeptidation **(B)** THCz-1 was added in molar rations of 1 to 8 with respect to the amount of the substrate lipid I or lipid II used in the individual test system.

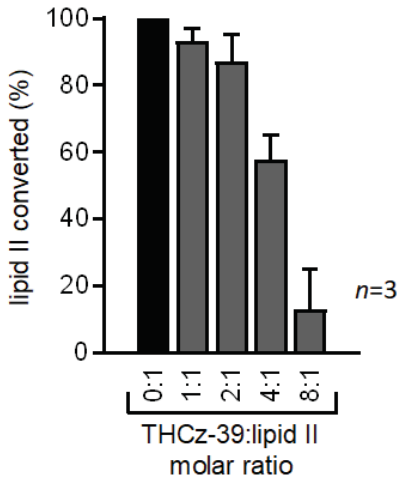

Figure S10. Impact of THCz-39 on PBP2- catalyzed lipid II transglycosylation. THCz-39 was added in molar ratios of 1 to 8 with respect to the amount of the substrate lipid II. Inhibition of PBP2-catalyzed reactions were quantified by the relative amount of C_{55}-PP formed. The error bars represent the standard deviation from the triplicate runs.

Reithuber, Wixe, Ludwig *et al.* (2021)
Proc. Natl. Acad. Sci., 118 (47), e2108244118

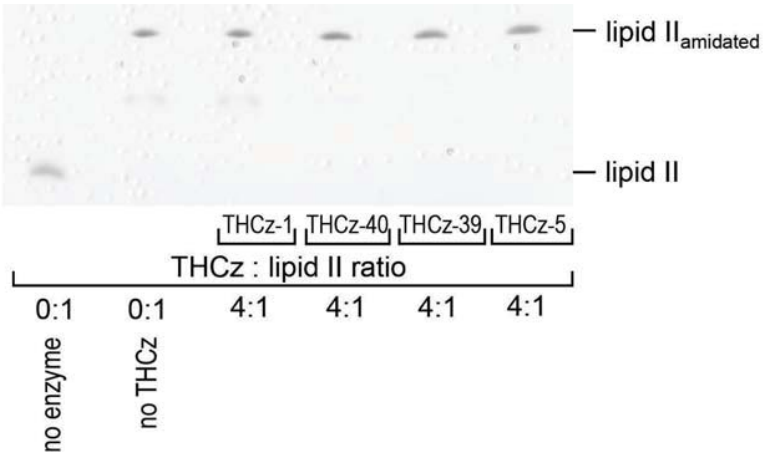

Figure S11. MurT-GatD-catalyzed amidation of lipid II is not inhibited by THCz *in vitro*. THCz-1, THCz-40, THCz-39, and THCz-5 were incubated at molar ratios of 4:1 with respect to the substrate lipid II. The reaction mixtures were extracted, analyzed by TLC and visualized by phosphomolybdic acid staining.

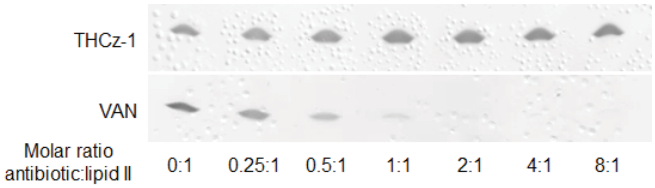

Figure S12. THCz-1 does not form extraction-stable complexes with lipid II. THCz-1 and vancomycin (VAN) were incubated with purified lipid II at increasing molar ratios. After extraction with BuOH/PyrAc lipid II in the solvent phase was separated by TLC. Binding of VAN is indicated by a reduction of the amount of free lipid II visible on the TLC and lipid II is almost fully locked in a complex at equimolar ratio. No complex formation was observed with THCz-1. The chromatograms are representative of two independent experiments.

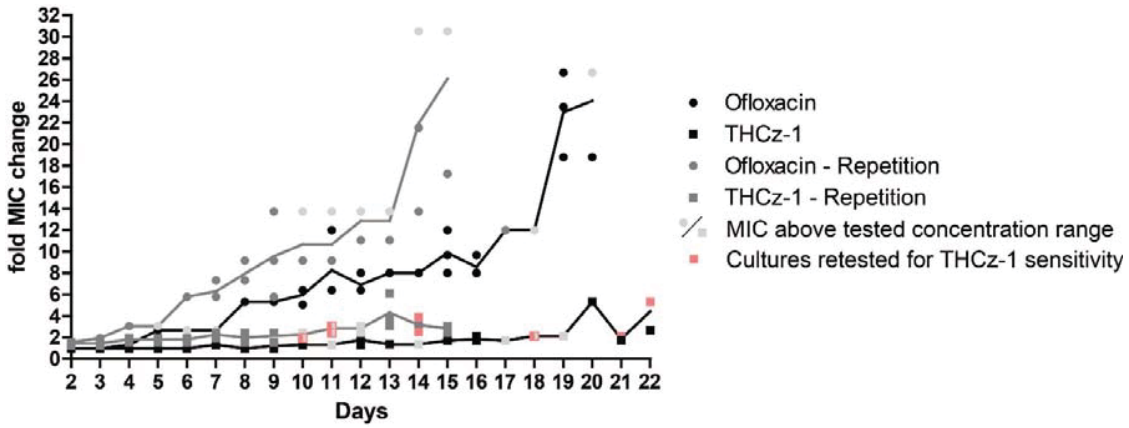

Figure S13. Resistance development in *S. aureus*. Serial culturing of *S. aureus* in small incrementing concentration steps of THCz-1 and ofloxacin was performed in two experiments (highlighted in black and dark grey). Cultures that had a MIC higher than the tested concentration range are indicated in grey (highest tested concentration is given). Bacteria from below MIC concentration cultures of a certain day that had been isolated and re-tested for THCz-1 sensitivity are indicated in red. The tested cultures were equally sensitive to THCz-1 as the wild type strain upon re-exposure.

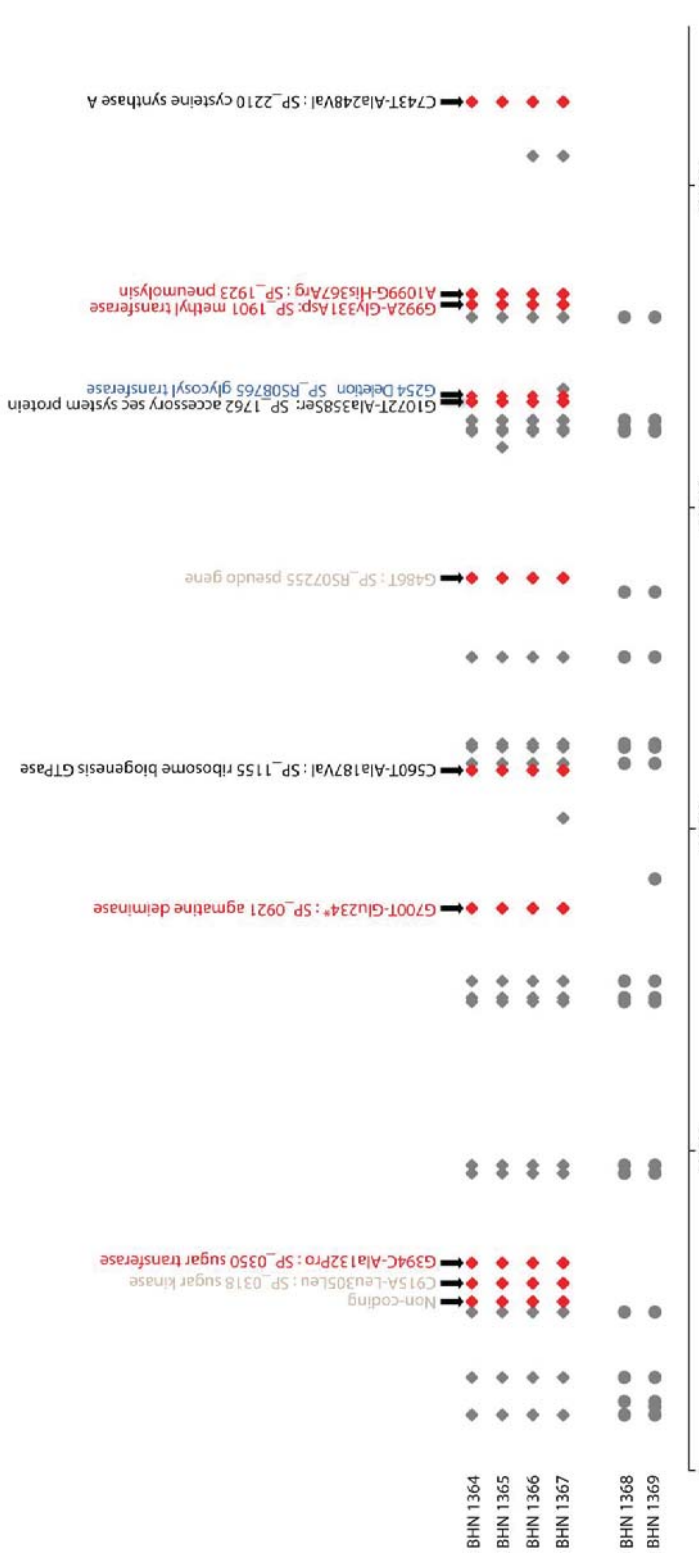

Visualization of the whole genome sequencing data investigating the molecular basis for reduced THCz-1 sensitivity. The genomic variants for two clones (BHN1368 and BHN1369) of a sensitive isolate (T4 derivative isolate #25 incubated and re-streaked on THY plates depicted in circles), and four clones (BHN1364, BHN1365, BHN1366, and BHN1367) of a reduced THCz-1 sensitivity isolate (T4 derivative isolate #22 incubated and re-streaked on THCz-1 containing plates shown in diamonds) are shown with reference to the NCBI annotated reference of the T4 genome (NC_003028.3). Mutations that were only present in clones with reduced THCz-1 sensitivity are highlighted in red, whereas other spontaneous mutations in relation to NC_003028.3 are colored in grey. Above each mutation that is found in strains with reduced sensitivity and absent in the sensitive isolates, the corresponding amino acid change as well as the gene number and the gene annotations are given along with a color code to provide information on the potential impact of the mutations for the encoded proteins. Mutations that resulted in a synonymous amino acid, affected codons in a pseudogene, or those present in a non-coding region are colored in brown. Non-synonymous mutations that resulted in changes to amino acids with similar biochemical properties are colored in black and a frame shift mutation is displayed in blue. Stop-codon mutations or non-synonymous mutations that resulted in amino acid changes with changed biochemical properties are indicated in red. For these mutations knockouts of the respective genes were constructed and tested but only the mutant of *cpsE* (*SP0350*) could reproduce the reduced THCz-1 sensitive phenotype.

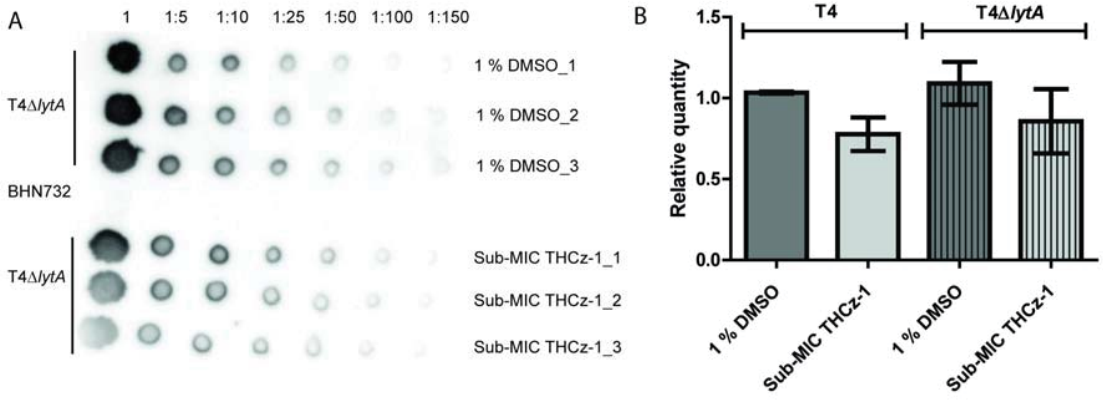

Figure S15. Phosphorylcholine amount in *S. pneumoniae* after sub-MIC THCz-1 passaging. (A) Dot blot probed for phosphorylcholine of one biological replicate including BHN732 unable to decorate the cell surface with phosphorylcholine (*15*). The blots were used as basis for **(B)** the relative quantification of phosphorylcholine in 1 % DMSO or 0.4 µM THCz-1 incubated pneumococci. The average and standard deviation of three biological replicates are displayed. For one biological replicate all untreated replicates were used once for relative quantification and an average of the respectively treated samples was calculated over several dilutions.

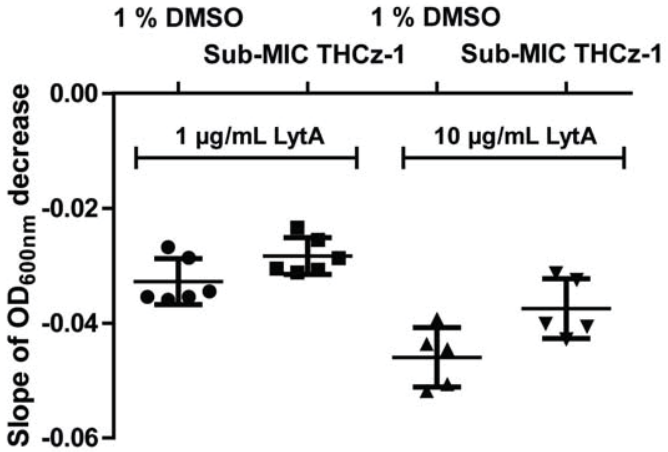

Figure S16. *S. pneumoniae* Δ*lytA* mutant sensitivity to externally added LytA after sub-MIC THCz-1 passaging. Degree of lysis in T4Δ*lytA* measured as the slope of OD_{600nm} decrease in the presence of 1 µg/mL or 10 µg/mL recombinant LytA after 3 µM THCz-1 treatment in early logarithmic phase.

Supplementary Tables

Investigation of modifications on the central core scaffold

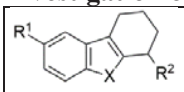

THCz-	R1[a]	X	R2[a]	MIC [b] [µM (µg / mL)]	Toxicity[c] [n]
1[d]		NH	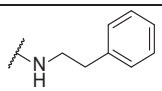	3.1 (1.3)	79.4 ± 16.4 [10]
2[d]		NH	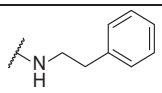	3.1 (1.1)	84.2 ± 10.5 [4]
3[d]		NH	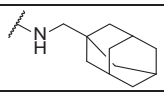	3.1 (1.2)	78.2 ± 20.4 [4]
5		NH	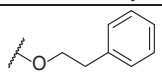	>100 (>29.1)	ND
6[e]		O	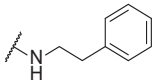	50 (18.4)	5.9 ± 7.8 [4]
10		NH		>100 (>26.6)	ND
11		NH	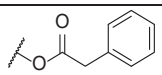	>100 (>38.4)	ND
17[e]		O		>100 (26.6)	ND
19		NH	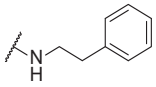	6.3 (1.9)	13 ± 14.8 [4]

Notes: **[a]** Cy - cyclohexyl; Ph - phenyl; Me - methyl; Br - bromo; Adm - adamantyl. **[b]** Minimal inhibitory concentration of THCz analogs for *S. pneumoniae* T4 in supplemented C+Y medium. Most abundant MIC is given. An overview of the observed MIC distribution is given in **Fig. S2**. **[c]** Non-viable A549 cells, after exposure to 50 µM of the respective THCz analogs for 23 h. Average ± Standard Deviation are given and the number of biological replicates is noted in brackets. **[d]** Original hit compounds from the screen; see also **Fig. 1** for structures. **[e]** For simplicity, we refer to all compounds studied here as THCz analogs, although these compounds are oxa-tetrahydrofluorenes. ND = Not determined.

Table S2. Structure-activity and toxicity relationship of THCz compounds: Investigation of modifications in R^2

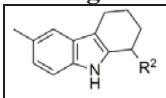

THCz-	R^2	MIC [a] [µM (µg / mL)]	Toxicity [b] [n]
23	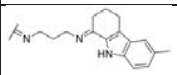	100 (43.7)	19.3 ± 10.1 [4]
24	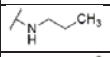	100 (22.8)	ND
26	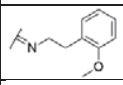	25 (8.3)	ND
27	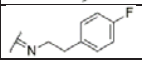	50 (16.0)	ND
29	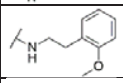	3.1 (1.0)	70.3 ± 6 [5]
30	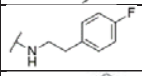	6.3 (2.0)	13.8 ± 14.9 [6]
31	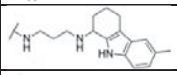	3.1 (1.4)	62.2 ± 27.3 [6]
32	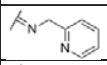	>100 (>28.9)	ND
33	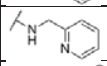	>100 (>29.1)	ND
34	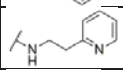	25 (7.6)	ND
35	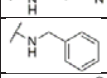	25 (8.2)	4.4 ± 6.3 [4]
36	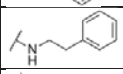	6.3 (2.2)	17.3 ± 14.7 [7]
37	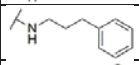	6.3 (2.0)	4.8 ± 4.2 [3]
38	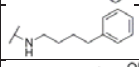	6.3 (2.1)	18.1 ± 15.2 [4]
39	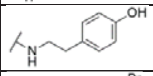	6.3 - 12.5 (2.0 - 4.0)	5.9 ± 7.1 [4]
40	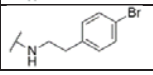	6.3 (2.4)	28.4 ± 24.5 [8]

Notes: [a]) Minimal inhibitory concentration of THCz analogs for *S. pneumoniae* T4 in supplemented C+Y medium. Most abundant MIC is given. An overview of the observed MIC distribution is given in Figure S2. **[b])** Non-viable A549 cells, after exposure to 50 µM of the respective THCz analogs for 23 h. Average ± Standard Deviation are given and the number of biological replicates is noted in brackets. ND = Not determined.

Table S3. Structure-activity and toxicity relationship of THCz compounds: Extended investigation of modifications in R^1 and R^2

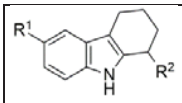

THCz-	R^1	R^2	MIC [a] [µM (µg / mL)]	Toxicity [b] [n]
41		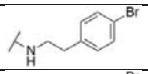	12.5 (4.8)	10.8 ± 9.6 [4]
42		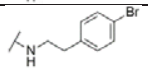	>100 (>45.9)	ND
43		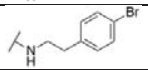	6.3 (3.1)	84.8 ± 10.9 [6]
44		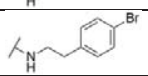	6.3 (3.1)	95.2 ± 4.8 [6]
45		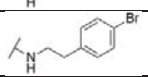	6.3 (2.6)	36.8 ± 24.2 [5]
46		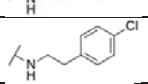	6.3 (2.4)	69.2 ± 26 [5]
47		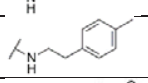	6.3 (2.3)	16.8 ± 13.1 [5]
48		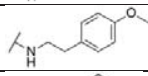	12.5 (8.4)	2.2 ± 2.5 [4]
49		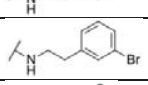	6.3 (2.7)	56.4 ± 20.1 [5]
50		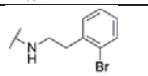	3.1 (1.3)	66.1 ± 11.1 [4]

Notes: [a]) Minimal inhibitory concentration of THCz analogs for *S. pneumoniae* T4 in supplemented C+Y medium. Most abundant MIC is given. An overview of the observed MIC distribution is given in Figure S2. **[b])** Non-viable A549 cells, after exposure to 50 µM of the respective THCz analogs for 23 h. Average ± Standard Deviation are given and the number of biological replicates is noted in brackets. ND = Not determined.

Table S4. Minimal inhibitory concentration of THCz-1 and -40 against antibiotic resistant pneumococcal strains determined with broth microdilution assay in supplemented C+Y medium

Strain[a]	Serotype	MIC[b] [µg / mL]		MIC[c] [µg / mL]					
		THCz-1	THCz-40	Pen	Ctx	Ery	Cli	Chl	Tet
T4	4	1.3	2.4	-	-	-	-	-	-
T4R	4	1.3	2.4	-	-	-	-	-	-
T4Δ*lytA*	4	1.3	2.4	-	-	-	-	-	-
1 (700669)	23F	1.3	2.4	2	0.5	0.06	0.06	16	32
2 (700670)	6B	1.3	2.4	2	1	0.12	0.12	16	32
3 (700671)	9V	1.3	2.4	2	1	0.12	0.12	2	≤0.5
9 (700676)	14	1.3	2.4	0.03	0.03	32	0.12	2	≤0.5
11 (700678)	19A	1.3	4.8	4	1	>32	>32	32	32
16 (BAA-343)	23F	1.3	2.4	8	8	>8	0.25	16	16
				2[d]	2[d]	0.5[d]	0.5[d]	8[d]	2[d]

Notes: **[a])** PMEN strain number according to McGee et al (*16*) with corresponding ATCC number in parenthesis**. [b])** MIC determined by broth microdilution assay in this study. **[c])** For reference, MIC of indicated antibiotics determined with E-tests (*16*); Pen, penicillin; Ctx, cefotoxamine; Cli, clindamycin; Chl, chloramphenicol; Tet, tetracyclin. **[d])** Breakpoint values for *S. pneumoniae* resistance (R) determined by EUCAST (*17*)

Table S5. Extended THCz analog bacterial sensitivity determination to THCz analogs

		MIC [µg / mL]									
		THCz-1			THCz-40			THCz-39			THCz-5
Species	**Strain**	**R/S[a]**	**R[a]**	**S[a]**	**R/S[a]**	**R[a]**	**S[a]**	**R/S[a]**	**R[a]**	**S[a]**	**R/S[a]**
S. pneumoniae	Tigr4 (T4)	1	5	3	2	5	2	2 - 4	8	2	>29
B. subtilis	168	2	2	2	4	4	2	16	8	16	512
	sacA::pCHlux101 (P_{liaI}-*lux*)	2	ND	ND	4	ND	ND	16	ND	ND	256 - 512
	amyE::pAC6 (P_{ypuA}-*lacZ*)	2	ND	ND	4	ND	ND	16	ND	ND	ND
	amyE::pAC6 (P_{yorB}-*lacZ*)	2	ND	ND	4	ND	ND	16	ND	ND	ND
	amyE::pAC6 (P_{yvgS}-*lacZ*)	2	ND	ND	4	ND	ND	16	ND	ND	ND
	amyE::pAC6 (P_{yheI}-*lacZ*)	2	ND	ND	4	ND	ND	16	ND	ND	ND
S. simulans	22	2	2	2	4	4	4	16	16	16	>16
S. epidermidis	CLB26329 (MRSE)	2	2	2	4	4	4	16	16	16	ND
S. aureus	ATCC 29213	2	2	2	4	4	4	16	16	16	>16
	SG511	2	2	2	4	4	2	16	16	16	>16
	USA300 JE2 (MRSA)	4	2	2	4	4	4	16	16	16	ND
	SG511 DAP^R	2	2	2	4	4	4	16	16	16	>16
	HG001	4	2	2	4	4	4	16	16	16	>16
	HG001 DAP^R	4	2	2	4	4	4	16	16	16	>16
	Mu50 (VISA)	2	2	2	4	4	4	16	16	16	>16
	Vc40 (VISA)	4	2	2	4	4	4	16	16	16	>16
	SA113	4	ND	ND	4	ND	ND	16	ND	ND	>16
	SA113Δ*atlA*	4	ND	ND	4	ND	ND	>16	ND	ND	>16
	SA113Δ*tarO*	4	ND	ND	4	ND	ND	>16	ND	ND	>16
E. faecalis	JH2-2	2	2	2	4	4	2	16	16	16	ND
E. faecium	BM4147 (VRE)	2	2	2	4	4	2	16	16	16	ND
M. luteus	DSM1790	1	1	1	2	2	2	8	8	8	128
E. coli	O-19592	>128	>128	>128	>128	>128	>128	>128	>128	>128	>128
	MB5746[b]	2	2	2	4	4	2	16	16	8	>32

Notes: [a]) activity of the racemate ((+)-(R)/(-)-(S)) and the purified enantiomer (+)-(R) and (-)–(S) form. **[b])** outer membrane hyper-permeable and efflux-deficient. ND, not determined

Table S6. Minimal inhibitory concentration of *S. pneumoniae* P-type ATPase deletion mutants

Strain	MIC [a]	
	Penicillin G [µg / mL]	**THCz-1 [µg / mL]**
T4Δ*SP1551*	0.0078 – 0.0313	0.6 – 1.3
T4Δ*SP1623*	0.0156 – 0.0313	1.3
T4Δ*SP2101*	0.0156 – 0.0313	1.3
T4Δ*SP0729*	0.0156 – 0.0313	1.3 – 2.6
T4Δ*SP1551*Δ*SP1623*Δ*SP2101*Δ*SP0729*	0.0156 – 0.0313	1.3
Note: [a]) MIC was determined in supplemented C+Y medium		

Table S7. List of PCR primers

Primer	Sequence (5'-3') [a]	Comment
SP0729up-frw-I	agagaagaaatcaagtgctgt	Anneals ~700 bp upstream of *SP0729* Orf
SP0729up-frw-II	caaggtttgttcccgtagga	Anneals ~800 bp upstream of *SP0729* Orf
SP0729up-rev-TetCassOH	TACATGATTACAAAGTATCTGTgccaca agaaaattcatgtcg	Anneals upstream of *SP0729* start codon. Overhang seq complimentary to 5'-end of *tetM* cassette
SP0729down-frw-TetCassOH	ATACGAGTGGATACTATACTaagtaatga ctagatttctttg	Anneals downstream of *SP0729* stop codon. Overhang seq complimentary to 3'-end of *tetM* cassette
SP0729down-rev-I	actggaatttcaacaacagct	Anneals ~700 bp downstream of *SP0729* Orf
SP0729down-rev-II	tttgtcgatttcaacttcgttc	Anneals ~800 bp downstream of *SP0729* Orf
TetCassFrw	acagatactttgtaatcatgt	Anneals at the 5' end of the *tetM* cassette
TetCassRev	agtatagtatccactcgtattc	Anneals at the 3' end of the *tetM* cassette
SP1551up-frw-I	tcagcgcattggagttggat	Anneals ~700 bp upstream of *SP1551* Orf
SP1551up-frw-II	tccacaatcggataattgaa	Anneals ~800 bp upstream of *SP1551* Orf
SP1551up-rev-ErmCassOH	GCAAGTCACACGAACACGAAagcttttca cgacaaacaaaaag	Anneals upstream of *SP1551* start codon. Overhang seq complimentary to 5'-end of *ermB* promoter
SP1551up-rev-ErmOrfOH	TATTTAACGGGAGGAAATAAgggaggttt cggatgtcagca	Anneals downstream of *SP1551* stop codon. Overhang seq complimentary to 3'-end of *ermB* Orf
SP1551down-rev-I	tccaagaattttgcagaacct	Anneals ~700 bp downstream of *SP1551* Orf
SP1551down-rev-II	ttaatttctgtataagttact	Anneals ~800 bp downstream of *SP1551* Orf
ErmCassFrw	ttcgtgttcgtgtgacttgc	Anneals upstream of *ermB* promoter
ErmOrfRev	ttatttcctcccgttaaataatag	Anneals at the end of *ermB* Orf
SP1623up-frw-I	ctgtttgaatacgattggcga	Anneals ~700 bp upstream of *SP1623* Orf
SP1623up-frw-II	ataatagcaaggatgagggca	Anneals ~800 bp upstream of *SP1623* Orf
SP1623up-rev-SpectORFOH	TTAATTTGTTCGTATGTATTCATaaattct attatatcatttttttaac	Anneals upstream of *SP1623* start codon. Overhang seq complimentary to 5'-end of spectinomycin Orf
SP1623down-frw-SpectOrfOH	TTTAAATAACAGATTAAAAAAATTA TAGatcaaaaccaccagtgtgaact	Anneals downstream of *SP1623* stop codon. Overhang seq complimentary to 3'-end of *spcR* Orf
SP1623down-rev-I	tccatagagcttttagcgtggt	Anneals ~700 bp downstream of *SP1623* Orf
SP1623down-rev-II	catcagatctacgatagatc	Anneals ~800 bp downstream of *SP1623* Orf
SpectOrfFrw	atgaatacatacgaacaaattaataaag	Anneals at the beginning of *spcR* Orf
SpectOrfRev	ctataatttttttaatctgttatttaa	Anneals at the end of *spcR* Orf
SP2101up-frw-I	aagcaagtcagatacagcatc	Anneals ~700 bp upstream of *SP2101* Orf
SP2101up-frw-II	atagaaagtttttttcagagt	Anneals ~800 bp upstream of *SP2101* Orf

Primer	**Sequence (5'-3')** [a]	**Comment**
SP2101up-rev-KanOrfOH	TGATATTCTCATTTTAGCCATattattcacc tataaggctatc	Anneals upstream of *SP2101* start codon. Overhang seq complimentary to 5'-end of *kanR* Orf
SP2101down-frw-KanOrfOH	TTACTGGATGAATTGTTTTAGatgagagtt attaacagcaaaaag	Anneals downstream of *SP2101* stop codon. Overhang seq complimentary to 3'-end of *kanR* Orf
SP2101down-rev-I	agactggtcacgttatcact	Anneals ~700 bp downstream of *SP2101* Orf
SP2101down-rev-II	gtccttaaccaagaccataatg	Anneals ~800 bp downstream of *SP2101* Orf
KanOrfFrw	atggctaaaatgagaatatca	Anneals at the beginning of *kanR* Orf
KanOrfRev	ctaaaacaattcatccagtaa	Anneals at the end of *kanR* Orf
aguA-up-frw-I	gtgcaccaggttctcgctttg	Anneals ~700 bp upstream of *aguA* Orf
aguA-up-frw-II	cgtaaacacggtccgcgttgt	Anneals ~800 bp upstream of *aguA* Orf
aguA-up-rev-ErmOrfOH	GTTTTGAGAATATTTTATATTTTTGTT CATgataatctccctttaaag	Anneals upstream of aguA start codon. Overhang seq complementary to 5'-end of *ermB* Orf
aguA-down-frw-ErmOrfOH	TATCTATTATTTAACGGGAGGAAATA Agagaaaaagatgagaaatgta	Anneals downstream of *SP2101* stop codon. Overhang seq complimentary to 3'-end of *ermB* Orf
aguA-down-rev-I	tctgtccgccattttcctcac	Anneals ~700 bp downstream of *aguA* Orf
aguA-down-rev-II	tcataagtagctaacagaaca	Anneals ~800 bp downstream of *aguA* Orf
ErmOrf-frw	atgaacaaaaatataaaatattctca	Anneals at the beginning of *ermB* Orf
ErmOrf-rev	ttatttcctcccgttaaataataga	Anneals at the end of *ermB* Orf
SP0350/1ig-up-frw-II	tattgagaactcatatattactga	Anneals ~800 bp upstream of the *SP0350* stop codon
SP0350/1ig-up-frw-I	tctgaaaatcattgagtgacca	Anneals ~700 bp upstream of the *SP0350* stop codon
SP0350/1ig-up-rev-ErmOrfOH	GAGAATATTTTATATTTTTGTTCATtta actttctttcttaccactac	Anneals at the 3' end of *SP0350* with overhang seq complementary to the 5' end of the *ermB* Orf
SP0350/1ig-down-frw-ErmOrfOH	ATTATTTAACGGGAGGAAATAAattgga caatgaaaatactatttgtttg	Anneals in the intergenic region (ig) of *SP0350* and *SP0351* just down-stream the *SP0350* stop codon with overhang seq complementary to the 3' end of the *ermB* Orf
SP0350/1ig-down-rev-I	tgtgctttgccaatattacca	Anneals ~700 bp downstream of the *SP0350* stop codon
SP0350/1ig-down-rev-II	cttgggtaaattggtattcttc	Anneals ~800 bp downstream of the *SP0350* stop codon
cpsE-up-frw-I	gtatcaccaaaccctacag	Anneals ~700 bp upstream of the *cpsE* Orf
cpsE-up-frw-II	cagggctaacagaatttttatc	Anneals ~800 bp upstream of the *cpsE* Orf
cpsE-up-rev-ErmOrfOH	GAATATTTTATATTTTTGTTCATaaacaa cctccaactataaattc	Anneals upstream of *cpsE* start codon. Overhang seq complimentary to 5'-end of *ermB* Orf
cpsE-down-frw-ErmOrfOH	CTATTATTTAACGGGAGGAAATAAatt ggacaatgaaaatactatttg	Anneals downstream of *cpsE* stop codon. Overhang seq complimentary to 3'-end of *ermB* Orf
cpsE-down-rev-I	ctttgccaatattaccagc	Anneals ~700 bp downstream of *cpsE* Orf

Primer	**Sequence (5'-3')** [a]	**Comment**
cpsE-down-rev-II	gtaccatctccaacaaaatg	Anneals ~800 bp downstream of *cpsE* Orf
SP1901-up-frw-I	gtatattgcttatcaagttccttg	Anneals ~700 bp upstream of the *SP1901* Orf
SP1901-up-frw-II	taagagcgcttgctatatcc	Anneals ~800 bp upstream of the *SP1901* Orf
SP1901-up-rev-ErmOrfOH	GAGAATATTTTATATTTTTGTTCATac ccctatcttatcacattttg	Anneals upstream of *SP1901* start codon. Overhang seq complimentary to 5'-end of *ermB* Orf
SP1901-down-frw-ErmOrfOH	CTATTATTTAACGGGAGGAAATaaaaaa gtagttgacaaagtttgaaa	Anneals downstream of *SP1901* stop codon. Overhang seq complimentary to 3'-end of *ermB* Orf
SP1901-down-rev-I	ctatgtatcgtcgccttg	Anneals ~700 bp downstream of *SP1901* Orf
SP1901-down-rev-II	cattgccgaagattcccta	Anneals ~800 bp downstream of *SP1901* Orf
ply-up-frw-I	agctgctacatagatttctac	Anneals ~1000 bp upstream of *ply* Orf
ply-up-frw-II	cagtgggaaagtatccagtca	Anneals ~1100 bp upstream of *ply* Orf
ply-up-rev-ErmOH	GCAAGTCACACGAACACGAActtctacct cctaataagttc	Anneals upstream of *ply* start codon. Overhang seq complimentary to 5'-end of *ermB* cassette
ply-down-frw-ErmOH	CTCGTCTTAATCAGCAACATgagaggag aatgcttgcgac	Anneals upstream of *ply* stop codon. Overhang seq complimentary to 3'-end of *ermB* cassette
ply-down-rev-I	agaagccgataaggaaaagatg	Anneals ~1000 bp downstream of *ply* Orf
ply-down-rev-II	cctttggctttatcaatcgct	Anneals ~1100 bp downstream of *ply* Orf
Note: [a]) Annealing sequences displayed in lower case letters and non-annealing overhang sequences in upper case letters.		

Table S8. Strains used in the study

Species	Strain	Identifyer	Genotype	Reference
S. pneumoniae	Tigr4 (T4)	BHN842	TIGR4, wild type, Serotype 4	This study
	Tigr4R (T4R)	BHN659	Unencapsulated derivative of T4	(*18*)
	T4Δ*lytA*::Erm	BHN433	Erythromycin resistance (*ermB*) cassette replacing *SP1937* Orf	(*18*)
	T4RΔ*lytA*::Erm	BHN434	Erythromycin resistance (Erm) cassette replacing SP1937 Orf	(*18*)
	PMEN1	ATCC 700669	Antibiotic resistant serotype 23F	(*16*)
	PMEN2	ATCC 700670	Antibiotic resistant serotype 6B	(*16*)
	PMEN3	ATCC 700671	Antibiotic resistant serotype 9V	(*16*)
	PMEN9	ATCC 700676	Antibiotic resistant serotype 14	(*16*)
	PMEN11	ATCC 700678	Antibiotic resistant serotype 19A	(*16*)
	PMEN16	ATCC BAA-343	Antibiotic resistant serotype 23F	(*16*)
	T4Δ*SP_0729*::Tet	BHN1685	Tetracyclin (*tetM*) resistance cassette (promoter and Orf) replacing *SP0729* Orf	This study
	T4Δ*SP_1551*::Erm	BHN1686	Erythromycin (*ermB*) resistance cassette (promoter and Orf) replacing *SP1551* Orf	This study
	T4Δ*SP_1623*::Spect	BHN1687	Spectinomycin resistance (*spcR*) Orf replacing *SP1623* Orf	This study
	T4Δ*SP_2101*::Kan	BHN1688	Kanamycin resistance (*kanR*) Orf replacing *SP2101* Orf	This study
	T4Δ*SP_0729*::TetΔ*SP_1551*::Erm Δ*SP_1623*::SpectΔ*SP_2101*::Kan	BHN1689	Quadruple deletion mutant with the same replacement constructs described for the single deletion mutants above	This study
	T4_22#1 / *THCz-1(RS)*	BHN1364	Clone #1 of isolate #22 with reduced sensitivity (RS) to THCz-1	This study
	T4_22#2 / THCz-1(RS)	BHN1365	Clone #2 of isolate #22 with reduced sensitivity (RS) to THCz-1	This study
	T4_22#3 / THCz-1(RS)	BHN1366	Clone #3 of isolate #22 with reduced sensitivity (RS) to THCz-1	This study
	T4_22#4 / THCz-1(RS)	BHN1367	Clone #4 of isolate #22 with reduced sensitivity (RS) to THCz-1	This study
	T4_25#2 / THCz-1(S)	BHN1368	Clone #2 of isolate #25, THCz-1 sensitive (S), serially passaged on THY plates	This study
	T4_25#3 / THCz-1(S)	BHN1369	Clone #3 of isolate #25, THCz-1 sensitive (S), serially passaged on THY plates	This study
	T4Δ*aguA*::Erm	BHN1371	Erythromycin Orf (*ermB*) replacing *aguA* (*SP0921*) Orf	This study
	T4Δ*cpsE*::Erm	BHN1690	Erythromycin Orf (*ermB*) replacing *cpsE* (*SP0350*) Orf	This study
	T4 *cps4E*^{G394C} Ω (*SP0350*-∇(*erm*Orf)-*SP0351*)	BHN1691	A SNP mutation (G394C) introduced in *cpsE* (*SP0350*). Erythromycin Orf (*ermB*) inserted in inter-genic region between *SP0350* and *SP0351*	This study
	T4 Ω (*SP0350*-∇(*erm*Orf)-*SP0351*)	BHN1692	Control strain with wild type sequence of SP0350 and with an erythromycin Orf (*ermB*) inserted in the inter-genic region between *SP0350* and *SP0351*	This study
	T4Δ*SP1901*::Erm	BHN1693	Erythromycin Orf (*ermB*) replacing *SP1901* Orf	This study
	T4Δ*ply*::Erm	BHN2043	Erythromycin cassette (*ermB*) replacing *ply* (*SP1923)* Orf	This study
	D39ChipLicA	BHN732	Choline-independent and unable to incorporate choline into teichoic acids	(*15*)
S. parasanguinis		ATCC 903		
S. pyogenes			Clinical isolate, serotype M1T1 isolate 5448	(*19*)

Species	Strain	Identifyer	Genotype	Reference
B. subtilis		ATCC 6051		
	168	ATCC 23857		
	168 *sacA*::pCHlux101 (P_{lial}-lux)			(*20*)
	168 *amyE*::pAC6 (P_{ypuA}-lacZ)			(*21*)
	168 *amyE*::pAC6 (P_{yorB}-lacZ)			(*21*)
	168 *amyE*::pAC6 (P_{yvgS}-lacZ)			(*21*)
	168 *amyE*::pAC6 (P_{yhel}-lacZ)			(*21*)
S. simulans	22			
S. epidermidis	CLB26329 (MRSE)			
S. aureus		ATCC 25923		
		ATCC 29213		
	SG511			(*22*)
	USA300 JE2 (MRSA)		USA300 LAC derivative with plasmids cured. Strain obtained from the NARSA strain collection.	(*23*)
	SG511 DAP^R			(*24*)
	HG001			(*25*)
	HG001 DAP^R			(*24*)
	Mu50 (VISA)		Clinical isolate	*(26)*
	VC40 (VISA)			(*27*)
	SA113		Derivative of NCTC 8325	(*28*)
	SA113Δ*atlA*			
	SA113Δ*tarO*			(*29*)
E. faecalis	JH2-2			
E. faecium	BM4147 (VRE)			
M. luteus		DSM1790, ATCC 10240		
M. bovis		ATCC 35734		
M. smegmatis		ATCC 70084		
M. catarrhalis			Clinical isolate	
E. coli		ATCC 11775		
	O-19592			
	MB5746[a]			
P. aeruginosa		ATCC 10145		
N. gonorrhoeae			Clinical isolate	

Supplementary References

1. L. L. Ling *et al.*, A new antibiotic kills pathogens without detectable resistance. *Nature* **517**, 455-459 (2015).
2. A. M. Bolger, M. Lohse, B. Usadel, Trimmomatic: a flexible trimmer for Illumina sequence data. *Bioinformatics* **30**, 2114-2120 (2014).
3. H. Li, R. Durbin, Fast and accurate short read alignment with Burrows-Wheeler transform. *Bioinformatics* **25**, 1754-1760 (2009).
4. A. McKenna *et al.*, The Genome Analysis Toolkit: a MapReduce framework for analyzing next-generation DNA sequencing data. *Genome Res* **20**, 1297-1303 (2010).
5. D. S. Orlov, T. Nguyen, R. I. Lehrer, Potassium release, a useful tool for studying antimicrobial peptides. *Journal of microbiological methods* **49**, 325-328 (2002).
6. P. Mellroth *et al.*, LytA, major autolysin of Streptococcus pneumoniae, requires access to nascent peptidoglycan. *J Biol Chem* **287**, 11018-11029 (2012).
7. H. Strahl, L. W. Hamoen, Membrane potential is important for bacterial cell division. *Proc Natl Acad Sci U S A* **107**, 12281-12286 (2010).
8. C. A. Schneider, W. S. Rasband, K. W. Eliceiri, NIH Image to ImageJ: 25 years of image analysis. *Nat Methods* **9**, 671-675 (2012).
9. W. Lennox, H. Qi, D.-h. Lee, S. Choi, Y.-c. Moon. (PTC Therapeutics, Inc. (South Plainfield, NJ, US) USA, 2006), vol. WO 2006065480 A2.
10. J. A. King, F. H. McMillan, The decarboxylative acylation of arylacetic acids. *Journal of the American Chemical Society* **73**, 4911-4915 (1951).
11. Y. C. Xu *et al.*, N-Methyl-5-tert-butyltryptamine: A novel, highly potent 5-HT1D receptor agonist. *J Med Chem* **42**, 526-531 (1999).
12. T. Akalaeva *et al.*, Antitubercular, antifungal, and antibacterial activity in vitro of 1-phenethylamino-1, 2, 3, 4-tetrahydrocarbazoles. *Pharmaceutical Chemistry Journal* **24**, 826-829 (1990).
13. X. Li, R. Vince, Conformationally restrained carbazolone-containing alpha,gamma-diketo acids as inhibitors of HIV integrase. *Bioorg Med Chem* **14**, 2942-2955 (2006).
14. S. D. Boggs *et al.*, Efficient asymmetric synthesis of N-[(1 R)-6-chloro-2, 3, 4, 9-tetrahydro-1 H-carbazol-1-yl]-2-pyridinecarboxamide for treatment of human papillomavirus infections. *Organic process research & development* **11**, 539-545 (2007).
15. F. Gehre *et al.*, Role of teichoic acid choline moieties in the virulence of Streptococcus pneumoniae. *Infect Immun* **77**, 2824-2831 (2009).
16. L. McGee *et al.*, Nomenclature of major antimicrobial-resistant clones of Streptococcus pneumoniae defined by the pneumococcal molecular epidemiology network. *Journal of clinical microbiology* **39**, 2565-2571 (2001).
17. h. w. e. o. The European Committee on Antimicrobial Susceptibility Testing. Breakpoint tables for interpretation of MICs and zone diameters. Version 7.1. (http://www.eucast.org).
18. P. Mellroth *et al.*, LytA, major autolysin of Streptococcus pneumoniae, requires access to nascent peptidoglycan. *Journal of Biological Chemistry* **287**, 11018-11029 (2012).
19. R. G. Kansal, A. McGeer, D. E. Low, A. Norrby-Teglund, M. Kotb, Inverse relation between disease severity and expression of the streptococcal cysteine protease, SpeB, among clonal M1T1 isolates recovered from invasive group A streptococcal infection cases. *Infect Immun* **68**, 6362-6369 (2000).

20. J. Radeck *et al.*, Anatomy of the bacitracin resistance network in B acillus subtilis. *Molecular Microbiology* **100**, 607-620 (2016).
21. H. Harms *et al.*, Antimicrobial Dialkylresorcins from marine-derived microorganisms: insights into their mode of action and putative ecological relevance. *Planta medica* **84**, 1363-1371 (2018).
22. P. Sass, G. Bierbaum, Native graS mutation supports the susceptibility of Staphylococcus aureus strain SG511 to antimicrobial peptides. *International Journal of Medical Microbiology* **299**, 313-322 (2009).
23. NARSA, Network on Antimicrobial Resistance in Staphylococcus aureus, library https://app1.unmc.edu/fgx/methods.html. (2020).
24. A. Müller *et al.*, Differential daptomycin resistance development in Staphylococcus aureus strains with active and mutated gra regulatory systems. *International Journal of Medical Microbiology* **308**, 335-348 (2018).
25. S. Herbert *et al.*, Repair of global regulators in Staphylococcus aureus 8325 and comparative analysis with other clinical isolates. *Infect Immun* **78**, 2877-2889 (2010).
26. K. Hiramatsu *et al.*, Methicillin-resistant Staphylococcus aureus clinical strain with reduced vancomycin susceptibility. *The Journal of antimicrobial chemotherapy* **40**, 135-136 (1997).
27. P. Sass *et al.*, Genome sequence of Staphylococcus aureus VC40, a vancomycin- and daptomycin-resistant strain, to study the genetics of development of resistance to currently applied last-resort antibiotics. *J Bacteriol* **194**, 2107-2108 (2012).
28. S. Iordanescu, M. Surdeanu, Two Restriction and Modification Systems in Staphylococcus aureusNCTC8325. *Microbiology* **96**, 277-281 (1976).
29. C. Weidenmaier *et al.*, Role of teichoic acids in Staphylococcus aureus nasal colonization, a major risk factor in nosocomial infections. *Nature medicine* **10**, 243-245 (2004).

Chapter 6

The dual mode of antibacterial action of the synthetic small molecule DCAP involves lipid II binding

The synthetic small molecule 2-((3-(3,6-dichloro-9H-carbazol-9-yl)-2-hydroxypropyl)amino)-2-(hydroxymethyl)propane-1,3-diol (DCAP) was previously identified in an *in vitro* high-throughput screening in search for cell division inhibitors (Eun *et al.*, 2012). The synthetic compound exhibits antibacterial activity against Gram-positive and Gram-negative bacteria. DCAP was previously suggested to increase permeability of the bacterial membrane leading to depolarization. DCAP shows structural similarity to lipid II-binding THCz (**chapter 5**), and the aim of this study was thus to revisit the proposed mechanism of action in search for a specific target.

Killing assays revealed the strong lytic activity of DCAP to be autolysin-mediated, pointing towards a more complex mode of action than previously anticipated. Remarkably, acquistion of resistance was not observed during serial passaging of *S. aureus* in presence of DCAP. Moreover, fluorescence microscopy of *Staphyloccous aureus* cells demonstrated mislocalization of the cell division proteins FtsZ and FtsW to aberrant septa in DCAP-treated cells. In constrast to the membrane-depolarizing ionophore carbonyl cyanide *m*-chlorophenylhydrazone (CCCP), DCAP treatment led to delocalization of the septal signal of the fluorescent D-amino acid HADA indicating a reduced transpeptidase activity and pointing towards a more direct interference with cell wall biosynthesis.

Bioreporters and characteristic cell-shape deformations of *Bacillus subtilis* revealed that DCAP targets cell wall biosynthesis and interferes with the lipid II cycle. Corroborating, the soluble peptidoglycan precursor UDP-*N*-acetylmuramic acid-pentapeptide accumulated in *S. aureus* cells indicating that DCAP blocks a late-stage peptidoglycan biosynthesis step. The impact of DCAP on cell wall biosynthesis reactions was investigated by use of purified recombinant biosynthetic enzymes of *S. aureus*. DCAP inhibited lipid II-consuming reactions as well as reactions that convert undecaprenyl pyrophosphate (C_{55}-PP)-coupled lipid substrates. In line with this observation, DCAP caused delocalization of the bifunctional penicillin-binding protein 2 (PBP2). A direct interaction of DCAP with the cell wall biosynthesis lipid substrates was further supported by the fact that addition of C_{55}-PP-containing lipid intermediates of peptidoglycan, wall teichoic acid and capsule biosyntheses antagonized the DCAP-induced cell wall stress response in *B. subtilis*.

The results of this study refine the mode of action of DCAP to exert a dual mode of action that combines membrane disturbance and specific binding to the peptidoglycan precursor lipid II. Like teixobactin, the compound's ability to bind to multiple cell wall intermediates, triggering rapid autolysin-mediated cell lysis, may account for the low propensity of resistance development. DCAP represents another chemically-synthesized lipid II-binding antibiotic amenable to derivatization for future development of antibiotics that can be used to combat multidrug-resistant bacterial infections.

K.C.L. performed all the experimental work apart from fluorescence microscopy and cytotoxicity assays, analyzed the data and wrote the manuscript with the input from the co-authors.

The dual mode of antibacterial action of the synthetic small molecule DCAP involves lipid II binding

Kevin C. Ludwig[†,⊥,#], Jan-Samuel Puls[†,#], Cruz L. Matos de Opitz[§], Jan Bornikoel[§], Melina Arts[†], Sebastian Krannich[†], Jan Straetener[§], Dominik Brajtenbach[‡], Beate Henrichfreise[†], Peter Sass[§,‖], Anna Müller[†], Heike Brötz-Oesterhelt[§,‖], Ulrich Kubitscheck[‡], Fabian Grein[†,⊥,*], and Tanja Schneider[†,⊥,*]

[†]Institute for Pharmaceutical Microbiology, University of Bonn, Meckenheimer Allee 168, 53115 Bonn, Germany
[‡]Institute for Physical and Theoretical Chemistry, University of Bonn, Wegelerstraße 12, 53115 Bonn, Germany
[§]Department of Microbial Bioactive Compounds, Interfaculty Institute of Microbiology & Infection Medicine, University of Tübingen, Auf der Morgenstelle 28, 72076 Tübingen, Germany
[‖]German Center for Infection Research (DZIF), partner site Tübingen, Tübingen, Germany
[⊥]German Center for Infection Research (DZIF), partner site Bonn-Cologne, Bonn, Germany

ABSTRACT: The synthetic small molecule DCAP is a chemically well characterized compound with antibiotic activity against Gram-positive and Gram-negative bacteria, including drug-resistant pathogens. Until now its mechanism of action was proposed to rely exclusively on targeting of bacterial membranes, thereby causing membrane depolarization, and increasing membrane permeability (Eun *et al.* 2012, *J. Am. Chem. Soc.* 134 (28), 11322– 11325, Hurley *et al.* 2015, *ACS Med. Chem. Lett.* 6, 466-471). Here we show that the antibiotic activity of DCAP results from a dual mode of action that is more multifaceted than previously anticipated. Using microbiological and biochemical assays in combination with fluorescence microscopy we provide evidence that DCAP interacts with undecaprenyl pyrophosphate-coupled cell envelope precursors, thereby blocking peptidoglycan biosynthesis and impairing cell division site organization. Our work discloses a concise model for the mode of action of DCAP exerting pleiotropic effects on cell wall biosynthetic and divisome machineries in accord with membrane effects.

The emergence of multi-drug resistance among most bacterial pathogens rises intensely and thwarts the efficacy and lifespan of antibiotics.[1,2] These days, 1,27 million people die per year due to infections attributable to antibiotic-resistant bacteria and it was estimated that, if the trend continues, this number will dramatically increase in the future.[3,4] Thus, there is a pressing need to develop new therapeutic drugs with new mechanisms of action capable of circumventing resistance development.

A previous *in vitro* high-throughput screening for novel cell division inhibitors identified the synthetic small molecule 2-((3-(3,6-**d**ichloro-9*H*-**c**arbazol-9-yl)-2-hydroxypropyl)**a**mino)-2-(hydroxymethyl)**p**ropane-1,3-diol (DCAP).[5] The compound was shown to be active against Gram-positive and Gram-negative bacteria and was found to be efficient at eradicating biofilm-associated cells.[5] Furthermore, DCAP was shown to reduce uropathogenic *Escherichia coli* infections by modulating autophagy.[2] The results of the original study pointed towards a multifaceted membrane-targeting mechanism of action, inducing the collapse of transmembrane potential, an increase of membrane permeability, and mislocalization of essential membrane-associated proteins.[5] Therefore, it was hypothesized, that DCAP combines membrane effects with specific target binding.[5] It has been speculated that the compound interacts with lipids or proteins in the bacterial membrane, however, no molecular target had been identified so far. Therefore, we set out to characterize the cellular consequences that lead to cell death upon DCAP treatment to ultimately identify a putative molecular target.

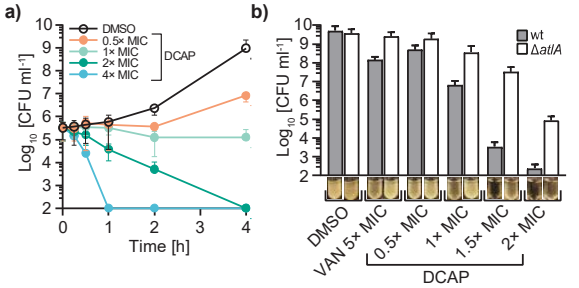

Figure 1. DCAP rapidly kills *S. aureus*. (a) Killing kinetics of early-exponential phase-grown *S. aureus* in the presence of DCAP. (b) DCAP treatment resulted in AtlA-mediated lysis as demonstrated with an Δ*atlA* mutant of *S. aureus* exhibiting markedly reduced lysis. Survival of exponential phase-grown *S. aureus* cells after 24 h of DCAP-treatment. Exemplary images of cultures are shown below the respective columns. Data of both graphs are representative of 3 independent experiments. Error bars represent the standard deviation (SD).

Previous studies already tested a variety of important bacterial pathogens and model organisms for their susceptibility against DCAP.[5,7] We expanded this list and observed moderate antibacterial activity against a variety of Gram-positive pathogens including drug-resistant *Staphylococcus aureus*, methicillin-resistant *S. epidermidis* (MRSE), and vancomycin-resistant enterococci (VRE). A slightly lower activity was observed against mycobacteria and Gram-negative species (Table S1). We next assessed the killing kinetics of DCAP and

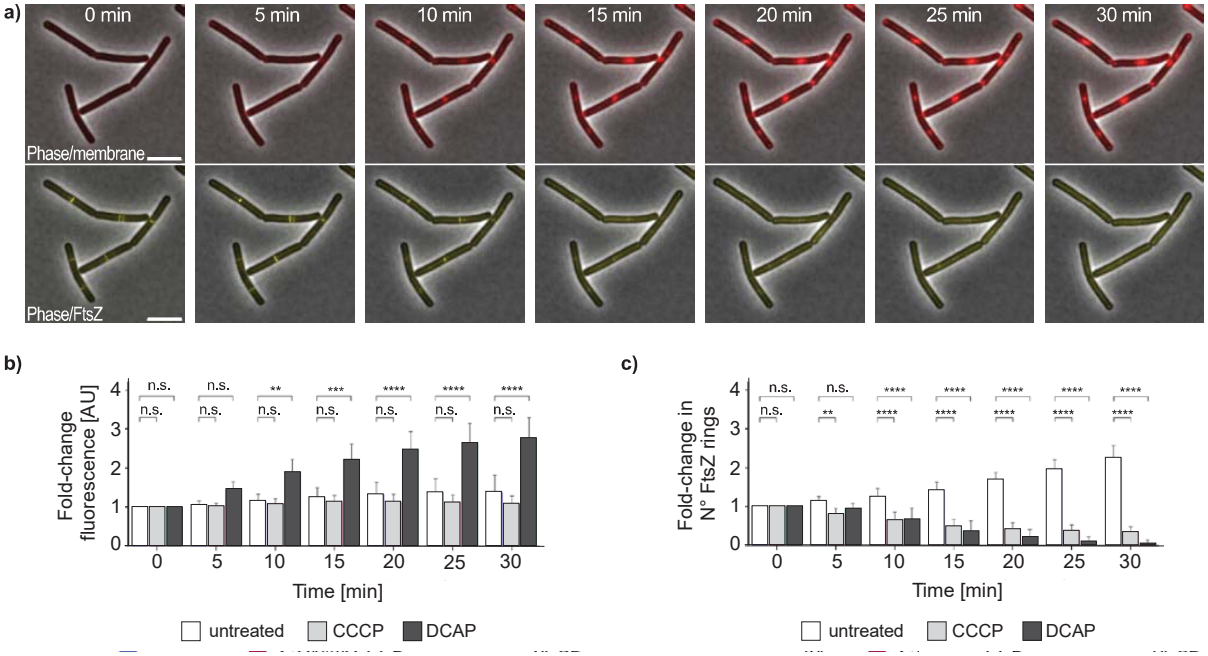

Figure 2. DCAP leads to localized membrane perturbation at the septum and subsequent delocalization of FtsZ. (a) Time-lapse fluorescence microscopy of exponentially growing *B. subtilis* 2020 cells treated with DCAP at 0.5× MIC. Images show channel overlays of phase contrast with either FM4-64-labelled cell membrane (upper panel, FM4-64/membrane in red) or GFP-tagged FtsZ (lower panel, in yellow). The micrographs show that DCAP treatment induces localized perturbation of the cell membrane at the septum area, which precedes the delocalization of FtsZ from mid-cell. Scale bars = 5 µm. Images are representative of at least three biological replicate cultures of *B. subtilis* 2020 with >700 septa/FtsZ rings monitored over time. A time-lapse video is provided by Supplementary movie 2. (b) Time-resolved fold change of the septal FM4-64 fluorescence signal during DCAP treatment. In contrast to the untreated or CCCP-treated controls, DCAP leads to a significant increase in fluorescence intensity of the lipophilic dye FM 4-64 at the septum, which is indicative for membrane perturbation in this area. Data are represented as mean values of three independent experiments analyzing >700 septa over time. Error bars represent the SD. Two-way ANOVA, ****p<0.0001. (c) Time-resolved fold change of the number of disintegrated FtsZ-rings during DCAP exposure. Data are represented as mean values of three independent experiments analyzing >700 FtsZ rings over time. Error bars represent the SD. Two-way ANOVA, ****p<0.0001.

found it to be rapidly bactericidal towards *S. aureus* (Figure 1a) and in line with the previously described bacteriolytic effect on *Caulobacter cresentus*,[5] we found that DCAP is also bacteriolytic towards *S. aureus.* DCAP caused lysis already at low concentrations and this lysis phenotype was largely mediated by the major *S. aureus* autolysin AtlA (Figure 1b). These observations supported the idea of a more complex mode of action that goes beyond an impact on the transmembrane potential as shown by the previous comparison of DCAP and the ionophore carbonyl cyanide *m*-chlorophylhydrazone (CCCP).[5]

To gain deeper insights into the membrane effects of DCAP, we next established a live-cell microscopy-based method that allows the simultaneous spatio-temporal visualization of membrane effects with effects on the integrity of FtsZ-rings as a measure of the transmembrane potential in *Bacillus subtilis*. In untreated cells, the membrane was uniformly stained by FM4-64 in the course of the experiment and FtsZ was found to form FtsZ-rings at the division sites (Figure S1a and Video S1). In contrast, DCAP led to localized membrane perturbation at the septum area and subsequent delocalization of FtsZ (Figure 2 and Video S2). Of note, such localized membrane effect was not observed for cells treated with CCCP (Figure S1b and Video S3). We therefore hypothesized that DCAP may first affect membrane integrity at the septum area in a specific, target-mediated manner, which then causes downstream effects on the overall membrane potential that leads to delocalization of FtsZ.

We next set out to acquire a better understanding of the distinctive cellular effects of DCAP on the cell phenotype of *S. aureus*. DCAP-treated cells displayed aberrant septa including multiple septation, failed cell separation and a unique bent septum phenotype, while CCCP had no significant effect on septum morphology (Figure 3a). As septum formation is closely linked to cell division and cell wall biosynthesis, we examined the effect of DCAP on FtsZ and the essential peptidoglycan (PGN) biosynthesis protein FtsW. We found both proteins localizing at misplaced or aberrant septa in almost 40% of the cells (Figure 3b,c) upon DCAP treatment. Furthermore, a considerable fraction of cells displayed complete disassembly of Z-rings with subsequent effects on FtsW localization. CCCP in contrast did not alter septum morphology significantly, but in line with its activity on the transmembrane potential induced disintegration of the Z-ring[8] more effectively than DCAP. Interestingly, the abundance of cells with Z-ring dissolution increased with higher concentrations of DCAP, while the effect on septum phenotype did not, indicating a higher efficiency of septum disorganization than of a general transmembrane potential disruption at low concentrations.

Disturbed septum formation as observed for DCAP treatment is a typical effect of cell wall biosynthesis machinery (CWBM)-inhibiting antibiotics.[9,10] We therefore studied the effect of DCAP on the transpeptidase activities of *S. aureus* and *B. subtilis* through the incorporation of the fluorescent amino acid HCC-amino-D-alanine (HADA) *in vivo*. While CCCP and DCAP both

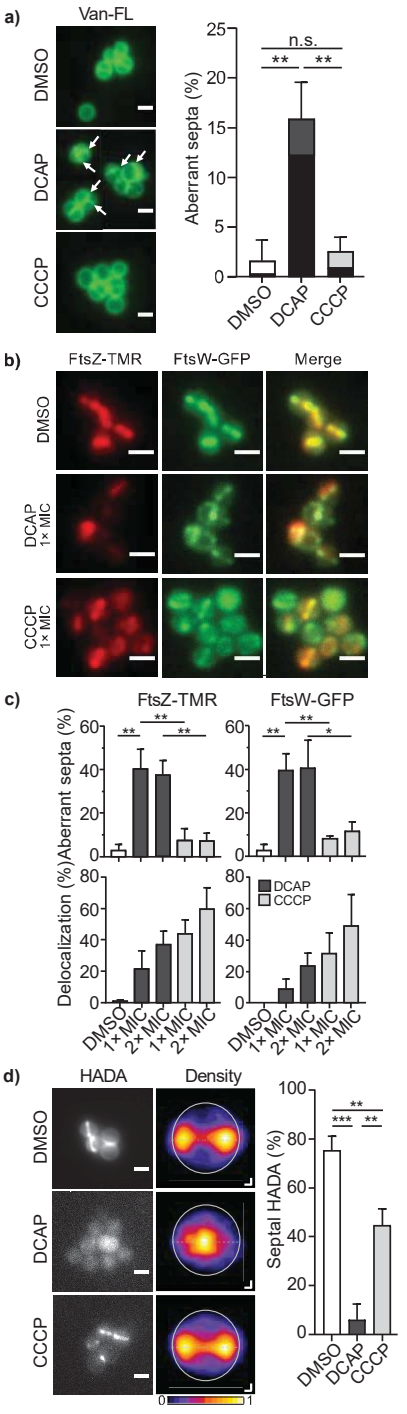

Figure 3. DCAP disrupts *S. aureus* cell division and cell wall biosynthesis. (a) DCAP (1× MIC) induces aberrated septum morphology (white bars), including multiple septation, impaired cell separation and a unique bent septum phenotype (black bars, white arrows). Cell morphology was visualized via vancomycin-FL cell wall staining. (b) and (c) FtsZ and FtsW localize at aberrant septa after DCAP treatment. Higher DCAP concentrations lead to additional Z-Ring disassembly with subsequent effects on FtsW localization. In contrast, CCCP does not alter septum morphology significantly, but affects Z-Ring disintegration more effectively compared to DCAP. Representative images shown for FtsZ-SNAP stained with SNAP-TMR-Star (red) and FtsW-GFP (green). (d) DCAP (2× MIC) causes diffuse distribution of fluorescent D-amino acid HADA incorporation, indicating inhibition of septal transpeptidase activity, which occurs across the leading edge of the developing septum. CCCP (2× MIC) does not alter HADA fluorescence distribution. Representative images (individually adjusted) and density rendering of HADA fluorescence maxima analysis. HADA density scale bar = 0.1 µm for x and y, respectively. All data quantified from $n \geq 300$ cells from 3 independent biological experiments ($n \geq 100$ per replicate).

reduced HADA fluorescence intensity (Figure S2 and S3), DCAP remarkably caused complete dislocation of the signal resulting in homogenous fluorescence distribution across the cell. CCCP instead had considerably less effect on spatial organization of the transpeptidase activity with most of the HADA fluorescence remaining septal (Figures 3c and S3). From these experiments we concluded that DCAP may directly impact the CWBM and indeed, cell wall biosynthesis was identified as the target pathway using pathway-selective *B. subtilis* bioreporters (Figures 4a and S4). Moreover, treatment with DCAP and other cell wall-targeting antibiotics resulted in similar characteristic membrane blebbing of methanol-acetic acid-fixed cells, whereas non-cell wall targeting and exclusively membrane-affecting compounds such as CCCP and valinomycin did not (Figures 4a and S5), reaffirming DCAP to impair cell wall integrity.[11]

Treating cells with compounds that interfere with late-stage PGN biosynthesis steps e.g. by binding to lipid II, usually leads to intracellular accumulation of the ultimate soluble PGN precursor UDP-*N*-acetylmuramic acid-pentapeptide (UDP-MurNAc-pp). Notably, we found a strong and dose-dependent accumulation of UDP-MurNAc-pp upon DCAP treatment (Figure 4b). It has been shown that treating *S. aureus* with the lipid II binding antibiotic vancomycin leads to a delocalization of the penicillin binding protein 2 (PBP2) in *S. aureus*.[12] Likewise, DCAP significantly decreased the fraction of cells with PBP2 present at the septum and reduced the ratio of septal to peripheral fluorescence in those cells (Figure S6).

From these results we hypothesized that DCAP may bind to lipid II and/or that it interferes with its biosynthesis. To test this hypothesis, we monitored the induction of the *B. subtilis* LiaRS two-component system (TCS), which is known to respond to lipid II cycle-interfering antibiotics.[13] Indeed, DCAP induced the LiaRS-mediated cell envelope stress response. Moreover, pre-incubation with purified lipid II was found to antagonize this response in a dose-dependent manner, indicating a direct and specific interaction of DCAP with lipid II (Figure 4c).

Having lipid II identified as a molecular target of DCAP, we next determined the minimal biding motif of DCAP. To this end, we tested different undecaprenyl pyrophosphate (C_{55}PP)-containing PGN biosynthesis precursors for their ability to antagonize the LiaRS activation. Lipid I, lipid II, the wall teichoic acid (WTA) precursor lipid III_{WTA}, and the streptococcal capsule biosynthesis precursor lipid II_{cap} (C_{55}PP-glucose-galactose) all antagonized the DCAP-induced LiaRS response at molar ratios of 2:1 (lipid:DCAP), suggesting that DCAP is likely to form dimers with lipids containing a C_{55}PP motif (Figures 4c and S7). The lipid II variant found in vancomycin-resistant enterococci and vancomycin-resistant *S. aureus* with the stem peptide ending in D-Ala-D-Lac antagonized the response as efficiently as the variant ending in D-Ala-D-Ala. Notably, the interaction with the first sugar moiety attached to C_{55}PP appears to be crucial for higher binding affinity since a 4:1 molar ratio was required for only C_{55}PP (Figure S7), as also observed for structure-

related tetrahydrocarbazoles (THCz).[14] In contrast, even at a 10:1 molar ratio, $C_{55}P$, the soluble precursor UDP-MurNAc-pp and UDP-GlcNAc did not antagonize the LiaRS response. These findings strongly pointed towards the lipid-bound pyrophosphate moiety as the minimal molecular binding motif of DCAP. To confirm this, we tested the impact of DCAP on a cascade of individual *S. aureus* cell wall biosynthesis reactions *in vitro*. The initial membrane-associated step of PGN synthesis is catalyzed by the glycosyltransferase MraY that links UDP-MurNAc-pp to the lipid carrier undecaprenyl phosphate ($C_{55}P$), yielding lipid I (Figure 4d).[15] This reaction, which does not involve $C_{55}PP$, was not inhibited. In contrast, the MurG-catalyzed synthesis of lipid II though addition of UDP-activated *N*-acetylglucosamine (GlcNAc) to lipid I was inhibited in a dose-dependent manner when DCAP was added (Figure 4d).[16] Likewise, the MurT-GatD-catalyzed amidation of lipid II[17] as well as the PBP2-mediated transglycosylation and PBP4-mediated carboxypeptidation of the PGN precursor were blocked.[18] Furthermore, DCAP inhibited dephosphorylation of $C_{55}PP$ to $C_{55}P$ (Figure 4d), an essential recycling step conducted by $C_{55}PP$ phosphatases such as the tested YbjG phosphatase.[19] Also, synthesis of the WTA precursor lipid IV_{WTA} catalyzed by the glycosyltransferase TarA was inhibited (Figure 4d).[20] All inhibited reactions were fully blocked at a 4-fold molar excess of DCAP with respect to the corresponding lipid substrate, clearly indicating that DCAP interacts with the lipid substrates rather than inhibiting one of the enzymes. In summary, all reactions where the lipid substrate contained a pyrophosphate group were inhibited, strongly suggesting that moiety to be the molecular binding motif of DCAP. In line with that, only those lipids antagonized the bactericidal effect of DCAP *in vivo*, which contained this pyrophosphate moiety while the length of the prenyl chain appeared to be not important (Table S2).

Combining *in vivo* and *in vitro* results we concluded, that DCAP directly interacts with all $C_{55}PP$-containing lipids of PGN, capsule, and WTA synthesis, including lipid II. This implies a potent primary binding event to multiple key biosynthesis precursors *in vivo*, resulting in a massively reduced chance for resistance and a more complex dual mode of action that exceeds the previously anticipated membrane activity of the DCAP scaffold by extending to an impaired cell division site and CWBM organization and direct PGN synthesis inhibition. Accordingly, we were unable to isolate resistant mutants of *S. aureus*, when serially passaged in the presence of sub-MIC levels of DCAP over a period of 25 days (Figure S8).

Finally, we expanded previous toxicity studies which found that DCAP is moderately toxic to rabbit red blood cells at 50 µM (20.7 µg ml^{-1}).[5] We assessed hemolysis in human red blood

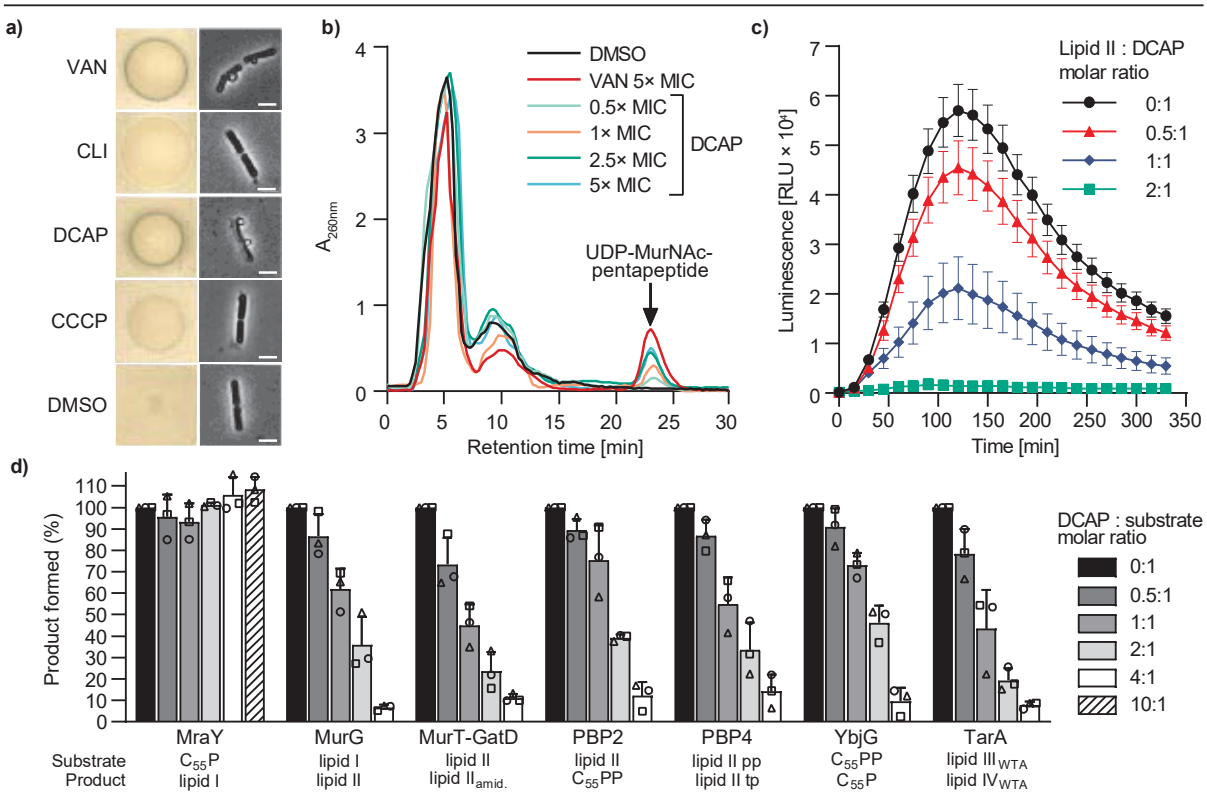

Figure 4: DCAP targets bacterial cell wall biosynthesis. (a) *Left:* DCAP activated the *B. subtilis ypuA* promotor, selectively responding to antibiotic interference with the cell wall biosynthesis pathway, as observed by a blue halo at the edge of the inhibition zone. *Right:* Phase-contrast microscopy of *B. subtilis* revealed that DCAP causes impairment of cell wall integrity as severe cell-shape deformations and characteristic membrane blebs were observed. Scale bar = 2 µm. (b) Cytoplasmic accumulation of the soluble peptidoglycan precursor UDP-*N*-acetylmuramic acid pentapeptide (UDP-MurNAc-pp, indicated by arrow) in DCAP-treated *S. aureus*. (c) Antagonization of DCAP-induced cell wall stress response of *B. subtilis* P_{liaI}-*lux* by lipid II. Full antagonization of the P_{liaI}-*lux* signal is achieved at a 2:1 molar ratio (lipid II:DCAP). Error bars represent the SD of three independent experiments (d) Impact of DCAP on individual cell wall biosynthesis reactions *in vitro* using purified substrates and *S. aureus* enzymes. DCAP inhibits all reactions with $C_{55}PP$-containing lipid substrates or $C_{55}PP$ in a dose-dependent manner and almost completely inhibits enzymatic activity when added in 4-fold molar excess. The amount of reaction product formed in the absence of DCAP was taken 100%. DCAP was added at molar ratios of 0.5 to 10:1 with respect to the lipid substrates as indicated. Data represent mean values from three independent experiments and error bars represent the SD. pp, pentapeptide; tp, tetrapeptide.

cells and found DCAP but not CCCP to be inert up to 128 µg ml^{-1} (Figure S9a). Time- and dose-dependent cytotoxic effects were observed in both human epithelial (HEp-2) and murine McCoy B cells upon treatment with DCAP (Figure S9b to e). Importantly, toxicity did not arise from major membrane lesions as no effect of DCAP on membrane integrity was found even at 4× IC_{50} (Figure S10a). The fact that membrane integrity of *B. subtilis* cells was severely impaired at the 4× MIC (Figure S10b) but not the membrane integrity of HEp-2 cells again points to the presence of a specific molecular target that is present in bacterial cells but absent in human cell membranes. As such, C_{55}PP is absent in human cell membranes but is present in bacteria and also in mitochondria. Interestingly, we found DCAP to depolarize mitochondria within HEp-2 cells at 4× IC_{50} (Figure S10c) which is well in line with previous observations in human epithelial kidney (HEK) cells.[5]

Based on our findings we propose that DCAP exerts a complex dual mode of action that involves both membrane integrity impairment and binding of essential lipid precursors of the cell wall biosynthesis including lipid II. Our findings suggest, that these two effects are independent from each other, leading to massive effects on the membrane potential as well as on cell division and cell wall biosynthesis organization to cumulate to a rapid cell death in a synergistic fashion (Figure S11).

DCAP provides an insightful example into the potentials of fully synthetic antimicrobial scaffolds. The results obtained in this study illustrate that the mode of action of these small synthetic molecules can be multifaceted and complex, despite the straightforward first impression of their antibiotic activity and their small size. Furthermore, the synthetic character of these molecules allows for easy optimization of their features and improved understanding of the building blocks required for different aspects of their molecular action. As such, Hurley *et al.* were able to improve antibacterial activity of the DCAP scaffold by increasing the hydrophobicity of the tail-region and were able to prove essentiality of the carbazole moiety for activity.[7] We suggest, that this moiety is responsible for interaction with pyrophosphate, probably in concert with the amino-linker. Structurally related THCz[14] share similar features of spatially close amino groups, while lacking the distinctive chlorine substitutions of DCAP, indicating an important role of the amines and a possible explanation for the difference in binding between one and two phosphates (meaning more negative charges to interact with the positively polarized amino groups). Further improvement of this molecular interaction combined with increased hydrophobi-city as shown by Hurley *et al.* could maximize the bactericidal action of the DCAP scaffold. Following the recently identified THCz, DCAP joins the class of small molecule lipid II-binding cell wall antibiotics and represents another promising candidate for further development.

ASSOCIATED CONTENT

Supporting Information

The Supporting Information is available free of charge on the xxxxx Publications website at DOI: xxxxx.

AUTHOR INFORMATION

Corresponding Authors

*grein@uni-bonn.de; tschneider@uni-bonn.de

Author Contributions

#K.C.L. and J.-S.P. contributed equally.

Funding Sources

Funding was provided by the German Research Foundation (DFG), TRR261, project ID 398967434.

Notes

The authors declare no competing financial interest.

ACKNOWLEDGMENT

We thank Vanessa Becker for preparation and purification of streptococcal lipid II_{cap} and Thorsten Mascher for providing strain TMB1617 *B. subtilis* W168 *sacA*::pCHlux101 (P_{lial}-*lux*).

ABBREVIATIONS

CWBM, cell wall biosynthesis machinery; PGN, peptidoglycan; TCS, two-component system; WTA, wall teichoic acid.

REFERENCES

(1) Tacconelli, E.; Carrara, E.; Savoldi, A.; Harbarth, S.; Mendelson, M.; Monnet, D. L.; Pulcini, C.; Kahlmeter, G.; Kluytmans, J.; Carmeli, Y.; Ouellette, M.; Outterson, K.; Patel, J.; Cavaleri, M.; Cox, E. M.; Houchens, C. R.; Grayson, M. L.; Hansen, P.; Singh, N.; Theuretzbacher, U.; Magrini, N.; Aboderin, A. O.; Al-Abri, S. S.; Awang Jalil, N.; Benzonana, N.; Bhattacharya, S.; Brink, A. J.; Burkert, F. R.; Cars, O.; Cornaglia, G.; Dyar, O. J.; Friedrich, A. W.; Gales, A. C.; Gandra, S.; Giske, C. G.; Goff, D. A.; Goossens, H.; Gottlieb, T.; Guzman Blanco, M.; Hryniewicz, W.; Kattula, D.; Jinks, T.; Kanj, S. S.; Kerr, L.; Kieny, M.-P.; Kim, Y. S.; Kozlov, R. S.; Labarca, J.; Laxminarayan, R.; Leder, K.; Leibovici, L.; Levy-Hara, G.; Littman, J.; Malhotra-Kumar, S.; Manchanda, V.; Moja, L.; Ndoye, B.; Pan, A.; Paterson, D. L.; Paul, M.; Qiu, H.; Ramon-Pardo, P.; Rodríguez-Baño, J.; Sanguinetti, M.; Sengupta, S.; Sharland, M.; Si-Mehand, M.; Silver, L. L.; Song, W.; Steinbakk, M.; Thomsen, J.; Thwaites, G. E.; van der Meer, J. W.; Van Kinh, N.; Vega, S.; Villegas, M. V.; Wechsler-Fördös, A.; Wertheim, H. F. L.; Wesangula, E.; Woodford, N.; Yilmaz, F. O.; Zorzet, A. *Lancet Infect. Dis.* **2018**, *18* (3), 318–327.

(2) Brown, E. D.; Wright, G. D. *Nature* **2016**, *529* (7586), 336–343.

(3) O'Neill, J. *Heal. Wealth Nations* **2014**, December, 1–16.

(4) Murray, C. J.; Ikuta, K. S.; Sharara, F.; Swetschinski, L.; Robles Aguilar, G.; Gray, A.; Han, C.; Bisignano, C.; Rao, P.; Wool, E.; Johnson, S. C.; Browne, A. J.; Chipeta, M. G.; Fell, F.; Hackett, S.; Haines-Woodhouse, G.; Kashef Hamadani, B. H.; Kumaran, E. A. P.; McManigal, B.; Agarwal, R.; Akech, S.; Albertson, S.; Amuasi, J.; Andrews, J.; Aravkin, A.; Ashley, E.; Bailey, F.; Baker, S.; Basnyat, B.; Bekker, A.; Bender, R.; Bethou, A.; Bielicki, J.; Boonkasidecha, S.; Bukosia, J.; Carvalheiro, C.; Castañeda-Orjuela, C.; Chansamouth, V.; Chaurasia, S.; Chiurchiù, S.; Chowdhury, F.; Cook, A. J.; Cooper, B.; Cressey, T. R.; Criollo-Mora, E.; Cunningham, M.; Darboe, S.; Day, N. P. J.; De Luca, M.; Dokova, K.; Dramowski, A.; Dunachie, S. J.; Eckmanns, T.; Eibach, D.; Emami, A.; Feasey, N.; Fisher-Pearson, N.; Forrest, K.; Garrett, D.; Gastmeier, P.; Giref, A. Z.; Greer, R. C.; Gupta, V.; Haller, S.; Haselbeck, A.; Hay, S. I.; Holm, M.; Hopkins, S.; Iregbu, K. C.; Jacobs, J.; Jarovsky, D.; Javanmardi, F.; Khorana, M.; Kissoon, N.; Kobeissi, E.; Kostyanev, T.; Krapp, F.; Krumkamp, R.; Kumar, A.; Kyu, H. H.; Lim, C.; Limmathurotsakul, D.; Loftus, M. J.; Lunn, M.; Ma, J.; Mturi, N.; Munera-Huertas, T.; Musicha, P.; Mussi-Pinhata, M. M.; Nakamura, T.; Nanavati, R.; Nangia, S.; Newton, P.; Ngoun, C.; Novotney, A.; Nwakanma, D.; Obiero, C. W.; Olivas-Martinez, A.; Olliaro, P.; Ooko, E.; Ortiz-Brizuela, E.; Peleg, A. Y.; Perrone, C.; Plakkal, N.; Ponce-de-Leon, A.; Raad, M.; Ramdin, T.; Riddell, A.; Roberts, T.; Robotham, J. V.; Roca, A.; Rudd, K. E.; Russell, N.; Schnall, J.; Scott, J. A. G.; Shivamallappa, M.; Sifuentes-Osornio, J.; Steenkeste, N.; Stewardson, A. J.; Stoeva, T.; Tasak, N.; Thaiprakong, A.; Thwaites, G.; Turner, C.; Turner, P.; van Doorn, H. R.; Velaphi, S.; Vongpradith, A.; Vu, H.; Walsh, T.; Waner, S.; Wangrangsimakul, T.; Wozniak, T.; Zheng, P.; Sartorius, B.; Lopez, A. D.; Stergachis, A.; Moore, C.; Dolecek, C.; Naghavi, M. *Lancet* **2022**, *6736* (21).

(5) Eun, Y. J.; Foss, M. H.; Kiekebusch, D.; Pauw, D. A.; Westler, W. M.; Thanbichler, M.; Weibel, D. B. *J. Am. Chem. Soc.* **2012**, *134* (28), 11322–11325.

(6) Allavena, G.; Debellis, D.; Marotta, R.; Joshi, C. S.; Mysorekar, I. U.; Grimaldi, B. *Cell Death Dis.* **2018**, *9* (7).

(7) Hurley, K. A.; Heinrich, V. A.; Hershfield, J. R.; Demons, S. T.; Weibel, D. B. *ACS Med. Chem. Lett.* **2015**, *6* (4), 466–471.

(8) Strahl, H.; Hamoen, L. W. *Proc. Natl. Acad. Sci. U. S. A.* **2010**, *107* (27), 12281–12286.

(9) Grein, F.; Müller, A.; Scherer, K. M.; Liu, X.; Ludwig, K. C.; Klöckner, A.; Strach, M.; Sahl, H.; Kubitscheck, U.; Schneider, T. *Nat. Commun.* **2020**, *11* (1), 1455.
(10) Lund, V. A.; Wacnik, K.; Turner, R. D.; Cotterell, B. E.; Walther, C. G.; Fenn, S. J.; Grein, F.; Wollman, A. J. M.; Leake, M. C.; Olivier, N.; Cadby, A.; Mesnage, S.; Jones, S.; Foster, S. J. *Elife* **2018**, *7*, 1–31.
(11) Schneider, T.; Kruse, T.; Wimmer, R.; Wiedemann, I.; Sass, V.; Pag, U.; Jansen, A.; Nielsen, A. K.; Mygind, P. H.; Raventós, D. S.; Neve, S.; Ravn, B.; Bonvin, A. M. J. J.; De Maria, L.; Andersen, A. S.; Gammelgaard, L. K.; Sahl, H.-G.; Kristensen, H.-H. *Science* **2010**, *328* (5982), 1168–1172.
(12) Pinho, M. G.; Errington, J. *Mol. Microbiol.* **2005**, *55* (3), 799–807.
(13) Mascher, T.; Zimmer, S. L.; Smith, T.-A.; Helmann, J. D. *Antimicrob. Agents Chemother.* **2004**, *48* (8), 2888–2896.
(14) Reithuber, E.; Wixe, T.; Ludwig, K. C.; Müller, A.; Uvell, H.; Grein, F.; Lindgren, A. E. G.; Muschiol, S.; Nannapaneni, P.; Eriksson, A.; Schneider, T.; Normark, S.; Henriques-Normark, B.; Almqvist, F.; Mellroth, P. *Proc. Natl. Acad. Sci.* **2021**, *118* (47), e2108244118.
(15) Ikeda, M.; Wachi, M.; Jung, H. K.; Ishino, F.; Matsuhashi, M.. *J. Bacteriol.* **1991**.
(16) Ha, S.; Gross, B.; Walker, S. E. Coli MurG: *Current drug targets. Infectious disorders*. 2001.
(17) Münch, D.; Roemer, T.; Lee, S. H.; Engeser, M.; Sahl, H. G.; Schneider, T. *PLoS Pathog.* **2012**, *8* (1), e1002509.
(18) Srisuknimit, V.; Qiao, Y.; Schaefer, K.; Kahne, D.; Walker, S. *J. Am. Chem. Soc.* **2017**, 139 (29), 9791–9794.
(19) Ginsberg, C.; Zhang, Y. H.; Yuan, Y.; Walker, S. *ACS Chem Biol.* **2006** Feb 17;1(1):25-8.
(20) Workman, S. D.; Strynadka, N. C. *J. Mol. Biol.* **2020**, 432 (18), 4964–4982.

Graphical abstract:

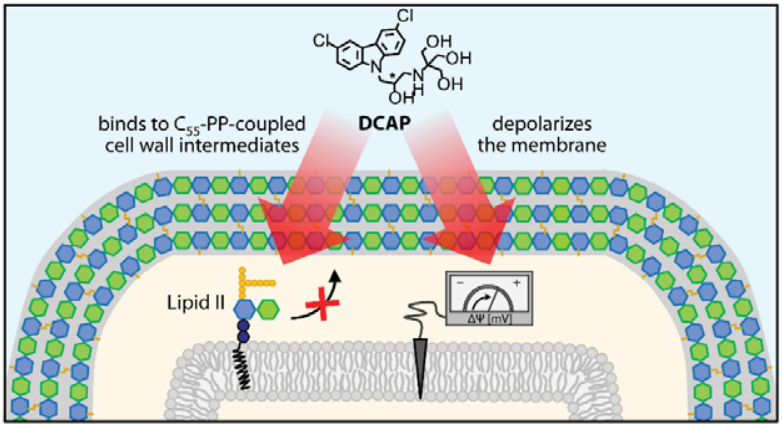

Supporting Information

The dual mode of antibacterial action of the synthetic small molecule DCAP involves lipid II binding

Kevin C. Ludwig[†,⊥], Jan-Samuel Puls[†,], Cruz L. Matos de Opitz[§], Jan Bornikoel[§], Melina Arts[†], Sebastian Krannich[†], Jan Straetener[§], Dominik Brajtenbach[‡], Beate Henrichfreise[†], Peter Sass[§,‖], Anna Müller[†], Heike Brötz-Oesterhelt[§,‖], Ulrich Kubitscheck[‡], Fabian Grein[†,⊥], and Tanja Schneider[†,⊥]

[†]Institute for Pharmaceutical Microbiology, University of Bonn, Meckenheimer Allee 168, 53115 Bonn, Germany
[‡]Institute for Physical and Theoretical Chemistry, University of Bonn, Wegelerstraße 12, 53115 Bonn, Germany
[§]Department of Microbial Bioactive Compounds, Interfaculty Institute of Microbiology & Infection Medicine, University of Tübingen, Auf der Morgenstelle 28, 72076 Tübingen, Germany
[‖]German Center for Infection Research (DZIF), partner site Tübingen, Tübingen, Germany
[⊥]German Center for Infection Research (DZIF), partner site Bonn-Cologne, Bonn, Germany

Material & methods

Antibiotic susceptibility testing

MIC was determined by broth microdilution according to CLSI guidelines[1], in polypropylene microtiter plates (Nunc brand) using cation-adjusted Mueller-Hinton broth (MHB, Oxoid).

Killing kinetics

S. aureus SA113 was grown in MHB at 37 °C to an OD_{600} of 0.5 and diluted 100-fold. 100 µL of bacteria were transferred to 96-well flat bottom plates containing 100 µL of MHB containing DCAP at concentrations corresponding to 0.5×, 1×, 2× and 4× MIC, or DMSO as negative control. At defined time points aliquots were removed, tenfold serially diluted and plated on Mueller-Hinton agar (MHA) plates. CFU ml^{-1} were determined after 24 h incubation at 37°C.

For qualitative analysis of lysis, 3 ml exponential phase-grown cell suspensions of *S. aureus* SA113 and the AtlA-deficient mutant *S. aureus* SA113 Δ*altA* (supplemented with 150 µg ml^{-1} spectinomycin) were adjusted to an OD_{600} of 1 and treated with DCAP at concentrations corresponding to 0.5×, 1×, 1.5× and 2× the MIC, with vancomycin at 5× the MIC, or with DMSO in glass test tubes. After 24 h, cell density was photographed, and aliquots for CFU determination were plated on MHA plates.

β-galactosidase reporter assays

B. subtilis β-galactosidase reporter assays were performed as previously described.[2] In short, reporter strains were grown in MHB containing 5 µg ml^{-1} chloramphenicol at 30 °C to an OD_{600} of 0.5. Subsequently, cells were poured at 1×10^7 CFU ml^{-1} in MHA plates supplemented with 5 µg ml^{-1} chloramphenicol and 75 µg ml^{-1} (cell wall reporter), 125 µg ml^{-1} (DNA reporter), and 250 µg ml^{-1} (RNA and protein reporters) 5-bromo-4-chloro-3-indolyl-β-D-galactopyranoside (X-gal), respectively. After solidification of the plates, 128 µg DCAP, 16 µg carbonyl cyanide *m*-chlorophylhydrazone (CCCP), and control antibiotics inducing the promotors were spotted (6 µg vancomycin for cell wall, 0.3 µg ciprofloxacin for DNA, 6 µg rifampicin for RNA, 3 µg clindamycin for protein). DMSO was used as solvent control. Results were documented after incubation overnight at 30 °C.

Luciferase reporter assays and antagonization

B. subtilis luciferase reporter assays were conducted as previously described.[2,3] Briefly, *B. subtilis* W168 *sacA*::pCHlux101 (P_{liaI}-*lux*) was grown in MHB containing 5 µg ml^{-1} chloramphenicol at 30 °C to an OD_{600} of 0.5. Cells were added to 96-well white wall chimney plates containing serially diluted antibiotics. For antagonization assays, cell wall precursors (UDP-GlcNAc, UDP-MurNAc-pentapeptide, $C_{55}P$, $C_{55}PP$, lipid I, lipid II, lipid II-D-Lac, lipid III_{WTA}, and lipid II_{cap}) were added in 0.5 to 10-fold molar excess with respect to DCAP (0.5× MIC), and were pre-incubated for 10 min prior to addition of the reporter strain. Luminescence measurements were performed at 30 °C in a microplate reader Spark 10M (Tecan). At least three independent biological replicate experiments were conducted.

Bacterial cell wall integrity assay

Bacterial cell wall integrity assays were adapted from previous work.[4] *B. subtilis* 168 cultures were grown in MHB at 30 °C to an OD_{600} of 0.3. Subsequently, cells were treated with 16 µg ml^{-1} DCAP, 2 µg ml^{-1} vancomycin, 2 µg ml^{-1} bacitracin, 2 µg ml^{-1} friulimicin, 0.5 µg ml^{-1} nisin, 2 µg ml^{-1} daptomycin, 128 µg ml^{-1} oxacillin, 4 µg mL^{-1} valinomycin (in presence of 300 mM KCl), 16 µg ml^{-1} CCCP, 2 µg ml^{-1} clindamycin, or DMSO and further incubated at 30 °C for 60 min. Lysozyme-treated (128 µg ml^{-1}) cells were incubated for 10 min. Cells were immediately fixed in a 1 ml 1:3 (v:v) mixture of acetic acid and methanol, and immobilized on thin 1% w/v agarose slides. Imaging was performed by phase contrast microscopy on a Zeiss Axio Observer Z1 microscope (Zeiss, Jena, Germany) equipped with HXP 120 V light source and an Axio Cam MR3 camera. Images were acquired with Zen 2 software (Zeiss) and analyzed and postprocessed using ImageJ v1.53e software (National Institutes of Health).[5]

Quantification of intracellular UDP-N-acetylmuramic acid-pentapeptide

To analyze the cytoplasmic nucleotide pool we adapted the protocol of Kohlrausch and Höltje.[6] *S. aureus* SA113 was grown in 15 ml MHB at 37°C to an OD_{600} of 0.6 and incubated with 130 µg ml^{-1} chloramphenicol for 15 min. DCAP was added at 0.5×, 1×, 2.5×, and 5× MIC and incubated for another 30 min. Lipid II-complexing vancomycin (5× MIC) was used as positive control. Extraction of nucleotide-linked peptidoglycan precursors and their analysis was performed by HPLC as described previously.[7] Corresponding fractions were confirmed by mass spectrometry.

Synthesis and purification of lipid intermediates

Large scale synthesis and purification of the peptidoglycan precursors lipid I, lipid II, and the wall teichoic acid precursor lipid III_{WTA} was performed as previously described.[8–10] UDP-MurNAc-pentapeptide was purified according to the protocol elaborated by Kohlrausch and Höltje.[6] For synthesis of the lipid II variant with a terminal D-Lac residue, UDP-MurNAc-pentapeptide (Ala-Glu-Lys-Ala-Lac) was purified from *Lactobacillus casei* ATCC393 as previously described.[11] Streptococcal lipid II_{cap} (serotype 14, undecaprenyl-pyrophosphoryl-glucose-galactose) was synthesized using 5 nmol $C_{55}P$, 1 mM UDP-β-glucose and 2 mM UDP-α-galactose in presence of 0.7 mg mL^{-1} 1,2-dioleoyl-*sn*-glycero-3-phosphoglycerol (DOPG), 50 mM Tris-HCl and 10 mM $MgCl_2$ at pH 7.5. The reaction was initiated by the addition of 1.7 µg recombinant His_6-CpsE and 1.5 µg co-purified CpsFG-His_6, and samples were incubated for 2 h at 30 °C. Lipid II_{cap} was extracted from the reaction mixture and purified as described for staphylococcal capsule intermediates.[12] Undecaprenyl phosphate ($C_{55}P$) and undecaprenyl diphosphate ($C_{55}PP$) were purchased from Larodan Fine Chemicals AB (Malmö, Sweden) and used without further purification. The concentration of purified peptidoglycan and wall teichoic acid precursors was quantified on the basis of their phosphate content as described.[13]

In vitro peptidoglycan synthesis reactions using purified S. aureus proteins and substrates

To determine the enzymatic activity of MraY-His_6 the assay was carried out in a total volume of 50 µL containing 5 nmol $C_{55}P$, 25 nmol of UDP-MurNAc-pp in 100 mM Tris-HCl, 10 mM $MgCl_2$, at pH 7.5, and 0.6% Triton X-100. The reaction was initiated by the addition of 2 µg of MraY-His_6 and incubated for 1.5 h at 30°C.

The *in vitro* MurG reaction was performed in a 30 µL reaction containing 2 nmol of purified lipid I and 25 nmol of UDP-*N*-acetyl glucosamine (UDP-GlcNAc) in 200 mM Tris-HCl, 5.7 mM $MgCl_2$, at pH 7.5, and 0.8% Triton X-100 with 2 µg of purified, recombinant MurG-His_6 enzyme. Reaction mixtures were incubated for 30 min at 30 °C.

In vitro amidation was assayed by incubating 2 nmol of lipid II in 160 mM Tris-HCl, 40 mM $MgCl_2$, 30 mM KCl, at pH 7.5, 0.26% Triton X-100, 6 mM ATP, and 6.6 mM glutamine in a total volume of 30 µL. The reaction was initiated by the addition of 3 µg of the *S. aureus* GatD-His_6/MurT complex and was incubated for 2 h at 30 °C.

The PBP2 and PBP4 activity assay was performed in a 50 µL reaction containing 2 nmol of purified lipid II, in 20 mM MES, 2 mM $MgCl_2$, and 2 mM $CaCl_2$, at pH 5.5 with 2 µg of purified, recombinant PBP2-His_6 or PBP4-His_6 enzyme. Reaction mixtures were incubated for 2 h at 30 °C.

Dephosphorylation of $C_{55}PP$ was determined using purified YbjG-His6 enzyme (SA0415). A total of 20 nmol of $C_{55}PP$ was incubated with 3 µg of YbjG-His_6 in 20 mM Tris-HCl, 150 mM NaCl, and 0.8% Triton X-100 at pH 7.5 in 50 µL for 30 min at 30 °C.

The lipid IV_{WTA} synthesis reaction was performed by incubating 2 nmol of lipid III_{WTA} in 200 mM Tris-HCl, 0.2% Triton X-100, 100 mM NaCl, and 1 mM UDP-GlcNAc, at pH 7.5 in 50 µL. The reaction was initiated by the addition of 3 µg of TarA-His_6 and 1 µg MnaA-His_6 and incubated for 4 h at 30 °C.

In all *in vitro* assays, DCAP was added in molar ratios from 0.5 to 4 (and to 10 for MraY) with respect to the respective substrate. $C_{55}P$-containing products were extracted with an equal volume of *n*-butanol/pyridine acetate, pH 4.2 (2:1, v/v) and analyzed by TLC using chloroform/methanol/water/ammonia (88:48:10:1, v/v/v/v) as the solvent[14] and phosphomolybdic acid staining.[10] The quantitative analysis of lipids extracted to the *n*-butanol phase was carried out using ImageJ v1.53e software (National Institutes of Health).[5] Experiments were performed at least in triplicates.

AlamarBlue cell viability assay

Cytotoxicity of DCAP on human epithelial type 2 (HEp-2) cells (ATCC® CCL-23™) and McCoy [McCoy B] (ATCC® CRL-1696™) mouse fibroblast cells was measured by using the non-fluorescent resazurin-based alamarBlue™ cell viability reagent (Invitrogen) which is converted into fluorescent resorufin by living cells. Cells were seeded at a density of 5×10^4 cells per well in 96-well flat base TC plates (Sarstedt), and incubated in Dulbecco's modified Eagle's medium (DMEM, Gibco) or Roswell Park Memorial Institute 1640 medium (RPMI, Gibco), respectively, supplemented with 1× MEM non-essential amino acids (Gibco) and 1× MEM vitamin solution (Gibco) in an atmosphere of 5% CO_2 at 37°C. After 48 h, the culture was treated with DCAP at serially diluted concentrations ranging from 1 to 128 µg ml^{-1}. After another incubation for 2, 4, 6, 17 or 30 h, medium was removed and the cell monolayer was washed twice with Hank's balanced salt solution (HBSS, Gibco). To indicate cell viability, alamarBlue™ reagent was added to a final concentration of 10% (v/v) and cells were incubated for 1 h at 37 °C and 5% CO_2. Fluorescence measurements (570 nm excitation and 585 nm emission) were performed in a microplate reader Spark 10M (Tecan). Relative cell viability was calculated as the percentage of untreated cells (set 100%). The 50% inhibitory concentration (IC_{50}) calculation was performed with GraphPad Prism 5.01 software using non-linear fit log(inhibitor) vs. response calculation with variable slope and constraints of 0% and 100% toxicity for top and bottom constraints respectively.

Red blood cell lysis assay

DCAP was serially diluted in phosphate buffered saline (PBS) in 96-well U-shaped plates (Greiner) at concentrations ranging from 1 to 128 µg mL^{-1}. Human red blood cells (RBCs) were washed three times with PBS immediately prior to addition of RBCs to the wells at a final concentration of 2.5% RBC per well. After 6, 17, or 30 h of incubation in an atmosphere of 5% CO_2 at 37°C, RBCs were pelleted by centrifugation (1500 × *g* for 10 min). Supernatants were diluted 5-fold in PBS in a new 96-well plate, and absorbance of the heme was measured at 405 nm in a microplate reader Spark 10M (Tecan). Relative hemolysis was calculated as the percentage of RBCs treated with 1% v/v Triton X-100 (set 100%).

Serial passaging

S. aureus SA113 was serially passaged in the presence of sub-MIC concentrations of DCAP (and ciprofloxacin as control) over a period of 25 days. Cells were incubated at 37 °C with agitation, and passaged at 24 h intervals in the presence of antibiotics at sub-inhibitory concentration. The well containing bacterial suspension at the DCAP concentration corresponding to 0.5× MIC was used as the inoculum for the second passage. For each passage, MICs were determined as described for *Antibiotic susceptibility testing*.

Fluorescence microscopy

For time-lapse fluorescence microscopy, cells of *B. subtilis* 2020 (*trpC2 spc amyE::*P_{xyl}*-gfp-ftsZ*) were grown at 37 °C to early-exponential phase (OD_{600} 0.1-0.2). For the expression of the GFP fusion protein, the P_{xyl} promoter was induced using 0.2% xylose. Then, cells were pre-stained with a vital concentration (0.2 µg ml^{-1}) of the lipophilic dye FM 4-64 (Molecular Probes), for 10 min at 37 °C. Bacteria were immobilized onto agarose-coated microscopy slides using gene frames (Life Technologies) and were then monitored by time-lapse microscopy. The slide composition consisted of a thin film of 1.5% w/v agarose in 25% LB containing DCAP at 0.5× MIC as well as the respective concentrations of the inducer and the membrane dye. The time elapsed between sampling and image acquisition did not exceed 10 min, with phase contrast and fluorescence images taken every 5 min. Of note, the DCAP concentration used allowed us to follow the cellular events upon antibiotic action before cells were starting to lyse. Additional controls included untreated cells as well bacteria exposed to 2.5 µg ml^{-1} of the ionophore CCCP. Time-lapse micrographs were obtained using a Nikon Eclipse Ti automated microscope equipped with a Perfect Focus system (Nikon Instruments Europe BV, Netherlands), an Orca Flash 4.0 camera (Hamamatsu, Photonics, Japan), and CFI Plan-Apo DM 100×/1.45 oil Ph3 objective (Nikon). For the evaluation of the effect of DCAP- or CCCP-treatment on bacterial septa and localization of FtsZ-rings compared to untreated cells, more than 700 septa/FtsZ-rings were evaluated for each condition.

For cell wall labeling and HCC-amino-D-alanine (HADA) incorporation assays, *S. aureus* SA113 was used. For co-visualization of FtsZ and FtsW, *S. aureus* RN4220 with chromosomal *ftsW-gfp* and pCQ11-*ftsZ*-SNAP was

used. For PBP2 delocalization studies, *S. aureus* RNpPBP2-31 with chromosomal *gfp-pbp2* fusion was used.[15] Cultures were grown in MHB at 37°C under constant shaking until reaching an OD_{600} of 0.5. For selection of pCQ11, 10 µg mL^{-1} erythromycin was added. Microscopy was performed on a Carl Zeiss AxioObserver Z1 equipped with an HXP 120 C lamp, an αPlan-Apo 100×/1.46 oil Ph3 objective and an AxioCam MRm camera. Standard filter sets were used for BODIPY-FL / GFP (450-490 nm excitation, 495 nm beam splitter and 500–500 nm emission), SNAP (538-562 nm excitation, 570 nm beam splitter and 570-640 nm emission), and HADA (335-390 nm excitation, 395 nm beam splitter and 420-470 nm emission). HADA was synthesized by EMC Microcollections (Tübingen).

FtsZ-SNAP expression in *S. aureus* was induced with 100 µM isopropyl β-D-1-thiogalactopyranoside (IPTG) for 4 h. Cells were then incubated with DCAP and CCCP at 1× and 2× MIC, or with DMSO for 1 h (30 min for GFP-PBP2), washed three times with MHB and were immobilized on microscope slides covered with a thin film of 1% w/v agarose. SNAP-tag® labelling was achieved by adding 200 nM SNAP-Cell® TMR-Star (NEB) to the culture 15 min prior to washing.

Cell wall labelling was achieved by adding a mixture of 0.5 µg mL^{-1} BODIPY-FL vancomycin (Van-FL, Thermo Fisher Scientific) and 4.5 µg mL^{-1} vancomycin or DMSO to the culture 15 min prior to washing.

HADA labelling of *S. aureus* was achieved by adding 500 µM of the fluorescent D-amino acid to the culture 15 min prior to washing.

For HADA labelling of *B. subtilis* 168, cells were grown in LB overnight at 37 °C with agitation (180 rpm), diluted 1:100 in fresh medium and grown at 37 °C to an OD_{600} 0.3-0.4. Aliquots of 500 µL were treated for 5 min with DCAP (1× MIC or 2× MIC) or CCCP (5 µM) at 37 °C and 500 rpm in a 24-well plate. DMSO (0.5%) served as a negative control. Then, samples were centrifuged (5000 × *g*, 5 min), most of the supernatant (450 µL) was removed, and cells were labelled in the remaining 50 µL with a final concentration of 1 mM HADA, mixed briefly and incubated for 3.5 min at 37°C. The reaction was stopped by adding 1 mL ice-cold PBS and unbound dye was removed by three washing steps with ice-cold PBS (16,000 × *g*, 3 min, 4°C). Subsequently, the cells were placed on microscopy slides covered with a thin layer of 1.2 w/v agarose and visualized by brightfield and fluorescence microscopy in a Zeiss Axio Observer Z1 LSM800 at 335-390 nm excitation, and 420-470 nm emission.

Pore formation of *B. subtilis* 168 was monitored using the Live/Dead BacLight bacterial viability kit (Molecular Probes). Cells were grown in LB at 37 °C to the exponential phase. Aliquots (100 µL) of the cells were treated for 15 min with DCAP (1× and 4× MIC, respectively), nisin (100 µg mL^{-1}, positive control) or DMSO (1%, negative control). Then 0.2 µL of a 1:1 mixture of syto9 and propidium iodide (PI) were added per 100 µL of culture and incubation was continued for 15 min at room temperature in the dark before microscopic analysis. Samples were visualized by brightfield and fluorescence microscopy at 483 nm excitation, 500 nm emission (syto9) and 305 nm excitation, 617 nm emission (PI) on microscope slides covered with a thin film of 1% w/v agarose using a Zeiss Axio Observer Z1 automated microscope. Images were acquired with an Orca Flash 4.0 V2 camera (Hamamatsu) and an αPlan-Apo 100×/1.46 oil Ph3 objective (Zeiss). Images were processed using the Zen 2 software (Zeiss).

For microscopy of eukaryotic cells, HEp-2 cells were seeded on CELLview cell culture slides (Greiner Bio-One) at 1 × 10^4 cells per well in 100 µL RPMI 1640 medium supplemented with 10% fetal bovine serum (assay medium) and incubated to adhere overnight at 37 °C, 5% CO_2, 95% relative humidity. Pore formation was monitored using the Live/Dead BacLight bacterial viability kit (Molecular Probes). To this end, the medium was aspirated and 100 µL fresh assay medium was added to each well, containing 0.4 % of a 1:1 mixture of syto9 and propidium iodide (PI) and either DCAP (8 µg ml^{-1} or 32 µg ml^{-1}; i.e., 1× and 4× IC_{50}, respectively), Triton X-100 (0.1%, positive control) or DMSO (1%, negative control). Samples were visualized after 30 min of treatment by brightfield and fluorescence microscopy at 483 nm excitation, 500 nm emission (syto9) and 305 nm excitation, 617 nm emission (PI) using a Zeiss Axio Observer Z1 automated microscope. Images were acquired with an Orca Flash 4.0 V2 camera (Hamamatsu) and an αPlan-Apo 100×/1.46 oil Ph3 objective (Zeiss). Images were processed using the Zen 2 software (Zeiss). The mitochondrial membrane potential was assessed using the JC-1 dye (Invitrogen). Therefore, the medium was aspirated and all wells were stained with fresh assay medium containing 5 µg ml^{-1} JC-1 dye and 1 µg ml^{-1} DAPI dye and incubated as above, protected from light for 15 min. Following staining, the medium was removed and each well was treated for 30 min with 100 µL assay medium containing DCAP (8 µg ml^{-1} or 32 µg ml^{-1}; i.e., 1× and 4× IC_{50} respectively), CCCP (50 µg ml^{-1}, positive control) or DMSO (1%, negative control). Samples were visualized by brightfield and fluorescence microscopy at an excitation wavelength (EX) of 554 nm and an emission wavelength (EM) of 600 nm (JC-1 red channel), EX 500 nm EM 542 nm (JC-1 green channel), EX 377 nm EM 447 nm (DAPI) using a Nikon Eclipse Ti-E microscope. Images were acquired with

an Orca Flash 4.0 LT camera (Hamamatsu) and processed using NIS Elements Advanced Research software (Nikon).

Image acquisition and analysis was performed with Zen 2 software (Zeiss), ImageJ v1.52p and the plug-in tool MicrobeJ v5.13l (20) beta.[5,16] MicrobeJ was used for cell identification and segmentation, extraction of fluorescence and size parameters, maxima detection and maxima heatmap density rendering. In MicrobeJ, the septum intensities were measured using the feature detection parameter, strip; whereas the localization of FtsZ was determined using the menu, find maxima. Conditions were kept identical in all conditions, for the evaluation of the different time points and between replicates. Microscopy data was obtained from at least three independent experiments and biological samples. Septal/peripheral ratios were determined using ImageJ stock tools. Semi-quantitative analysis of cell phenotypes was performed manually. Statistical analysis was carried out using GraphPad Prism 9.0.0. Depending on the experimental set-up, statistical significance was determined using unpaired or paired two-tailed Student's t-tests (95% confidence interval), or two-way ANOVA. Differences between groups, i.e., treated and untreated cells were evaluated using Dunnett's multiple comparison test.

Supplementary figures

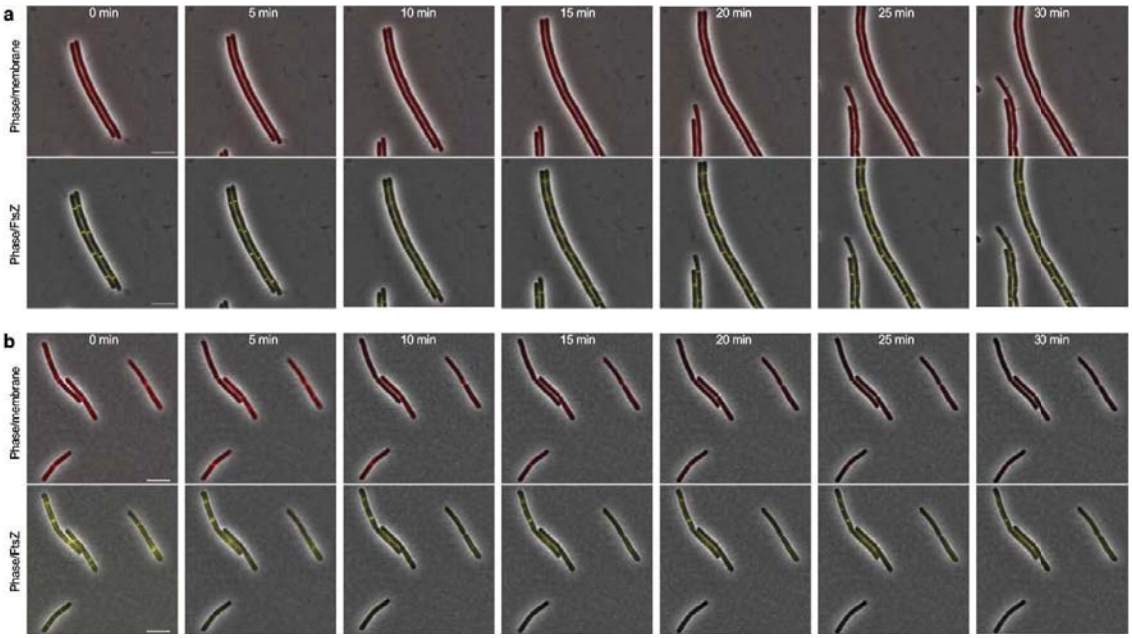

Figure S1: Time-lapse fluorescence microscopy of exponentially growing *B. subtilis* 2020 in the absence (a, untreated control cells) or presence of 2.5 µg mL^{-1} CCCP (b, ionophore-treated control cells). Images show channel overlays of phase contrast with either FM4-64-labelled cell membrane (upper panel, FM4-64/membrane in red) or GFP-tagged FtsZ (lower panel, in yellow). The micrographs show a uniform staining of the membrane by FM4-64 and mid-cell localization of FtsZ in untreated cells (a). In cells treated with the ionophore CCCP (b), in contrast to DCAP-treated cells (Fig. 2), no localized membrane effect was observed. Scale bars, 5 µm. Images are representative of at least three biological replicate cultures of *B. subtilis* 2020 with >700 septa/FtsZ rings monitored over time for each condition (untreated, DCAP-, or CCCP-treated). Corresponding time-lapse videos are provided by Supplementary movies 1 and 3.

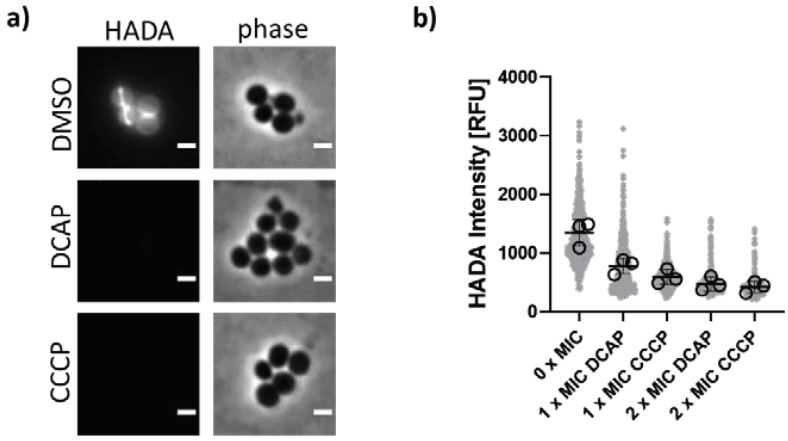

Figure S2: DCAP and CCCP reduce HADA incorporation in *S. aureus*. a) Left: Representative Images of HADA intensity shown in Fig. 3b with brightness and contrast adjusted to the untreated control. Right: Phase contrast images of cell shapes for intelligibility. Scale bar = 1 µm. b) Quantification of HADA fluorescence intensity of individual cells (light grey small dots). The resulting means of three independent biological experiments are shown as large circles. Mean ± SD of the three biological replicates are shown as line and error bars. Data quantified from $n \geq 300$ cells from 3 independent biological experiments ($n \geq 100$ per replicate).

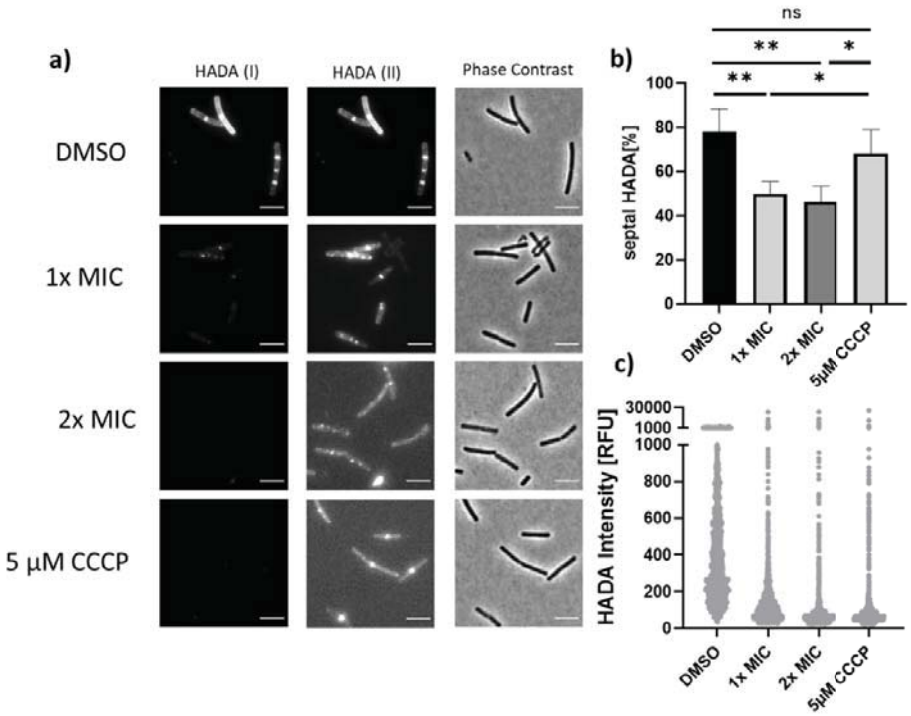

Figure S3: DCAP interferes with distribution of HADA incorporation in *B. subtilis.* a) Representative images of *B. subtilis* 168 after 5 min of exposure to DMSO (0.5%), DCAP (16 µg/ml, 1x MIC or 32 µg/ml, 2x MIC) or CCCP (5 µM, 1.6x MIC), followed by a short pulse of HADA. Brightness and contrast of HADA fluorescence images are adjusted (I) to the DMSO control or (II) to the individual image grey values. Microscopic settings were selected to yield a good signal in the DMSO control and then kept constant for all micrographs. Scale bar, 5 µm. b) Relative frequencies of cells with a septal HADA signal after 5 min pre-treatment with the indicated compounds as described above. Error bars represent the SD of four biological replicates. c) Quantification of HADA fluorescence intensity of individual cells (light grey small dots). The resulting means of three independent biological experiments are shown as large circles. Mean ± SD of the four biological replicates are shown as line and error bars. Data quantified from $n \geq 1146$ cells from 4 independent biological experiments ($n \geq 222$ per replicate).

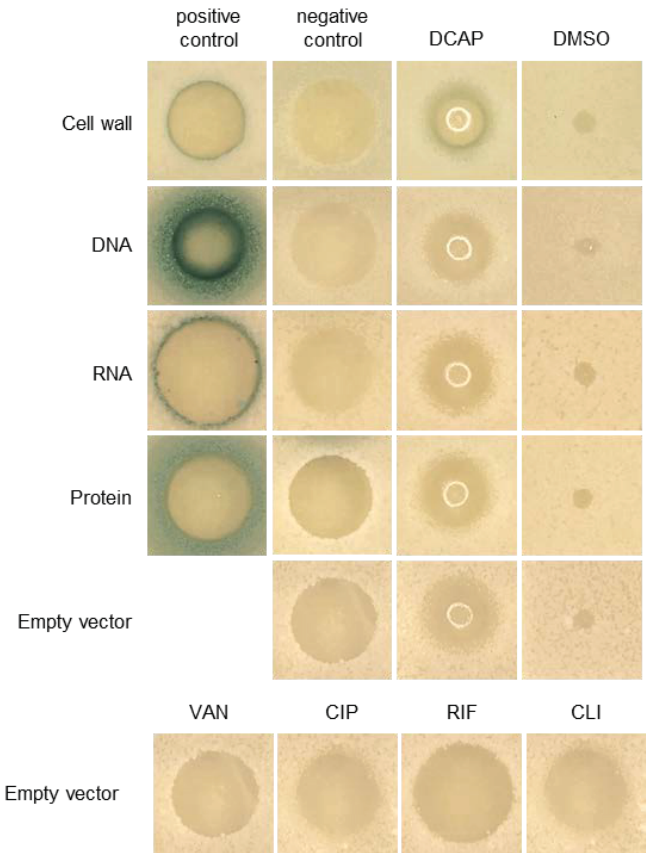

Figure S4: Impact of DCAP on major biosynthesis pathways in *B. subtilis*. *B. subtilis* bioreporter strains with selected promotor-*lacZ* gene fusions were used to identify interference with DNA (P_{yorB}), RNA (P_{yvgS}), protein (P_{yhel}), and cell wall (P_{ypuA}) biosynthesis. Induction of a specific stress response results in expression of β-galactosidase indicated by a blue halo surrounding the inhibition zone. Antibiotics vancomycin (VAN), ciprofloxacin (CIP), clindamycin (CLI), and rifampicin (RIF) were used as positive controls. The corresponding amount of DMSO was taken as solvent control.

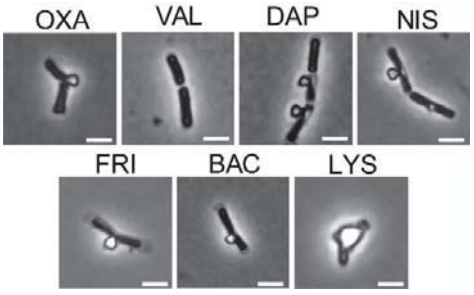

Figure S5: Phase-contrast microscopy of methanol:acetic acid-fixed *B. subtilis*. Treatment with cell wall-active antibiotics, such as oxacillin (OXA), daptomycin (DAP), nisin (NIS), friulimicin (FRI), bacitracin (BAC) and lysozyme (LYS) impair *B. subtilis* cell wall integrity as severe cell-shape deformations and a characteristic blebbing phenotype were observed. The ionophore valinomycin (VAL) did not induce the formation of membrane blebs. Scale bars = 2 µm.

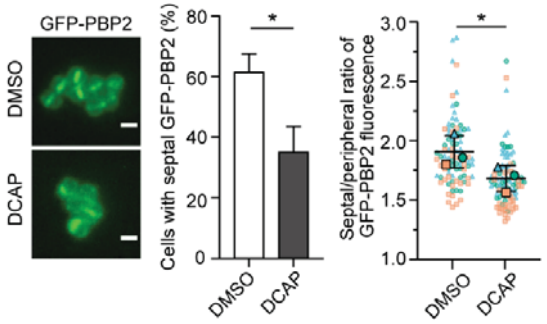

Figure S6: DCAP delocalizes GFP-PBP2 in *S. aureus*. a) Representative images of *S. aureus* GFP-PBP2 fluorescence after incubation with DMSO (control) or DCAP (2× MIC), Scale bar = 1 µm. b) DCAP reduces the percentage of cells with GFP-PBP2 at the septum. c) In cells with GFP-PBP2 at the septum, DCAP leads to more GFP-PBP2 signal in the peripheral membrane and less GFP-PBP2 signal at the septal membrane. All data quantified from n = 90 cells from 3 independent biological experiments.

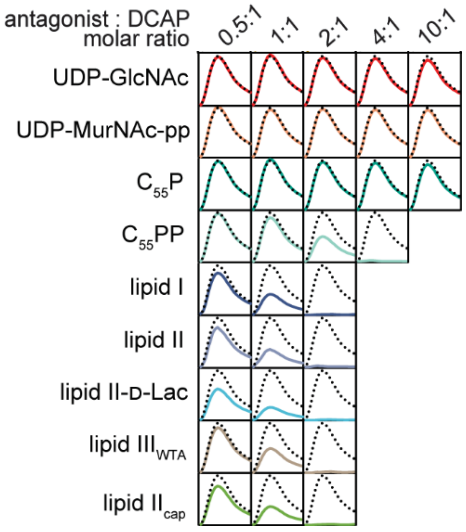

Figure S7: The DCAP-induced LiaRS cell wall stress response in *B. subtilis* (P_{liaI}-*lux*; dotted line) is antagonized by C_{55}PP-containing cell wall precursors (colored lines). Y-axis represents luminescence with a maximum at 6 × 10^4 RLU, x-axis represents time line with a maximum of 330 min. GlcNAc, *N*-acetylglucosamine; MurNAc, *N*-acetylmuramic acid; pp, pentapeptide.

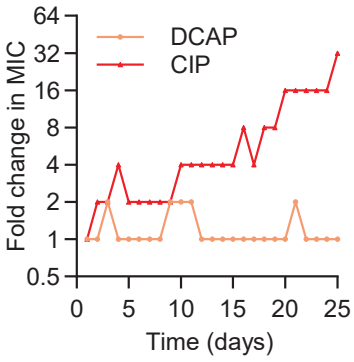

Figure S8: Resistance acquisition of *S. aureus* during serial passaging in the presence of sub-MIC levels of antibiotics over 25 days. For ciprofloxacin (CIP), 32× MIC was the highest concentration tested. The figure is representative of 3 independent experiments.

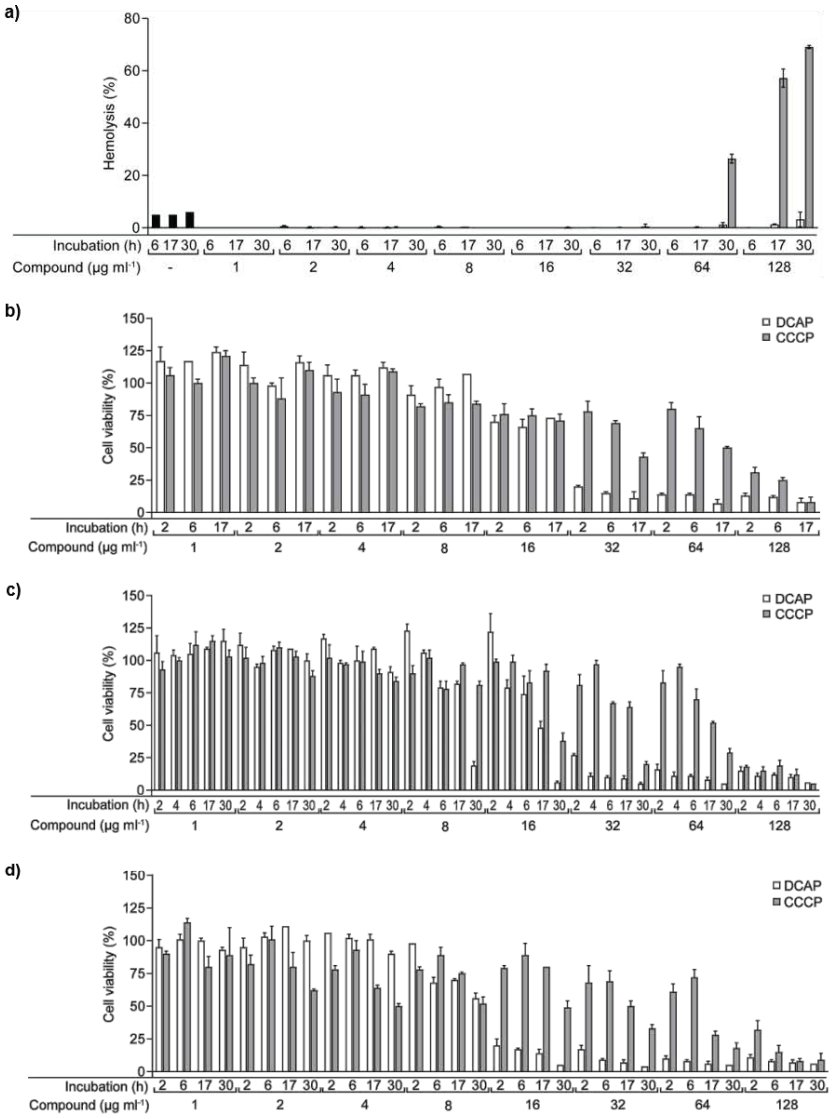

e)

Cell type, medium	IC_{50} [µg/ml] 2 h DCAP	2 h CCCP	4 h DCAP	4 h CCCP	6 h DCAP	6 h CCCP	17 h DCAP	17 h CCCP	30 h DCAP	30 h CCCP
HEp-2, RPMI	24.4 ± 1.3	91.2 ± 1.2	n.d.	n.d.	20.8 ± 1.3	63.8 ± 1.2	21.8 ± 1.4	37.1 ± 1.2	10.6 ± 1.4	18.9 ± 1.3
HEp-2, DMEM	41.0 ± 1.5	111.4 ± 1.3	21.2 ± 1.3	136.0 ±1.4	20.7 ± 1.2	70.8 ± 1.2	15.7 ± 1.3	55.0 ± 1.2	7.0 ± 1.3	14.5 ± 1.1
McCoy B, DMEM	13.2 ± 1.3	67.0 ± 1.2	n.d.	n.d.	11.3 ± 1.2	73.9 ± 1.2	10.1 ± 1.3	24.9 ± 1.2	8.2 ± 1.2	9.4 ± 1.2

Figure S9: Hemolysis and cytotoxicity. (a) Human red blood cell (RBC) hemolysis following treatment with DCAP (white bars) and CCCP (grey bars) expressed relative to Triton X-100-induced RBC lysis (set 100 %). DMSO vehicle-treated cells are shown with black bars. RBCs were challenged with serially diluted concentrations of inhibitors for 6, 17, and 30 h, respectively. In contrast to CCCP, DCAP did not show hemolytic activity towards human RBCs within the tested range up to 128 µg/ml. Cell viability of HEp-2 cells grown in (b) RPMI and (c) DMEM medium and (d) McCoy B cells grown in DMEM medium after treatment with DCAP and CCCP. Cells were incubated with serially diluted concentrations of inhibitors for 2, 4, 6, 17 or 30 h. Metabolically active cells reduced resazurin to resorufin and fluorescence was measured. (e) 50% inhibitory concentrations (IC_{50}) of DCAP and CCCP against HEp-2 and McCoy B cells. DCAP and CCCP showed concentration and time dependent cytotoxic effects in both cell lines and culture media. Error bars indicate ± standard deviation (n = 3). (n.d.: not determined).

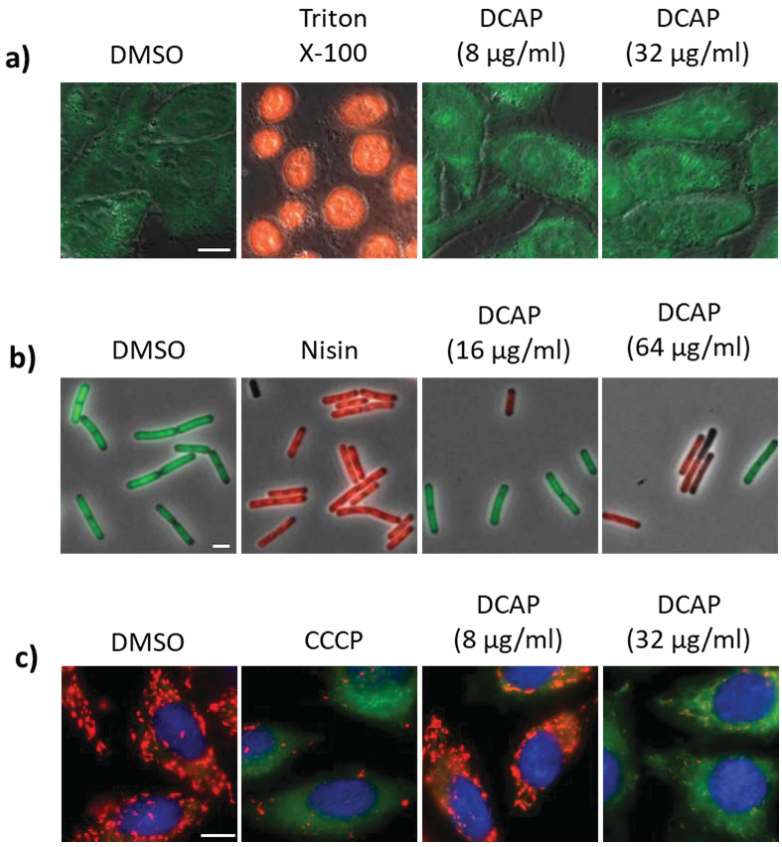

Figure S10: Impact of DCAP on the integrity of the cytoplasmic membrane of HEp-2 and *B. subtilis* cells and of the membrane potential of HEp-2 cells. (a) Effect of DCAP (at 1× or 4× IC_{50}, 8 and 32 µg ml^{-1}, respectively), Triton X-100 (0.1%, positive control) or DMSO (1%, negative control) after 30 min of treatment as detected by Syto9 (green) and propidium iodide (PI, red) staining. Images represent merged brightfield, Syto9 and PI channels. Scale bar = 10 µm. (b) Effect of DCAP (at 1× or 4× MIC, 16 and 64 µg ml^{-1}, respectively), nisin (100 µg ml^{-1}, positive control) or DMSO (1%, negative control) after 30 min of treatment as detected by Syto9 (green) and propidium iodide (PI, red) staining. Images represent merged brightfield, Syto9 and PI channels. Scale bar = 2 µm. (c) Effect on membrane potential of the inner mitochondrial membrane in HEp-2 cells determined by JC-1 staining. DCAP was applied at 1× or 4× IC_{50}, 8 and 32 µg ml^{-1}, respectively. CCCP (50 µM) was used as a positive control, DMSO (1%) as a negative control. Energized mitochondria stained red, depolarized mitochondria stained green. DAPI was used as a reference staining for DNA. Images represent merged JC-1 (red and green) and DAPI channels. Scale bar = 10 µm.

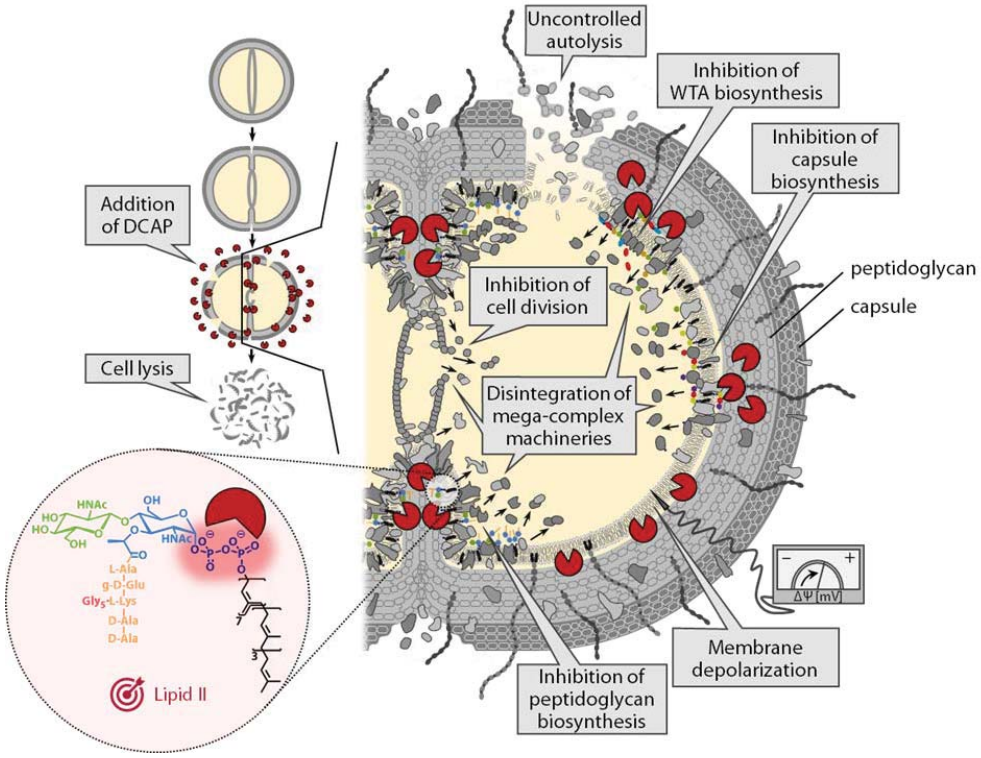

Figure S11: Proposed model for the mechanism of action of DCAP in *S. aureus*.

Table S1: Minimum inhibitory concentrations (MIC) of DCAP against pathogenic bacteria

Organism and genotype	DCAP MIC (μg ml^{-1})
Micrococcus luteus ATCC® 10240™	4
Bacillus subtilis 168	16
Bacillus subtilis 2020	16
Staphylococcus simulans 22	16
Staphylococcus aureus SG511	16
Staphylococcus aureus SG511 (DAP^{R})	16
Staphylococcus aureus HG001	32
Staphylococcus aureus HG001 (DAP^{R})	16
Staphylococcus aureus USA300 JE2 (MRSA)	32
Staphylococcus aureus COL (MRSA)	16
Staphylococcus aureus Mu50 (VISA)	16
Staphylococcus aureus VC40 (VISA)	16
Staphylococcus aureus RN4220	16
Staphylococcus aureus SA113	32
Staphylococcus aureus SA113 Δ*atlA*	32
Staphylococcus epidermidis ATCC® 14990™	16
Staphylococcus epidermidis CLB26329 (MRSE)	16
Streptococcus pyogenes ATCC® 10389™	16
Enterococcus faecalis JH2-2	16
Enterococcus faecalis ATCC® 51299™ (VRE)	16
Enterococcus faecium BM4147 (VRE)	16
Escherichia coli ATCC® 10536™	64
Escherichia coli O-19592	64
Escherichia coli MB5746 Δ*tolC ΔlpxC*	8
Pseudomonas aeruginosa ATCC® 10145™	64
Pseudomonas aeruginosa PAO1	64
Klebsiella pneumoniae ATCC® 27736™	32
Moraxella catarrhalis ATCC® 43617™	32
Mycobacterium bovis BCG 1260	64
Mycobacterium smegmatis ATCC® 700084™	32

Table S2: Antagonistic effect of cell wall biosynthesis lipid precursors and phospholipids on antimicrobial activity of DCAP. DCAP at 5×MIC was exposed to precursors for 10 min in the indicated molar ratios prior to mixture with *M. luteus* DSM1790 (5×10^5 cfu/ml) in MHB. Visible bacterial growth was recorded after 20 h incubation. Results of three independent experiments are summarized. +, antagonization; –, no antagonization; n.d., not determined.

	molar ratio antagonist : DCAP					
Antagonist	**0:1**	**0.5:1**	**1:1**	**2:1**	**4:1**	**10:1**
C_{15}-P	–	–	–	–	–	–
C_{20}-P	–	–	–	–	–	–
C_{55}-P	–	–	–	–	–	–
C_{15}-PP	–	–	–	–	+	+
C_{20}-PP	–	–	–	–	+	+
C_{55}-PP	–	–	–	–	+	+
lipid I	–	–	–	+	n.d.	n.d.
lipid II (L-Lys)	–	–	–	+	+	n.d.
lipid II (*m*DAP)	–	–	–	+	+	n.d.
lipid II-D-Lac	–	–	–	+	+	n.d.
lipid III_{WTA}	–	–	–	+	n.d.	n.d.
lipid II_{cap}	–	–	–	+	n.d.	n.d.
UDP-MurNAc-pentapeptide	–	–	–	–	–	–
UDP-GlcNAc	–	–	–	–	–	–

References

(1) Clinical Laboratory Standards Institute. Methods for Dilution Antimicrobial Susceptibility Tests for Bacteria That Grow Aerobically ; Approved Standard — Tenth Edition. CLSI Document M07-A9. *Clin. Lab. Standars Inst.* **2015**.

(2) Harms, H.; Klöckner, A.; Schrör, J.; Josten, M.; Kehraus, S.; Crüsemann, M.; Hanke, W.; Schneider, T.; Schäberle, T. F.; König, G. M. Antimicrobial Dialkylresorcins from Marine-Derived Microorganisms: Insights into Their Mode of Action and Putative Ecological Relevance. *Planta Med.* **2018**, *84* (18), 1363–1371.

(3) Tan, S.; Ludwig, K. C.; Müller, A.; Schneider, T.; Nodwell, J. R. The Lasso Peptide Siamycin-I Targets Lipid II at the Gram-Positive Cell Surface. *ACS Chem. Biol.* **2019**, *14* (5), 966–974.

(4) Schneider, T.; Kruse, T.; Wimmer, R.; Wiedemann, I.; Sass, V.; Pag, U.; Jansen, A.; Nielsen, A. K.; Mygind, P. H.; Raventós, D. S.; Neve, S.; Ravn, B.; Bonvin, A. M. J. J.; De Maria, L.; Andersen, A. S.; Gammelgaard, L. K.; Sahl, H.-G.; Kristensen, H.-H. Plectasin, a Fungal Defensin, Targets the Bacterial Cell Wall Precursor Lipid II. *Science* **2010**, *328* (5982), 1168–1172.

(5) Schneider, C. A.; Rasband, W. S.; Eliceiri, K. W. NIH Image to ImageJ: 25 Years of Image Analysis. *Nat. Methods* **2012**, *9* (7), 671–675.

(6) Kohlrausch, U.; Höltje, J. V. Analysis of Murein and Murein Precursors during Antibiotic-Induced Lysis of Escherichia Coli. *J. Bacteriol.* **1991**, *173* (11), 3425–3431.

(7) Schneider, T.; Gries, K.; Josten, M.; Wiedemann, I.; Pelzer, S.; Labischinski, H.; Sahl, H.-G. The Lipopeptide Antibiotic Friulimicin B Inhibits Cell Wall Biosynthesis through Complex Formation with Bactoprenol Phosphate. *Antimicrob. Agents Chemother.* **2009**, *53* (4), 1610–1618.

(8) Ling, L. L.; Schneider, T.; Peoples, A. J.; Spoering, A. L.; Engels, I.; Conlon, B. P.; Mueller, A.; Schäberle, T. F.; Hughes, D. E.; Epstein, S.; Jones, M.; Lazarides, L.; Steadman, V. A.; Cohen, D. R.; Felix, C. R.; Fetterman, K. A.; Millett, W. P.; Nitti, A. G.; Zullo, A. M.; Chen, C.; Lewis, K. A New Antibiotic Kills Pathogens without Detectable Resistance. *Nature* **2015**, *517* (7535), 455–459.

(9) Müller, A.; Ulm, H.; Reder-Christ, K.; Sahl, H.-G.; Schneider, T. Interaction of Type A Lantibiotics with Undecaprenol-Bound Cell Envelope Precursors. *Microb. Drug Resist.* **2012**, *18* (3), 261–270.

(10) Schneider, T.; Senn, M. M.; Berger-Bächi, B.; Tossi, A.; Sahl, H. G.; Wiedemann, I. In Vitro Assembly of a Complete, Pentaglycine Interpeptide Bridge Containing Cell Wall Precursor (Lipid II-Gly5) of Staphylococcus Aureus. *Mol. Microbiol.* **2004**, *53* (2), 675–685.

(11) Münch, D.; Engels, I.; Müller, A.; Reder-Christ, K.; Falkenstein-Paul, H.; Bierbaum, G.; Grein, F.; Bendas, G.; Sahl, H.-G.; Schneider, T. Structural Variations of the Cell Wall Precursor Lipid II and Their Influence on Binding and Activity of the Lipoglycopeptide Antibiotic Oritavancin. *Antimicrob. Agents Chemother.* **2015**, *59* (2), 772–781.

(12) Rausch, M.; Deisinger, J. P.; Ulm, H.; Müller, A.; Li, W.; Hardt, P.; Wang, X.; Li, X.; Sylvester, M.; Engeser, M.; Vollmer, W.; Müller, C. E.; Sahl, H. G.; Lee, J. C.; Schneider, T. Coordination of Capsule Assembly and Cell Wall Biosynthesis in Staphylococcus Aureus. *Nat. Commun.* **2019**, *10* (1), 1404.

(13) Rouser, G.; Fkeischer, S.; Yamamoto, A. Two Dimensional Thin Layer Chromatographic Separation of Polar Lipids and Determination of Phospholipids by Phosphorus Analysis of Spots. *Lipids* **1970**, *5* (5), 494–496.

(14) Rick, P. D.; Hubbard, G. L.; Kitaoka, M.; Nagaki, H.; Kinoshita, T.; Dowd, S.; Simplaceanu, V.; Ho, C. Characterization of the Lipid-Carrier Involved in the Synthesis of Enterobacterial Common Antigen (ECA) and Identification of a Novel Phosphoglyceride in a Mutant of Salmonella Typhimurium Defective in ECA Synthesis. *Glycobiology* **1998**, *8* (6), 557–567.

(15) Pinho, M. G.; Errington, J. Recruitment of Penicillin-Binding Protein PBP2 to the Division Site of Staphylococcus Aureus Is Dependent on Its Transpeptidation Substrates. *Mol. Microbiol.* **2005**, *55* (3), 799–807.

(16) Ducret, A.; Quardokus, E. M.; Brun, Y. V. MicrobeJ, a Tool for High Throughput Bacterial Cell Detection and Quantitative Analysis. *Nat. Microbiol.* **2016**.

V. Discussion

" The purified lipid intermediate contained: glutamic acid, alanine, lysine, glycine, MurNAc, GlcNAc, and organic phosphate. […] The mass spectrum of the lipid identified it conclusively as an undecaprenyl alcohol. "

With this citation from 1967 Higashi, Strominger, and Sweely first described the chemical structure, and thus, the differential interaction sites of the probably most targeted molecule in natural microbial ecosystems, lipid II (Higashi *et al.*, 1967). Lipid II is a membrane-standing cell wall precursor that is a unique trait among almost all bacteria (Errington, 2013). The inhibition of cell wall biosynthesis through lipid II binding is an evolutionary ancient and validated antimicrobial strategy for combatting competing microbes, as evidenced by the identification of antibiotic BGCs and resistance genes in metagenomes from permafrost sediments (D'Costa *et al.*, 2011; Waglechner *et al.*, 2021). Moreover, the antimicrobial activity of some eukaryotic host defense peptides from the evolutionary ancient, non-specific innate immune sytem of different kingdoms of life were demonstrated to bind to lipid II (Schneider *et al.*, 2010).

Nature created numerous potent lipid II-binding antibiotics, but only a few of them entered the clinics. These include the glycopeptide vancomycin (1958), and the semi-synthetic lipoglycopeptides teicoplanin (1987), telavancin (2009), dalbavancin, and oritavancin (both 2014). Although in clinical use since 2003, the ability of the lifesaving second-line lipopeptide daptomycin to bind to lipid II (see **chapter 2**) remained long-time enigmatic. All clinical lipid II binders serve as agents of last-resort for the treatment of certain types of infections with multidrug-resistant Gram-positive pathogens. In 2004, another lipid II-binding antibiotic, the lipoglycodepsipeptide ramoplanin A_2, received fast-track approval from the FDA for phase III clinical trials aiming at oral treatment of VRE and *C. difficile* infections. Currently there is no recent information about ongoing clinical trials with ramoplanin (Upert *et al.*, 2021). Further lipid II-binding antibiotics are in preclinical stages of development (Malin and De Leeuw, 2019).

Why is lipid II such an exceptional target?

The fact that lipid II acts as a most relevant target structure for a variety of naturally occurring compounds from diverse chemical classes emphasizes that lipid II binding is a widespread and powerful antibiotic mechanism.

The essential PGN precursor represents an effective target for several reasons: it is highly conserved among bacteria and has no homologs in eukaryotes. It is readily accessible on the extracellular surface and represents a central weak spot for antibiotic attack, particularly in Gram-positive bacteria (Schneider and Sahl, 2010). Importantly, resistance acquisition against lipid II-binding antibiotics is strongly hampered as the non-protein target is generally difficult to be altered by mutation (Ulm and Schneider, 2016). Apart from being a mere PGN building block, current research points to broader cellular roles of lipid II. The lipid intermediate is supposed to drive the spatial organization of the cell wall biosynthetic/cell division machinery through membrane recruitment of the *B. subtilis* actin-like

MreB filaments (Schirner *et al.*, 2015; Strahl *et al.*, 2014). Likewise, localization of PBPs was shown to depend on availability of the lipid II substrate (Pinho and Errington, 2005) and is likely involved in the organization of cell wall biosynthetic machineries. In addition, lipid II serves as a signal molecule of the serine/threonine kinase PknB in *S. aureus* and *M. tuberculosis*, which is involved in crosstalk with the WalKR TCS and FtsZ, proteins coordinating autolysis and cell division, respectively (Hardt *et al.*, 2017; Kaur *et al.*, 2019). In addition, the synthesis of lipid II also requires tight coordination with other cell wall biosynthesis pathways such as WTA or CP biosyntheses, as they share precursor pools of which only limited numbers are available in the bacterial cell.

In summary, direct binding of the lipid II target does not only render it unavailable as a substrate for PGN biosynthesis (**immediate/ primary effect**), but also provokes a cascade of a multide of destructive cellular processes (**downstream/ secondary effects**) that lead to irreversible physical damage and subsequent cell death. The latter include disintegration of septal multi-enzyme complexes (e.g. PGN biosynthetic machinery), defective cell division, malfunctioning of regulatory systems and autolysis, and depending on the lipid II binder's physicochemical features disturbance of the cytoplasmic membrane integrity. Thus, binding of the PGN precursor appears to exhibit a composite mechanism of primary and multifaceted secondary effects that largely differ between individual lipid II-binding antibiotics.

Lipid II-binding antibiotics: Same target, various modes of action, various modes of resistance

Lipid II is a validated target for at least five different chemical classes of antibiotics and the number of newly discovered lipid II is constantly growing (Müller *et al.*, 2017; this thesis). Although interacting with the same target, the potency of antimicrobial activities of lipid II-binding antibiotics substantially varies depending on the interaction with the **differential binding sites on lipid II** (Figure 10). The interaction site on lipid II is relevant for binding affinity, dimerization, conformational stability, membrane insertion, and the propensity for resistance development (Ulm and Schneider, 2016). As lipid II is embedded in the cytoplasmic membrane, binding of the precursor may also involve disturbance of membrane functions or cause massive phospholipid rearrangements depending on the physicochemical properties of the lipid II-targeting antibiotics.

Interaction with the lipid II stem peptide is likely to provoke resistance

The glycopeptide vancomycin, for example, specifically binds to the terminal D-Ala-D-Ala residue of the lipid II stem peptide, which is driven by the formation of five hydrogen bonds (Jia *et al.*, 2011; Reynolds, 1989). However, modifications of the stem peptide can be found in vancomycin-resistant strains, that emerged 30 years after the introduction of vancomycin into the clinics (Leclercq *et al.*, 1988). The first vancomycin-resistant phenotype was described for enterococci (VRE; Arthur *et al.*, 1996) and was acquired most probably by the uptake of mobile genetic elements of glycopeptide-producing streptomycetes or other soil-borne microbes, that use the resistance cassette for producer self-resistance (Marshall *et al.*, 1997). Currently, 11 gene clusters (*vanA-G*, *vanI*, *vanL-N*) are known, that encode for the key enzymes involved in the synthesis of a modified lipid II variant with the stem peptide terminating in D-Ala-D-Lac or D-Ala-D-Ser (Cong *et al.*, 2020). In case lipid II ends in D-Lac, one of the five hydrogen bonds cannot form, resulting in a 1000-fold decrease in binding affinity of vancomycin to lipid II

(Bugg *et al.*, 1991). Unlike resistance to enzyme-inhibitors (e.g. quinolones or D-cycloserine), which is rapidly acquired by single-point mutations (Bhatnagar and Wong, 2019; Chen *et al.*, 2017a), vancomycin-resistant strains occured after a comparably long time, and high-level resistance is not (easily) achieved *in vitro* (Starikova *et al.*, 2013; Young *et al.*, 2019). In contrast, the emergence of vancomycin-resistant strains relies on horizontal gene transfer via mobile genetic elements. Vancomycin-resistance is most prevalent among enterococci and represents a global threat for patient care constituting roughly 68% and average 22% of all clinical isolates in the US and Europe, respectively (OneHealthTrust, as of December 1th, 2022).

Occasionally, the *vanA* cluster spreads to *S. aureus* (VRSA), generating currently 52 isolates worldwide in year 2020 (Cong *et al.*, 2020). VRSA pose an immediate threat limiting treatment options. However, high-level vancomycin-resistance is rarely observed in *S. aureus* since the modified lipid II D-Lac variant is a poor substrate for the Fem peptidyltransferases catalyzing the pentaglycine crossbridge formation (Münch *et al.*, 2015). Indeed, VRSA are deficient of pentaglycine crossbridges (Severin *et al.*, 2004). Moreover, the acquisition of *vanA*-type resistance causes high fitness costs for *S. aureus* (Foucault *et al.*, 2009).

So-called "vancomycin-intermediate-resistant" strains of *S. aureus* (VISA) can be generated *in vitro*, with usually a 2- to 8-fold increase in minimum inhibitory concentration (MIC). Even though resistance is low, infections caused by VISA strains are harder to treat with vancomycin. Unlike high-level vancomycin resistance, the VISA phenotype is based on gradual accumulation of single-point mutations and does not synthesize an altered gene cluster-derived lipid II molecule. In general, VISA strains are characterized by a reduced autolysis and a thickened and less cross-linked cell wall with altered charge that limits access of vancomycin to membrane-bound lipid II (Cui *et al.*, 2006; Howden *et al.*, 2010). On the other hand, the reduced cross-linking leads to an increased number of free D-Ala-D-Ala termini to which vancomycin is bound. This "clogging effect" limits binding to the lipid II target. Even more mechanisms are linked to the reduced vancomycin susceptibility of VISA, which are correlated to mutations in 35 genes, but most frequently in genes of the *graRS*, *vraRS*, or *walKR* operons, that regulate e.g. autolysis, WTA alanylation, CP expression, biofilm formation, and exotoxin expression (Mwangi *et al.*, 2007). The exact underlying molecular mechanisms of VISA development and how these are exactly interlinked are unknown so far (Hu *et al.*, 2016).

In summary, binding of an antibiotic to the D-Ala-D-Ala terminus of the lipid II stem peptide provokes resistance development, either by the comparably slow evolution and spread of a gene operon that modifies lipid II and thus prevents antibiotic interaction (VRE, VRSA) or by gradual acquisition of single-point mutations conferring an altered cell envelope preventing access to the lipid II target site (VISA).

The second-generation semi-synthetic glycopeptide oritavancin that features additional hydrophobic moieties (a short acyl chain and a 4'-chlorobiphenylmethyl group) displays enhanced antibacterial activity compared to vancomycin (Sarkar and Haldar, 2019). The lipophilic side chain is likely to insert into the cytoplasmic membrane disrupting integrity and facilitating surface-templated binding to both, D-Ala-D-Ala and D-Ala-D-Lac residues of vancomycin-resistant species and thus has resistance-breaking properties (Allen, 2010; Belley *et al.*, 2010). The potent binding affinity of

oritavancin is due to secondary interactions with amidated D-Glu in position 2 and interpeptide bridges linked to position 3 of the lipid II stem peptide (Kim *et al.*, 2008; Münch *et al.*, 2015; Patti *et al.*, 2009). Moreover, oritavancin dimerizes ~13,000-fold more strongly than vancomycin and acts as a dimer which further contributes to high-affinity binding to lipid II (Allen, 2010). However, mutants resistant to second-generation glycopeptides already emerged in the clinic, including all types of vancomycin-resistant strains: VRE, VRSA and VISA. Remarkably, high-level oritavancin resistance did not occur thus far (Arthur *et al.*, 1999; Bozdogan *et al.*, 2004).

Amidation of the D-Glu residue in position 2 of the lipid II stem peptide confers another type of high-level resistance towards the lipid II-binding fungal defensin plectasin, as the modification results in a drastically reduced binding affinity of plectasin to lipid II (Münch *et al.*, 2012). NMR-data and computational modelling showed that plectasin not only interacts with lipid II via hydrogen bonding to the pyrophosphate group and the first sugar, but also via a crucial salt bridge formation to D-Glu_2 of the stem peptide. In line with this, the defensin does not bind to WTA precursors (Schneider *et al.*, 2010). Amidation of D-Glu_2 is mediated by the MurT-GatD bi-enzyme complex which is strongly conserved among a subset of pathogenic bacteria, such as *S. aureus*, *S. pneumoniae* and *M. tuberculosis* (Maitra *et al.*, 2021; Morlot *et al.*, 2018; Nöldeke *et al.*, 2018; Zapun *et al.*, 2013). Mutants that are deficient of lipid II amidation were characterized by a reduced degree of PGN cross-linking resulting in a higher susceptibility to e.g. β-lactams and the first-line host defense factor lysozyme (Boyle-Vavra *et al.*, 2001; Figueiredo *et al.*, 2014; Gustafson *et al.*, 1994; Zapun *et al.*, 2013). Taken together, amidation of the lipid II stem peptide poses an effective mechanism for immune evasion. Unlike plectasin, another fungal defensin, copsin, requires the third amino acid (L-Lys of Gram-positive or *m*DAP of Gram-negative bacteria) of the stem peptide for high-affinity lipid II binding (Essig *et al.*, 2014).

Interaction with the lipid II pyrophosphate group triggers various detrimental cellular effects

In contrast to glycopeptides, resistance acquisition to antibiotics that interact with the pyrophosphate moiety is minimized. The pyrophosphate motif is present in precursors of several pathways, including PGN, WTA, CP, AG, LPS O-antigen and ECA biosyntheses, thus, creating a vast spectrum of putative targets. Generally, resistance mechanisms towards antibiotics that interact with the pyrophosphate moiety are limited compared to antibiotics that interact with the stem peptide moiety that can be more variable.

One such lipid II binder that employs the pyrophosphate group is the lantibiotic nisin. Nisin wraps its lanthionine rings A and B around the pyrophosphate moiety by generating five hydrogen bonds, resulting in the assembly of a complex that forms lethal pores of 2 nm diameter in the cytoplasmic membrane (Hasper *et al.*, 2004; Hsu *et al.*, 2004). The complex was postulated to contain eight nisin and four lipid II molecules (Hasper *et al.*, 2004). In addition, formation of the pore complex causes the aggregation of virtually thousands of nisin and lipid II molecules leading to massive clusters that render lipid II unavailable for the PGN biosynthesis (Hasper *et al.*, 2006; Scherer *et al.*, 2013, 2015). Nisin was also found to induce pore formation upon binding to the lipid intermediates of WTA biosynthesis, lipid III_{WTA} and lipid IV_{WTA} (Müller *et al.*, 2012).

Resistance to nisin is achieved by alterations of the cell wall structure and charge or membrane composition as observed for VISA-type resistance, but also by nisin-degrading enzymes and efflux pumps (Draper *et al.*, 2015). More recently, the BceAB-type transporter *Sa*NsrFP of *Streptococcus agalactiae* was suggested to flip the lipid II target back to the cytosolic site to prevent target binding of nisin, which was earlier demonstrated for C_{55}-PP in bacitracin resistance (Kingston *et al.*, 2014; Zaschke-Kriesche *et al.*, 2020). Similarly, other BceAB-like transporters have been associated with nisin resistance, but the mechanism of how BceAB confers resistance is not fully understood.

Another mode of lipid II binding is demonstrated by daptomycin. In order to bind to lipid II and other undecaprenyl-coupled cell wall intermediates Ca^{2+}-daptomycin depends on the interaction with the anionic membrane phospholipid PG, as demonstrated in **chapter 2**. The antibacterial activity is suggested to rely on formation of daptomycin oligomers of at least six daptomycin molecules which is induced by a conformational change upon PG binding (Kreutzberger *et al.*, 2017; Muraih *et al.*, 2011; Taylor and Palmer, 2016). These oligomers are supposed to form complexes with the undecaprenyl-bound cell wall lipid intermediates and trigger disintegration of the cell wall biosynthetic machinery (**chapter 2**). The often-described membrane-disruptive property of daptomycin is observed after prolonged treatment (Silverman *et al.*, 2003), and thus, represents a secondary effect upon disintegrative membrane arrangements that follow PG and lipid II binding. Corroborating, daptomycin preferably associates with fluid membrane domains, i.e. so-called regions of increased fluidity (RIFs), and clusters them togheter which causes massive phospholipid rearrangements and displacement of cell wall biosynthetic enzymes. Oligomerization is assumed to potentiate the effect (Müller *et al.*, 2016).

Although daptomycin exerts multiple effects on bacterial physiology, the requirement of PG for target binding and the association with RIFs make daptomycin-treated strains particularly prone to resistance development. Resistance is acquired by alteration of the cell envelope and membrane structure as well as PG modification. Clinically relevant daptomycin-resistant *S. aureus* and enterococci strains frequently harbor mutations in *dltABCD*, *pgsA*, *mprF, cls2* and *walKR* genes. As observed for VISA, mutations in the latter lead to a decreased autolysis expression resulting in a thickened cell wall that limits access of daptomycin to the membrane. Generally, there is a high diversity of mutations in the *walRK* locus, which were also identified in strains resistant to other lipid II-targeting antibiotics, including VISA (Howden *et al.*, 2010), nisin-resistant (Draper *et al.*, 2015), and siamycin-resistsant strains (**chapter 1**). Mutations in *dltABCD* increase the degree of D-alanylated teichoic acids, resulting in an overall reduction in the negatively-charged bacterial surface and an increased capacity for electrostatic repulsion of Ca^{2+}-daptomycin (Bertsche *et al.*, 2011, 2013). Likewise, gain-of-function mutations in the *mprF* gene contribute to this effect, as MprF-mediated lysinylation of PG is increased, yielding more positively charged phospholipids within the membrane, leading to antibiotic repulsion. Mutations that mask the anionic charge of the bacterial envelope are also found as resistance mechanisms against other lipid II binders, including lantibiotics and defensins (Draper *et al.*, 2015; Gottlieb *et al.*, 2008). Importantly, the modification of anionic structures is tightly regulated and only active in the presence of the corresponding antibiotic (Peschel and Sahl, 2006).

Loss-of function mutations in the *pgsA* gene encoding for the PG synthase reduce the amount of daptomycin's anionic target (Khatib *et al.*, 2016; Mishra and Bayer, 2013; Peleg *et al.*, 2012; Yang *et al.*,

2013). Similarly, mutations in the gene for the CL synthase Cls2 reduce the PG amount through consumption of two PG molecules to form one CL molecule (Tran *et al.*, 2015). In addition, CL has been suggested to increase rigidity of the cytoplasmic membrane, thus preventing membrane insertion of daptomycin into RIFs and affecting binding affinity to lipid II (Lewis and McElhaney, 2009).

Blocking multiple cell wall biosynthetic pathways contributes to rapid lysis and killing

Intringuingly, no detectable resistance was found so far for teixobactin and the teixobactin-like depsipeptides hypeptin and clovibactin, which have the pyrophosphate interaction site of lipid II in common. This suggests that the mere interaction with this motif is not sufficient for the highly potent antibacterial activity of these peptides which, indeed, involves substantially different and even more deleterious cellular effects compared to the aforementioned lipid II binders. Unlike other lipid II-targeting peptides such as nisin, ramoplanin or siamycin-I, teixobactin and the teixobactin-like peptides do not show any cross-resistance to strains resistant to other lipid II-binding antibiotics, e.g. VRE, VISA or daptomycin-resistant *S. aureus*, emphasizing that modulation of the cell envelope or membrane characteristics does not affect teixobactin potency (Ling *et al.*, 2015; **chapters 3 and 4**).

Teixobactin-like depsipeptides were shown to simultaneously sequester the pyrophosphate-containing lipid intermediates from different cell wall biosynthetic pathways, including WTA biosynthesis, which is suggested to trigger the unique rapid bacteriolytic effect due to uncontrolled liberation of WTA-associated autolysins (Homma *et al.*, 2016). Notably, a similar mode of action was found for the depsipeptides ramoplanin and lysobactin (Lee *et al.*, 2016b), that are both active against VRE and VISA (Fulco and Wenzel, 2006; Maki *et al.*, 2001). For ramoplanin, the pyrophosphate group was reported to be the minimal binding motif for interaction with lipid II (Walker *et al.*, 2005). Unlike for lysobactin, it was possible to obtain a ramoplanin-resistant isolate *in vitro* (Schiffer *et al.*, 2018; Schmidt *et al.*, 2010). The mutant displayed cross-resistance to vancomycin and nisin and was characterized by thickened cell walls and a decreased autolysin expression. However, the identification of the exact mutations that confer resistance to ramoplanin in these isolates has not been elucidated so far.

It seems that the rapid killing mechanism of teixobactin-like depsipeptides most likely contributes to prevent the accumulation of resistance-conferring mutations. Thus, resistance development to these compounds will probably take longer to occur compared to vancomycin, and could eventually occur via acquistion of resistance genes via horizontal transfer of teixobactin-inactivating enzymes, such as D-stereospecific peptidases (Li *et al.*, 2018). Eventually, such resistance determinants already exist but have not been identified so far, as exemplified by the isolation of ancient *Streptomyces* esterases from a Mexican cave which were demonstrated to inactivate daptomycin via hydrolytic ring cleavage (Bhullar *et al.*, 2012). In general, the simultaneously blockade of multiple targets, also termed "polypharmacology" or "multi-targeting", is suggested to lower the propensity of spontaneous target-related resistance development (Brötz-Oesterhelt and Brunner, 2008; Silver, 2007).

The recent elucidation of lipid II binding of teixobactin and clovibactin in complex with lipid II in membranes suggests that these compounds sit on top of the membrane and specifically interact with the pyrophosphate group via the amino groups of their depsi-cycles (Shukla *et al.*, 2022;, **chapter 4**).

Moreover, it demonstrates the importance of the crucial order of L- and D-amino acids of the linear *N*-terminus for separation of hydrophilic (water-exposed) and hydrophobic (membrane-exposed) amino acid residues, that was previously shown to be indispensable for antibacterial activity (Abdel Monaim *et al.*, 2016; Chen *et al.*, 2017b; Parmar *et al.*, 2017).

Interestingly, the partly different modes of action of clovibactin and teixobactin (e.g. stronger bacteriolysis and higher binding affinity of clovibactin to C_{55}-PP compared to teixobactin) might be based on the structural diversities of the peptides. Although both antibiotics appear to interact in an equal manner with membrane-associated lipid II, the depsi-cycle of clovibactin (with a *C*-terminal Leu_7 residue) interacts less specific with the MurNAc sugar than teixobactin (with a *C*-terminal End_{10} residue; **chapter 4**). Interestingly, clovibactin and Leu_{10}-teixobactin demonstrated a similar difference in lipid II binding affinity compared to natural End_{10}-teixobactin (Shukla *et al.*, 2022), which emphasizes the structural importance of the *C*-terminus for target interaction. The fact that clovibactin coordinates the pyrophosphate group with three backbone amino protons of the depsi-cycle (β-OH-D-Asn_5, L-Ala_6, L-Leu_8) compared to two amino protons of teixobactin's depsi-cycle (D-Thr_8, L-Ile_{11}) might explain why clovibactin has higher binding affinity to C_{55}-PP compared to teixobactin (**chapter 4**; Ling *et al.*, 2015). Moreover, the highly rigid End_{10}-*C*-terminus of natural teixobactin theoretically contributes enthalpically by formation of hydrogen bonds and electrostatic interactions, whereas the Leu_7-*C*-terminus of clovibactin contributes mostly entropically by stripping of water molecules and eventually by hydrophobic interactions with the sugars. Indeed, Leu_{10}-teixobactin exhibits a more favorable entropy compared to End_{10}-teixobactin (Shukla *et al.*, 2022). Recent experiments of our group confirmed a stronger interaction of Leu_{10}-teixobactin to C_{55}-PP compared to End_{10}-teixobactin. Remarkably, we found that clovibactin also interacts with monophosphorylated C_{55}-P. However, the binding affinity appears to be less strong compared to C_{55}-PP. The importance of the clovibactin Leu_7-*C*-terminus in binding to C_{55}-P is supported by the finding that Leu_{10}-teixobactin showed equal interaction to C_{55}-P. Likewise, the newly discovered lipopeptide antibiotic cilagicin that inhibits cell wall biosynthesis shows ability to bind to both, C_{55}-P and C_{55}-PP, but not to lipid II (Wang *et al.*, 2022). Unlike clovibactin, cilagicin displays a higher binding affinity to C_{55}-P compared to C_{55}-PP. Additionally, the compound exerts bacteriolytic activity of the same strength as teixobactin-like depsipeptides and lacks resistance development.

Lipid II binding is proposed to favor the assembly of supramolecular structures

As observed for daptomycin and nisin, teixobactin captures lipid II molecules in clusters, leading to disintegration of the cell wall biosynthetic machinery (Hasper *et al.*, 2006; Kreutzberger *et al.*, 2017; Shukla *et al.*, 2020). Particularly, teixobactin forms antiparallel fiber-like β-sheets upon lipid II binding with one lipid II molecule doubly-coordinated by two teixobactin molecules. Closer examination revealed lipid II cluster-associated membrane perturbations in liposomes and bacterial cells. MD simulations further created a model in which the hydrophobic side of a teixobactin molecule displaces the polar headgroups of the membrane phospholipids and concentrates the polyprenyl tails of the clustered lipid II molecules, resulting in a compromised membrane integrity by thinning the bilayer (Shukla *et al.*, 2022). This membrane thinning phenomenom is described for several amphipathic

antimicrobial peptides (Grage *et al.*, 2016), e.g. oligomerization-dependent but lipid II-independent membrane interaction of nisin (Prince *et al.*, 2016).

Microscopic analyses (TEM, HS-AFM, and cryo-EM) revealed that the antiparallel β-sheet alignments of teixobactin molecules that are formed upon lipid II binding result in the assembly of supramolecular fibrillar structures reminiscent of amyloid-like structures (Hurst *et al.*, 2021; Shukla *et al.*, 2022; Yang *et al.*, 2018). Likewise, these fibrillar structures were formed in the presence of clovibactin and lipid II. In contrast to teixobactin, clovibactin supramolecular structures did not affect membrane integrity. That might be explained by the increased distance of clovibactin fibrils to the membrane surface compared to teixobactin (**chapter 4**). The lacking membrane-disturbing effect of clovibactin could also account for its less potent antibacterial activity compared to teixobactin.

In addition to teixobactins, solid-state NMR suggested that also plectasin oligomerizes in the lipid II-bound state in its physiologically relevant membrane environment (Jekhmane, 2020). However, microscopic analysis of a self-assembled fibril structure is missing so far. The formation of amyloid-like fibrils was also reported for ramoplanin in aqueous solution, lacking a membrane environment (Cudic *et al.*, 2002; Lo *et al.*, 2000). Fibril formation of ramoplanin was induced upon binding to shortened lipid I and lipid II, UDP-MurNAc-5p, and UDP-MurNAc-tripeptide, suggesting that an intact amide bond between the lactyl ether side chain of MurNAc and the first L-Ala amino acid are required. Unlike teixobactin, ramoplanin forms C_2-symmetric dimers (with each monomer adopting an antiparallel β-sheet structure), whose self-association is suggested to be induced upon membrane insertion (Hamburger *et al.*, 2009; Lo *et al.*, 2001). Crystallization experiments suggest that two ramoplanin dimers interact with the pyrophosphate group of a single lipid II molecule and enable the binding of one additional lipid II molecule at each uncomplexed end of these dimers. This allows the recruitment of additional dimers (so-called ligand-bridged dimer-dimer interactions), that favors the self-assembly of a polymeric fibrillar structure with a ramoplanin-lipid II stoichiometry of 2:1 (Hamburger *et al.*, 2009).

Self-assembled nanostructures are found for a large number of naturally occurring antimicrobial peptides of all kingdoms of life, however, little is known about their function (Lee *et al.*, 2020; Simonson *et al.*, 2020; Tian *et al.*, 2015). The self-assembly of amyloid-like fibrillar structures is primarily associated with neurodegenerative and systemic diseases, including Alzheimer's disease, Parkinson's disease, type II diabetes, amyotrophic lateral sclerosis, and prion diseases (Eisenberg and Jucker, 2012). Amyloids have been shown to exhibit cytotoxicity against human cells by disrupting cell membranes (Bucciantini *et al.*, 2002; Engel *et al.*, 2008; Friedman *et al.*, 2009; Marshall *et al.*, 2014; Milanesi *et al.*, 2012). Moreover, the membrane-affecting properties confer them antimicrobial activity against opportunistic bacterial and fungal pathogens, providing defense against infection (Engelberg and Landau, 2020; Moir *et al.*, 2018; Soscia *et al.*, 2010; Spitzer *et al.*, 2016; Welling *et al.*, 2015). Fibrillar structures were suggested to physically entrap the pathogens, to form fibrillar ion channels in their membranes, or to elicit a host immune response upon interaction with host cells (Kagan *et al.*, 2012; Simonson *et al.*, 2020). Particularly, lipid-binding serum apolipoproteins promote or form themselves fibrillar structures (Frankel *et al.*, 2022; Xia *et al.*, 2021; Yamazaki *et al.*, 2019) and apolipoprotein-derived host defense peptides were recently shown to induce fibril formation-mediated antibacterial activity upon contact with LTA or LPS (Gaglione *et al.*, 2021). Another recent study demonstrated that

the antibacterial activities of the lipid II-binding antibiotics lysocin E and nisin are both potentiated via the interaction with apolipoprotein A-I (ApoA-I; Hamamoto *et al.*, 2021). In addition, it was shown that lysocin E- or nisin-bound lipid II promoted the coordinated interaction between ApoA-I and the respective antibiotic, resulting in an enhanced membrane disruption activity and loss of membrane potential. The increased membrane-damaging activity could eventually result from an ApoA-I-induced fibrillar structure. However, the study did not include the investigation of a polymeric structure.

Apart from host factors, the ability of some antimicrobial peptides to form amyloid-like fibrils is of crucial importance as this property might affect host immunity. In general, antimicrobial peptides were shown to exhibit multifaceted immunomodulatory activities (Mookherjee *et al.*, 2020). Signaling of the innate immune system through self-assembled supramolecular fibrils can either be mediated by direct binding to immune receptors, i.e. Toll-like receptors (TLRs), or by functioning as chaperones that interact with immune ligands prior to TLR binding (Lee *et al.*, 2020).

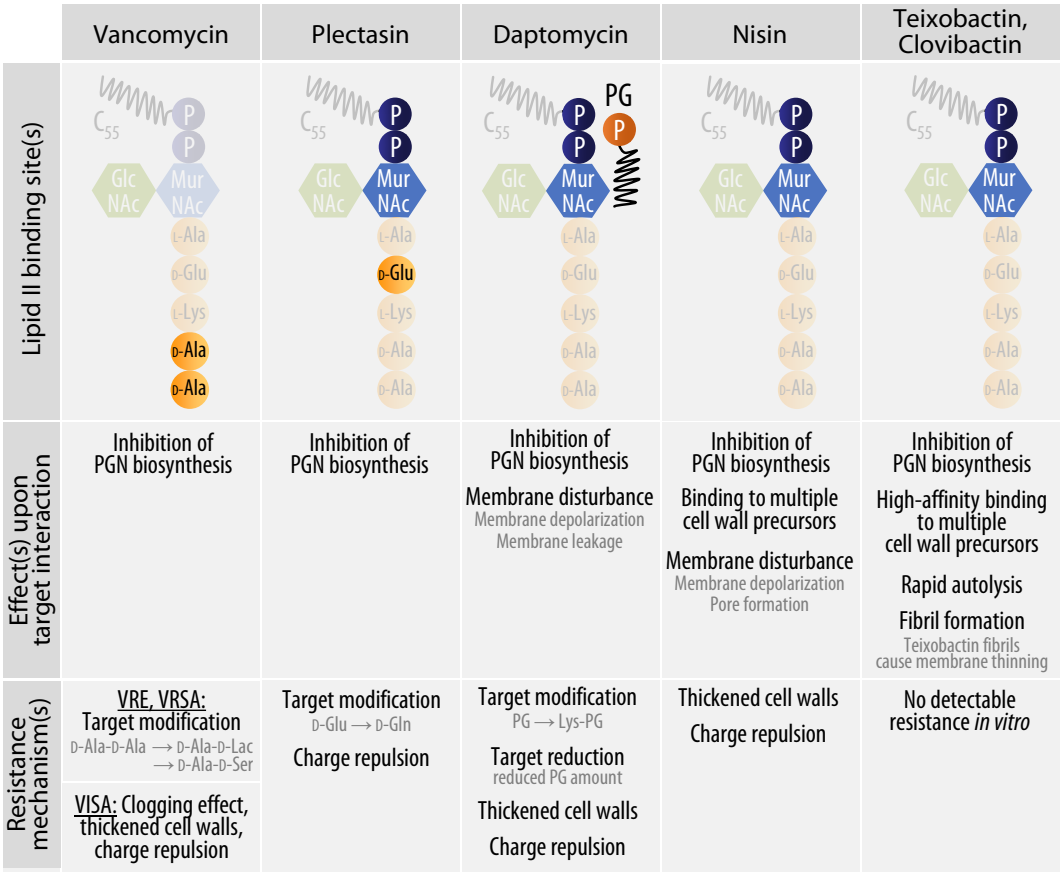

Figure 10. Lipid II interaction site-dependent antibiotic activities beyond the mere blocking of PGN biosynthesis. Despite binding to the same target molecule, even structurally similar lipid II-binding antibiotics can induce a coalescence of differential cellular effects, which affect antibiotic potency and the propensity for resistance development. The figure illustrates the differential lipid II binding sites of five different chemical classes: Glycopeptides (vancomycin), defensins (plectasin), lipopeptides (daptomycin), lantibiotics (nisin), depsipeptides (teixobactin and clovibactin).

Receptor binding may induce inflammasome pathways, leading to the secretion of pro-inflammatory cytokines and/or chemokines (Gustot *et al.*, 2015; Haney *et al.*, 2017; Yates *et al.*, 2000). It remains to be seen whether supermolecular structures of antibiotics, such as teixobactin-like depsipeptides and ramoplanin, have consequences for immune signaling and inflammation, which may lead to immunity disorders, autoimmune diseases, or anaphylaxis (Peavy and Metcalfe, 2008; Yang *et al.*, 2020).

Albeit representing a prerequisite for antimicrobial activity, the propensity to form supramolecular structures might eventually limit their application for systemic use, in case that fibril formation is associated with aggregation and gelation issues. Gelation is currently limiting intravenous administration of both teixobactin and ramoplanin (Zong *et al.*, 2018). Therefore, attempts to overcome this limitation include the development of formulations based on fat emulsions and cyclodextrins, and the synthesis of analogues ("prodrugs") with improved tolerability (Cadete Pires *et al.*, 2019; Jones *et al.*, 2022; Nowick and Yang, 2019; Parenti *et al.*, 2004; Pelzer and Vente, 2008; Zhang *et al.*, 2021; Zong *et al.*, 2018). In general, peptide-based antibiotics exhibit a high propensity to aggregate, resulting in decreased potency, stability, and/or cytotoxicity (Frokjaer and Otzen, 2005).

Future prospects for lipid II-binding antibiotics

Lipid II serves as a unique and most relevant target structure as antibiotic attack combines PGN biosynthesis inhibitory activity with subsequent multifaceted cellular effects. Lipid II-binding antibiotics are widespread in nature and mostly bind to the immutable pyrophosphate group instead of the mutable stem peptide which makes them ultra-robust towards high-level resistance development.

Nevertheless, not many lipid II binders entered the clinics yet, but several candidates are in pre-clinical development including teixobactin, plectasin-derivative NZ2114, cyclic depsipeptides and diverse lantibiotics (Malin and De Leeuw, 2019). Currently, only the glycopeptide prototype vancomycin, second-generation glycopeptides and the lipopeptide daptomycin represent clinically-used lipid II-binding antibiotics that serve for first-line treatment against infections caused by Gram-positive bacteria. However, vancomycin is also infamous for several disadvantages, including nephrotoxicity or the solely intravenous administration every 12 hours, which makes an early release from hospital with subsequent treatments in an out-patient setting impossible (Malin and De Leeuw, 2019).

Despite their high efficacy, the relatively small number of clinically-developed lipid II binders may rely on their chemical structure: Lipid II-targeting antibiotics tend to be of peptidic nature and considerable large size (with molecular masses higher than 1 kDa). These properties render them only active against Gram-positive bacteria and often solely applicable for intravenous injection. The latter is often associated with suboptimal efficacy and safety. In general, the complex peptidic scaffolds of lipid II binders that often consist of unusual non-proteinogenic D-amino acids make it hard to chemically synthesize or modify them and generate high production costs. Moreover, they mostly exhibit poor PK/PD and show tendencies for aggregation (Fosgerau and Hoffmann, 2015). The antibacterial activity of lipid II binders often relies on amphiphilicity and an overall positive charge. However, these cAMP features often correlate with unspecific cytotoxicity towards host cells (Ciumac *et al.*, 2019).

In order to improve their chances for rational development to next-generation antibiotics and to add them to the limited clinical arsenal against pathogens, future studies on lipid II binders should follow a common strategy. These studies should aim at **(i.)** the comprehensive understanding of the currently underexplored modes of action, including their decisive primary and secondary effects, the knowledge of the interdependencies and the cellular consequences of these effects in the bacterial cell, **(ii.)** the broadening of the antibacterial spectrum, in particular to encompass multidrug-resistant Gram-negative species and mycobacteria, and at **(iii.)** gaining knowledge about the efficacy of these compounds in hosts as well as the impact on host toxicity and immunity.

(i.) During antibiotic development, medicinal chemistry has to follow the molecular understanding of the lipid II-associated antibacterial characteristics (Parkes, 2020; Pawlowski *et al.*, 2016). So far, structural knowledge on the molecular interactions of antibiotics with lipid II is scarce due to physicochemical limitations of lipid II binders in aqueous complex (i.e. poorly solubility, micelle-forming tendency of full-length lipid II). In overcoming the limited structural determinations using truncated lipid II variants, solid-state NMR has been proven a valuable technology that provides more information on the native binding modes (such as the importance of a fixed D/L-amino acid stereochemistry or the assembly of supramolecular structures for antibiotic activity of teixobactin) by employing a physiologically-relevant membrane environment (Medeiros-Silva *et al.*, 2018; Shukla *et al.*, 2020, 2022; **chapter 4**).

(ii.) To expand the antibacterial activity of lipid II binders to highly problematic strains of Gram-negative bacteria and mycobacteria it is important to adapt the physicochemical nature of antibiotics regarding species-specific target modifications and permeability barriers. Lipid II-binding antibiotics are usually to large to pass through porins of the outer membrane or mycomembrane. Given the fact that these membranes confer intrinsic resistance to Gram-negative bacteria and mycobacteria, respectively, the evolution of such protective barriers may have been driven by lipid II-targeting peptides (Grein *et al.*, 2019). Currently, there are no lipid II binders known to cross these membranes, except for tridecaptin A_1 (Kato *et al.*, 1978). This lipopeptide is suggested to interact with outer membrane-anchored LPS, followed by outer membrane-crossing and binding to lipid II (Cochrane *et al.*, 2016). NMR analysis of the tridecaptin A_1-lipid II complex indicates interactions with D-Glu_2, *m*DAP_3, D-Ala_4, and D-Ala_5 of the lipid II stem peptide. In contrast to Gram-positive lipid II-L-Lys, Gram-negative lipid II-*m*DAP is exclusively bound with high affinity, which is reflected by the fact that tridecaptin A_1 is not active against Gram-positive bacteria (Cochrane and Vederas, 2014; Cochrane *et al.*, 2014). Indeed, the combinatorial treatment of Gram-negative bacteria with outer membrane-acting peptides (such as tridecaptin A_1 or polymyxins) and lipid II binders (such as vancomycin, nisin, or teixobactin) has already been proven successful (Chiorean *et al.*, 2020; Li *et al.*, 2021; Ng *et al.*, 2018). Other approaches aim at the development of hybrid antibiotics, in which lipid II-binding antibiotics are covalently linked to an outer membrane-disrupting compound (Domalaon *et al.*, 2018; Lei *et al.*, 2022; Surur and Sun, 2021). In addition, lipid II binders could eventually enter the bacterial cell by the so-called "trojan horse strategy" by which the lipid II-binding compound is conjugated to moieties that are naturally used for nutrient uptake, such as siderophores (Negash *et al.*, 2019). In this way, daptomycin was

turned into an antibiotic, which is active against the Gram-negative bacterium *A. baumannii* (Ghosh and Haldar, 2015). Another possibility to enter the Gram-negative or mycobacterial cell is the passage through unspecific, β-barrel-shaped porins, which are permeable for small molecules with molecular masses of less than 600 Da (Vergalli *et al.*, 2020). Recently, the Hergenrother group predicted the molecular properties required to overcome the restrictive permeability barrier of *E. coli* by investigation of more than 180 distinct small molecules (Richter *et al.*, 2017). Likewise, the Brown group collected physicochemical data of 4,500 small molecule inhibitors that were capable of entering *E. coli* cells (El Zahed *et al.*, 2021). Interestingly, small molecules that have been able to overcome the outer membrane were amphiphilic, showed high rigidity (i.e. less rotatable bonds), were of planar shape, and contained a positively charged amine group. The latter is already given for the lipid II-binding small molecules THCz and DCAP (**chapters 5 and 6**), yet they are of hydrophobic nature. Further development of these compounds holds promise for the development of orally available lipid II binders while limiting adverse systemic effects to a minimum.

(iii.) The development of safe lipid II-binding antibiotics requires a fundamental knowledge about their efficiacy, cytotoxicity, and immunomodulatory activities within the host environment. Current research shows that host serum proteins positively or negatively influence the activity of an antibiotic (Hamamoto *et al.*, 2021; Tickle *et al.*, 2022; Wang *et al.*, 2022), suggesting that standard antibiotic susceptibility testing in broth fails to detect novel therapeutically effective antibiotics (Ersoy *et al.*, 2017; Nussbaumer-Pröll and Zeitlinger, 2020). Notably, the antibiotic activity can be enhanced through suppression of pro-inflammatory cytokines and recruitment and activation of neutrophils or macrophages (Drayton *et al.*, 2021). Evaluation of antibiotic efficacy in host constituents and organotypic models in early stages of drug development allows to mitigate any physiological relevant hurdles, e.g. aggregation tendency, or unexpected cytotoxic effects in animal or clinical studies (Schäfer-Korting *et al.*, 2021). It further reflects the effect of virulence factors, immune recognition and resistance to host defenses.

The past three decades of effort demonstrated that it is incredibly difficult to find broad-spectrum antibiotics that are highly-effective and safe. If this trend continues, the global number of deaths attributed to antibiotic resistance will dramatically increase in the future (O'Neill, 2014). While the obstacle to better understand the complex biology of antibiotics, and their interplay with pathogens and hosts remain to be fully addressed, it is reasonable to predict that lipid II binders are likely to play an utmost important clinical role as next-generation antibiotics dealing with antimicrobial resistance.

VI. References

Abdel Monaim, S.A.H., Jad, Y.E., Ramchuran, E.J., El-Faham, A., Govender, T., Kruger, H.G., de la Torre, B.G., and Albericio, F. (2016). Lysine Scanning of Arg_{10}–Teixobactin: Deciphering the Role of Hydrophobic and Hydrophilic Residues. ACS Omega *1*, 1262–1265.

Acosta-Gutiérrez, S., Bodrenko, I. V., and Ceccarelli, M. (2021). The Influence of Permeability through Bacterial Porins in Whole-Cell Compound Accumulation. Antibiotics *10*, 635.

Akalaeva, T. V., Amel'kin, L.Y., Baklanova, O. V., Bokanov, A.I., Ivanov, P.Y., Padeiskaya, E.N., Radkevich, T.P., Filitis, L.N., and Shvedov, V.I. (1990). Antitubercular, antifungal, and antibacterial activity *in vitro* of 1-phenethylamino-1,2,3,4-tetrahydrocarbazoles. Pharm. Chem. J. *24*, 826–829.

Alborn, W.E., Allen, N.E., and Preston, D.A. (1991). Daptomycin disrupts membrane potential in growing *Staphylococcus aureus*. Antimicrob. Agents Chemother. *35*, 2282–2287.

Alcorlo, M., Martínez-Caballero, S., Molina, R., and Hermoso, J.A. (2017). Carbohydrate recognition and lysis by bacterial peptidoglycan hydrolases. Curr. Opin. Struct. Biol. *44*, 87–100.

Allen, N. (2010). From Vancomycin to Oritavancin: The Discovery and Development of a Novel Lipoglycopeptide Antibiotic. Antiinfect. Agents Med. Chem. *9*, 23–47.

Allen, N.E., Hobbs, J.N., and Alborn, W.E. (1987). Inhibition of peptidoglycan biosynthesis in gram-positive bacteria by LY146032. Antimicrob. Agents Chemother. *31*, 1093–1099.

Allen, N.E., Alborn, W.E., and Hobbs, J.N. (1991). Inhibition of membrane potential-dependent amino acid transport by daptomycin. Antimicrob. Agents Chemother. *35*, 2639–2642.

Ammerlaan, H.S.M., Harbarth, S., Buiting, A.G.M., Crook, D.W., Fitzpatrick, F., Hanberger, H., Herwaldt, L.A., van Keulen, P.H.J., Kluytmans, J.A.J.W., Kola, A., *et al.* (2013). Secular trends in nosocomial bloodstream infections: antibiotic-resistant bacteria increase the total burden of infection. Clin. Infect. Dis. *56*, 798–805.

Anderson, J.S., and Strominger, J.L. (1965). Isolation and utilization of phospholipid intermediates in cell wall glycopeptide synthesis. Biochem. Biophys. Res. Commun. *21*, 516–521.

Anderson, J.S., Matsuhashi, M., Haskin, M.A., and Strominger, J.L. (1967). Biosythesis of the peptidoglycan of bacterial cell walls. II. Phospholipid carriers in the reaction sequence. J. Biol. Chem. *242*, 3180–3190.

Antignac, A., Sieradzki, K., and Tomasz, A. (2007). Perturbation of cell wall synthesis suppresses autolysis in *Staphylococcus aureus*: Evidence for coregulation of cell wall synthetic and hydrolytic enzymes. J. Bacteriol. *189*, 7573–7580.

Arbeit, R.D., Karakawa, W.W., Vann, W.F., and Robbins, J.B. (1984). Predominance of two newly described capsular polysaccharide types among clinical isolates of *Staphylococcus aureus*. Diagn. Microbiol. Infect. Dis. *2*, 85–91.

Arranz-Trullén, J., Lu, L., Pulido, D., Bhakta, S., and Boix, E. (2017). Host antimicrobial peptides: The promise of new treatment strategies against tuberculosis. Front. Immunol. *8*.

Arthur, M., Reynolds, P., and Courvalin, P. (1996). Glycopeptide resistance in enterococci. Trends Microbiol. *4*, 401–407.

Arthur, M., Depardieu, F., Reynolds, P., and Courvalin, P. (1999). Moderate-level resistance to glycopeptide LY333328 mediated by genes of the *vanA* and *vanB* clusters in enterococci. Antimicrob. Agents Chemother. *43*, 1875–1880.

Asensio, A., Alvarez-Espejo, T., Fernandez-Crehuet, J., Ramos, A., Vaque-Rafart, J., Bishopberger, C., Hernandez Navarrete, M., Calbo-Torrecillas, F., Campayo, J., Canton, R., *et al.* (2011). Trends in yearly prevalence of third-generation cephalosporin and fluoroquinolone resistant *Enterobacteriaceae* infections and antimicrobial use in Spanish hospitals, Spain, 1999 to 2010. Euro Surveill. *16*.

Atanasov, A.G., Zotchev, S.B., Dirsch, V.M., Orhan, I.E., Banach, M., Rollinger, J.M., Barreca, D., Weckwerth, W., Bauer, R., Bayer, E.A., *et al.* (2021). Natural products in drug discovery: advances and opportunities. Nat. Rev. Drug Discov. *20*, 200–216.

Atilano, M.L., Pereira, P.M., Yates, J., Reed, P., Veiga, H., Pinho, M.G., and Filipe, S.R. (2010). Teichoic acids are temporal and spatial regulators of peptidoglycan cross-linking in *Staphylococcus aureus*. Proc. Natl. Acad. Sci. U. S. A. *107*, 18991–18996.

Baddiley, J. (1970). Structure, Biosynthesis, and Function of Teichoic Acids. Acc. Chem. Res. *3*, 98–105.

Badet, B., Vermoote, P., Haumont, P.Y., Lederer, F., and LeGoffic, F. (1987). Glucosamine synthetase from *Escherichia coli*: purification, properties, and glutamine-utilizing site location. Biochemistry *26*, 1940–1948.

Badurina, D.S., Zolli-Juran, M., and Brown, E.D. (2003). CTP:glycerol 3-phosphate cytidylyltransferase (TarD) from *Staphylococcus aureus* catalyzes the cytidylyl transfer via an ordered Bi-Bi reaction mechanism with micromolar K_m values. Biochim. Biophys. Acta *1646*, 196–206.

Ball, L.-J., Goult, C.M., Donarski, J.A., Micklefield, J., and Ramesh, V. (2004). NMR structure determination and calcium binding effects of lipopeptide antibiotic daptomycin. Org. Biomol. Chem. *2*, 1872–1878.

Baltz, R.H. (2005). Antibiotic discovery from Actinomycetes: Will a renaissance follow the decline and fall. SIM News *55*, 186–196.

Baltz, R.H., Miao, V., and Wrigley, S.K. (2005). Natural products to drugs: daptomycin and related lipopeptide antibiotics. Nat. Prod. Rep. *22*, 717.

Baltzer, S.A., and Brown, M.H. (2011). Antimicrobial peptides: promising alternatives to conventional antibiotics. J. Mol. Microbiol. Biotechnol. *20*, 228–235.

Baquero, F., and Levin, B.R. (2021). Proximate and ultimate causes of the bactericidal action of antibiotics. Nat. Rev. Microbiol. *19*, 123–132.

Barák, I., Muchová, K., Wilkinson, A.J., O'Toole, P.J., and Pavlendová, N. (2008). Lipid spirals in Bacillus subtilis and their role in cell division. Mol. Microbiol. *68*, 1315–1327.

Barreteau, H., Magnet, S., Ghachi, M. El, Touzé, T., Arthur, M., Mengin-Lecreulx, D., and Blanot, D. (2009). Quantitative high-performance liquid chromatography analysis of the pool levels of undecaprenyl phosphate and its derivatives in bacterial membranes. J. Chromatogr. B Anal. Technol. Biomed. Life Sci. *877*, 213–220.

Batt, S.M., Burke, C.E., Moorey, A.R., and Besra, G.S. (2020). Antibiotics and resistance: the two-sided coin of the mycobacterial cell wall. Cell Surf. *6*, 100044.

Belley, A., McKay, G.A., Arhin, F.F., Sarmiento, I., Beaulieu, S., Fadhil, I., Parr, T.R., and Moeck, G. (2010). Oritavancin disrupts membrane integrity of *Staphylococcus aureus* and vancomycin-resistant enterococci to effect rapid bacterial killing. Antimicrob. Agents Chemother. *54*, 5369–5371.

Ben-Yehuda, S., and Losick, R. (2002). Asymmetric cell division in *B. subtilis* involves a spiral-like intermediate of the cytokinetic protein FtsZ. Cell *109*, 257–266.

Benson, T.E., Marquardt, J.L., Marquardt, A.C., Etzkorn, F.A., and Walsh, C.T. (1993). Overexpression, purification, and mechanistic study of UDP-*N*-acetylenolpyruvylglucosamine reductase. Biochemistry *32*, 2024–2030.

Bentley, S.D., Aanensen, D.M., Mavroidi, A., Saunders, D., Rabbinowitsch, E., Collins, M., Donohoe, K., Harris, D., Murphy, L., Quail, M.A., *et al.* (2006). Genetic analysis of the capsular biosynthetic locus from all 90 pneumococcal serotypes. PLoS Genet. *2*, 0262–0269.

Bera, A., Biswas, R., Herbert, S., Kulauzovic, E., Weidenmaier, C., Peschel, A., and Götz, F. (2007). Influence of wall teichoic acid on lysozyme resistance in *Staphylococcus aureus*. J. Bacteriol. *189*, 280–283.

Berendonk, T.U., Manaia, C.M., Merlin, C., Fatta-Kassinos, D., Cytryn, E., Walsh, F., Bürgmann, H., Sørum, H., Norström, M., Pons, M.-N., *et al.* (2015). Tackling antibiotic resistance: the environmental framework. Nat. Rev. Microbiol. *13*, 310–317.

Bertsche, U., Weidenmaier, C., Kuehner, D., Yang, S.-J., Baur, S., Wanner, S., Francois, P., Schrenzel, J., Yeaman, M.R., and Bayer, A.S. (2011). Correlation of daptomycin resistance in a clinical *Staphylococcus aureus* strain with increased cell wall teichoic acid production and D-alanylation. Antimicrob. Agents Chemother. *55*, 3922–3928.

Bertsche, U., Yang, S.-J., Kuehner, D., Wanner, S., Mishra, N.N., Roth, T., Nega, M., Schneider, A., Mayer, C., Grau, T., *et al.* (2013). Increased cell wall teichoic acid production and D-alanylation are common phenotypes among daptomycin-resistant methicillin-resistant *Staphylococcus aureus* (MRSA) clinical isolates. PLoS One *8*, e67398.

Bhasin, N., Albus, A., Michon, F., Livolsi, P.J., Park, J.S., and Lee, J.C. (1998). Identification of a gene essential for *O*-acetylation of the *Staphylococcus aureus* type 5 capsular polysaccharide. Mol. Microbiol. *27*, 9–21.

Bhatnagar, K., and Wong, A. (2019). The mutational landscape of quinolone resistance in *Escherichia coli*. PLoS One *14*, e0224650.

Bhullar, K., Waglechner, N., Pawlowski, A., Koteva, K., Banks, E.D., Johnston, M.D., Barton, H.A., and Wright, G.D. (2012). Antibiotic resistance is prevalent in an isolated cave microbiome. PLoS One *7*, e34953.

Bierbaum, G., and Sahl, H.G. (1985). Induction of autolysis of staphylococci by the basic peptide antibiotics Pep 5 and nisin and their influence on the activity of autolytic enzymes. Arch. Microbiol. *141*, 249–254.

Birch, H.L., Alderwick, L.J., Bhatt, A., Rittmann, D., Krumbach, K., Singh, A., Bai, Y., Lowary, T.L., Eggeling, L., and Besra, G.S. (2008). Biosynthesis of mycobacterial arabinogalactan: Identification of a novel α(1→3)-arabinofuranosyltransferase. Mol. Microbiol. *69*, 1191–1206.

Boaretti, M., and Canepari, P. (1995). Identification of daptomycin-binding proteins in the membrane of *Enterococcus hirae*. Antimicrob. Agents Chemother. *39*, 2068–2072.

Boaretti, M., Canepari, P., Lleò, M.M., and Satta, G. (1993). The activity of daptomycin on *Enterococcus faecium* protoplasts: indirect evidence supporting a novel mode of action on lipoteichoic acid synthesis. J. Antimicrob. Chemother. *31*, 227–235.

Bogaert, D., Hermans, P.W.M., Adrian, P. V., Rümke, H.C., and de Groot, R. (2004). Pneumococcal vaccines: an update on current strategies. Vaccine *22*, 2209–2220.

Bolla, J.R., Sauer, J.B., Wu, D., Mehmood, S., Allison, T.M., and Robinson, C. V. (2018). Direct observation of the influence of cardiolipin and antibiotics on lipid II binding to MurJ. Nat. Chem. *10*, 363–371.

Borisova, M., Gaupp, R., Duckworth, A., Schneider, A., Dalügge, D., Mühleck, M., Deubel, D., Unsleber, S., Yu, W., Muth, G., *et al.* (2016). Peptidoglycan Recycling in Gram-Positive Bacteria Is Crucial for Survival in Stationary Phase. MBio *7*.

Boucher, H.W., Talbot, G.H., Bradley, J.S., Edwards, J.E., Gilbert, D., Rice, L.B., Scheld, M., Spellberg, B., and Bartlett, J. (2009). Bad bugs, no drugs: No ESKAPE! An update from the Infectious Diseases Society of America. Clin. Infect. Dis. *48*, 1–12.

Boyle-Vavra, S., Labischinski, H., Ebert, C.C., Ehlert, K., and Daum, R.S. (2001). A spectrum of changes occurs in peptidoglycan composition of glycopeptide-intermediate clinical *Staphylococcus aureus* isolates. Antimicrob. Agents Chemother. *45*, 280–287.

Bozdogan, B., Ednie, L., Credito, K., Kosowska, K., and Appelbaum, P.C. (2004). Derivatives of a vancomycin-resistant *Staphylococcus aureus* strain isolated at Hershey Medical Center. Antimicrob. Agents Chemother. *48*, 4762–4765.

van den Brink-van der Laan, E., Boots, J.P., Spelbrink, R.E.J., Kool, G.M., Breukink, E., Killian, J.A., and de Kruijff, B. (2003). Membrane interaction of the glycosyltransferase MurG: a special role for cardiolipin. J. Bacteriol. *185*, 3773–3779.

Brott, A.S., Jones, C.S., and Clarke, A.J. (2019). Development of a High Throughput Screen for the Identification of Inhibitors of Peptidoglycan *O*-Acetyltransferases, New Potential Antibacterial Targets. Antibiotics *8*, 65.

Brötz-Oesterhelt, H., and Brunner, N.A. (2008). How many modes of action should an antibiotic have? Curr. Opin. Pharmacol. *8*, 564–573.

Brown, S., Xia, G., Luhachack, L.G., Campbell, J., Meredith, T.C., Chen, C., Winstel, V., Gekeler, C., Irazoqui, J.E., Peschel, A., *et al.* (2012). Methicillin resistance in *Staphylococcus aureus* requires glycosylated wall teichoic acids. Proc. Natl. Acad. Sci. U. S. A. *109*, 18909–18914.

Bublitz, M., Kjellerup, L., Cohrt, K.O.H., Gordon, S., Mortensen, A.L., Clausen, J.D., Pallin, T.D., Hansen, J.B., Fuglsang, A.T., Dalby-Brown, W., *et al.* (2018). Tetrahydrocarbazoles are a novel class of potent P-type ATPase inhibitors with antifungal activity. PLoS One *13*, e0188620.

Bucciantini, M., Giannoni, E., Chiti, F., Baroni, F., Taddei, N., Ramponi, G., Dobson, C.M., and Stefani, M. (2002). Inherent toxicity of aggregates implies a common mechanism for protein misfolding diseases. Nature *416*, 507–511.

Bugg, T.D.H., Dutka-Malen, S., Arthur, M., Courvalin, P., and Walsh, C.T. (1991). Identification of vancomycin resistance protein VanA as a D-alanine:D-alanine ligase of altered substrate specificity. Biochemistry *30*, 2017–2021.

Bush, K., and Bradford, P.A. (2016). β-Lactams and β-Lactamase Inhibitors: An Overview. Cold Spring Harb. Perspect. Med. *6*.

Butler, M.S., Gigante, V., Sati, H., Paulin, S., Al-Sulaiman, L., Rex, J.H., Fernandes, P., Arias, C.A., Paul, M., Thwaites, G.E., *et al.* (2022). Analysis of the Clinical Pipeline of Treatments for Drug-Resistant Bacterial Infections: Despite Progress, More Action Is Needed. Antimicrob. Agents Chemother. *66*.

Cadete Pires, A.C., Duan, A.R., and Ling, L.L. (2019). Pharmaceutical compositions comprising teixobactin. International patent WO2019160719A1.

Cama, J., Leszczynski, R., Tang, P.K., Khalid, A., Lok, V., Dowson, C.G., and Ebata, A. (2021). To Push or to Pull? in a Post-COVID World, Supporting and Incentivizing Antimicrobial Drug Development Must Become a Governmental Priority. ACS Infect. Dis. *7*, 2029–2042.

Campbell, J., Singh, A.K., Santa Maria, J.P., Kim, Y., Brown, S., Swoboda, J.G., Mylonakis, E., Wilkinson, B.J., and Walker, S. (2011). Synthetic lethal compound combinations reveal a fundamental connection between wall teichoic acid and peptidoglycan biosyntheses in *Staphylococcus aureus*. ACS Chem. Biol. *6*, 106–116.

Campbell, J., Singh, A.K., Swoboda, J.G., Gilmore, M.S., Wilkinson, B.J., and Walker, S. (2012). An antibiotic that inhibits a late step in wall teichoic acid biosynthesis induces the cell wall stress stimulon in *Staphylococcus aureus*. Antimicrob. Agents Chemother. *56*, 1810–1820.

Canepari, P., Boaretti, M., Del Mar Lleo, M., and Satta, G. (1990). Lipoteichoic acid as a new target for activity of antibiotics: Mode of action of daptomycin (LY146032). Antimicrob. Agents Chemother. *34*, 1220–1226.

Cao, L., Do, T., and Link, A.J. (2021). Mechanisms of action of ribosomally synthesized and posttranslationally modified peptides (RiPPs). J. Ind. Microbiol. Biotechnol. *48*.

Cassini, A., Högberg, L.D., Plachouras, D., Quattrocchi, A., Hoxha, A., Simonsen, G.S., Colomb-Cotinat, M., Kretzschmar, M.E., Devleesschauwer, B., Cecchini, M., *et al.* (2019). Attributable deaths and disability-adjusted life-years caused by infections with antibiotic-resistant bacteria in the EU and the European Economic Area in 2015: a population-level modelling analysis. Lancet Infect. Dis. *19*, 56–66.

Chambers, H.F. (2001). The changing epidemiology of *Staphylococcus aureus*? Emerg. Infect. Dis. *7*, 178–182.

Chan, Y.G.Y., Frankel, M.B., Dengler, V., Schneewind, O., and Missiakas, D. (2013). *Staphylococcus aureus* Mutants Lacking the LytR-CpsA-Psr Family of Enzymes Release Cell Wall Teichoic Acids into the Extracellular Medium. J. Bacteriol. *195*, 4650–4659.

Chan, Y.G.Y., Kim, H.K., Schneewind, O., and Missiakas, D. (2014). The capsular polysaccharide of *Staphylococcus aureus* is attached to peptidoglycan by the LytR-CpsA-Psr (LCP) family of enzymes. J. Biol. Chem. *289*, 15680–15690.

Chatterjee, A.N. (1969). Use of bacteriophage-resistant mutants to study the nature of the bacteriophage receptor site of *Staphylococcus aureus*. J. Bacteriol. *98*, 519–527.

Chauhan, J., Cardinale, S., Fang, L., Huang, J., Kwasny, S.M., Ross Pennington, M., Basi, K., Ditargiani, R., Capacio, B.R., MacKerell, A.D., *et al.* (2016). Towards development of small molecule Lipid II inhibitors as novel antibiotics. PLoS One *11*, 1–19.

Chen, H., Nyantakyi, S.A., Li, M., Gopal, P., Aziz, D.B., Yang, T., Moreira, W., Gengenbacher, M., Dick, T., and Go, M.L. (2018). The mycobacterial membrane: A novel target space for anti-tubercular drugs. Front. Microbiol. *9*, 1–11.

Chen, J., Zhang, S., Cui, P., Shi, W., Zhang, W., and Zhang, Y. (2017a). Identification of novel mutations associated with cycloserine resistance in *Mycobacterium tuberculosis*. J. Antimicrob. Chemother. *72*, 3272–3276.

Chen, K.H., Le, S.P., Han, X., Frias, J.M., and Nowick, J.S. (2017b). Alanine scan reveals modifiable residues in teixobactin. Chem. Commun. *53*, 11357–11359.

Chen, L., Hou, W.T., Fan, T., Liu, B., Pan, T., Li, Y.H., Jiang, Y.L., Wen, W., Chen, Z.P., Sun, L., *et al.* (2020). Cryo-electron microscopy structure and transport mechanism of a wall teichoic acid ABC transporter. MBio *11*, 1–13.

Chiorean, S., Antwi, I., Carney, D.W., Kotsogianni, I., Giltrap, A.M., Alexander, F.M., Cochrane, S.A., Payne, R.J., Martin, N.I., Henninot, A., *et al.* (2020). Dissecting the Binding Interactions of Teixobactin with the Bacterial Cell-Wall Precursor Lipid II. ChemBioChem *21*, 789–792.

Cho, H., Wivagg, C.N., Kapoor, M., Barry, Z., Rohs, P.D.A., Suh, H., Marto, J.A., Garner, E.C., and Bernhardt, T.G. (2016). Bacterial cell wall biogenesis is mediated by SEDS and PBP polymerase families functioning semi-autonomously. Nat. Microbiol. *1*, 16172.

Chokekijchai, S., Kojima, E., Anderson, S., Nomizu, M., Tanaka, M., Machida, M., Date, T., Toyota, K., Ishida, S., Watanabe, K., *et al.* (1995). NP-06: A novel anti-human immunodeficiency virus polypeptide produced by a *Streptomyces* species. Antimicrob. Agents Chemother. *39*, 2345–2347.

Chugunov, A., Pyrkova, D., Nolde, D., Polyansky, A., Pentkovsky, V., and Efremov, R. (2013). Lipid-II forms potential "landing terrain" for lantibiotics in simulated bacterial membrane. Sci. Rep. *3*, 1–11.

Ciumac, D., Gong, H., Hu, X., and Lu, J.R. (2019). Membrane targeting cationic antimicrobial peptides. J. Colloid Interface Sci. *537*, 163–185.

Clarke, A.J., and Dupont, C. (1992). *O*-Acetylated peptidoglycan: Its occurrence, pathobiological significance, and biosynthesis. Can. J. Microbiol. *38*, 85–91.

Clatworthy, A.E., Pierson, E., and Hung, D.T. (2007). Targeting virulence: a new paradigm for antimicrobial therapy. Nat. Chem. Biol. *3*, 541–548.

Cochrane, S.A., and Vederas, J.C. (2014). Unacylated tridecaptin A_1 acts as an effective sensitiser of Gram-negative bacteria to other antibiotics. Int. J. Antimicrob. Agents *44*, 493–499.

Cochrane, S.A., Lohans, C.T., Brandelli, J.R., Mulvey, G., Armstrong, G.D., and Vederas, J.C. (2014). Synthesis and structure-activity relationship studies of *N*-terminal analogues of the antimicrobial peptide tridecaptin A_1. J. Med. Chem. *57*, 1127–1131.

Cochrane, S.A., Findlay, B., Bakhtiary, A., Acedo, J.Z., Rodriguez-Lopez, E.M., Mercier, P., and Vederas, J.C. (2016). Antimicrobial lipopeptide tridecaptin A_1 selectively binds to Gram-negative lipid II. Proc. Natl. Acad. Sci. U. S. A. *113*, 11561–11566.

Cong, Y., Yang, S., and Rao, X. (2020). Vancomycin-resistant *Staphylococcus aureus* infections: A review of case updating and clinical features. J. Adv. Res. *21*, 169–176.

Cook, D., Brown, D., Alexander, R., March, R., Morgan, P., Satterthwaite, G., and Pangalos, M.N. (2014). Lessons learned from the fate of AstraZeneca's drug pipeline: A five-dimensional framework. Nat. Rev. Drug Discov. *13*, 419–431.

Cooper, S., and Hsieh, M.L. (1988). The rate and topography of cell wall synthesis during the division cycle of *Escherichia coli* using *N*-acetylglucosamine as a peptidoglycan label. J. Gen. Microbiol. *134*, 1717–1721.

Craik, D.J., Fairlie, D.P., Liras, S., and Price, D. (2013). The Future of Peptide-based Drugs. Chem. Biol. Drug Des. *81*, 136–147.

Cudic, P., Kranz, J.K., Behenna, D.C., Kruger, R.G., Tadesse, H., Wand, A.J., Veklich, Y.I., Weisel, J.W., and McCafferty, D.G. (2002). Complexation of peptidoglycan intermediates by the lipoglycodepsipeptide antibiotic ramoplanin: Minimal structural requirements for intermolecular complexation and fibril formation. Proc. Natl. Acad. Sci. U. S. A. *99*, 7384–7389.

Cui, L., Iwamoto, A., Lian, J.Q., Neoh, H.M., Maruyama, T., Horikawa, Y., and Hiramatsu, K. (2006). Novel mechanism of antibiotic resistance originating in vancomycin-intermediate *Staphylococcus aureus*. Antimicrob. Agents Chemother. *50*, 428–438.

Cuthbertson, L., Kos, V., and Whitfield, C. (2010). ABC transporters involved in export of cell surface glycoconjugates. Microbiol. Mol. Biol. Rev. *74*, 341–362.

Czarny, T.L., and Brown, E.D. (2016). A Small-Molecule Screening Platform for the Discovery of Inhibitors of Undecaprenyl Diphosphate Synthase. ACS Infect. Dis. *2*, 489–499.

D'Costa, V.M., King, C.E., Kalan, L., Morar, M., Sung, W.W.L., Schwarz, C., Froese, D., Zazula, G., Calmels, F., Debruyne, R., *et al.* (2011). Antibiotic resistance is ancient. Nature *477*, 457–461.

D'Elia, M.A., Millar, K.E., Beveridge, T.J., and Brown, E.D. (2006a). Wall teichoic acid polymers are dispensable for cell viability in *Bacillus subtilis*. J. Bacteriol. *188*, 8313–8316.

D'Elia, M.A., Pereira, M.P., Chung, Y.S., Zhao, W., Chau, A., Kenney, T.J., Sulavik, M.C., Black, T.A., and Brown, E.D. (2006b). Lesions in teichoic acid biosynthesis in *Staphylococcus aureus* lead to a lethal gain of function in the otherwise dispensable pathway. J. Bacteriol. *188*, 4183–4189.

Daniel-Ivad, M., Hameed, N., Tan, S., Dhanjal, R., Socko, D., Pak, P., Gverzdys, T., Elliot, M.A., and Nodwell, J.R. (2017). An Engineered Allele of *afsQ1* Facilitates the Discovery and Investigation of Cryptic Natural Products. ACS Chem. Biol. *12*, 628–634.

Deak, D., Outterson, K., Powers, J.H., and Kesselheim, A.S. (2016). Progress in the Fight Against Multidrug-Resistant Bacteria? A Review of U.S. Food and Drug Administration-Approved Antibiotics, 2010-2015. Ann. Intern. Med. *165*, 363–372.

Debono, M., Barnhart, M., Carrell, C.B., Hoffmann, J.A., Occolowitz, J.L., Abbott, B.J., Fukuda, D.S., Hamill, R.L., Biemann, K., and Herlihy, W.C. (1987). A21978C, a complex of new acidic peptide antibiotics: isolation, chemistry, and mass spectral structure elucidation. J. Antibiot. (Tokyo). *40*, 761–777.

Debono, M., Abbott, B.J., Molloy, R.M., Fukuda, D.S., Hunt, A.H., Daupert, V.M., Counter, F.T., Ott, J.L., Carrell, C.B., and Howard, L.C. (1988). Enzymatic and chemical modifications of lipopeptide antibiotic A21978C: the synthesis and evaluation of daptomycin (LY146032). J. Antibiot. (Tokyo). *41*, 1093–1105.

Deighton, M.A., and Balkau, B. (1990). Adherence measured by microtiter assay as a virulence marker for *Staphylococcus epidermidis* infections. J. Clin. Microbiol. *28*, 2442–2447.

Dengler, V., Meier, P.S., Heusser, R., Kupferschmied, P., Fazekas, J., Friebe, S., Staufer, S.B., Majcherczyk, P.A., Moreillon, P., Berger-Bächi, B., *et al.* (2012). Deletion of hypothetical wall teichoic acid ligases in *Staphylococcus aureus* activates the cell wall stress response. FEMS Microbiol. Lett. *333*, 109–120.

Derouaux, A., Turk, S., Olrichs, N.K., Gobec, S., Breukink, E., Amoroso, A., Offant, J., Bostock, J., Mariner, K., Chopra, I., *et al.* (2011). Small molecule inhibitors of peptidoglycan synthesis targeting the lipid II precursor. Biochem. Pharmacol. *81*, 1098–1105.

Dheman, N., Mahoney, N., Cox, E.M., Farley, J.J., Amini, T., and Lanthier, M.L. (2020). An Analysis of Antibacterial Drug Development Trends in the United States, 1980–2019. Clin. Infect. Dis. 1–7.

DiMasi, J.A., Grabowski, H.G., and Hansen, R.W. (2016). Innovation in the pharmaceutical industry: New estimates of R&D costs. J. Health Econ. *47*, 20–33.

Do, T., Page, J.E., and Walker, S. (2020a). Uncovering the activities, biological roles, and regulation of bacterial cell wall hydrolases and tailoring enzymes. J. Biol. Chem. *295*, 3347–3361.

Do, T., Schaefer, K., Santiago, A.G., Coe, K.A., Fernandes, P.B., Kahne, D., Pinho, M.G., and Walker, S. (2020b). *Staphylococcus aureus* cell growth and division are regulated by an amidase that trims peptides from uncrosslinked peptidoglycan. Nat. Microbiol. *5*, 291–303.

Domalaon, R., Idowu, T., Zhanel, G.G., and Schweizer, F. (2018). Antibiotic Hybrids: the Next Generation of Agents and Adjuvants against Gram-Negative Pathogens? Clin. Microbiol. Rev. *31*.

Domínguez-Escobar, J., Wolf, D., Fritz, G., Höfler, C., Wedlich-Söldner, R., and Mascher, T. (2014). Subcellular localization, interactions and dynamics of the phage-shock protein-like Lia response in *Bacillus subtilis*. Mol. Microbiol. *92*, 716–732.

Donahue, E.H., Dawson, L.F., Valiente, E., Firth-Clark, S., Major, M.R., Littler, E., Perrior, T.R., and Wren, B.W. (2014). *Clostridium difficile* has a single sortase, SrtB, that can be inhibited by small-molecule inhibitors. BMC Microbiol. *14*, 1–14.

Draper, L.A., Cotter, P.D., Hill, C., and Ross, R.P. (2015). Lantibiotic Resistance. Microbiol. Mol. Biol. Rev. *79*, 171–191.

Drayton, M., Deisinger, J.P., Ludwig, K.C., Raheem, N., Müller, A., Schneider, T., and Straus, S.K. (2021). Host Defense Peptides: Dual Antimicrobial and Immunomodulatory Action. Int. J. Mol. Sci. *22*, 11172.

Dubrac, S., and Msadek, T. (2004). Identification of Genes Controlled by the Essential YycG/YycF Two-Component System of *Staphylococcus aureus*. J. Bacteriol. *186*, 1175–1181.

Dubrac, S., Boneca, I.G., Poupel, O., and Msadek, T. (2007). New insights into the WalK/WalR (YycG/YycF) essential signal transduction pathway reveal a major role in controlling cell wall metabolism and biofilm formation in *Staphylococcus aureus*. J. Bacteriol. *189*, 8257–8269.

Dulberger, C.L., Rubin, E.J., and Boutte, C.C. (2020). The mycobacterial cell envelope — a moving target. Nat. Rev. Microbiol. *18*, 47–59.

Egan, A.J.F., Cleverley, R.M., Peters, K., Lewis, R.J., and Vollmer, W. (2017). Regulation of bacterial cell wall growth. FEBS J. *284*, 851–867.

Egan, A.J.F., Errington, J., and Vollmer, W. (2020). Regulation of peptidoglycan synthesis and remodelling. Nat. Rev. Microbiol. *18*, 446–460.

von Eiff, C., Taylor, K.L., Mellmann, A., Fattom, A.I., Friedrich, A.W., Peters, G., and Becker, K. (2007). Distribution of capsular and surface polysaccharide serotypes of *Staphylococcus aureus*. Diagn. Microbiol. Infect. Dis. *58*, 297–302.

Eisenberg, D., and Jucker, M. (2012). The amyloid state of proteins in human diseases. Cell *148*, 1188–1203.

Eliopoulos, G.M., Thauvin, C., Gerson, B., and Moellering, R.C. (1985). *In vitro* activity and mechanism of action of A21978C1, a novel cyclic lipopeptide antibiotic. Antimicrob. Agents Chemother. *27*, 357–362.

Ellwood, D.C. (1970). The wall content and composition of *Bacillus subtilis* var. *niger* grown in a chemostat. Biochem. J. *118*, 367–373.

Emami, K., Guyet, A., Kawai, Y., Devi, J., Wu, L.J., Allenby, N., Daniel, R.A., and Errington, J. (2017). RodA as the missing glycosyltransferase in *Bacillus subtilis* and antibiotic discovery for the peptidoglycan polymerase pathway. Nat. Microbiol. *2*, 1–8.

Engel, M.F.M., Khemtémourian, L., Kleijer, C.C., Meeldijk, H.J.D., Jacobs, J., Verkleij, A.J., De Kruijff, B., Killian, J.A., and Höppener, J.W.M. (2008). Membrane damage by human islet amyloid polypeptide through fibril growth at the membrane. Proc. Natl. Acad. Sci. U. S. A. *105*, 6033–6038.

Engelberg, Y., and Landau, M. (2020). The Human LL-37(17-29) antimicrobial peptide reveals a functional supramolecular structure. Nat. Commun. *11*, 1–10.

Epand, R.M. (1997). Biophysical studies of lipopeptide-membrane interactions. Biopolymers *43*, 15–24.

Epand, R.M. (2019). Anionic Lipid Clustering Model. pp. 65–71.

Epand, R.M., Walker, C., Epand, R.F., and Magarvey, N.A. (2016). Molecular mechanisms of membrane targeting antibiotics. Biochim. Biophys. Acta - Biomembr. *1858*, 980–987.

Errington, J. (2013). L-form bacteria, cell walls and the origins of life. Open Biol. *3*, 120143.

Ersoy, S.C., Heithoff, D.M., Barnes, L., Tripp, G.K., House, J.K., Marth, J.D., Smith, J.W., and Mahan, M.J. (2017). Correcting a Fundamental Flaw in the Paradigm for Antimicrobial Susceptibility Testing. EBioMedicine *20*, 173–181.

Essig, A., Hofmann, D., Münch, D., Gayathri, S., Künzler, M., Kallio, P.T., Sahl, H.-G., Wider, G., Schneider, T., and Aebi, M. (2014). Copsin, a novel peptide-based fungal antibiotic interfering with the peptidoglycan synthesis. J. Biol. Chem. *289*, 34953–34964.

Eun, Y.J., Foss, M.H., Kiekebusch, D., Pauw, D.A., Westler, W.M., Thanbichler, M., and Weibel, D.B. (2012). DCAP: A broad-spectrum antibiotic that targets the cytoplasmic membrane of bacteria. J. Am. Chem. Soc. *134*, 11322–11325.

Ezzell, J.W., and Welkos, S.L. (1999). The capsule of Bacillus anthracis, a review. J. Appl. Microbiol.

Farha, M.A., Leung, A., Sewell, E.W., D'Elia, M.A., Allison, S.E., Ejim, L., Pereira, P.M., Pinho, M.G., Wright, G.D., and Brown, E.D. (2013). Inhibition of WTA synthesis blocks the cooperative action of PBPs and sensitizes MRSA to β-lactams. ACS Chem. Biol. *8*, 226–233.

Farha, M.A., Czarny, T.L., Myers, C.L., Worrall, L.J., French, S., Conrady, D.G., Wang, Y., Oldfield, E., Strynadka, N.C.J., and Brown, E.D. (2015). Antagonism screen for inhibitors of bacterial cell wall biogenesis uncovers an inhibitor of undecaprenyl diphosphate synthase. Proc. Natl. Acad. Sci. U. S. A. *112*, 11048–11053.

Figueiredo, T.A., Ludovice, A.M., and Sobral, R.G. (2014). Contribution of peptidoglycan amidation to β-lactam and lysozyme resistance in different genetic lineages of *Staphylococcus aureus*. Microb. Drug Resist. *20*, 238–249.

Fischer, W. (1988). Physiology of Lipoteichoic Acids in Bacteria. Adv. Microb. Physiol.

Fischer, W. (1994). Lipoteichoic acid and lipids in the membrane of *Staphylococcus aureus*. Med. Microbiol. Immunol. *183*, 61–76.

Fleeman, R.M., Macias, L.A., Brodbelt, J.S., and Davies, B.W. (2020). Defining principles that influence antimicrobial peptide activity against capsulated *Klebsiella pneumoniae*. Proc. Natl. Acad. Sci. U. S. A. *117*, 27620–27626.

Fleming, A. (1929). On the antibacterial action of cultures of a penicillium, with special reference to their use in the isolation of *B. influenzae*. Br. J. Exp. Pathol. *10*, 226–236.

Fletcher, S., Yu, W., Huang, J., Kwasny, S.M., Chauhan, J., Opperman, T.J., Mackerell, A.D., and De Leeuw, E.P. (2015). Structure–activity exploration of a small-molecule lipid II inhibitor. Drug Des. Devel. Ther. *9*, 2383–2394.

Flores-Kim, J., Dobihal, G.S., Fenton, A., Rudner, D.Z., and Bernhardt, T.G. (2019). A switch in surface polymer biogenesis triggers growth-phase-dependent and antibiotic-induced bacteriolysis. Elife *8*, 1–23.

Fosgerau, K., and Hoffmann, T. (2015). Peptide therapeutics: Current status and future directions. Drug Discov. Today *20*, 122–128.

Foucault, M.L., Courvalin, P., and Grillot-Courvalin, C. (2009). Fitness cost of VanA-type vancomycin resistance in methicillin-resistant *Staphylococcus aureus*. Antimicrob. Agents Chemother. *53*, 2354–2359.

Frankel, R., Sparr, E., and Linse, S. (2022). On the Aggregation of Apolipoprotein A-I. Int. J. Mol. Sci. *23*, 8780.

Friedman, R., Pellarin, R., and Caflisch, A. (2009). Amyloid Aggregation on Lipid Bilayers and Its Impact on Membrane Permeability. J. Mol. Biol. *387*, 407–415.

Frokjaer, S., and Otzen, D.E. (2005). Protein drug stability: A formulation challenge. Nat. Rev. Drug Discov. *4*, 298–306.

Fukuchi, K., Kasahara, Y., Asai, K., Kobayashi, K., Moriya, S., and Ogasawara, N. (2000). The essential two-component regulatory system encoded by *yycF* and *yycG* modulates expression of the *ftsAZ* operon in *Bacillus subtilis*. Microbiology *146*, 1573–1583.

Fulco, P., and Wenzel, R.P. (2006). Ramoplanin: a topical lipoglycodepsipeptide antibacterial agent. Expert Rev. Anti. Infect. Ther. *4*, 939–945.

Gaglione, R., Smaldone, G., Cesaro, A., Rumolo, M., De Luca, M., Di Girolamo, R., Petraccone, L., Del Vecchio, P., Oliva, R., Notomista, E., *et al.* (2021). Impact of a Single Point Mutation on the Antimicrobial and Fibrillogenic Properties of Cryptides from Human Apolipoprotein B. Pharmaceuticals *14*, 631.

Gänzle, M.G. (2004). Reutericyclin: Biological activity, mode of action, and potential applications. Appl. Microbiol. Biotechnol. *64*, 326–332.

Geno, K.A., Gilbert, G.L., Song, J.Y., Skovsted, I.C., Klugman, K.P., Jones, C., Konradsen, H.B., and Nahm, M.H. (2015). Pneumococcal capsules and their types: Past, present, and future. Clin. Microbiol. Rev. *28*, 871–899.

Geno, K.A., Saad, J.S., and Nahm, M.H. (2017). Discovery of Novel Pneumococcal Serotype 35D, a Natural WciG-Deficient Variant of Serotype 35B. J. Clin. Microbiol. *55*, 1416–1425.

El Ghachi, M., Howe, N., Huang, C.Y., Olieric, V., Warshamanage, R., Touzé, T., Weichert, D., Stansfeld, P.J., Wang, M., Kerff, F., *et al.* (2018). Crystal structure of undecaprenyl-pyrophosphate phosphatase and its role in peptidoglycan biosynthesis. Nat. Commun. *9*, 1–13.

Ghosh, C., and Haldar, J. (2015). Membrane-Active Small Molecules: Designs Inspired by Antimicrobial Peptides. ChemMedChem *10*, 1606–1624.

Ghuysen, J.-M., and Strominger, J.L. (1963). Structure of the Cell Wall of *Staphylococcus aureus*, Strain Copenhagen. II. Separation and Structure of Disaccharides. Biochemistry *2*, 1119–1125.

Ginsberg, C., Zhang, Y.-H., Yuan, Y., and Walker, S. (2006). *In vitro* reconstitution of two essential steps in wall teichoic acid biosynthesis. ACS Chem. Biol. *1*, 25–28.

Gottlieb, C.T., Thomsen, L.E., Ingmer, H., Mygind, P.H., Kristensen, H.-H., and Gram, L. (2008). Antimicrobial peptides effectively kill a broad spectrum of *Listeria monocytogenes* and *Staphylococcus aureus* strains independently of origin, sub-type, or virulence factor expression. BMC Microbiol. *8*, 205.

Gould, S.W., Cuschieri, P., Rollason, J., Hilton, A.C., Easmon, S., and Fielder, M.D. (2010). The need for continued monitoring of antibiotic resistance patterns in clinical isolates of *Staphylococcus aureus* from London and Malta. Ann. Clin. Microbiol. Antimicrob. *9*, 20.

Grage, S.L., Afonin, S., Kara, S., Buth, G., and Ulrich, A.S. (2016). Membrane thinning and thickening induced by membrane-active amphipathic peptides. Front. Cell Dev. Biol. *4*.

Grein, F., Schneider, T., and Sahl, H.-G. (2019). Docking on Lipid II-A Widespread Mechanism for Potent Bactericidal Activities of Antibiotic Peptides. J. Mol. Biol. *431*, 3520–3530.

Gross, M., Cramton, S.E., Götz, F., and Peschel, A. (2001). Key role of teichoic acid net charge in *Staphylococcus aureus* colonization of artificial surfaces. Infect. Immun. *69*, 3423–3426.

Gudmundsson, K.S., Sebahar, P.R., Richardson, L.D.A., Catalano, J.G., Boggs, S.D., Spaltenstein, A., Sethna, P.B., Brown, K.W., Harvey, R., and Romines, K.R. (2009). Substituted tetrahydrocarbazoles with potent activity against human papillomaviruses. Bioorg. Med. Chem. Lett. *19*, 3489–3492.

Guo, Y., Pfahler, N.M., Völpel, S.L., and Stehle, T. (2021). Cell wall glycosylation in *Staphylococcus aureus*: targeting the *tar* glycosyltransferases. Curr. Opin. Struct. Biol. *68*, 166–174.

Gustafson, J., Strassle, A., Hachler, H., Kayser, F.H., and Berger-Bachi, B. (1994). The *femC* locus of *Staphylococcus aureus* required for methicillin resistance includes the glutamine synthetase operon. J. Bacteriol. *176*, 1460–1467.

Gustot, A., Gallea, J.I., Sarroukh, R., Celej, M.S., Ruysschaert, J.M., and Raussens, V. (2015). Amyloid fibrils are the molecular trigger of inflammation in Parkinson's disease. Biochem. J. *471*, 323–333.

Gwynn, M.N., Portnoy, A., Rittenhouse, S.F., and Payne, D.J. (2010). Challenges of antibacterial discovery revisited. Ann. N. Y. Acad. Sci. *1213*, 5–19.

Hamamoto, H., Panthee, S., Paudel, A., Ishii, K., Yasukawa, J., Su, J., Miyashita, A., Itoh, H., Tokumoto, K., Inoue, M., *et al.* (2021). Serum apolipoprotein A-I potentiates the therapeutic efficacy of lysocin E against *Staphylococcus aureus*. Nat. Commun. *12*, 6364.

Hamburger, J.B., Hoertz, A.J., Lee, A., Senturia, R.J., McCafferty, D.G., and Loll, P.J. (2009). A crystal structure of a dimer of the antibiotic ramoplanin illustrates membrane positioning and a potential Lipid II docking interface. Proc. Natl. Acad. Sci. U. S. A. *106*, 13759–13764.

Hammerschmidt, S., Wolff, S., Hocke, A., Rosseau, S., Müller, E., and Rohde, M. (2005). Illustration of pneumococcal polysaccharide capsule during adherence and invasion of epithelial cells. Infect. Immun. *73*, 4653–4667.

Haney, E.F., Wu, B. (Catherine), Lee, K., Hilchie, A.L., and Hancock, R.E.W. (2017). Aggregation and Its Influence on the Immunomodulatory Activity of Synthetic Innate Defense Regulator Peptides. Cell Chem. Biol. *24*, 969-980.e4.

Hanson, B.R., and Neely, M.N. (2012). Coordinate regulation of Gram-positive cell surface components. Curr. Opin. Microbiol. *15*, 204–210.

Hardt, P., Engels, I., Rausch, M., Gajdiss, M., Ulm, H., Sass, P., Ohlsen, K., Sahl, H.-G., Bierbaum, G., Schneider, T., Grein, F. (2017). The cell wall precursor lipid II acts as a molecular signal for the Ser/Thr kinase PknB of *Staphylococcus aureus*. Int. J. Med. Microbiol. *307*, 1–10.

Harms, A., Maisonneuve, E., and Gerdes, K. (2016). Mechanisms of bacterial persistence during stress and antibiotic exposure. Science *354*.

Hashimoto, M., Ooiwa, S., and Sekiguchi, J. (2012). Synthetic lethality of the *lytE cwlO* genotype in *Bacillus subtilis* is caused by lack of D,L-endopeptidase activity at the lateral cell wall. J. Bacteriol. *194*, 796–803.

Hasper, H.E., De Kruijff, B., and Breukink, E. (2004). Assembly and stability of nisin-Lipid II pores. Biochemistry *43*, 11567–11575.

Hasper, H.E., Kramer, N.E., Smith, J.L., Hillman, J.D., Zachariah, C., Kuipers, O.P., De Kruijff, B., and Breukink, E. (2006). An alternative bactericidal mechanism of action for lantibiotic peptides that target lipid II. Science *313*, 1636–1637.

van Hecke, O., Wang, K., Lee, J.J., Roberts, N.W., and Butler, C.C. (2017). Implications of Antibiotic Resistance for Patients' Recovery From Common Infections in the Community: A Systematic Review and Meta-analysis. Clin. Infect. Dis. *65*, 371–382.

Hegemann, J.D. (2020). Factors Governing the Thermal Stability of Lasso Peptides. ChemBioChem *21*, 7–18.

Hegemann, J.D., Zimmermann, M., Xie, X., and Marahiel, M.A. (2015). Lasso peptides: an intriguing class of bacterial natural products. Acc. Chem. Res. *48*, 1909–1919.

van Heijenoort, Y., Gómez, M., Derrien, M., Ayala, J., and van Heijenoort, J. (1992). Membrane intermediates in the peptidoglycan metabolism of *Escherichia coli*: possible roles of PBP 1b and PBP 3. J. Bacteriol. *174*, 3549–3557.

Henrich, E., Ma, Y., Engels, I., Münch, D., Otten, C., Schneider, T., Henrichfreise, B., Sahl, H.-G., Dötsch, V., and Bernhard, F. (2016). Lipid Requirements for the Enzymatic Activity of MraY Translocases and *in vitro* Reconstitution of the Lipid II Synthesis Pathway. J. Biol. Chem. *291*, 2535–2546.

Higashi, Y., Strominger, J.L., and Sweeley, C.C. (1967). Structure of a lipid intermediate in cell wall peptidoglycan synthesis: a derivative of a C55 isoprenoid alcohol. Proc. Natl. Acad. Sci. U. S. A. *57*, 1878–1884.

Higashi, Y., Strominger, J.L., and Sweeley, C.C. (1970). Biosynthesis of the peptidoglycan of bacterial cell walls. XXI. Isolation of free C_{55}-isoprenoid alcohol and of lipid intermediates in peptidoglycan synthesis from *Staphylococcus aureus*. J. Biol. Chem. *245*, 3697–3702.

Ho, S.W., Jung, D., Calhoun, J.R., Lear, J.D., Okon, M., Scott, W.R.P., Hancock, R.E.W., and Straus, S.K. (2008). Effect of divalent cations on the structure of the antibiotic daptomycin. Eur. Biophys. J. *37*, 421–433.

Höltje, J. V (1998). Growth of the stress-bearing and shape-maintaining murein sacculus of Escherichia coli. Microbiol. Mol. Biol. Rev. *62*, 181–203.

Homma, T., Nuxoll, A., Gandt, A.B., Ebner, P., Engels, I., Schneider, T., Götz, F., Lewis, K., and Conlon, B.P. (2016). Dual Targeting of Cell Wall Precursors by Teixobactin Leads to Cell Lysis. Antimicrob. Agents Chemother. *60*, 6510–6517.

Honarnejad, K., Daschner, A., Gehring, A.P., Szybinska, A., Giese, A., Kuznicki, J., Bracher, F., and Herms, J. (2014). Identification of tetrahydrocarbazoles as novel multifactorial drug candidates for treatment of Alzheimer's disease. Transl. Psychiatry *4*.

Hoover, D.G., and Gray, R.J. (1977). Function of cell wall teichoic acid in thermally injured *Staphylococcus aureus*. J. Bacteriol. *131*, 477–485.

Horwitz, M.A., and Silverstein, S.C. (1980). Influence of the *Escherichia coli* capsule on complement fixation and on phagocytosis and killing by human phagocytes. J. Clin. Invest. *65*, 82–94.

Howden, B.P., Davies, J.K., Johnson, P.D.R., Stinear, T.P., and Grayson, M.L. (2010). Reduced vancomycin susceptibility in *Staphylococcus aureus*, including vancomycin-intermediate and heterogeneous vancomycin-intermediate strains: Resistance mechanisms, laboratory detection, and clinical implications. Clin. Microbiol. Rev. *23*, 99–139.

Howden, B.P., McEvoy, C.R.E., Allen, D.L., Chua, K., Gao, W., Harrison, P.F., Bell, J., Coombs, G., Bennett-Wood, V., Porter, J.L., *et al.* (2011). Evolution of Multidrug Resistance during *Staphylococcus aureus* Infection Involves Mutation of the Essential Two Component Regulator WalKR. PLoS Pathog. *7*, e1002359.

Hsu, S.T.D., Breukink, E., Tischenko, E., Lutters, M.A.G., De Kruijff, B., Kaptein, R., Bonvin, A.M.J.J., and Van Nuland, N.A.J. (2004). The nisin-lipid II complex reveals a pyrophosphate cage that provides a blueprint for novel antibiotics. Nat. Struct. Mol. Biol. *11*, 963–967.

Hu, Q., Peng, H., and Rao, X. (2016). Molecular Events for Promotion of Vancomycin Resistance in Vancomycin Intermediate *Staphylococcus aureus*. Front. Microbiol. *7*.

Hu, Y., Helm, J.S., Chen, L., Ginsberg, C., Gross, B., Kraybill, B., Tiyanont, K., Fang, X., Wu, T., and Walker, S. (2004). Identification of selective inhibitors for the glycosyltransferase MurG via high-throughput screening. Chem. Biol. *11*, 703–711.

Huber, J., Donald, R.G.K., Lee, S.H., Jarantow, L.W., Salvatore, M.J., Meng, X., Painter, R., Onishi, R.H., Occi, J., Dorso, K., *et al.* (2009). Chemical genetic identification of peptidoglycan inhibitors potentiating carbapenem activity against methicillin-resistant *Staphylococcus aureus*. Chem. Biol. *16*, 837–848.

Hübscher, J., McCallum, N., Sifri, C.D., Majcherczyk, P.A., Entenza, J.M., Heusser, R., Berger-Bächi, B., and Stutzmann Meier, P. (2009). MsrR contributes to cell surface characteristics and virulence in *Staphylococcus aureus*. FEMS Microbiol. Lett. *295*, 251–260.

Hurley, K.A., Heinrich, V.A., Hershfield, J.R., Demons, S.T., and Weibel, D.B. (2015). Membrane-Targeting DCAP Analogues with Broad-Spectrum Antibiotic Activity against Pathogenic Bacteria. ACS Med. Chem. Lett. *6*, 466–471.

Hurst, P.J., Morris, M.A., Graham, A.A., Nowick, J.S., and Patterson, J.P. (2021). Visualizing Teixobactin Supramolecular Assemblies and Cell Wall Damage in *B. Subtilis* Using CryoEM. ACS Omega *6*, 27412–27417.

Hussein, M., Karas, J.A., Schneider-Futschik, E.K., Chen, F., Swarbrick, J., Paulin, O.K.A., Hoyer, D., Baker, M., Zhu, Y., Li, J., *et al.* (2020). The Killing Mechanism of Teixobactin against Methicillin-Resistant *Staphylococcus aureus*: an Untargeted Metabolomics Study. MSystems *5*.

Igarashi, M., Watanabe, T., Hashida, T., Umekita, M., Hatano, M., Yanagida, Y., Kino, H., Kimura, T., Kinoshita, N., Inoue, K., *et al.* (2013). Waldiomycin, a novel WalK-histidine kinase inhibitor from *Streptomyces* sp. MK844-mF10. J. Antibiot. (Tokyo). *66*, 459–464.

Inokoshi, J., Nakamura, Y., Hongbin, Z., Uchida, R., Nonaka, K.I., Masuma, R., and Tomoda, H. (2013). Spirohexalines, new inhibitors of bacterial undecaprenyl pyrophosphate synthase, produced by *Penicillium brasilianum* FKI-3368. J. Antibiot. (Tokyo). *66*, 37–41.

Inokoshi, J., Nakamura, Y., Komada, S., Komatsu, K., Umeyama, H., and Tomoda, H. (2016). Inhibition of bacterial undecaprenyl pyrophosphate synthase by small fungal molecules. J. Antibiot. (Tokyo). *69*, 798–805.

Ishimoto, N., and Strominger, J.L. (1966). Polyribitol phosphate synthetase of *Staphylococcus aureus*. J. Biol. Chem. *241*, 639–650.

Jackson, M. (2014). The mycobacterial cell envelope-lipids. Cold Spring Harb. Perspect. Med. *4*, 1–22.

Jekhmane, S. (2020). Solid-state NMR studies on therapeutic peptides. Utrecht University.

Jia, Z., O'Mara, M.L., Zuegg, J., Cooper, M.A., and Mark, A.E. (2011). The effect of environment on the recognition and binding of vancomycin to native and resistant forms of lipid II. Biophys. J. *101*, 2684–2692.

Jones, C. (2005). Revised structures for the capsular polysaccharides from *Staphylococcus aureus* Types 5 and 8, components of novel glycoconjugate vaccines. Carbohydr. Res. *340*, 1097–1106.

Jones, C.R., Guaglianone, G., Lai, G.H., and Nowick, J.S. (2022). Isobactins: *O*-acyl isopeptide prodrugs of teixobactin and teixobactin derivatives. Chem. Sci. *13*, 13110–13116.

Jorgenson, M.A., MacCain, W.J., Meberg, B.M., Kannan, S., Bryant, J.C., and Young, K.D. (2019). Simultaneously inhibiting undecaprenyl phosphate production and peptidoglycan synthases promotes rapid lysis in *Escherichia coli*. Mol. Microbiol. *112*, 233–248.

Joshi, V.S., Bajaj, I.B., Survase, S.A., Singhal, R.S., and Kennedy, J.F. (2009). Meningococcal polysaccharide vaccines: A review. Carbohydr. Polym. *75*, 553–565.

Jung, D., Rozek, A., Okon, M., and Hancock, R.E.W. (2004). Structural transitions as determinants of the action of the calcium-dependent antibiotic daptomycin. Chem. Biol. *11*, 949–957.

Jung, D., Powers, J.P., Straus, S.K., and Hancock, R.E.W. (2008). Lipid-specific binding of the calcium-dependent antibiotic daptomycin leads to changes in lipid polymorphism of model membranes. Chem. Phys. Lipids *154*, 120–128.

Kaeberlein, T., Lewis, K., and Epstein, S.S. (2002). Isolating "uncultivable" microorganisms in pure culture in a simulated natural environment. Science (80-.). *296*, 1127–1129.

Kagan, B.L., Jang, H., Capone, R., Teran Arce, F., Ramachandran, S., Lal, R., and Nussinov, R. (2012). Antimicrobial properties of amyloid peptides. Mol. Pharm. *9*, 708–717.

Kant, S., Asthana, S., Missiakas, D., and Pancholi, V. (2017). A novel STK1-targeted small-molecule as an "antibiotic resistance breaker" against multidrug-resistant *Staphylococcus aureus*. Sci. Rep. *7*, 1–19.

Karinou, E., Schuster, C.F., Pazos, M., Vollmer, W., and Gründling, A. (2019). Inactivation of the Monofunctional Peptidoglycan Glycosyltransferase SgtB Allows *Staphylococcus aureus* To Survive in the Absence of Lipoteichoic Acid. J. Bacteriol. *201*.

Kato, T., Hinoo, H., and Shoji, J. (1978). The structure of tridecaptin A (studies on antibiotics from the genus *Bacillus*. XXIV). J. Antibiot. (Tokyo). *31*, 652–661.

Kaur, P., Rausch, M., Malakar, B., Watson, U., Damle, N.P., Chawla, Y., Srinivasan, S., Sharma, K., Schneider, T., Jhingan, G.D., *et al.* (2019). LipidII interaction with specific residues of *Mycobacterium tuberculosis* PknB extracytoplasmic domain governs its optimal activation. Nat. Commun. *10*, 1231.

Kawai, Y., Marles-Wright, J., Cleverley, R.M., Emmins, R., Ishikawa, S., Kuwano, M., Heinz, N., Bui, N.K., Hoyland, C.N., Ogasawara, N., *et al.* (2011). A widespread family of bacterial cell wall assembly proteins. EMBO J. *30*, 4931–4941.

Khatib, T.O., Stevenson, H., Yeaman, M.R., Bayer, A.S., and Pokorny, A. (2016). Binding of daptomycin to anionic lipid vesicles is reduced in the presence of lysyl-phosphatidylglycerol. Antimicrob. Agents Chemother. *60*, 5051–5053.

Kim, S.J., Cegelski, L., Stueber, D., Singh, M., Dietrich, E., Tanaka, K.S.E., Parr, T.R., Far, A.R., and Schaefer, J. (2008). Oritavancin exhibits dual mode of action to inhibit cell-wall biosynthesis in *Staphylococcus aureus*. J. Mol. Biol. *377*, 281–293.

Kim, S.J., Singh, M., Sharif, S., and Schaefer, J. (2017). Desleucyl-Oritavancin with a Damaged D-Ala-D-Ala Binding Site Inhibits the Transpeptidation Step of Cell-Wall Biosynthesis in Whole Cells of *Staphylococcus aureus*. Biochemistry *56*, 1529–1535.

Kim, W., Fricke, N., Conery, A.L., Fuchs, B.B., Rajamuthiah, R., Jayamani, E., Vlahovska, P.M., Ausubel, F.M., and Mylonakis, E. (2016). NH125 kills methicillin-resistant *Staphylococcus aureus* persisters by lipid bilayer disruption. Future Med. Chem. *8*, 257–269.

Kim, W., Zou, G., Hari, T.P.A., Wilt, I.K., Zhu, W., Galle, N., Faizi, H.A., Hendricks, G.L., Tori, K., Pan, W., *et al.* (2019). A selective membrane-targeting repurposed antibiotic with activity against persistent methicillin-resistant *Staphylococcus aureus*. Proc. Natl. Acad. Sci. U. S. A. *116*, 16529–16534.

King, B.F., and Wilkinson, B.J. (1981). Binding of human immunoglobulin G to protein A in encapsulated *Staphylococcus aureus*. Infect. Immun. *33*, 666–672.

Kingston, A.W., Zhao, H., Cook, G.M., and Helmann, J.D. (2014). Accumulation of heptaprenyl diphosphate sensitizes *Bacillus subtilis* to bacitracin: Implications for the mechanism of resistance mediated by the BceAB transporter. Mol. Microbiol. *93*, 37–49.

Kiser, K.B., Bhasin, N., Deng, L., and Lee, J.C. (1999). *Staphylococcus aureus cap5P* encodes a UDP-*N*-acetylglucosamine 2-epimerase with functional redundancy. J. Bacteriol. *181*, 4818–4824.

Knappe, T.A., Linne, U., Zirah, S., Rebuffat, S., Xie, X., and Marahiel, M.A. (2008). Isolation and structural characterization of capistruin, a lasso peptide predicted from the genome sequence of *Burkholderia thailandensis* E264. J. Am. Chem. Soc. *130*, 11446–11454.

Kneidinger, B., O'Riordan, K., Li, J., Brisson, J.-R., Lee, J.C., and Lam, J.S. (2003). Three highly conserved proteins catalyze the conversion of UDP-*N*-acetyl-D-glucosamine to precursors for the biosynthesis of O antigen in *Pseudomonas aeruginosa* O11 and capsule in *Staphylococcus aureus* type 5. Implications for the UDP-*N*-acetyl-L-fucosamine. J. Biol. Chem. *278*, 3615–3627.

Kohga, H., Mori, T., Tanaka, Y., Yoshikaie, K., Taniguchi, K., Fujimoto, K., Fritz, L., Schneider, T., and Tsukazaki, T. (2022). Crystal structure of the lipid flippase MurJ in a "squeezed" form distinct from its inward- and outward-facing forms. Structure *30*, 1088-1097.e3.

Kotsogianni, I., Wood, T.M., Alexander, F.M., Cochrane, S.A., and Martin, N.I. (2021). Binding Studies Reveal Phospholipid Specificity and Its Role in the Calcium-Dependent Mechanism of Action of Daptomycin. ACS Infect. Dis. *7*, 2612–2619.

Koyama, N., Tokura, Y., Münch, D., Sahl, H.G., Schneider, T., Shibagaki, Y., Ikeda, H., and Tomoda, H. (2012). The nonantibiotic small molecule cyslabdan enhances the potency of β-lactams against MRSA by inhibiting pentaglycine interpeptide bridge synthesis. PLoS One *7*.

Kresse, H., Belsey, M.J., and Rovini, H. (2007). The antibacterial drugs market. Nat. Rev. Drug Discov. *6*, 19–20.

Kreutzberger, M.A., Pokorny, A., and Almeida, P.F. (2017). Daptomycin-Phosphatidylglycerol Domains in Lipid Membranes. Langmuir *33*, 13669–13679.

Kunin, C.M., Beard, M. V., and Halmagyi, N.E. (1962). Evidence for a Common Hapten Associated with Endotoxin Fractions of *E. coli* and other *Enterobacteriaceae*. Exp. Biol. Med. *111*, 160–166.

Labischinski, H. (1992). Consequences of the interaction of β-lactam antibiotics with penicillin binding proteins from sensitive and resistant *Staphylococcus aureus* strains. Med. Microbiol. Immunol. *181*, 241–265.

Laganas, V., Alder, J., and Silverman, J.A. (2003). *In vitro* bactericidal activities of daptomycin against *Staphylococcus aureus* and *Enterococcus faecalis* are not mediated by inhibition of lipoteichoic acid biosynthesis. Antimicrob. Agents Chemother. *47*, 2682–2684.

Larsson, D.G.J., and Flach, C.-F. (2022). Antibiotic resistance in the environment. Nat. Rev. Microbiol. *20*, 257–269.

Lawrence, W.S., Peel, J.E., Sivasubramani, S.K., Baze, W.B., Whorton, E.B., Beasley, D.W.C., Comer, J.E., Hughes, D.E., Ling, L.L., and Peterson, J.W. (2020). Teixobactin provides protection against inhalation anthrax in the rabbit model. Pathogens *9*, 1–13.

Leclercq, R., Derlot, E., Duval, J., and Courvalin, P. (1988). Plasmid-mediated resistance to vancomycin and teicoplanin in *Enterococcus faecium*. N. Engl. J. Med. *319*, 157–161.

Lee, E.Y., Srinivasan, Y., de Anda, J., Nicastro, L.K., Tükel, Ç., and Wong, G.C.L. (2020). Functional Reciprocity of Amyloids and Antimicrobial Peptides: Rethinking the Role of Supramolecular Assembly in Host Defense, Immune Activation, and Inflammation. Front. Immunol. *11*, 1–15.

Lee, S.H., Wang, H., Labroli, M., Koseoglu, S., Zuck, P., Mayhood, T., Gill, C., Mann, P., Sher, X., Ha, S., *et al.* (2016a). TarO-specific inhibitors of wall teichoic acid biosynthesis restore β-lactam efficacy against methicillin-resistant staphylococci. Sci. Transl. Med. *8*, 329ra32.

Lee, T.K., Tropini, C., Hsin, J., Desmarais, S.M., Ursell, T.S., Gong, E., Gitai, Z., Monds, R.D., and Huang, K.C. (2014). A dynamically assembled cell wall synthesis machinery buffers cell growth. Proc. Natl. Acad. Sci. U. S. A. *111*, 4554–4559.

Lee, W., Schaefer, K., Qiao, Y., Srisuknimit, V., Steinmetz, H., Müller, R., Kahne, D., and Walker, S. (2016b). The Mechanism of Action of Lysobactin. J. Am. Chem. Soc. *138*, 100–103.

de Leeuw, E.P.H. (2014). Efficacy of the small molecule inhibitor of Lipid II BAS00127538 against *Acinetobacter baumannii*. Drug Des. Devel. Ther. *8*, 1061–1064.

Lei, E., Tao, H., Jiao, S., Yang, A., Zhou, Y., Wang, M., Wen, K., Wang, Y., Chen, Z., Chen, X., *et al.* (2022). Potentiation of Vancomycin: Creating Cooperative Membrane Lysis through a "derivatization-for-Sensitization" Approach. J. Am. Chem. Soc. *144*, 10622–10639.

Lennarz, W.J., and Scher, M.G. (1972). Metabolism and function of polyisoprenol sugar intermediates in membrane-associated reactions. Biochim. Biophys. Acta - Rev. Biomembr. *265*, 417–441.

Łeski, T.A., and Tomasz, A. (2005). Role of penicillin-binding protein 2 (PBP2) in the antibiotic susceptibility and cell wall cross-linking of *Staphylococcus aureus*: evidence for the cooperative functioning of PBP2, PBP4, and PBP2A. J. Bacteriol. *187*, 1815–1824.

Lewis, K. (2020). The Science of Antibiotic Discovery. Cell *181*, 29–45.

Lewis, R.N.A.H., and McElhaney, R.N. (2009). The physicochemical properties of cardiolipin bilayers and cardiolipin-containing lipid membranes. Biochim. Biophys. Acta - Biomembr. *1788*, 2069–2079.

Li, F.K.K., Rosell, F.I., Gale, R.T., Simorre, J.P., Brown, E.D., and Strynadka, N.C.J. (2020). Crystallographic analysis of *Staphylococcus aureus* LcpA, the primary wall teichoic acid ligase. J. Biol. Chem. *295*, 2629–2639.

Li, Q., Cebrián, R., Montalbán-López, M., Ren, H., Wu, W., and Kuipers, O.P. (2021). Outer-membrane-acting peptides and lipid II-targeting antibiotics cooperatively kill Gram-negative pathogens. Commun. Biol. *4*, 31.

Li, W.-J., Xu, P., Zhang, L.-P., Tang, S.-K., Cui, X.-L., Mao, P.-H., Xu, L.-H., Schumann, P., Stackebrandt, E., and Jiang, C.-L. (2003). *Streptomonospora alba* sp. nov., a novel halophilic actinomycete, and emended description of the genus *Streptomonospora* Cui *et al.* 2001. Int. J. Syst. Evol. Microbiol. *53*, 1421–1425.

Li, W., Ulm, H., Rausch, M., Li, X., O'Riordan, K., Lee, J.C., Schneider, T., and Müller, C.E. (2014). Analysis of the *Staphylococcus aureus* capsule biosynthesis pathway *in vitro*: Characterization of the UDP-GlcNAc C6 dehydratases CapD and CapE and identification of enzyme inhibitors. Int. J. Med. Microbiol. *304*, 958–969.

Li, Y.X., Zhong, Z., Hou, P., Zhang, W.P., and Qian, P.Y. (2018). Resistance to nonribosomal peptide antibiotics mediated by d-stereospecific peptidases. Nat. Chem. Biol. *14*, 381–387.

Lin, T.Y., and Weibel, D.B. (2016). Organization and function of anionic phospholipids in bacteria. Appl. Microbiol. Biotechnol. *100*, 4255–4267.

Lin, P.F., Samanta, H., Bechtold, C.M., Deminie, C.A., Patick, A.K., Alam, M., Riccardi, K., Rose, R.E., White, R.J., and Colonno, R.J. (1996). Characterization of siamycin I, a human immunodeficiency virus fusion inhibitor. Antimicrob. Agents Chemother. *40*, 133–138.

Ling, L.L., Schneider, T., Peoples, A.J., Spoering, A.L., Engels, I., Conlon, B.P., Mueller, A., Schäberle, T.F., Hughes, D.E., Epstein, S., *et al.* (2015). A new antibiotic kills pathogens without detectable resistance. Nature *517*, 455–459.

Lipinski, C.A., Lombardo, F., Dominy, B.W., and Feeney, P.J. (2012). Experimental and computational approaches to estimate solubility and permeability in drug discovery and development settings. Adv. Drug Deliv. Rev. *64*, 4–17.

Livermore, D.M. (2004). The need for new antibiotics. Clin. Microbiol. Infect. *10 Suppl 4*, 1–9.

Llobet, E., Tomás, J.M., and Bengoechea, J.A. (2008). Capsule polysaccharide is a bacterial decoy for antimicrobial peptides. Microbiology *154*, 3877–3886.

Lo, M., Men, H., Branstrom, A., Helm, J., Yao, N., Goldman, R., and Walker, S. (2000). A New Mechanism of Action Proposed for Ramoplanin. J. Am. Chem. Soc. *122*, 3540–3541.

Lo, M., Helm, J.S., Sarngadharan, G., Pelczer, I., and Walker, S. (2001). A New Structure for the Substrate-Binding Antibiotic Ramoplanin. J. Am. Chem. Soc. *123*, 8640–8641.

Loskill, P., Pereira, P.M., Jung, P., Bischoff, M., Herrmann, M., Pinho, M.G., and Jacobs, K. (2014). Reduction of the peptidoglycan crosslinking causes a decrease in stiffness of the *Staphylococcus aureus* cell envelope. Biophys. J. *107*, 1082–1089.

Lovering, A.L., Lin, L.Y.-C., Sewell, E.W., Spreter, T., Brown, E.D., and Strynadka, N.C.J. (2010). Structure of the bacterial teichoic acid polymerase TagF provides insights into membrane association and catalysis. Nat. Struct. Mol. Biol. *17*, 582–589.

Lund, V.A., Wacnik, K., Turner, R.D., Cotterell, B.E., Walther, C.G., Fenn, S.J., Grein, F., Wollman, A.J.M., Leake, M.C., Olivier, N., *et al.* (2018). Molecular coordination of *Staphylococcus aureus* cell division. Elife *7*, 1–31.

Ma, P., Nishiguchi, K., Yuille, H.M., Davis, L.M., Nakayama, J., and Phillips-Jones, M.K. (2011). Anti-HIV siamycin I directly inhibits autophosphorylation activity of the bacterial FsrC quorum sensor and other ATP-dependent enzyme activities. FEBS Lett. *585*, 2660–2664.

Mainardi, J.L., Villet, R., Bugg, T.D., Mayer, C., and Arthur, M. (2008). Evolution of peptidoglycan biosynthesis under the selective pressure of antibiotics in Gram-positive bacteria. FEMS Microbiol. Rev. *32*, 386–408.

Maitra, A., Nukala, S., Dickman, R., Martin, L.T., Munshi, T., Gupta, A., Shepherd, A.J., Arnvig, K.B., Tabor, A.B., Keep, N.H., *et al.* (2021). Characterization of the MurT/GatD complex in Mycobacterium tuberculosis towards validating a novel anti-tubercular drug target. JAC-Antimicrobial Resist. *3*, 1–10.

Mak, P., Pohl, J., Dubin, A., Reed, M.S., Bowers, S.E., Fallon, M.T., and Shafer, W.M. (2003). The increased bactericidal activity of a fatty acid-modified synthetic antimicrobial peptide of human cathepsin G correlates with its enhanced capacity to interact with model membranes. Int. J. Antimicrob. Agents *21*, 13–19.

Maki, H., Miura, K., and Yamano, Y. (2001). Katanosin B and plusbacin A_3, inhibitors of peptidoglycan synthesis in methicillin-resistant *Staphylococcus aureus*. Antimicrob. Agents Chemother. *45*, 1823–1827.

Maksimov, M.O., Pan, S.J., and James Link, A. (2012). Lasso peptides: Structure, function, biosynthesis, and engineering. Nat. Prod. Rep. *29*, 996–1006.

Malin, J.J., and De Leeuw, E. (2019). Therapeutic compounds targeting Lipid II for antibacterial purposes. Infect. Drug Resist. *12*, 2613–2625.

Manat, G., Roure, S., Auger, R., Bouhss, A., Barreteau, H., Mengin-Lecreulx, D., and Touzé, T. (2014). Deciphering the metabolism of undecaprenyl-phosphate: The bacterial cell-wall unit carrier at the membrane frontier. Microb. Drug Resist. *20*, 199–214.

Mann, P.A., Müller, A., Xiao, L., Pereira, P.M., Yang, C., Ho Lee, S., Wang, H., Trzeciak, J., Schneeweis, J., Dos Santos, M.M., *et al.* (2013). Murgocil is a highly bioactive staphylococcal-specific inhibitor of the peptidoglycan glycosyltransferase enzyme MurG. ACS Chem. Biol. *8*, 2442–2451.

Marshall, C.G., Broadhead, G., Leskiw, B.K., and Wright, G.D. (1997). D-Ala-D-Ala ligases from glycopeptide antibiotic-producing organisms are highly homologous to the enterococcal vancomycin-resistance ligases VanA and VanB. Proc. Natl. Acad. Sci. U. S. A. *94*, 6480–6483.

Marshall, K.E., Marchante, R., Xue, W.F., and Serpell, L.C. (2014). The relationship between amyloid structure and cytotoxicity. Prion *8*, 192–196.

Martin, J.K., Sheehan, J.P., Bratton, B.P., Moore, G.M., Mateus, A., Li, S.H.-J., Kim, H., Rabinowitz, J.D., Typas, A., Savitski, M.M., *et al.* (2020). A Dual-Mechanism Antibiotic Kills Gram-Negative Bacteria and Avoids Drug Resistance. Cell *181*, 1518-1532.e14.

Marx, C.E. (2018). Characterization and mode of action analysis of the antibiotic hypeptin. University of Bonn.

Mascher, T., Zimmer, S.L., Smith, T., and Helmann, J.D. (2004). Antibiotic-inducible promoter regulated by the cell envelope stress-sensing two-component system LiaRS of *Bacillus subtilis*. Antimicrob. Agents Chemother. *48*, 2888–2896.

Matano, L.M., Morris, H.G., Wood, B.M.K., Meredith, T.C., and Walker, S. (2016). Accelerating the discovery of antibacterial compounds using pathway-directed whole cell screening. Bioorganic Med. Chem. *24*, 6307–6314.

McDonald, L.C. (2006). Trends in antimicrobial resistance in health care-associated pathogens and effect on treatment. Clin. Infect. Dis. *42*, 65–71.

McKenna, M. (2020). The antibiotic paradox: why companies can't afford to create life-saving drugs. Nature *584*, 338–341.

McKenney, D., Hübner, J., Muller, E., Wang, Y., Goldmann, D.A., and Pier, G.B. (1998). The *ica* locus of *Staphylococcus epidermidis* encodes production of the capsular polysaccharide/adhesin. Infect. Immun. *66*, 4711–4720.

Medeiros-Silva, J., Jekhmane, S., Paioni, A.L., Gawarecka, K., Baldus, M., Swiezewska, E., Breukink, E., and Weingarth, M. (2018). High-resolution NMR studies of antibiotics in cellular membranes. Nat. Commun. *9*, 3963.

Medeiros-Silva, J., Jekhmane, S., Breukink, E., and Weingarth, M. (2019). Towards the Native Binding Modes of Antibiotics that Target Lipid II. ChemBioChem *20*, 1731–1738.

Meeske, A.J., Riley, E.P., Robins, W.P., Uehara, T., Mekalanos, J.J., Kahne, D., Walker, S., Kruse, A.C., Bernhardt, T.G., and Rudner, D.Z. (2016). SEDS proteins are a widespread family of bacterial cell wall polymerases. Nature *537*, 634–638.

Mengin-Lecreulx, D., and van Heijenoort, J. (1994). Copurification of glucosamine-1-phosphate acetyltransferase and *N*-acetylglucosamine-1-phosphate uridyltransferase activities of *Escherichia coli*: characterization of the *glmU* gene product as a bifunctional enzyme catalyzing two subsequent steps in the pathway for UDP-*N*-acetylglucosamine synthesis. J. Bacteriol. *176*, 5788–5795.

Mengin-Lecreulx, D., and van Heijenoort, J. (1996). Characterization of the essential gene *glmM* encoding phosphoglucosamine mutase in *Escherichia coli*. J. Biol. Chem. *271*, 32–39.

Mengin-Lecreulx, D., Allen, N.E., Hobbs, J.N., and van Heijenoort, J. (1990). Inhibition of peptidoglycan biosynthesis in *Bacillus megaterium* by daptomycin. FEMS Microbiol. Lett. *57*, 245–248.

Meredith, T.C., Swoboda, J.G., and Walker, S. (2008). Late-stage polyribitol phosphate wall teichoic acid biosynthesis in *Staphylococcus aureus*. J. Bacteriol. *190*, 3046–3056.

Metelev, M., Tietz, J.I., Melby, J.O., Blair, P.M., Zhu, L., Livnat, I., Severinov, K., and Mitchell, D.A. (2015). Structure, bioactivity, and resistance mechanism of streptomonomicin, an unusual lasso Peptide from an understudied halophilic actinomycete. Chem. Biol. *22*, 241–250.

Michie, A.J., and Zintel, H.A. (1949). The nephrotoxicity of bacitracin in man. Surgery *26*, 626–632.

Miethke, M., Pieroni, M., Weber, T., Brönstrup, M., Hammann, P., Halby, L., Arimondo, P.B., Glaser, P., Aigle, B., Bode, H.B., *et al.* (2021). Towards the sustainable discovery and development of new antibiotics. Nat. Rev. Chem. *5*, 726–749.

Milanesi, L., Sheynis, T., Xue, W.F., Orlova, E. V., Hellewell, A.L., Jelinek, R., Hewitt, E.W., Radford, S.E., and Saibil, H.R. (2012). Direct three-dimensional visualization of membrane disruption by amyloid fibrils. Proc. Natl. Acad. Sci. U. S. A. *109*, 20455–20460.

Milani, R. V, Wilt, J.K., Entwisle, J., Hand, J., Cazabon, P., and Bohan, J.G. (2019). Reducing inappropriate outpatient antibiotic prescribing: normative comparison using unblinded provider reports. BMJ Open Qual. *8*, e000351.

Mileykovskaya, E., and Dowhan, W. (2005). Role of membrane lipids in bacterial division-site selection. Curr. Opin. Microbiol. *8*, 135–142.

Mishra, N.N., and Bayer, A.S. (2013). Correlation of cell membrane lipid profiles with daptomycin resistance in methicillin-resistant *Staphylococcus aureus*. Antimicrob. Agents Chemother. *57*, 1082–1085.

Miyafusa, T., Caaveiro, J.M.M., Tanaka, Y., and Tsumoto, K. (2013). Dynamic elements govern the catalytic activity of CapE, a capsular polysaccharide-synthesizing enzyme from *Staphylococcus aureus*. FEBS Lett. *587*, 3824–3830.

Moir, R.D., Lathe, R., and Tanzi, R.E. (2018). The antimicrobial protection hypothesis of Alzheimer's disease. Alzheimer's Dement. *14*, 1602–1614.

Monnet, D.L. (2005). Antibiotic development and the changing role of the pharmaceutical industry. Int. J. Risk Saf. Med. *17*, 133–145.

Montalbán-López, M., Scott, T.A., Ramesh, S., Rahman, I.R., Van Heel, A.J., Viel, J.H., Bandarian, V., Dittmann, E., Genilloud, O., Goto, Y., *et al.* (2021). New developments in RiPP discovery, enzymology and engineering. Nat. Prod. Rep. *38*, 130–239.

Monteiro, J.M., Fernandes, P.B., Vaz, F., Pereira, A.R., Tavares, A.C., Ferreira, M.T., Pereira, P.M., Veiga, H., Kuru, E., VanNieuwenhze, M.S., *et al.* (2015). Cell shape dynamics during the staphylococcal cell cycle. Nat. Commun. *6*, 8055.

Monteiro, J.M., Pereira, A.R., Reichmann, N.T., Saraiva, B.M., Fernandes, P.B., Veiga, H., Tavares, A.C., Santos, M., Ferreira, M.T., Macário, V., *et al.* (2018). Peptidoglycan synthesis drives an FtsZ-treadmilling-independent step of cytokinesis. Nature *554*, 528–532.

Monteiro, J.M., Covas, G., Rausch, D., Filipe, S.R., Schneider, T., Sahl, H., and Pinho, M.G. (2019). The pentaglycine bridges of *Staphylococcus aureus* peptidoglycan are essential for cell integrity. Sci. Rep. *9*, 5010.

Mookherjee, N., Anderson, M.A., Haagsman, H.P., and Davidson, D.J. (2020). Antimicrobial host defence peptides: functions and clinical potential. Nat. Rev. Drug Discov. *19*, 311–332.

Moreira, R., and Taylor, S.D. (2022). The Chiral Target of Daptomycin Is the 2R,2'S Stereoisomer of Phosphatidylglycerol. Angew. Chem. Int. Ed. Engl. *61*, e202114858.

Morlot, C., Straume, D., Peters, K., Hegnar, O.A., Simon, N., Villard, A.M., Contreras-Martel, C., Leisico, F., Breukink, E., Gravier-Pelletier, C., *et al.* (2018). Structure of the essential peptidoglycan amidotransferase MurT/GatD complex from *Streptococcus pneumoniae*. Nat. Commun. *9*, 1–12.

Mott, J.E., Shaw, B.A., Smith, J.F., Bonin, P.D., Romero, D.L., Marotti, K.R., and Miller, A.A. (2008). Resistance mapping and mode of action of a novel class of antibacterial anthranilic acids: Evidence for disruption of cell wall biosynthesis. J. Antimicrob. Chemother. *62*, 720–729.

Müller, A., Ulm, H., Reder-Christ, K., Sahl, H.-G., and Schneider, T. (2012). Interaction of type A lantibiotics with undecaprenol-bound cell envelope precursors. Microb. Drug Resist. *18*, 261–270.

Müller, A., Wenzel, M., Strahl, H., Grein, F., Saaki, T.N. V., Kohl, B., Siersma, T., Bandow, J.E., Sahl, H.-G., Schneider, T., Hamoen, L.W. (2016). Daptomycin inhibits cell envelope synthesis by interfering with fluid membrane microdomains. Proc. Natl. Acad. Sci. U. S. A. *113*, E7077–E7086.

Müller, A., Klöckner, A., and Schneider, T. (2017). Targeting a cell wall biosynthesis hot spot. Nat. Prod. Rep. *34*, 909–932.

Münch, D., Roemer, T., Lee, S.H., Engeser, M., Sahl, H.G., and Schneider, T. (2012). Identification and *in vitro* analysis of the GatD/MurT enzyme-complex catalyzing lipid II amidation in *Staphylococcus aureus*. PLoS Pathog. *8*, e1002509.

Münch, D., Engels, I., Müller, A., Reder-Christ, K., Falkenstein-Paul, H., Bierbaum, G., Grein, F., Bendas, G., Sahl, H.-G., and Schneider, T. (2015). Structural variations of the cell wall precursor lipid II and their influence on binding and activity of the lipoglycopeptide antibiotic oritavancin. Antimicrob. Agents Chemother. *59*, 772–781.

Munita, J.M., and Arias, C.A. (2016). Mechanisms of Antibiotic Resistance. Microbiol. Spectr. *4*, 1–24.

Munos, B. (2009). Lessons from 60 years of pharmaceutical innovation. Nat. Rev. Drug Discov. *8*, 959–968.

Muñoz, K.A., and Hergenrother, P.J. (2021). Facilitating Compound Entry as a Means to Discover Antibiotics for Gram-Negative Bacteria. Acc. Chem. Res. *54*, 1322–1333.

Muraih, J.K., Pearson, A., Silverman, J., and Palmer, M. (2011). Oligomerization of daptomycin on membranes. Biochim. Biophys. Acta - Biomembr. *1808*, 1154–1160.

Murray, C.J., Ikuta, K.S., Sharara, F., Swetschinski, L., Robles Aguilar, G., Gray, A., Han, C., Bisignano, C., Rao, P., Wool, E., *et al.* (2022). Global burden of bacterial antimicrobial resistance in 2019: a systematic analysis. Lancet *6736*.

Muthaiyan, A., Silverman, J.A., Jayaswal, R.K., and Wilkinson, B.J. (2008). Transcriptional profiling reveals that daptomycin induces the *Staphylococcus aureus* cell wall stress stimulon and genes responsive to membrane depolarization. Antimicrob. Agents Chemother. *52*, 980–990.

Mwangi, M.M., Wu, S.W., Zhou, Y., Sieradzki, K., de Lencastre, H., Richardson, P., Bruce, D., Rubin, E., Myers, E., Siggia, E.D., *et al.* (2007). Tracking the *in vivo* evolution of multidrug resistance in *Staphylococcus aureus* by whole-genome sequencing. Proc. Natl. Acad. Sci. U. S. A. *104*, 9451–9456.

Nair, D.R., Chen, J., Monteiro, J.M., Josten, M., Pinho, M.G., Sahl, H.G., Wu, J., and Cheung, A. (2017). A quinolinol-based small molecule with anti-MRSA activity that targets bacterial membrane and promotes fermentative metabolism. J. Antibiot. (Tokyo). *70*, 1009–1019.

Nakayama, J., Tanaka, E., Kariyama, R., Nagata, K., Nishiguchi, K., Mitsuhata, R., Uemura, Y., Tanokura, M., Kumon, H., and Sonomoto, K. (2007). Siamycin attenuates fsr quorum sensing mediated by a gelatinase biosynthesis-activating pheromone in *Enterococcus faecalis*. J. Bacteriol. *189*, 1358–1365.

Nanra, J.S., Buitrago, S.M., Crawford, S., Ng, J., Fink, P.S., Hawkins, J., Scully, I.L., McNeil, L.K., Aste-Amézaga, J.M., Cooper, D., *et al.* (2013). Capsular polysaccharides are an important immune evasion mechanism for *Staphylococcus aureus*. Hum. Vaccin. Immunother. *9*, 480–487.

Nar, H., Schmid, A., Puder, C., and Potterat, O. (2010). High-resolution crystal structure of a lasso peptide. ChemMedChem *5*, 1689–1692.

Nathan, C. (2004). Antibiotics at the crossroads. Nature *431*, 899–902.

Nathan, C., and Goldberg, F. (2005). The profit problem in antibiotic R&D. Nat. Rev. Drug Discov. *4*, 887–891.

Negash, K.H., Norris, J.K.S., and Hodgkinson, J.T. (2019). Siderophore-Antibiotic Conjugate Design: New Drugs for Bad Bugs? Molecules *24*.

Neuhaus, F.C. (1971). Initial translocation reaction in the biosynthesis of peptidoglycan by bacterial membranes. Acc. Chem. Res. *4*, 297–303.

Ng, V., Kuehne, S.A., and Chan, W.C. (2018). Rational Design and Synthesis of Modified Teixobactin Analogues: *In vitro* Antibacterial Activity against *Staphylococcus aureus*, *Propionibacterium acnes* and *Pseudomonas aeruginosa*. Chem. - A Eur. J. *24*, 9136–9147.

Nichols, D., Cahoon, N., Trakhtenberg, E.M., Pham, L., Mehta, A., Belanger, A., Kanigan, T., Lewis, K., and Epstein, S.S. (2010). Use of ichip for high-throughput *in situ* cultivation of "uncultivable" microbial species. Appl. Environ. Microbiol. *76*, 2445–2450.

Nikaido, H. (2003). Molecular basis of bacterial outer membrane permeability revisited. Microbiol. Mol. Biol. Rev. *67*, 593–656.

Nikaido, H., and Vaara, M. (1985). Molecular basis of bacterial outer membrane permeability. Microbiol. Rev. *49*, 1–32.

Nilsson, I.M., Lee, J.C., Bremell, T., Rydén, C., and Tarkowski, A. (1997). The role of staphylococcal polysaccharide microcapsule expression in septicemia and septic arthritis. Infect. Immun. *65*, 4216–4221.

Nöldeke, E.R., Muckenfuss, L.M., Niemann, V., Müller, A., Störk, E., Zocher, G., Schneider, T., and Stehle, T. (2018). Structural basis of cell wall peptidoglycan amidation by the GatD/MurT complex of *Staphylococcus aureus*. Sci. Rep. *8*, 1–15.

Nowick, J.S., and Yang, H. (2019). Antimicrobial compositions. US Patent US20190112335.

von Nussbaum, F., Brands, M., Hinzen, B., Weigand, S., and Häbich, D. (2006). Antibacterial natural products in medicinal chemistry - exodus or revival? Angew. Chem. Int. Ed. Engl. *45*, 5072–5129.

Nussbaumer-Pröll, A., and Zeitlinger, M. (2020). Use of Supplemented or Human Material to Simulate PD Behavior of Antibiotics at the Target Site *In vitro*. Pharmaceutics *12*.

O'Neill, J. (2014). Review on Antibiotic resisitance. Antimicrobial Resistance : Tackling a crisis for the health and wealth of nations. Heal. Wealth Nations 1–16.

O'Shea, R., and Moser, H.E. (2008). Physicochemical properties of antibacterial compounds: Implications for drug discovery. J. Med. Chem. *51*, 2871–2878.

OECD (2020). Health at a Glance: Europe 2020.

OECD, WHO, FAO, and OIE (2017). Tackling Antimicrobial Resistance Ensuring Sustainable R&D.

Oku, Y., Kurokawa, K., Matsuo, M., Yamada, S., Lee, B.-L., and Sekimizu, K. (2009). Pleiotropic roles of polyglycerolphosphate synthase of lipoteichoic acid in growth of *Staphylococcus aureus* cells. J. Bacteriol. *191*, 141–151.

De Oliveira, D.M.P., Forde, B.M., Kidd, T.J., Harris, P.N.A., Schembri, M.A., Beatson, S.A., Paterson, D.L., and Walker, M.J. (2020). Antimicrobial Resistance in ESKAPE Pathogens. Clin. Microbiol. Rev. *33*.

Oliver, P.M., Crooks, J.A., Leidl, M., Yoon, E.J., Saghatelian, A., and Weibel, D.B. (2014). Localization of anionic phospholipids in *Escherichia coli* cells. J. Bacteriol. *196*, 3386–3398.

Oluwole, A.O., Corey, R.A., Brown, C.M., Hernández-Rocamora, V.M., Stansfeld, P.J., Vollmer, W., Bolla, J.R., and Robinson, C. V. (2022). Peptidoglycan biosynthesis is driven by lipid transfer along enzyme-substrate affinity gradients. Nat. Commun. *13*, 1–12.

OneHealthTrust (2022). ResistanceMap: Antibiotic resistance.

Orskov, I., Orskov, F., Jann, B., and Jann, K. (1977). Serology, chemistry, and genetics of O and K antigens of *Escherichia coli*. Bacteriol. Rev. *41*, 667–710.

Öster, C., Walkowiak, G.P., Hughes, D.E., Spoering, A.L., Peoples, A.J., Catherwood, A.C., Tod, J.A., Lloyd, A.J., Herrmann, T., Lewis, K., *et al.* (2018). Structural studies suggest aggregation as one of the modes of action for teixobactin. Chem. Sci. *9*, 8850–8859.

Over, B., Heusser, R., McCallum, N., Schulthess, B., Kupferschmied, P., Gaiani, J.M., Sifri, C.D., Berger-Bächi, B., and Stutzmann Meier, P. (2011). LytR-CpsA-Psr proteins in *Staphylococcus aureus* display partial functional redundancy and the deletion of all three severely impairs septum placement and cell separation. FEMS Microbiol. Lett. *320*, 142–151.

Pan American Health Organization (2022). Antimicrobial Resistance, Fueled By the Covid-19 Pandemic. 1–14.

Parenti, F., Candiani, G., Ciabatti, R., and Cavaleri, M. (2004). Injectable formulations containing ramoplanin. US Patent US-6720305-B1.

Parkes, A.L. (2020). Antibacterial medicinal chemistry–what can we design for? Expert Opin. Drug Discov. *15*, 1005–1013.

Parmar, A., Iyer, A., Prior, S.H., Lloyd, D.G., Leng Goh, E.T., Vincent, C.S., Palmai-Pallag, T., Bachrati, C.Z., Breukink, E., Madder, A., *et al.* (2017). Teixobactin analogues reveal enduracididine to be non-essential for highly potent antibacterial activity and lipid II binding. Chem. Sci. *8*, 8183–8192.

Pasquina, L., Santa Maria, J.P., McKay Wood, B., Moussa, S.H., Matano, L.M., Santiago, M., Martin, S.E.S., Lee, W., Meredith, T.C., and Walker, S. (2016). A synthetic lethal approach for compound and target identification in *Staphylococcus aureus*. Nat. Chem. Biol. *12*, 40–45.

Patin, D., Boniface, A., Kovač, A., Hervé, M., Dementin, S., Barreteau, H., Mengin-Lecreulx, D., and Blanot, D. (2010). Purification and biochemical characterization of Mur ligases from *Staphylococcus aureus*. Biochimie *92*, 1793–1800.

Patti, G.J., Kim, S.J., Yu, T.-Y., Dietrich, E., Tanaka, K.S.E., Parr, T.R., Far, A.R., and Schaefer, J. (2009). Vancomycin and oritavancin have different modes of action in *Enterococcus faecium*. J. Mol. Biol. *392*, 1178–1191.

Pawlowski, A.C., Johnson, J.W., and Wright, G.D. (2016). Evolving medicinal chemistry strategies in antibiotic discovery. Curr. Opin. Biotechnol. *42*, 108–117.

Payne, D.J., Gwynn, M.N., Holmes, D.J., and Pompliano, D.L. (2007). Drugs for bad bugs: Confronting the challenges of antibacterial discovery. Nat. Rev. Drug Discov. *6*, 29–40.

Peavy, R.D., and Metcalfe, D.D. (2008). Understanding the mechanisms of anaphylaxis. Curr. Opin. Allergy Clin. Immunol. *8*, 310–315.

Peleg, A.Y., Miyakis, S., Ward, D. V., Earl, A.M., Rubio, A., Cameron, D.R., Pillai, S., Moellering, R.C., and Eliopoulos, G.M. (2012). Whole genome characterization of the mechanisms of daptomycin resistance in clinical and laboratory derived isolates of *Staphylococcus aureus*. PLoS One *7*, e28316.

Pelzer, S., and Vente, A. (2008). New lipoglycodepsipeptide compositions. European Patent EP1994938A1.

Pereira, M.P., and Brown, E.D. (2004). Bifunctional catalysis by CDP-ribitol synthase: convergent recruitment of reductase and cytidylyltransferase activities in *Haemophilus influenzae* and *Staphylococcus aureus*. Biochemistry *43*, 11802–11812.

Peschel, A., and Sahl, H.-G. (2006). The co-evolution of host cationic antimicrobial peptides and microbial resistance. Nat. Rev. Microbiol. *4*, 529–536.

Peschel, A., Otto, M., Jack, R.W., Kalbacher, H., Jung, G., and Götz, F. (1999). Inactivation of the *dlt* operon in *Staphylococcus aureus* confers sensitivity to defensins, protegrins, and other antimicrobial peptides. J. Biol. Chem. *274*, 8405–8410.

Peschel, A., Vuong, C., Otto, M., and Gotz, F. (2000). The D-alanine residues of *Staphylococcus aureus* teichoic acids alter the susceptibility to vancomycin and the activity of autolytic enzymes. Antimicrob. Agents Chemother. *44*, 2845–2847.

Peukert, S., Sun, Y., Zhang, R., Hurley, B., Sabio, M., Shen, X., Gray, C., Dzink-Fox, J., Tao, J., Cebula, R., *et al.* (2008). Design and structure-activity relationships of potent and selective inhibitors of undecaprenyl pyrophosphate synthase (UPPS): tetramic, tetronic acids and dihydropyridin-2-ones. Bioorg. Med. Chem. Lett. *18*, 1840–1844.

Piepenbreier, H., Diehl, A., and Fritz, G. (2019). Minimal exposure of lipid II cycle intermediates triggers cell wall antibiotic resistance. Nat. Commun. *10*, 2733.

Pier, G.B. (2003). Promises and pitfalls of *Pseudomonas aeruginosa* lipopolysaccharide as a vaccine antigen. Carbohydr. Res. *338*, 2549–2556.

Pinho, M.G., and Errington, J. (2003). Dispersed mode of *Staphylococcus aureus* cell wall synthesis in the absence of the division machinery. Mol. Microbiol. *50*, 871–881.

Pinho, M.G., and Errington, J. (2005). Recruitment of penicillin-binding protein PBP2 to the division site of *Staphylococcus aureus* is dependent on its transpeptidation substrates. Mol. Microbiol. *55*, 799–807.

Pless, D.D., and Neuhaus, F.C. (1973). Initial membrane reaction in peptidoglycan synthesis. Lipid dependence of phospho-*N*-acetylmuramyl-pentapeptide translocase (exchange reaction). J. Biol. Chem. *248*, 1568–1576.

Pogliano, J., Pogliano, N., and Silverman, J.A. (2012). Daptomycin-mediated reorganization of membrane architecture causes mislocalization of essential cell division proteins. J. Bacteriol. *194*, 4494–4504.

Portolés, M., Kiser, K.B., Bhasin, N., Chan, K.H., and Lee, J.C. (2001). *Staphylococcus aureus* Cap5O has UDP-ManNAc dehydrogenase activity and is essential for capsule expression. Infect. Immun. *69*, 917–923.

Prince, A., Sandhu, P., Kumar, P., Dash, E., Sharma, S., Arakha, M., Jha, S., Akhter, Y., and Saleem, M. (2016). Lipid-II Independent Antimicrobial Mechanism of Nisin Depends on Its Crowding and Degree of Oligomerization. Sci. Rep. *6*, 1–15.

Qin, Z., Zhang, J., Xu, B., Chen, L., Wu, Y., Yang, X., Shen, X., Molin, S., Danchin, A., Jiang, H., *et al.* (2006). Structure-based discovery of inhibitors of the YycG histidine kinase: New chemical leads to combat *Staphylococcus epidermidis* infections. BMC Microbiol. *6*, 1–18.

Radeck, J., Gebhard, S., Orchard, P.S., Kirchner, M., Bauer, S., Mascher, T., and Fritz, G. (2016). Anatomy of the bacitracin resistance network in *Bacillus subtilis*. Mol. Microbiol. *100*, 607–620.

Rai, A.K., and Mitchell, A.M. (2020). Enterobacterial common antigen: Synthesis and function of an enigmatic molecule. MBio *11*, 1–19.

Rausch, M., Deisinger, J.P., Ulm, H., Müller, A., Li, W., Hardt, P., Wang, X., Li, X., Sylvester, M., Engeser, M., Vollmer, W., Müller. C.E., Sahl, H.-G., Lee, J.C., Schneider T. (2019). Coordination of capsule assembly and cell wall biosynthesis in *Staphylococcus aureus*. Nat. Commun. *10*, 1404.

Reed, P., Veiga, H., Jorge, A.M., Terrak, M., and Pinho, M.G. (2011). Monofunctional transglycosylases are not essential for *Staphylococcus aureus* cell wall synthesis. J. Bacteriol. *193*, 2549–2556.

Reeves, P.R., Hobbs, M., Valvano, M.A., Skurnik, M., Whitfield, C., Coplin, D., Kido, N., Klena, J., Maskell, D., Raetz, C.R.H., *et al.* (1996). Bacterial polysaccharide synthesis and gene nomenclature. Trends Microbiol. *4*, 495–503.

Reichmann, N.T., Tavares, A.C., Saraiva, B.M., Jousselin, A., Reed, P., Pereira, A.R., Monteiro, J.M., Sobral, R.G., VanNieuwenhze, M.S., Fernandes, F., *et al.* (2019). SEDS–bPBP pairs direct lateral and septal peptidoglycan synthesis in *Staphylococcus aureus*. Nat. Microbiol. *4*, 1368–1377.

Reith, J., and Mayer, C. (2011). Peptidoglycan turnover and recycling in Gram-positive bacteria. Appl. Microbiol. Biotechnol. *92*, 1–11.

Reithuber, E. (2021). Targeting cell envelope synthesis of *Streptococcus pneumoniae* and microfluidic diagnostic tool development. Karolinska Institutet Stockholm.

Reynolds, P.E. (1989). Structure, biochemistry and mechanism of action of glycopeptide antibiotics. Eur. J. Clin. Microbiol. Infect. Dis. *8*, 943–950.

Rice, L.B. (2008). Federal funding for the study of antimicrobial resistance in nosocomial pathogens: no ESKAPE. J. Infect. Dis. *197*, 1079–1081.

Richter, M.F., Drown, B.S., Riley, A.P., Garcia, A., Shirai, T., Svec, R.L., and Hergenrother, P.J. (2017). Predictive compound accumulation rules yield a broad-spectrum antibiotic. Nature *545*, 299–304.

Roemer, T., Schneider, T., and Pinho, M.G. (2013). Auxiliary factors: A chink in the armor of MRSA resistance to β-lactam antibiotics. Curr. Opin. Microbiol. *16*, 538–548.

Roney, I.J., and Rudner, D.Z. (2022). Two broadly conserved families of polyprenyl-phosphate transporters. Nature *22*, 303–310.

Rotondi, K.S., and Gierasch, L.M. (2005). A well-defined amphipathic conformation for the calcium-free cyclic lipopeptide antibiotic, daptomycin, in aqueous solution. Biopolymers *80*, 374–385.

Rubino, F.A., Mollo, A., Kumar, S., Butler, E.K., Ruiz, N., Walker, S., and Kahne, D.E. (2020). Detection of Transport Intermediates in the Peptidoglycan Flippase MurJ Identifies Residues Essential for Conformational Cycling. J. Am. Chem. Soc. *142*, 5482–5486.

Sachla, A.J., and Helmann, J.D. (2021). Resource sharing between central metabolism and cell envelope synthesis. Curr. Opin. Microbiol. *60*, 34–43.

Sacksteder, K.A., Protopopova, M., Barry, C.E., Andries, K., and Nacy, C.A. (2012). Discovery and development of SQ109: a new antitubercular drug with a novel mechanism of action. Future Microbiol. *7*, 823–837.

Salzberg, L.I., Powell, L., Hokamp, K., Botella, E., Noone, D., and Devine, K.M. (2013). The WalRK (YycFG) and σI RsgI regulators cooperate to control CwlO and LytE expression in exponentially growing and stressed *Bacillus subtilis* cells. Mol. Microbiol. *87*, 180–195.

Sangshetti, J.N., Joshi, S.S., Patil, R.H., Moloney, M.G., and Shinde, D.B. (2017). Mur Ligase Inhibitors as Anti-bacterials: A Comprehensive Review. Curr. Pharm. Des. *23*, 3164–3196.

Sarkar, P., and Haldar, J. (2019). Glycopeptide Antibiotics. In Antibiotic Drug Resistance, (Wiley), pp. 73–95.

Sauermann, R., Rothenburger, M., Graninger, W., and Joukhadar, C. (2008). Daptomycin: a review 4 years after first approval. Pharmacology *81*, 79–91.

Schaefer, K., Matano, L.M., Qiao, Y., Kahne, D., and Walker, S. (2017). *In vitro* reconstitution demonstrates the cell wall ligase activity of LCP proteins. Nat. Chem. Biol. *13*, 396–401.

Schaefer, K., Owens, T.W., Page, J.E., Santiago, M., Kahne, D., and Walker, S. (2021). Structure and reconstitution of a hydrolase complex that may release peptidoglycan from the membrane after polymerization. Nat. Microbiol. *6*, 34–43.

Schäfer-Korting, M., Maria-Engler, S.S., and Landisedel, R. (2021). Organotypic Models in Drug Development (Cham: Springer International Publishing).

Schatz, A., and Waksman, S.A. (1944). Effect of Streptomycin and Other Antibiotic Substances upon *Mycobacterium tuberculosis* and Related Organisms. Exp. Biol. Med. *57*, 244–248.

Scheffers, D.-J., and Pinho, M.G. (2005). Bacterial cell wall synthesis: new insights from localization studies. Microbiol. Mol. Biol. Rev. *69*, 585–607.

Scherer, K., Wiedemann, I., Ciobanasu, C., Sahl, H.G., and Kubitscheck, U. (2013). Aggregates of nisin with various bactoprenol-containing cell wall precursors differ in size and membrane permeation capacity. Biochim. Biophys. Acta - Biomembr. *1828*, 2628–2636.

Scherer, K.M., Spille, J.H., Sahl, H.G., Grein, F., and Kubitscheck, U. (2015). The lantibiotic nisin induces Lipid II aggregation, causing membrane instability and vesicle budding. Biophys. J. *108*, 1114–1124.

Schiffer, G., Fälker, S., Daube, G., Wiehl, W., and Köbbering, J. (2018). Combination of lysobactin and aminoglycosides against diseases caused by gram-positive and gram-negative bacteria in non-human animals. European Patent EP3548059.

Schirner, K., Eun, Y.-J., Dion, M., Luo, Y., Helmann, J.D., Garner, E.C., and Walker, S. (2015). Lipid-linked cell wall precursors regulate membrane association of bacterial actin MreB. Nat. Chem. Biol. *11*, 38–45.

Schlag, M., Biswas, R., Krismer, B., Kohler, T., Zoll, S., Yu, W., Schwarz, H., Peschel, A., and Götz, F. (2010). Role of staphylococcal wall teichoic acid in targeting the major autolysin Atl. Mol. Microbiol. *75*, 864–873.

Schleifer, K.H., and Kandler, O. (1972). Peptidoglycan types of bacterial cell walls and their taxonomic implications. Bacteriol. Rev. *36*, 407–477.

Schmidt, J.W., Greenough, A., Burns, M., Luteran, A.E., and McCafferty, D.G. (2010). Generation of ramoplanin-resistant *Staphylococcus aureus*. FEMS Microbiol. Lett. *310*, 104–111.

Schneider, T., and Sahl, H.-G. (2010). An oldie but a goodie - cell wall biosynthesis as antibiotic target pathway. Int. J. Med. Microbiol. *300*, 161–169.

Schneider, T., Senn, M.M., Berger-Bächi, B., Tossi, A., Sahl, H.G., and Wiedemann, I. (2004). *In vitro* assembly of a complete, pentaglycine interpeptide bridge containing cell wall precursor (lipid II-Gly_5) of *Staphylococcus aureus*. Mol. Microbiol. *53*, 675–685.

Schneider, T., Kruse, T., Wimmer, R., Wiedemann, I., Sass, V., Pag, U., Jansen, A., Nielsen, A.K., Mygind, P.H., Raventós, D.S., *et al.* (2010). Plectasin, a fungal defensin, targets the bacterial cell wall precursor Lipid II. Science *328*, 1168–1172.

Severin, A., Tabei, K., Tenover, F., Chung, M., Clarke, N., and Tomasz, A. (2004). High level oxacillin and vancomycin resistance and altered cell wall composition in *Staphylococcus aureus* carrying the staphylococcal mecA and the enterococcal *vanA* gene complex. J. Biol. Chem. *279*, 3398–3407.

Sewell, E.W.C., and Brown, E.D. (2014). Taking aim at wall teichoic acid synthesis: New biology and new leads for antibiotics. J. Antibiot. (Tokyo). *67*, 43–51.

Sham, L.-T., Butler, E.K., Lebar, M.D., Kahne, D., Bernhardt, T.G., and Ruiz, N. (2014). Bacterial cell wall. MurJ is the flippase of lipid-linked precursors for peptidoglycan biogenesis. Science *345*, 220–222.

Shoji, J., Hinoo, H., Hattori, T., Hirooka, K., Kimura, Y., and Yoshida, T. (1989). Isolation and characterization of hypeptin from *Pseudomonas* sp. J. Antibiot. (Tokyo). *42*, 1460–1464.

Shukla, R., Medeiros-Silva, J., Parmar, A., Vermeulen, B.J.A., Das, S., Paioni, A.L., Jekhmane, S., Lorent, J., Bonvin, A.M.J.J., Baldus, M., *et al.* (2020). Mode of action of teixobactins in cellular membranes. Nat. Commun. *11*, 1–10.

Shukla, R., Lavore, F., Maity, S., Derks, M.G.N., Jones, C.R., Vermeulen, B.J.A., Melcrová, A., Morris, M.A., Becker, L.M., Wang, X., *et al.* (2022). Teixobactin kills bacteria by a two-pronged attack on the cell envelope. Nature *608*, 390–396.

Siewert, G., and Strominger, J.L. (1968). Biosynthesis of the peptidoglycan of bacterial cell walls. XI. Formation of the isoglutamine amide group in the cell walls of *Staphylococcus aureus*. J. Biol. Chem. *243*, 783–790.

Silver, L.L. (2003). Novel inhibitors of bacterial cell wall synthesis. Curr. Opin. Microbiol. *6*, 431–438.

Silver, L.L. (2007). Multi-targeting by monotherapeutic antibacterials. Nat. Rev. Drug Discov. *6*, 41–55.

Silver, L.L. (2011). Challenges of antibacterial discovery. Clin. Microbiol. Rev. *24*, 71–109.

Silver, L.L., and Mobashery, S. (2014). Challenges In Overcoming Antibiotic Resistance. In Technological Challenges in Antibiotic Discovery and Development: A Workshop Summary, (National Academies Press (US)), pp. 7–12.

Silverman, J.A., Perlmutter, N.G., and Shapiro, H.M. (2003). Correlation of daptomycin bactericidal activity and membrane depolarization in *Staphylococcus aureus*. Antimicrob. Agents Chemother. *47*, 2538–2544.

Simonsen, G.S. (2018). Antimicrobial resistance surveillance in Europe and beyond. Euro Surveill. *23*.

Simonson, A.W., Aronson, M.R., and Medina, S.H. (2020). Supramolecular Peptide Assemblies as Antimicrobial Scaffolds. Molecules *25*.

Sinko, W., Wang, Y., Zhu, W., Zhang, Y., Feixas, F., Cox, C.L., Mitchell, D.A., Oldfield, E., and McCammon, J.A. (2014). Undecaprenyl diphosphate synthase inhibitors: Antibacterial drug leads. J. Med. Chem. *57*, 5693–5701.

Sit, B., Srisuknimit, V., Bueno, E., Zingl, F.G., Hullahalli, K., Cava, F., and Waldor, M.K. (2022). Undecaprenyl phosphate translocases confer conditional microbial fitness. Nature 1–2.

Snowden, M.A., Perkins, H.R., Wyke, A.W., Hayes, M. V., and Ward, J.B. (1989). Cross-linking and O-acetylation of newly synthesized peptidoglycan in *Staphylococcus aureus* H. J. Gen. Microbiol. *135*, 3015–3022.

Soldo, B., Lazarevic, V., and Karamata, D. (2002a). tagO is involved in the synthesis of all anionic cell-wall polymers in *Bacillus subtilis* 168. Microbiology *148*, 2079–2087.

Soldo, B., Lazarevic, V., Pooley, H.M., and Karamata, D. (2002b). Characterization of a *Bacillus subtilis* thermosensitive teichoic acid-deficient mutant: gene *mnaA* (*yvyH*) encodes the UDP-*N*-acetylglucosamine 2-epimerase. J. Bacteriol. *184*, 4316–4320.

Soscia, S.J., Kirby, J.E., Washicosky, K.J., Tucker, S.M., Ingelsson, M., Hyman, B., Burton, M.A., Goldstein, L.E., Duong, S., Tanzi, R.E., *et al.* (2010). The Alzheimer's disease-associated amyloid β-protein is an antimicrobial peptide. PLoS One *5*, 1–10.

Spellberg, B., Powers, J.H., Brass, E.P., Miller, L.G., and Edwards, J.E. (2004). Trends in antimicrobial drug development: implications for the future. Clin. Infect. Dis. *38*, 1279–1286.

Spitzer, P., Condic, M., Herrmann, M., Oberstein, T.J., Scharin-Mehlmann, M., Gilbert, D.F., Friedrich, O., Grömer, T., Kornhuber, J., Lang, R., *et al.* (2016). Amyloidogenic amyloid-β-peptide variants induce microbial agglutination and exert antimicrobial activity. Sci. Rep. *6*, 1–11.

Srisuknimit, V., Qiao, Y., Schaefer, K., Kahne, D., and Walker, S. (2017). Peptidoglycan Cross-Linking Preferences of *Staphylococcus aureus* Penicillin-Binding Proteins Have Implications for Treating MRSA Infections. J. Am. Chem. Soc. *139*, 9791–9794.

Stariha, L.M., and McCafferty, D.G. (2021). Discovery of the Class I Antimicrobial Lasso Peptide Arcumycin. ChemBioChem *22*, 2632–2640.

Starikova, I., Al-Haroni, M., Werner, G., Roberts, A.P., Sørum, V., Nielsen, K.M., and Johnsen, P.J. (2013). Fitness costs of various mobile genetic elements in *Enterococcus faecium* and *Enterococcus faecalis*. J. Antimicrob. Chemother. *68*, 2755–2765.

Stewardson, A.J., Allignol, A., Beyersmann, J., Graves, N., Schumacher, M., Meyer, R., Tacconelli, E., De Angelis, G., Farina, C., Pezzoli, F., *et al.* (2016). The health and economic burden of bloodstream infections caused by antimicrobial-susceptible and non-susceptible *Enterobacteriaceae* and *Staphylococcus aureus* in European hospitals, 2010 and 2011: a multicentre retrospective cohort study. Euro Surveill. *21*.

Stewardson, A.J., Marimuthu, K., Sengupta, S., Allignol, A., El-Bouseary, M., Carvalho, M.J., Hassan, B., Delgado-Ramirez, M.A., Arora, A., Bagga, R., *et al.* (2019). Effect of carbapenem resistance on outcomes of bloodstream infection caused by *Enterobacteriaceae* in low-income and middle-income countries (PANORAMA): a multinational prospective cohort study. Lancet. Infect. Dis. *19*, 601–610.

Strahl, H., Bürmann, F., and Hamoen, L.W. (2014). The actin homologue MreB organizes the bacterial cell membrane. Nat. Commun. *5*, 3442.

Straus, S.K., and Hancock, R.E.W. (2006). Mode of action of the new antibiotic for Gram-positive pathogens daptomycin: Comparison with cationic antimicrobial peptides and lipopeptides. Biochim. Biophys. Acta - Biomembr. *1758*, 1215–1223.

Strominger, J.L. (1958). Enzymic transfer of pyruvate to uridine diphosphoacetylglucosamine. Biochim. Biophys. Acta *30*, 645–646.

Su, L., Li, J., Zhou, Z., Huang, D., Zhang, Y., Pei, H., Guo, W., Wu, H., Wang, X., Liu, M., *et al.* (2019). Design, synthesis and evaluation of hybrid of tetrahydrocarbazole with 2,4-diaminopyrimidine scaffold as antibacterial agents. Eur. J. Med. Chem. *162*, 203–211.

Su, M., Xia, D., Teng, P., Nimmagadda, A., Zhang, C., Odom, T., Cao, A., Hu, Y., and Cai, J. (2017). Membrane-Active Hydantoin Derivatives as Antibiotic Agents. J. Med. Chem. *60*, 8456–8465.

Surur, A.S., and Sun, D. (2021). Macrocycle-Antibiotic Hybrids: A Path to Clinical Candidates. Front. Chem. *9*, 659845.

Süssmuth, R.D., and Mainz, A. (2017). Nonribosomal Peptide Synthesis—Principles and Prospects. Angew. Chemie - Int. Ed.

Suzuki, T., Campbell, J., Kim, Y., Swoboda, J.G., Mylonakis, E., Walker, S., and Gilmore, M.S. (2012). Wall teichoic acid protects *Staphylococcus aureus* from inhibition by Congo red and other dyes. J. Antimicrob. Chemother. *67*, 2143–2151.

Swoboda, J.G., Meredith, T.C., Campbell, J., Brown, S., Suzuki, T., Bollenbach, T., Malhowski, A.J., Kishony, R., Gilmore, M.S., and Walker, S. (2009). Discovery of a small molecule that blocks wall teichoic acid biosynthesis in *Staphylococcus aureus*. ACS Chem. Biol. *4*, 875–883.

T'Hart, P., Kleijn, L.H.J., de Bruin, G., Oppedijk, S.F., Kemmink, J., and Martin, N.I. (2014). A combined solid- and solution-phase approach provides convenient access to analogues of the calcium-dependent lipopeptide antibiotics. Org. Biomol. Chem. *12*, 913–918.

T'Hart, P., Oppedijk, S.F., Breukink, E., and Martin, N.I. (2016). New Insights into Nisin's Antibacterial Mechanism Revealed by Binding Studies with Synthetic Lipid II Analogues. Biochemistry *55*, 232–237.

Tacconelli, E., Carrara, E., Savoldi, A., Harbarth, S., Mendelson, M., Monnet, D.L., Pulcini, C., Kahlmeter, G., Kluytmans, J., Carmeli, Y., *et al.* (2018). Discovery, research, and development of new antibiotics: the WHO priority list of antibiotic-resistant bacteria and tuberculosis. Lancet Infect. Dis. *18*, 318–327.

Taguchi, A., Welsh, M.A., Marmont, L.S., Lee, W., Sjodt, M., Kruse, A.C., Kahne, D., Bernhardt, T.G., and Walker, S. (2019). FtsW is a peptidoglycan polymerase that is functional only in complex with its cognate penicillin-binding protein. Nat. Microbiol.

Tahlan, K., Wilson, R., Kastrinsky, D.B., Arora, K., Nair, V., Fischer, E., Barnes, S.W., Walker, J.R., Alland, D., Barry, C.E., *et al.* (2012). SQ109 Targets MmpL3, a Membrane Transporter of Trehalose Monomycolate Involved in Mycolic Acid Donation to the Cell Wall Core of *Mycobacterium tuberculosis*. Antimicrob. Agents Chemother. *56*, 1797–1809.

Tan, S. (2022). Remodeling of Peptidoglycan Biosynthesis in *Staphylococcus aureus* for Enhanced Antimicrobial Activity and Novel Drug Discovery University of Toronto.

Tan, S., Moore, G., and Nodwell, J. (2019). Put a Bow on It: Knotted Antibiotics Take Center Stage. Antibiotics *8*, 117.

Taylor, C.M., and Roberts, I.S. (2004). Capsular Polysaccharides and Their Role in Virulence. In Concepts in Bacterial Virulence, (Basel: Karger), pp. 55–66.

Taylor, S.D., and Palmer, M. (2016). The action mechanism of daptomycin. Bioorg. Med. Chem. *24*, 6253–6268.

Thakker, M., Park, J.S., Carey, V., and Lee, J.C. (1998). *Staphylococcus aureus* serotype 5 capsular polysaccharide is antiphagocytic and enhances bacterial virulence in a murine bacteremia model. Infect. Immun. *66*, 5183–5189.

Tian, X., Sun, F., Zhou, X.R., Luo, S.Z., and Chen, L. (2015). Role of peptide self-assembly in antimicrobial peptides. J. Pept. Sci. *21*, 530–539.

Tickle, A., Ledger, E.V.K., and Edwards, A.M. (2022). Human serum induces daptomycin tolerance in *Enterococcus faecalis* and viridans group streptococci. BioRxiv 2022.10.12.511873.

Tietz, J.I., Schwalen, C.J., Patel, P.S., Maxson, T., Blair, P.M., Tai, H.C., Zakai, U.I., and Mitchell, D.A. (2017). A new genome-mining tool redefines the lasso peptide biosynthetic landscape. Nat. Chem. Biol. *13*, 470–478.

Tipper, D.J., and Strominger, J.L. (1966). Isolation of 4-o-β-*N*-acetylmuramyl-*N*-acetylglucosamine and 4-O-β-*N*,6-0-diacetylmuramyl-*N*-acetylglucosamine and the structure of the cell wall polysaccharide of *Staphylococcus aureus*. Biochem. Biophys. Res. Commun. *22*, 48–56.

Tommasi, R., Brown, D.G., Walkup, G.K., Manchester, J.I., and Miller, A.A. (2015). ESKAPEing the labyrinth of antibacterial discovery. Nat. Rev. Drug Discov. *14*, 529–542.

Touzé, T., Tran, A.X., Hankins, J. V., Mengin-Lecreulx, D., and Trent, M.S. (2008). Periplasmic phosphorylation of lipid A is linked to the synthesis of undecaprenyl phosphate. Mol. Microbiol. *67*, 264–277.

Tran, T.T., Munita, J.M., and Arias, C.A. (2015). Mechanisms of drug resistance: Daptomycin resistance. Ann. N. Y. Acad. Sci. *1354*, 32–53.

Tsunakawa, M., Hu, S.L., Hoshino, Y., Detlefson, D.J., Hill, S.E., Furumai, T., White, R.J., Nishio, M., Kawano, K., Yamamoto, S., *et al.* (1995). Siamycins I and II, New Anti-HIV Peptides: I. Fermentation, Isolation, Biological Activity and Initial Characterization. J. Antibiot. (Tokyo). *48*, 433–434.

U.S. Committee on the Judiciary, S. on A. and M. (1961). Administered Prices, Drugs (U.S. Government Printing Office).

U.S. Federal Trade Commission (1958). Economic Report on Antibiotics Manufacture (U.S. Government Printing Office).

Ulm, H., and Schneider, T. (2016). Targeting bactoprenol-coupled cell envelope precursors. Appl. Microbiol. Biotechnol. *100*, 7815–7825.

Um, S., Kim, Y.J., Kwon, H., Wen, H., Kim, S.H., Kwon, H.C., Park, S., Shin, J., and Oh, D.C. (2013). Sungsanpin, a lasso peptide from a deep-sea streptomycete. J. Nat. Prod. *76*, 873–879.

Upert, G., Luther, A., Obrecht, D., and Ermert, P. (2021). Emerging peptide antibiotics with therapeutic potential. Med. Drug Discov. *9*, 100078.

Ushijima, T. (1967). Fine Structure of Strictly Anaerobic, Non-Spore-Forming, Gram-Negative Bacilli. Jpn. J. Microbiol. *11*, 275–287.

Varney, K.M., Bonvin, A.M.J.J., Pazgier, M., Malin, J., Yu, W., Ateh, E., Oashi, T., Lu, W., Huang, J., Diepeveen-de Buin, M., *et al.* (2013). Turning Defense into Offense: Defensin Mimetics as Novel Antibiotics Targeting Lipid II. PLoS Pathog. *9*, e1003732.

Ventola, C.L. (2015). The antibiotic resistance crisis: part 1: causes and threats. P T *40*, 277–283.

Vergalli, J., Bodrenko, I. V., Masi, M., Moynié, L., Acosta-Gutiérrez, S., Naismith, J.H., Davin-Regli, A., Ceccarelli, M., van den Berg, B., Winterhalter, M., *et al.* (2020). Porins and small-molecule translocation across the outer membrane of Gram-negative bacteria. Nat. Rev. Microbiol. *18*, 164–176.

Vollmer, W. (2008). Structural variation in the glycan strands of bacterial peptidoglycan. FEMS Microbiol. Rev. *32*, 287–306.

Vollmer, W., and Seligman, S.J. (2010). Architecture of peptidoglycan: more data and more models. Trends Microbiol. *18*, 59–66.

Vollmer, W., Blanot, D., and de Pedro, M.A. (2008). Peptidoglycan structure and architecture. FEMS Microbiol. Rev. *32*, 149–167.

Waglechner, N., Culp, E.J., and Wright, G.D. (2021). Ancient Antibiotics, Ancient Resistance. EcoSal Plus *9*, 157–159.

Wale, L.J., Shelton, A.P., and Greenwood, D. (1989). Scanning electronmicroscopy of *Staphylococcus aureus* and *Enterococcus faecalis* exposed to daptomycin. J. Med. Microbiol. *30*, 45–49.

Walker, S., Chen, L., Hu, Y., Rew, Y., Shin, D., and Boger, D.L. (2005). Chemistry and biology of ramoplanin: A lipoglycodepsipeptide with potent antibiotic activity. Chem. Rev. *105*, 449–475.

Wang, B., Pachaiyappan, B., Gruber, J.D., Schmidt, M.G., Zhang, Y.M., and Woster, P.M. (2016a). Antibacterial Diamines Targeting Bacterial Membranes. J. Med. Chem. *59*, 3140–3151.

Wang, H., Gill, C.J., Lee, S.H., Mann, P., Zuck, P., Meredith, T.C., Murgolo, N., She, X., Kales, S., Liang, L., *et al.* (2013). Discovery of wall teichoic acid inhibitors as potential anti-MRSA β-lactam combination agents. Chem. Biol. *20*, 272–284.

Wang, Q.M., Peery, R.B., Johnson, R.B., Alborn, W.E., Yeh, W.K., and Skatrud, P.L. (2001). Identification and characterization of a monofunctional glycosyltransferase from *Staphylococcus aureus*. J. Bacteriol. *183*, 4779–4785.

Wang, Y., Desai, J., Zhang, Y., Malwal, S.R., Shin, C.J., Feng, X., Sun, H., Liu, G., Guo, R.T., and Oldfield, E. (2016b). Bacterial Cell Growth Inhibitors Targeting Undecaprenyl Diphosphate Synthase and Undecaprenyl Diphosphate Phosphatase. ChemMedChem *11*, 2311–2319.

Wang, Z., Koirala, B., Hernandez, Y., Zimmerman, M., and Brady, S.F. (2022). Bioinformatic prospecting and synthesis of a bifunctional lipopeptide antibiotic that evades resistance. Science *376*, 991–996.

Watanabe, T., Hashimoto, Y., Yamamoto, K., Hirao, K., Ishihama, A., Hino, M., and Utsumi, R. (2003). Isolation and characterization of inhibitors of the essential histidine kinase, YycG in *Bacillus subtilis* and *Staphylococcus aureus*. J. Antibiot. (Tokyo). *56*, 1045–1052.

Weidenmaier, C., and Peschel, A. (2008). Teichoic acids and related cell-wall glycopolymers in Gram-positive physiology and host interactions. Nat. Rev. Microbiol. *6*, 276–287.

Weidenmaier, C., Kokai-Kun, J.F., Kristian, S.A., Chanturiya, T., Kalbacher, H., Gross, M., Nicholson, G., Neumeister, B., Mond, J.J., and Peschel, A. (2004). Role of teichoic acids in *Staphylococcus aureus* nasal colonization, a major risk factor in nosocomial infections. Nat. Med. *10*, 243–245.

Weidenmaier, C., Kokai-Kun, J.F., Kulauzovic, E., Kohler, T., Thumm, G., Stoll, H., Götz, F., and Peschel, A. (2008). Differential roles of sortase-anchored surface proteins and wall teichoic acid in *Staphylococcus aureus* nasal colonization. Int. J. Med. Microbiol. *298*, 505–513.

Weintraub, A. (2003). Immunology of bacterial polysaccharide antigens. Carbohydr. Res. *338*, 2539–2547.

Welling, M.M., Nabuurs, R.J.A., and Van Der Weerd, L. (2015). Potential role of antimicrobial peptides in the early onset of Alzheimer's disease. Alzheimer's Dement. *11*, 51–57.

Wenzel, M., and Bandow, J.E. (2011). Proteomic signatures in antibiotic research. Proteomics *11*, 3256–3268.

Whitfield, C., Wear, S.S., and Sande, C. (2020). Assembly of Bacterial Capsular Polysaccharides and Exopolysaccharides. Annu. Rev. Microbiol. *74*, 521–543.

WHO (2017). Global priority list of antibiotic-resistant bacteria to guide research, discovery, and development of new antibiotics.

WHO (2020). Global Tuberculosis Report.

WHO (2021). Bacterial vaccines in clinical and preclinical development 2021.

Wiedemann, I., Breukink, E., Van Kraaij, C., Kuipers, O.P., Bierbaum, G., De Kruijff, B., and Sahl, H.G. (2001). Specific binding of nisin to the peptidoglycan precursor lipid II combines pore formation and inhibition of cell wall biosynthesis for potent antibiotic activity. J. Biol. Chem. *276*, 1772–1779.

Willing, S., Schneewind, O., and Missiakas, D. (2021). Regulated Cleavage of Glycan Strands by the Murein Hydrolase SagB in *Staphylococcus aureus* Involves a Direct Interaction with LyrA (SpdC). J. Bacteriol. *203*.

Wilmes, M., Cammue, B.P.A., Sahl, H.G., and Thevissen, K. (2011). Antibiotic activities of host defense peptides: More to it than lipid bilayer perturbation. Nat. Prod. Rep. *28*, 1350–1358.

Wirtz, D.A. (2022). Biochemical and structural characterization of β-hydroxylases in non-ribosomal peptide biosynthesis. University of Bonn.

Woldringh, C.L., Huls, P., Pas, E., Brakenhoff, G.J., and Nanninga, N. (1987). Topography of Peptidoglycan Synthesis during Elongation and Polar Cap Formation in a Cell Division Mutant of *Escherichia coli* MC4100. Microbiology *133*, 575–586.

Wolf, D., Kalamorz, F., Wecke, T., Juszczak, A., Mäder, U., Homuth, G., Jordan, S., Kirstein, J., Hoppert, M., Voigt, B., *et al.* (2010). In-depth profiling of the LiaR response of *Bacillus subtilis*. J. Bacteriol. *192*, 4680–4693.

Woodward, R., Yi, W., Li, L., Zhao, G., Eguchi, H., Sridhar, P.R., Guo, H., Song, J.K., Motari, E., Cai, L., *et al.* (2010). *In vitro* bacterial polysaccharide biosynthesis: Defining the functions of Wzy and Wzz. Nat. Chem. Biol. *6*, 418–423.

Workman, S.D., and Strynadka, N.C.J. (2020). A Slippery Scaffold: Synthesis and Recycling of the Bacterial Cell Wall Carrier Lipid. J. Mol. Biol. *432*, 4964–4982.

Workman, S.D., Worrall, L.J., and Strynadka, N.C.J. (2018). Crystal structure of an intramembranal phosphatase central to bacterial cell-wall peptidoglycan biosynthesis and lipid recycling. Nat. Commun. *9*, 1159.

Wright, G.D. (2010). Q&A: Antibiotic resistance: where does it come from and what can we do about it? BMC Biol. *8*, 123.

Wyke, A.W., Ward, J.B., Hayes, M. V, and Curtis, N.A. (1981). A role *in vivo* for penicillin-binding protein-4 of *Staphylococcus aureus*. Eur. J. Biochem. *119*, 389–393.

Xia, G., Maier, L., Sanchez-Carballo, P., Li, M., Otto, M., Holst, O., and Peschel, A. (2010). Glycosylation of wall teichoic acid in *Staphylococcus aureus* by TarM. J. Biol. Chem. *285*, 13405–13415.

Xia, Z., Prescott, E., Leah, T., Dakin, H., Dimou, E., Zuo, E., Zhang, Y.P., Lam, J.Y.L., Danial, J.S.H., Jiang, H., *et al.* (2021). Co-aggregation with Apolipoprotein E modulates the function of Amyloid-β in Alzheimer's disease. BioRxiv 2021.07.13.452239.

Yamamoto, T., Matsui, H., Yamaji, K., Takahashi, T., Øverby, A., Nakamura, M., Matsumoto, A., Nonaka, K., Sunazuka, T., Ōmura, S., *et al.* (2016). Narrow-spectrum inhibitors targeting an alternative menaquinone biosynthetic pathway of *Helicobacter pylori*. J. Infect. Chemother. *22*, 587–592.

Yamazaki, Y., Zhao, N., Caulfield, T.R., Liu, C.C., and Bu, G. (2019). Apolipoprotein E and Alzheimer disease: pathobiology and targeting strategies. Nat. Rev. Neurol. *15*, 501–518.

Yang, H., Wierzbicki, M., Du Bois, D.R., and Nowick, J.S. (2018). X-ray Crystallographic Structure of a Teixobactin Derivative Reveals Amyloid-like Assembly. J. Am. Chem. Soc. *140*, 14028–14032.

Yang, L., Wang, G., and Xia, H. (2020). Molecular mechanism for impaired suppressive function of Tregs in autoimmune diseases: A summary of cell-intrinsic and cell-extrinsic factors. J. Cell. Mol. Med. *24*, 11056–11063.

Yang, S.-J.J., Mishra, N.N., Rubio, A., and Bayer, A.S. (2013). Causal role of single nucleotide polymorphisms within the *mprF* gene of *Staphylococcus aureus* in daptomycin resistance. Antimicrob. Agents Chemother. *57*, 5658–5664.

Yano, K., Toki, S., Nakanishi, S., Ochiai, K., Ando, K., Yoshida, M., Matsuda, Y., and Yamasaki, M. (1996). MS-271, a novel inhibitor of calmodulin-activated myosin light chain kinase from *Streptomyces* sp. - I. Isolation, structural determination and biological properties of MS-271. Bioorganic Med. Chem. *4*, 115–120.

Yates, S.L., Burgess, L.H., Kocsis-Angle, J., Antal, J.M., Dority, M.D., Embury, P.B., Piotrkowski, A.M., and Brunden, K.R. (2000). Amyloid β and amylin fibrils induce increases in proinflammatory cytokine and chemokine production by THP-1 cells and murine microglia. J. Neurochem. *74*, 1017–1025.

Yother, J. (2011). Capsules of *Streptococcus pneumoniae* and other bacteria: Paradigms for polysaccharide biosynthesis and regulation. Annu. Rev. Microbiol.

Young, S., Rohr, J.R., and Harwood, V.J. (2019). Vancomycin resistance plasmids affect persistence of *Enterococcus faecium* in water. Water Res. *166*, 115069.

El Zahed, S.S., French, S., Farha, M.A., Kumar, G., and Brown, E.D. (2021). Physicochemical and Structural Parameters Contributing to the Antibacterial Activity and Efflux Susceptibility of Small-Molecule Inhibitors of Escherichia coli. Antimicrob. Agents Chemother. *65*.

Zapun, A., Philippe, J., Abrahams, K.A., Signor, L., Roper, D.I., Breukink, E., and Vernet, T. (2013). *In vitro* reconstitution of peptidoglycan assembly from the gram-positive pathogen *Streptococcus pneumoniae*. ACS Chem. Biol. *8*, 2688–2696.

Zaschke-Kriesche, J., Unsleber, S., Voitsekhovskaia, I., Kulik, A., Behrmann, L. V., Overbeck, N., Stühler, K., Stegmann, E., and Smits, S.H.J. (2020). Mechanism of BceAB-type transporter: Resistance by lipid II flipping. BioRxiv 2020.03.05.978734.

Zhang, Y., Carney, D., Henninot, A., and Srinivasan, K. (2021). Novel High-Throughput Strategy for the Aqueous Solubility Assessment of Peptides and Proteins Exhibiting a Propensity for Gelation: Application to the Discovery of Novel Antibacterial Teixobactin Analogues. Mol. Pharm. *18*, 469–474.

Zhu, W., Zhang, Y., Sinko, W., Hensler, M.E., Olson, J., Molohon, K.J., Lindert, S., Cao, R., Li, K., Wang, K., *et al.* (2013). Antibacterial drug leads targeting isoprenoid biosynthesis. Proc. Natl. Acad. Sci. U. S. A. *110*, 123–128.

Zong, Y., Sun, X., Gao, H., Meyer, K.J., Lewis, K., and Rao, Y. (2018). Developing Equipotent Teixobactin Analogues against Drug-Resistant Bacteria and Discovering a Hydrophobic Interaction between Lipid II and Teixobactin. J. Med. Chem. *61*, 3409–3421.

Zuttion, F., Colom, A., Matile, S., Farago, D., Pompeo, F., Kokavecz, J., Galinier, A., Sturgis, J., and Casuso, I. (2020). High-speed atomic force microscopy highlights new molecular mechanism of daptomycin action. Nat. Commun. *11*, 1–16.

VII. Acknowledgements

The past years have been an amazing journey and there are many people that I would like to acknowledge for making it such a great experience.

Foremost, I would like to express my warmest gratitude to my supervisor Prof. Dr. Tanja Schneider for bringing the weight of her immense experience and knowledge to this thesis. Thank you for guiding me through all stages of this project and for the stimulating scientific discussions!

I would also like to thank the members of my promotion committee, Prof. Dr. Lukas Schreiber, Priv.-Doz. Dr. Christiane Dahl, and Prof. Dr. Ulrich Kubitscheck for reading and evaluating the thesis.

The completion of this thesis could not have been achieved without the expertise of Dr. Anna Müller. Thank you for teaching me several new techniques, for all your valuable advice and for introducing me into the lab when I started in Bonn.

Dr. Fabian Grein, Dr. Beate Henrichfreise, Prof. Dr. Hans-Georg Sahl, Prof. Dr. Gabriele Bierbaum, and Dr. Marvin Rausch, thank you for your continuous support and for the interesting discussions! I have learned a lot from you.

I sincerely thank all collaboration partners and co-authors of the included publications. Thank you for the pleasant teamwork. The list of these people is composed of smart and kind scientists of many interdisciplinary fields.

I want to thank my fellow labmates for the nice atmosphere, the moral support and for all the amazing conversations. Thanks goes also to the technichians, especially to Isabel Bodenstein and Michaele Josten who was involved in most of the studies. I was also lucky to supervise a large number of brainy students. I am grateful for all your helpful contributions!

I would like to give a very special thanks to my wife Franziska Ludwig and my family as a whole for their continuous support and understanding when undertaking my research. Their belief in me has kept my spirits and motivation high during the past years.

Lastly, I would be remiss in not acknowledging my eternal companion *Staphylococcus aureus*, without whom this study could not have been possible.